THE GEOCHEMISTRY AND MINERALOGY OF PACIFIC SEDIMENTS, BAJA CALIFORNIA

by

GRAHAM BARRY SHIMMIELD, B.Sc.

A thesis submitted for the degree of

DOCTOR OF PHILOSOPHY

at the University of Edinburgh

October, 1984

DECLARATION

I certify that the work described in this thesis is my own, except where otherwise stated, and has not been previously submitted for a degree at this, or any other, University.

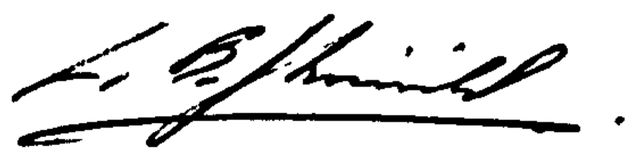

Graham B. Shimmield

ABSTRACT

The geochemical composition, mineralogy and radiochemistry of a suite of box-cores traversing the Pacific margin of the Baja California peninsula has been investigated. In particular, the role of diagenesis in influencing geochemical transformations is assessed.

The Baja California margin is situated at the confluence of the California Current and California Undercurrent. Resulting upwelling and high surface productivity results in a substantial flux of organic matter to the shelf and hemipelagic environment.

Detrital element geochemistry (Si, Zr, K, Mg, Fe, Rb) and mineralogy indicates that clay contents increase oceanwards, the hemipelagic and pelagic environment being dominated by smectite. Within hemipelagic sediments, grain size increases with depth (>20 cm), attributed to enhanced detrital sedimentation during the last glacial episode. Biogenic elements (Ca, Sr) are also elevated in glacial sediment although the enrichment may be due to either increased biological productivity or an increase in detrital carbonate. Ba is believed to result from biological vectoring but is diluted in concentration in glacial sediment.

Organic matter diagenesis results in a sequence of diagenetic zones within hemipelagic and pelagic sediment. With increasing diagenesis N, I and Br are more labile than in the fully oxic pelagic sediment where clay fixation is prominent. On the shelf, heavy metals (Cr, Ni, Cu, Zn, Mo, Pb), do not appear to be associated with the high levels of organic matter found, whilst grain size effectively controls the depth distribution of organic C.

The remobilisation of Mn and associated trace metals (Ni, Cu, Zn, Mo) during diagenesis is well displayed in hemipelagic sediments. The depth to the onset of Mn reduction occurs within bioturbated sediment defined by the distribution of ^{230}Th and ^{231}Pa. The oxidation state of the Mn is always high ($\sim MnO_{1.8}$) above the redoxcline although reduction in microenvironments at the sediment/water interface results in slightly lower oxidation states ($\sim MnO_{1.75}$). The level of trace metal enrichment is Mo>Ni>Zn=Cu, the same as their relative concentrations in seawater. With increasing diagenesis Ni decreases relative to Mn^{4+}. Following Mn reduction smectite absorbtion of released trace metals is important. Mo is lost prior to Mn remobilisation probably to the dissolved organic carbon pool or to monosulphide precipitation.

Measured $^{230}Th_{excess}/^{231}Pa_{excess}$ activity ratios decrease monotonically landwards. This is indication of preferential ^{231}Pa removal at ocean margins. With time the flux of particles has varied, resulting in changing initial activity ratios within the sediment. Long-lived isotopes are therefore unsuitable to the measurement of sedimentation rate in areas subject to variable particle flux.

Diagenetic mineral formation occurs in a variety of depositional environments. The precipitation of both apatite and manganese carbonate occurs in coarser-grained sediment, apatite forming on the shelf resulting from PO_4^{3-} generation during organic matter decomposition, and manganese carbonate forming at depth in the hemipelagic sediment after reduction of MnO_2. Glaucony forms at sites of local reduction prior to SO_4^{2-} reduction. Dolomite forms in slowly-accumulating, organic-rich

sediments of the hemipelagic and slope environments prior to extensive SO_4^{2-} reduction. Pyrite formation is an important sink for Fe in reducing shelf sediments.

TABLE OF CONTENTS

APPENDICES

CHAPTER 1

INTRODUCTION

In recent years our knowledge of the chemistry of deep-sea sediments has increased, due in part to the use of high technology apparatus, and in part to the rise in number of researchers in this field and the growing awareness of its importance as a scientific subject. Large-scale, multi-million dollar projects have been funded (Deep Ocean Mining Environmental Study, DOMES; Manganese Nodule Program, MANOP) in order to tackle the problems of sedimentary geochemistry with a view to exploiting the mineral resources of the deep-sea. Similar projects in this country consider aspects of nuclear waste disposal in marine sediments. However, a fully integrated study of deep-sea processes has yet to be realised and the MANOP concept of studying several areas of the Pacific ocean characterised by different types of sediment input has been effectively terminated due to the present economic situation. Instead, the onus has again been placed on individual researchers to undertake studies, which by their very nature and complexity, involve only one or two components of a multi-faceted natural system. In the last few years the vogue has been to investigate aspects of the oceanic system by use of numerical models which often necessitate approximations and assumptions which are not fully justified. In particular, the role of ocean margins *vis-a-vis* the open ocean in controlling many processes which were once considered homogeneous is worthy of critical examination. The Baja California continental margin provides a possibly unique setting in which to observe the geochemistry of a range of sediment types in a variety of depositional and environmental habitats.

Fundamental to the study of sedimentary geochemistry is the characterisation of detrital input material and its spatial

and temporal variability. Due to geographic and oceanographic controls the major source of detrital material off Baja California is from terrigenous weathering processes, whilst biological productivity in surface waters provides a considerable flux of organic matter to the sea bed. Low overall sediment accumulation rates and decomposition of organic material conspire to establish a suite of diagenetic environments, each having distinct chemical signatures, reaction rates, and mineral assemblages.

With these factors in mind the geochemical investigation of the Baja California shelf, slope and oceanic sediments proceeds by studying the bulk geochemistry of detrital elements in order to elucidate the type and variation of input in a range of environments and with time. In particular, changes in sedimentation between the last glacial episode, the Wisconsin, and the present-day interglacial merits attention. Characterisation of diagenetic environments by geochemical indicators (oxygen, nitrate, manganese and iron oxides) and the quantity and quality of organic matter is examined. Organic matter contains several elements (N, P, I, Br) which behave differently depending on the degree and/or rate of diagenesis. These rates are quantified using simple kinetic models in order to identify the labile and refractory components of the organic system and to relate organic matter flux, depositional environment and sedimentation rate in an effort to outline controls on organic matter preservation.

The association of heavy metals (Ni, Cu, Pb, Zn) with organic-rich sediments in the geological record has often been discussed and debated. Shelf sediments off Baja California

containing large amounts of organic matter are investigated both with regard to their metal content and also their textural relationships. Findings are compared with studies made on other modern, organic-rich, shelf facies.

Murray and Irvine (1895) were the first to recognise the mobilisation of manganese in deep-sea sediments in the presence of organic matter. Since then many authors have documented the occurence of Mn-rich surficial sediments in the hemipelagic realm, often in association with minor metals. These studies have relied on the evaluation of solid phase profiles and sometimes their associated pore waters to understand the mechanisms of remobilisation and reprecipitation. In this study the importance of identifying the mineralogy and oxidation state of the host Mn oxide and its quantification with respect to minor metal uptake is stressed. In particular, the minor metal/Mn ratio through a range of sediments responding to increasing diagenesis is investigated.

The vectoring of radionuclides (^{230}Th and ^{231}Pa) laterally and vertically in the open ocean and ocean margins is receiving critical appraisal. In this thesis accumulation of these radionuclides in oceanic sediments off Baja California is assessed in the context of theoretical supply rates of these radionuclides (by radioactive decay from uniformly distributed U isotopes), and the particle flux characteristics of ocean margins. The conclusions of such an approach not only pertain to the present day oceanic system, but to the use of these particular radionuclides in any situation where particle flux may have changed substantially through time.

Finally, the manifestation of diagenesis through mineral formation in marine sediments is investigated. Controls

governing the precipitation of apatite, manganese carbonate, glauconite, dolomite and pyrite are discussed. The validity of extrapolating laboratory-simulated conditions for crystal growth to the natural system operating on a time-scale of hundreds of years, rather than days or months, in questionable. With further insight into the mechanism of diagenetic mineral formation at the present day we will have a potentially valuable tool in extrapolating and deciphering palaeo-environmental conditions of formation and sediment accumulation, of great importance to the hydrocarbon industry.

The geochemistry and mineralogy presented in this thesis is the result of analysis of a suite of box-cores collected along a transect normal to the strike of the Baja California peninsula during cruise TGT-163 of the R/V *Thomas G. Thompson* in November, 1981. The stations sample a range of environments found on the shelf, slope and abyssal plain (Figure 1.1) at a variety of water depths (Table 1.1). Methods of core collection, core descriptions and sample preparation may be found in Appendix A; analytical techniques and results in Appendices B and C, respectively. Throughout the thesis comparison is made with published analyses from the previous year's cruise, TGT-145, and work from the Deep Sea Drilling Project (DSDP), DOMES and MANOP projects. The location of these studies is shown in Figure 1.2.

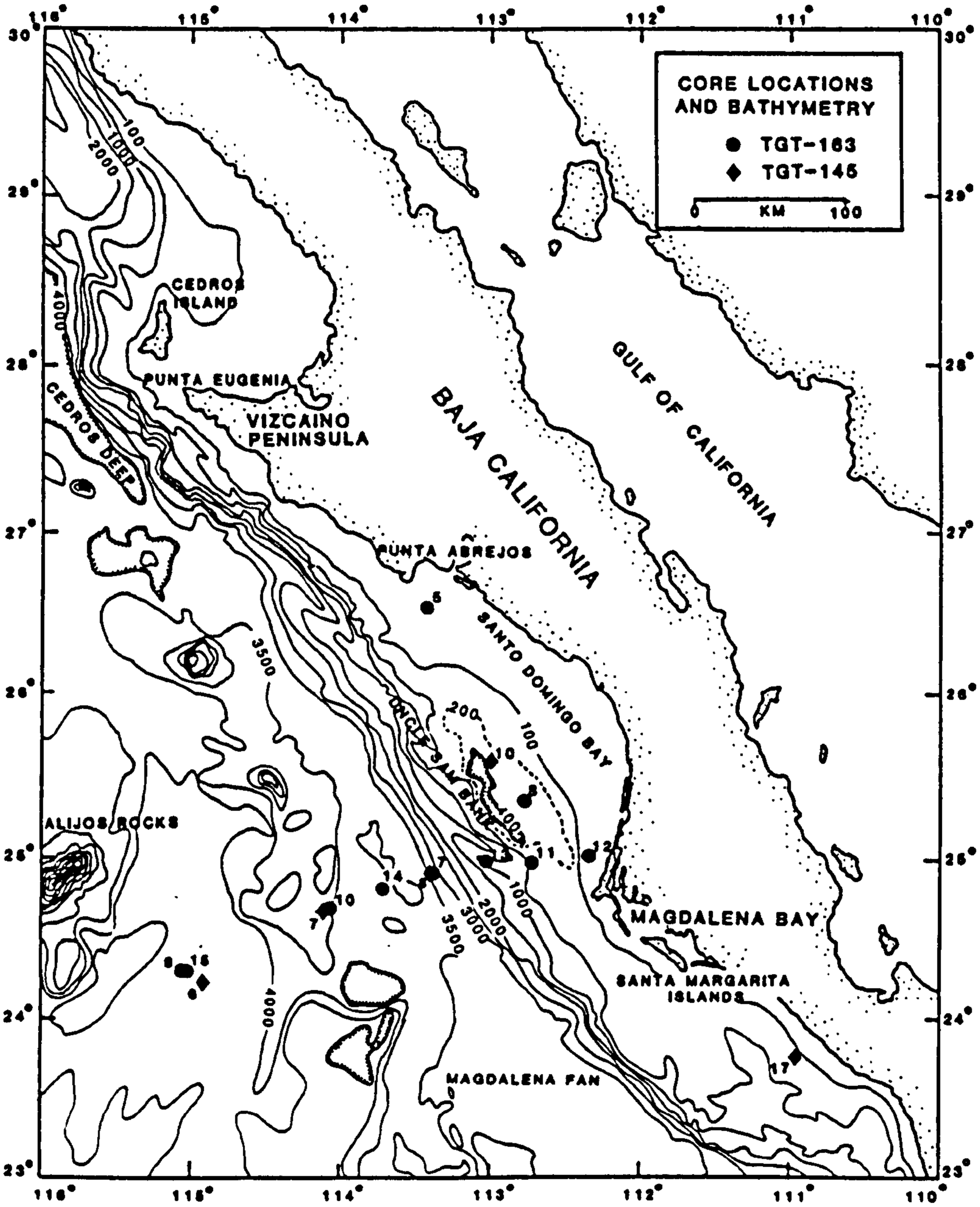

FIGURE 1.1 Locations of cores studied in this thesis. Bathymetry in meters.

TABLE 1.1

CORE LOCATIONS

CRUISE	CORE NO.	LATITUDE (N)	LONGITUDE (W)	WATER DEPTH (m)
TGT-145	5	23°-29.1'	117°-01.3'	3987
"	6	24°-17.0'	114°-59.0'	3643
"	7	24°-41.9'	114°-06.4'	3639
"	8	24°-54.9'	113°-25.1'	3655
"	17	23°-45.0'	111°-00.0'	200
TGT-163	15	24°-16.1'	115°-02.5'	3936
"	9	24°-16.0'	115°-03.7'	3685
"	10	24°-41.7'	114°-04.0'	3462
"	14	24°-49.4'	113°-44.8'	3168
"	7	24°-54.8'	113°-25.0'	3647
"	13	24°-58.3'	113°-03.1'	992
"	11	24°-58.8'	112°-45.9'	262
"	12	25°-02.2'	112°-20.6'	75
"	8	25°-22.5'	112°-47.2'	311
"	5	26°-30.6'	113°-27.3'	71

Station locations and approximate water depths of sediment cores collected during cruises TGT-145 and TGT-163. All samples were obtained by box-core except 145-6. Suspended particulate material was collected at stations 145-5, 145-6 and 145-7.

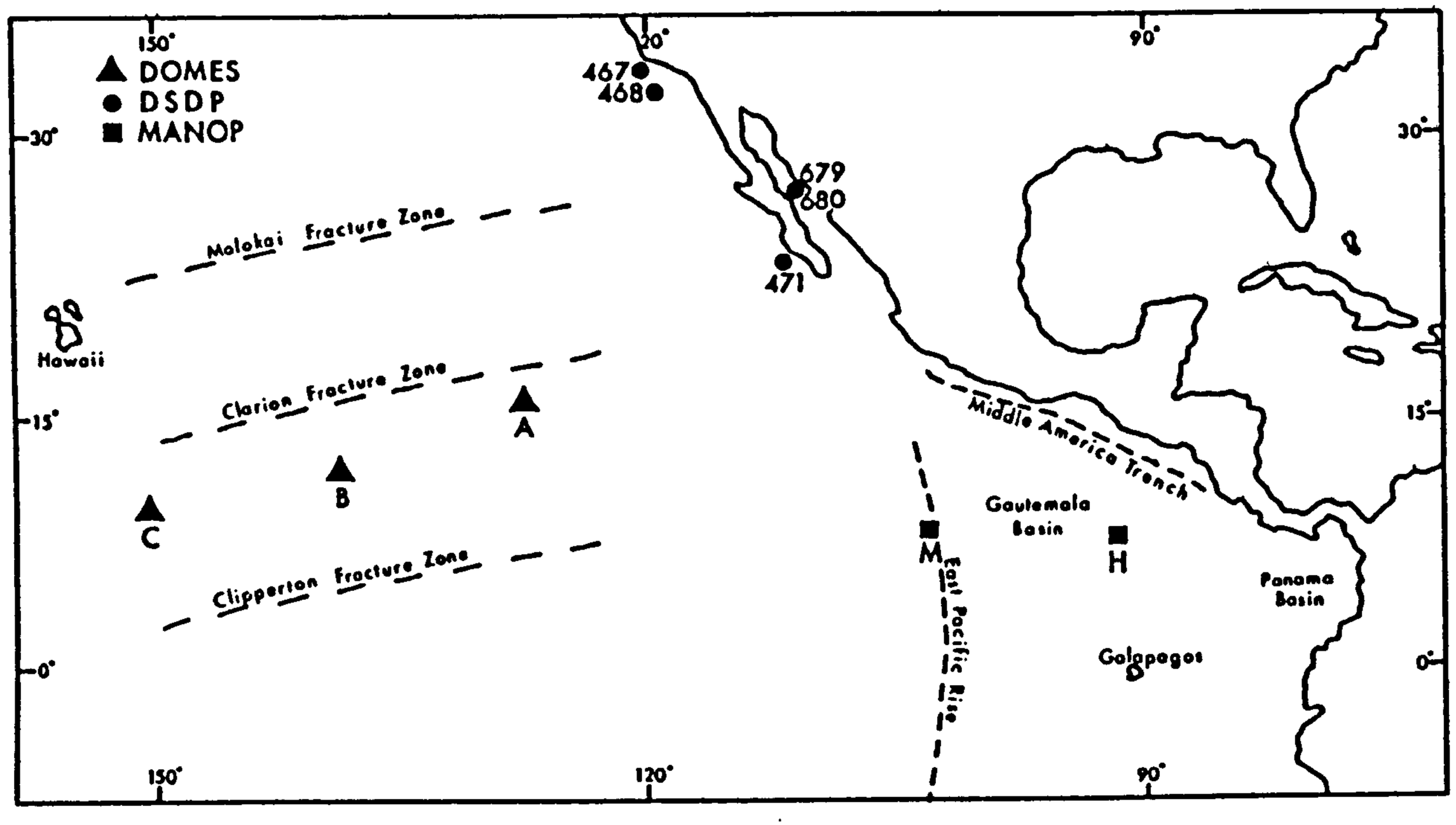

FIGURE 1.2 Locations of other sample sites referred to in this thesis.

CHAPTER 2

THE STUDY AREA

2.1 REGIONAL TECTONICS, GEOLOGY AND BATHYMETRY

The Pacific margin of Baja California can be divided into two main structural provinces. The NW-SE trending basin-and-ridge topography of the California continental borderland (Shepard and Emery, 1941; Emery, 1960) extends as far south as the Vizcaino Peninsula (Figure 1.1). Farther south, off Magdalena Bay, topographic relief is more subdued and the margin narrower than in the borderland province. This morphology reflects three distinct Cenozoic tectonic events (Krause, 1965; Spencer and Normark, 1979). The late Mesozoic and early Cenozoic subduction of the Farallon plate which continued into the Miocene and was succeeded by right-lateral transform faulting along the Pacific-North American plate boundary (Atwater, 1970; Doyle and Bandy, 1972; Atwater and Molnar, 1973; Spencer and Normark, 1979). The southward migrating ridge-trench-transform fault triple junction "jumped" eastwards about 4.5 Ma ago, forming the Gulf of California and leaving Baja California in a relatively passive intraplate setting (Larson, 1972). Seismic reflection data (Normark, 1977; Spencer and Normark, 1979) has revealed a continuous fault zone (the "Tosco-Abrejos Fault Zone") extending for 400 km along the continental margin south of the Vizcaino Peninsula, believed to mark the Neogene transform fault plate boundary between the Pacific and North America plates. Submarine ridges (eg Uncle Sam Bank) bounded on the east by faults and basins (D'Anglejan, 1967) extend NW-SE off Magdalena Bay (Figure 1.1). Recent seismicity (Sykes, 1968) and the uneven seafloor indicate that many of the faults are still active.

Evidence of previous subduction is found in the Franciscan-like terrain of Cedros Island, western Vizcaino Peninsula,

Magdalena and Santa Margarita Islands (Figure 1.1). The rocks around Magdalena Bay are predominantly sheared gabbro, serpentinites and variegated thin-bedded cherts, typical of a highly sheared ophiolite (Yeats *et al*, 1981). The continental shelf is underlain by Neogene sedimentary rocks that may overlie part of the accretionary wedge basement. On land, east of Magdalena Bay, exists a large area of Quaternary sands with economically important placer deposits of phosphorite, often in association with shelly coquinas. The bedrock is composed of shallow-water, shelf sands of the Eocene Tepetate Formation overlain by diatomaceous cherts and phosphorite bands of the Miocene Monterey Formation and its shallow-water, proximal facies equivalent, the San Isidro Formation. A marked erosional, transgressive unconformity separates these lithologies from the andesitic conglomerates and breccias of the Commondu Volcanics which form the mountainous backbone of southern Baja California. To the north and south of the peninsula Mesozoic granitic batholiths form upstanding plateaus, further extensions of which may be buried beneath the Commondu Volcanics. Deep Sea Drilling Project (DSDP) studies and acoustic profiling have revealed 15 Ma diabase beneath the sedimentary cover at the foot of the slope, indicative of the oceanic basement belonging either to the Pacific plate, or a fragment of the Farallon plate that was not consumed (Spencer and Normark, 1979).

The bathymetry west of Baja California is dominated by three main elements; the Guadalupe Arrugado to the north of the study area, the Cedros Deep and the Magdalena Fan (Figure 1.1). The Guadalupe Arrugado or "Rolling Plain" (Krause, 1965) is separated from the Baja California continental margin by the

Cedros Deep. It is a relatively flat area of the sea floor, some 3500 m deep, and was the site of the Experimental Mohole project in 1961. The Cedros Deep is a 4000 m deep, sediment-filled, flat-floored depression extending some 60-80 km seaward from the base of the continental slope. It may well be a remnant of the subduction trench formed during the consumation of the Farallon plate. The Magdalena Fan ia a broadly convex feature extending SW from the foot of the continental slope, between latitudes 23.3^{o}N and 24.1^{o}N, delineated by the 3200 m contour. Most of the sediment forming the fan was deposited prior to 13 Ma (Yeats and Haq, 1981) since when it has become a fossil feature. Exactly whether this shut-off of sediment supply was due to the opening of the Gulf of California, isolating the major source area of the Sierra Madre Occidental mountains on mainland Mexico, or that it was transported by right-lateral strike-slip from opposite the present position of the mouth of the Gulf of California, is debatable as both scenarios are not strongly supported by ages of events around the Gulf.

The shelf off Baja California between the Vizcaino Peninsula and Magdalena Bay is some 13,000 km^{2}, 80 km wide and less than 200 m deep. A faulted basin (113^{o}W, 25.5^{o}N) about three times the depth of the shelf is flanked to the west by a 100 km long line of ridges which form a sill limiting the free exchange of water between the shelf and open ocean.

2.2 CLIMATE

The semi-arid climate of the Baja California peninsula is characterised by 12 cm of rainfall per year (Aschman, 1959), which falls mostly during summer and autumn. Very few running streams cut the western coastal plain to enter the Pacific,

except during thunderstorms over the mountains when flash floods may occur. However, the deeply entrenched canyons, or "arroyos" suggest a wetter climate in the past (Arnold, 1957), perhaps during the last glacial episode. The undulating coastal plain sustains a desertic vegetation of cacti and hardy shrubs. Along the coast, north of Magdalena Bay, coastal dunes and lagoons become developed colonised by abundant mangroves. At present, the climate and transport processes conspire to prevent very little terrigenous supply to the outer shelf and hemipelagic environment.

2.3 CIRCULATION AND PRODUCTIVITY

The oceanic hydrography off Baja California is influenced by two large scale features of the east Pacific circulation pattern; the California Current and the California Undercurrent (Reid *et al*, 1958; Reid, 1963; Wooster and Jones, 1970). The undercurrent is restricted to a narrow longituidinal zone adjacent to the coast (Wooster and Jones, 1970) and interferes with the California Current to produce a complex eddy structure (Figure 2.1). Flow appears to be confined to the upper 500 m, transporting 15×10^6 m^3/s of water in a broad, weak southward movement (Wooster and Reid, 1963; Knauss, 1978).

During the summer the Pacific subtropical high-pressure cell intensifies and moves north along the western seaboard. Heating of the continental landmass develops a thermal low which further increases the coastal pressure gradient. The net result is a persistent coastal surface wind field that has a mean direction from the NNW (Breaker and Gilliland, 1981). The

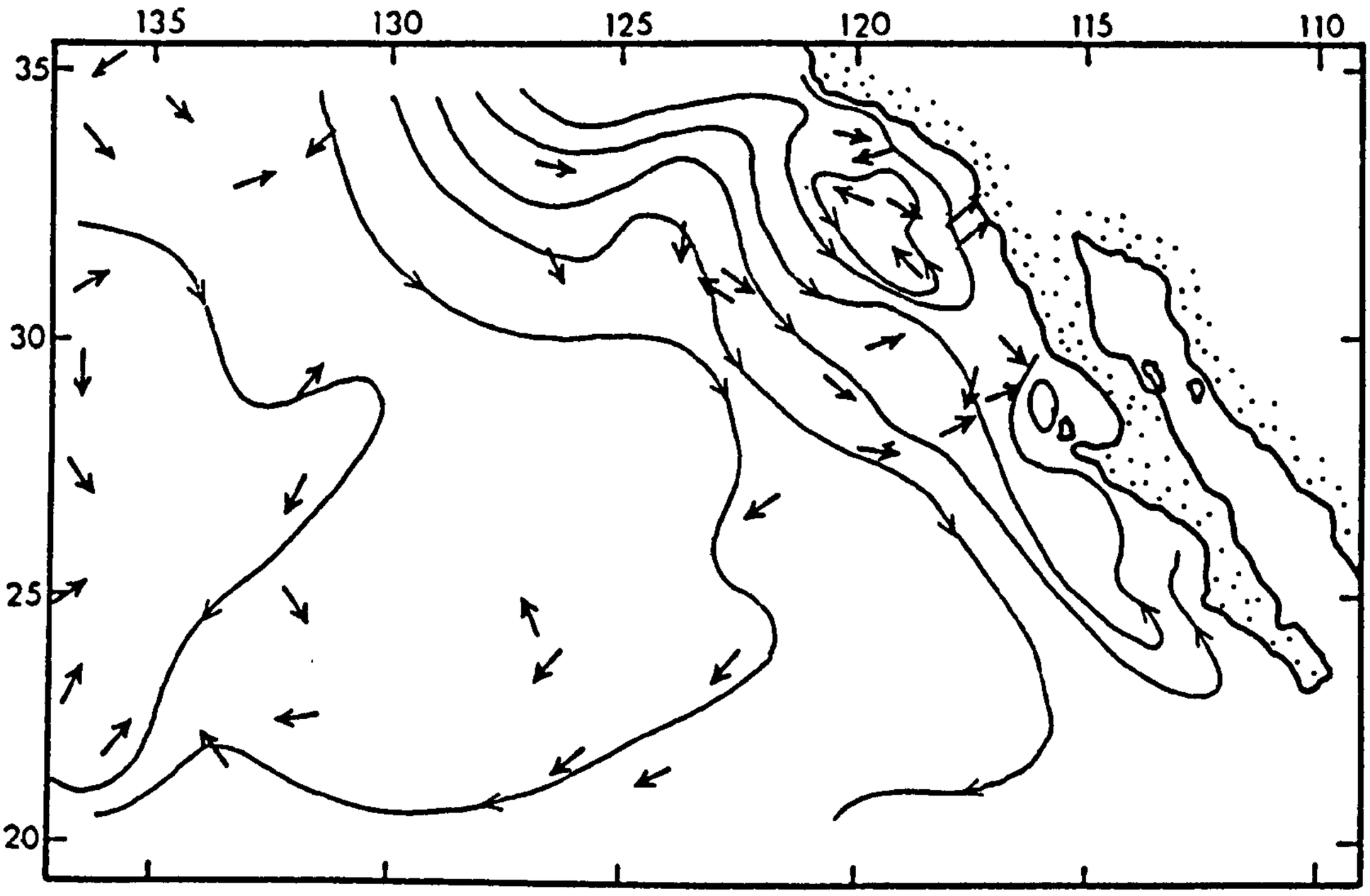

FIGURE 2.1 The complex eddy structure in the California Current off Baja California in March, 1954. The lines indicate the geostrophic flow pattern as calculated from temperature and salinity observations. Independant current measurements are shown by arrows (after Knauss, 1978).

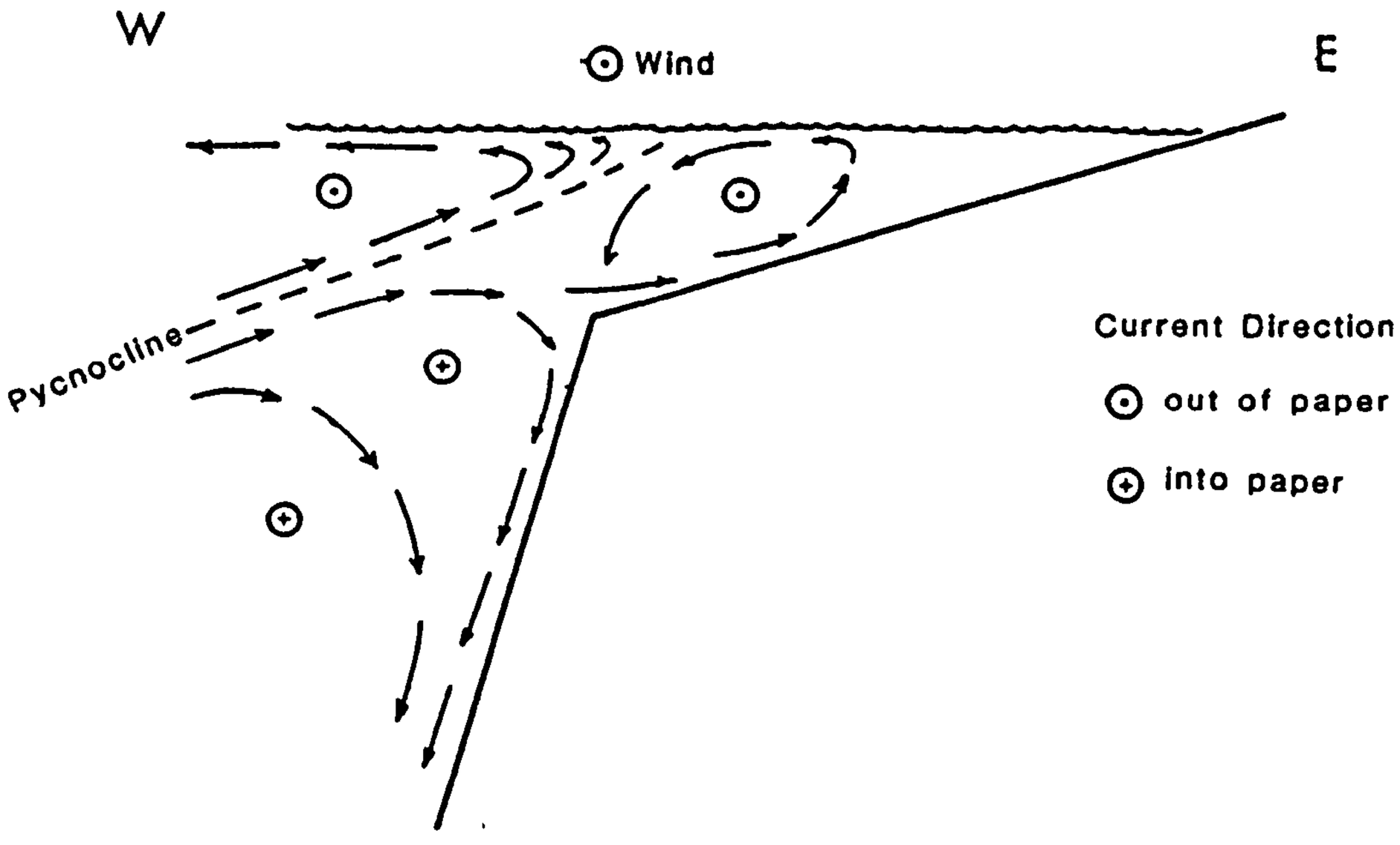

FIGURE 2.2 Diagrammatic representation of the interaction between the southward flowing California Current and the northward undercurrent off Baja California, resulting in density stratification and upwelling.

boundary between the California Current and undercurrent represents a trough in the sea surface, along the axis of these northerly winds. Off Baja California this trough and axis is farther offshore than in the California Bight (Munk, 1950). Resulting wind shear on the surface waters is at a maximum off southern Baja California during April, May and June (D'Anglejan, 1967) resulting in upwelling which is particularly intense off Punta Eugenia and Punta Abrejos (Figure 1.1). The southward flowing cold waters of the California Current override the more saline, oxygen depleted, nutrient-rich waters of the California Undercurrent (Ried *et al*, 1958; Murray *et al*, 1983) shown diagrammatically in Figure 2.2. With density stratification along the pycnocline an oxygen-minimum (<0.2 ml/l O_2) and nutrient maximum layer develop at about 200 m depth (D'Anglejan, 1967), somewhat shallower than farther north off southern California. As the edge of the shelf is also at about 200 m depth the oxygen depleted waters override the longitudinal sills at times of maximum upwelling, leading to low O_2 levels in the near bottom waters of the shelf and O_2 starvation in the basins (D'Anglejan, 1967). However, Phleger and Soutar (1973) found O_2 concentrations of these near-bottom waters to fluctuate strongly, being minimal during July and August.

In deeper water off the shelf (station 145-7, Figure 2.3) NO_3^- distribution mirrors the dissolved O_2 with a maximum concentration ~500 m deeper than the lowest dissolved O_2 (Murray *et al*, 1983), although denitrification at shallower depths may be responsible for the discrepancy. Dissolved silicate increases with depth and attains a broad concentration maximum ~1000 m above the seafloor.

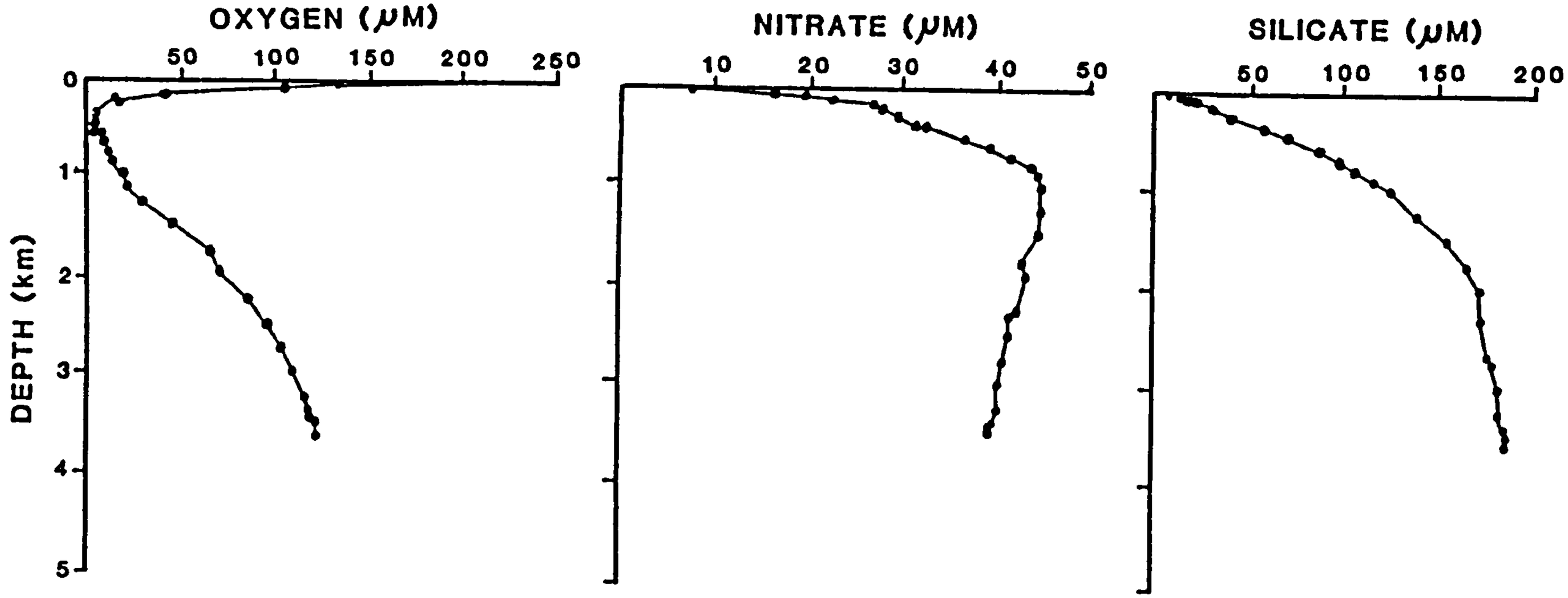

FIGURE 2.3 Nutrient profiles from TGT-145, station 7 (Murray *et al*, 1982).

On an areal distribution chlorophyll-*a* follows that of NO_3^- in the California Current (Bernal and McGowan, 1981). There is a concentration gradient that decreases both south and west (Figure 2.4a). Zooplankton also follow this general trend, although their distribution tends to be more patchy (Figure 2.4b; Smith, 1971). By using time series spectral analysis on biological and physical data for the California Current over the last 21 years Bernal and McGowan (1981) has come up with the surprising result that zooplankton biomass is uncorrelated with upwelling. Instead, advective transport of cold, low-salinity, high-nutrient water coming horizontally from the north in the main body of the California Current has a dominating influence. While this appears to be the general mechanism for the northern segment of the California Current, off Baja California local upwelling and mixing will have an important effect on introducing nutrients to the euphotic zone augmenting primary productivity.

Standing stocks of benthic foraminifera on the low-O_2 shelf are very large (Pheleger and Soutar, 1973). The population is dominated by the genera *Bolivina, Uvigerina* and *Bulimina* (Plate 2.1a), the foraminifera being small and thin-shelled, a characteristic of large standing stocks in areas of high production. The very high level of organic detritus causes the sediment to become anoxic immediately beneath the sediment/water interface. Nevertheless, the basin near station 163-8 (Figure 1.1) has a higher standing stock of benthic foraminifera (4300) than the Santa Barbara basin (2100-2300) or off Peru (1200) (all units in live forams per 20 cm^2 of surface sediment; Pheleger and Soutar, 1973).

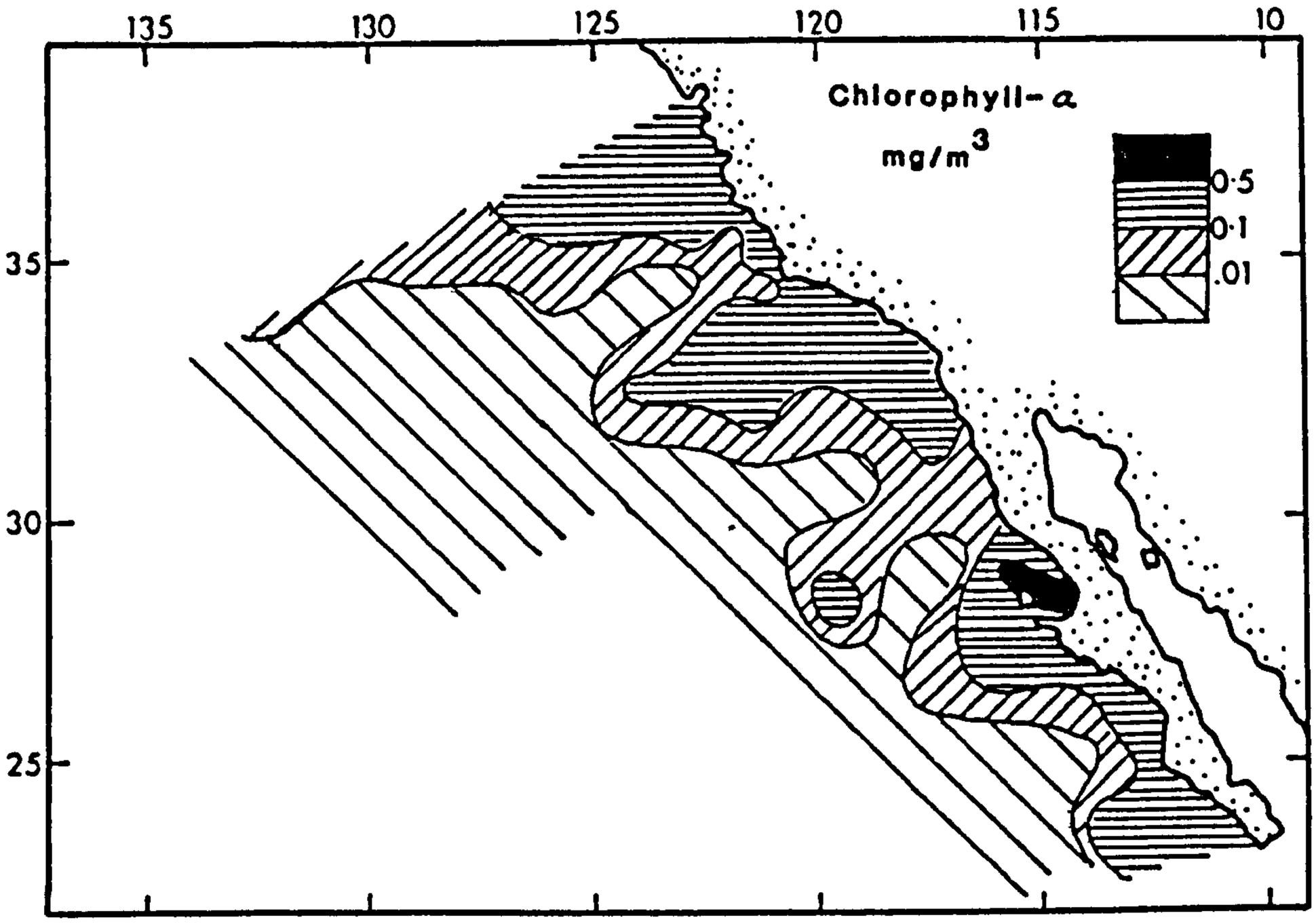

FIGURE 2.4 (a) Contoured concentrations of chlorophyll-a at 10 m depth.

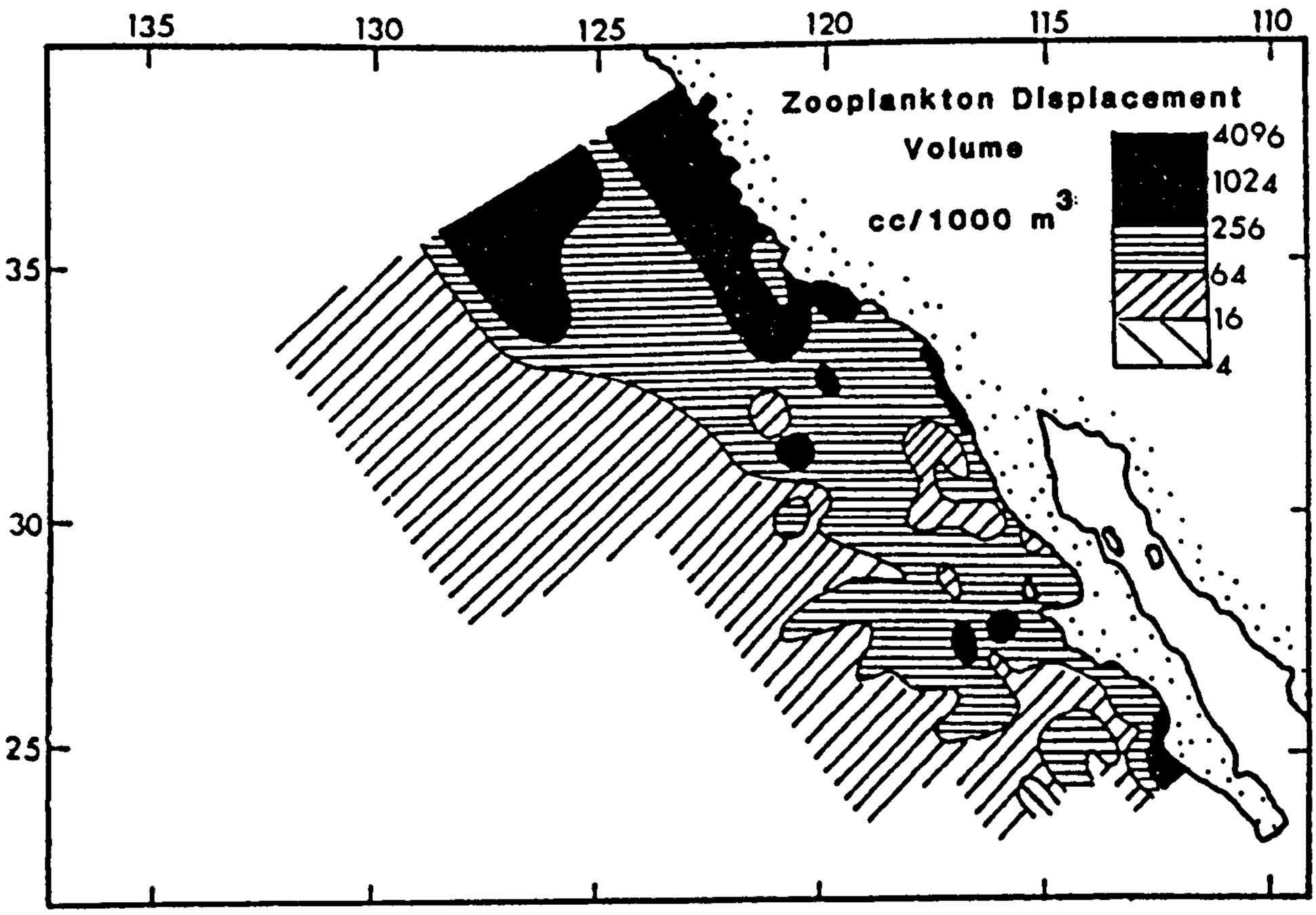

FIGURE 2.4 (b) Contoured zooplankton biomass. Data from CalCOFI cruise 6304 in April/May 1963 (Bernal and McGowan, 1981).

2.4 SEDIMENT TYPE AND DISTRIBUTION

2.4.1 *Mineralogy*

In order to assess changes in bulk geochemistry between the various cores taken on the continental shelf and rise off Baja California it is necessary to have some knowledge of the distribution and type of sediment deposited in each environment. Although the only samples taken were from localities shown in Figure 1.1 it is possible to outline the sediment type and distribution with reference to D'Anglejan's (1967) work. He found that sediments on the shelf are relatively fine grained in the clay-silt range, with occasional tongues of coarser sediment radiating outwards in the central and northern parts of Santo Domingo bay (Figure 1.1). In the present study the coarsest sediments are found at stations 163-5, 163-12 and 145-17. These sediments, deposited in less than 100 m of water (Table 1.1), are olive drab in colour and contain many fragments of bivalves, gastropods, scaphapods and siliceous and calcareous microfossils. Abundant evidence of bioturbation was noted, whilst the rippled upper surface of 163-5 indicates that some sediment transport occurs. The abundant macrofauna and bioturbation suggests that the sediment surface was in contact with oxygenated waters at the time of collection. Smear slide investigation reveals poorly sorted, abundant quartz and feldspar, the grains being sub-rounded to well-rounded. Appreciable quantities of glauconite are present. Core 145-17, obtained from the previous year's cruise of the R/V *Thomas Thompson*, contains diagenetic apatite, (Chapter 8). Minor mineral constituents in these cores include hypersthene,

hornblende, zircon, sphene, garnet, epidote, magnetite and phosphorite pellets.

The sediments in the intrashelf basin (163-8) are characterised by fine-grained, dark green-black ooze producing H_2S at depth. *Bolivina* is quite common. Core 163-8 is the most organic-rich (Figure 2.5) of the sediments analysed, although an attempt at coring station 163-6 revealed a very soft, H_2S-rich, ooze in which the box core overpenetrated. Unfortunately no sample was retained. Figure 2.6 displays a characteristic X-ray diffraction (XRD) trace for 163-8 indicating quartz and feldspar as primary detrital mineral components with some clay, and calcite contribution fom benthic foraminifera. Although undetected by this XRD trace, pyrite framboids and spherules occur throughout this core.

The most carbonate-rich of the shelf cores, 163-11, is situated on the outer bank (Figure 1.1) in an area rich in foraminifera, gastropods and glauconite (D'Anglejan, 1967). Most of the forams are benthonic and include the genera *Bolivina*, *Uvigerina* and *Bulimina* (Plate 2.1a). XRD (Figure 2.6) reveals detrital quartz and feldspar with little clay.

On the slope, station 163-13 is characterised by a lag deposit overlying stiff, dark grey-green clay containing abundant glauconite pellets and dolomite (Chapter 8). The ~15 cm coarse lag contains large blocks of basalt and old phosphorite bored by gastropods and covered with a Mn-Fe patina. The remainder of the lag comprises pellets of glauconite and phosphorite, detrital quartz and feldspar, heavy minerals, sulphides and benthic foraminifera. The XRD trace in Figure 2.6 displays the abundance of dolomite (Plate 2.1b) in

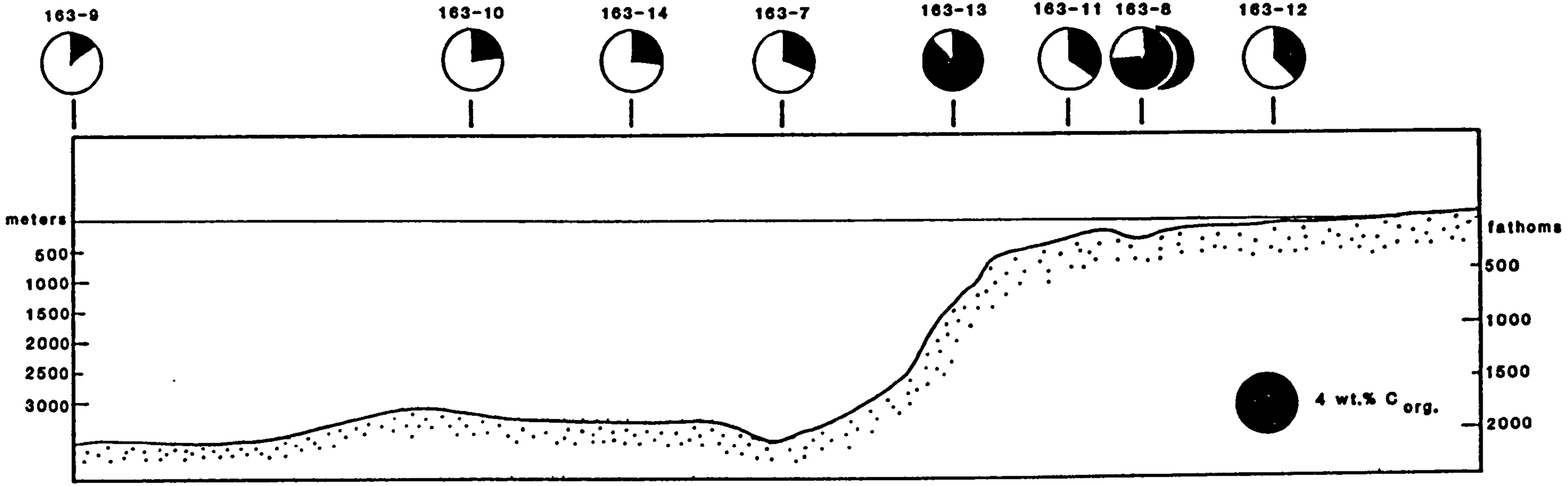

FIGURE 2.5 Bathymetry and organic carbon content of surface sediments along the TGT-163 transect. Station positions are normalised to the line of the transect.

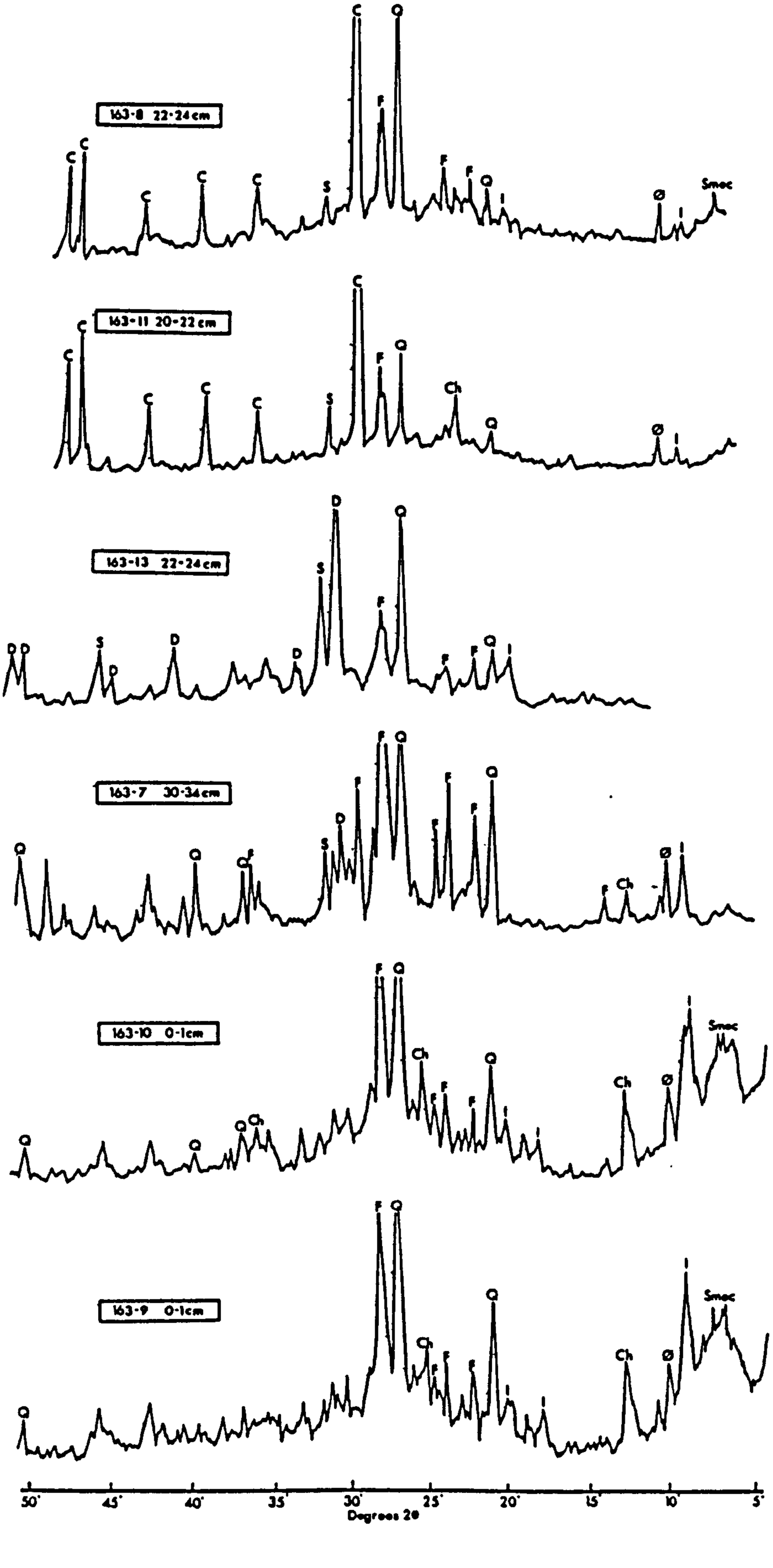

FIGURE 2.6 X-ray diffractograms of selected samples indicating the variation in mineralogy along the Baja California transect.

C - calcite Ch - chlorite D - dolomite F - feldspar
I - illite Q - quartz S - smectite Ø - spurious reflection

the underlying clay. Glauconite pellets containing dolomite, pyritised worm tubes and occasional large crystals of gypsum also occur. The mineralogy and origin of these phases is discussed in Chapter 8. The unstable tectonic environment in the vicinity of 163-13 (Section 2.1) may be responsible for the erosional process now occuring, a result of increased current action winnowing away the fines leaving only the very coarse material as a lag.

The predominantly lithogenous sediments of the oceanic environment have been divided into hemipelagic and pelagic facies. The hemipelagic sediments are characterised by a red-brown oxidising layer overlying grey-green reduced sediment. The upper oxic zone contains high levels of Mn (Chapter 6) and associated trace metals, whilst a $CaCO_3$ increase is observed at depth in the more reduced sediment (Chapter 3). In the pelagic setting the sediments are red-brown and oxidising throughout. Mushroom-shaped manganese nodules are found both on the sediment surface and buried to a depth of 10 cm. The surface nodules have a knobbly undersurface in contact with the sediment as opposed to a smooth upper surface covered with encrusting organisms above the sediment/water interface.

This oceanic environment is characterised by a marked increase in the clay fraction of the sediment. XRD (Figure 2.6) for the surface samples of 163-10 and 163-9 reveal that smectite, illite and chlorite are all present together with detrital quartz and feldspar. Whilst the smectite displays a rather broad peak characteristic or poor crystallinity and possible mixed layers the illite is quite crystalline and well-defined. Chlorite is asymetric towards lower angles.

With depth (Figure 2.6; 163-7:30-34 cm) in the three

hemipelagic cores there is some evidence to suggest that detrital quartz, feldspar and minor illite and chlorite assume greater importance, although this would require an exhaustive XRD study to prove conclusively. These deeper sediments also contain measurable quantities of diagenetic dolomite (Chapter 8) and manganese carbonate (cores 163-14 and 163-10; Chapter 8). Little identifiable biogenic debris is seen in the oceanic cores, despite the $CaCO_3$ increase (Figure 3.2) observed below ~15 cm in the three hemipelagic cores. Diatoms are rare and sponge spicules are nearly all dissolved away at depth.

2.4.2 *Geotechnical propeties*

In geochemical studies of recent sediments the volume of pore space, or porosity, may significantly influence rates and mechanisms of nutrient release to overlying waters (Berner, 1975; Martens and Klump, 1980; Reimers, 1982) and diffusion of chemical species (Berner, 1980). The bulk dry sediment density is often required for calculations of input on a weight per unit time basis. With increasing time and depth of burial the reduction in porosity varies considerably among the different sediment types and is primarily controlled by physico-chemical conditions and the depositional environment rather than simply overburden stress (Bennett *et al*, 1981).

Water content, and hence porosity, was determined for the samples collected off Baja California by drying at 60^{o}C (Appendix A). Porosity was calculated according to Berner (1971)*. This was done for all cores collected on cruise TT-163; for the TT-145 samples water content is taken as being

approximately proportional to the Cl concentration. The measured water content is used to calculate the contribution of sea salt in each sample interval, assuming a constant salinity of 35 $^{o}/_{oo}$ throughout the core (Appendix B.2). Figure 2.7 displays the water content of selected cores to illustrate the dependance of porosity on facies type. The lowest water contents are found in the near shore shelf sands (163-5 and 163-12). The foraminiferal sands of the outer shelf (163-11) have ~10 % more water in them. These shelf deposits are unusual in that water contents increase downcore (Figure 2.7). This effect is attributed to changes in grain size and an increasing clay component with depth. (Further discussion of this statement may be found in Chapter 3). In contrast to the low water content in these silty sediments, 163-8 has the highest (~70%) of any core measured reflecting its depositional environment. This intrashelf basin receives large amounts of organic matter (Chapter 4; Figure 2.5) and probably has one of the highest sedimentation rates of the Baja California transect. Busch and Keller (1981) found that extremely organic-rich sediments of the upper slope mud lens on the Peruvian margin had very high water contents. They attributed this to the organic matter adsorbing water and forming an open sediment fabric, resulting in an increase in the Atterberg limits (water

---

$$* \quad \Phi = \frac{W.p_s}{W.p_s + (1-W).p_w}$$

where: W = % H_2O (wet wt.)/100
p_s = dry density of solid sediment (gcm-3), taken to be 2.7 gcm-3
p_w = density of interstitial water, taken to be 1.025 gcm-3

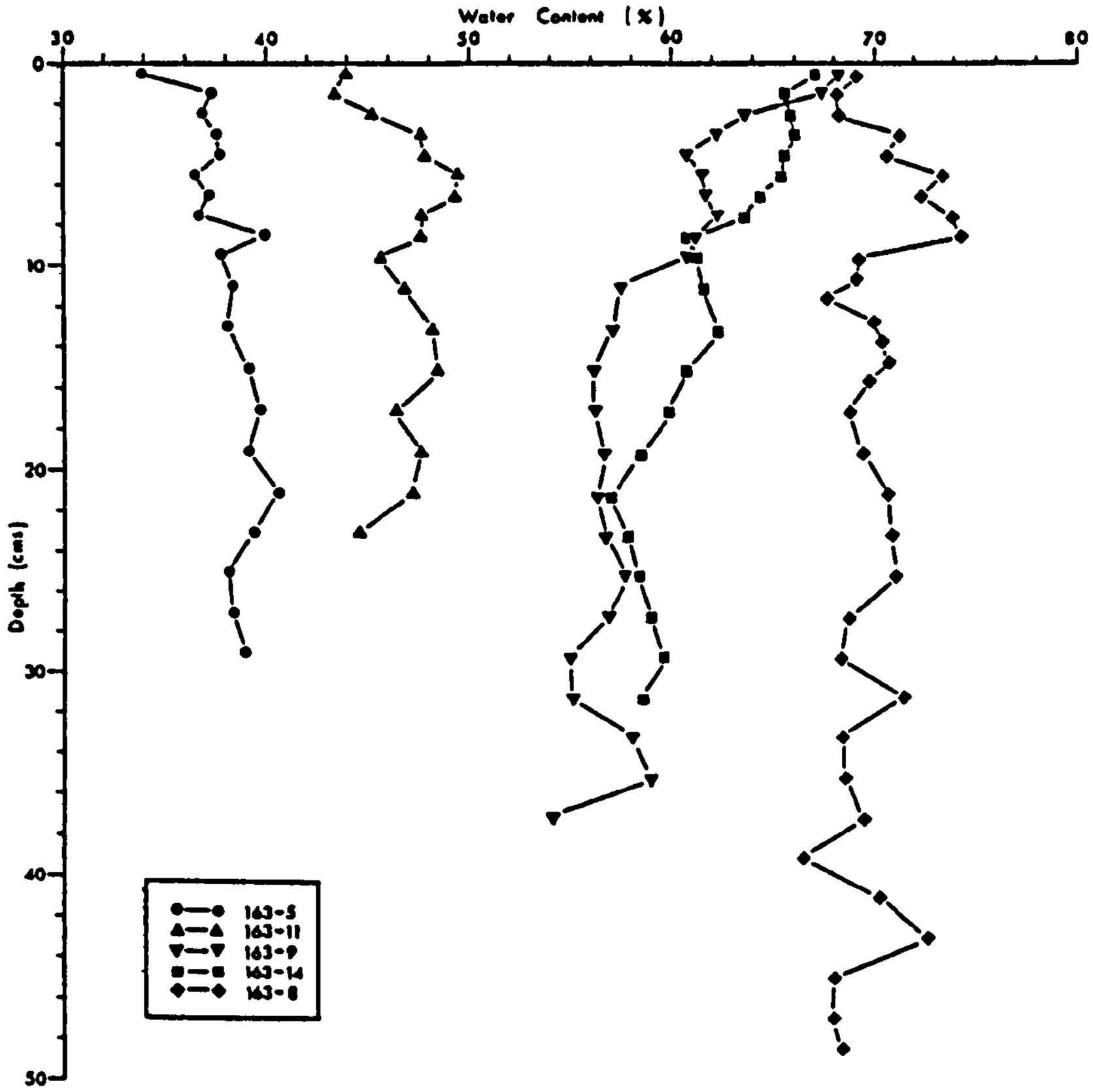

FIGURE 2.7 Water content (% of wet weight) of selected cores along the Baja California transect.

contents that correspond to different states of consistency of a remoulded sediment; Lambe and Whitman, 1969).

In the oceanic environment (163-7, 163-14, 163-10, 163-9, 163-15) water contents are approximately similar, ranging from 62.2 - 69.1 % at the surface to 53.9 - 58.6 % at depth. There is evidence to suggest that slowly accumulating pelagic sediments (163-9, 163-15) have high water contents at the surface which rapidly decrease with depth. Moore's (1964) work on the Mohole project farther north, showed that low shear strength and therefore high water content was found in sediments that accumulated more slowly than high shear strength, rapidly accumulating sediments.

PLATE 2.1a Photomicrograph of benthic foraminifera, *Bolivina*, *Uvigerina* and Bulimina, occuring in sediment from core 163-11 on the outer shelf off Baja California. The foraminifera are small and thin-shelled, a characteristic of large standing stocks in areas of high production.

PLATE 2.1b Photomicrograph of abundant, euhedral dolomite rhombs occuring in the basal clay of core 163-13, beneath the overlying lag deposit.

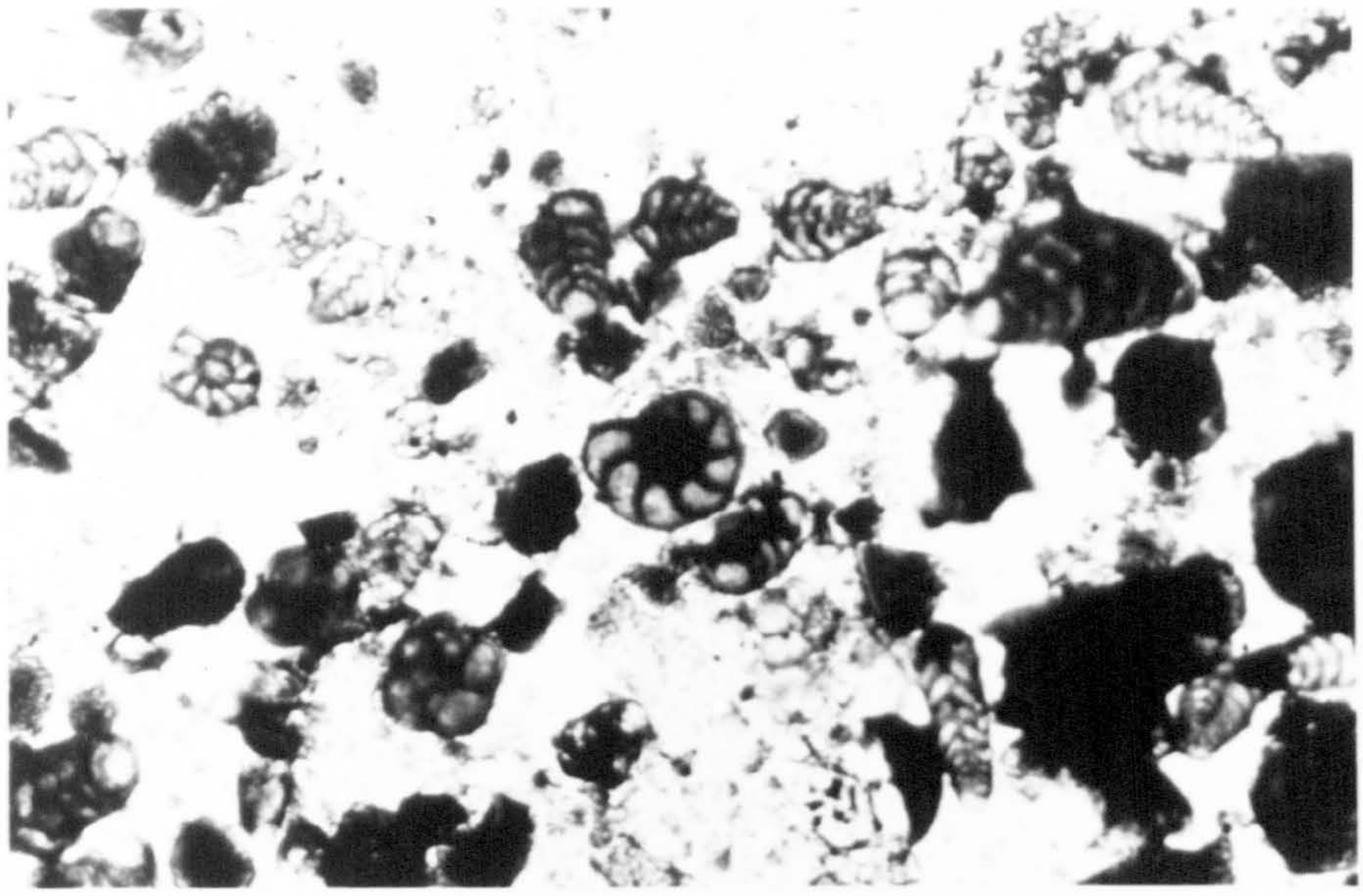

500 µm

a

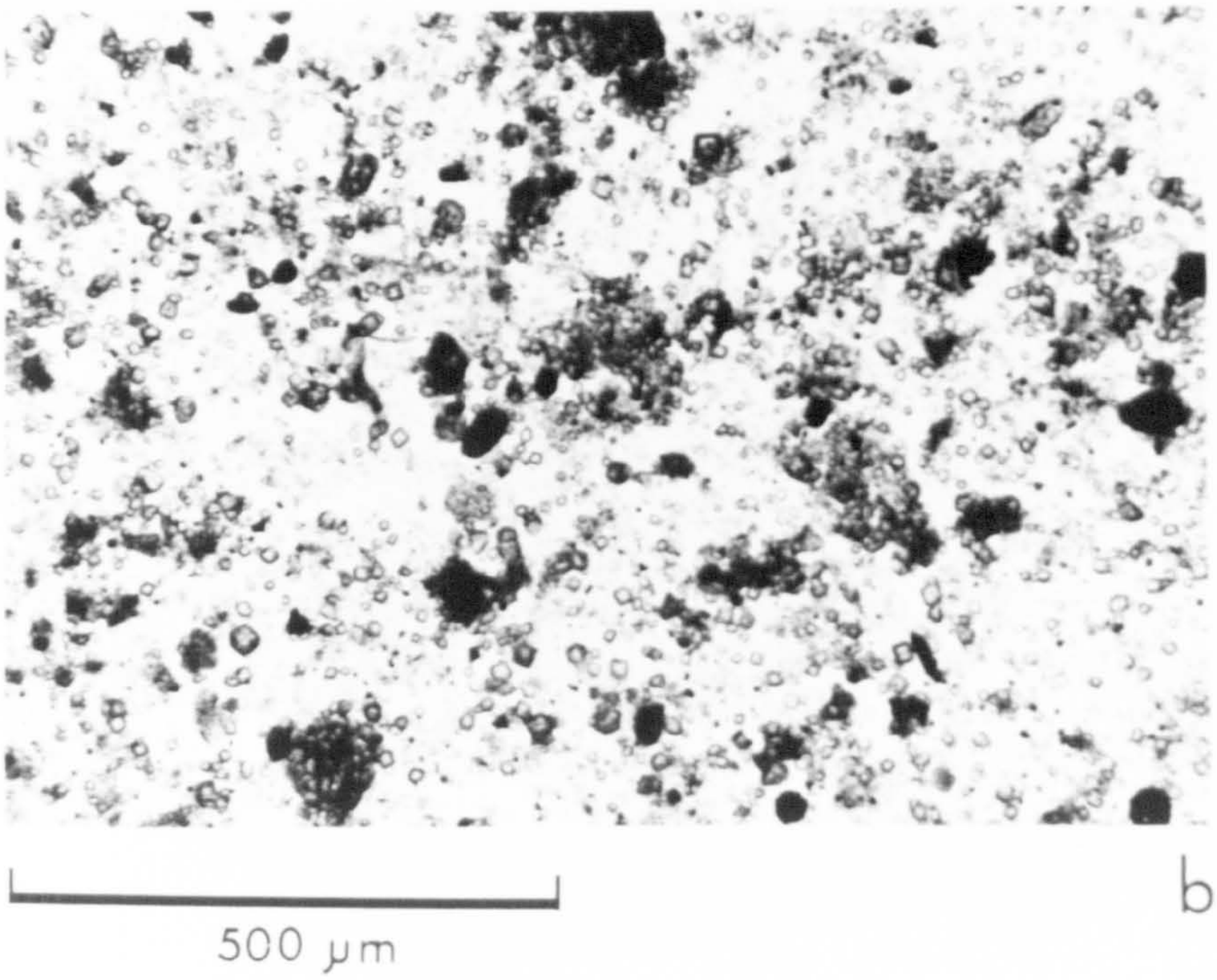

500 µm

b

CHAPTER 3

THE DISTRIBUTION AND BEHAVIOUR OF DETRITAL AND BIOGENIC ELEMENTS

3.1 INTRODUCTION

Aside from hydrogenous and diagenetic precipitation and redistribution (Chapter 6) the important controls on the distribution of major and trace elements in marine sediments are the inputs of terrigenous minerals and biogenic detritus. This chapter will be concerned with identifying the geochemistry of these primary inputs, and the relationship between element distributions in time and space.

Off Baja California sediment supply is partitioned between inorganic and biogenic phases. In order to exclude the effects of dilution of one or other phase, the element distribution is frequently reported on a ratio basis, usually with respect to Al. The distribution of Al in marine sediments is almost exclusively controlled by detrital aluminosilicates, either from the continents or submarine vulcanism (Chester and Aston, 1976) and is not incorporated into biogenic material to any significant degree. As a result Al has been used as an indicator of terrigenous debris (Arrhenius, 1952; Landergren, 1964; Bostrom *et al*, 1969; Chester and Aston, 1976, Bischoff *et al*, 1979) allowing element/Al ratios to be interpreted as mineralogical changes in the sediment free from induced correlation resulting from dilution by biogenic, detrital, hydrogenous and diagenetic components.

In addition, concentrations of several major elements (Na, Mg, Ca and K) and Br are affected by contributions from sea salt during sample preparation. These have been corrected for by the method outlined in Appendix B.2 together with a correction for total dilution for all elements by the salt present. Analysis techniques are fully described in Appendix B.

The sequence of elements considered in this chapter is

determined by the major phase in which they are incorporated. Detrital geochemistry is divided into those elements concentrated in the heavy mineral fraction, Ti and Zr, and those associated with detrital clay or feldspar, Si, K, Mg, Fe and Rb. The final section deals with biogenic geochemistry, identifying the distribution of biogenic opal, Ca, $CaCO_3$, Sr and Ba. These geochemical divisions are not mutually exclusive and some elements are governed by several processes, however, they provide a framework with which to desribe their distribution.

3.2 INORGANIC ELEMENT GEOCHEMISTRY

3.2.1 *Heavy mineral geochemistry*

Titanium

Although Ti may occur within a number of phases within deep-sea sediments (terrigenous material, basaltic debris, hydrogenous precipitates and biogenic material) it is primarily concentrated in continentally-derived minerals, especially the oxides ilmenite, rutile and anatase (Rankama and Sahama, 1950; Chester and Aston, 1976). In sediments with very high Ti contents (> ~0.70 wt.%) the contributor is almost always basaltic debris (Goldberg and Arrhenius, 1958). Although biogenic Ti has been found in marine organisms (Nicholls *et al*, 1959; Martins and Knauer, 1973; Bostrom *et al*, 1974) the lack of abnormal Ti/Al ratios in biogenic sediments of the equatorial Pacific productivity belt (Goldberg and Arrhenius, 1958; Pedersen, 1979) suggests that is not an important source especially in the predominantly lithogenous sediments off Baja

California. Authigenic Ti, either due to post depositional migration to form anatase, or to relace Al in clay mineral lattices (Correns, 1954) may occur. Similarly, hydrogenous sorption of dissloved Ti by ferric oxides in nodules (Goldberg, 1954; Cronan, 1972) has been documented.

TABLE 3.1

Sample	Depth	Al	Ti	Zr	Ti/Al	Zr/Al
	cm	wt.%	wt.%	ppm		$x10^{-4}$
163-5	0-1	6.49	0.35	175	0.054	27.0
163-12	0-1	7.83	0.37	140	0.047	17.9
145-17	0-1	6.57	0.30	205	0.046	31.2
163-8	0-1	4.79	0.28	78	0.059	16.3
163-11*	0-1	3.27	0.15	69	0.046	21.1
163-13*	0-1	2.67	0.18	85	0.067	31.8
163-7	0-1	7.43	0.41	125	0.055	16.8
163-14	0-1	7.67	0.43	135	0.056	17.6
163-10	0-1	7.91	0.43	138	0.054	17.5
163-9	0-1	7.92	0.44	154	0.055	19.5
163-15	0-1	7.75	0.43	142	0.055	18.3
Turekian and Wedepohl (1961)+		8.70	0.48	157	0.055	18.0

* lag deposit
\+ Salt-corrected from presented Cl analysis

The concentration of Ti in surface sediments (Table 3.1) ranges from 0.15 wt.% in the foraminiferal sand of 163-11, to 0.44 wt.% in the oceanic red clay of 163-9. Relative to Al (Figure 3.1) the ratio is very constant without any marked increase in nearshore shelf sands. The similarity in ratio between the different facies indicates the uniformity of Ti incorporation, probably in detrital ilmenite and rutile, the absolute concentration being diluted by clay, quartz, feldspar,

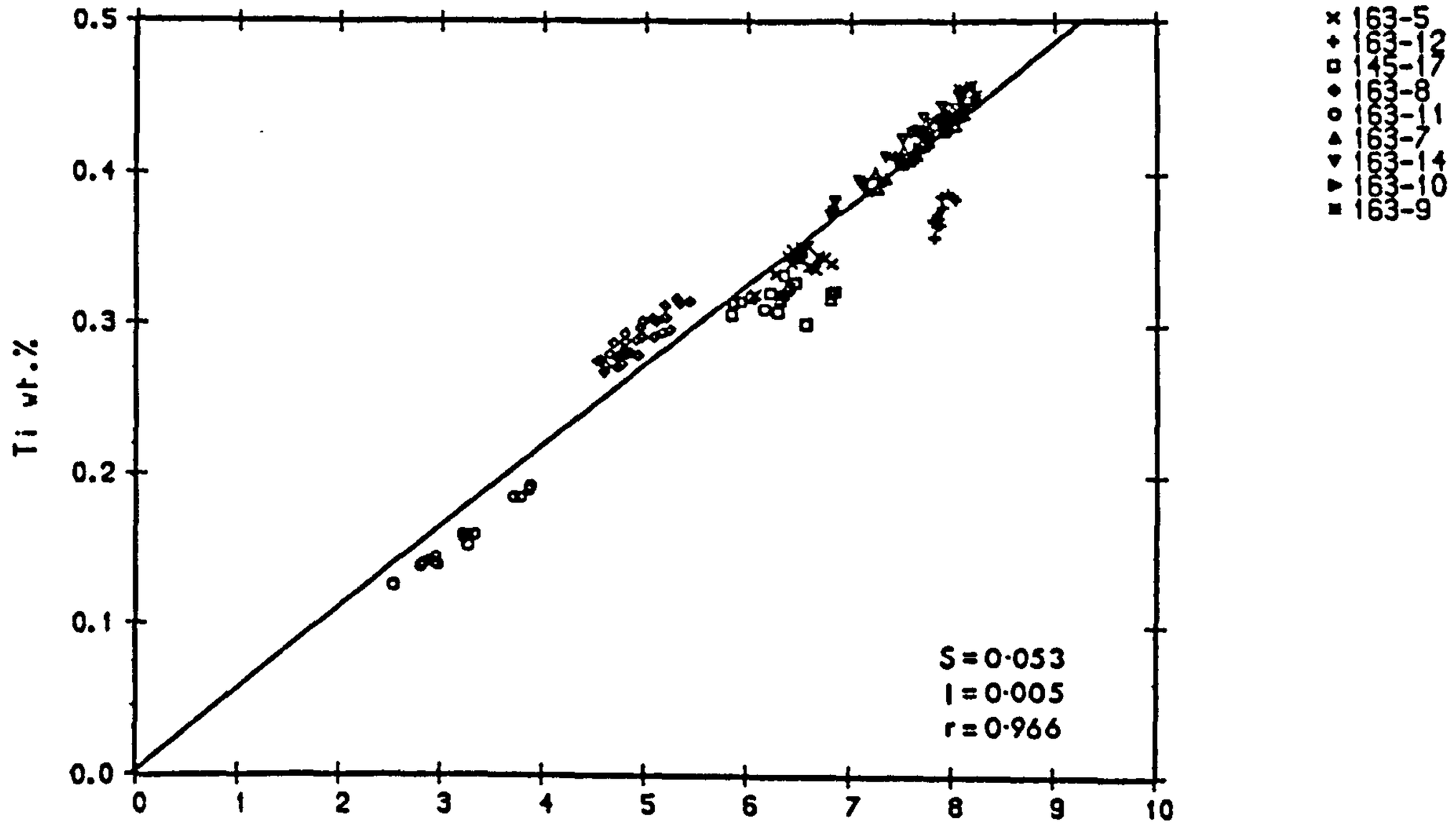

FIGURE 3.1 The correlation between Ti and Al for sediments along the Baja California transect (salt-free).

carbonate and organic matter. The slightly higher Ti/Al ratios in the oceanic sediment may be due to some oxyhydroxide absorption of Ti.

Zirconium

Zirconium concentrations range from 69 to 205 ppm in the surface sediments off Baja California (Table 3.1). Relative to Al the shelf sediments, especially the nearshore stations of 163-5 and 145-17, have the highest ratios indicating the placer enrichment of zircon in these shallow-water coarse silts (Chapter 2). In the deeper water environment the ratio increases offshore as coarser-grained, feldspathic detritus gives way to fine-grained clays. However, the depth distribution of Zr in these cores is very interesting, and reveals detail concerning changes in terrigenous input into the hemipelagic environment. The Zr/Al ratio in four cores (163-7, 163-14, 163-10 and 163-9) has been normalised to the surface ratio and plotted against depth in Figure 3.2, together with the appropriate $CaCO_3$ profile (Section 3.3). In the hemipelagic sediments both carbonate and normalised Zr/Al abrubtly increase about 15 cm below the surface. The change in Zr/Al ratio is accentuated towards the coast. Given that both Zr and Al are little affected by redox reactions the change in ratio can result from a variation in grain size of terrigenous input (Goldschmidt, 1954; Taylor 1965). This may be interpreted as an increase in the coarse-grained terrigenous component with depth (time) in the core. Further discussions on changes in mineralogical input and productivity with time may be found in Section 3.4.

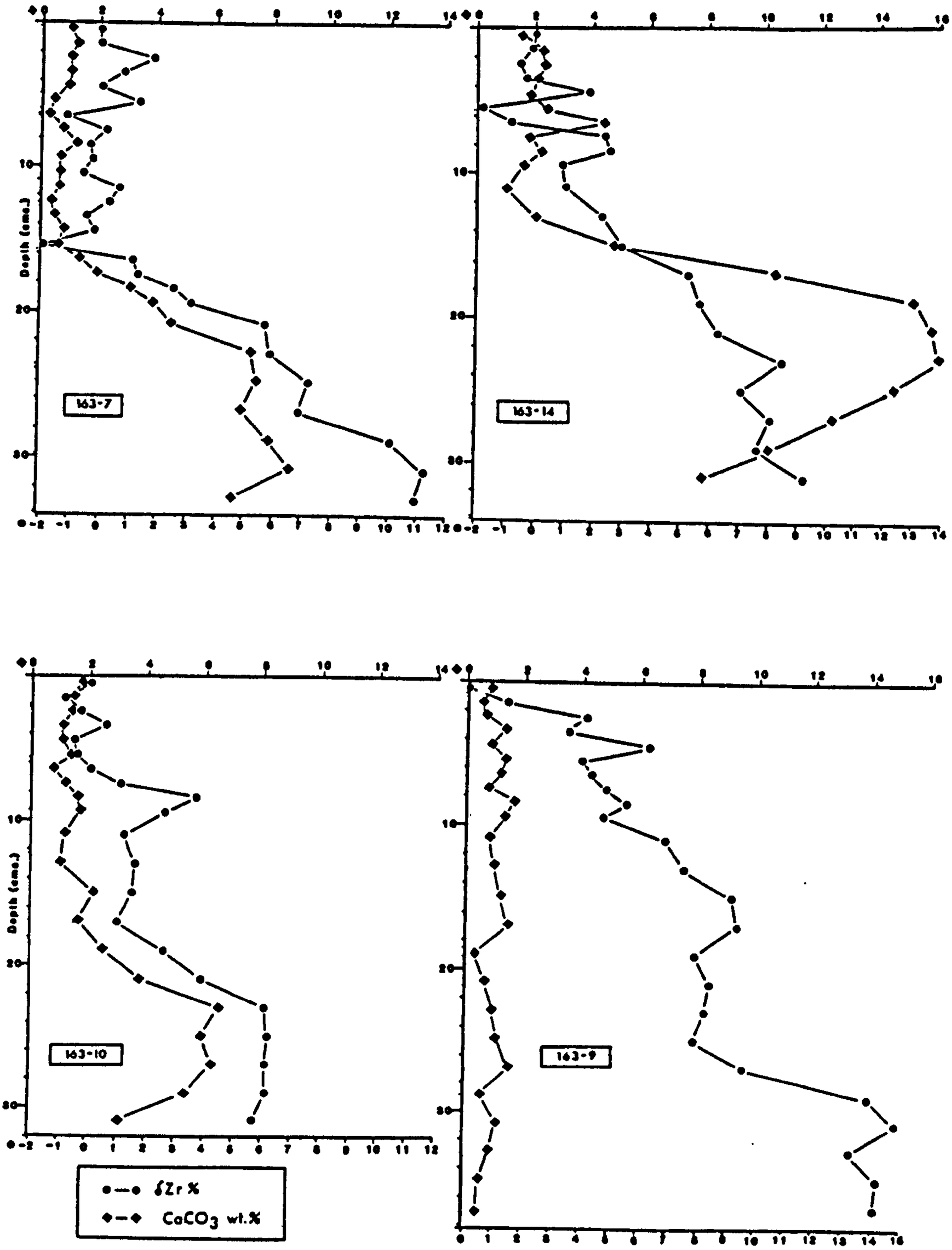

FIGURE 3.2 Normalised Zr (lower axis) and $CaCO_3$ (upper axis) with depth in the four oceanic cores (salt-free).

$$dZr\% = \left(\frac{Zr/Al}{Zr/Al_{surface}} - 1 \right) \times 100$$

3.2.2 *Aluminosilicate and Clay Geochemistry*

Silicon

Si can be partitioned between terrigenous and biogenic phases. In terrigenous material Si is a primary component of feldspar and clays, as well as occuring as free quartz. Off Baja California aeolian sedimentation (Rex and Goldberg, 1958; Bonatti and Arrhenius, 1965) is characterised by a high proportion of quartz, plagioclase and mica. The distribution of Si relative to terrigenous Al in all the sediments is shown in Figure 3.3. The samples define a Si/Al ratio of 3.26, slightly in excess of 3.0 in average lithogenous pelagic clay (Turekian and Wedepohl, 1961), and near a line defining the average Si/Al for sites A, B and C of the DOMES area further to the west (Bischoff *et al*, 1979), with the exception of 163-5 and samples from the upper decimeter of 145-17. These two stations lie off the main cruise transect (north and south respectively) and are very close to shore.

With depth subtle changes in the Si/Al ratio become more apparent (Figures 3.4 and 3.5). The shelf sediments, particularly 145-17 and 163-5, do indeed have high ratios although falling rapidly with depth. Comparison with Figure 2.7 indicates that the lower Si/Al ratios correspond to an increase in water and organic matter content with depth, suggesting that Si/Al is an indicator of grain size; there being coarser, quartz-rich sediment in the upper ~5 cm. The extremely high and variable Si/Al ratio in 163-13 (Figure 3.4) is also evidence of quartz concentration in this lag-type deposit. Zr/Al ratios (Appendix C) reinforce the hypothesis of coarse, heavy mineral concentration at the surface of 145-17, 163-5 and 163-13.

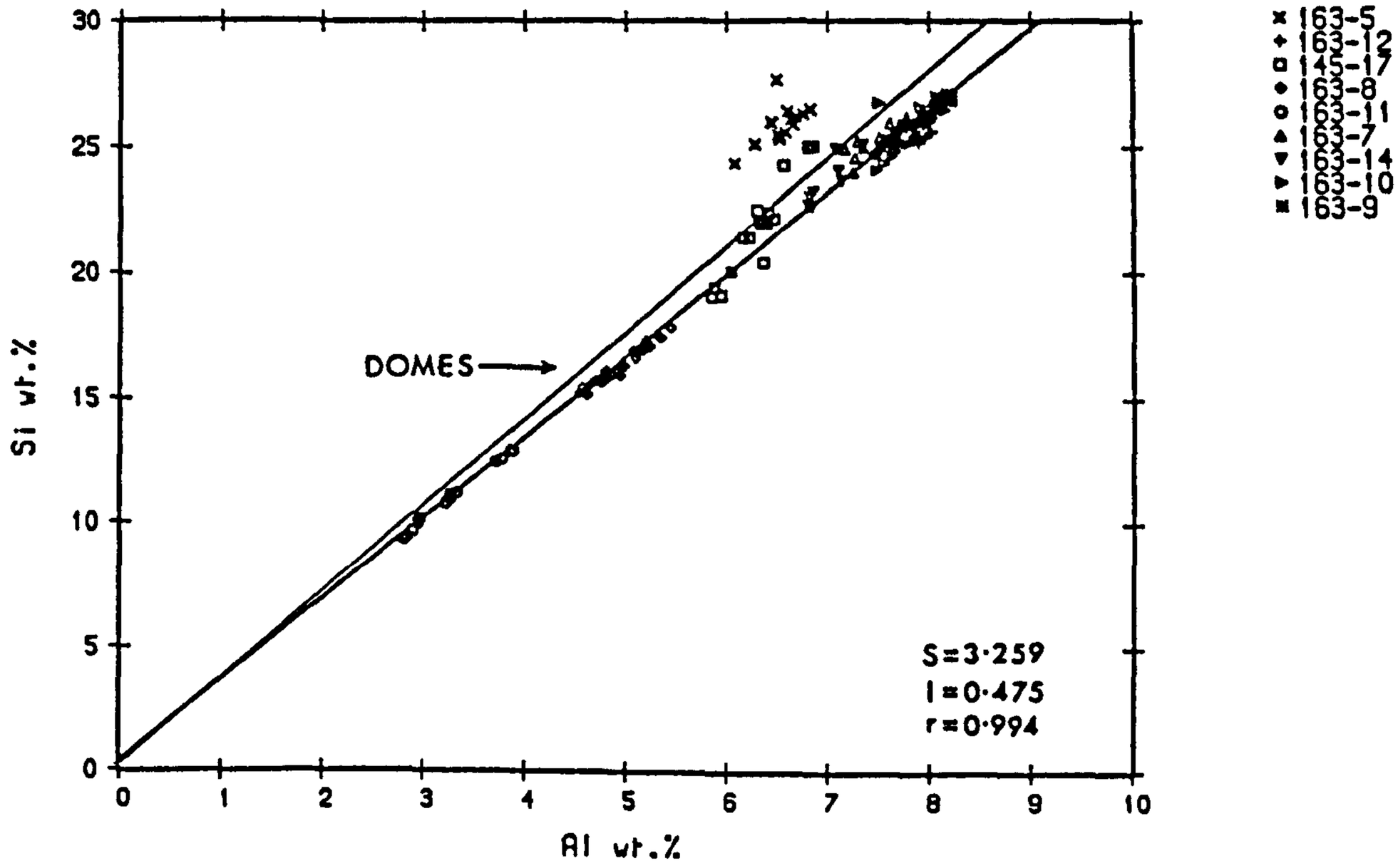

FIGURE 3.3 The correlation between Si and Al for sediments along the Baja California transect (salt-free). The DOMES line (average of sites A, B and C) has a ratio of 3.49 (Bischoff *et al*, 1979).

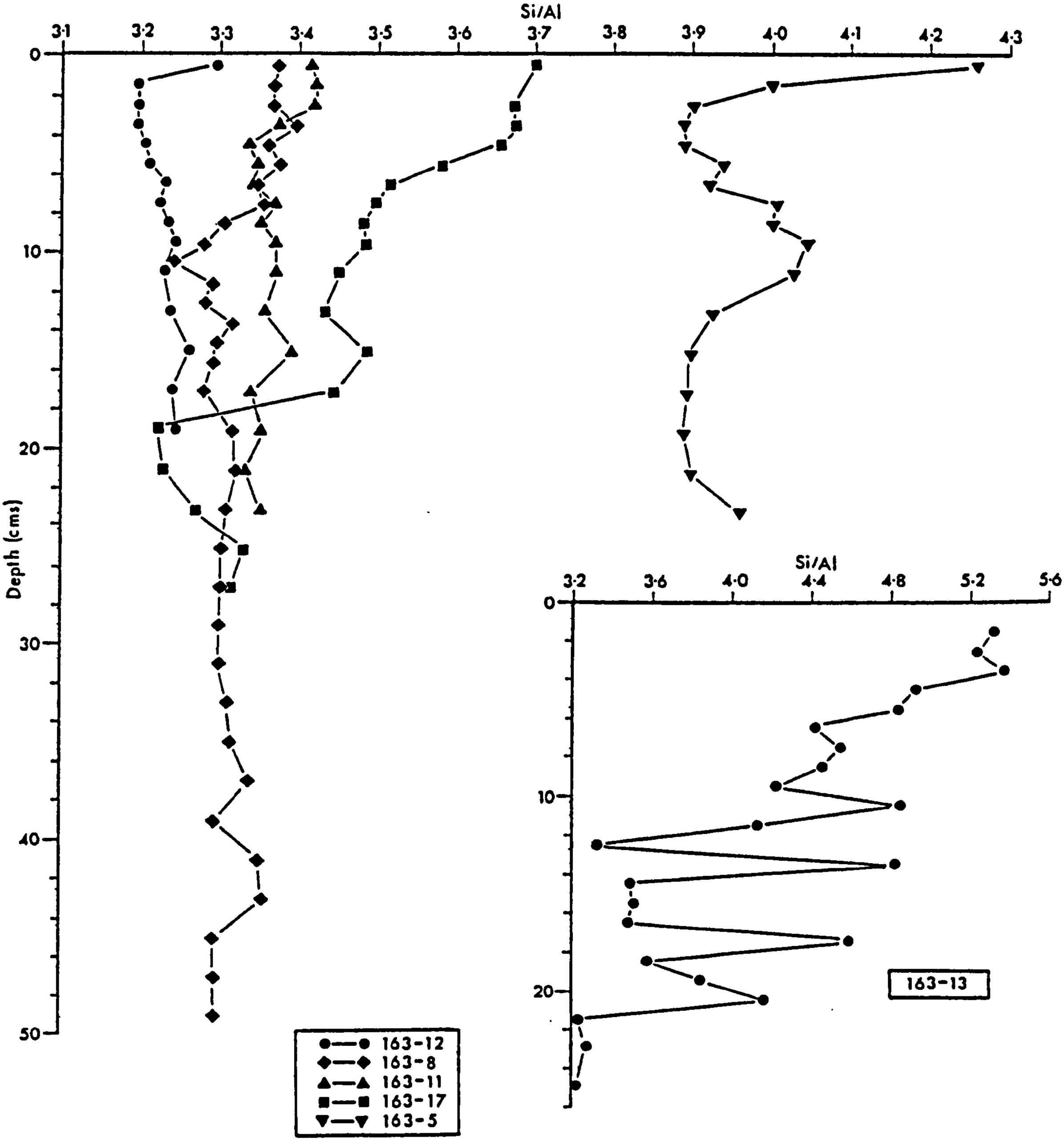

FIGURE 3.4 Profiles of Si/Al with depth for the Baja California shelf sediments (salt-free). Note the scale change for core 163-13 (inset).

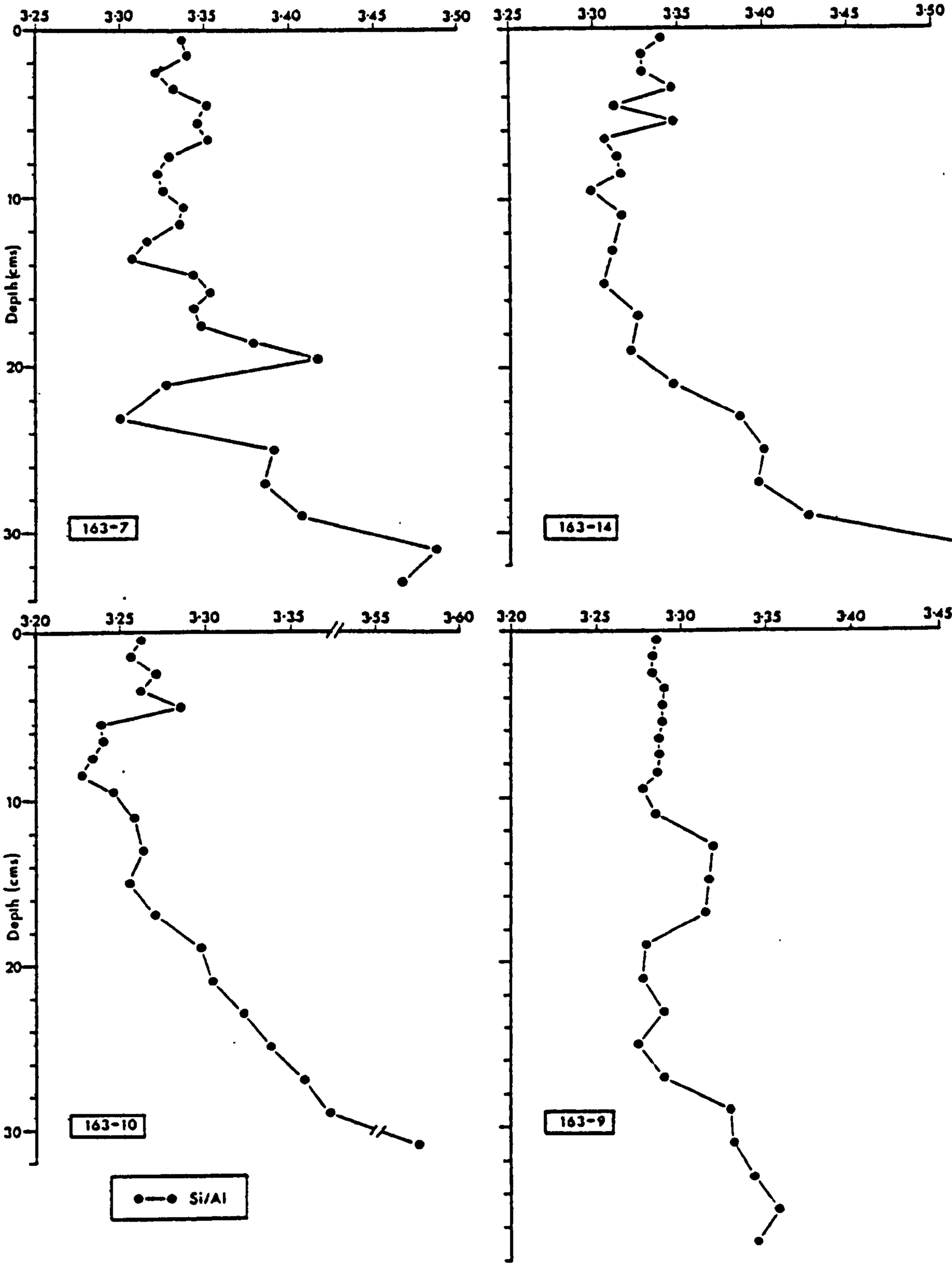

FIGURE 3.5 Profiles of Si/Al with depth for the Baja California oceanic sediments (salt-free). Note the break in scale for core 163-10.

In the oceanic environment (Figure 3.5) Si/Al ratios increase downcore in a manner similar to Zr/Al (Figure 3.2). However, extreme elevations are evident in the basal sample of 163-14 and 163-10 accompanied by increases in Fe, K and Mg (see below) without a concomitant increase in normalised Zr/Al. This may be due to a lithologic change, such as an ash band, which may have prevented further penetration of the corer. The changing Si/Al ratio with depth possibly records a change in depositional mechanism and associated sedimentation rates accompanying changes in Quaternary climate. This hypothesis is discussed in Section 3.4.

The slightly elevated average Si/Al ratio of the DOMES area over pelagic clay defined by Turekian and Wedepohl (1961) (Figure 3.3) has been taken to indicate a contribution of biogenic silica in the sediments (Bischoff *et al*, 1979). They estimate that 6% of the total Si content is biogenic at site C, increasing SW towards the equatorial productivity belt (Figure 1.2). However, using the normative calculation of Leinen (1977) based on the proportion of Al and Mg in the sediment, the percentage of biogenic Si off Baja California is negligible. Indeed, SEM evidence indicates dissolution of siliceous tests at a very early stage during sediment burial. Instead, free quartz of detrital origin is believed responsible for the slightly higher Si/Al ratio relative to Pacific pelagic clay observed off Baja California.

Potassium

The distribution of K relative to Al is quite striking (Figure 3.6) showing a dramatic increase in surface K/Al from 0.16-0.17 in shallow-water, shelf sediments to 0.26-0.30 in the

distal red-clay of the pelagic environment (Table 3.2). The lowest K/Al ratios (Figure 3.7) are found in the foraminiferal silt of 163-11 (~0.08) and the anoxic organic-rich mud of 163-8 (~0.04), the latter being very erratic*. Apart from the latter core the K/Al ratio with depth on the shelf is generally constant at 0.16-0.17. In the hemipelagic and pelagic environment the K/Al ratio increases very slightly with distance from the coast (Table 3.2). An enrichment in Al relative to K is seen in core 163-12. This shallow-water, nearshore station (Figure 1.1) may be receiving local inputs of detrital minerals. The lack of K and Mg but increase in Ca (Section 3.3) in this core may represent an input of calcic plagioclase. Inspection of beach sands from Santo Domingo Bay indicate the abundance of this mineral, probably as a result of weathering of the Commondu Volcanics.

In the oceanic sediments (Figure 3.8) K/Al increases in 163-7 from 0.240 at the surface to 0.264 at 32-34 cm depth; 163-14 increases from 0.240 to 0.292 at 28-30 cm but displays a K/Al minimum of 0.186 at 18-20 cm depth*; 163-10 has elevated K/Al at 30-32 cm depth corresponding to an increase in the Si/Al ratio (Figure 3.5). In the red-clay of 163-9 K/Al increases from 0.263 at the surface to 0.298 at 36-38 cm depth, similarly in 163-15 an increase from 0.258 to 0.297 is observed.

*It should be noted that there may be a loss of alkalies during the preparation of fused discs which have a high Ca and organic C content relative to Al. For further details see Appendix B.1.1. This artifact in sample preparation may result in the low K values for cores 163-11, 163-8 and the lower 15-32 cm of 163-14 shown in Figures 3.6, 3.7 and 3.8.

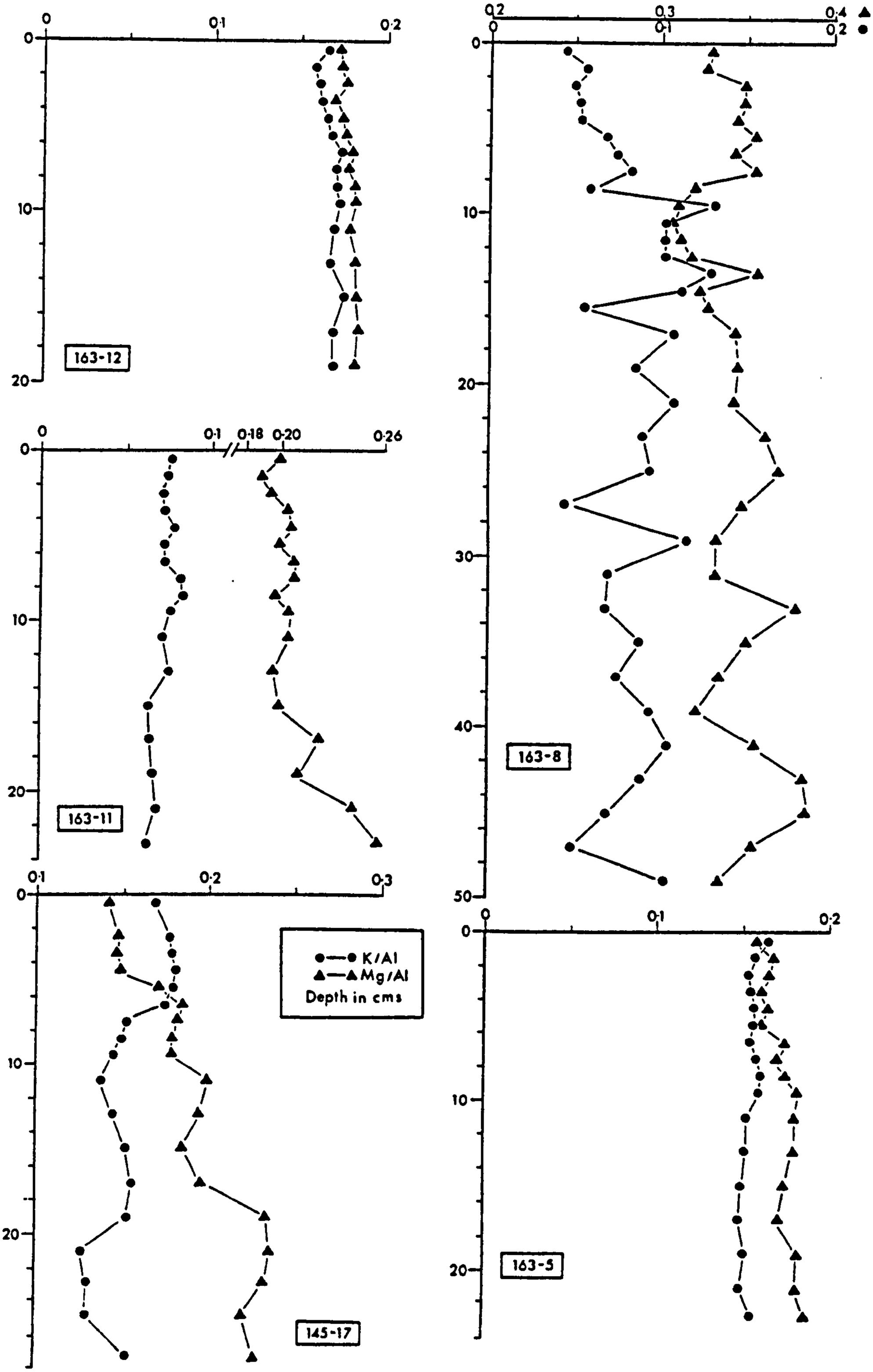

FIGURE 3.7 Profiles of K/Al and Mg/Al with depth for the Baja California shelf sediments (salt-free).

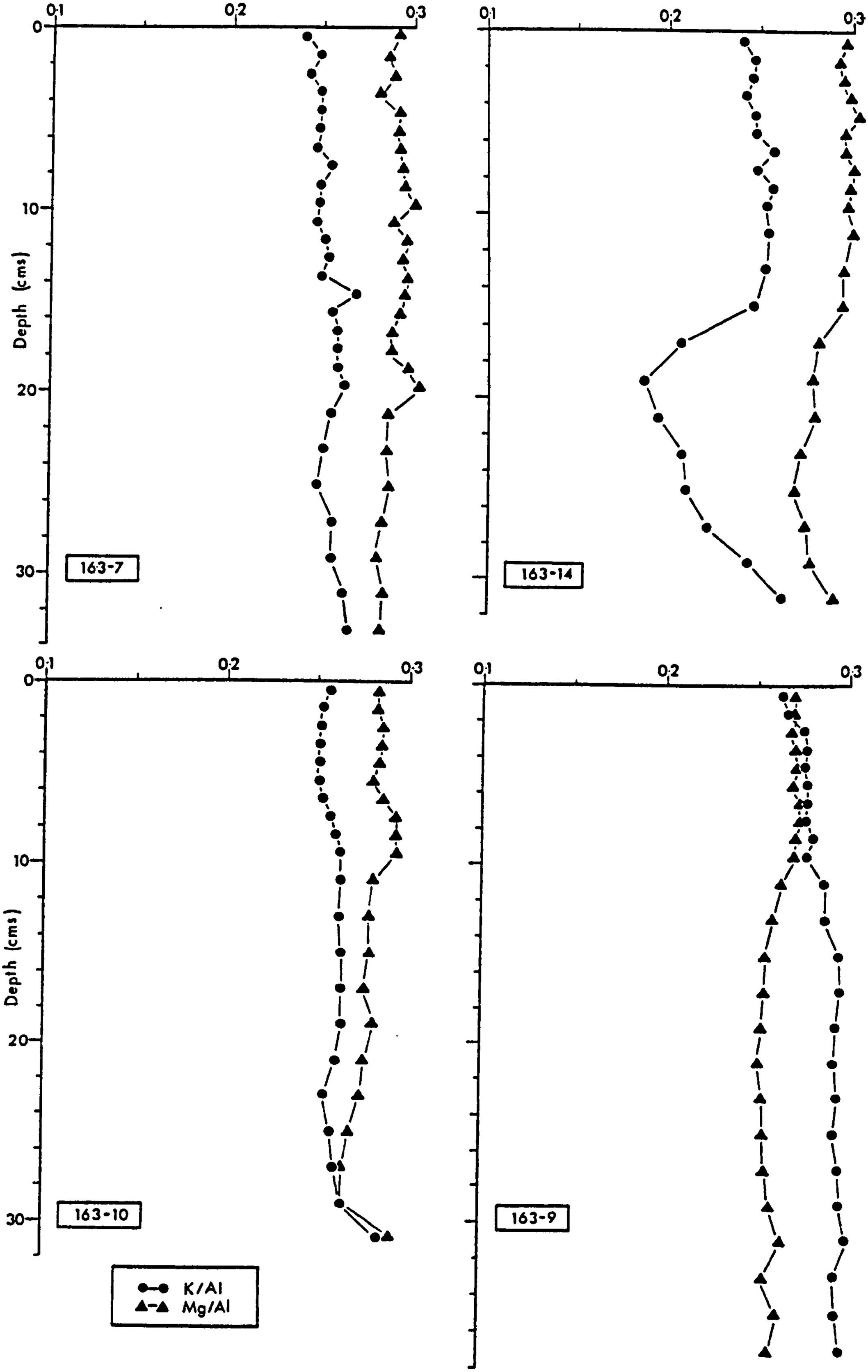

FIGURE 3.8 Profiles of K/Al and Mg/Al with depth for the Baja California oceanic sediments (salt-free).

TABLE 3.2

Sample	Depth cm	K/Al	Mg/Al	Fe/Al	K/Rb
163-5	0-1	0.165	0.159	0.284	297
163-12	0-1	0.165	0.171	0.314	369
145-17	0-1	0.169	0.143	0.299	185
163-8	0-1	0.044	0.323	0.514	48
163-11	0-1	0.076	0.199	0.385	125
163-7	0-1	0.240	0.292	0.599	221
163-14	0-1	0.240	0.296	0.618	209
163-10	0-1	0.257	0.283	0.608	233
163-9	0-1	0.263	0.271	0.706	207
163-15	0-1	0.258	0.274	0.703	225
Turekian and Wedepohl (1961)[+]		0.300	0.230	0.780	226

[+] Salt-corrected from presented Cl analysis

Magnesium

The highest surface Mg/Al ratios (~0.33) off Baja California are found in the organic-rich, anoxic sediments of the intrashelf basin, 163-8 (Table 3.2; Figure 3.9). The other shelf sediments (163-5, 163-11, 163-12) display Mg/Al ratios in the range 0.16-0.20, except for the lower 10 cm of 163-11 (Figure 3.7). In core 145-17 Mg/Al ratios steadily increase from 0.123 at the surface to 0.226 at depth (Figure 3.7), corresponding to a decrease in Si/Al (Figure 3.4), but an increase in C_{org} (Figure 4.2).

In the oceanic environment surface Mg/Al ratios decrease offshore from 0.292 at station 163-7 to 0.271 at station 163-9 (Table 3.2). Similarly, Mg/Al ratios decrease slightly downcore (Figure 3.8), in an antipathetic manner relative to K/Al. the major K/Al decrease at 18-20 cm depth in 163-14 is not shown by Mg/Al, however, the basal elevation at 30-32 cm in this core and 163-10 is complemented. In the red-clay of 163-9, after an

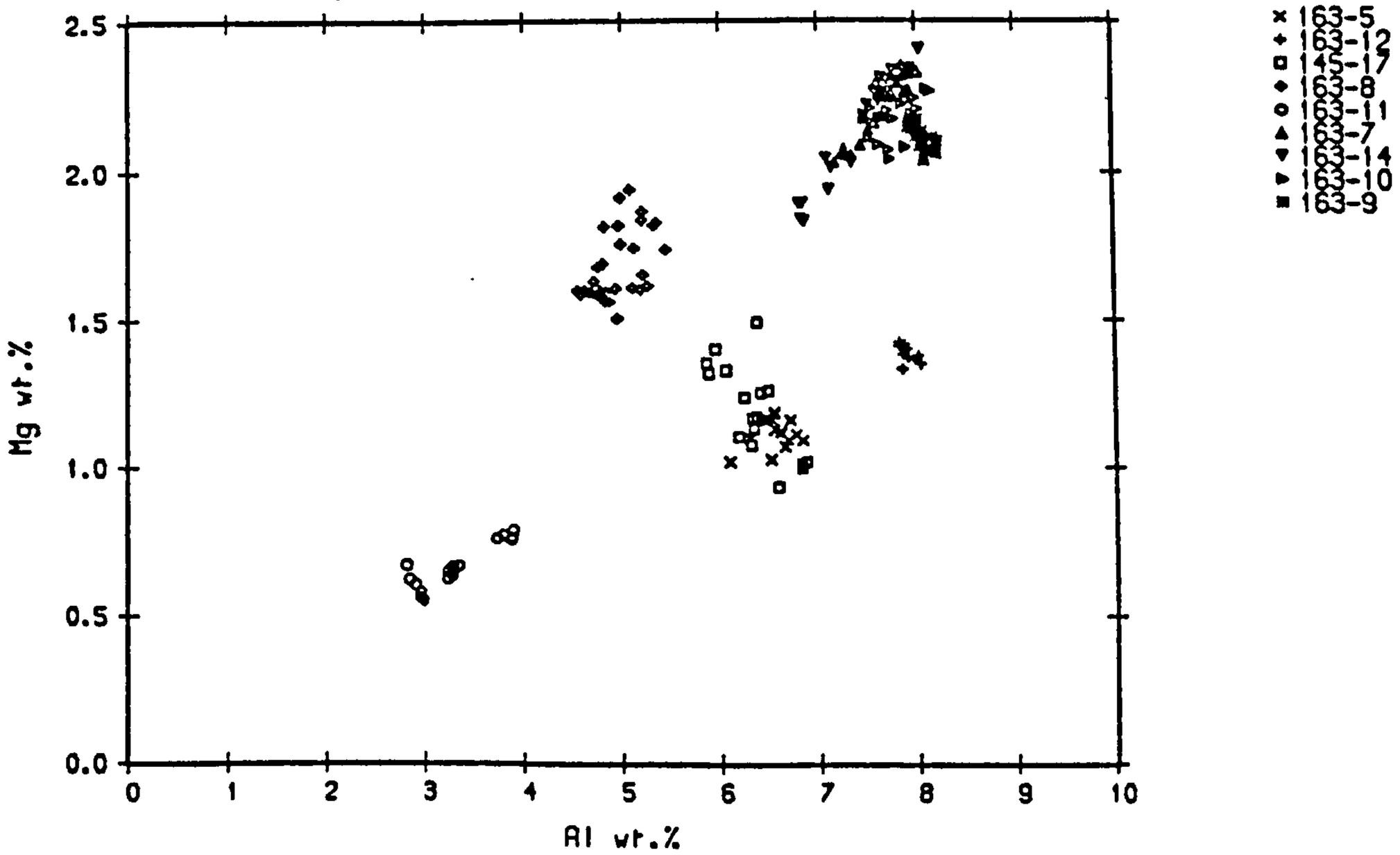

FIGURE 3.9 The relationship between Mg and Al for sediments along the Baja California transect (salt-free).

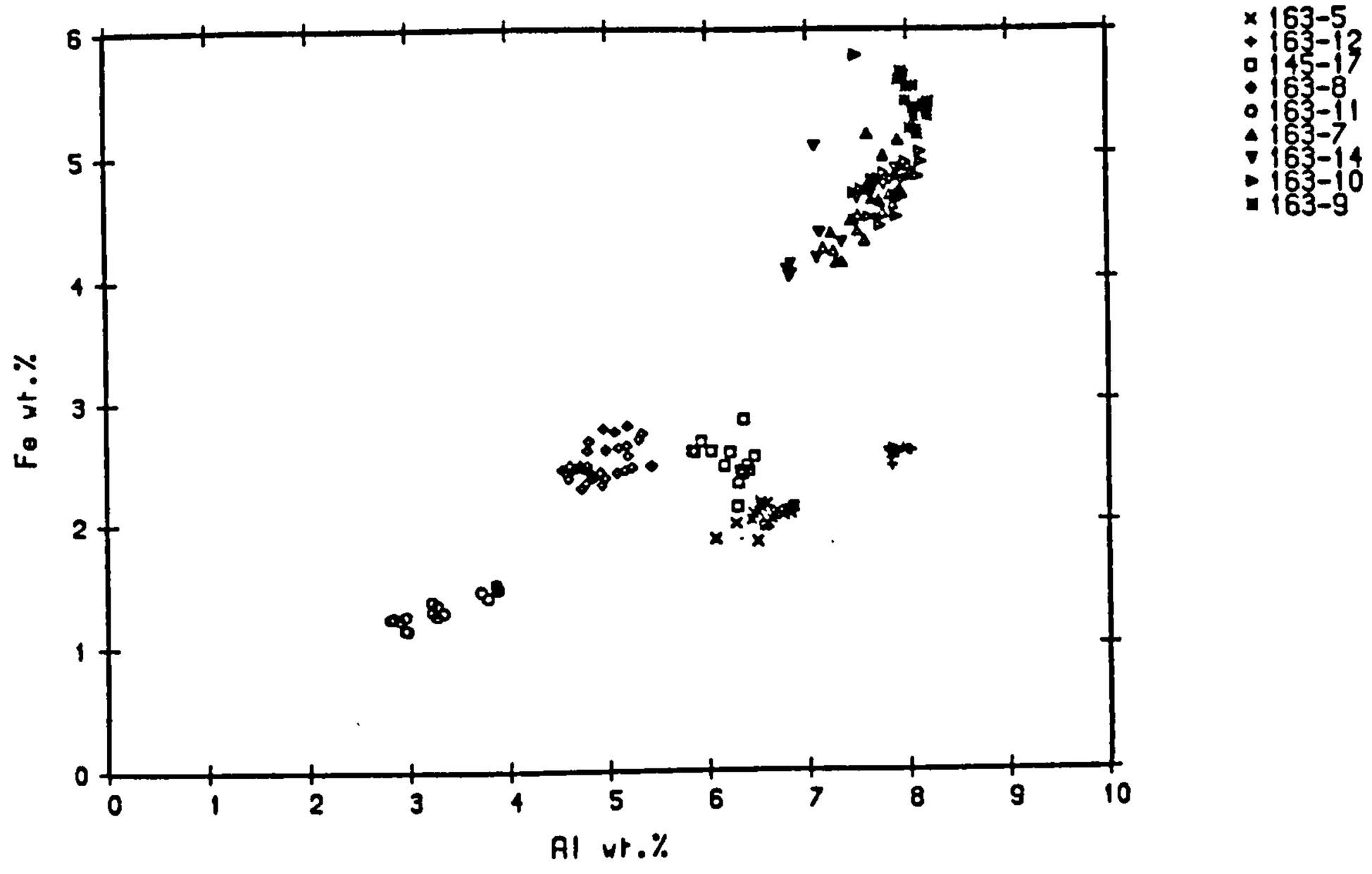

FIGURE 3.10 The relationship between Fe and Al for sediments along the Baja California transect (salt-free).

intial ratio of ~0.27, Mg/Al decreases rapidly below 10-12 cm depth to a core minimum of 0.252 at 20-22 cm before increasing slightly at depth.

Iron

Fe distribution, relative to Al, off Baja California is quite variable (Table 3.2; Figure 3.10) depending on the environmental conditions of sediment deposition. The two nearshore silt-sands, 163-5 and 163-12 (Figure 3.11) have Fe/Al ratios averaging 0.3-0.33, changing very little with depth. In contrast, the finer-grained, organic-rich cores, in particular 163-8, have much higher Fe/Al ratios varying erratically with depth (Figure 3.11). The transition from silt to mud in 145-17 is marked by a large increase in Fe/Al from 0.299 at the surface to a core maximum of 0.447 at 18-20 cm depth. Likewise 163-11, the foraminiferal ooze, increases from 0.385 at the surface to 0.458 at 22-24 cm depth. The high Fe/Al ratio in the organic-rich sediment of 163-8 averages 0.51, but is quite variable.

In the oceanic environment, the hemipelagic cores (163-7, 163-14 and 163-10; Figure 3.12) have lower surface Fe/Al ratios (~0.605) than the oceanic red-clays (163-9, 163-15; Table 3.2), which are ~0.1 higher. Overall, Fe/Al decreases downcore (Figure 3.12) at all these stations, but some perturbations exist. A double subsurface spike occurs between 14-20 cm in 163-7, reaching a maximum ratio of 0.679. In 163-14 and 163-10 the basal metal enrichment, relative to Al, displayed by K, Mg and Si is well shown by Fe. In the red-clay of 163-9 Fe/Al is quite constant over the uppermost ~8 cm (~0.705) before

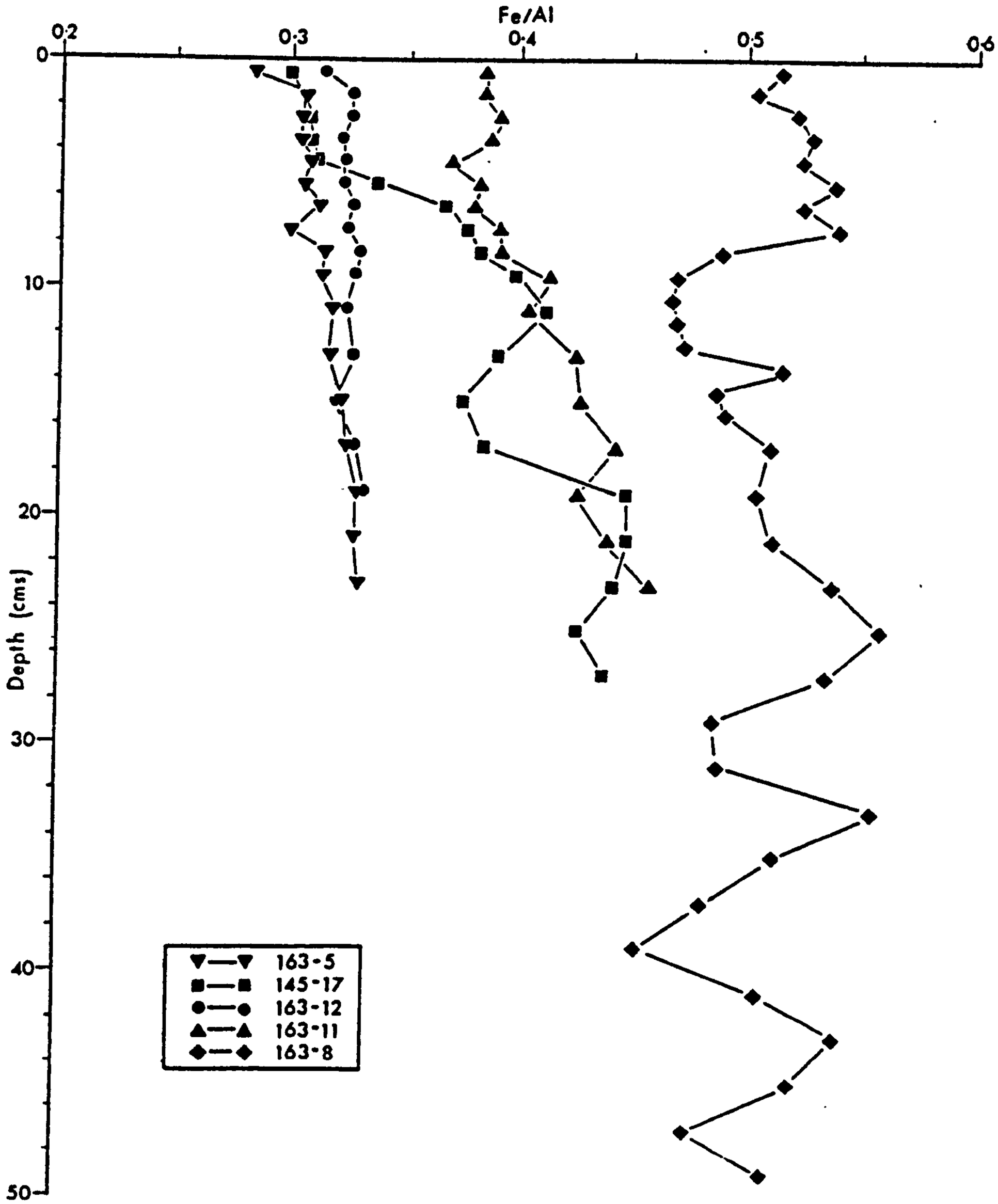

FIGURE 3.11 Profiles of Fe/Al with depth for the Baja California shelf sediments (salt-free).

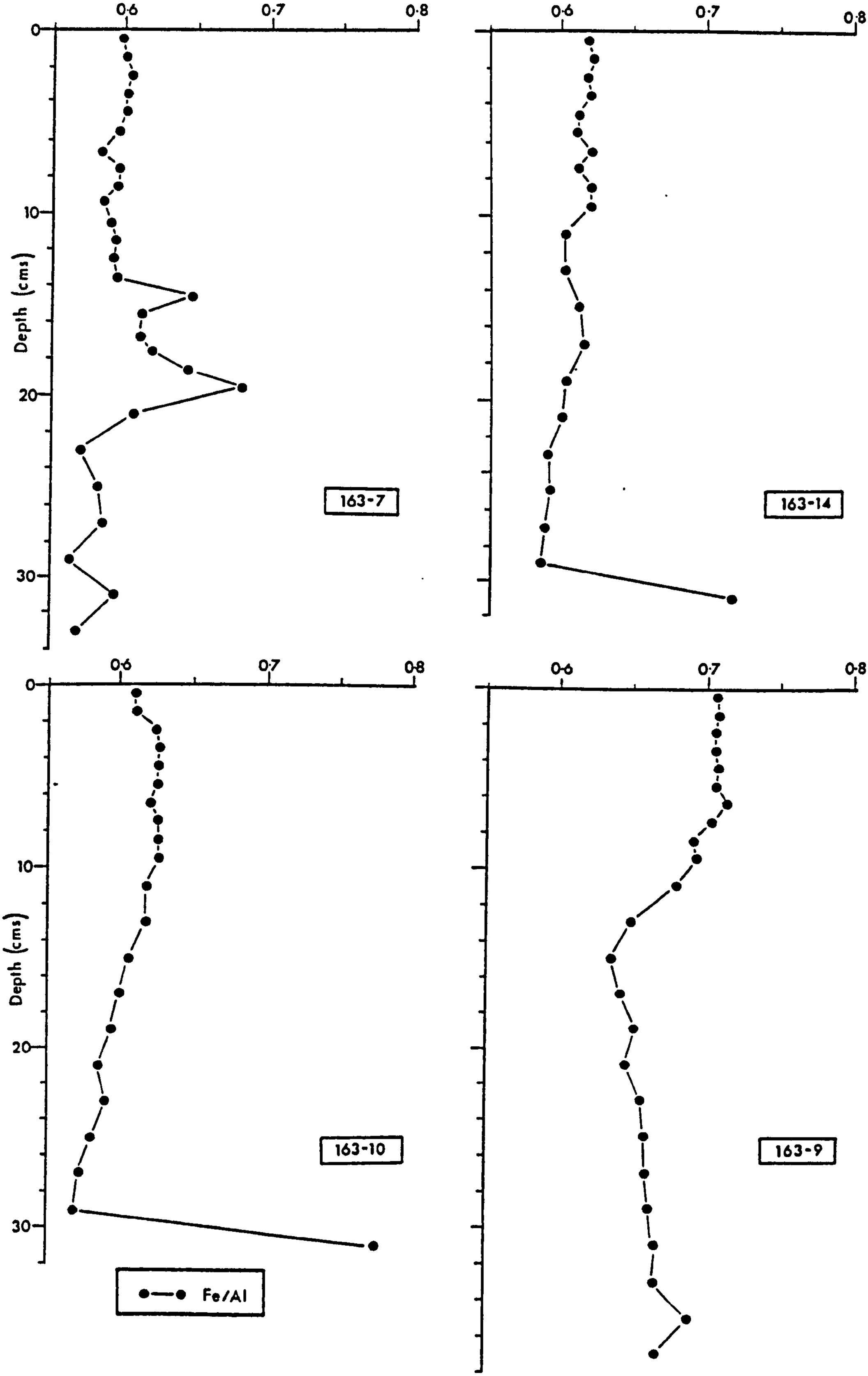

FIGURE 3.12 Profiles of Fe/Al with depth for the Baja California oceanic sediments (salt-free).

decreasing to a core minimum of 0.636 at 14-16 cm depth, similar to Mg/Al and opposite to the increase in K/Al.

Rubidium

The geochemistry of the trace element Rb approximately parallels that of K as shown by Figure 3.13. In typical marine sediments the diadochous relationship is mainly due to their similarity in ionic radii (1.48 Å for Rb^+ and 1.33 Å for K^+) enabling Rb^+ to substitute for K^+ in potassic clays (eg illite) and feldspar. However, Figure 3.13 also indicates that alkali loss in the organic-rich sediments of 163-8, 163-11 and the lower part of core 145-17, and in the high $CaCO_3$ portion of 163-14, occurs causing these samples to deviate from linearity. Nevertheless, the K/Rb ratio for oceanic sediments (Table 3.2) is very close to that of Turekian and Wedepohl (1961) indicating the uniformity of this ionic substitution in deep sea clays.

In the shelf sediments the Rb to Al ratio is variable; station 163-8 has an average Rb/Al of ~9.0×10^{-4} (Appendix C), whilst 145-17 increases from 9.14×10^{-4} in the surface silt to to 12.10×10^{-4} at depth. Similarly, the foraminiferal ooze of 163-11 has relatively higher Rb/Al ratios averaging ~6.5×10^{-4} compared with ~$5.5\text{-}4.6 \times 10^{-4}$ in the sandy-silts of nearshore cores 163-5 and 163-12. These ratios may reflect grain size as Calvert (1976) has suggested that Rb is enriched in finer-grained sediment.

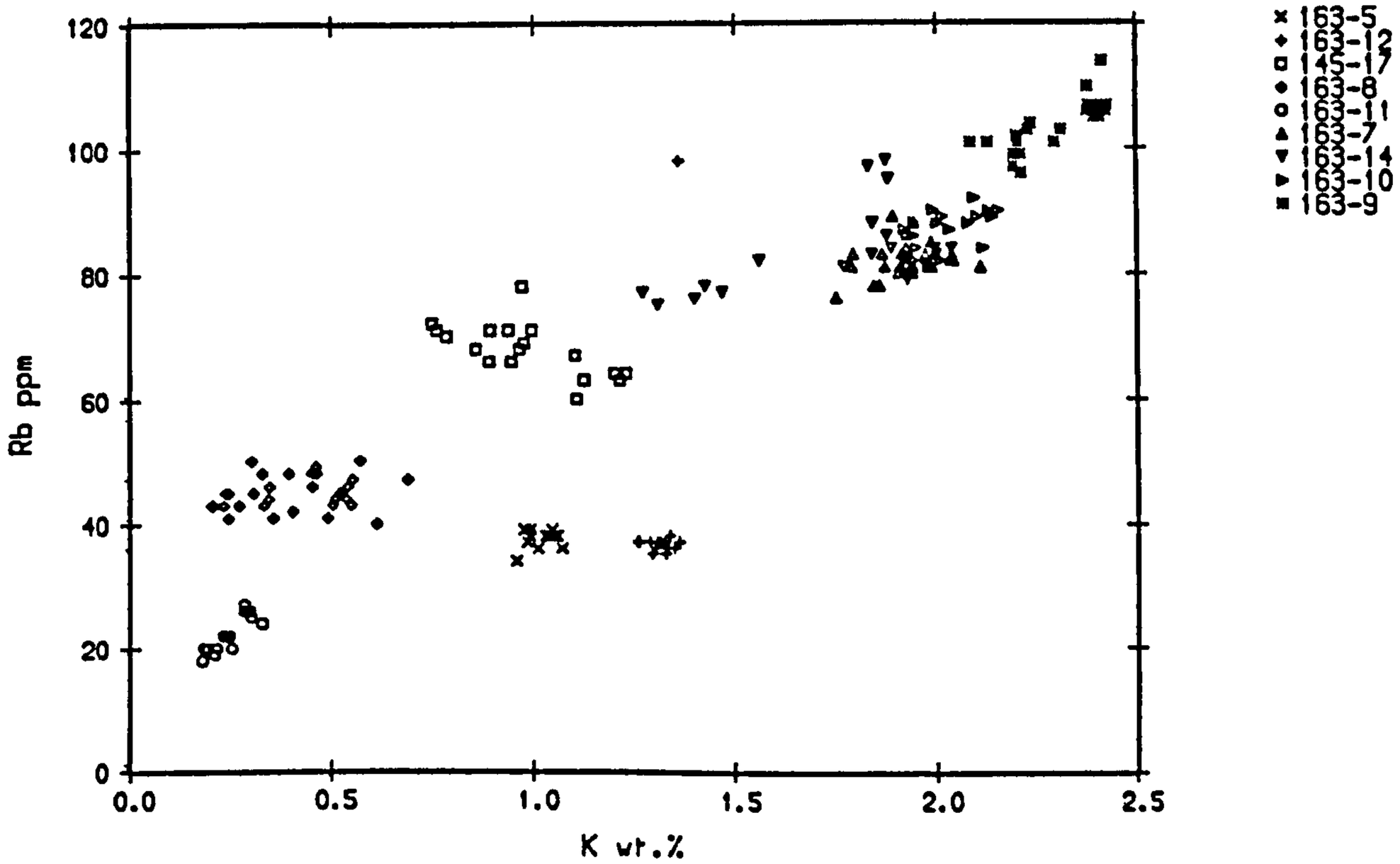

FIGURE 3.13 The relationship between Rb and K for sediments along the Baja California transect (salt-free).

3.2.3 *Discussion*

Si distribution off Baja California is primarily controlled by the distribution of quartz, feldspar and clay; biogenic input being very small. Four mineral hosts for K may be identified from XRD analysis (Figure 2.6); illite, feldspar, chlorite and smectite (in decreasing importance). Glauconite will also contribute to the K level in some of the nearshore sands but it does not occur in sufficient concentration to significantly affect the bulk geochemistry. Mg is commonly found to be enriched in smectites (Table 3.3) relative to other clays and is important in the diagenetic formation of dolomite (Chapter 8). Fe is distributed between smectites, chlorites and sulphides as well as occuring in oxyhydroxides. The range of environments off Baja California causes the bulk geochemistry to be dependant, to some extent, on the distribution and formation of these mineral phases.

Clay Geochemistry

Many studies of marine sediments have concluded that clay minerals are primarily detrital in origin and reflect the composition of their source area. Brief XRD evidence presented in Chapter 2 suggests that much of the illite and chlorite off Baja California, and perhaps some of the smectite, is detrital in nature. Due to the proximity of continental sources of detritus it is probable that variations in clay mineralogy and the resulting geochemical signature is influenced by changes in rate and method of supply of the clays to the shelf and oceanic environment The distribution of illite in the Baja California oceanic sediments may be portrayed by variations in the K/Al ratio (Boyle, 1983), which increase with greater concentrations

TABLE 3.3

ELEMENTAL RATIOS FOR DEEP-SEA SMECTITES

Reference	Mg/Al	Si/Al	K/Al	Ca/Al	Ti/Al	Fe/Al	Origin
Bischoff (1972)	0.64	15.33	0.59	0.32	-	*20.00	1
Nelson and Thompson (1973)	0.64	3.13	0.22	0.04	0.03	0.76	3
	1.84	3.46	0.23	0.07	0.03	2.05	
	0.42	3.55	0.22	0.07	0.30	2.61	
	1.40	2.34	0.22	0.07	0.33	0.56	
Aoki *et al* (1974)	0.59-0.68	5.61-6.93	0.14-0.18	0.02-0.18	0.08-0.25	1.82-2.97	4
Drever (1976)	0.24	2.79	-	0.09	-	0.73	5
	0.26-0.41	2.96-3.76	0.08-0.20	0.15-0.50	-	0.76-1.50	3
Kastner (1976)	-	-	-	-	-	*0.50	3
	-	-	-	-	-	1.70	
Seyfried *et al* (1976)	3.80	7.77	0.31	0.06	0.05	4.23	2
Heath & Dymond (1977)	-	18.93	-	-	-	16.10	4
Scheideger & Stakes (1977)	1.41-2.10	4.62-5.84	0.15-0.34	0.28-0.42	0.08	* 1.96-3.12	3
Hein & Scholl (1978)	-	-	-	-	0.13	*0.45	3
	-	-	-	-	0.29	1.07	
Hein *et al* (1979)	0.42	2.86	0.25	0.08	0.05	0.87	4
	0.50	-	-	0.50	0.13	2.50	

Origin: 1 hydrothermal precipitation
2 low temperature precipitation at spreading centres
3 alteration of volcanic debris
4 chemical combination of Fe oxyhydroxides and Si
5 detrital smectite (for comparison)

(after Hein *et al*, 1979)

of illite relative to other clay minerals.

The slight increase in K/Al with depth in 163-7, 163-10 and 163-9 (Figure 3.8) corresponds to a marked increase in Si/Al (Figure 3.5) suggesting that the proportion of illite may well increase with depth in these cores together with quartz. The causitive factor behind this change in detrital mineralogy is discussed in Section 3.4 . The large decrease in K/Al at depth in 163-14 may be an artifact of sample preparation (Appendix B.1.1); coincidence with the large increase in $CaCO_3$ (Figure 3.2) should not affect the K/Al ratio. If illite is the dominant K bearing mineral on the shelf, rather than feldspar, the increase in K/Al with depth in 145-17 and 163-11 (Figure 3.7) is futher evidence of a decrease in grain size.

In contrast to illite, the distribution of smectite and its chemical composition is affected by both detrital and aggradation processes. The predominance of a smectite component is characteristic of Pacific sediments along the California margin and in the east Equatorial Pacific (Griffin and Goldberg, 1963, 1969; Heath, 1969; Heath *et al* , 1974; Pedersen, 1979; Hein *et al*, 1979; Rateev *et al*, 1981). There is considerable evidence to suggest that appreciable quantities of smectite can form diagenetically in the abyssal environment (Griffin *et al*, 1968; Heath, 1969; Windom, 1969; Sayles and Bischoff, 1973; Aoki *et al*, 1974; Hein *et al*, 1979). Griffin and Goldberg (1963) have suggested that smectite forms from *in situ* alteration of volcanic debris. Off Baja California it is uncertain if detrital smectite from weathered andesitic source terranes (the Commondu Volcanics, Section 2.1) or *in situ* formation is the primary factor, although diagenetic formation

certainly seems to occur from physical (Plate 3) and chemical (Chapters 3 and 6) evidence.

Mg/Al is taken as the primary indicator of this mineral phase given the abundance of Mg^{2+} in marine smectites (Table 3.3). Apart from core 163-13, dolomite concentrations are not sufficiently high to influence the bulk Mg content. The higher Mg/Al ratios in the oceanic environment suggests greater concentrations of smectite, supported by XRD evidence (Figure 2.6). The antipathetic trend between Mg and K relative to Al (Figure 3.8) may be interpreted as indicating the relative importance of smectite over illite with time. In the hemipelagic sediments there has been a general increase in the level of smectite (Mg/Al) from the past to the present day. In the pelagic red-clay such a change occurs suddenly at ~10 cm depth.

The Multifarious Role of Iron

In the oceanic sediments, Fe displays an increase oceanwards (Table 3.2) in the same direction as increasing clay content. The plot of Fe against Al (Figure 3.10) indicates that aluminosilicate minerals, probably Fe-rich smectite, host nearly all the Fe apart from two exceptions.

(1) The highest Fe/Al of the shelf sediments occurs in the anoxic basin, 163-8, and may be due to the formation of iron sulphide in the presence of H_2S. Similarly, sulphide formation may well be responsible for the rise in Fe/Al with depth in 145-17 and 163-11. The parallel behaviour of Mg/Al (compare Figure 3.7 and 3.11) in these cores may be a

consequence of this process.* Drever (1971) found that non-exchangeable Mg increased in anoxic sediments of Banderas Bay, Mexico, which he believed to result from Fe release from smectite during sulphate reduction to form sulphides, enabling Mg to enter the vacant structural site. High Mg concentrations in diatomaceous, organic-rich sediments of the Nambian shelf have been attributed to the same process (Calvert, 1976). However, organic matter itself may be an important source of Mg in anoxic sediments without the need to envoke Mg substitution into smectite. Chapters 5 and 8 present futher geochemical (Fe, Mo, S) and mineralogical evidence of sulphide formation in the Baja California shelf sediments.

(2) The increase in Fe/Al in the oceanic sediments oceanwards may be due to a greater proportion of iron oxide in the less reducing sediment, due to decreasing organic matter content (Chapter 4) and correspondingly slower diagenetic reactions. Fe is a redox-controlled element, commonly existing as insoluble Fe^{3+} in oxidising sediment and on reduction to Fe^{2+} becomes solubilised. The element behaves in much the same way as Mn (Chapter 6) undergoing dissolution/reprecipitation reactions during diagenesis, but at a lower Eh. The redox change is also marked by a colour change from brown, oxidised sediment to grey-green, reduced sediment (Bezrukov, 1960; Lynn and Bonatti, 1965; Lyle, 1983). Recent work (Rozenson and Heller-Kallai, 1976a,b; Russell *et al*, 1979) has shown that this colour change is both reversible, and unique to Fe-rich smectites. In contrast, aluminous smectites only darken from

---

* No dolomite was observed in these cores (Chapter 8) enabling this source of Mg to be discounted.

off-white to grey (Rozenson and Heller-Kallai, 1976a) while iron oxyhydroxides do not show a reversible reaction (Lyle, 1983).

In the hemipelagic sediments (163-7, 163-14, 163-10) such colour changes are seen (Appendix A) despite no distinct change in Fe/Al gradient at the colour change depth as one might expect if large quantities of Fe were released into solution at the critical Eh level. In fact, Russell *et al* (1979) suggest that only 10% of Fe in typical smectites need be reduced to incur a colour change. The lack of a surficial maximum in Fe/Al for these sediments indicates that Fe oxyhydroxides are only a minor component (as opposed to Mn oxyhydroxides; Chapter 6) and that aluminosilicates do indeed host most of the Fe. Several studies (Table 3.3) on authigenic smectites in the Pacific have shown high Fe/Al ratios, although this may be partly attributable to their mode of formation. The sharp increase in Fe/Al at the base of 163-14 and 163-10 (Figure 3.12) is reflected by smaller increases in K/Al and Mg/Al (Figure 3.8) and may represent a lithological variation, such as an ash band. In addition, the lack of any "excess" Fe is evidence that diagenetic precipitation of ferriphosphate is unlikely. In the pelagic red-clay cores (163-9, 163-15) the higher Fe/Al ratios probably indicate that oxyhydroxides are a more important component in this more oxic environment; no colour change is seen in these cores.

PLATE 3 Scanning electron micrograph of "cornflake" textured diagenetic smectite overgrowing detrital grains. The sample is from the base of core 163-10 at the site of a possible ash band. The interval between the ticks on the scale bar is 10 μm.

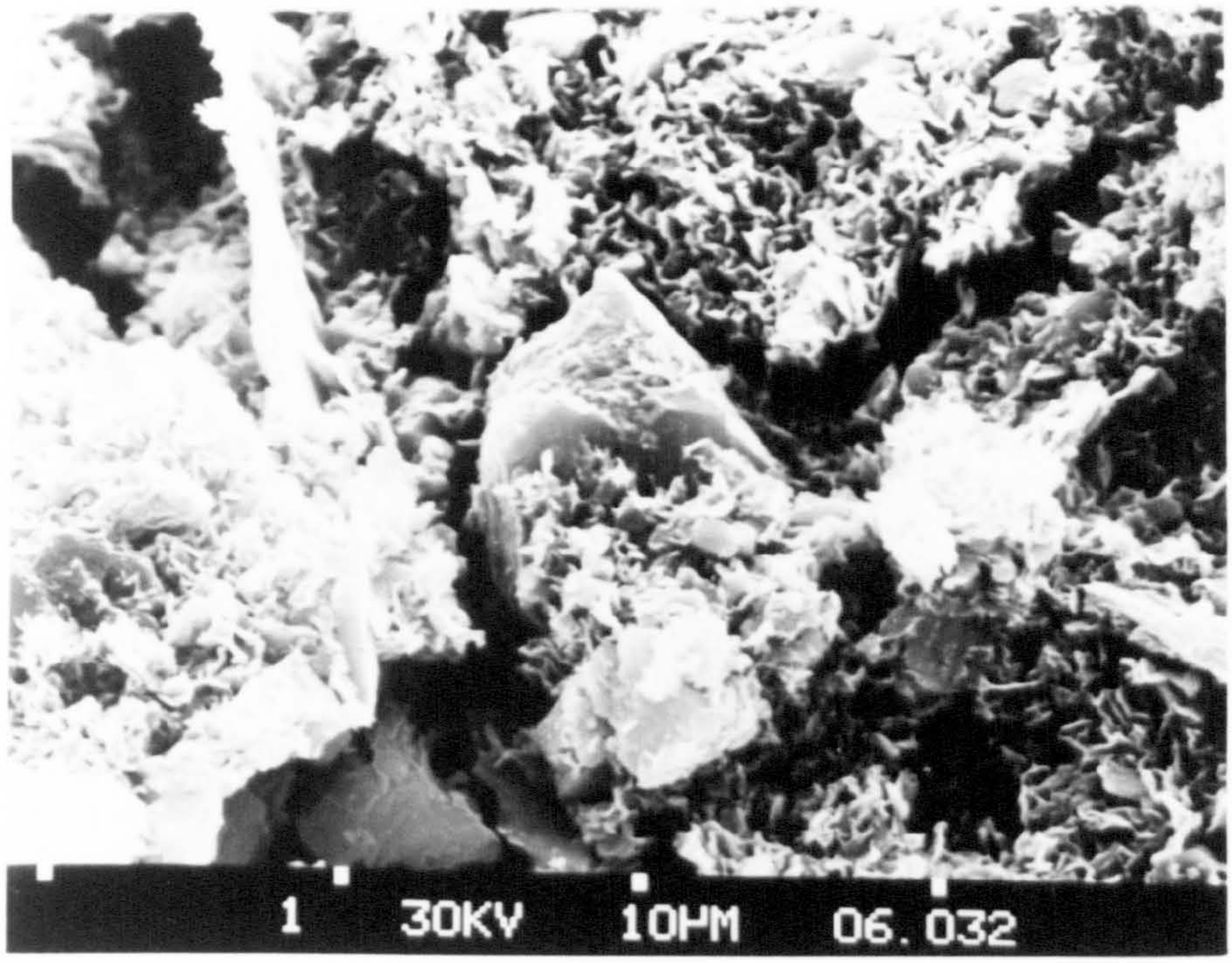
1 30KV 10UM 06.032

3.3 BIOGENIC ELEMENT GEOCHEMISTRY

Calcium

Ca, like Si, is partitioned between both biogenic and terrigenous phases. However, unlike Si which is terrigenously dominated, the Ca distribution of Baja California is primarily controlled by biogenic $CaCO_3$. Ca was measured by XRF techniques (Appendix B.1); $CaCO_3$ by difference between total C and organic C using a Perkin-Elmer Elemental Analyser and a Leco induction furnace respectively (Appendix B.5). Figure 3.14 shows the correlation between the two methods, indicating the control on Ca distribution by $CaCO_3$ in the oceanic sediments. The intercept on the ordinate (~1.0 wt.%) represents Ca in detrital aluminosilicate (feldspar). Table 3.4 indicates the decreasing surface Ca/Al offshore, shown for all samples in Figure 3.15.

TABLE 3.4

Sample	Depth	Ca	$CaCO_3$	C_{org}	Sr	Ba	Ca/Al	Sr/Al	Ba/Al
	cm	wt.%	wt.%	wt.%	ppm	ppm		$x10^{-4}$	$x10^{-4}$
163-5	0-1	6.84	-	1.70	556	441	1.054	85.7	68.0
163-12	0-1	6.85	-	1.35	744	501	0.875	95.0	64.0
145-17	0-1	8.91	-	1.97	579	561	1.357	88.2	85.5
163-8	0-1	12.84	-	6.90	712	279	2.681	148.7	58.3
163-11	0-1	23.18	-	1.39	866	157	7.089	264.8	48.0
163-7	0-1	1.58	1.08	1.24	365	3473	0.213	49.1	468.0
163-14	0-1	1.69	1.58	1.12	387	3684	0.221	50.4	480.2
163-10	0-1	1.53	1.75	0.96	383	4041	0.194	48.4	510.9
163-9	0-1	1.31	0.75	0.61	415	5588	0.165	52.4	705.6
163-15	0-1	1.43	-	0.79	368	4629	0.185	47.5	597.3
Clay*		3.00	-	-	188	2400	0.340	21.6	275.9
Carbonate*		32.65	-	-	2090	198	15.620	1000.0	94.7

*Turekian and Wedepohl (1961) Salt-corrected using presented Cl analysis

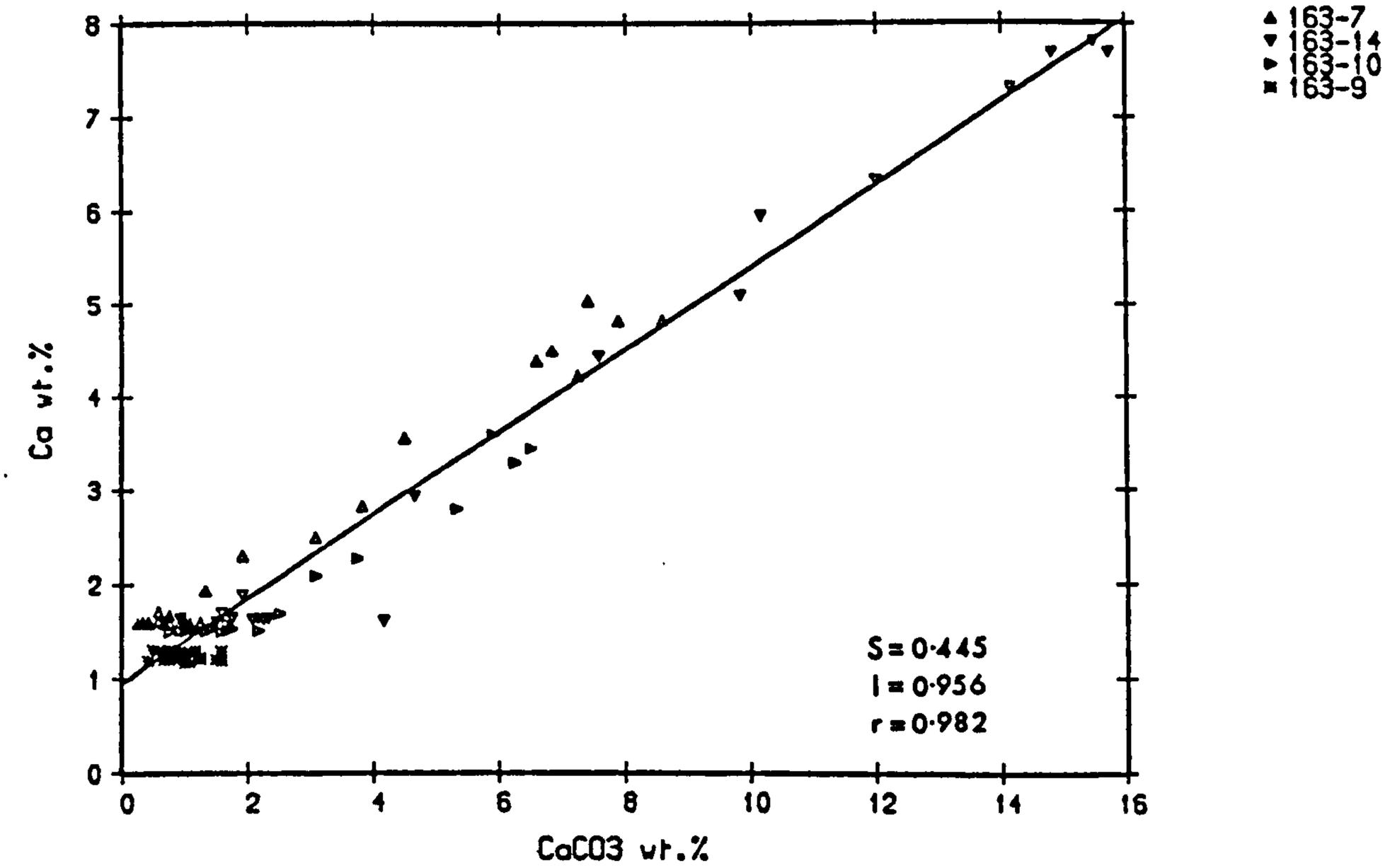

FIGURE 3.14 The correlation between Ca and $CaCO_3$ in oceanic sediments off Baja California (salt-free).

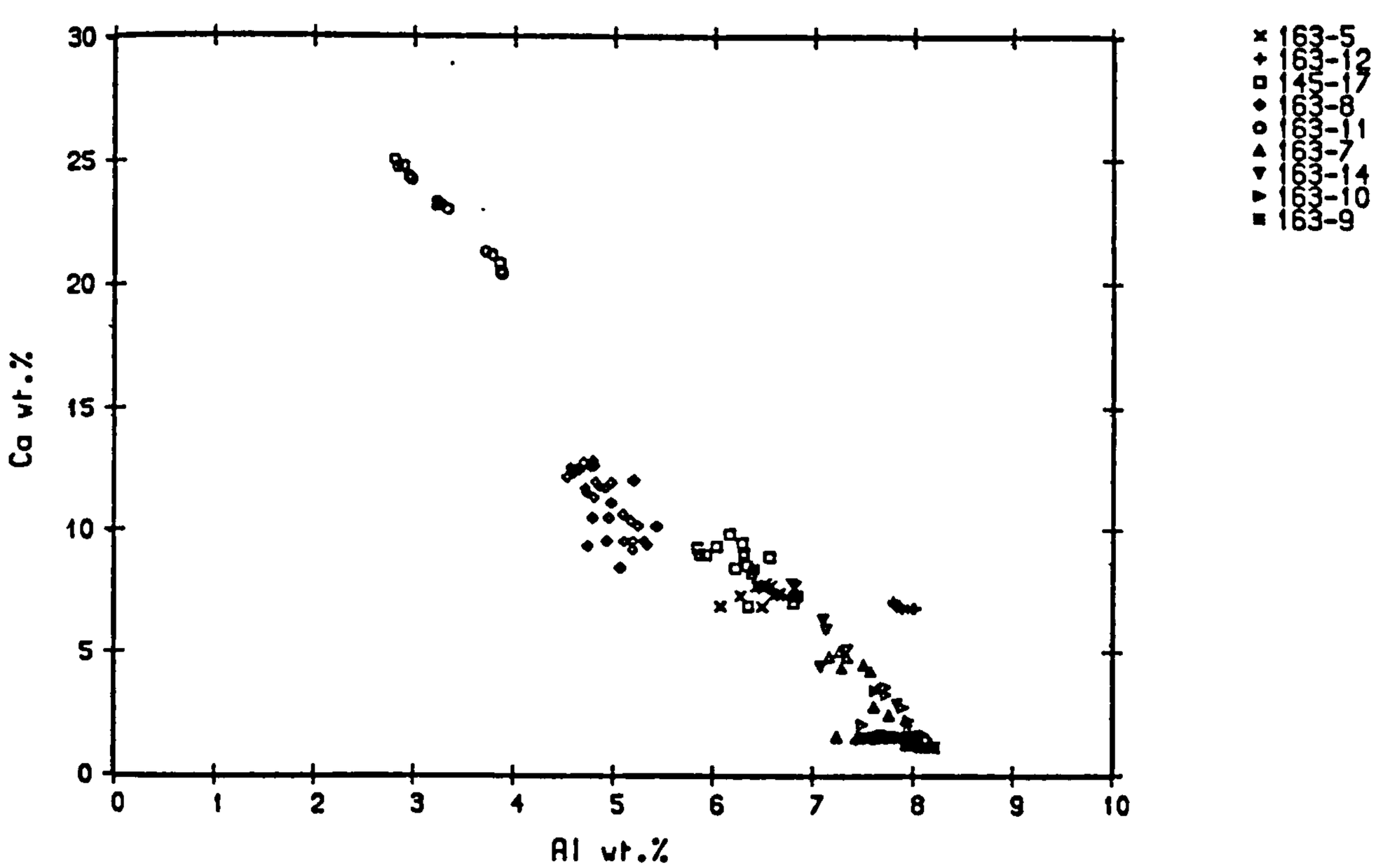

FIGURE 3.15 The inverse relationship between Ca and Al for sediments along the Baja California transect (salt-free).

The antipathetic trend between terrigenous aluminosilicate indicated by Al, and biogenic input indicated by Ca, shows clearly the dual incorporation mechanisms each acting as a dilutent of the other, although deviations from this trend indicate the presence of other components. For instance, the high organic matter content of 163-8 reduces both Ca and Al in this case, whilst the calcic plagioclase in the nearshore environment of 163-12 lies above the dilution line.

The high Ca/Al ratios of the shelf sediments occur in deposits containing abundant benthic, calcareous foraminifera (Plate 2.1a), especially in the organic-rich basin (163-8, Ca/Al = 2.681) and towards the outer part of the shelf (163-11, Ca/Al = 7.089). In the deeper water of the hemipelagic and pelagic setting the surface Ca/Al are much lower than expected (0.221-0.165; Table 3.4) given the abundant productivity in the surface waters. This suggests that dissolution of $CaCO_3$, especially planktonic foraminifera, occurs in the water column with the sediment being deposited below the calcite compensation depth (CCD). The actual depth of this horizon is unknown. Station 163-14 has the highest surface Ca/Al ratio (0.221) of the five oceanic cores, and is situated on a slight topographic rise (3229 m), about 500 m shallower than the other stations (Table 1.1). In addition, the high degree of carbonate solution may result from the high dissolved organic matter content, lower CO_3^{2-}, and high CO_2 production within the sediment (Berger, 1970).

With depth the distribution of Ca/Al (Figure 3.16) is marked by a striking increase at ~15 cm depth in the hemipelagic cores, and an absence of this increase in the red-clay of cores 163-9 and 163-15. In 163-7 the maximum Ca/Al is

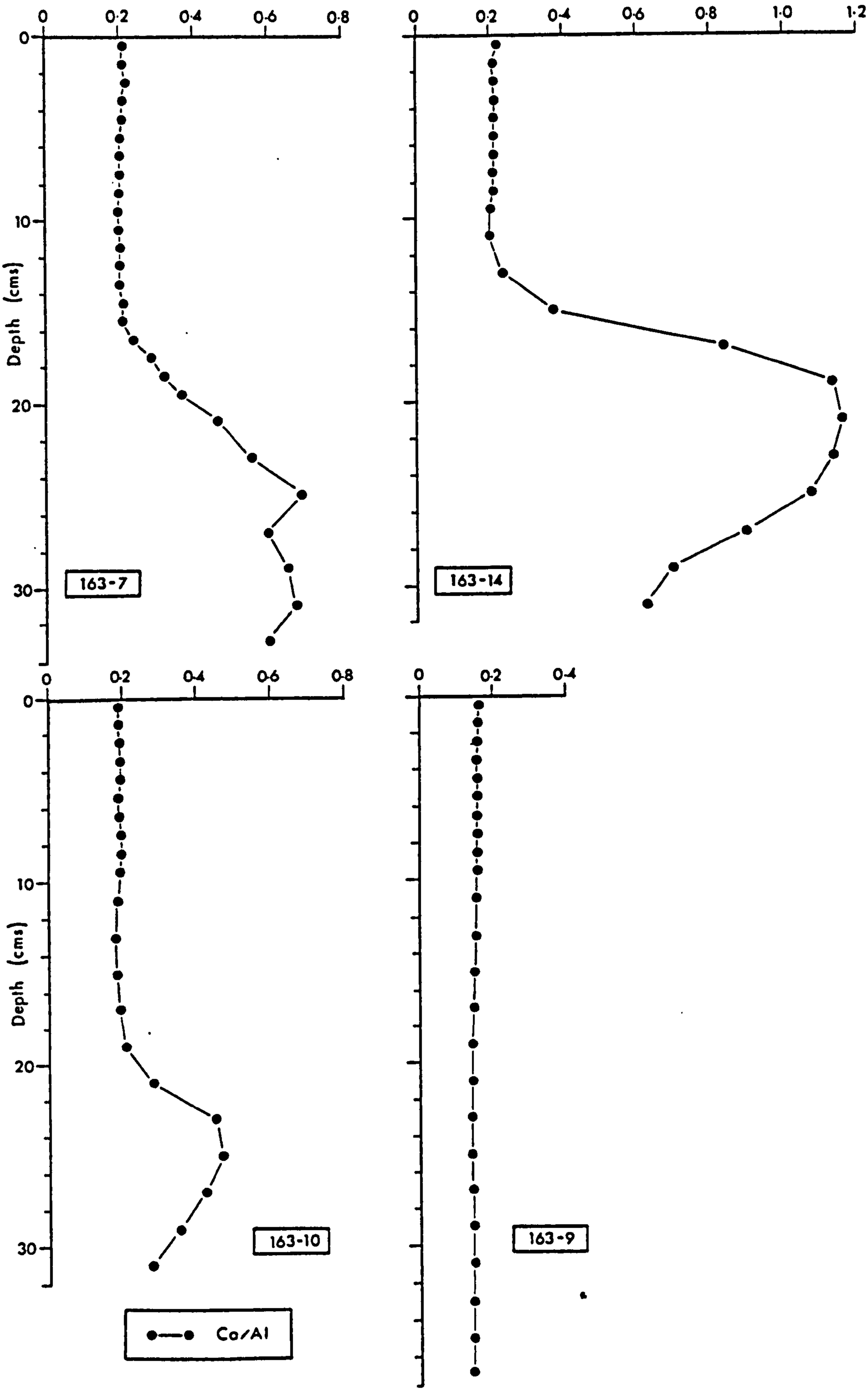

FIGURE 3.16 Profiles of Ca/Al with depth for the Baja California oceanic sediments (salt-free).

0.694 and maintains a slightly lower ratio to the base of the core. In contrast, 163-14 and 163-10 display well-defined maxima, having the largest Ca/Al ratio of 1.151 at 20-22 cm depth in 163-14, and 0.466 at 24-26 cm depth in 163-10. The two pelagic cores, 163-9 and 163-15, display a slight decrease in Ca/Al with depth, and no maxima. The hemipelagic depth profiles suggest that major changes in the flux of carbonate to the seafloor has occured over the time interval of the cores. This subject is discussed in detail below (Section 3.4).

Strontium

The distribution of Sr off Baja California is partitioned between four phases; carbonate (calcite), barite, apatite, and aluminosilicates (clay and feldspar). Figure 3.17 indicates the inverse relationship between Sr and Ca for all sediments along the transect, each of which have varying proportions of the four Sr-bearing phases. Calcite occurs in both the foraminiferal debris of the shelf (eg 163-11), and at depth in the three hemipelagic cores, particularly 163-14. The highest Ca value in 163-11 is 25.8 wt.% (22-24 cm depth, Appendix C) corresponding to approximately 65 wt.% $CaCO_3$. Taking Turekian and Wedepohl's (1961, Table 3.4) Sr analysis for average lithogenous clay, this corresponds to ~66 ppm of Sr in the 35% clay fraction of this core, or 1430 ppm Sr in pure $CaCO_3$ (Line A, Figure 3.17). This core contains little or no barite and/or apatite unlike the oceanic sediments (see below) or core 145-17 (Chapter 8) respectively. Barite apparently increases oceanwards in the deep-water sediments, reaching a maximum concentration in 163-9, but is reduced in the glacial sediment

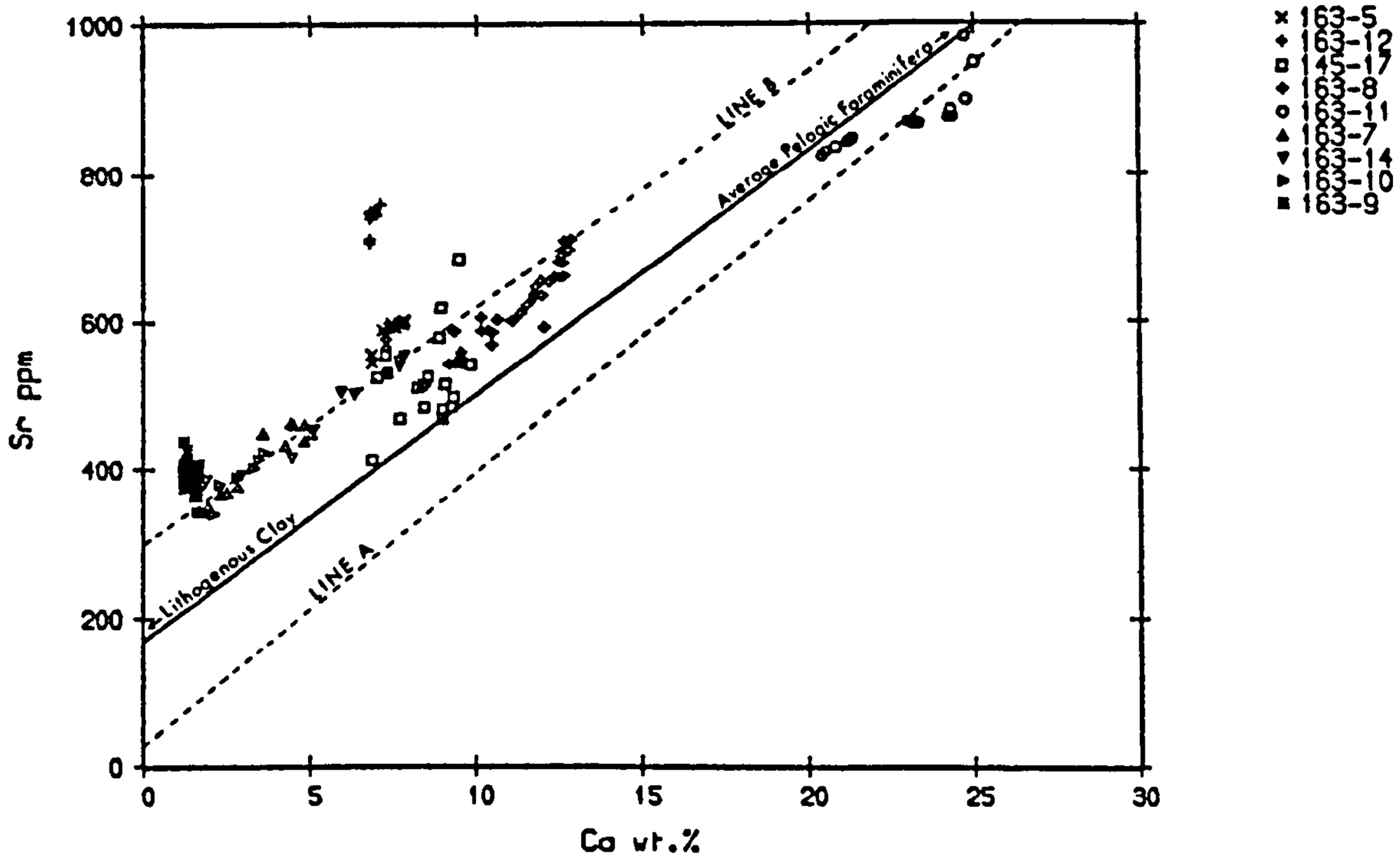

FIGURE 3.17 The relationship between Sr and Ca for sediments along the Baja California transect (salt-free). The tie-line connects Sr in lithogenous clay to Sr in average pelagic carbonate (Turekian and Wedepohl, 1961). Line A represents the Sr/Ca ratio in clay-free carbonate in 163-11; Line B the Sr/Ca ratio for the carbonate maxima in the three hemipelagic cores.

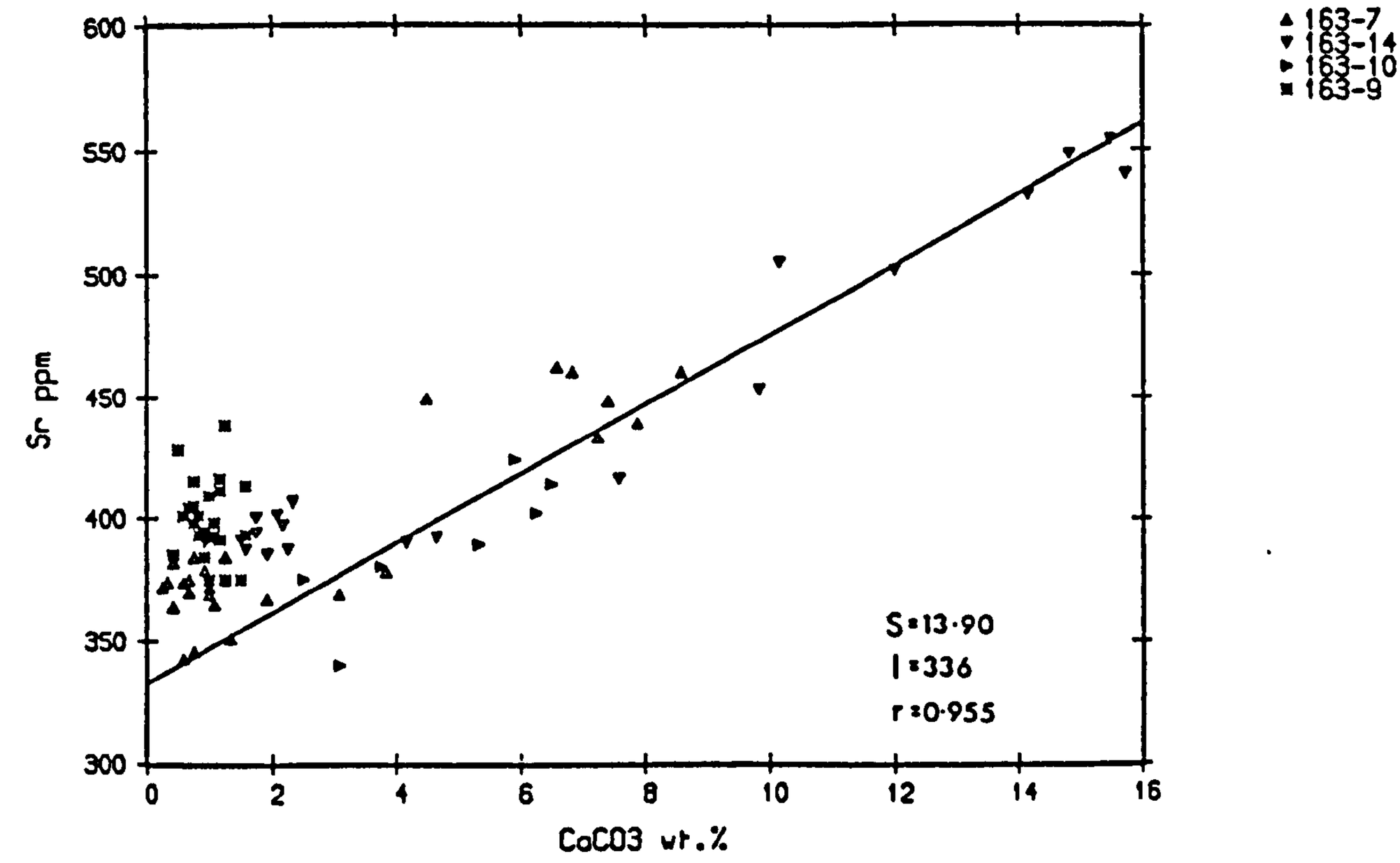

FIGURE 3.18 The correlation between Sr and $CaCO_3$ for the carbonate maxima in the three hemipelagic cores off Baja California (salt-free).

of the lower decimeter of the three hemipelagic cores where $CaCO_3$ concentrations are greatest (Figure 3.22). The Sr concentration in 100% $CaCO_3$ has been calculated for these sediments by fitting a regression line to Ca (Figure 3.17) and $CaCO_3$ (Figure 3.18) data from the lower 20 cm in 163-7 and 163-14, and the lower 14 cm in 163-10. In this case 300-336 ppm of Sr is held in the non-carbonate fraction, whilst 1054-1287 ppm occurs in pure calcite. This regression data indicates the similarity in Sr content of the $CaCO_3$ fraction of the Baja California sediments with that found by Turekian (1964) and other workers who have analysed pelagic foraminifera tests (Table 3.5). Figure 3.17 also indicates that other sediments without barite or apatite (eg 163-8) fall parallel to, and between, lines A and B according to the degree of carbonate dilution by aluminosilicate debris or organic matter.

TABLE 3.5

Sr CONCENTRATION OF PELAGIC FORAMINIFERA TESTS

Author	Sr (ppm)
Emiliani (1955)	1200
Thompson and Chow (1956)	1300
Turekian (1957)	1200
Krinsley (1960)	1150
Turekian (1964)	655
This study - by extrapolation:	
163-11	1430
163-7, 163-14, 163-10	1054-1287

The quantity of Sr held in barite is estimated from 163-9. In this core a maximum Ba concentration of 6036 ppm is matched by 438 ppm Sr at 30-32 cm depth (Appendix C). As carbonate is negligible in this core the enrichment in Sr relative to average lithogenous clay (Table 3.4) must be due to the presence of barite. Thus approximately 5.7 wt.% of Sr is held in one mole of barite, or 6.5 mole% of $SrSO_4$. Church (1979) found Sr to range from 0.2-3.4 mole% with an average of 1 mole% in marine barites.

Core 163-12 indicates that substantial Sr is held in excess of possible barite or calcite. The presence of calcic plagioclase (see above) may be responsible for this Sr enrichment. The extreme elevation of Sr relative to Ca in 145-17 is due to the formation of diagenetic apatite (Chapter 8).

Barium

The occurrence of barite in marine sediments, existing as large concretions, was first documented by Murray and Renard (1898) during the *Challenger* expedition. Similar concretions off southern California have been attributed to reaction between magmatic fluids containing dissolved Ba and interstitial water of the sediments (Cortecci and Longinelli, 1972). Vinogradov (1953) found barite crystals and nodules in the Indian Ocean associated with benthic protozoans of the order Xenophyphorida. Futher work identified dispersed, but ubiquitous, microcrystals underlying the equatorial productivity belt of the eastern Pacific, and occasionally the Atlantic (Goldberg and Arrhenius, 1958; Turekian and Tausch, 1964; Bostrom *et al*, 1973). In addition, high concentrations of

Ba have been found in the vicinity of active spreading ridges (Arrhenius and Bonatti, 1965; Bostrom and Peterson, 1966) and in metalliferous Fe-Mn sediments (Bostrom and Peterson, 1966; Sayles and Bischoff, 1973). The most recent work on Ba has identified particulate Ba enrichment in the water column (Dehairs *et al*, 1980) with the highest contents of suspended barite just below the euphotic zone, and may correlate with biological productivity.

Off Baja California the distribution of Ba seems to be controlled by two important mechanisms (Figure 3.19).

(1) The shelf sediments (163-5, 163-11, 163-12, 145-17, 163-8) display a correlation between Ba and Al (Figure 3.20) suggesting that detrital aluminosilicate (probably K-feldspar) hosts most of the Ba in the nearshore, shallow-water environment. Note however, that station 163-12 and possibly 163-5, have a different behaviour relating to the aluminous nature of these sediments (see also Figures 3.1, 3.6, 3.9, 3.10, 3.13) and the increase in Ca (Figure 3.15) and Sr (Figure 3.17). Previously, it was noted that core 163-12 may contain an abundance of calcic plagioclase relative to the other shelf sediments. If this is the case, the lack of Ba in these sediments may be attributable to Ba^{2+} substitution for K^{+} (ionic radius 1.34 Å for Ba^{2+}, 1.33 Å for K^{+}) in potassic orthoclase (Taylor, 1965) which may be the primary feldspar on the shelf but not in the local nearshore environment sampled by 163-12. The positive Al intercept indicates that some of the aluminosilicate debris does not contain any Ba. On the shelf no relation is observed between the level of Ba and organic matter (Table 3.4). The concentration of organic C broadly reflects primary productivity in the surface waters, indicating

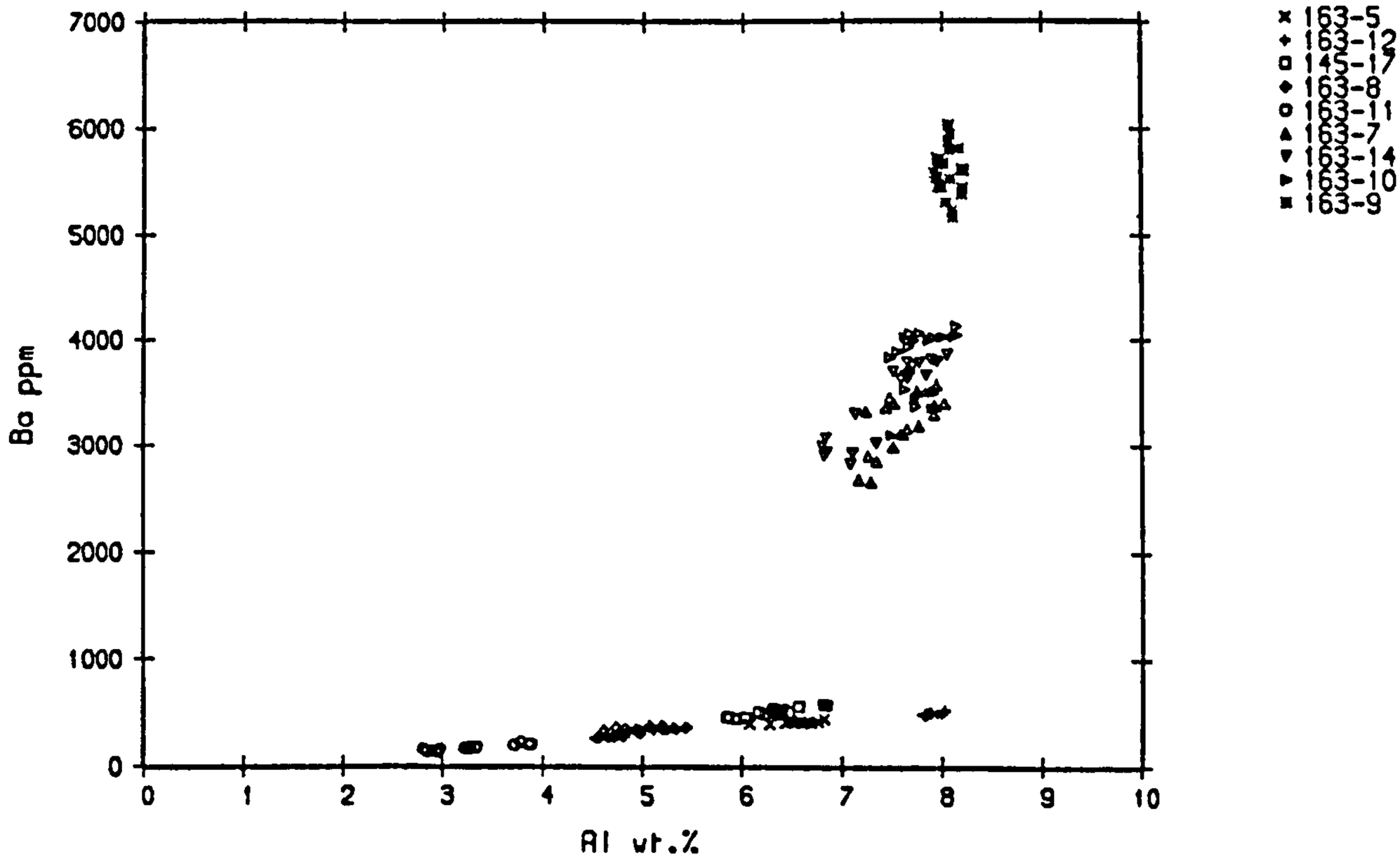

FIGURE 3.19 The disparate relationship of Ba relative to Al between the shelf and oceanic sediments off Baja California (salt-free).

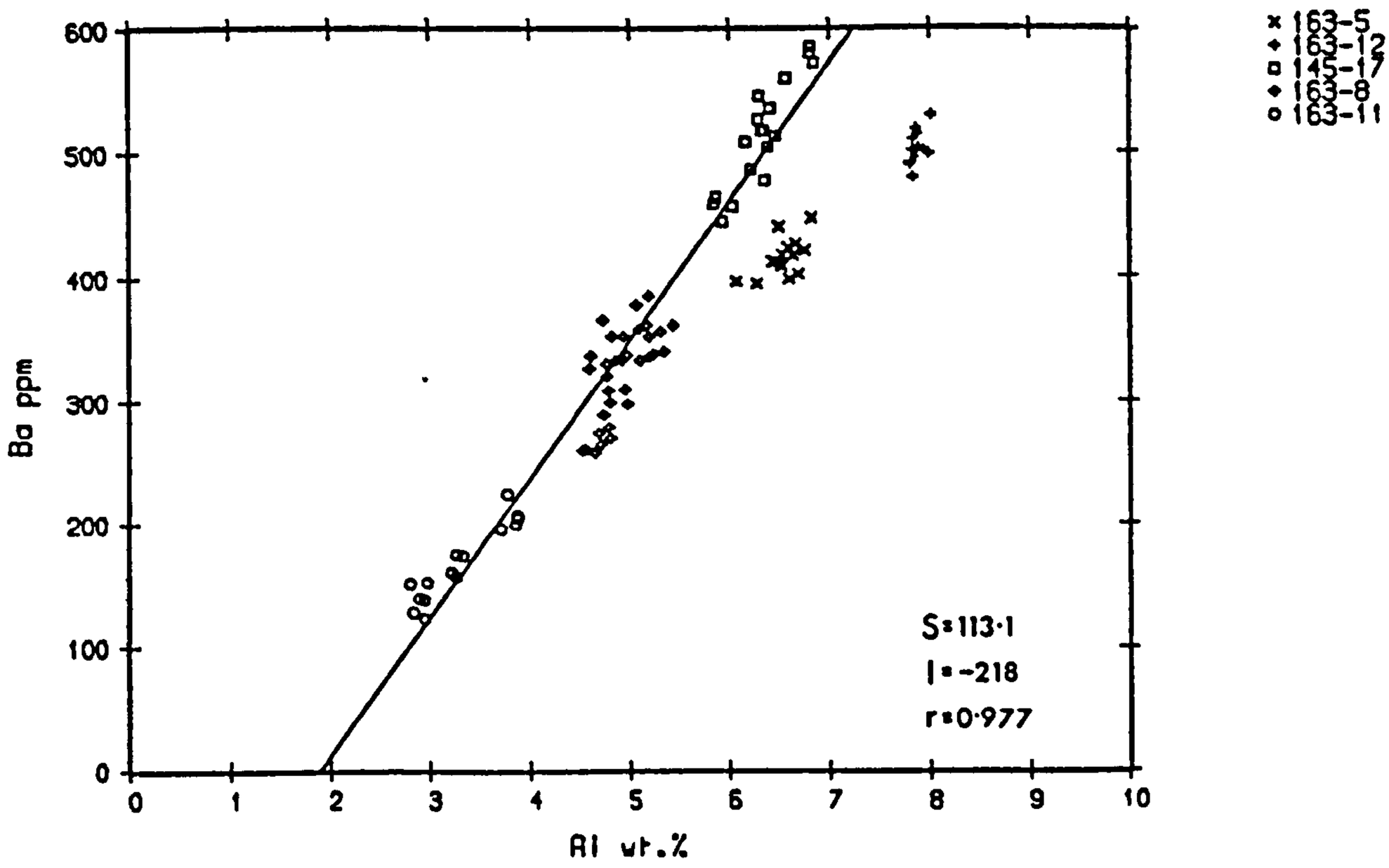

FIGURE 3.20 The correlation between Ba and Al for the Baja California shelf sediments (salt-free) (Stations 145-17, 163-8 and 163-11).

that Ba is not intimately associated with the flux of organic matter to the sediments.

(2) In the oceanic environment concentrations of Ba are much higher than on the shelf, and apparently independant of both Ca and Al (Figures 3.16 and 3.19). The oceanic concentration increases seawards from 3473 ppm at the surface of 163-7 to a maximum of 5588 ppm in 163-9 (Table 3.4). Again no correlation with the level of organic matter in the sediment is seen.

While it seems that Ba distribution on the shelf can be accounted for in terms of terrigenous supply the lack of correlation between Ba and biogenic components ($CaCO_3$, Ca, C_{org}) in the offshore environment is difficult to explain. However, the absence of metalliferous sediment (Chapter 2) and large distance from any volcanogenic Ba source indicates that some biogenic agent must be operating. When the Ba distribution of high productivity areas are studied in detail anomalies begin to appear. Along the equatorial productivity belt Ba concentrations rapidly diminish westwards whereas opaline Si concentrations continue uniterrupted (Bostrom *et al*, 1973). Brongersma-Sanders (1966) suggested that Ba-containing diatoms dissolve easily leaving Ba in the sediments and accounting for the lack of source organisms, but this appears unlikely. Church (1970, 1979) suggests that Ba concentrations are correlated with $CaCO_3$ and organic matter on the East Pacific Rise. He proposes that pelagic barite results from a concentration of Ba in the biological cycle, and is subsequently precipitated after biogenic degradation and release of Ba^{2+} to sulphate-rich microenvironments. The water column flux would contribute half

of the sedimentary barite, the remainder coming from diagenetic growth within the sediment during further organic degradation.

In order to assess these proposals Ba is plotted against salt-corrected S (Figure 3.21), and normalised against Al with depth in Figure (3.22). S exists in excess of the maximum concentration of stoichiometric barite because of the possible presence of micro-framboids of sulphide. With depth Ba/Al decreases in the three hemipelagic cores, dropping by 21.3% in 163-7, 16.5% in 163-14 and 18.7% in 163-10. In each case the maximum change in gradient of the Ba/Al profiles occurs at depth; 14 cm in 163-7, 10 cm in 163-14 and 16-18 cm in 163-10. In the pelagic sediment of 163-9, Ba/Al decreases down to 14-16 cm before increasing again to a core maximum of 748.5×10^{-4} at 30-32 cm depth.

The decrease in Ba/Al with depth would suggest that Church's (1979) hypothesis of diagenetic precipitation is not occuring to a significant degree. Dehairs *et al*'s (1980) work referred to above identified micron sized barite particles in suspended matter throughout the world's oceans. They claim that barite is introduced into surface waters by biological processes, and that the degree of biological productivity correlates with the particulate Ba content; barite formation proceeds by direct secretion within planktonic organisms and by precipitation within microenvironments of decaying organic debris. It is therefore possible that changes in the Ba/Al ratio reflect the degree of dilution by terrigenous debris of biogenic Ba deposited on the ocean floor.

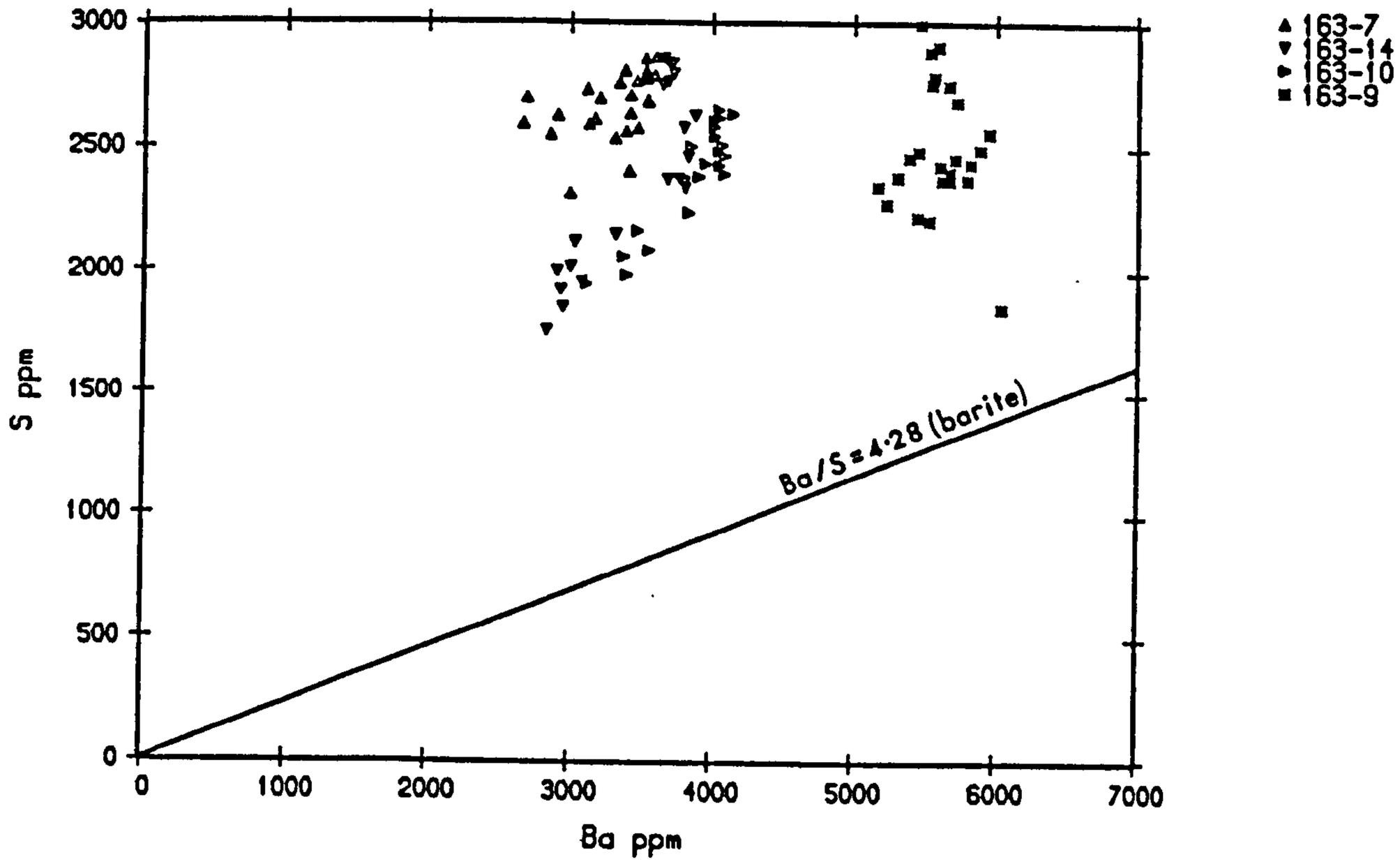

FIGURE 3.21 The relationship between S and Ba in oceanic sediments off Baja California (salt-free). The line represents the empirical Ba/S ratio (4.28) in pure barite.

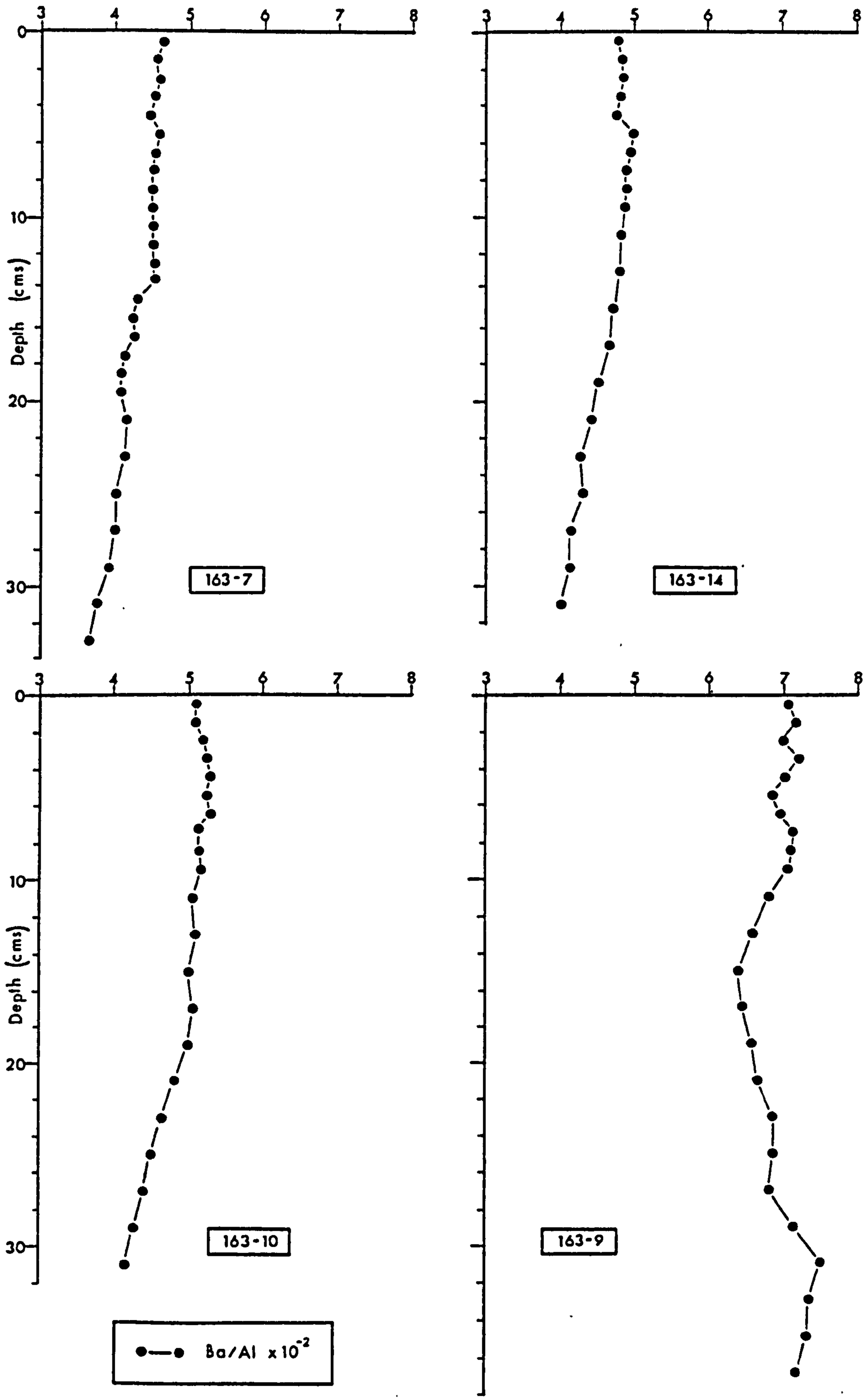

FIGURE 3.22 Profiles of Ba/Al ($x10^{-2}$) with depth in oceanic sediments off Baja California (salt-free).

3.4 THE GEOCHEMICAL RECORD OF CLIMATIC FLUCTUATION OFF BAJA CALIFORNIA

Since Arrhenius (1952) first proposed that cyclic variations in $CaCO_3$ with depth in the eastern equatorial Pacific were due to climatic extremes during the Pleistocene, there have been many studies on this phenomenon (Ericson *et al*, 1956; Broecker *et al*, 1958; Broecker, 1971; Berger, 1973; Thompson and Saito, 1974; Damuth, 1975; Luz and Shackleton, 1975; Adelseck and Anderson, 1978; Volat *et al*, 1980; Pedersen, 1983; Bacon, 1984). The cause of these $CaCO_3$ variations is uncertain, particularly as a universal explanation is certainly not applicable to all locations and depths in the world's oceans. In the Atlantic dissolution cycles are the opposite to the Indo-Pacific. Three oceanographic factors influence the carbonate content of a sediment: (1) biological productivity of calcareous organisms; (2) dissolution of carbonate pre- and post-deposition; (3) dilution by non-carbonate material. In addition off Baja California, a fourth factor, the supply of detrital carbonate, may be considered.

Important to the evaluation of the effect of these mechanisms on the Baja California sediments is the establishment of a chronological time scale. Sawlan (1982) obtained ^{14}C dates for two cores (145-7 and 145-8) from the previous cruise, TT-145. At 26-35 cm depth in 145-7 (approximately the same position as 163-10; Figure 1.1) a date of 14,090 + 150 years was reported. For the intervals 0-6 cm and 26-34 cm in 145-8 (equivalent to 163-7) dates of 2,700 and 10,400 years were measured. From these dates sediment accumulation rates of 2.2 cm kyr^{-1} for 145-8 and 3.5 cm kyr^{-1} were calculated (Sawlan, 1982). These dates indicate that the

elevated $CaCO_3$ (Figures 3.2 and 3.16), Si/Al, normalised Zr/Al and K/Al, and the decrease in Mg/Al and Ba/Al at >~15 cm depth in the hemipelagic cores, occur in sediment deposited during the last glacial episode, the Wisconsin. Thus changes in climate may have directly or indirectly affected sediment geochemistry and mineralogy in the oceanic environment off Baja California. It remains to assess the importance of the four factors outlined above.

3.4.1 *Calcareous plankton productivity*

Arrhenius (1952) proposed that high carbonate contents in Pacific equatorial sediments result from increased atmospheric and oceanic circulation due to compression of climatic belts with ice advance, intensifying upwelling and productivity. This hypothesis has recieved considerable support from other Pacific workers (Broecker *et al*, 1958; Hays *et al* 1969; Quinn, 1971; Gardner and Hays, 1976; Valencia, 1977; Pedersen, 1983). Fundamental to this arguement is whether primary productivity actually results in a higher carbonate content in the sediment. A greater degree of upwelling of nutrient-rich waters is likely to increase siliceous productivity, which may dilute the carbonate content of the sediment, and organic matter flux resulting in greater organic oxidation, production of CO_2 and therefore carbonate dissolution (Berger, 1970). Quantification of these processes is extremely difficult, especially as sedimentation rate (tending to protect tests from solution) and the long term balance of carbonate in the oceans may vary through climatic episodes.

However, various authors, Arrhenius (1952) and Pedersen

(1983) in the equatorial Pacific and Heath *et al* (unpub. report) at MANOP site H, have dated $CaCO_3$ increases in the sediment column as being of Wisconsin age. In particular, Pedersen (1983) dates carbonate maxima in the Panama Basin as occuring 14,000-19,000 years B.P. Comparison of Sawlan's (1982) ^{14}C dates with $CaCO_3$ (Figure 3.2) and Ca/Al (Figure 3.16) profiles for the three hemipelagic cores indicates the strong possibilty that the profiles result from an increase in productivity during the Wisconsin.

In the previous section it was noted that Ba is probably biologically vectored. If this is the case, one might expect Ba/Al to increase in sympathy with Ca/Al if the two elements are limited by biological processes in the oceanic environment. As they do not correlate, either Ba and Ca respond to different biosystems, or the high productivity influence on carbonate is augmented by an alternative detrital source, diluting the productivity signal of Ba (see below).

3.4.2 *Calcium carbonate dissolution*

A great deal of literature centers on aspects of carbonate dissolution since Berger (1968, 1970, 1971, 1973) constructed the carbonate-solution model based on the equilibrium process of carbonate supply to the ocean, and carbonate removal by organisms. Various authors have felt that most dissolution of calcareous organisms occurs at the sea bed rather than in the water column (Berger and Piper, 1972; Volat *et al*, 1980). In this respect sedimentation rate is of great importance. Organism type is also of consequence; coccoliths may be more resistant to solution than planktonic foraminifera (Hay, 1970;

McIntyre and McIntyre, 1971).

The influence of bottom currents and their corrosive attitude towards carbonate has been remarked on (Edmond, 1974). Ruddiman and Heezen (1967) and Berger (1968) point out the coincidence between Antarctic Bottom Water and carbonate dissolution features. The resulting dissolution cycles are a subject of great debate (Volat *et al*, 1980), outside the scope of this chapter, save to indicate that dissolution has undoubtedly affected, and will continue to affect, the carbonate profiles off Baja California.

3.4.3 *Dilution by non-carbonate material*

Although some parts of the world's oceans are heavily influenced by biogenic silica production, this is not the case off Baja California (Section 3.2.2) and therefore dilution occurs primarily by terrigenous debris. Several lines of evidence have indicated an increase in terrigenous components during glacial episodes: (1) by atmospheric processes (Parkin and Shackleton, 1973; Diester-Haas, 1976; Sarnthein *et al*, 1981; Janecek and Rea, 1983); (2) by eustatic sealevel changes (Damuth and Kumar, 1975; Damuth and Embley, 1981; Nardin *et al*, 1981; Nardin, 1983). Damuth and Kumar (1975) suggest that during the last glaciation (the Wisconsin) the continental shelf off the Amazon River was emergent and that most of the sediment load transported by the river was fed directly to the head of the Amazon Submarine Canyon. With sea-level rise the continental shelf became flooded and the locus of sedimentation moved some 300-350 km inland from the shelf-break. Sediment is

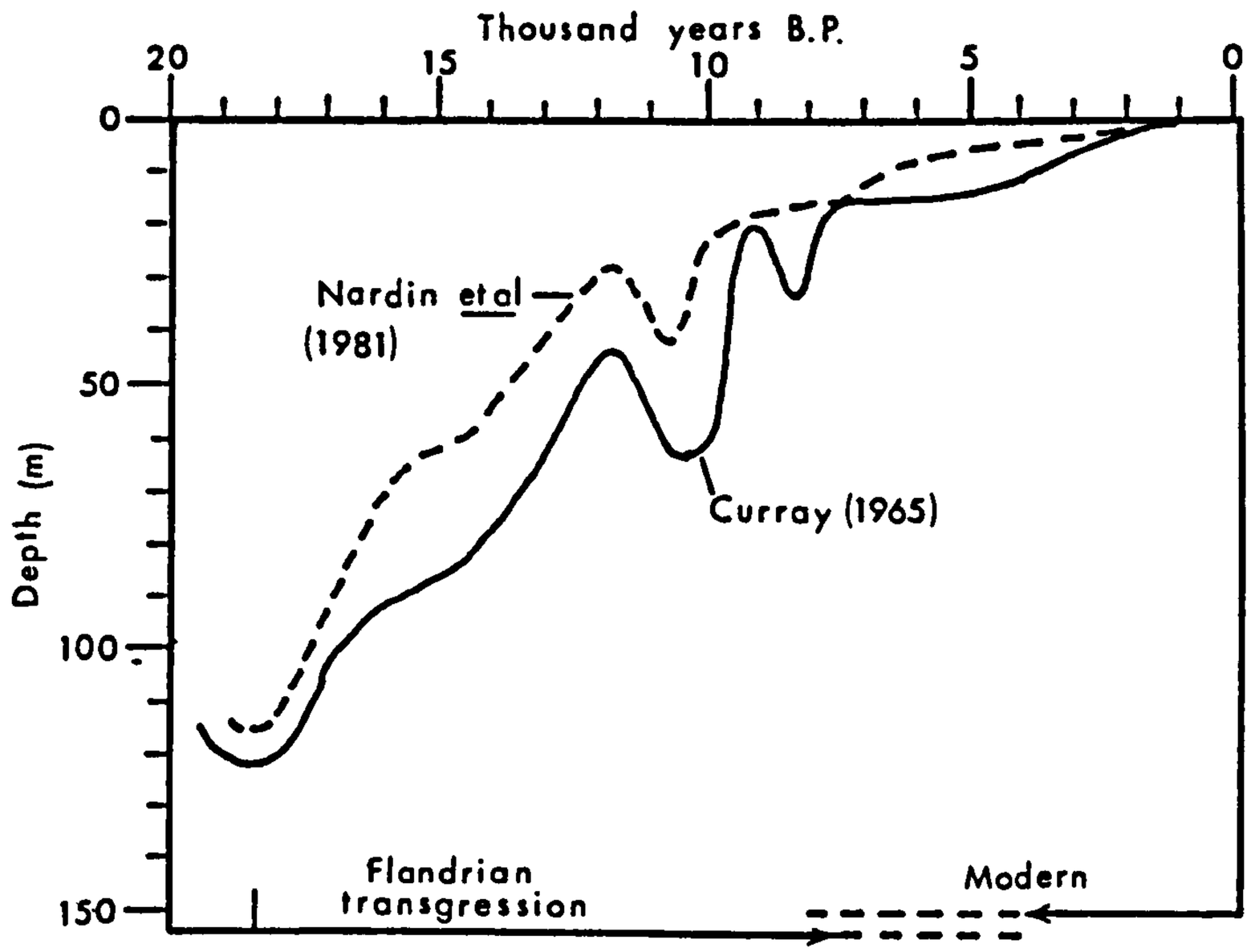

FIGURE 3.23 Flandrian sea-level fluctuations for Texas (Curray, 1965) and southern California (Nardin *et al*, 1981) shelves. Prior to 10,000 years BP time control is poorer.
(after Nardin *et al*, 1981)

now deposited in the river estuary or transported NW by longshore currents, so that the Amazon Cone has become essentially inactive. Boyle (1983) has shown that the relationship between changes in climate and variation in detrital input is far from simple. It is felt that eustatic sea level changes are likely to dominate the marginal setting described here, whereas atmospheric processes have undoubtedly played an important role in the more open ocean environment.

Evidence from the Baja California hemipelagic sediments suggests that detrital sedimentation was indeed higher during the latter stages of the Wisconsin. The concomitant increase in Zr/Al and Si/Al, and to a lesser extent the possible increase in detrital illite (represented by K/Al) supports this theory in showing a higher quantity of coarser-grained debris at depth. Boyle (1983) used the total change in Ti/Al ratio of sediments from the Peruvian margin to delineate changes in detrital input with time. Unfortunately, without high-precision Ti analyses such changes are undefined off Baja California.

An inspection of published late Quaternary sea level curves (Bloom, 1977) shows that no single curve can be applied worldwide due to changes in tectonic environment, and a significant isostatic component related to loading of the seafloor by glacial meltwater (Wellman, 1962; Nardin *et al*, 1981). Nevertheless, Nardin *et al* (1981) have shown that a eustatic sea level curve for the California continental borderland is similar in shape, if not amplitude, to other studies. Their proposed curve is illustrated in Figure 3.23 and indicates that the Flandrian trangression commenced some 18,000 years ago when sea level was 120 m below its present level. If

this were the case off Baja California then large areas of the continental shelf would have been exposed to wave scour and/or terrestrial erosion. Large quantities of detritus could have been shed into deep water by turbid, sediment-laden plumes supported by density stratification (Komar *et al*, 1974; Kulm *et al*, 1975) and/or increased aeolian transport resulting in coarser-grained and higher sedimentation rates in the hemipelagic environment.

Apart from the ^{14}C dates from Sawlan (1983) chronologic control on the relation between geochemical profiles and the actual age of the sediment is poor. However, the abrupt uniformity in Ca/Al, Si/Al and Zr/Al at 14-16 cm depth in 163-7, 10-12 cm in 163-14 and 12-14 cm in 163-10 (Ca/Al is slightly out of step in this core) suggests a chronostratigraphic time plane, perhaps relating to submergence of most of the shelf below the influence of wave and wind action. The sea level curve of Nardin *et al* (1981) (Figure 3.23) indicates a waning of the Flandrian transgression towards the present, however, sea level was 10 m lower some 6,000 years B.P. This indicates that the sedimentation rate in the hemipelagic environment is much lower during the present interglacial episode, as one might expect.

The balance between enhanced carbonate production and preservation during the glacial high productivity episode, and dilution by terrigenous debris is extremely fine. Barite production during the Wisconsin was apparently not sufficient to overcome dilution, resulting in decreasing Ba/Al ratios with depth and towards the coast. With regard to $CaCO_3$ either primary production was greater and/or higher sedimentation rates prevented substantial seabed dissolution, or low sea

level stands allowed detrital carbonate (foraminifera, molluscs, etc.) from the shelf to enter the deeper water environment and augment the carbonate content. No recognisable benthic carbonate debris has been found in these cores to resolve this possibility, nor is the resolution in the determination of the Sr content (Section 3.3) in the two environments sufficient to provide any conclusive evidence.

CHAPTER 4

THE DIAGENESIS OF ORGANIC CARBON AND RELATED ELEMENTS

4.1 INTRODUCTION

An important process in the geochemical evolution of marine sediments is the occurrence of diagenetic reactions near the sediment/water interface. Characterised by oxidation-reduction, these reactions influence the distribution and behaviour of many trace metals, nutrients, major ions and, indirectly, carbonates. The driving force behind these geochemical transformations is primarily the presence of organic carbon (C_{org}) and its rate of oxidation or mineralisation.

Environment plays a critical role in limiting the degree of diagenesis that occurs, by governing the input of marine organic matter and the availability of major oxidants (especially O_2). There is an extensive literature on diagenesis in organic-rich, anoxic marine sediments where reactions involve the consumption of SO_4^{2-} and the generation of CO_2, CH_4, alkalinity, PO_4^{3-}, NH_4^- and metal reaction (Rittenberg *et al*, 1955; Richards and Vaccaro, 1956; Richards, 1965; Berner *et al*, 1970; Bischoff and Ku, 1971; Nissenbaum *et al*, 1972; Sholkovitz, 1973; Martens and Berner, 1974; Kaplan, 1974; Reeburgh, 1976; Barnes and Goldberg, 1976; Martens and Berner, 1977; Goldhaber *et al*, 1977; Murray *et al*, 1978; Jahnke, Emerson and Murray, 1982). Where C_{org} contents are lower and the sediment overlain by oxygenated waters, such as in the hemipelagic and pelagic environments, there has been less work (Lynn and Bonatti, 1965; Presley *et al*, 1967; Li *et al*, 1969; Bischoff and Ku, 1970; Bender *et al*, 1977; Froelich *et al*, 1979) although there has been great interest in the last few years with the advent of *in situ* pore water samplers,

eliminating pressure and temperature artifacts (Murray *et al*, 1980; Emerson and Bender, 1981; Grundmanis and Murray, 1982; Sawlan and Murray, 1983; Liu and Kaplan, 1984). In these types of sediments the slow rate of water exchange and low levels of organic matter mean that utilisation of oxidants occurs within the sediments, not the water column. Off Baja California the overall sedimentation rate and the level of C_{org} in the hemipelagic and pelagic environments conspire to allow the observation of oxidant utilisation over a depth range of some 30-40 cm within the sediment. On the shelf, small intrashelf basins and the presence of an oxygen minimum in the water column (Chapter 2) cause rapid depletion of O_2 and NO_3^- leading to SO_4^{2-} reduction and anoxia in the sediments at a much shallower depth; a useful end-member process to compare with the oxic conditions of the pelagic realm.

The availability of C_{org} and related elements, N, P, I and Br, and its reactivity, is exceedingly complex, dependant on many oceanographic controls both in the water column and in the sediment. Organic matter settling through the water column is susceptible to oxidation and elemental fractionation, especially the removal of labile organic compounds (lipids and amino acids) containing N and P (Rittenberg *et al*, 1955; Holm-Hansen *et al*, 1966; Gordon, 1971; Bishop *et al*, 1977; Knauer *et al*, 1979; Wakeham *et al*, 1984). On arrival at the sea floor much of the organic detritus is converted into biomass by benthic organisms (Smith, 1978; Wishner, 1980; Smith *et al*, 1983) which tend to concentrate P and N relative to C (Grundmanis and Murray, 1982). Organic matter reconstituted in this way is then available for benthic heterotrophic organisms and accompanying diagenetic redox reactions. To a first

approximation the level of C_{org} that finally enters the sediment column is geographically related to areas of high primary productivity in the surface waters (Koblentz-Mishke *et al*, 1970; Premuzic *et al*, 1982) and high sedimentation rate which enhances the preservation of C_{org} (Toth and Lerman, 1977; Heath *et al*, 1977; Muller and Suess, 1979; Reimers and Suess, 1983).

This chapter presents data describing the distribution of organic matter between the shelf, hemipelagic and pelagic environments and the elemental partitioning of C_{org}, N, P, I and Br with depth in the sediment column. From this three main areas of discussion will follow:

(1) To describe and infer diagenetic reactions resulting from organic matter decomposition and utilisation of available oxidants.

(2) To attempt to quantify the rate of these decomposition reactions using published kinetic and advection-diffusion models.

(3) The relationship between primary productivity and sedimentation rate leading to organic matter preservation areally along the transect, and with time down the sediment column.

4.2 THE DISTRIBUTION OF ORGANIC C, N, P, I AND Br

4.2.1 *Organic Carbon*

The surface concentrations of C_{org} and related elements on a salt-free basis are presented in Table 4.1. In a similar way Figure 2.5 illustrates the increase in concentration of C_{org}

TABLE 4.1

THE CONCENTRATION OF ORGANIC CARBON AND RELATED ELEMENTS IN SURFACE SEDIMENTS (SALT-FREE)

Core	Depth	C_{org}	N	P	I	Br	C/N	C/P	I/C_{org}	Br/C_{org}
	cm	wt.%	wt.%	wt.%	ppm	ppm			$x10^{-4}$	$x10^{-4}$
163-5	0-1	1.70	-	0.40	224	123	-	4.25	132	72
163-12	0-1	1.35	-	0.25	123	110	-	5.40	91	81
145-17	0-1	1.97	-	0.60	260	202	-	3.28	132	103
163-8	0-1	6.90	-	0.26	523	654	-	26.54	76	95
163-11	0-1	1.39	-	0.23	424	148	-	6.04	305	106
163-7	0-1	1.24	0.22	0.17	333	87	5.64	7.29	269	70
163-14	0-1	1.12	0.18	0.17	212	110	6.22	6.59	189	98
163-10	0-1	0.96	0.13	0.15	172	95	5.33	6.40	179	99
163-9	0-1	0.61	0.12	0.13	116	71	5.08	4.69	190	116
163-15	0-1	0.79	-	0.13	87	44	-	6.08	110	56

from the open ocean (0.61 wt.%) to the shelf (max. 6.90 wt.%). In detail, this increase is due to a number of environmental factors. The high productivity in the surface waters (Chapter 2) over the outer part of the shelf not only contributes to a higher flux of organic matter to the sea bed but also to the maintenance of a pronounced oxygen minimum zone between 200 and 800 meters depth which intersects the shelf (Chapter 2). As a result the waters of the intrashelf basins are depleted in O_2; with the substantial carbon flux and the highest sedimentation rates of the Baja California transect (10 cm kyr^{-1}; Kim (1983) cited in Jahnke *et al*, 1983), C_{org} preservation is at its

maximum. The lack of any rivers debouching onto the shelf and the arid climate make the likelihood of terrestrial carbon input unlikely for the southern Baja California margin.

In the hemipelagic and pelagic environments there is a monotonic decrease in surface C_{org} away from the coast (Table 4.1). In addition, approximate sedimentation rates decrease in the same direction from 3.5 cm kyr^{-1} (Sawlan, 1982), at approximately the location of 163-7, to 0.45 cm kyr^{-1} in 163-9 (Chapter 7). A consequence of this decreasing C_{org} oceanwards is the increase in thickness of the oxic, red-brown top of these cores (see core descriptions in Appendix A) in a manner similar to that described by Lynn and Bonatti (1965) and Lyle (1983).

Vertical distributions of C_{org} in these sediments are displayed in Figures 4.1 and 4.2. Only 163-9 displays the expected exponential decrease in C_{org} from 0.61 wt.% at the surface to 0.26 wt.% at 36-38 cm depth if decomposition is expected to follow first-order kinetics mediated by bacterial breakdown (Muller and Mangini, 1980; Waples and Sloan, 1980; Reimers and Suess, 1983). In the three hemipelagic cores the initial decrease in C_{org} is modified by greater concentrations at depth. As a result, in 163-10 a steady decrease from 0.96 wt.% at the surface to 0.70 wt.% at 8-9 cm depth is followed by an increase to a C_{org} maximum in this core of 1.10 wt.% at 12-14 cm depth before decreasing more gradually with depth. In 163-14 the subsurface decrease occurs over 6-7 cm from 1.12 wt.% at the surface to 0.73 wt.%, before increasing to a core maximum of 1.23 wt.% and decreasing again. Finally, in the most nearshore of the three hemipelagic cores, 163-7, C_{org} decreases

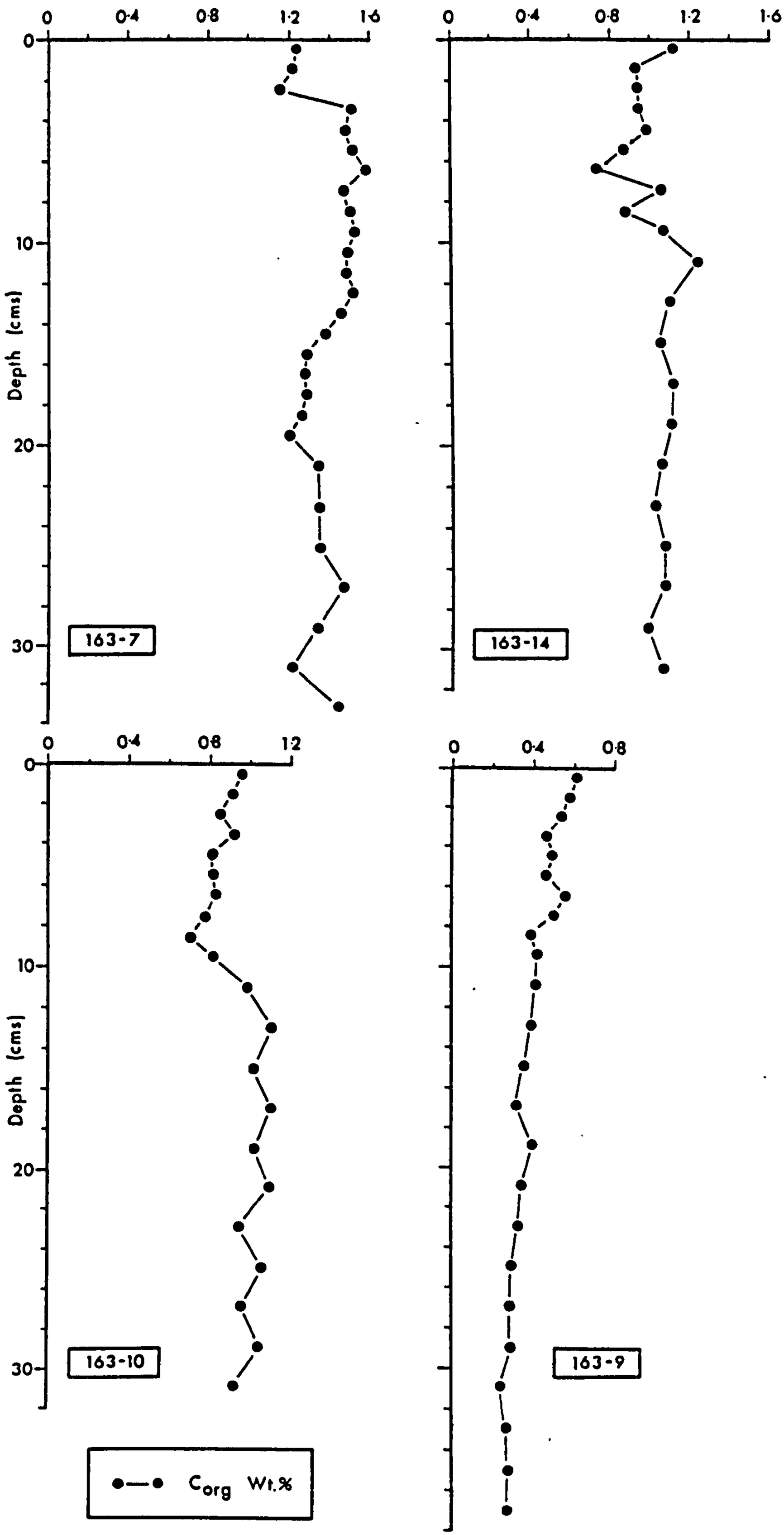

FIGURE 4.1 Depth profiles of C_{org} with depth for the Baja California oceanic sediments (salt-free).

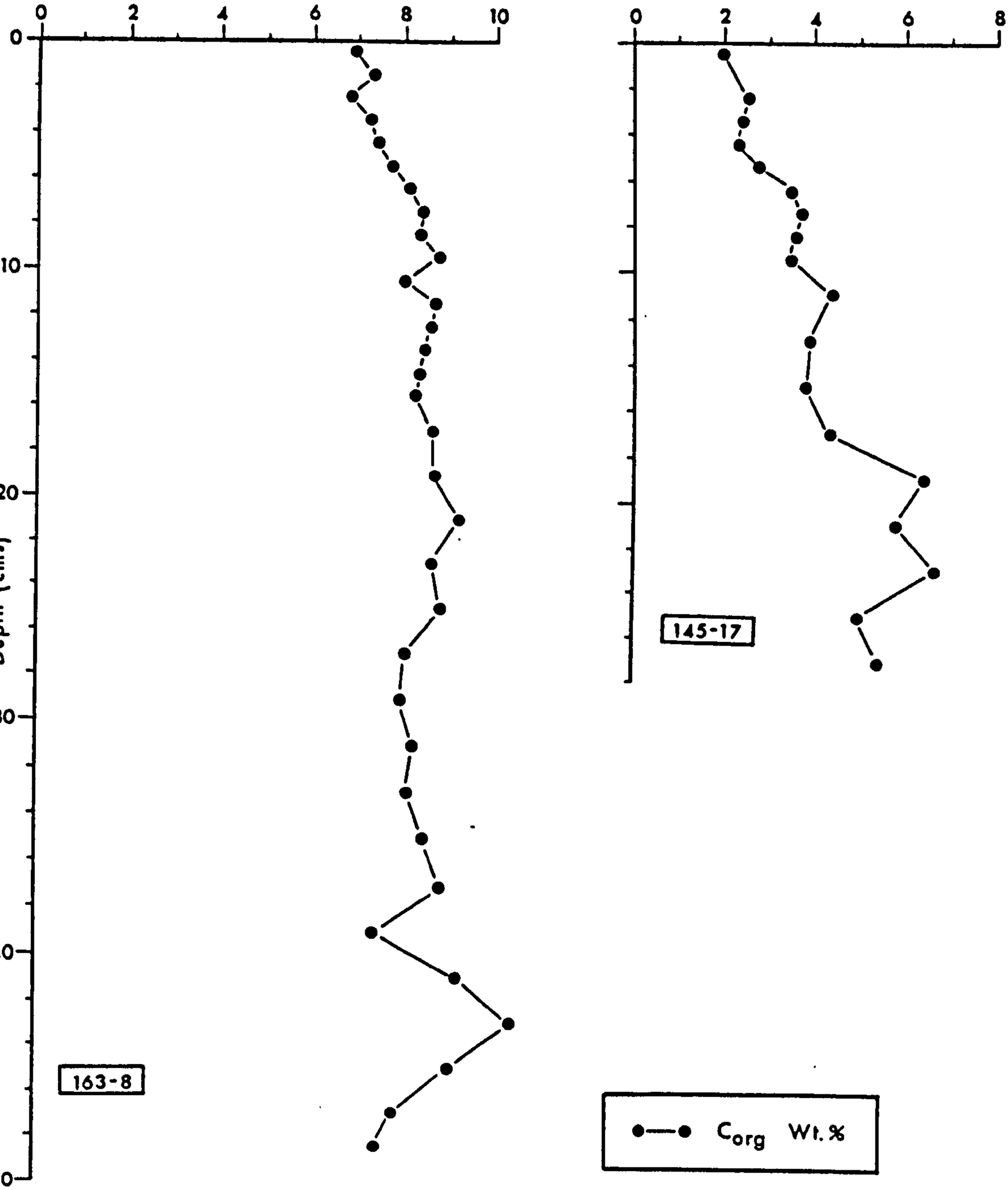

FIGURE 4.2 Profiles of C_{org} with depth for two cores from the Baja California shelf (salt -free).

over 2-3 cm from 1.24 wt.% at the surface to 1.16 wt.%, before increasing rapidly to 1.51 wt.% and decreasing again to 1.43 wt.% at depth, with occasional, minor perturbations.

The reason why these hemipelagic profiles appear not to be in steady state is a major problem, but the maximum depth of O_2 diffusion, the degree of bioturbation and the feeding/excretion characteristics of the infaunal benthos may all contribute in some way.

The two shallow-water, shelf stations, 163-8 and 145-17, also present unusual C_{org} profiles (Figure 4.2). Not only are the C_{org} profiles exremely high (6.90 wt.% and 1.97 wt.% at the surface of 163-8 and 145-17 respectively) but they increase with depth to a maximum of 10.37 wt.% at 42-44 wt.% in 163-8 and 6.57 wt.% in 145-17. Jahnke *et al* (1983) found C_{org} to behave exactly the same way in their analysis for the latter core. They note that 145-17 is situated at the upper boundary of the oxygen minimum and that the bottom water O_2 concentration does not exceed 10 umoles/kg. However, O_2 is still available for C_{org} oxidation, whereas in the past the O_2 minimum may have shifted allowing greater organic matter preservation and accounting for the positive gradient in C_{org} with depth. This explanation ignores the possibility that productivity and sediment input (grain size) fluctuations may also be responsible for the increasing C_{org} profile with depth (Chapter 5).

4.2.2 *Nitrogen*

The distribution of N in marine sediments tends to follow that of C_{org} indicating its incorporation in the amino groups of the organic molecule. Amino acids are the building

blocks of proteins and the largest reservoir of organic N in most organisms (Wakeham *et al*, 1984) and as such may be used to characterise various types of organic matter. Protein has an atomic C/N ratio of about 3, so organisms rich in protein have low C/N ratios eg. polychaetes (3.4), fish and fish larvae (3.9) and copepods (4.3) (Beers, 1966). In contrast, Redfield *et al* (1963) and Bordovskiy (1965,a) have determined the C/N ratio of zooplankton as 5.4 and 5.9 respectively (Table 4.2). The benthic community of macro and micro-organisms is also rich in protein showing C/N ratios of 4-5 (Bordovskiy, 1965,a,b). Higher land plants are low in protein and therefore display high C/N ratios of 25-30 (Marlett and Erdman, 1959; Muller, 1977).

TABLE 4.2

ELEMENTAL COMPOSITION OF MARINE ORGANISMS

Organism	Author	Content %dry weight					Atomic ratio	
		ash	C	H	N	P	C/N	C/P
diatoms	1	57.81	18.68	3.65	2.49	0.60	8.75	80.43
peridineans	1	5.20	33.49	5.58	4.61	0.57	8.48	151.78
copepods	1	10.10	45.52	7.22	9.96	1.03	5.33	114.17
bacteria	1	5.50	50.40	6.78	12.30	-	4.78	-
benthos	1	9.14	51.55	7.67	12.32	-	4.88	-
Atomic ratios in plankton								
zooplankton	2	-	103	-	16.5	1	6.24	103
phytoplankton	2	-	108	-	15.5	1	6.97	108
average	2	-	106	-	16.0	1	6.63	106

1 Data from various authors given in Bordovskiy (1965,a)

2 Fleming (1940); Redfield *et al* (1963)

In the oceanic sediments the total surface N measured decreases oceanwards (Table 4.1) and at depth closely follows C_{org} (compare profiles in Figure 4.3 with Figure 4.1). In all cases the total N content decreases downcore but the subsurface minima seen in C_{org} at 2-3 cm in 163-7 and 8-9 cm in 163-10 (Figure 4.1) are also defined by N. As these two elements were measured by two separate methods (Appendix B) it is concluded that these profiles are real and not an artifact of sample analysis.

In the hemipelagic sediments the C/N ratios increase with depth. This is most marked in 163-7 where the surface C/N (atomic) of 6.58 increases to 9.26 at 32-34 cm depth. In contrast, the pelagic red clay of core 163-9 displays a decrease in C/N from 5.93 at the surface to 5.05 at depth. Despite the cummulative experimental inaccuracies involved in obtaining the atomic C/N ratio it is remarkable how consistent the surface ratios are, and indicates that the same source of organic matter supplies the four cores and that similar degradation processes operate on the particulate organic matter as it descends through the water column. These surface ratios also indicate the absence of terrestrial organic matter in the sediment with its attendant high C/N value. The possible diagenetic mechanisms operating on the organic matter leading to a lowering or raising of the ratio with depth are discussed below in Section 4.4.1.

4.2.3 *Phosphorus*

Phosphorus is a principal component of the organic molecule, albeit in low concentrations. Assuming a Redfield

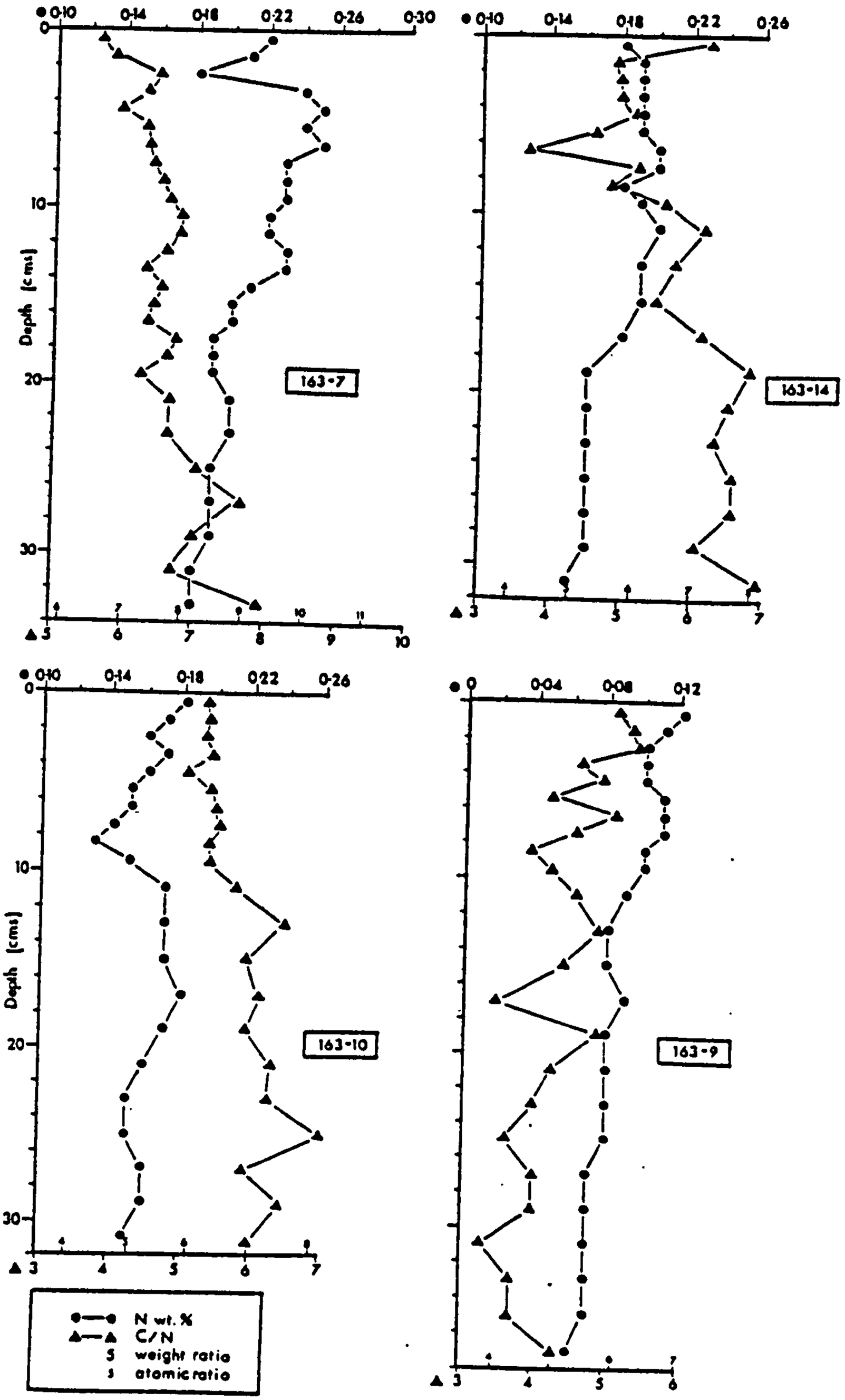

FIGURE 4.3 Profiles of N (upper axis) and C/N ratio (lower axis, weight and atomic ratio) with depth for the Baja California oceanic sediments (salt-free). Note that the origins for N in 163-9 and C/N in 163-7 are different.

composition for degradable organic matter (Redfield *et al*, 1963) the C/P atomic ratio is 106 (Table 4.2). P forms molecules of great physiological importance to organisms and its release during microbial breakdown may play an important part in the formation of diagenetic mineral phases such as apatite (Kazakov, 1938; McConnell, 1965; Burnett, 1977; Froelich *et al*, 1982; Jahnke *et al*, 1983). In addition, P is also concentrated in the skeletal debris of marine organisms (Arrhenius, 1963; Lowenstam, 1974; Doyle and Reidel, 1979; Suess, 1981), whilst "average" biogenic $CaCO_3$ may contain 300 ± 80 ppm of P (El Wakeel and Riley, 1961; Froelich *et al*, 1982). Inorganic phases such as ferriphosphate coatings on grains (Berner, 1973, Froelich *et al*, 1977) and detrital apatite also contribute to the total P sink in the sediment column.

In an attempt to partition the total P measured here, various contributions relating to organic, detrital and authigenic fractions were calculated using published ratios to C_{org} (Redfield *et al*, 1963) and Al (Turekian and Wedepohl, 1961). This partitioning for the surface sediment of each core is presented in Table 4.3. Authigenic P is defined as total P - (organic P + detrital P), and thus will include contributions from authigenic phases (apatite and ferriphosphates) and P in skeletal debris. These calculations indicate that whilst all the environments along the Baja California transect receive similar proportions of detrital P, the major area of authigenic enrichment is on the open shelf (145-17 and 163-5) where apatite formation is thought to occur (D'Anglejan, 1967; Jahnke *et al*, 1983).

TABLE 4.3

THE PARTITIONING OF PHOSPHORDUS IN SURFACE SEDIMENTS OFF BAJA CALIFORNIA

Sample	Depth	C_{org}	P_{total}	P_{org}	$P_{detrital}$	P_{excess}
163-5	0-1	1.70	0.40	0.041	0.057	0.302
163-12	0-1	1.35	0.25	0.033	0.069	0.148
145-17	0-1	1.97	0.60	0.048	0.057	0.495
163-8	0-1	6.90	0.26	0.168	0.042	0.050
163-11	0-1	1.39	0.23	0.034	0.029	0.167
163-7	0-1	1.24	0.171	0.030	0.065	0.076
163-14	0-1	1.12	0.170	0.027	0.067	0.076
163-10	0-1	0.96	0.148	0.023	0.069	0.056
163-9	0-1	0.61	0.130	0.015	0.069	0.046
163-15	0-1	0.79	0.133	0.019	0.068	0.046

$P_{org} = (C_{org}/41.0)$

$P_{detrital} = (Al \times 0.00875)$

$P_{excess} = P_{total} - (P_{org} + P_{detrital})$

The vertical distribution of salt-free P in the hemipelagic and pelagic cores and two representative cores from the shelf are shown in Figures 4.4 and 4.5. In Figure 4.4 the total P concentration deceases over the length of the four cores, although in each case the upper decimeter or so, displays relatively constant values with the average P content decreasing offshore. In the same way that the surface values were partitioned in Table 4.3 so too have the depth values. A source of error here is the changing C/P ratio for the organic matter which is likely to increase with depth during organic matter diagenesis. Indeed, it is well established that significant elevations in the C/P ratio occur in settling organic matter due to degradation within the water column. However, it is possible that the formation of large organic-containing particles, such as faecal pellets and marine snow flocculles, sink so rapidly (McCave, 1975; Shanks and Trent,

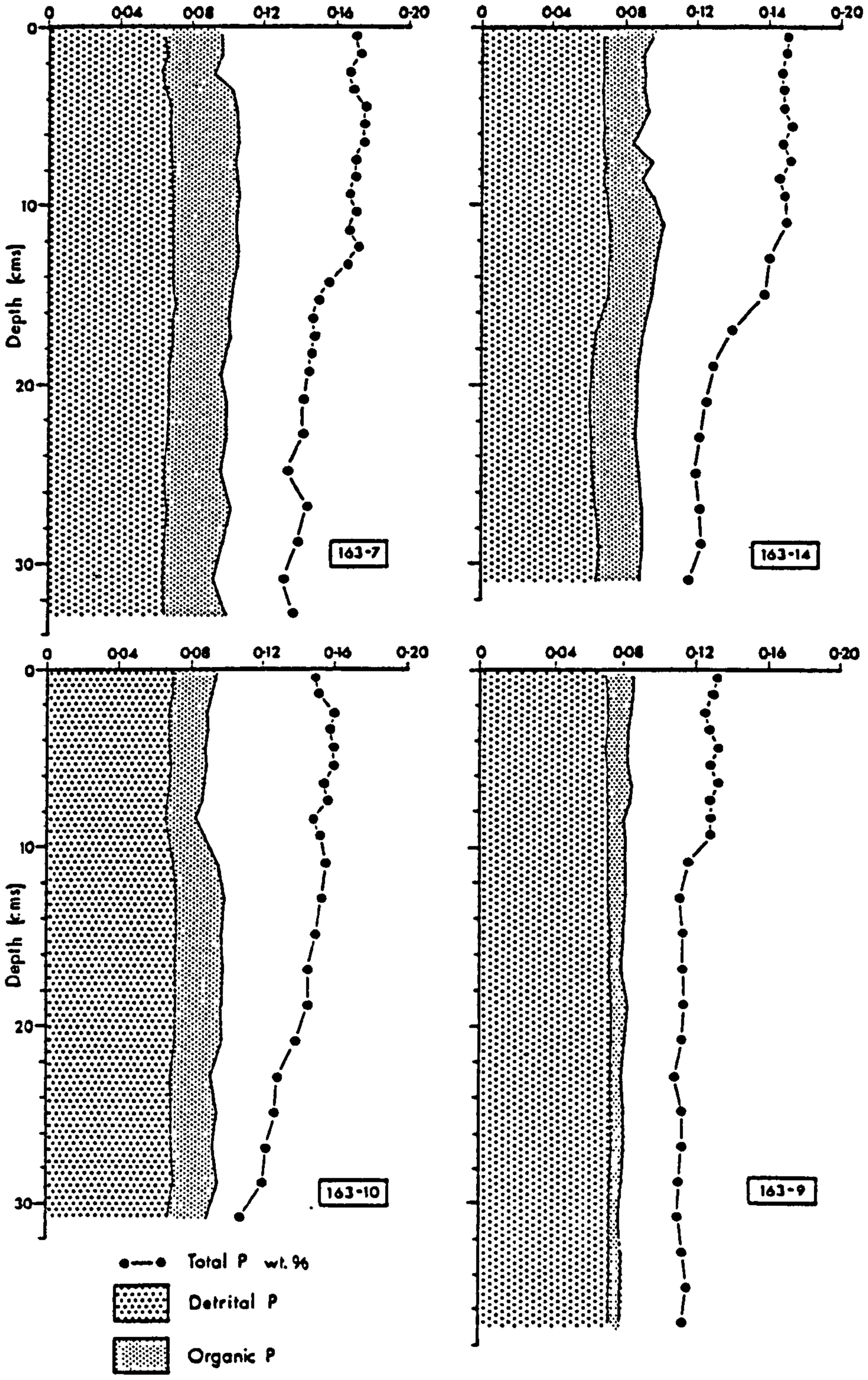

FIGURE 4.4 Profiles of total P and its partitioning with depth in the Baja California oceanic sediments (salt-free). The detrital P component is defined by the average P/Al ratio in shale (0.00875; Turekian and Wedepohl, 1961), whilst organic P is defined by the Redfield composition for marine organic matter (C/P weight ratio of 41.0).

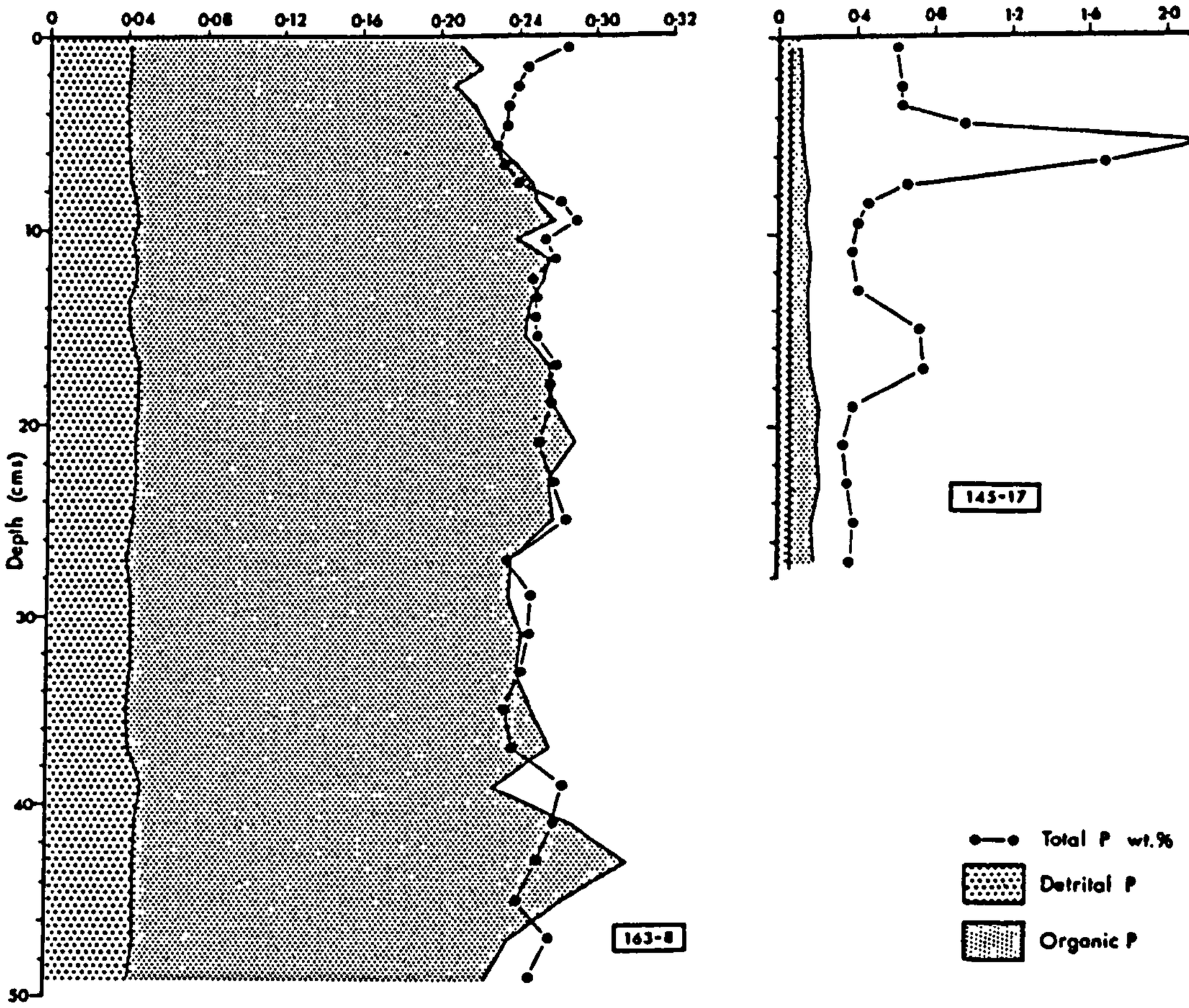

FIGURE 4.5 Profiles of total P and its partitioning with depth in the Baja California shelf sediments (salt-free). Partitioning ratios are as for Figure 4.4. Note the change in scale for 145-17.

1980) that regeneration is reduced during their short residence time (Knauer *et al*, 1979; Honjo, 1980) so that organic matter arriving at the sea-floor will have an almost unaltered C/P ratio.

From a large compilation of literature data Froelich *et al* (1982) tried to estimate the burial ratio of organic matter in marine sediments. They showed that P_{org} in organic-rich sediments is deficient relative to the Redfield ratio, in contrast to an excess in organic-poor sediments (< 0.5 % C_{org}). This suggests that in these latter sediments stable, P-rich, organic compounds exist, such as inositol phosphates (White and Miller, 1976). Alternatively, the production of biomass carbon at the sediment/water interface referred to above, may concentrate P-containing compounds, lowering the C/P ratio. A surface C/P of ~12 is required to produce the observed P_{total} (assuming a detrital P concentation relative to Al of 0.00875) which is clearly excessive. It therefore seems that the "excess" P is due either to skeletal debris, or the diagenetic formation of ferriphosphate. The former seems to be more attractive as the amount of Fe present relative to Al in the surface sediments of the four bathyal cores is less than the lithogenic clay average for pelagic sediments given by Turekian and Wedepohl (1961). This makes the P contribution in ferriphosphate very small or absent. The implication that skeletal debris is the main source of this "excess" P is plausible. Suess (1981) showed that P from fish debris dissolution supplied three times as much P to the dissolved nutrient pool as does organic matter, primarily due to the ability of skeletal debris to survive water column and sediment

surface degradation. He does point out that this situation is probably peculiar to coastal upwelling zones.

In the two shelf cores the vertical distribution of total P is very different (Figure 4.5). The suboxic/anoxic intrashelf basin (163-8) displays reasonably constant values of approximately 0.25 wt.% ± 0.02, whereas the open shelf, shallow water station of 145-17 clearly shows marked subsurface maxima of 2.159 wt.% at 5-6 cm and approximately 0.71 wt.% at the deeper depth of 14-18 cm. The partitioning of P clearly indicates the strong influence of C_{org} on the P concentration in the anoxic mud of the basin (163-8) whereas the subsurface spikes in 145-17 have been attributed to the diagenetic formation of apatite by Jahnke *et al* (1983). The lack of "excess" P in 163-8 due to skeletal debris may result from a high sedimentation rate in this core which effectively dilutes any detrital skeletal source of P. Further discussion on the P relationships in the hemipelagic and pelagic cores may be found below (Section 4.4) and on apatite formation in Chapter 8.

4.2.4 *Iodine and Bromine*

Of the two halogens condidered here, I has received the most attention in the literature. However, measurements have tended to be confined to near-shore and continental margin sediments where high concentrations of I (Vinogradov, 1939; Shishkina and Pavlova, 1965; Price *et al*, 1970; Pavlova and Shishkina, 1973; Price and Calvert, 1973; Price and Calvert, 1977; Ullman and Aller, 1983) and Br (Vinogradov, 1939; Price *et al*, 1970; Price and Calvert, 1977) have been found in

association with organic matter underlying zones of high productivity. These studies have shown that for I in oxic sediments the relationship with C_{org} is linear; this is not the case for Br which displays little redox control. In hemipelagic sediments there has been far less work, an exception being Pedersen and Price's (1980) study of the two halogens in the Panama Basin, where they found both I and Br to correlate strongly with the level of C_{org} in the surface sediments in a ratio similar to the shallow water sediments of the Barents Sea (Price *et al*, 1970).

With depth the concentration of I and Br apparently decrease during early diagenesis (Shishkina and Pavlova, 1965; Pavlova and Shishkina, 1973; Price and Calvert, 1977; Pedersen and Price, 1980). Iodine seems more labile than C_{org} in contrast to the more refractory behaviour of Br, suggesting bonding by different organic ligands with I being more diagenetically mobile than Br (Pedersen and Price, 1980). It is worth noting that salt corrections for Br can introduce a greater degree of error than with I determinations.

In the different environmental settings off Baja California the distribution of the two halogens is quite complex. The minimum surface concentration (Table 4.1) of I is 87 ppm at station 163-15 in oxidising pelagic red clay to a maximum of 523 ppm in the suboxic/anoxic intrashelf basin of 163-8. Br increases in the same way from 71 ppm at 163-9 to 654 ppm in 163-8. These variations are in the same order as the increase in C_{org} (Table 4.1).

With depth in the more oxidising environments of 163-9,

163-10, 163-14, and 163-7 (Figure 4.6) both halogens decrease in concentration with some perturbations. In the completely oxidising sediment of 163-9 both I and Br show exponential decreases resulting in a 20.7% loss for I at 36-38 cm depth from its surface value of 116 ppm, and a 54.9% decrease for Br from an initial concentration of 71 ppm. In 163-14 and 163-10 Br decreases more steadily than I; a 40.9% decrease from 110 ppm in 163-14 and a 34.7% decrease from 95 ppm in 163-10. The I in these two cores, whilst decreasing overall, displays subsurface maxima of 251 ppm at 5-6 cm, and 248 ppm at 16-18 cm depth in 163-14, and 224 ppm at 8-9 cm depth in 163-10. In the near-shore hemipelagic core of 163-7 the greatest variations with depth are seen; Br increases from its surface concentration to a maximum of 151 ppm at 6-7 cm depth, decreasing by 45% at 30-32 cm depth. I displays some near-surface scatter before decreasing to a minimum value of 180 ppm at 19-20 cm depth followed by a subsurface culmination of 218 ppm at 26-28 cm depth.

The depth distributions of I and Br on the shelf (Figure 4.7) are exemplified by 163-8 and 145-17, for which C_{org} has also been measured. Both halogens show similar profiles with subsurface maxima paralleling the distribution of C_{org} (Figure 4.2).

4.3 THE SEQUENCE OF ORGANIC MATTER OXIDATION

4.3.1 *Introduction*

There have been many published models to account for the observed distribution of oxidants, reductants and metabolites in pore waters (Richards, 1965; Sholkovitz, 1973; Bender *et al*,

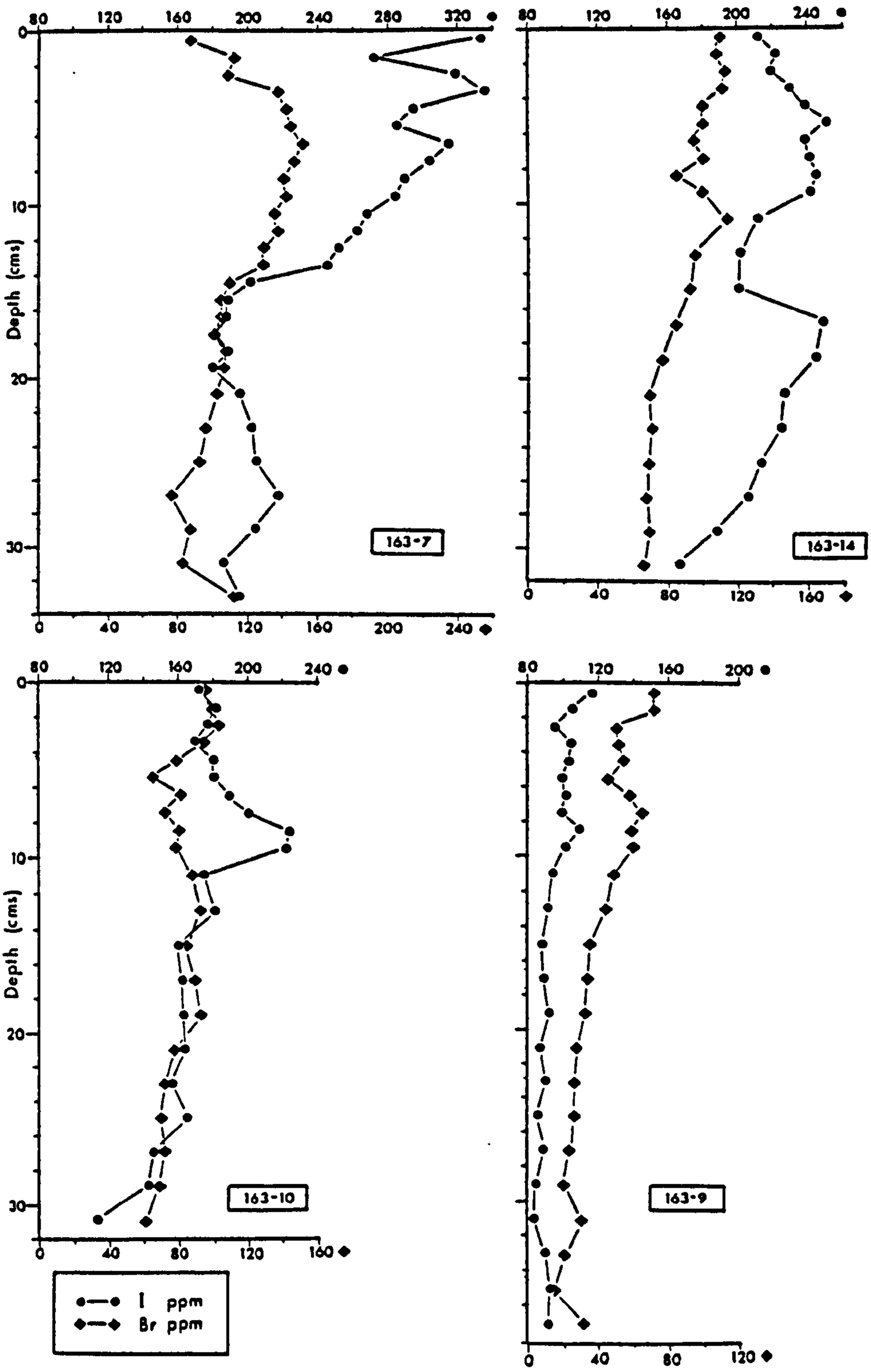

FIGURE 4.6 Profiles of I (upper axis) and Br (lower axis) with depth in the Baja California oceanic sediments (salt-free).

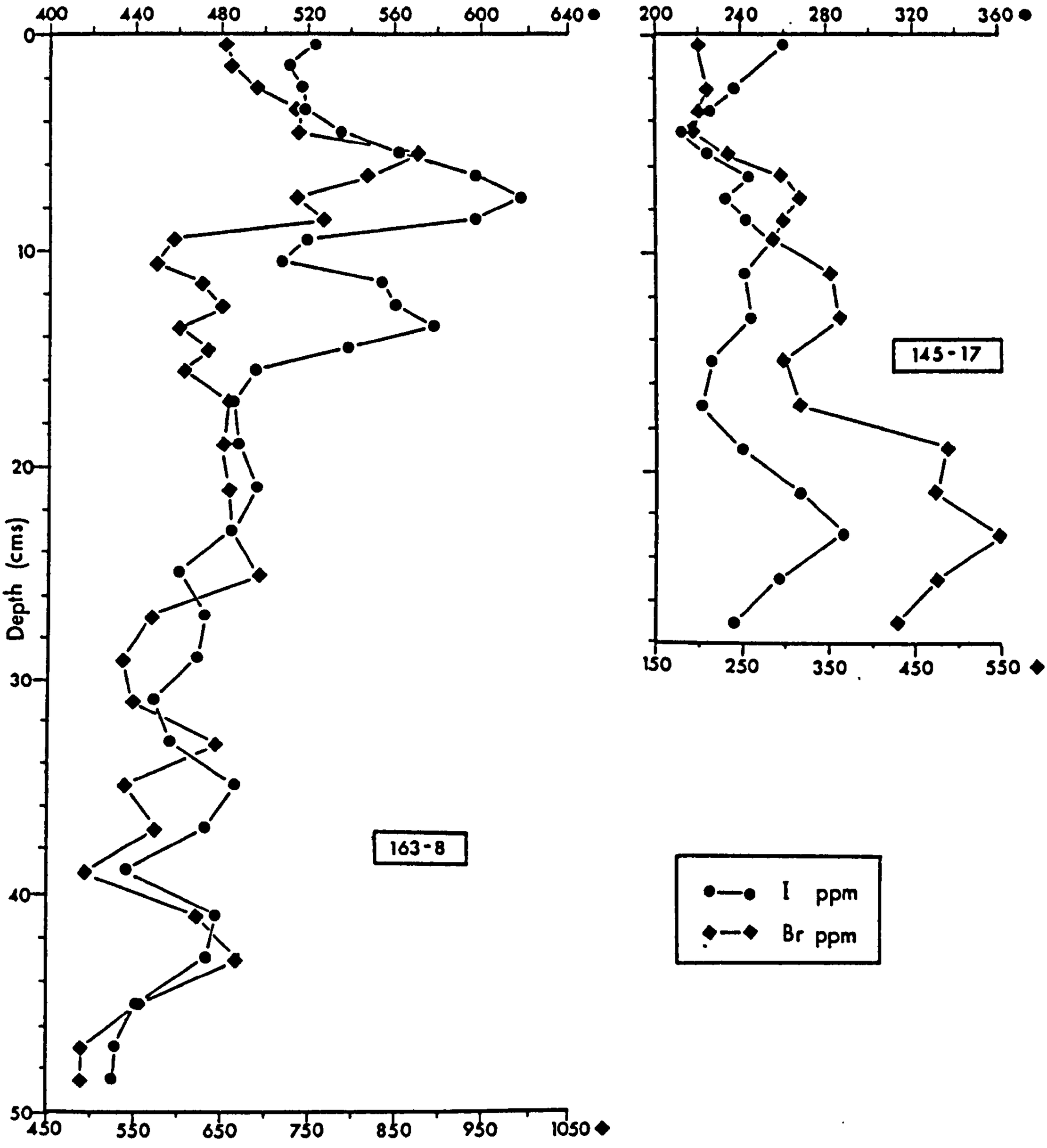

FIGURE 4.7 Profiles of I (upper axis) and Br (lower axis) with depth in two cores from the Baja California shelf (salt-free). Note the change in origin for I and Br between the two cores.

1977; Vanderborght *et al*, 1977a,b; Froelich *et al*, 1979; Emerson *et al*, 1980; Grundmanis and Murray, 1982; Jahnke *et al*, 1982a,b; Burdidge and Giekes, 1983). In the simplest terms, organic matter, assumed to be of Redfield composition (Redfield *et al*, 1963), is oxidised by the oxidant yielding the greatest free energy change (ΔG^{o}) per mole of organic carbon oxidised, and mediated by the microbial population in the sediment (Stumm and Morgan, 1970, p.334). Theory predicts that as each oxidant is depleted, oxidation will proceed by the next most easily utilised oxidant (ie the most energy producing). Such a sequence is outlined in Table 4.4 with the appropriate free energy yields calculated from published thermodynamic data.

In sediments overlain by oxygenated waters the complete oxidation of organic matter would require 276 atoms of oxygen, liberating 1 phosphate ion, 16 nitrate ions and 106 molecules of carbon dioxide. This represents complete oxidation, but it is clear that nitrogen intermediates, NH_4^+, NO_2^- and urea, can form within 10 cm of the sediment water interface (Suess *et al*, 1980; Emerson *et al*, 1980; Jahnke *et al*, 1982b) in oxic sediment. Ammonia is oxidised to NO_2^- by *Nitrosomonas* and then to NO_3^- by *Nitrobacter* (Grundmanis and Murray, 1982); slow reaction kinetics for this oxidation may result in the subsurface maxima of nitrogen intermediates observed (Emerson *et al*, 1980). (During the deeper reduction of SO_4^{2-}, NH_3 is released and accumulates in the sulphide-rich environment without being oxidised; Richards, 1965).

NO_3^- reduction (denitrification) commences at low, but not zero, levels of O_2 (Richards, 1965) even though stoichiometric models for NO_3^- reduction (Vanderborght and Billen, 1975;

Jahnke *et al*, 1982b) usually assume that complete O_2 consumption has occured for mathematical simplicity. On a thermodynamic basis the product of denitrification controls its position in the diagenetic reaction sequence. Reaction 2a (Table 4.4) is theoretically favourable (all NO_3^- to N_2) and has been shown to occur in nature in the Cariaco Trench and Dramsfjord (Richards and Benson, 1961) and in Saanich Inlet (Richards, 1965). In this case the reaction will overlap with the reduction of MnO_2, occuring almost simultaneously (Froelich *et al*, 1979). Alternatively, NH_3 release (Reaction 2b) will occur after the reduction of reactive MnO_2. For the hemipelagic sediments off Baja California denitrification is confined to the sediment column (Jahnke *et al*, 1982b; Sawlan and Murray, 1983), although the shelf sediments have very little NO_3^- if at all (Emerson *et al*, 1980; Jahnke *et al*, 1982b) tending to be characterised by large increases in interstitial NH_4^+ instead.

After the reduction of O_2, and possibly NO_3^-, the utilisation of MnO_2 as the next preferred electron acceptor is thermodynamically favourable (Equation 3, Table 4.4; Emerson *et al*, 1980; Burdidge and Gieskes, 1983). Whilst this explanation is well documented from the solid phase (Lynn and Bonatti, 1965; Li *et al*, 1969; Froelich *et al*, 1979; Berger *et al* 1983; Kalhorn and Emerson, 1984; Graybeal and Heath, 1984, Murray *et al*, 1984) and pore water data (Presley *et al*, 1967; Bischoff and Ku, 1970; Bender *et al*, 1977; Froelich *et al*, 1979; Klinkhammer, 1980; Sawlan and Murray, 1983) the data are also consistent with changes in the Eh-pH of the system. The lowering of Eh in the sediment, produced by the bacterial mediation of O_2 and NO_3^- reduction, results in Mn^{2+} being favoured over the less soluble Mn^{4+} in manganese oxyhydroxides

(Stumm and Morgan, 1970; Burdige and Gieskes, 1983). The question of thermodynamic versus Eh control on Mn diagenesis is still debated. However, the qualitative result of subsurface, solid-phase Mn spikes undergoing dissolution (at the Mn "redoxcline") is indicative of the stage in the reaction sequence of Table 4.4*.

Iron oxyhydroxide reduction is dependant on similar thermodynamic/Eh controls, however, the small proportion of FeOOH to total Fe in sediments off Baja California means that the spectacular subsurface profiles for solid-phase Mn are less detectable. It should be noted that the highest concentration of Fe^{2+} and Mn^{2+} in the pore water is controlled by the solubility of $FeCO_{3(s)}$ and $MnCO_{3(s)}$ respectively (Stumm and Morgan, 1970).

Sulphate reduction and methane generation by disproportionation occur after complete, or nearly complete, consumption of O_2, NO_3^-, MnO_2 and Fe_2O_3. Wheatland (1954), cited in Richards (1965), showed that SO_4^{2-} reduction is negligible in the presence of more than 0.11 ml/l (and probably less) of dissolved O_2. The reaction is biologically mediated by bacteria, such as *Desulfovibrio*, and as such must operate below a pE of -3 (Stumm and Morgan, 1970).

These thermodynamic and Eh controlled reactions should therefore define a sequence of diagenetic zones in the sediment column. The zone between the sediment/water interface and the disappearance of dissolved O_2 (Reaction 1) is termed the *oxic*

---

*The Mn redoxcline may be formally defined as the first appearance of manganous ions in the pore water, usually at low, but not zero, levels of nitrate. The redoxcline is manifested by a sudden change in the solid phase Mn profile (dMn/dZ = max).

TABLE 4.4

Adapted from Froelich *et al* (1979). Gibbs free energy changes are calculated at standard conditions and at the biochemical reference state (pH 7) and presented as kilojoules per mole of glucose. Multiplication by 17.67 converts to kJ per Redfield molecule.

Assumptions: (1) Organic matter represented by the Redfield molecule.

(2) O_2, NO_3^-, MnO_2, Fe_2O_3 or FeOOH and SO_4^{2-} are the only electron acceptors.

(3) Organic matter is the only electron donor.

(4) Ammonia released during reaction 1 is quantitatively oxidised to NO_3^-; all organic N oxidised in reactions 2 and 3 is converted to N_2, and all ammonia released in subsequent reactions remains unoxidised.

TABLE 4.4

AEROBIC RESPIRATION

1. $(CH_2O)_{106}(NH_3)_{16}(H_3PO_4) + 138\ O_2 \rightarrow 106\ CO_2 + 16\ HNO_3 + H_3PO_4 + 122\ H_2O$

$\Delta G^0 = -3190$ kJ/mole of glucose

DENITRIFICATION

2a. $(CH_2O)_{106}(NH_3)_{16}(H_3PO_4) + 94.4\ HNO_3 \rightarrow 106\ CO_2 + 55.2\ N_2 + H_3PO_4 + 177.2\ H_2O$

$\Delta G^0 = -3030$ kJ/mole

2b. $(CH_2O)_{106}(NH_3)_{16}(H_3PO_4) + HNO_3 \rightarrow 106\ CO_2 + 42.4\ N_2 + 16\ NH_3 + H_3PO_4 + 148.4\ H_2O$

$\Delta G^0 = -2750$ kJ/mole

MANGANESE REDUCTION

3. $(CH_2O)_{106}(NH_3)_{16}(H_3PO_4) + 236\ MnO_2 + 472\ H^+ \rightarrow 236\ Mn^{2+} + 106\ CO_2 + N_2 + H_3PO_4 + 366\ H_2O$

$\Delta G^0 = -3090$ kJ/mole BIRNESSITE
-3030 kJ/mole NSUTITE
-2920 kJ/mole PYROLUSITE

IRON REDUCTION

4. $(CH_2O)_{106}(NH_3)_{16}(H_3PO_4) + 212\ Fe_2O_3$ (or $424\ FeOOH$) $+ 848\ H^+ \rightarrow$
$424\ Fe2+ + 106\ CO_2 + 16\ NH_3 + H_3PO_4 + 530\ H_2O$ (or $742\ H_2O$)

$\Delta G^0 = -1410$ kJ/mole (HEAMATITE, Fe_2O_3)
-1330 kJ/mole (LIMONITIC GOETHITE, FeOOH)

SULPHATE REDUCTION

5. $(CH_2O)_{106}(NH_3)_{16}(H_3PO_4) + 53\ SO_4^{2-} \rightarrow 106\ CO_2 + 16\ NH_3 + 53\ S^{2-} + H_3PO_4 + 106\ H_2O$
$\Delta Go = -380$ kJ/mole

DISPROPORTIONATION

6. $(CH_2O)_{106}(NH_3)_{16}(H_3PO_4) \rightarrow 53\ CO_2 + 53\ CH_4 + 16\ NH_3 + H_3PO_4$

$\Delta G^0 = -350$ kJ/mole

zone; the zone between Mn^{2+} appearance and the onset of SO_4^{2-} reduction is the *suboxic zone*; during consumption of SO_4^{2-} the sediments become *anoxic* (Froelich *et al*, 1979). The depth to each of these zones in the sediment column is dictated by the organic matter content, sediment type (porosity and permeability), and availability of oxidants. Sediments which are suffering rapid diagenesis usually show compressed, or absent, oxic and suboxic zones.

However, the vertical zonation is not always clear. Physical processes of bioturbation and irrigation serve to disrupt and diffuse the geochemical boundaries. Several investigators have attempted to model these effects (Goldhaber *et al*, 1977; Grundmanis and Murray, 1977; Schink and Guinasso, 1977; Vanderborght *et al*, 1977,a,b; Grundmanis and Murray, 1982) but they are limited by our mathematical description of bioturbation as approximating to a diffusion coefficient (Officer, 1982). The assumption of a constant biodiffusion coefficient over a given depth interval probably does not adequately describe the decrease with depth of the activity and numbers of organisms present in the sediment.

In a similar way, the stoichiometry of the degrading organic matter will also constrain the reactions defined in Table 4.4. Although the Redfield C:N:P molar ratio of 106:16:1 is used there are numerous instances of deviations from this idealised formula. Schemes showing the variation of metabolite and oxidant concentrations during organic matter oxidation in a closed system (Bender *et al*, 1977; Froelich *et al*, 1979; Emerson *et al*, 1980) rely on unchanging C:N:P ratios; clearly a simplification of the organic molecule breakdown process,

although the two layer model of denitrification and sulphate reduction of Vanderborght *et al* (1977b) makes some effort to rectify this. Off Baja California changing C:N:P ratios seem to depend on the rate and degree of diagenesis (see below) so that completely oxidising sediment cores (163-9) display relatively constant C/N ratios, whilst rapid O_2 utilisation and denitrification (163-7) alter the molecular makeup proportionately.

4.4 THE BEHAVIOUR OF ORGANIC CARBON AND N, P, I AND Br DURING DIAGENESIS

The degree or rate of organic matter degradation and accompanying organic-element release will depend on the input of detrital organic matter, the rate of sedimentation, or both. The reactivity and behaviour of buried organic material in oxic, suboxic and anoxic conditions within the sediments has been assessed using some simple kinetic equations outlining the effect of various oxidants on the behaviour of C_{org} and related elements.

4.4.1 *Oxic diagenesis (Aerobic respiration)*

The red clay of 163-9 and the oxic tops of the three hemipelagic cores, 163-10, 163-14 and 163-7, provide the opportunity to study organic matter mineralisation in the

presence of oxygen. Although pore water nutrient data was not collected, NO_3^- concentrations measured by Jahnke *et al* (1982b) and Sawlan and Murray (1983) for core 145-6 at approximately the same location as 163-7 (Figure 1.1) indicates that denitrification is yet to occur and therefore dissolved O_2 exists throughout the length of the core. NO_3^- increases from a bottom water value of 38 µmol/kg to approximately 50 µmol/kg with the maximum increase in gradient over the top 4-6 cm of the sediment column (Sawlan and Murray, 1983). In the hemipelagic environment core 145-7, equivalent to 163-10, measurable but decreasing NO_3^- occurs over the length of the core, whereas total NO_3^- consumption occurs by 15 cm depth in 145-8 (equivalent to 163-7). Obviously, the increase in C_{org} landwards (Figure 2.5) is accompanied by a greater degree of diagenesis. Dissolved O_2 was not measured directly in these cores but the position of the Mn redoxcline in the hemipelagic sediments (Chapter 6) indicates the maximum depth of O_2 penetration in these sediments (2-3 cm in 163-7; 8-9 cm in 163-14 and 163-10).

Organic Carbon

Organic carbon in these sediments is made up of two fractions; (1) an inert refractory residue probably composed of geopolymers, such as kerogen and humics (Grundmanis and Murray, 1982) and N-rich, P-poor organic matter adsorbed by clay minerals (Muller and Mangini, 1980; Suess and Muller, 1980); (2) a reactive component composed of rapidly-transported, relatively fresh organic matter (McCave, 1975; Shanks and Trent, 1980; Honjo, 1980). Thus the reactive carbon, C_{diag},

available for diagenetic reactions, can be calculated from the total C_{org} by assuming a refractory residue, $C_{org}/Al = 0.029$, the minimum value in 163-9 which has suffered major oxic degradation (Appendix C). This ratio is almost the same as the one used by Grundmanis and Murray (1982) of 0.028, but higher than Muller and Mangini's (1980) value of 0.010. These higher ratios are probably due to the shortness of the cores in that they have not penetrated to the depth of constant C_{org} identified by Muller and Mangini (1980). Nevertheless, changes in C_{diag} (total C_{org} - (Al x 0.029)), will reflect early diagenesis in the top 40 cms or so of these cores. Figure 4.8 displays the profiles of C_{diag} calculated for the three hemipelagic cores and the oxic red clay of 163-9. Also marked are the depths of the estimated diagenetic zones.

The decomposition of organic matter, whatever the oxidant, is thought to follow first order kinetics (Stumm and Morgan, 1970; Berner, 1980; Muller and Mangini, 1980; Waples and Sloan, 1980; Reimers and Suess, 1983). Assuming that the input of C_{diag} has remained constant with depth (ie time, but see discussion in Chapter 3), is stationary within the sediment column (ie no bioturbation), and is at steady state then:

$$- W \frac{d C_{diag}}{d x} - k_C . C_{diag} = 0 \qquad (1)$$

where: x is the depth in the sediment (+ down the core)

W is the sedimentation rate

k_C is the first-order rate constant

C_{diag} is the reactive C_{org} fraction.

If compaction is ignored, solution of equation 1 with the following boundary conditions:

$$C_{diag} = C_{diag,0} \qquad x = 0$$

$$C_{diag} \rightarrow 0 \qquad x \rightarrow \infty$$

($C_{diag,0}$ is the surface concentration of C_{diag}) yields:

$$C_{diag,x} = C_{diag,0} \exp(-k_C/W.x) \qquad (2a)$$

in terms of depth, or in terms of time:

$$C_{diag,t} = C_{diag,0} \exp(-k_C.t) \qquad (2b)$$

By fitting equation 2a to the C_{diag} profile of 163-9 (Figure 4.8) using least-squares regression a rate constant, k_C, of 0.033 kyr^{-1} for oxic degradation in the pelagic environment off Baja California is obtained, using a sedimentation rate of 0.45 cm kyr^{-1} (Chapter 7). This is compared with other published C_{org} oxic degradation rates in Table 4.5. Muller and Mangini (1980), Waples and Sloan (1980) and Reimers and Suess (1983) all neglect sediment mixing; the first two because the data pertains to more deeply buried C_{org} (hence the longer half-lives, especially the North Phillipine Sea data which is in metres; Waples and Sloan, 1980), the latter on non-uniformity of feeding behaviour of the benthic community.

In contrast, oxic diagenesis at the surface of the three hemipelagic cores proceeds in sediment that is actively being bioturbated. In this instance the application of a biodiffusion-advection-decay model (Berner, 1980) is more appropriate. Again under steady state conditions and assuming

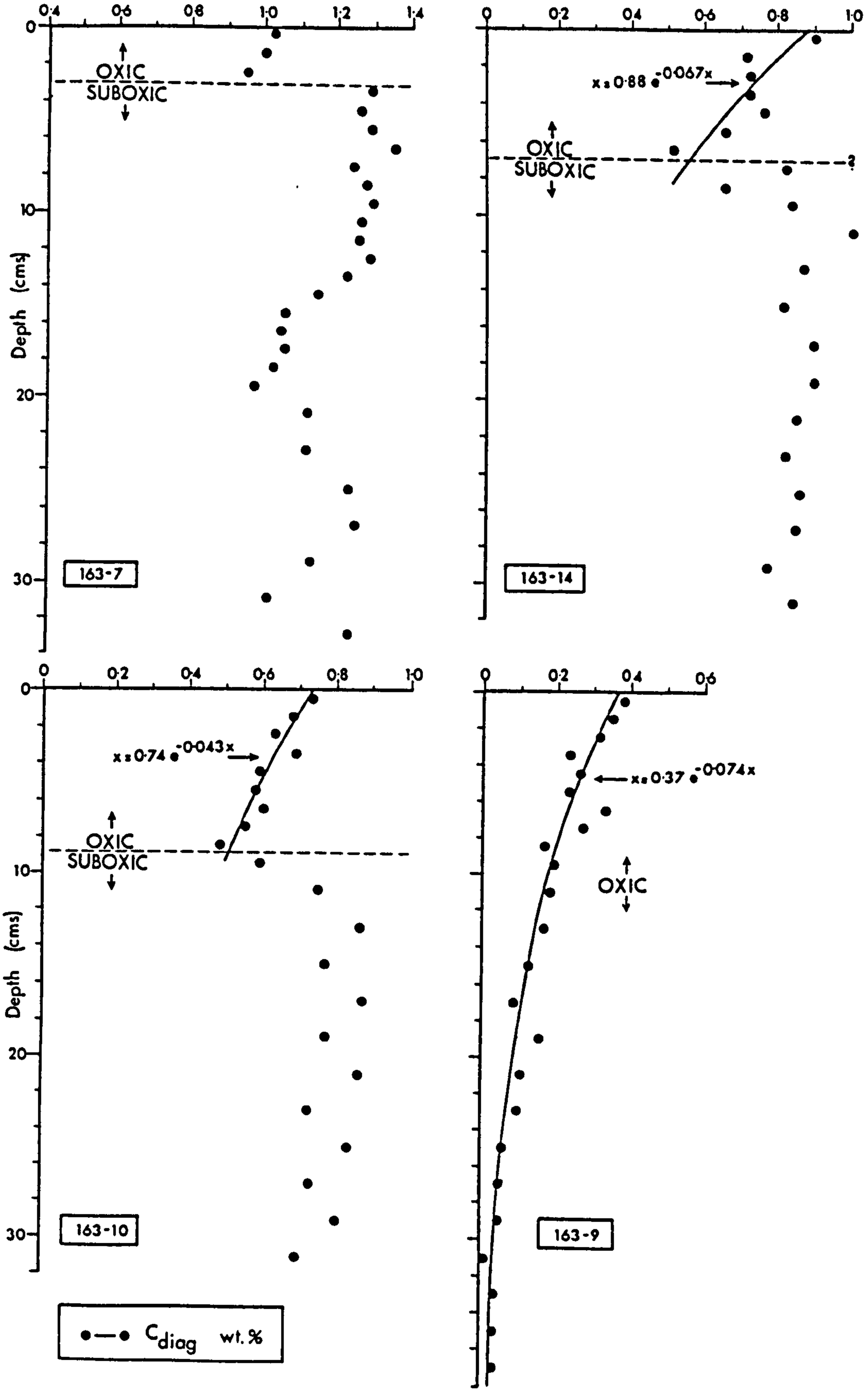

FIGURE 4.8 Profiles of C_{diag} with depth and the corresponding diagenetic zones for the Baja California oceanic sediments (salt-free), $C_{diag} = C_{org} - (Al * 0.029)$. Least-squares exponential fits are to data within the oxic zone (x = depth in cm). See text for further details.

TABLE 4.5

ORGANIC CARBON OXIDATION RATES AND HALF-LIVES

Locality	Author	Core	Section cm	N cm kyr^{-1}	k_c kyr^{-1}	$t_{1/2}$ kyr
Baja Calif.	This study	163-9	0-38	0.45	0.033	21
Pacific Manganese Nodule Belt (DOMES)	Muller & Mangini (1980)	10176-1	8-90	0.15	0.00310	220
		10127-2	0-40	0.19	0.00874	220
		10175-1	0-20	0.23	0.00779	89
		10145-1	0-30	0.32	0.0128	54
		10141-1	0-18	0.36	0.0158	44
		10140-1	0-13	0.41	0.0177	39
		10147-1	0-30	0.43	0.0275	25
		10132-1	0-30	0.58	0.0275	25
North Phillipine Sea	Waples & Sloan (1980)	443	0-450(m)	60.0	0.0008	866
		442	0-300(m)	60.0	0.0010	693
		445	0-750(m)	25.0	0.0010	693
		444	0-280(m)	20.0	0.0014	495
South flank Pacific-Antarctic Ridge	Reimers & Suess (1983)	7812-10	0-12	2.58	0.413	1.68
		7812-07	0-10	1.80	0.306	2.27
North flank		7812-05	0-12	5.88	0.764	0.91

constant porosity, sedimentation rate and first-order kinetics for organic matter decay:

$$D \frac{d^2 C_{diag}}{d x^2} - N \frac{d C_{diag}}{d x} - k_C . C_{diag} = 0 \quad (3)$$

where D is the bioturbation mixing coefficient and the other symbols are as for equation 2.

The solution of equation 3 at the boundary conditions:

$$C_{diag} = C_{diag,0} \qquad x = 0$$

$$C_{diag} \rightarrow 0 \qquad x \rightarrow \infty$$

is:

$$C_{diag,x} = C_{diag,0} \exp \left[\left(\frac{W - (W^2 + 4k_C D)^{1/2}}{2D} \right) . x \right] \quad (4)$$

taking: $$B_c = \frac{W - (W^2 + 4k_C D)^{1/2}}{2D} \quad (5)$$

least-squares curve fitting to the equation:

$$C_{diag,x} = C_{diag,0} \exp (-B_c . x)$$

for the oxic zone, C_{diag} data in cores 163-10 and 163-14 (163-7 displays a minimal oxic zone) results in B_c coefficients of -0.043 cm^{-1} for 163-10 and -0.067 cm^{-1} for 163-14 (Figure 4.8).

Over the oxic zone the downward flux due to biomixing is likely to outweigh the sedimentation flux. Using the dimensionless number, D/LW (L is the depth of biomixing) it can be shown that for W less than 2 cm kyr^{-1}, biomixing over a depth L of about 10 cm, dominates the distribution profile for $D > 20$ $cm^2 kyr^{-1}$ (Grundmanis and Murray, 1982). The biodiffusion coefficient has not been measured directly in these sediments but, by analogy with data in the literature (Guinasso and Schink, 1975; Nozaki *et al*, 1977; Peng *et al*, 1979; Cochran and Krishnaswami, 1980; Berner, 1980; Grundmanis and Murray, 1982) an average coefficient of 100 ± 50 $cm^2 kyr^{-1}$ for the deep-sea seems likely. (Note that the values used by Sawlan and Murray

(1983) seem unrealistically slow). At these high biomixing rates B_c may be approximated by $(k_C/D)^{1/2}$ (Grundmanis and Murray, 1982; Sawlan and Murray, 1983).

Table 4.6 indicates the importance of obtaining mixing coefficients as k_C defined here has an uncertainty of 50%. Nevertheless, oxic diagenesis in the hemipelagic sediments seems to degrade C_{org} approximately 6 (163-10) to 14 (163-14) times more quickly compared with the pelagic environment (163-9). This is probably due to the longer residence time of detrital organic matter at the sediment/water interface in more slowly accumulating sediments, allowing greater oxidation of C_{org} before burial. Figure 4.9 indicates the relationship between the sedimentation rate, W, and the rate constant, k_C, for different diagenetic environments. Muller and Mangini (1980) point out that the oxic decay constant increases by a factor of 30 with each 10-fold increase in sedimentation rate which is compatible with the results shown here.

TABLE 4.6

Hemipelagic oxic degradation rate constants,
subject to different biodiffusion rates

Core	Interval	B_c	D	k_C	$t_{1/2}$
	cm	cm^{-1}	$cm^2 kyr^{-1}$	kyr^{-1}	kyr
163-10	0-9	-0.043	100	0.185	3.7
		"	50	0.092	7.5
		"	150	0.277	2.5
163-14	0-7	-0.067	100	0.449	1.5
		"	50	0.224	3.1
		"	150	0.673	1.0

B_c approximated from $(k_C/D)^{1/2}$; k_C, the first-order rate constant is derived from least-squares fits to C_{diag} data (Figure 4.8). See text for further details.

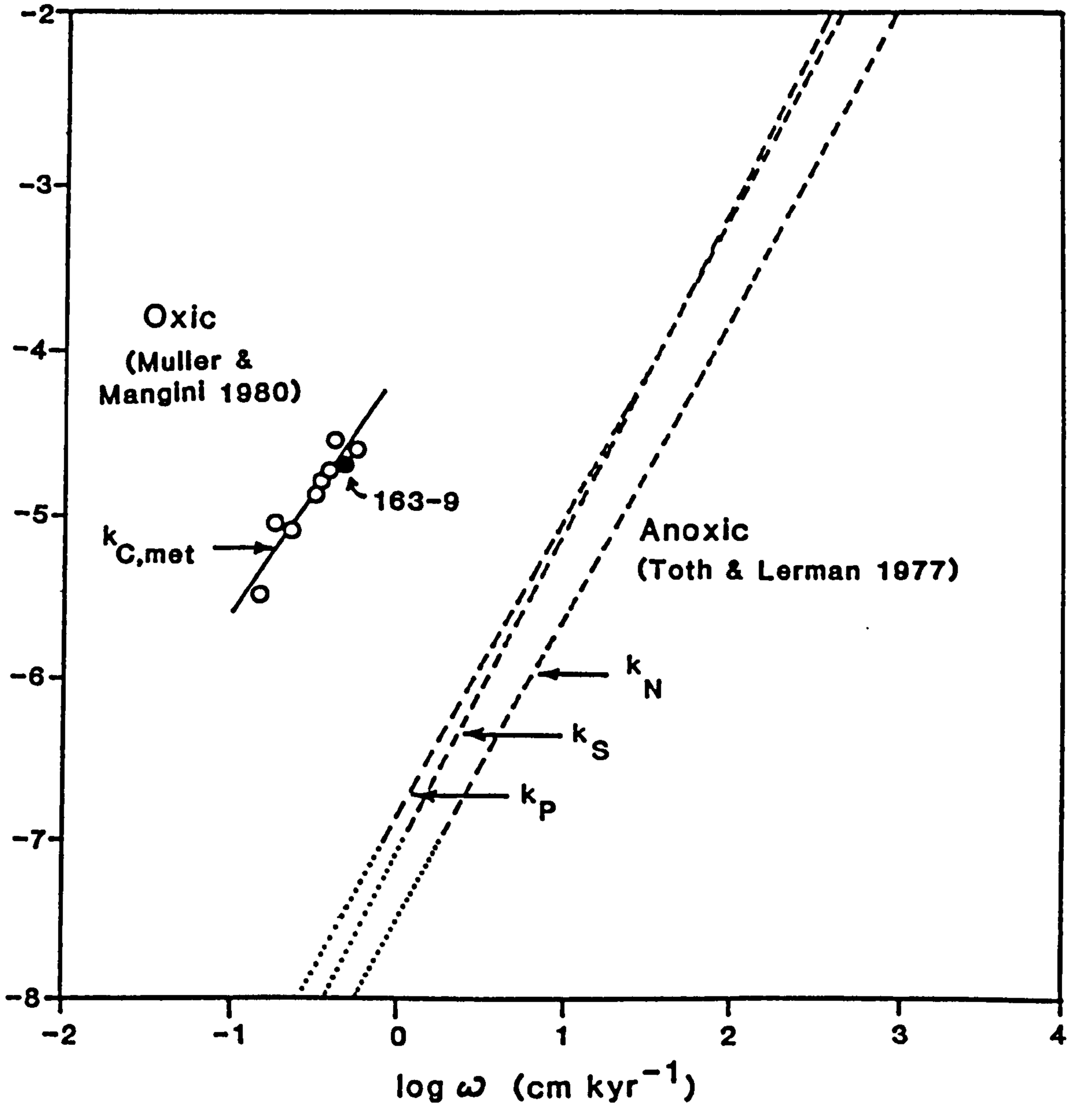

FIGURE 4.9 Log-log plot for the decay constant of C_{diag} *versus* sedimentation rate for 163-9 and data from the DOMES area given by Muller and Mangini (1980). Dashed lines indicate the relationship for sulphate reduction (k_S) and ammonia (k_N and phosphate (k_P) formation in anoxic sediments (Toth and Lerman, 1977). Extrapolation to similar sedimentation rates suggests faster decomposition for oxic environments.

Nitrogen

Figure 4.10 displays the regression line for oxic C/N ratios in the hemipelagic and pelagic surface sediments. The slope of the line indicates the similarity of surface organic matter to the Redfield composition. Holm-Hansen *et al* (1966) and Gordon (1971) report particulate C/N ratios close to that of marine plankton in the surface waters of the California Current and the Central Pacific, respectively. However, at depth the C/N ratio rises to > 15, attributed to preferential protein utilisation compared with carbohydrate. Off Baja California the sediment surface C/N ratio does not reflect this detrital composition, probably because the bottom fauna rejuvenate the organic matter (Smith, 1978; Wishner, 1980; Smith *et al*, 1983) enriching it in N and P (Muller, 1977; Grundmanis and Murray, 1982).

In some of the first measurements on C/N ratios in Pacific pelagic clays Arrhenius (1952) descibed decreasing C/N ratios with increasing sediment depth. Since then Hartman *et al* (1973) and Muller (1977) have also described decreasing C/N ratios, typically ranging from an atomic C_{org}/N_{total} of 3.8 at the surface, to 1.8 at depth (Muller, 1977; core 10132-1).

Considerable amounts of ammonium may become entrapped in the interstices formed by hexagonal oxygen rings within the lattice structures of clay minerals (Stevenson and Cheng, 1972) so that the ammonium content of sediments may be related to the clay mineral content and composition (Stevenson and Dharwial, 1959; Stevenson *et al* 1967). It seems likely that some of the total N measured off Baja California reflects an inorganic component, although the excellent correlation with C_{org} (Figures 4.10 and 4.11) indicates that this component is small.

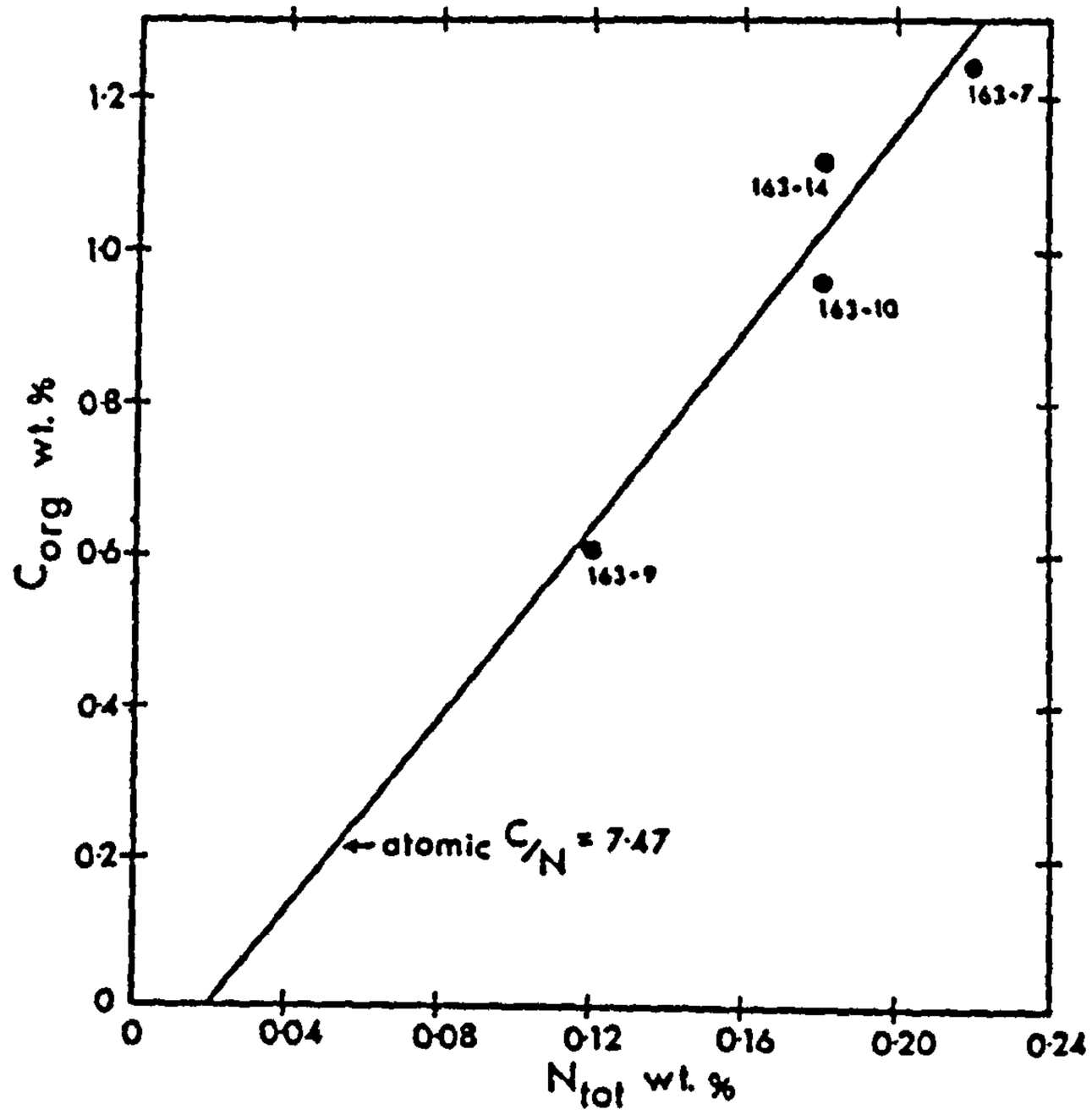

FIGURE 4.10 The relationship between C_{org} and N_{Tot} in the surface samples of oceanic sediments off Baja California (salt-free). The slope of the best-fit line indicates an atomic C/N ratio of 7.47, close to the Redfield ratio of 6.63. The N_{Tot} intercept of ~0.02 wt.% may represent NH_4 fixed in clays.

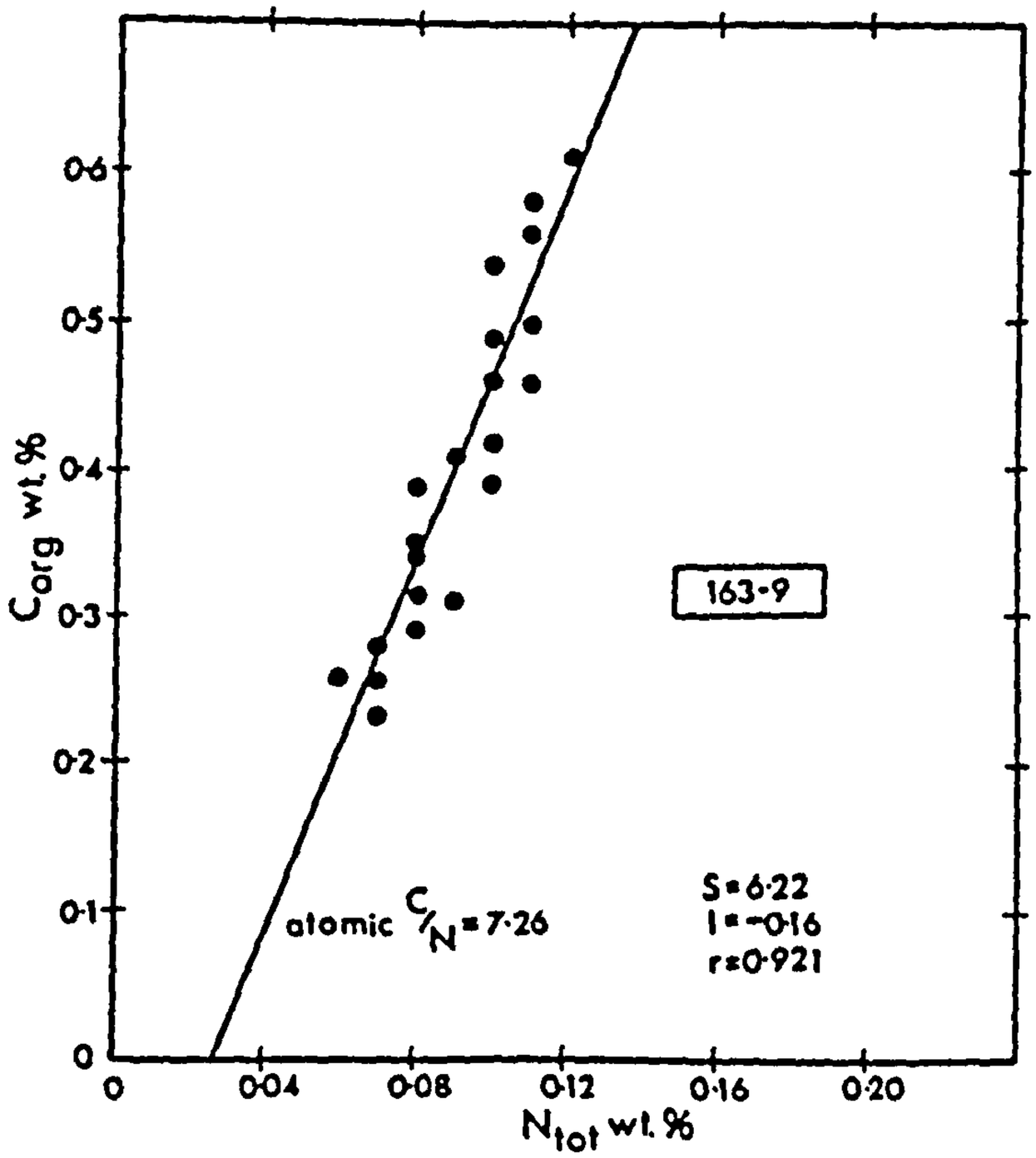

FIGURE 4.11 The correlation between C_{org} and N_{Tot} in samples from the oxic sediment of 163-9 (salt-free). The best-fit line has an atomic C/N ratio (7.26) similar to the samples indicated in Figure 4.10 (7.47) and a corresponding N_{Tot} intercept possibly due to NH_4 fixation by clays.

The positive N_{total} intercept in Figure 4.11 may well represent ammonium fixed in illites, representing some 22% of N_{total} at the surface.

Oxic degradation of organic matter in 163-9, whilst reducing the level of C_{org} and N_{total}, decreases the C/N ratio with depth. During diagenesis the released labile amino groups will be available for uptake by smectites or other swelling clays as described by Weiss (1969). As a result of this absorbtion, organic substances are protected from further bacterial attack (Muller, 1977). It would seem that the quantity of swelling clay (smectites) within the sediment column available for the uptake of these organic substances, could control the relative proportions during diagenesis.

Iodine and bromine

I and Br are biogeochemically active elements having distinct solution chemistries, reactivities and non-volatile stable forms (Whitehead, 1974; Truesdale, 1975; Neal and Truesdale, 1976; Harvey, 1980; Wong, 1980). Despite the common occurrence or I and Br in association with organic matter mentioned above, it is apparent that the geochemistry of I in oxic sediment behaves as a single class of organic compounds, while Br geochemistry is much more diverse (Harvey, 1980). I and Br, initially associated with biogenic matter, is subject to diagenetic release and redistribution during organic matter diagenesis (Price and Calvert, 1977; Krom and Sholkovitz, 1977; Ullman and Aller, 1980; Elderfield *et al*, 1981), although this is better documented for I than Br. It is the redox-dependant

solution chemistry of I and the sediment characteristics for each diagenetic zone, that ultimately controls the distribution of this element. The contrasting behaviour of I between oxic and anoxic sedimentary environments (Price and Calvert, 1977; Ullman and Aller, 1980) support the treatment of the halogen data in terms of diagenetic environment, as is used here.

As I is known to exist in more than one oxidation state in natural waters its chemistry has been extensively studied (Sugawara *et al*, 1958; Barkley and Thompson, 1960; Tsunogai, 1971; Truesdale and Spencer, 1974; Truesdale, 1975; Wong and Brewer, 1974, 1977; Elderfield and Truesdale, 1980; Wong, 1980; Ullman and Aller, 1980). Both IO_3^- and I^- exist, although the latter is more thermodynamically unstable. The average concentration of total dissolved I in seawater is 0.5 μM (Wong, 1980) with strong variations in the proportion of IO_3^- to I^- depending on the environment; anoxic water being enriched in I^- (Wong and Brewer, 1977). The oxidation of I^- to IO_3^- is assumed to occur in oceans although the process is still not well understood (Wong, 1980). Interconvertion between the two species occurs at a pE of +12.5, just below that of NO_3^- reduction (+12.65) making the redox behaviour of I very important in the early diagenetic environment:

$$IO_3^- + 6H^+ + 6e^- = I^- + 3H_2O \quad (pE = +12.5;\ pH = 8.1) \quad (1)$$

As a result it can act as an electron acceptor or donor in heterotrophic or chemoautotrophic microbial metabolic activity (Ullman and Aller, 1983). The only I species capable of reacting with organic N in organic matter is hypoiodite (IO^-) (Harvey, 1980; Wong, 1980) forming I^- (equation 2) or iodinated

organic species (equation 3)

$$IO^- + \text{reducing agent} = I^- \quad (2)$$

$$HIO + R = RI \quad (3)$$

These reactions of hypoiodite (and hypochlorite and hypobromite) with organic matter in natural waters have been long recognised (Wong and Davidson, 1977; Harvey, 1980; Wong, 1980) and can only occur in the presence of oxygenated waters, not under conditions of anoxia.

F, Cl and Br are the only elements to have negative oxidation states in oxygenated seawater (Sillen, 1961; Bruland, 1983). In contrast to the complicated behaviour of I, Br is one of the major anions, behaves conservatively, and is present in a concentration of 0.84 mmol kg^{-1} (at 35 $^{o}/_{oo}$ salinity).

From our knowledge of the chemical behaviour of the two halogens we would predict a strong redox control on I, and a negligible effect on Br. This is well illustrated by Figures 4.12 and 4.13 in which the surface concentration of salt-corrected I and Br, and C_{org} are plotted together. Whilst Br concentrations linearly increase with C_{org}, regardless of environment (oxic conditions typified by 163-9; suboxic/anoxic by 163-8), I displays linearity only for oxic conditions (although, mineralogical control is also active in these sediments; see below). The average ratio of Br/C_{org}, 96, compares with 146 in the Panama Basin (Pedersen and Price, 1980) and 120 in the Barents Sea (Price *et al*, 1970). I/C_{org} for the oxic sediments is 412 off Baja California, compared to 395 for the Panama Basin and 380 for the Barents Sea (all $\times 10^{-4}$).

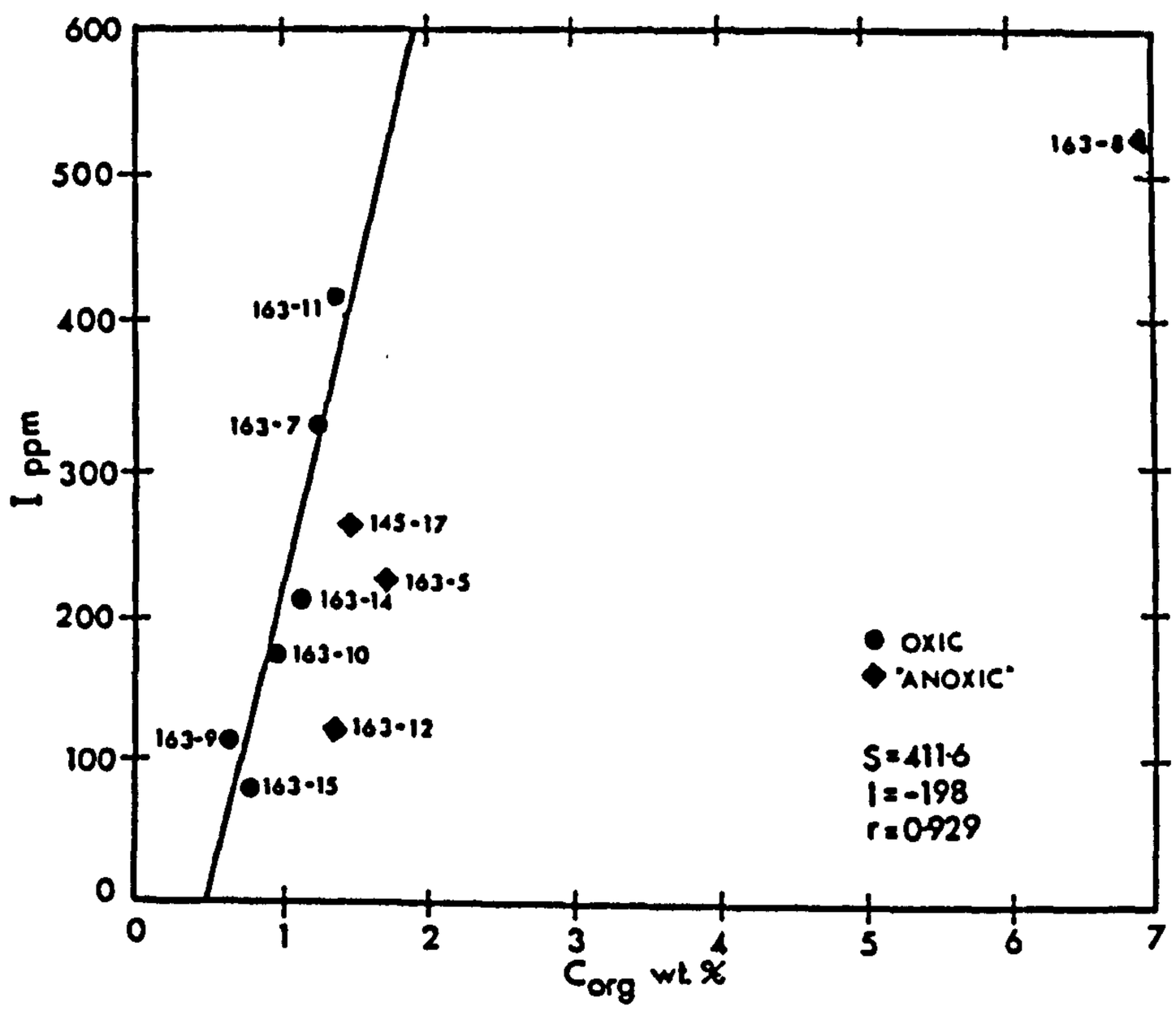

FIGURE 4.12 The correlation between I and C_{org} in surface samples off Baja California (salt-free). Only oxic sediments (circles) are used in the regression data. The definitions of oxic and anoxic sediment relate to the depositional environment, position of the O_2 minimum, and level of C_{org} in the sediment.

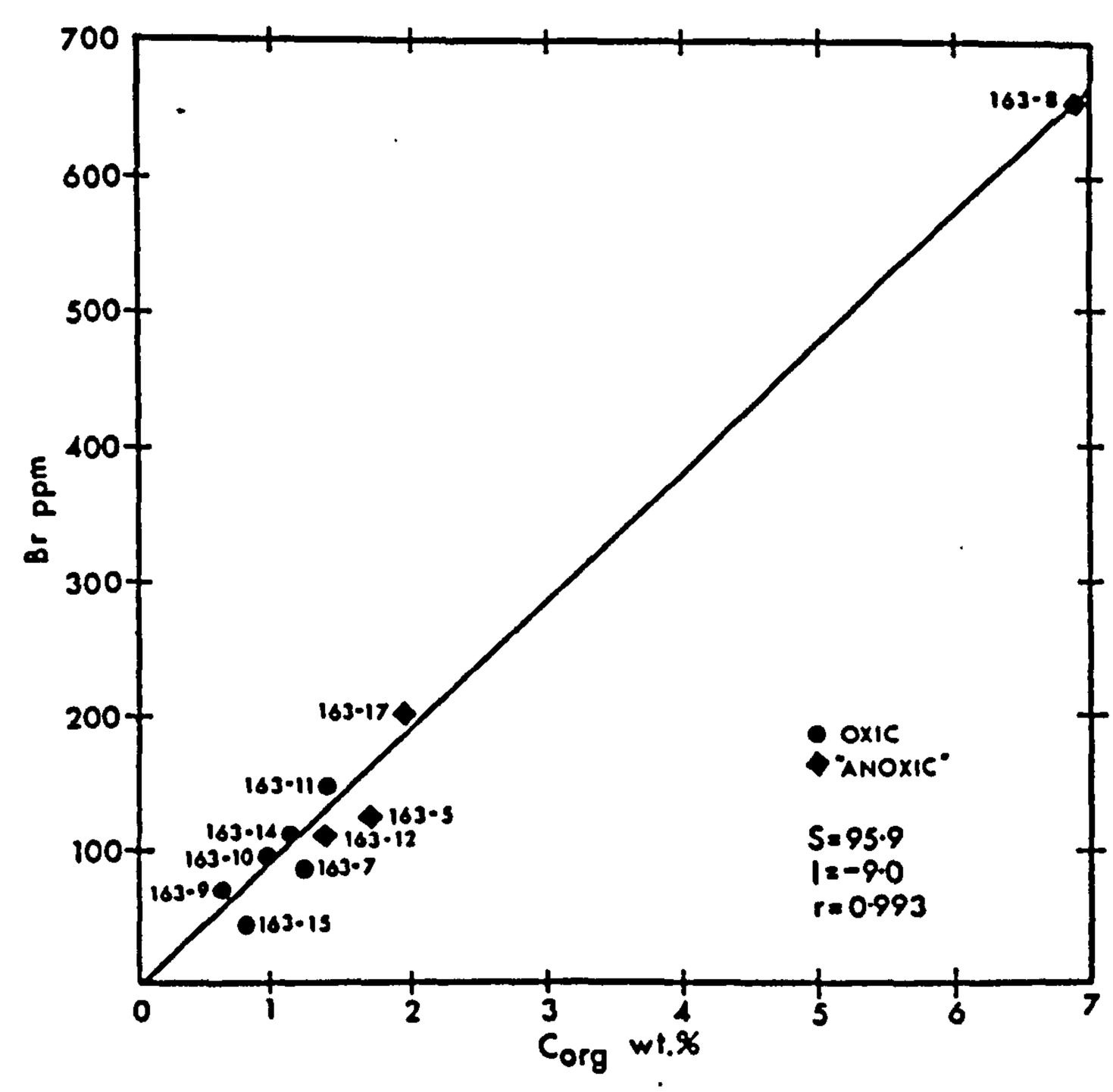

FIGURE 4.13 The correlation between Br and C_{org} in surface samples off Baja California (salt-free). All samples are used in the regression data.

Although the I and Br profiles in Figure 4.6 decrease with depth in 163-9, suggesting that oxic diagenesis releases halogens which migrate upwards and are lost from the sediment (Shishkina and Pavlova, 1965; Price and Calvert, 1977) normalised I to C_{org} increases with depth (Figure 4.14) whilst Br/C_{org} slightly decreases. The first-order rate constants for total I, total Br and total C_{org} are displayed in Table 4.7. I has the slowest rate of decay which is responsible for the rising I/C_{org} with depth. Also to be explained is the subsurface increase in I and I/C_{org} (Figure 4.14) at, or just above, the Mn redoxcline in the oxic zone of the hemipelagic sediments.

TABLE 4.7

FIRST-ORDER RATE CONSTANTS FOR 163-9

$k_{C,total}$ (cm^{-1})	$k_{I,total}$ (cm^{-1})	$k_{Br,total}$ (cm^{-1})
-0.024	-0.006	-0.035
$k_{C,diag}^{+}$	$k_{I,diag}^{@}$	$k_{Br,diag}^{*}$
-0.074	-0.098	-0.064

$^{+}$ C,diag = C,total - (Al x 0.029)

$^{@}$ I,diag = I,total - (Al x 11.14)

* Br,diag = Br,total - (Al x 1.86)

refractory element/Al ratios taken from the lower samples of the core

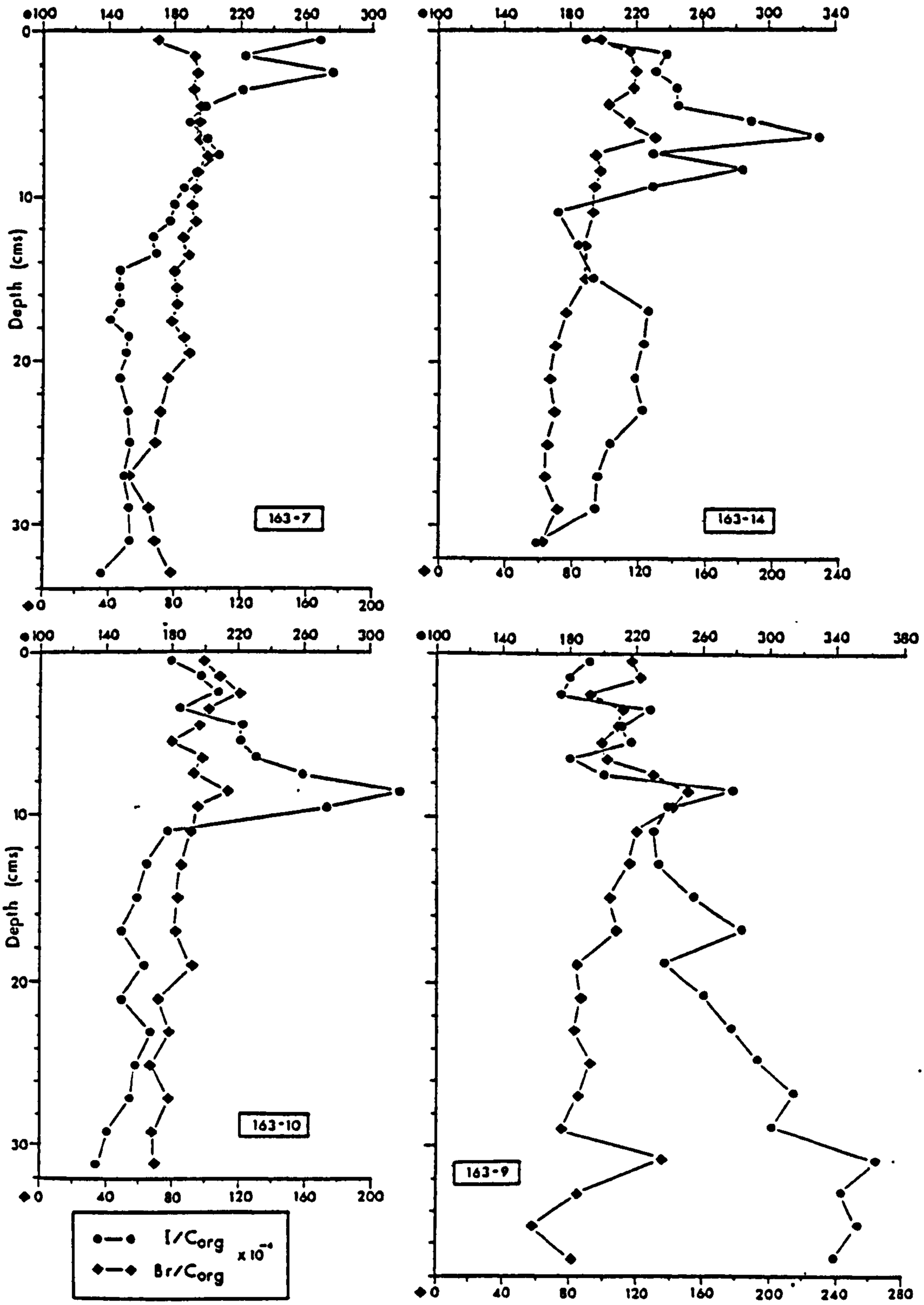

FIGURE 4.14 Profiles of I/C_{org} (upper axis) and Br/C_{org} (lower axis) with depth in the Baja California oceanic sediments.

TABLE 4.8

I/C RATIOS IN OCEANIC COMPONENTS

Component	I/C ($\times 10^{-4}$)	Author
From regression of total I against phosphate in seawater	1.0	Elderfield and Truesdale (1980)
Plankton composition*		
Pacific ocean	1.0	Elderfield and
$5^{o}15.7'N$ $79^{o}44.5'W$	1.5	Truesdale (1980)
Faecal pellets from sediment traps		Spencer *et al* (1981)
"green" pellets	3.1	
"red" pellets	1.6	
Stoichiometric relationships in pore water - Narragansett Bay	4.8	Elderfield and Truesdale (1980)
Marine sediments+		
Barents Sea	380	Price *et al* (1970)
Panama Basin	395	Pedersen and Price (1980)
Baja California	412	This study

*Duplicates represent separate plankton tows.
+Regression data from a number of stations.

Measurements of specific total-iodine and specific phosphate (Elderfield and Truesdale, 1980) suggest the direct coupling of I and nutrients within the water column, in an I/C assimilation ratio of ~1.0 x 10^{-4} when a Redfield-type stoichiometric model is used (Table 4.8). This ratio is the same as that obtained for Pacific plankton (Elderfield and Truesdale, 1980) and similar to that of faecal pellet material obtained from sediment traps (Spencer *et al*, 1978). In addition, pore water analyses from Narragansett Bay sediments (Elderfield *et al*, 1981) display a similar ratio, in complete contrast to oxidised marine sediment at the sediment/water

interface. In a somewhat analogous way to N and P, benthic processes are also likely to play an important part in modifying the chemistry of the degrading organic matter. Two possible mechanisms to account for not only the high surface I/C_{org} ratio but also the elevated I/C_{org} ratios at depth, either throughout the length of the pelagic core, or in the oxic zone of the hemipelagic sediment, are (1) biochemical and (2) geochemical absorbtion processes.

(1) Price and Calvert (1977) proposed a biochemical mechanism for the absorbtion of I at the surface of oxic sediments. I is absorbed as I^- (the degree of uptake being limited by the available I^- concentration; Shaw, 1962; Tsunogai and Sase, 1969) probably after reaction 2 (above) in the presence of suitable nitrate-reducing organisms. An enzyme, "iodide-oxidase" (Kylin, 1930) occuring at the surface of many algae (Shaw, 1962) oxidises I^- to I_2 which is subsequently hydrolysed to IO^-, diffuses through the cell wall and is reduced back to I^- (Reaction 2). This reaction can only occur in oxic conditions (see above). The two major classes of sedimentary organic matter having amide bonds to react with I in this manner are polypeptides and chitin (N-acetylglucosamine) (Harvey, 1980). The section on the behaviour of organic N (above) described the uptake of organic nitrogenous compounds by smectites (Weiss, 1969). In a similar way, an abundance of smectite and fully oxic conditions may cause I to be held for longer in the sediment during decomposition in preference to C_{org}, resulting in a rising I/C_{org} ratio, even though total I decreases with C_{org}. The rate constants for these two reactions ($k_{I,diag}$ and $k_{I,total}$ versus

$k_{C,diag}$ and $k_{C,total}$) are shown in Table 4.7.

(2) Geochemical absorbtion processes are more active in the hemipelagic cores (163-10, 163-14, 163-7) where the oxic zone is greatly enriched by diagenetic oxyhydroxides (Chapter 6), especially those of Mn. However, similar, more subdued, absorbtion may also occur throughout the oxic red clay of 163-9 and 163-15 augmenting the total I content in these cores. I species, especially IO_3^-, can react with Fe-hydroxides under these conditions (Sugawara *et al*, 1958; Goldschmidt, 1954 ;Whitehead, 1974; Neal and Truesdale, 1976; Ullman and Aller, 1980). In addition $CaCO_3$ (Whitehead, 1974) and kaolinite (Neal and Truesdale, 1976) are found to have sorbitive capacities, although the presence of soluble salts can inhibit sorbtion by clays. Ullman and Aller's (1980) study on pore water I in sediments from Mud Bay, South Carolina, suggests that I is released during degradation of organic matter at depth, but that the oxic sediment top acts as an efficient sink for this remobilised I and can greatly reduce the dissolved flux across the sediment/water interface. Without doubt, such a mechanism operates in the hemipelagic setting off Baja California accounting for the subsurface enrichment in I and the resulting elevated I/C_{org} ratios. This diagenetic enrichment of the solid phase profiles of I makes it impossible to accurately calculate the rate constant for I release in this environment.

In contrast to I, little is known about Br absorbtion processes. Many Br compounds exist in marine sediments (Harvey, 1980), each having different coordination and binding energies. Qualitative interpretation of the Baja California data suggests that redox control is not important, that diagenetic release from organic matter is less rapid than for I ($k_{Br,diag}$ <

$k_{I,diag}$; Table 4.7), but that absorbtion is not important ($k_{Br,total} > k_{C,total} > k_{I,total}$).

4.4.2 *Suboxic Diagenesis*

Off Baja California the suboxic environment is represented by the lower sections of the three hemipelagic cores as shown in Figure 4.8. Unfortunately, these cores also display evidence of changing detrital and biogenic input with time (Chapter 3) making it difficult to isolate changes in concentration of elements due to diagenesis, and changes due to productivity fluctuation. The most obvious indicator of change in these cores is the $CaCO_3$ profile (Figures 3.2 and 3.16) possibly representing the last glacial episode (Chapter 3). At this time C_{org} may have increased due to enhanced primary production (Stevenson and Cheng, 1973; Pedersen, 1983) although not necessarily synchronously. Application of kinetic models to diagenesis in this zone is impossible as the primary assumption of constant input is invalid. Nevertheless, qualitative assessment of the biogenic element/C_{org} ratio (assuming both entered the sediment in the same ratio through time) may be used to define the relative decay rates.

<u>Nitrogen</u>

N is apparently released from the sediment more rapidly than C_{org} in this zone (Figure 4.3 displays increasing C/N ratios with depth). Although the oxidant efficiency is less, the labile nature of the amino groups in the organic molecule causes it to be lost at a greater rate. As the overall

diagenetic rate is faster due to higher levels of organic matter and increased sedimentation rates, the nitrogenous compounds released are rapidly remobilised and not sorbed at depth. The rate of change of the increasing C/N ratio with depth is greatest in sediments with high organic matter content (ie 163-7 displays a more rapid increase than 163-10). This selective loss of nitrogenous compounds has been shown to occur in many hemipelagic sediments (Rittenberg *et al*, 1963; Degens *et al*, 1964; Emery *et al*, 1964; Bordovskiy, 1965c; Stevenson and Tilo, 1970) and through glacial/interglacial cycles (Stevenson and Cheng, 1973).

<u>Iodine and bromine</u>

Both halogens display decreasing ratios relative to C_{org} beneath the Mn redoxcline (except for I/C_{org} in 163-14 between 17 and 23 cm depth). This is indicative of the labile nature of the two halogens and the lack of a suitable substrate for either biochemical or geochemical absorbtion processes, as both depend on oxic conditions. Qualitatively, the rate of release is similar in both 163-7 and 163-10.

4.4.3 *Anoxic Diagenesis*

Organic matter degradation in the absence of O_2 and NO_3^- is exemplified by two cores from the Baja California continental shelf; 163-8 and 145-17. Both show complicated C_{org} profiles due to changes in detrital and biogenic input, sedimentation rate and availability of oxidants. The formation

of diagenetic mineral phases resulting from the high levels of C_{org} and element availability are widespread (eg apatite, glauconite, pyrite) and are discussed in Chapter 8. P is dominated by diagenetic mineral formation in 145-17, whilst N has not been measured in these cores.

The distribution of the halogens provides useful information on their redox behaviour. From Figure 4.12 it was noted that I concentrations relative to C_{org} are much lower in anoxic sediments. Here, the sorbitive mechanisms referred to above are unable to operate and the ratio is lower. In addition, the core from the intrashelf basin, 163-8, displays little change in the I/C_{org} with depth (Figure 4.15). Similar phenomena has been observed in the anoxic environment of the Black Sea (Calvert and Batchelor, 1977) and Namibia (Price and Calvert, 1977). The fluctuating C_{org}, I and Br profiles in Figures 4.2 and 4.7 for core 163-8 suggest that while input or dilution of organic matter may have varied, the incorporation of I into the sediment, the rate of diagenesis and its subsequent release, is extremely low in this environment, reflecting the lack of an efficient oxidant. If the lower C_{org} values in the upper 10-15 cm of 145-17 do represent a change to more oxygenated bottom water conditions* (Jahnke *et al*, 1983) then the higher I/C_{org} ratio over this region of the core is yet further evidence of redox control on the distribution of this halide.

---

*Detrital element geochemistry (Si/Al, Zr) and water contents indicate that a change to finer grained sediment at depth occurs, accounting for the increase in C_{org} (Chapter 5).

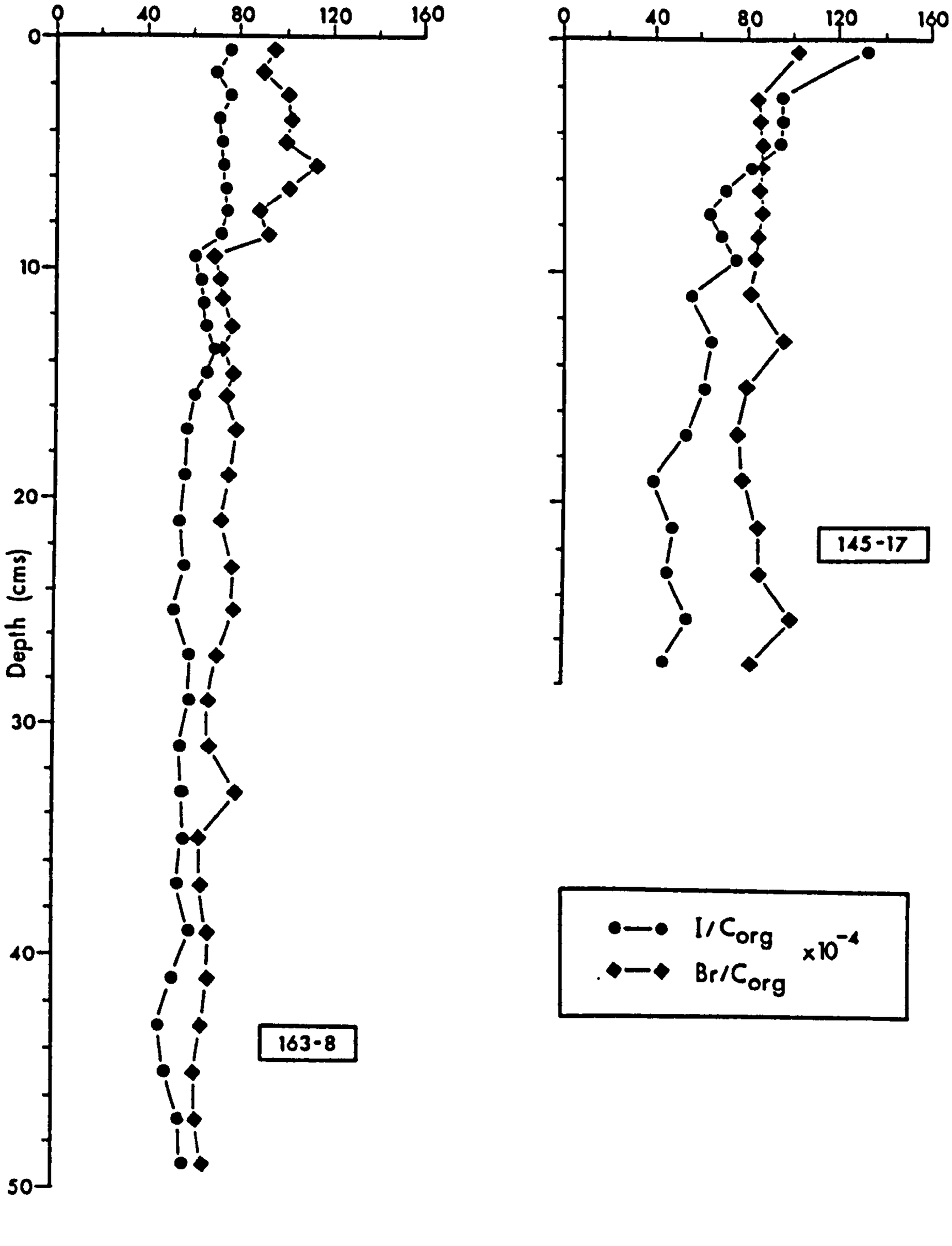

FIGURE 4.15 Profiles of I/C_{org} and Br/C_{org} with depth in two cores from the Baja California shelf (salt-free). Both ratios are relative to the abcissa scale.

4.5 THE PARTITIONING OF CARBON FLUXES BETWEEN PRODUCTION AND PRESERVATION

The partitioning of C_{org} during its post-formational history may be accomplished by the use four major factors: C_{prod}, the rate of primary production of C_{org} in the euphotic zone; C_{flux}, the flux of C_{org} at any depth as measured by sediment traps; $C_{pre-burial}$, the rate of C_{org} utilisation by benthic processes before burial; C_{acc}, the rate of C_{org} accumulation in the sediment as determined from the flux across the sediment/water interface.

The fertility of the sea is determined by oceanic circulation, biological processes of uptake and mineralisation, settling of organic debris and regeneration of nutrients, and migration of organisms. As a result, the spatial distribution of organic detritus is extremely variable and subject to the above controls. Without entering the themantics of primary production measurement it has been shown by Suess (1980) that an empirical relationship exists between C_{prod} and C_{flux}, *viz*:

$$C_{flux\ (z)} = \frac{C_{prod}}{0.0238z + 0.212} \qquad (1)$$

where C_{prod} and C_{flux} are in units of ($gC/m^2/yr$) and z (>50) is the water depth in meters at which the traps were moored.

A complication arises in defining the fraction of the net vertical flux (C_{flux}) accumulating in the sediment, and therefore available for early diagenesis (C_{acc}), *versus* the fraction consumed by benthic organisms and/or oxidation prior to burial (Jorgensen, 1978; Sorensen *et al*, 1979; Wishner, 1980), $C_{pre-burial}$, which is often higher than the accumulating

C_{org} flux estimates. Hence the total benthic carbon budget may be defined:

$$C_{flux} = C_{pre\text{-}burial} + C_{acc}$$

The partitioning of these fluxes is displayed in Table 4.9 illustrating the importance of pre-burial benthic processes in degrading ~95% of the organic detrital flux. Reimers and Suess (1983) found up to 85% of C_{org} reaching the seafloor in any one year is oxidised or consumed before burial. Wishner (1980) showed that only ~1.3% of the C_{org} flux in the abyssal plain environment is incorporated in the top 1 cm of sediment.

Obviously, these calculations given here have large errors, especially the estimation of C_{prod}. Variations in seasonal productivity and uncertainties in the conversion of surface production to production over the entire euphotic zone may be a major source of error (Suess, 1980). In addition, the sedimentation rates are not accurately known for the hemipelagic cores (Chapter 7).

Wishner (1980) also showed that 37 to 20% of the C_{flux} is respired by benthos and benthopelagic plankton leaving some 63-80% of the C_{flux} unaccounted for. In addition to the consumption by macro- and microfauna the high degree of pre-burial utilisation may be due to multiple cycling of organic matter across the sediment/water interface. Gardner (1977), cited in Wishner (1980), found a large proportion of the near-bottom organic flux consisted of resuspended material. The calculated flux of C_{org} from the bottom of core 163-9 is 0.007 $gC/m^2/yr$, assuming a constant sedimentation rate through time. If C_{flux} has also remained constant then ~30% of buried C_{org} has been lost through oxic diagenesis in some 85,000 years.

The changes in the C_{org} profiles with depth in the hemipelagic cores represent fluctuating C_{org} inputs and/or preservation. Variation in C_{org} during glacial/interglacial episodes has been noted by Arrhenius, 1952; Stevenson and Cheng, 1973; Hartmann *et al*, 1976; Pedersen, 1983. Figure 4.9 supports the qualitative interpretation of a 30-fold increase in decay rate ($k_{C,diag}$) with each 10-fold increase in sedimentation rate (Muller and Mangini, 1980), suggesting that higher sedimentation rates favour preservation of labile organic compounds.

Two possibilities arise concerning fluctuations in C_{org} with time in the hemipelagic and shelf sediments. Firstly, that changes in the diagenetic regime occured, particularly the supply of oxidants. Jahnke *et al* (1983) argued that a shifting O_2 minimum, causing greater oxygenation of the overlying water column at the present day, is responsible for the lower C_{org} in the top decimeter of 145-17. Secondly, and more probably, the rate of sediment and/or organic supply changed.

Changes in the diagenetic environment would be expected to have a profound influence on the I/C_{org} ratio (Section 4.4.1). Such changes are not as prominent below the Mn redoxcline in the hemipelagic sediments. Likewise, the steadily decreasing I/C_{org} ratio in the suboxic/anoxic sediment of 163-8 (Figure 4.15) mitigates against fluctuating diagenetic environment causing the changes in C_{org} with depth. These smooth I/C_{org} profiles suggest instead increasing organic matter accumulation, either through sediment input changes and/or productivity events. In the hemipelagic environment such changes occured during the last glacial episode, the Wisconsin.

TABLE 4.9

THE PARTITIONING OF ORGANIC CARBON FLUXES TO THE SEA FLOOR OFF BAJA CALIFORNIA

Station	9	10	14	7
	all values in $gCm^{-2}yr^{-1}$			
C_{prod} [1]	50	100	150	250
C_{flux} [2]	0.569	1.203	1.984	2.873
$C_{pre\text{-}burial}$ [3]	0.56	1.13-1.08	1.94-1.87	2.79-2.72
C_{acc} [4]	0.01	0.12-0.08	0.10-0.05	0.15-0.08
% C_{org} oxidised at sediment surface before burial	98	94-90	93-95	95-97
% C_{org} incorporated into the sediment	1.8	10.0-6.7	5.0-2.5	5.2-2.8
θ (ρ_{sed} = 2.7)	0.850	0.812	0.843	0.847
C_{org} (surface)	0.61	0.96	1.12	1.24
Sedimentation rate [5] ($cm\ kyr^{-1}$)	0.45	2.5-1.55	2.0-1.0	3.0-1.55

[1] Estimated from Van Andel *et al* (1975); Wooster and Ried (1963) give values of 87.6-328.5 $gCm^{-2}yr^{-1}$ for the California Current; El Sayed and Taguchi (1979) give ~48 $gCm^{-2}yr^{-1}$ for the DOMES area.

[2] Suess (1980) $\dfrac{C_{prod}}{0.02382z + 0.212}$ z = water depth

[3] $C_{pre\text{-}burial} = C_{flux} - C_{acc}$

[4] C_{acc} - flux of C_{org} across the sediment/water interface

$$C_{acc} = \frac{\% \rho_{sed} C_{org} (1-\theta)}{10}$$

[5] Station 9 from radionuclide data (Chapter 7); hemipelagic stations from $CaCO_3$ profiles and ^{14}C measurements by Sawlan (1982).

At that time (12,000-17,000 years BP) carbonate accumulation increased and a lower sea level stand resulted in a greater degree of sediment transport off the shelf into the more distal hemipelagic environment (Chapter 3). In contrast, the rapidly increasing I/C_{org} ratio towards the top of 145-17 may substantiate a change to more oxic conditions being responsible for greater surface degradation of organic matter.

CHAPTER 5

ON THE BIOPHILIC NATURE OF TRACE METALS IN SHELF SEDIMENTS OFF BAJA CALIFORNIA

5.1 INTRODUCTION

The mechanism of high trace metal enrichment in black, bituminous sediments in the geological record has been the subject of much debate (Brongersma-Sanders, 1966; Vine and Tourtelot, 1970; Wedepohl *et al*, 1978; Holland, 1979; Tourtelot, 1979; Brumsack, 1980; Spears and Amin, 1981). Explanations for syngenetic metal enrichment have varied from uptake of metals from seawater (Holland, 1979; Brumsack, 1980; Brumsack and Lew, 1982) to supply of metals from plankton in areas of upwelling (Brongersma-Sanders, 1966; Brongersma-Sanders *et al*, 1980), or from undifferentiated organic components including plankton and faecal pellets (Chester *et al*, 1978). Often a trace metal-organic matter association is cited (Curtis, 1966; Calvert and Price, 1970, Calvert, 1976; Spears and Amin, 1981) because of correlation between the two. However, both grain size and the presence of sulphides are known to affect, or even dominate, the metal-organic matter relationship. With these words of warning the organic-rich sediments on the Baja California shelf have been investigated *a propos* their distribution and trace metal content.

5.2 THE ASSOCIATION OF THE TRACE METALS, Cr, Cu, Mo, Ni, Pb, V, and Zn WITH ORGANIC CARBON IN TWO SHELF STATIONS, 145-17 AND 163-8

The distribution of organic carbon (C_{org}) on the shelf has already been outlined in Chapter 4. Profiles of C_{org} with depth are presented in Figure 4.2, for the two shelf sediments, 145-17, a silt-mud which may be oxidising at the surface Jahnke *et al* (1983) (Section 4.5), and 163-8 from the intrashelf basin

which is a suboxic/anoxic mud.

Figures 5.1 and 5.2 present the relationship between Cr, Cu, Mo, Ni, Pb, V and Zn with C_{org} in stations 145-17 and 163-8. There appears to be a clear association between Cr, Cu, Ni, V and Zn, and C_{org}, but less so for Mo and Pb. Using the data for 145-17 a 10 wt.% increase in C_{org} is accompanied by ~90 ppm increase in Cr, ~45 ppm increase in Cu, ~110 ppm increase in Ni, ~150 ppm increase in V, and ~90 ppm increase in Zn. However, before statements can be made concerning the trace metal content of the organic matter in these shelf sediments, some investigation of the factors causing the large variation in the C_{org} is required.

5.2.1 *Factors affecting the organic matter content of the shelf sediments*

It is well known that sediment particle size can influence the level of C_{org} in sediments (Trask, 1953; Van Andel, 1964; Bordovskiy, 1965,b). Clays from the Gulf of California (Van Andel, 1964) and the Peruvian margin (Busch and Keller, 1981) contain proportionately more organic matter and water than coarser-grained sediments having the same biogenic input. Figure 5.3 displays the strong inverse relationship between C_{org} and Si/Al, and Zr/Al, especially in 145-17. The increasing Si/Al and Zr/Al are probably due to greater proportions of quartz and zircon relative to Al-containing clay* (Chapters 2 and 3). This suggests that C_{org} is definitely enriched in clay,

---

* The higher organic C values for 163-8 indicate that enhanced organic matter production and preservation occurs in this suboxic/anoxic basin, in addition to any sedimentological control.

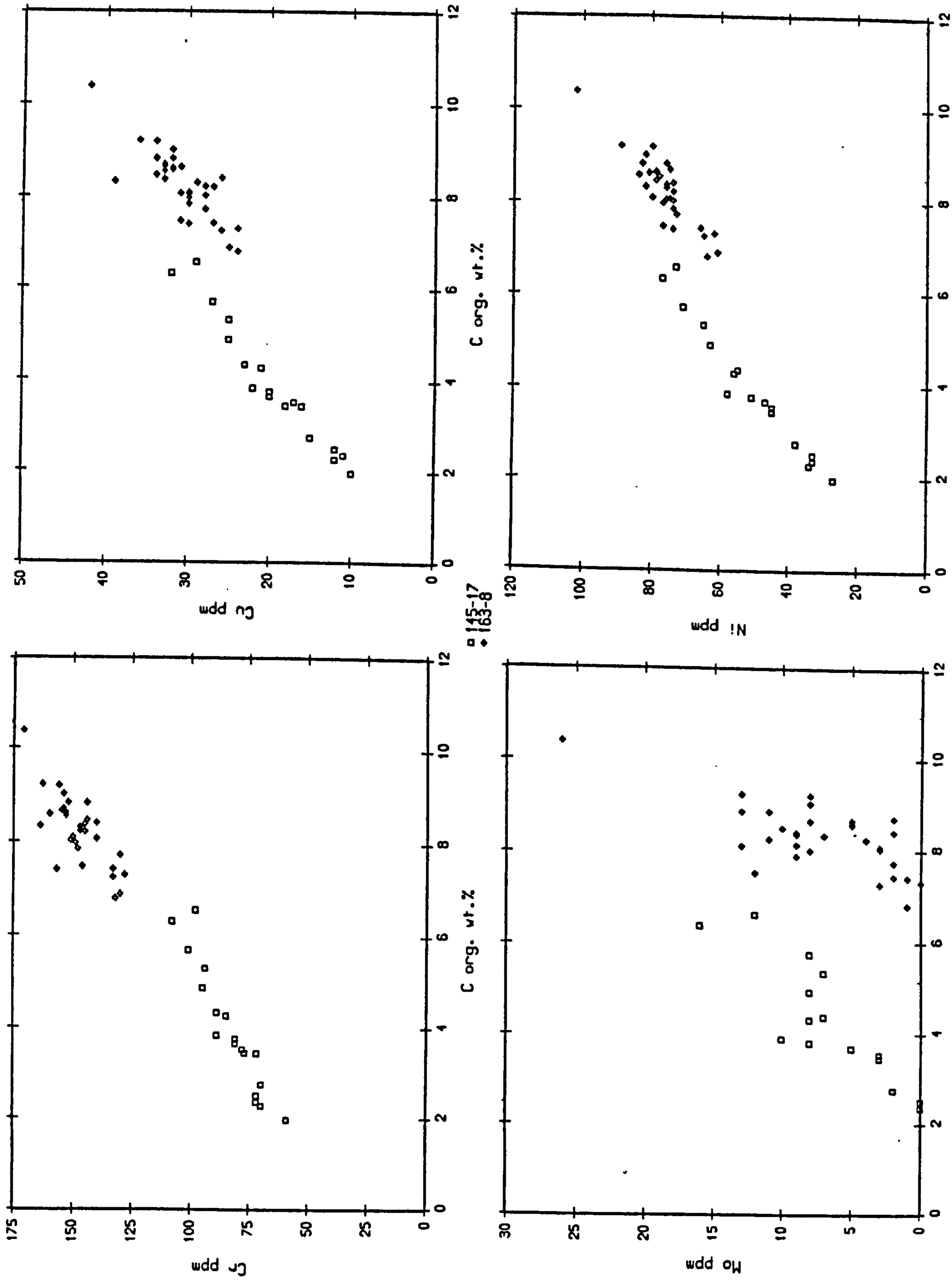

FIGURE 5.1 The relationship between Cr, Cu, Mo and Ni with organic C in two Baja California shelf sediments (salt-free).

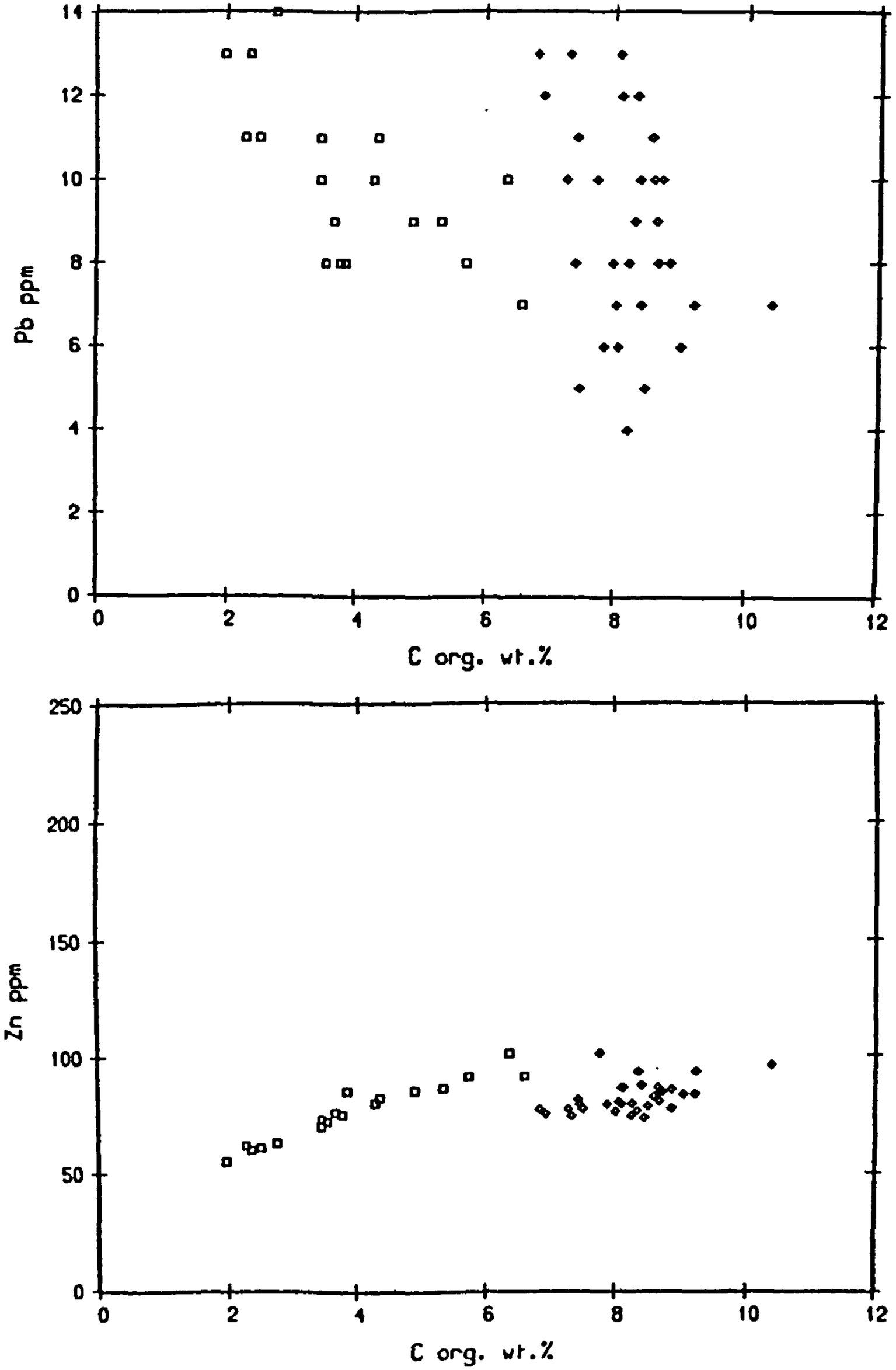

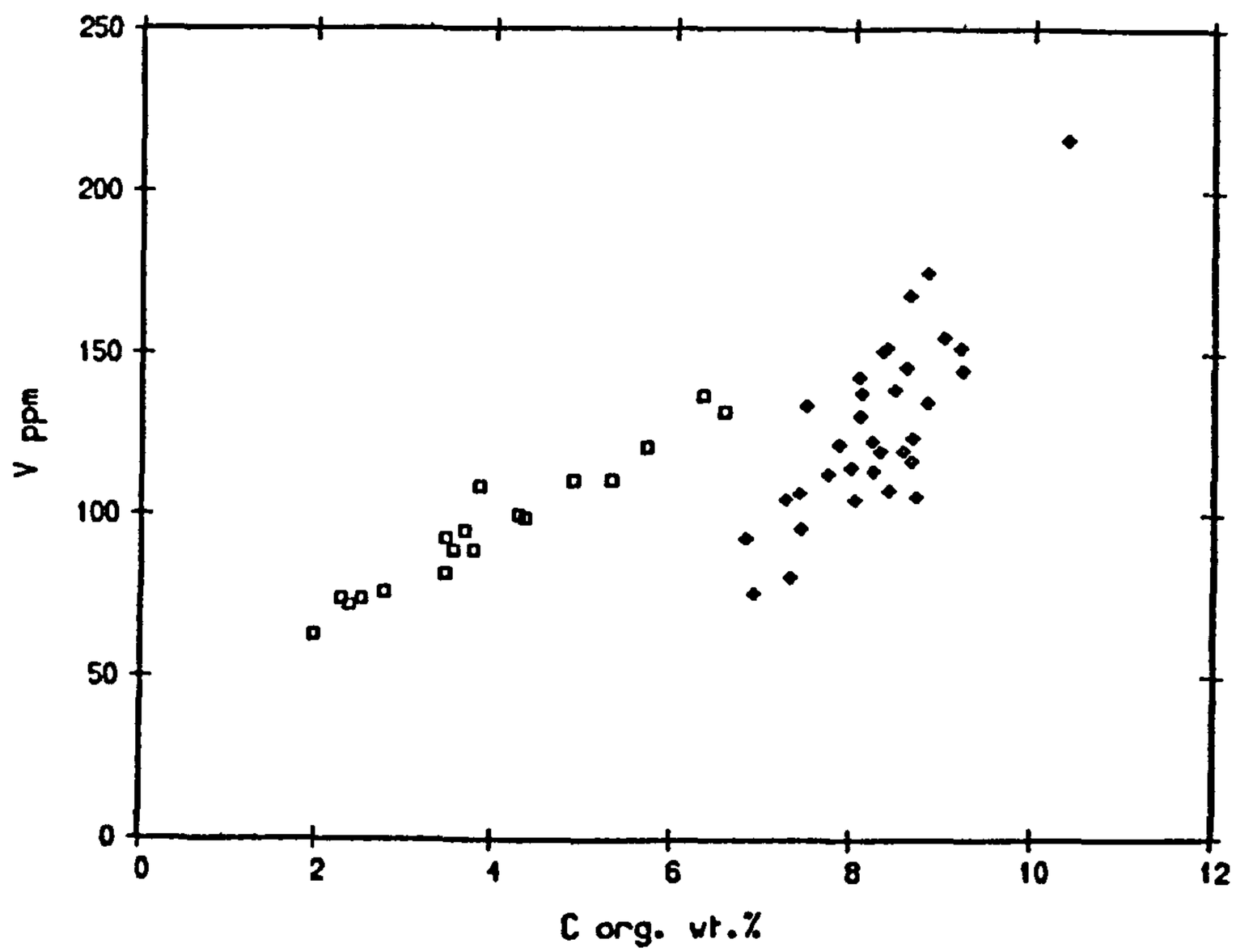

□ 145-17
◆ 163-8

FIGURE 5.2 The relationship between Pb, V and Zn with organic C in two Baja California shelf sediments (salt-free).

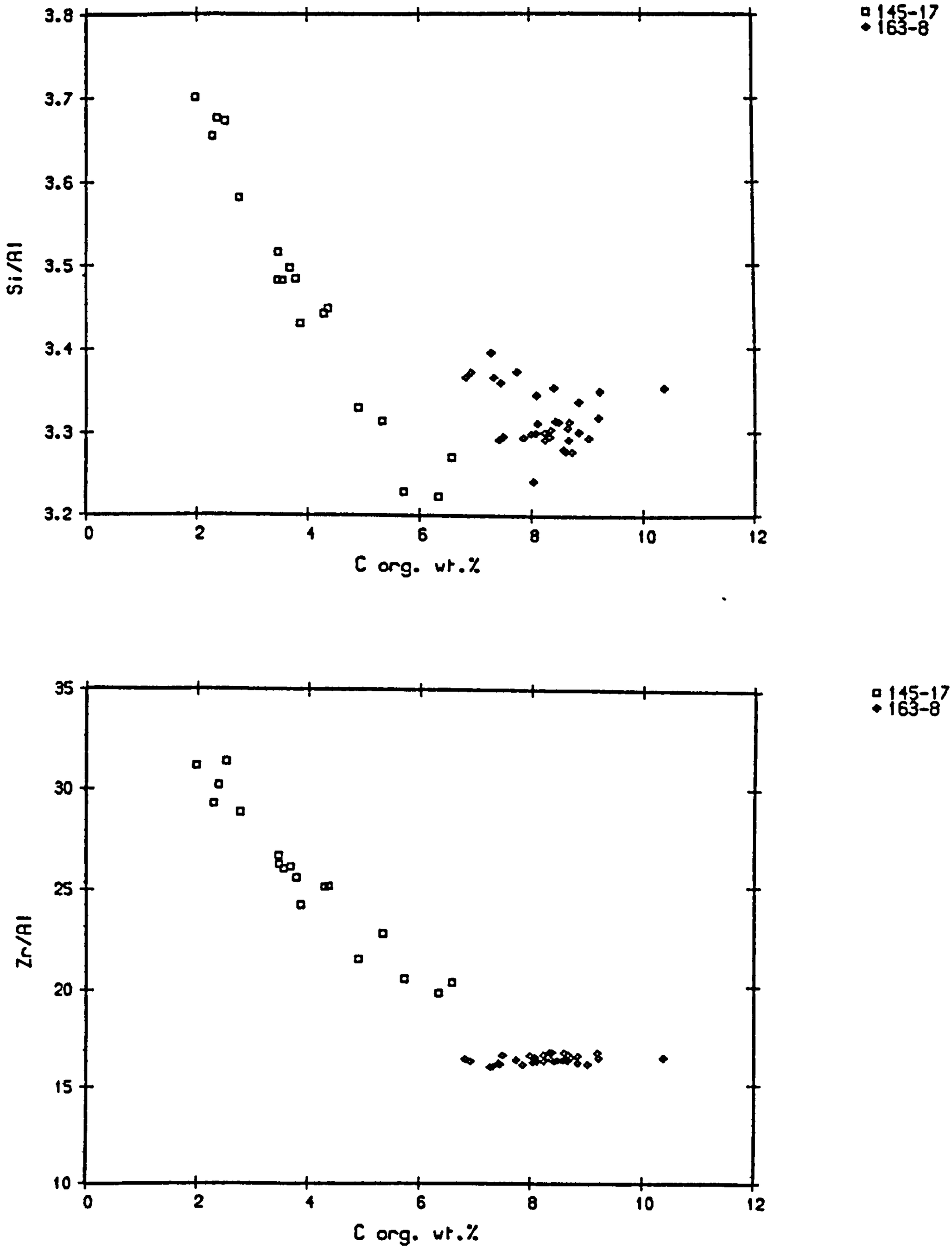

FIGURE 5.3 The inverse relationship between Si/Al and Zr/Al with organic C in station 145-17 (salt-free). The relationship suggests grain size control on organic C, although excess organic matter occurs in 163-8.

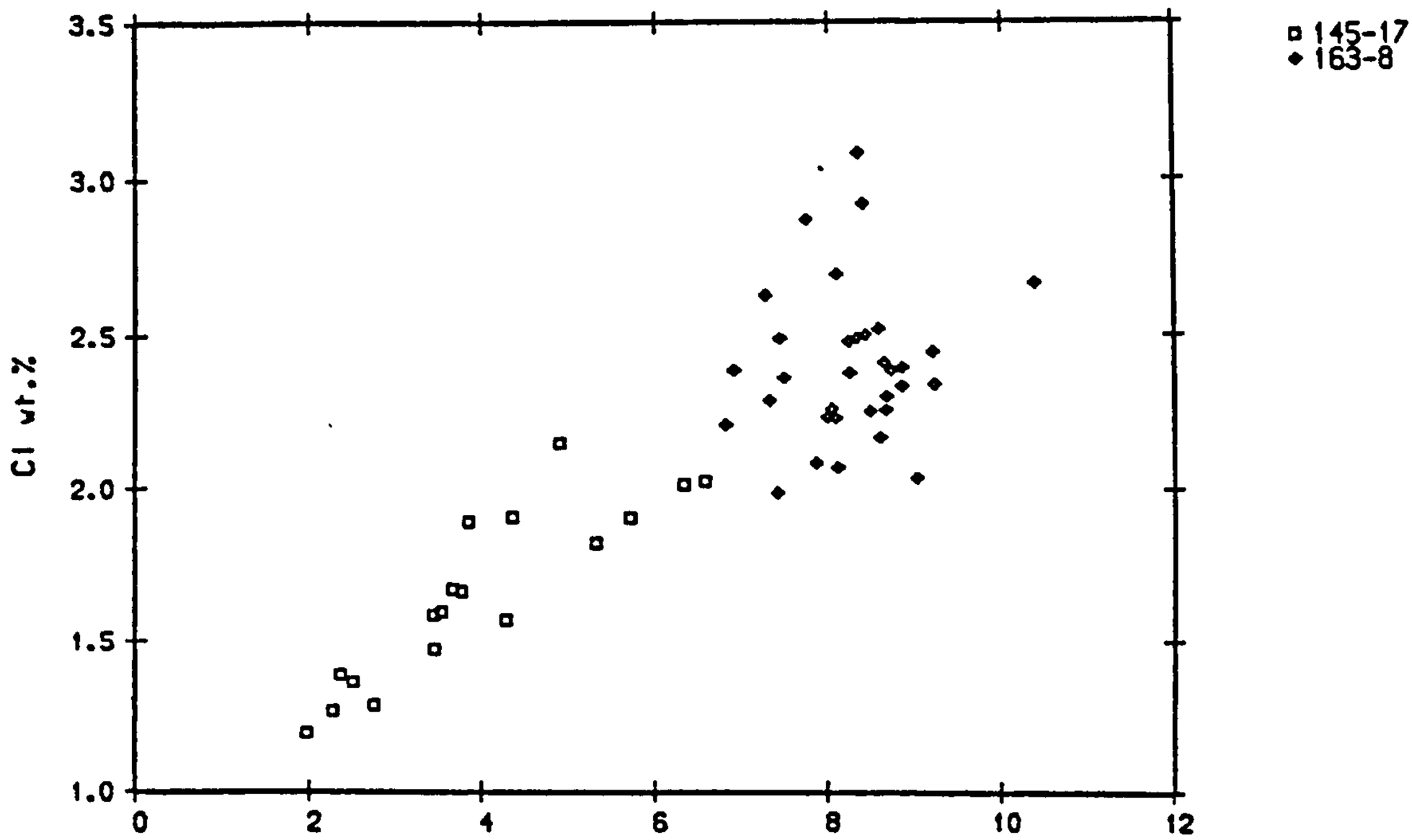

FIGURE 5.4 The relationship between Cl and organic C in stations 145-17 and 163-8. Cl is taken as an indicator of water content (see text for details) suggesting grain-size control on the organic C distribution.

but to confirm this hypothesis the same relationship should be found with water content. Unfortunately the water content of 145-17 was not measured, nevertheless the level of Cl in the sediments should be proportional to the pore water content (Chapter 2; Appendix C). Thus the correlation between C_{org} and Cl content in Figure 5.4 establishes the dominance of grain size and clay content in controlling the distribution of organic matter in the two shelf localities.

5.2.2 *The problem of trace metal enrichment*

With some knowledge of the sedimentological control on the distribution of C_{org} it is important to ascertain if the metal-organic C relationship in Figures 5.1 and 5.2 are due to trace metal incorporation by organic matter, or if the level of clay in the sediment is proportional to the metal content.

The trace metal contents and their ratios to Al for several near-shore environments are presented in Table 5.1. In addition, the average shale composition determined by Turekian and Wedepohl (1961) and the average metal contents for 145-17 and 163-8 are reproduced. In order to avoid dilution effects comparison should be made between the metal/Al ratios. Despite the high C_{org} contents of these two shelf sediments the trace metal enrichments are not particularly high with respect to average shale, except for Mo. The similarity in Pb/Al to Si/Al and Zr/Al downcore (Appendix C) suggests that this metal is concentrated in the coarse, detrital fraction.

The lack of trace metal enrichment, particularly Cu, Pb and Zn, is surprising as Brongersma-Sanders (1965, 1966) has

TABLE 5.1

THE DETRITAL GEOCHEMISTRY OF NEAR-SHORE SEDIMENTS

Element	Gulf of Paria platform sands[1]	Gulf of Paria basin clays[1]	Buzzards Bay[2]	Oregon-Washington Shelf[3]	Average Shale[4]	This study[5] 145-17	163-8
Al	3.24	8.79	3.68	6.88	8.00	6.33	4.92
Cr	31	93	33	191	90	83	148
Cu	7	17	18	28	45	20	31
Ni	16	31	11	100	68	51	76
Pb	13	22	25	10	20	10	9
V	79	146	45	93	130	96	128
Zn	-	-	-	-	95	76	81
Mo	-	-	-	-	2.6	6	7
Cr/Al	9.57	10.60	8.97	27.76	11.25	13.11	30.08
Cu/Al	2.16	1.93	4.89	4.07	5.63	3.16	6.30
Ni/Al	4.94	3.53	2.99	14.53	8.50	8.06	15.45
Pb/Al	4.01	2.50	6.79	1.45	2.50	1.58	1.83
V/Al	24.40	16.61	12.23	13.52	16.25	15.17	26.01
Zn/Al	-	-	-	-	11.90	12.01	16.46
Mo/Al	-	-	-	-	0.33	0.95	1.42

Al in wt.%, trace elements in ppm.

[1] Hirst (1962,a,b); Mean of 12 platform sands and 6 basin clays; analysis by wet chemistry (Al) and emission spectroscopy.
[2] Moore (1963); Mean of 125 sands and muddy sands, analysis by emission spectroscopy.
[3] White (1970); Mean of 45 sands and silts; analysis by XRF (Al) and emission spectroscopy.
[4] Turekian and Wedepohl (1961)
[5] Average of core 145-17 and 163-8; analysis by XRF.

ascribed the enrichment of these metals in bituminous shales, such as the Permian Kupferschiefer of northern Germany, to supply by plankton in regions of upwelling. Likewise, the large trace metal concentrations seen in Cretaceous Atlantic black shales (Brumsack, 1980; Brumsack and Lew, 1982) and attributed to uptake by the sediments from seawater under anoxic conditions is not evident. As the supply of organic matter to the Baja California shelf is undoubtedly from plankton rather than refractory, terrigenous derivation (Chapter 4) the analyses of 145-17 and 163-8 are compared with the data of Calvert and Price (1983) for surface, organic-rich, diatomaceous ooze recovered from the Namibian shelf off south west Africa (Figure 5.5). Their analyses reveal metal/Al ratios far in excess of average shale (marked by the arrow on the ordinate) supporting their contention that these metals are intimately associated with the organic fraction of the sediments. In contrast the Baja California sediments have much lower Cu, Ni and Zn relative to Al, but display a much greater correlation with C_{org}.

As the ratio of Cr, Cu, Ni, V and Zn to Al is close to that of shale in the Baja California sediments, and that the grain size of the sediment appears to be the major control on organic matter content, it is postulated that the correlation between metal and C_{org} is fortuitous; the level of clay in the sediment being the dominant factor in this instance. The implication for studies that have relied solely on metal/C_{org} correlation (Curtis, 1966; Spears and Amin, 1982) as evidence of initial organic input of trace metals is obvious.

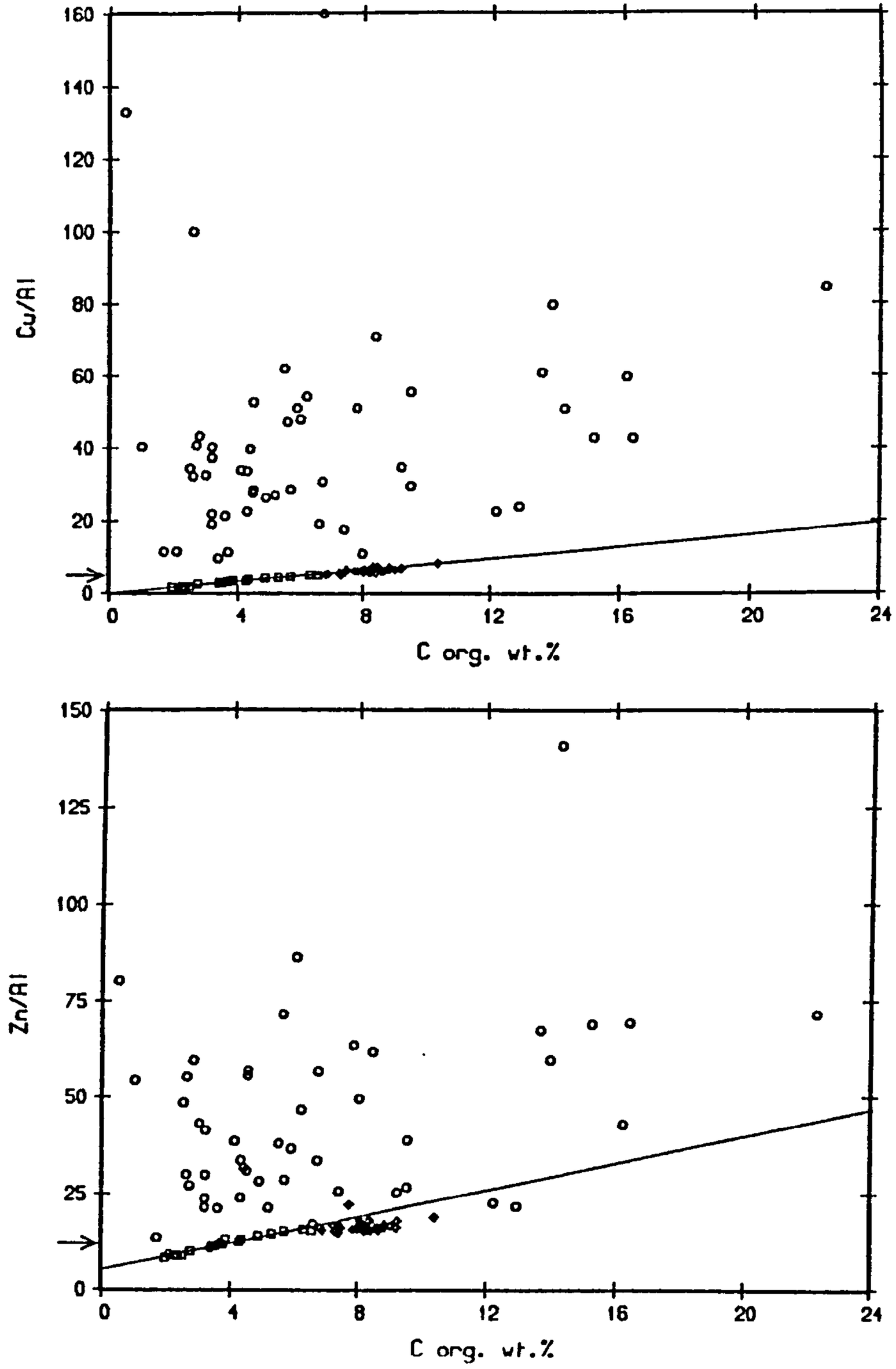

FIGURE 5.5 The correlation between Cu/Al, Ni/Al and Zn/Al with organic C in station 145-17 together with data from station 163-8 and diatomaceous, organic-rich sediments from the Namibian shelf (Calvert and Price, 1983), on a salt-free basis. The arrow on the ordinate marks the metal/Al ratio in average shale (Turekian and Wedepohl, 1961).

Regression data for station 145-17

	Slope	Intercept	r
Cu/Al *versus* C_{org}	0.806	-0.029	0.986
Ni/Al *versus* C_{org}	1.914	0.577	0.987
Zn/Al *versus* C_{org}	1.723	5.287	0.979

5.3 DISCUSSION

5.3.1 *Organic controls on trace metal geochemistry*

If clay hosts the majority of the metal concentration in the Baja California shelf sediments, why is the organic matter relatively barren in metals compared with the Namibian shelf? A comparison of the composition of marine organisms, mainly plankton, which are uncontaminated (Table 5.2) shows that only in the case of Zn can a direct contribution from plankton represent a significant proportion of the metal in the sediment (Calvert and Price, 1983). This casts further doubt on the biogenic enrichment mechanism suggested by Brongersma-Sanders (1965, 1966).

Nissenbaum and Swaine (1976) have drawn attention to the role of humic substances (of the humic acid and fulvic acid type) which comprise 40% of more of the organic matter in Recent sediments. Nissenbaum and Kaplan (1972) and Nissenbaum (1974) have shown marine humates to be genetically related to degraded planktonic material and to have high concentrations of trace metals: 600-4000 ppm Cu, 100-1000 ppm Ni, up to 600 ppm Pb, and up to 4000 ppm Zn (Nissenbaum and Swaine, 1976). The ability of soil humates to mobilise trace metals during diagenesis has been previously recognised by Baker (1973) and Rashid and Leonard (1973). If diagenetic uptake of metals by humics were to operate in the marine system either large quantities of planktonic matter would need to be decomposed, or metals would have to be leached from an inorganic carrier. Nissenbaum and Swaine (1976) felt that the inordinate amount of organic matter degradation required to produce the levels of trace metal enrichment in humics observed rules out the first option, concentrating on leaching as a possible mechanism. On

TABLE 5.2

THE ELEMENTAL COMPOSITION OF MARINE ORGANISMS

Author	Organism	Cr	Cu	Mo	Ni	Pb	V	Zn
Nicholls *et al* (1959)	plankton	-	238	3	65	83	-	-
Sugawara *et al* (1961)	plankton	-	-	0.38	-	-	-	-
Vinogradova Koval'skiy (1962)	plankton	-	200	10	36	5	-	2600
Bowen (1966)	brown algae	-	11	0.45	3	8	-	150
Yamamoto and Fujita (1966)	seaweed	1.2	14	0.3	2.8	-	3.1	150
Presley *et al* (1972)	plankton (diatoms)	-	13	5	9	-	-	165
Martin and Knauer (1973)	zoo- and microplankton	1	11.5-57.5	-	8.4-11.6	2.1-31	3.1	180-780
Bostrom *et al* (1974)	plankton	54	340	-	83	160	4.2	3700
Fowler (1977)	zooplankton	4.9	39	-	8.1	11	-	483
Moore and Bostrom (1978)	plankton	55	280	56	93	64	21	880

All trace elements in ppm.

the Namibian shelf the reverse seems more likely, as mineralogical components are scarce whilst plankton availability is very great. Brumsack and Geiskes (1983) found dissolved organic matter to be enriched in Mo (prior to sulphide diagenesis) and Cr in interstitial waters from anoxic sediments of the Gulf of California. Mo incorporation occurs due to the reduction of Mo^{6+} to Mo^{5+} which is easily sorbed (Szilagyi, 1967) by the organic humics acting as both a reducing agent and absorption or ion exchange sites. Cr redox chemistry is similar; Yamazaki *et al* (1980) have shown that Cr^{3+} forms uncharged and/or negatively charged organic complexes in the presence of humics within the neutral pH range.

Despite this knowledge the mechanism of metal enrichment off Namibia is unresolved (Calvert and Price, 1983). Price (pers. comm.) indicates that in some of the very organic-rich cores metal concentrations decrease below the surface. This, together with the extremely fluid, acoustically transparent (Calvert and Price, 1983) nature of the sediment, suggests a boundary zone, above the solid sediment/water interface, where high levels of reactive organic matter undergo condensation and polymerisation forming organic substances (humics). These are available to take up metals being recycled diagenetically during plankton degradation. Such conditions can only exist on a protected shelf underlying high productivity waters. It may be that metal concentrations are maintained in this "organic soup" without being incorporated into the sediment column; the sediments themselves reflecting only high C_{org} levels and trace metals associated with sulphide enrichment. The shelf sediments

off Baja California have been subjected to a large detrital input and/or current winnowing in the recent past shown by the high surface Si/Al and Zr/Al ratios (Figure 3.4; Appendix C). Any surficial organic-rich veneer may have been removed leaving only relatively refractory C_{org} in the sediment column.

5.3.2 *Sulphide control on trace metal geochemistry*

In addition to possible organo-metallic reactions occuring at an early stage in the sediment depositional history, the formation of diagenetic Fe sulphides represents an important sink for trace metals. Pyrite (FeS_2) is the most ubiquitous sulphide, often occuring as framboids or spherules (Chapter 8). The mechanism of its formation is now well understood (Berner, 1964, 1970, 1982, 1984). However, less is known about the coprecipitation of trace metals. Calvert (1976) has suggested that the Mo enrichment often seen in anoxic sediments (eg the Baltic, Black Sea, Oslo Fjord and South-west Africa) occurs by a coprecipitation reaction with FeS, after the work by Korolev (1958) and Bertine (1972). Certainly, Mo has the greatest enrichment over shale values in the shelf sediments off Baja California and the correlation between Fe and S (Figure 5.6), and Mo and S (Figure 5.7) supports the removal of Mo from seawater by this coprecipitation mechanism with Fe monosulphide under anoxic conditions:

$$FeS\ (amorph) + MoO_2S_2^{2-} + H_2S + H^+ \rightarrow FeS.MoS_3\ (amorph) + 2H_2O$$

$$FeS.MoS_3\ (amorph) \rightarrow FeS\ (tetr.) + MoS_3$$

The S intercept in Figure 5.7 may represent pyrite which does

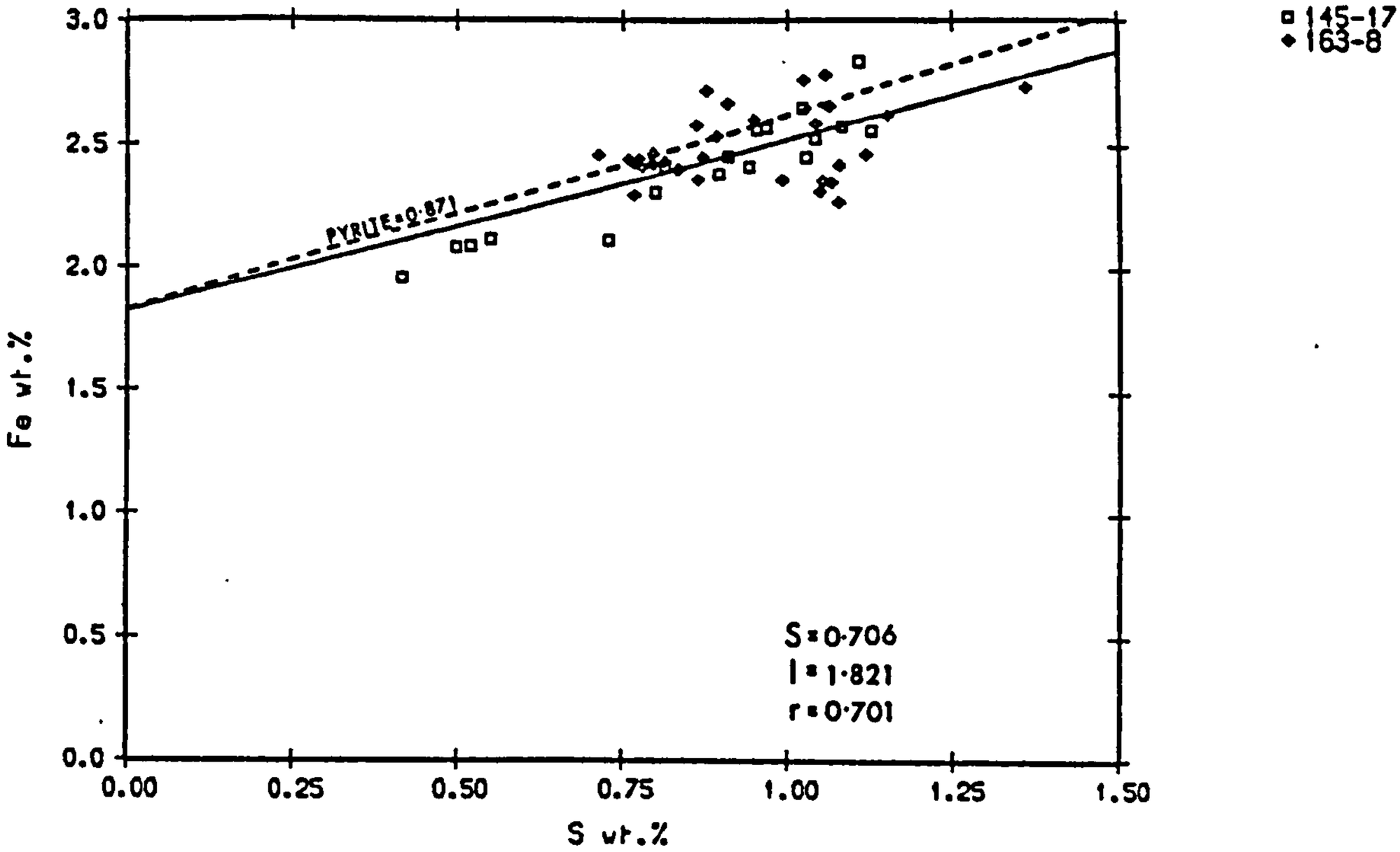

FIGURE 5.6 The correlation between Fe and S in two cores from the Baja California shelf (salt-free). The dashed line indicates stoichiometric FeS_2 (pyrite), using the same Fe intercept.

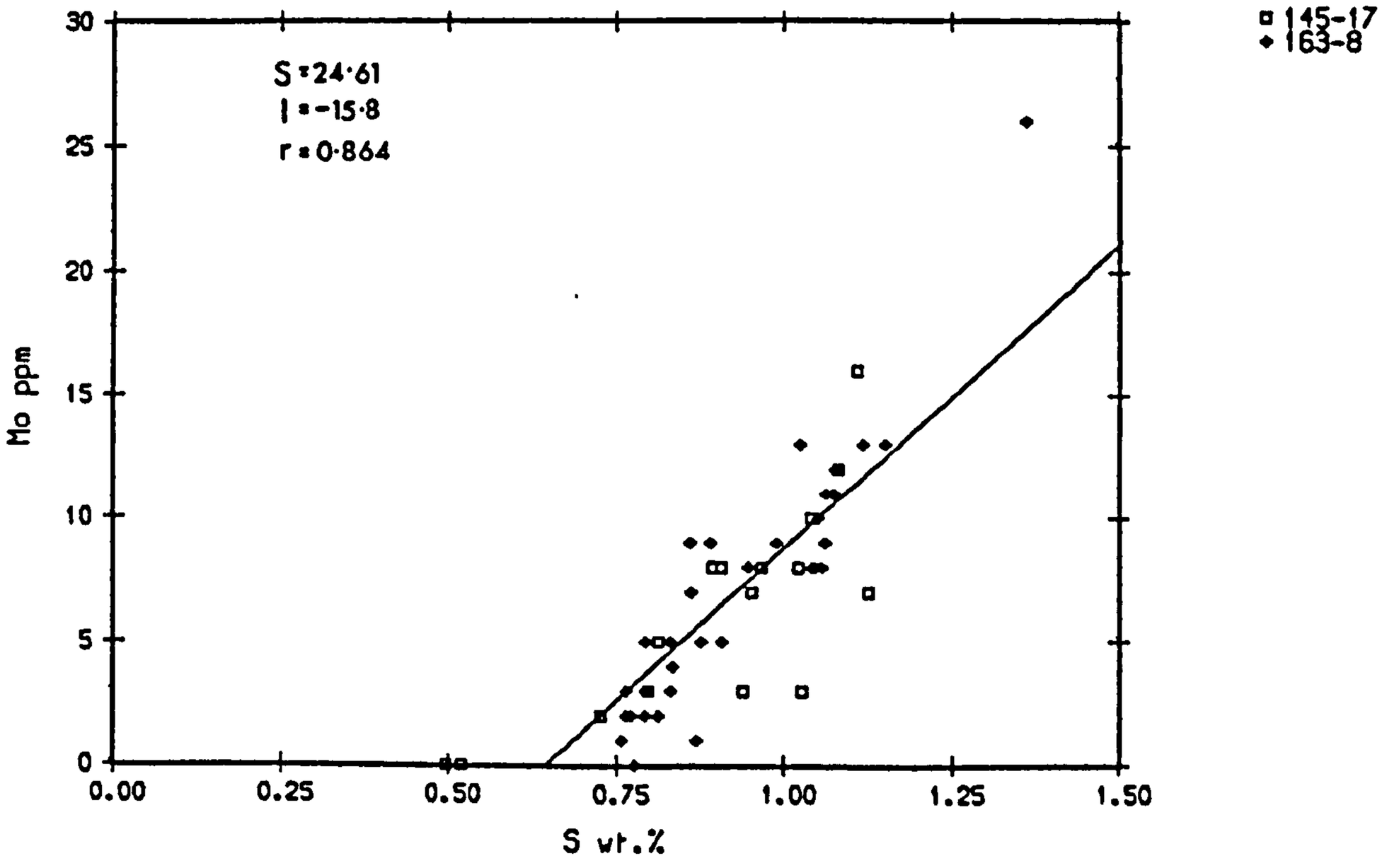

FIGURE 5.7 The correlation between Mo and S in two cores from the Baja California shelf (salt-free).

not hold any Mo in its structure.

The relative partitioning of Mo between sulphide phases and humics (Nissenbaum and Swaine, 1976) is unresolved. Volkov and Fomina (1974) have suggested that in Black Sea sediments a large proportion of Mo is fixed by organic substances although sulphide may host Mo in the surface sediments; however this is not supported by their surface Mo/S correlation. Similarly, no correlation was found with Ni and Cu, only Co showed a relationship with total S in sapropelic muds. Calvert (1976) believes that most Mo in H_2S-bearing seawater is removed by coprecipitation with FeS, whereas most of that in anoxic sediments is associated with organic materials. This simplistic model requires further work, but obviously the cycling of organic matter and the transfer of Mo to the sulphide phase in surface sediments is very important.

Data on other trace metals incorporated during pyrite formation is sparse. Volkov and Fomina (1974) found CoO, NiO and CuO to comprise on average 0.017%, 0.15% and 0.128% of the pyrite formed in Black Sea sediments. Thus enrichments of these metals due to pyrite formation in Baja California shelf sediments is undetectable.

CHAPTER 6

THE DIAGENESIS OF MANGANESE AND RELATED METALS

6.1 INTRODUCTION

Detailed solid phase analysis of manganese and associated trace metals (Mo,Ni,Zn,Cu) was carried out to elucidate processes controlling metal composition and distribution. The aim of this study is; (1) To investigate the distribution of Mn and related trace metals in sediments from the organic-rich hemipelagic environment to the red clay of the oceanic environment; (2) To ascertain the importance of mineralogy in modifying trace metal uptake and release during redox processes; (3) To examine the behaviour of trace metals with Mn in a range of diagenetic environments both horizontally and vertically in time and space.

6.2 RESULTS

6.2.1 *Description of manganese enrichment*

Figures 6.1 and 6.2 show the clear surficial enrichment of Mn in the hemipelagic region off the Baja California continental margin typified by stations 163-7, 163-14 and 163-10. Similar enrichments have been described by Sawlan and Murray (1983) at stations 145-7 and 145-8. A variation in the degree of enrichment for the surface samples is seen, increasing landwards from 1.83 wt.% in 163-10, through 2.40 wt.% in 163-14 to 3.58 wt.% in 163-7 (Table 6.1). Each of these three profiles display subsurface maxima, here defined as the Mn redoxcline (see also Chapter 4). The depth of this redoxcline decreases landwards, from 9 cm in both 163-10 and 163-14 to 3 cm in 163-7.

TABLE 6.1

MANGANESE AND TRACE METAL CONCENTRATIONS IN OCEANIC SEDIMENTS OFF BAJA CALIFORNIA

Station	depth	Mn	Mo	Ni	Zn	Cu	Mn/Al	Mo/Al	Ni/Al	Zn/Al	Cu/Al
	cm	wt.%	ppm	ppm	ppm	ppm		$x10^{-3}$	$x10^{-3}$	$x10^{-3}$	$x10^{-3}$
OXIC METAL CONCENTRATIONS											
163-7	0-1	3.58	63	238	287	287	0.482	0.85	3.20	3.86	3.86
163-14	0-1	2.40	37	431	333	294	0.313	0.48	5.62	4.34	3.83
163-10	0-1	1.83	17	267	255	317	0.232	0.22	3.38	3.22	4.01
163-9	0-1	1.43	21	302	208	357	0.180	0.27	3.81	2.63	4.51
163-9	20-22	1.07	18	215	182	264	0.130	0.22	2.62	2.22	3.22
SUBOXIC METAL CONCENTRATIONS											
163-7	20-22	0.08	n.d.	167	281	219	0.010	n.d.	2.19	3.68	2.87
163-14	20-22	0.48	n.d.	148	209	182	0.070	n.d.	2.18	3.08	2.68
163-10	20-22	0.86	n.d.	217	251	283	0.108	n.d.	2.73	3.16	3.54
average shale (Turekian and Wedepohl, 1961)		0.085	27	68	165	45	0.011	0.34	0.85	2.06	0.56

n.d. - not detectable

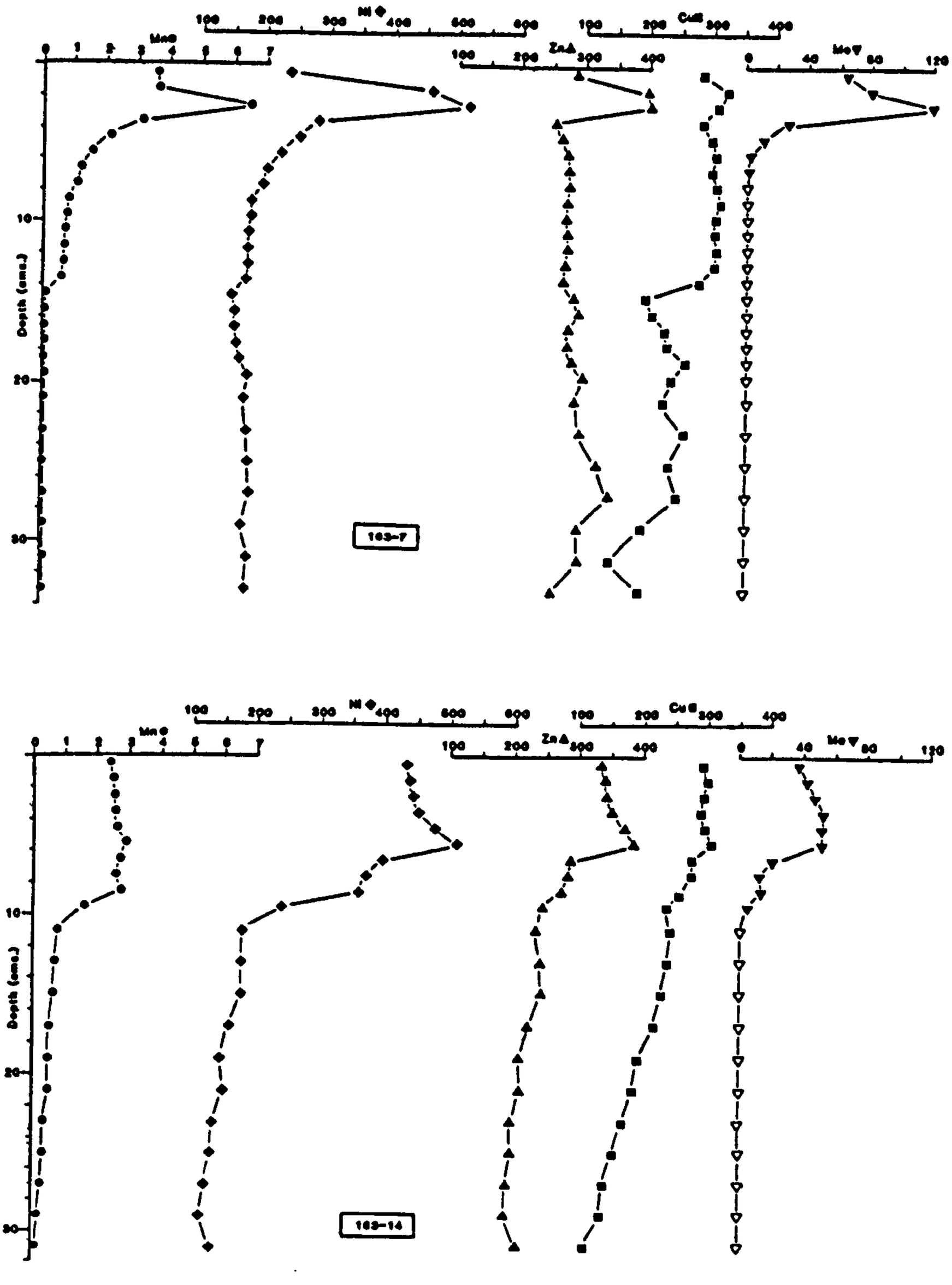

FIGURE 6.1 Profiles of Mn (wt.%), Ni (ppm), Zn (ppm), Cu (ppm) and Mo (ppm) with depth in hemipelagic cores 163-7 and 163-14 off Baja California (salt-free).

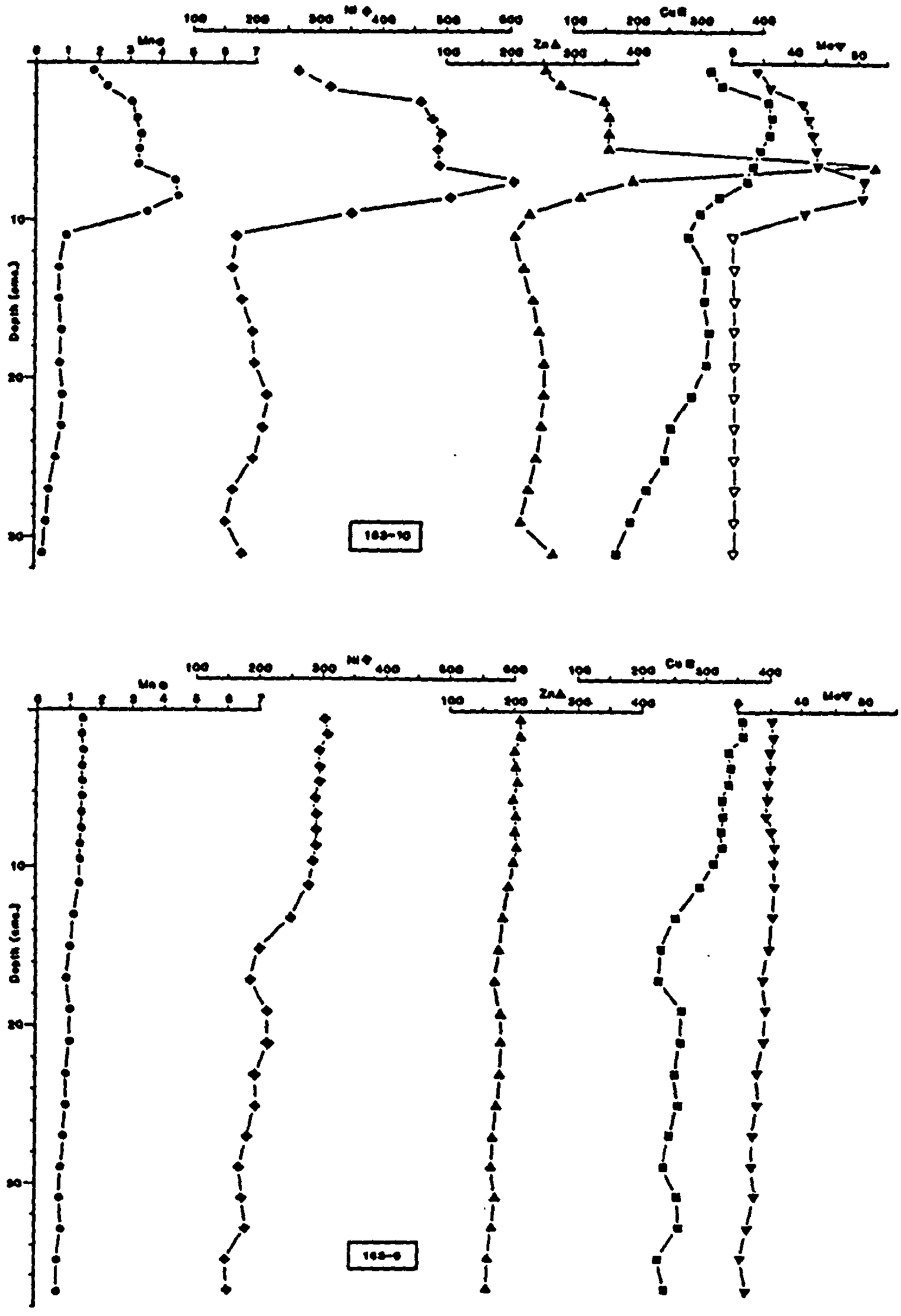

FIGURE 6.2 Profiles of Mn (wt.%), Ni (ppm), Zn (ppm), Cu (ppm) and Mo (ppm) with depth in core 163-10 (hemipelagic) and 163-9 (pelagic) off Baja California (salt-free).

Beneath this level the concentration of Mn in these three hemipelagic cores is also very different. In 163-10 Mn increases slightly from 0.73 wt.% at 13 cm depth to 0.86 wt.% at 21 cm depth, before falling to 0.23 wt.% at the bottom of the core. Station 163-14 displays a monotonic decrease from 0.74 wt.% below the redoxcline to 0.12 wt.% at the base of the core. In contrast, 163-7 is best described by a quasi-exponential decrease in Mn from 6.49 wt.% at the redoxcline to 0.61 wt.% at 14 cm depth where it steps down to a uniform concentration of 0.08 wt.% as far as the core base.

Profiles of Mn^{4+} (for analysis method see Appendix B.6) in Figure 6.3 closely mimic that of total Mn with initial concentrations ranging from 1.37 wt.% in 163-10 to 1.83 wt.% in 163-14 and 2.43 wt.% in 163-7. Mn^{4+} concentrations decreases sharply at the redoxcline, but maintain measurable quantities until 30 cm depth in 163-10 and 163-14 and 15 cm depth in 163-7. Recalculated in terms of manganese oxide stoichiometry* (Figure 6.3) all three profiles have lower x values in the top 3 cm of the sediment column, reaching a maximum above the redoxcline in 163-10 and 163-14, and below in 163-7. A steady decrease in oxidation state below the redoxcline is observed in 163-10 and 163-14, and from 9 cm depth in 163-7. This latter core is noted by its sharp decrease in oxidised Mn below 15 cm,

*The oxidation state of Mn is expressed as MnO_x (Murray and Balistieri, 1983) where

$$x = 1 + 1/2 \frac{[\,2Mn^{4+} + Mn^{3+}\,]}{[\,Mn^{4+} + Mn^{3+} + Mn^{2+}\,]}$$

By this notation samples of pure Mn^{4+}, Mn^{3+} and Mn^{2+} have values of 2.0, 1.5 and 1.0 respectively. As this method cannot distinguish between Mn^{4+} and Mn^{3+}, MnO_x has been expressed as if all the oxidative capacity of the sample is due to Mn^{4+}.

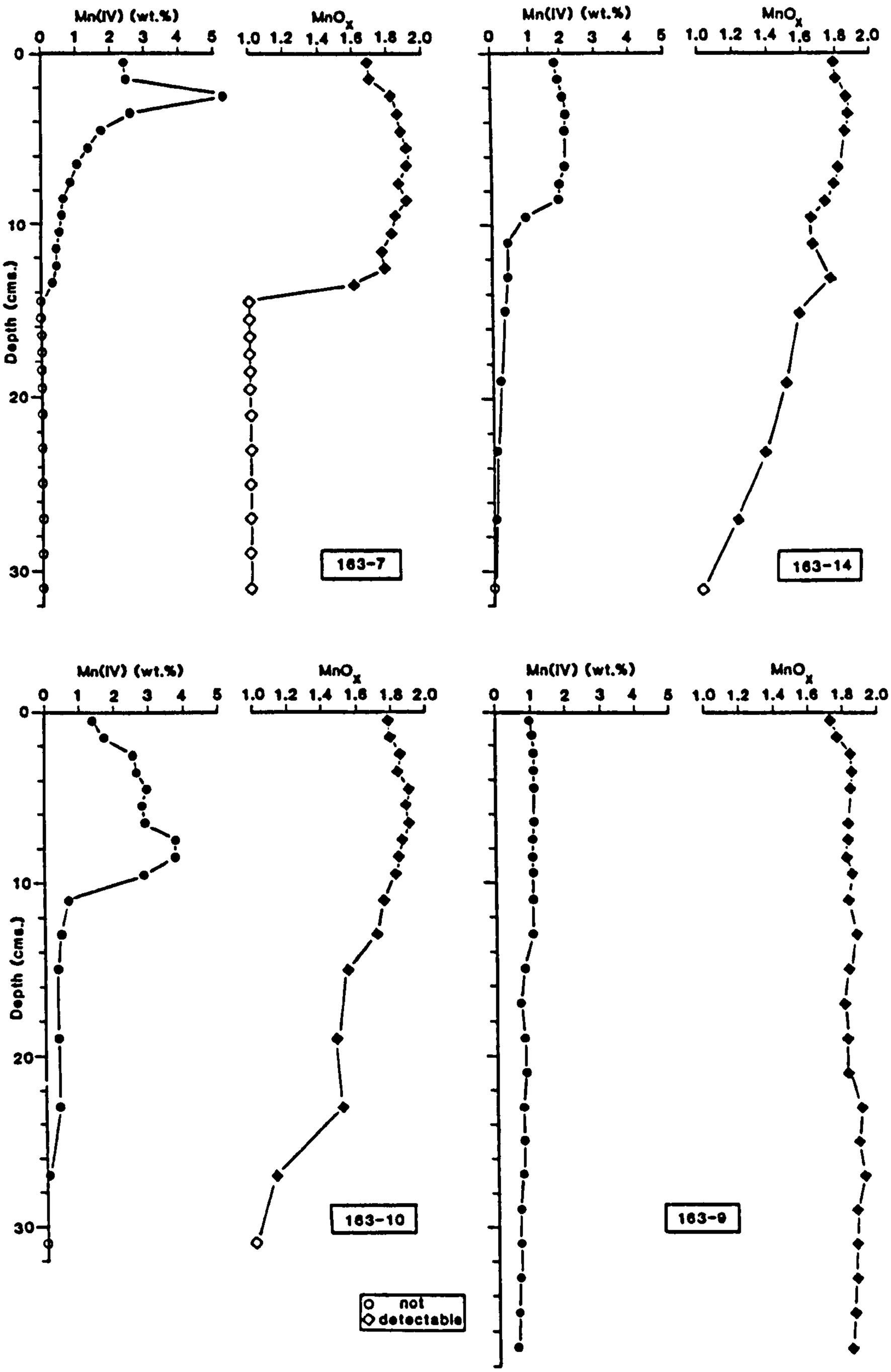

FIGURE 6.3 Profiles of Mn^{4+} and Mn oxide stoichiometry (see text for details) with depth in oceanic sediments off Baja California (salt-free).

whereas the other two hemipelagic cores reveal the presence of oxidised Mn species down to 30 cm depth. The behaviour of Mn in the oceanic environment has been studied with reference to core 163-9. In this core total Mn decreases steadily from 1.43 wt.% at the surface to 0.72 wt.% at 38 cm depth (Figure 6.2). No redoxcline is evident. Mn^{4+} is again closely related having a surface value of 0.97 wt.% and 0.53 wt.% in the deepest sample (Figure 6.3). Apart from an increase of 1.73 to 1.85 over the top 3 cm of the sediment column there is essentially no change in the oxidation state of the Mn in core 163-9.

The shelf and slope sediments, 163-5, 163-12, 163-8, 163-11, 145-17 and 163-13 all have constant total Mn values of 0.02-0.04 wt.%. Mn oxidation states have not been measured on these cores.

6.2.2 Description of Mn-associated trace metal enrichments

Mo, Ni and Zn closely follow the distribution of total Mn and Mn^{4+} in the hemipelagic and oceanic environment off Baja California (Figures 6.1 and 6.2). Surficial concentrations of these metals, together with Mn, are presented in Table 6.1. In the hemipelagic sediments all three metals fall in concentration at the Mn redoxcline, however their suboxic baseline concentrations are very different (Table 6.1). Mo collapses to undetectable values; Ni falls to 140-200 ppm but shows a slight increase at 22-24 cm depth in 163-7 and 163-10. Zn falls to 250-280 ppm with subsurface enrichments at 26-28 cm depth in 163-7 and 163-10. The large Zn value (775 ppm) at 6-7 cm depth seems real based on repeat analysis and examination of XRF raw count data.

Cu exhibits somewhat different behaviour. In 163-7 the subsurface peak is just above that of Mn, whilst a fall-off from 276 ppm to 192 ppm occurs where Mn^{4+} disappears. Station 163-14 has Cu enrichment coinciding with the Mn^{4+}profile, whilst in 163-10, Cu surficial enrichment is clearly seen above the redoxcline, together with a small peak at 16-20 cm depth.

In the oceanic sediment of core 163-9 Mo, Ni and Zn also decrease steadily with total Mn and Mn^{4+}. No pronounced maxima are seen and Mo is always detectable. Cu behaves similarly in this core. In contrast, 163-15 shows spikes of these metals (Appendix C) interpreted as micronodules that were not removed prior to analysis.

Due to the absence of Mn in the shelf and slope environment the behaviour of Mo, Ni, Zn and Cu are not discussed here but have been described in Chapter 5.

6.3 THE DISTRIBUTION OF MANGANESE AND RELATED TRACE METALS

6.3.1 *Introduction*

The early work of Krauskopf (1956) suggested that MnO_2 is one of the most important solid phases controlling trace metal concentrations in natural sea water environments. Mn is a transition metal capable of existing in a number of different oxidation states (2+,3+,4+,6+,7+), however, 2+ and 4+ are the lowest and highest found in nature. It is possible that ephemeral intermediate states (eg. hausmannite containing

Mn^{3+}) may exist metastably (Bricker, 1965). Usually, Mn oxide minerals contain more than one oxidation state of Mn but whether 3+ occurs in the solid state or through equal distribution of 2+ and 4+ is open to debate (Bricker, 1965).

Since the work of Lynn and Bonatti (1965) in which they proposed that Mn dissolves upon burial in reduced sediments, then slowly migrates to accumulate in an enriched surficial oxidised zone, there have been many such studies (Li *et al*, 1969; Krishnaswami, 1976; Froelich *et al*, 1979; Heath and Lyle, 1981; Burdige and Geiskes, 1983; Sawlan and Murray, 1983; Graybeal and Heath, 1984) addressing the problems of distribution, mobilisation, precipitation and kinetics of this transition metal. Froelich *et al* (1979) have presented detailed pore water analyses in conjunction with solid phase data from the north equatorial Atlantic. This trend has continued with the work of Sawlan and Murray (1983) on sediments from the Guatemala basin and the Baja California margin. The association of Ni and Zn with Mn was noted by Krishnaswami (1976) before being looked at experimentally by Balistrieri and Murray (1984), who investigated the nature of the sorption of various trace metals onto MANOP site H interfacial sediments. Bischoff *et al* (1979) used normative calculations to partition the sediment geochemistry of DOMES sites A, B and C. Graybeal and Heath (1984) report on the passive behaviour of Ni and Zn with Mn during its remobilisation at MANOP sites M and H.

Sawlan and Murray (1983) report dissolved concentrations of Ni and Cu together with Mn and NO_3^- for the Baja California margin. Three studies by Klinkhammer (1980), Klinkhammer *et al*

(1982) and Callender and Bowser (1980) provide additional data on the distribution of dissolved Cu and Ni in abyssal sediments. These workers have shown conclusively that the distribution of oxidants, reductants and metabolites in marine sediments is related to the oxidation sequence of organic matter (Chapter 4) (Bender *et al*, 1977; Froelich *et al*, 1979; Emerson *et al*, 1980). In this model the oxidation of organic matter proceeds by the oxidant producing the greatest free energy change (ΔG^{o}) (Table 4.4). The depth at which these reactions occur is governed by the interplay between the level of organic matter, sedimentation rate, oxygen content of the overlying sea water and the availability of other oxidants.

The distribution of metals in the dissolved and solid phases with depth provide a valuable insight into their behaviour with diagenesis. Klinkhammer (1980) defines two groups; Group A (Mn, Ni, Fe) metal concentrations are dominated by dissolved concentration gradients below the oxidised zone. The correlation between Ni and Mn in the pore waters suggests that Ni is closely associated with Mn oxides being reduced in the sediments. Group B elements have pore water profiles that change within the oxic zone. Cu is an example of a metal with this behaviour, increasing in concentration just below the subsurface (Sawlan and Murray, 1983). However, Cu also seems to be released by Mn oxide reduction, though not to the same extent as Ni. During Fe reduction both metals decrease in concentration in the pore waters suggesting that early formed sulphides may act as a sink for these metals.

The analyses for Mn, Mo, Ni, Zn and Cu presented here support the established model. As C_{org} content of the sediment

increases landwards, so the thickness of the oxidised Mn layer becomes less; however, the colour change of these sediments (Appendix A) does not correspond to this solid phase Mn spike. This discrepancy may be due to the brown-green colour change resulting from Fe^{3+} to Fe^{2+} reduction (Lyle, 1983), occurring at a deeper depth than Mn reduction. Work by Sawlan and Murray (1983) has shown that whilst NO_3^- and MnO_2 reduction follow the proposed model there appears to be a zone of diffusion separating the depth of NO_3^- and Mn^{2+} oxidation from the depths of NO_3^- and MnO_2 reduction, manifested by the top of the Mn^{2+} ion gradient occurring within the linear portion of the NO_3^- gradient. They suggest that the discontinuous nature of the reactions may be due to limits on the amount of utilisable C_{org} in the sediment. Indeed, the maximum dissolved Mn^{2+} (ie when $dMn^{2+}/dZ = 0$) in 145-7 is 45 µmol/kg compared with 80 µmol/kg in 145-8, corresponding to an increase in C_{org} landwards. In their cores 145-7 and 145-8 (Figure 1.1; approximately equivalent to 163-10 and 163-7 respectively) then complete NO_3^- consumption occurs at 30 cm and 18 cm respectively, whilst Mn^{2+} occurs at 6 cm in both. In their red clay station, 145-6, (equivalent to 163-9) NO_3^- is present throughout the core, whilst no Mn^{2+} is detectable.

Figures 6.1 and 6.2 indicate that the redox behaviour of Mn in sediments containing organic matter strongly affects the solid concentrations of Ni, Zn and Mo and to a lesser extent, Cu. However, data on the mechanism by which Mn adsorbs trace metals in the natural environment, and then releases them to solution during reduction, is somewhat limited. Whilst information on the adsorbtion chemistry of manganese oxides is readily available, details on the redox state of MnO_2 in the

oceanic environment have only recently appeared (Balistrieri and Murray, 1982; Kalhorn and Emerson, 1984; Murray *et al*, 1984) save for a few early analyses by El Wakeel and Riley (1961).

Here, I will attempt to interpret my data on the oxidation state of Mn through the early diagenetic cycle as outlined above and in Chapter 4.

6.3.2 *The mineralogy and oxidation state of solid phase manganese*

Klinkhammer and Bender (1980) argue on thermodynamic grounds that the solid, oxidised form of Mn that is most likely to be in equilibrium concentrations in ocean water (a pH of 8.2) is hausmannite (Mn_3O_4). Morgan (1967) and Stumm and Giovanoli (1976) also present evidence from XRD that hausmannite is often the initial precipitate in laboratory experiments. Hausmannite is a metastable, mixed valence, oxide which should undergo further oxidation to a more stable phase on ageing (Stumm and Morgan, 1970). Similarly, Kalhorn and Emerson (1984), after work by Hem (1981), suggest that the metastable Mn oxyhydroxide, fietknechite, may be the intial precipitate and it too to increase in oxidation state with age. In contrast, Chukhrov *et al* (1979) and Burns and Burns (1979) state that the main oceanic mineral of oceanic sediments is vernadite, a poorly crystallised manganese oxide identical to *d*-MnO_2. Chukhrov *et al* (1979) claim that vernadite, as described by Betekhtin (1940) has precedence over *d*-MnO_2, and

following the example of Burns and Burns (1979) its usage is retained here for naturally-formed *d*-MnO_2. One should note the opposite opinion of Giovanoli (1980) on the subject of vernadite and its structure.

Much of the work on Mn mineralogy in the marine environment has been based on nodules. Early work on these Mn nodules (Buser and Grutter, 1956) identified the primary Mn phase as *d*-MnO_2 characterised by the absence of basal reflections and disordering of the structure. Since then nodules from different oceanic environments have been found which are characterised by different Mn minerals. Nodules from deep sea abyssal plains tend to be composed of todorokite ("10 Å manganite") and birnessite ("7 Å manganite") (Burns, 1976), whilst seamount nodules are predominantly *d*-MnO_2 (Barnes, 1967). Today vernadite is often considered synonymous with disordered birnessite having broad, diffuse XRD lines at about 2.40 and 1.42 Å, with little or no suggestion of additional lines at around 7.0-7.2 Å and 3.5-3.6 Å which are the diagnostic basal planes of birnessite (Burns, 1976).

Structurally, vernadite and birnessite are similar in that they are composed of edge shared $[MnO_6]$ octahedra formed into sheets. Two structural models exist; chalcophanite and lithiophorite (Wadsley, 1952, 1955). In chalcophanite single sheets of water molecules lie between layers of edge-shared $[MnO_6]$ octahedra, with Zn atoms located between the water layer and the oxygens of the $[MnO_6]$ layer. The spacing between the two $[MnO_6]$ layers is 7.17 Å. In lithiophorite the edge-shared $[MnO_6]$ octahedra alternate with layers of $(Al,Li)(OH)_6$ octahedra, resulting in a spacing of 9.5 Å between layers.

Natural chalcophanites differ from their ideal formula of

$Zn^{2+}Mn_3{}^{4+}O_7.3H_2O$. Often water contents are variable whilst a deficiency in Mn^{4+} ions usually leads to the number of cations exceeding 4 in the formula unit. Mn^{2+} can substitute for Mn^{4+} in the linked octahedra, whilst additional cations can occur between the H_2O layers and the $[MnO_6]$ layers (Burns, 1976).

In vernadite the crystallites are only 2-3 atomic layers thick; virtually two dimensional (Buser and Graf, 1955). Consequently, these fragments of the chalcophanite structure have a high proportion of vacancies on their exterior surface available for the adsorbtion of cations, as well as within the sheets of edge-shared $[MnO_6]$ octahedra. This results in a strongly negatively-charged surface which is very acidic compared with other oxide surfaces in the marine environment (Balistrieri and Murray, 1982). These observations have been verified experimentaly by Morgan and Stumm (1964) who showed that synthetic δ-MnO_2 has a zero point of charge (ZPC) at a pH of 2.8 in the absence of absorbed ions other than H^+ and OH^-. As the pH rises so the cation exchange capacity increases. δ-MnO_2 adsorbs Mn^{2+} strongly (>0.5 mol of Mn^{2+} per mol of MnO_2 in the alkaline range), whilst approximately 1 mole of H^+ is released per mol of Mn^{2+} adsorbed. The chemistry of this mineral forms the basis for explaining the uptake and fixation of trace metals by manganese oxides in the marine environment.

6.3.3 *Discussion*

El Wakeel and Riley (1961) could see no systematic variation in Mn oxidation state for their analyses which ranged from $MnO_{1.60}$ to $MnO_{2.00}$ for those samples in the Pacific. Their closest sample to the Baja California margin (sample 25;

$31^{o}05'N$, $135^{o}24'W$, described as a red clay) was also their lowest value, $MnO_{1.60}$. Murray *et al* (1984) analysed a suite of Mn nodules and sediments and found that in the sediments x stays uniformly high (1.90-1.95) until dissolved Mn^{2+} increases in the pore water and then x decreases. They conclude that the adsorption of Mn^{2+} appears to cause the decrease in x. Kalhorn and Emerson (1984) found similar phenomena in addition to a subsurface minima (1.5 cm depth) in MnO_x at MANOP site H.

It follows that any model proposed to describe the mechanism of trace metal enrichment in hemipelagic sediments off Baja California will have to account for the following:

(1) An intially low value of MnO_x (approximately 1.75) increasing to 1.85 within 3-4 cm of the sediment/water interface.

(2) A maximum value of MnO_x that does not always coincide with the Mn redoxcline.

(3) The presence of Mn including Mn^{4+} below the redoxcline.

(4) The behaviour of trace metal to Mn^{4+} and trace metal to total Mn accumulation for the oxic zone along the Baja California transect.

The oxidation state of freshly precipitated Mn and its early diagenesis

If Klinkhammer and Bender (1980) and Kalhorn and Emerson (1984) are correct in their conclusion that hausmannite, or fietknechite, is the stable form of the solid-phase Mn oxide in ocean water then the Mn phase accumulating on the sea floor may have an inherent low stoichiometry. In contrast, Chukhrov *et al*

(1979) and Burns and Burns (1979) believe vernadite to be the accumulating phase, in which case lower oxidation states might be expected due to bacterial degradation of organic matter behaving as a binding agent for the particles (Hunter, 1980; Kristofferson *et al* , 1982). There is evidence to suggest that the majority of organic matter reaching the sea floor suffers degradation within millimeters of the sediment/water interface (Chapter 4), however one must account for Mn being the utilised oxidant, rather than oxygen which would be kinetically favoured. Kalhorn and Emerson (1984) suggest that microenvironments may develop in which organic matter degradation proceeds faster than the supply of O_2 by molecular diffusion, causing MnO_2 to be reduced.

The profile of MnO_x

The position of the maximum oxidation state of Mn is likely to be just above the first appearance of Mn^{2+} in the pore water. As noted by Morgan and Stumm (1964) *d*-MnO_2 has a strong affinity for Mn^{2+} which will result in a lowering of its oxidation state. The occurrence of the Mn redoxcline <u>below</u> the appearance of Mn^{2+} in pore waters was also noted by Sawlan (1982) and may be related to mineralogical (see below) or lithologic control on the precipitation of vernadite.

As Mn is precipitated by upward diffusion of Mn^{2+} in the pore water it will have a large surface area and a corresponding large number of cation vacancies (Section 6.3.2) which will attract cations from organic matter release and from sea water by diffusion.

Bricker (1965) and Hem (1978) outline a possible process

by which valence electrons in hausmannite can rearrange themselves to give *d*-MnO_2 and Mn^{2+} as follows:

$$Mn_3O_4 + 4\ H^+ = d\text{-}MnO_2 + 2\ Mn^{2+} + 2\ H_2O$$

This may occur immediately at the sediment surface, but Mn^{2+} produced during disproportionation probably does not leave the oxide surface and O_2 from sea water can readily oxidise it to Mn_3O_4. This can give rise to the autocatalytic effect observed by various investigators (Bricker, 1965; Hem, 1978). Thermodynamically, this reaction is favourable; the flux of upward migrating Mn^{2+} meeting the dissolved O_2 (at a pH buffered by sea water) representing an un-equilibrated free-energy input that keeps the disproportionation process going and building up a layer of vernadite (*d*-MnO_2).

The presence of Mn^{4+} at a depth greater than the redoxcline in 163-14 and 163-10 is at odds with the data of Balzer (1982) in which excess Mn was solubilised in a 100 day experiment by an upward-moving redox front. Excess Mn at depth may be explained by the formation of a mixed carbonate phase (Chapter 8) exerting a Mn solubility control. Sawlan and Murray (1983) found that $MnCO_{3(s)}$ saturation is theoretically reached in hemipelagic cores from this transect. However, they point out problems of alkalinity artifacts during sampling and with data on the apparent solubility product of rhodochrosite in sea water (Chapter 8). SEM evidence (Plate 8.1) for the formation of manganese carbonates at the base of 163-14 and 163-10 has been found, but it does not explain the total Mn profiles (including Mn^{4+}) for the lower parts of these cores.

Observations on the distribution of solid phase Mn^{4+} and pore water Mn^{2+} (Froelich *et al*, 1979) suggest that Mn is reduced (and solubilised) more easily (at higher Eh) than Fe, but is slow to reprecipitate following a gradient to more oxic conditions (Stumm and Morgan, 1970; Hem, 1978; Wilson, 1980). Thus, metastable high concentrations of Mn^{2+} concentrations are found in oxic waters and Mn^{2+} can escape from the oxic layers of coastal sediments (Sundby, *et al*, 1981). Therefore, the steepest solid phase Mn gradient ($dMn/dZ=max$) does not necessarily represent the redox level of $Mn^{4+} = Mn^{2+}$, which should occur between an Eh of +470 and +410 mV (Stumm and Morgan, 1970). Even given the slow oxidation of Mn^{2+} and the retarding effects of soluble organics complexing the oxidisable species (Wilson, 1980) it remains to be explained how Mn^{4+} exists so far beneath the redoxcline. Indeed, Sawlan and Murray (1983) point out that the reduction reaction is complicated because dissolved Mn^{2+} is produced in a series of steps after NO_3^- has been consumed. Clearly, some stabilisation of the vernadite has occured allowing it to metastably enter lower redox zones.

Hem (1978) suggests that ionic substitution for the vacant lattice positions in the freshly deposited vernadite may be thermodynamically favourable if such substitution increases the stability of the lattice. Table 6.2 shows that the preferential substitution for Mn^{2+} in the lattice, based on ionic radii criteria, would be Mo > Ni > Cu > Zn. Such substitution would result in an increase of Mn^{2+} in solution as shown by Loganathan and Burau (1973), Burns (1976) and Murray and Dillard (1979). The strength of the electrostatic attraction between cation and oxide "sites" is dependant on the charge of

the cation and the distance of closest approach between cation and anion (Anderson *et al*, 1973). Another method of identifying the distance of closest approach, other than the ionic radii, is the "ionic potential" of the ion involved (Krauskopf, 1979, p.483). This is defined as the quotient of the positive charge of the ion divided by its radius. In theory, Mo should most readily precipitate with Mn oxyhydroxide having an ionic potential >9.5 (Krauskopf, 1979). In practice, the transition metals, because of their tendency to form covalent bonds, distort the large O^{2-} anion so that absorbtion is not simply dependant on charge and radius.

TABLE 6.2

IONIC RADII OF THE TRANSITION METALS

Species	Radius, Å
Mn^{4+}	0.62
Mn^{3+}	0.73
Mn^{2+}	0.91
Mo^{6+}	0.68
Mo^{4+}	0.73
Ni^{2+}	0.77
Cu^{2+}	0.81
Zn^{2+}	0.83

Radius for 6-coordination ("octahedral")
Whittaker and Muntus (1970)

The substitution of ions into the lattice could result in a spinel-type structure (Hem, 1978) having a general formula unit $2XO.ZO_2$ (where X is a di- and Z a trivalent cation). Some minerals with spinel-type structures (eg. ferrites) are highly resistant to solution. Hem (1978) states that

> "Thermodynamic data for corresponding manganites does not exist, but one might expect structures that are relatively stable thermodynamically would form where the metal ions having favourable dimensions are available".

If this were the case then cation-containing vernadite may well be stabilised to lower redox levels in the sediment, only dissolving slowly and producing a step-shaped pore-water gradient. This occurs in 163-14 and 163-10, but in 163-7 the high C_{org} content of the sediment and its attendant reduction is too severe to allow the meta-stable existence of oxyhydroxide below the redoxcline, except by physical biomixing. In fact the stoichiometry of the MnO_x decreases within the biomixed zone of all three hemipelagic cores indicating that the kinetics of Mn^{4+} reduction exceeds the rate of bioturbation (Chapter 7). In 163-7 the mixed zone extends down to 15 cm and beneath this depth Mn^{4+} is undetectable.

6.4 THE AFFINITY OF TRACE METALS (Mo, Ni, Zn, Cu) FOR MANGANESE OXIDES

6.4.1 *Introduction*

Whilst the association of the trace metals, Mo, Ni, Zn and Cu with Mn-rich sediments and nodules has been long known, their post-depositional behaviour during diagenesis has only

recently been looked at in detail (Graybeal and Heath, 1984). The partioning of trace metal-bearing Mn phases into diagenetic, hydrogenous (authigenic) or hydrothermal end members has been attempted by both mathematical and chemical methods. In the former, statistical factoring (Graybeal and Heath, 1984) and linear programming (Heath and Dymond, 1977, 1981; Dymond, 1981) have been extensively used. However, all the models make some assumptions about the singular behaviour of certain key elements (ie detrital=Al, hydrothermal=Fe, authigenic=Co, biogenic=Cu, solution residue=Ba; Dymond,1981) which may not always be the case. Variations in sediment composition relative to these key elements are used to infer diagenesis. This approach has been adopted by Graybeal and Heath (1984) for MANOP sites M and H, and has led to problems in the characterisation of the biogenic component.

The chemically leachable fraction of the sediment has also been used to examine the effect of diagenesis on metal distributions. However, the variability between leaching techniques and reagents (Heath and Dymond, 1977; Graybeal and Heath, 1984) means that inter-laboratory comparisons are often difficult. The excess of leachable metal implies mobilisation and precipitation, or adsorbtion by an oxide, usually MnO_2.

In order to ascertain the relative trace metal enrichment of hydrogenous Mn as opposed to diagenetic Mn in oxic sediments a different approach is used here. Samples from cores 163-9, 163-10, 163-14 and 163-7 are compared with published values from Sawlan (1982) and Sawlan and Murray (1983) for cruise TGT-145. These cores span the oceanic and hemipelagic environment; hydrogenous processes dominating the former, diagenetic the latter. Variations in trace metal behaviour between these

environments may be interpreted as being due to the relative importance of one process over the other.

TABLE 6.3

DIAGENETIC TRACE METAL ENRICHMENTS AT THE Mn REDOXCLINE

Station	Depth cm	Mn wt.%	Mo ppm	Ni ppm	Zn ppm	Cu ppm
163-7	2-3	6.49 (15.1)	117 (12)	514 (2.4)	399 (2.4)	305 (1.3)
163-14	5-6	2.89 (6.7)	51 (5.1)	509 (2.4)	383 (2.3)	306 (1.3)
163-10	8-9	4.53 (10.5)	82 (8.2)	504 (2.4)	308 (1.9)	328 (1.4)
Pacific pelagic clay (Bischoff *et al*, 1979)		0.43 (1)	10 (1)	210 (1)	165 (1)	230 (1)
Shale (Turekian and Wedepohl, 1961)		0.085 (0.2)	2.6 (0.3)	68 (0.3)	95 (0.6)	45 (0.1)

Numbers in parentheses refer to enrichment relative to Pacific pelagic clay.

Table 6.3 illustrates the degree of enrichment of trace metals at the Mn redoxcline, relative to average Pacific pelagic clay (Bischoff *et al*, 1979). Trace metal to Mn atomic ratios for the sediments off Baja California are given in Table 6.4. Figures 6.4 and 6.5 indicate the relative behaviour of the trace metals to Mn^{4+} in the oxic tops of the hemipelagic cores and the oceanic oxic sediment of 163-9. Here the enrichment factor is defined as,

$$E.F. = \frac{(Me/Al)}{(Me/Al)_{min}}$$

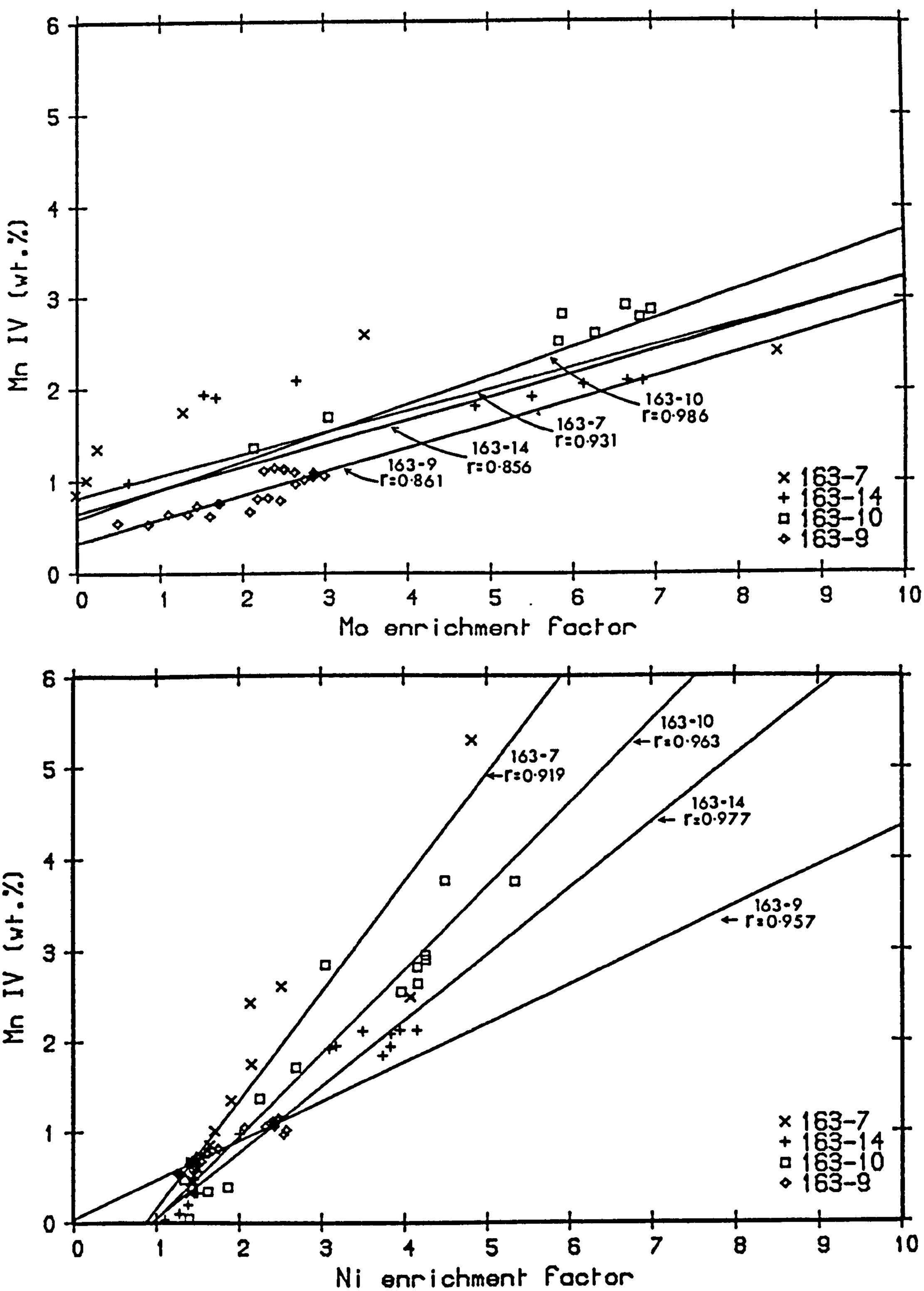

FIGURE 6.4 The correlation between Mn^{4+} and Mo and Ni enrichment in oceanic sediments off Baja California (salt-free). The enrichment factor is defined by the increase in Me/Al above the Mn redoxcline to the ~lowest Me/Al ratio in the reduced sediment below (Mo/Al=0.0, all stations; $Ni/Al=15 \times 10^{-4}$, station 163-14).

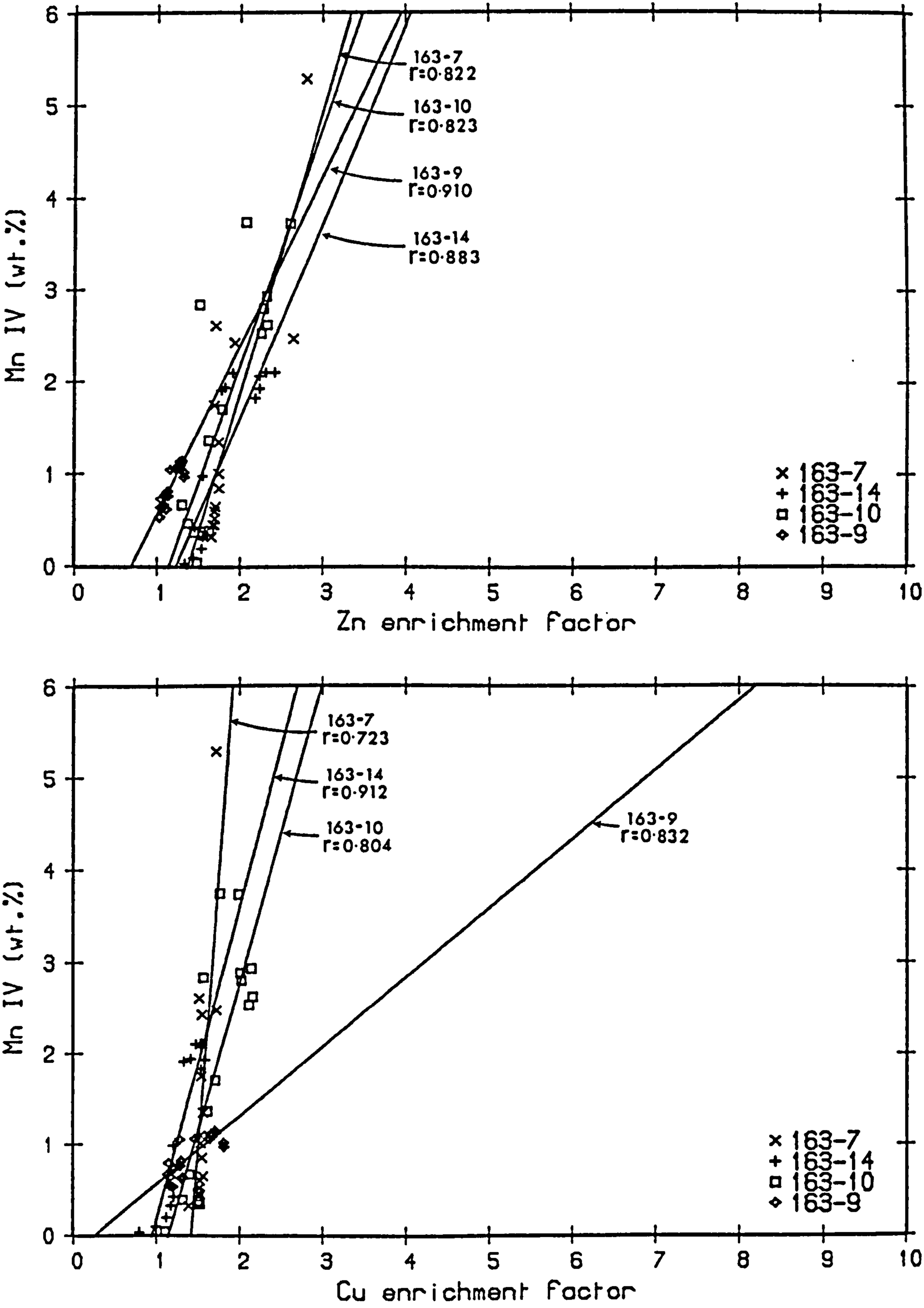

FIGURE 6.5 The correlation between Mn^{4+} and Zn and Cu enrichment in oceanic sediments off Baja California (salt-free). The enrichment factor is defined as in Figure 6.4 ($Zn/Al=20 \times 10^{-4}$, station 163-9; $Cu/Al=25 \times 10^{-4}$, all stations). The gradient of the regression lines in Figure 6.4 and the plots above indicate a relative trace metal enrichment of Mo > Ni > Zn > Cu in Mn oxide.

where "min" is the is the ~lowest Me/Al in either the hemipelagic or pelagic sediment (Mo/Al = 0, all stations; Ni/Al = 15 x 10^{-4}, station 163-14; Zn/Al = 20 x 10^{-4}, station 163-9; Cu/Al = 25 x 10^{-4}, all stations) and Me is the trace metal being studied. By taking this common denominator the enrichment in trace metal in the oxic zone may be compared between cores. A similar relationship is seen with Me *versus* Mn^{4+} plots, however the Me intercept will vary according to the level of fixation at depth, below the redoxcline (see below).

Table 6.3 and Figures 6.4 and 6.5 indicate the same phenomena; that the relative degree of trace metal enrichment is Mo > Ni > Zn = Cu, the same as their natural abundance in bottom waters (Table 6.5) and very similar to atomic radii and ionic potential predictions. This seems to indicate that hydrogenous Mn scavenges as many cations as it can from seawater in order to balance its negative surface charge (Section 6.3.2). During diagenesis this simple relationship becomes more complicated. Table 6.4 and Figure 6.6 indicate that the behaviour of Ni towards Mn^{4+} varies systematically, the level of Ni uptake decreasing with increasing organic carbon (ie with increasing diagenesis). Thus, Mn reprecipitating in the oxic zone of the hemipelagic cores shows a depletion in Ni (and to a lesser extent Zn and Cu) corresponding to the degree of diagenetic remobilisation of the host Mn. In contrast, hydrogenous Mn precipitating in the open ocean, red clay environment is effectively saturated with respect to trace metal uptake.

TABLE 6.4

TRACE METAL/Mn ATOMIC RATIOS IN HEMIPELAGIC AND OCEANIC SEDIMENTS

TOGETHER WITH SURFACE ORGANIC CARBON (AT THE Mn REDOXCLINE)

Station/Type	Author	Ni/Mn ($\times 10^{-3}$)	Cu/Mn ($\times 10^{-3}$)	C_{org} (wt.%)
145-3-R	Sawlan & Murray (1983)	43.8	35.1	0.197
145-4-R	"	43.0	32.7	0.467
145-5-R	"	22.7	25.7	0.425
163-9-R (36-38 cm)	This study	20.4	28.8	0.61
145-6-R	Sawlan & Murray (1983)	21.2	20.3	0.571
145-7-H	"	11.1	8.2	1.200
163-10-H (8-9 cm)	This study	10.4	6.3	0.96
163-14-H (5-6 cm)	"	16.5	9.2	1.12
163-7-H (2-3 cm)	"	7.4	4.1	1.24
145-8-H	Sawlan & Murray (1983)	6.7	6.6	1.519
Average hemipelagic ferromanganese nodule	Cronan (1977)	2.93	1.83	
Average pelagic ferromanganese nodule	"	30.1	19.1	

R - red clay

H - hemipelagic

$C_{org.}$ in wt.%

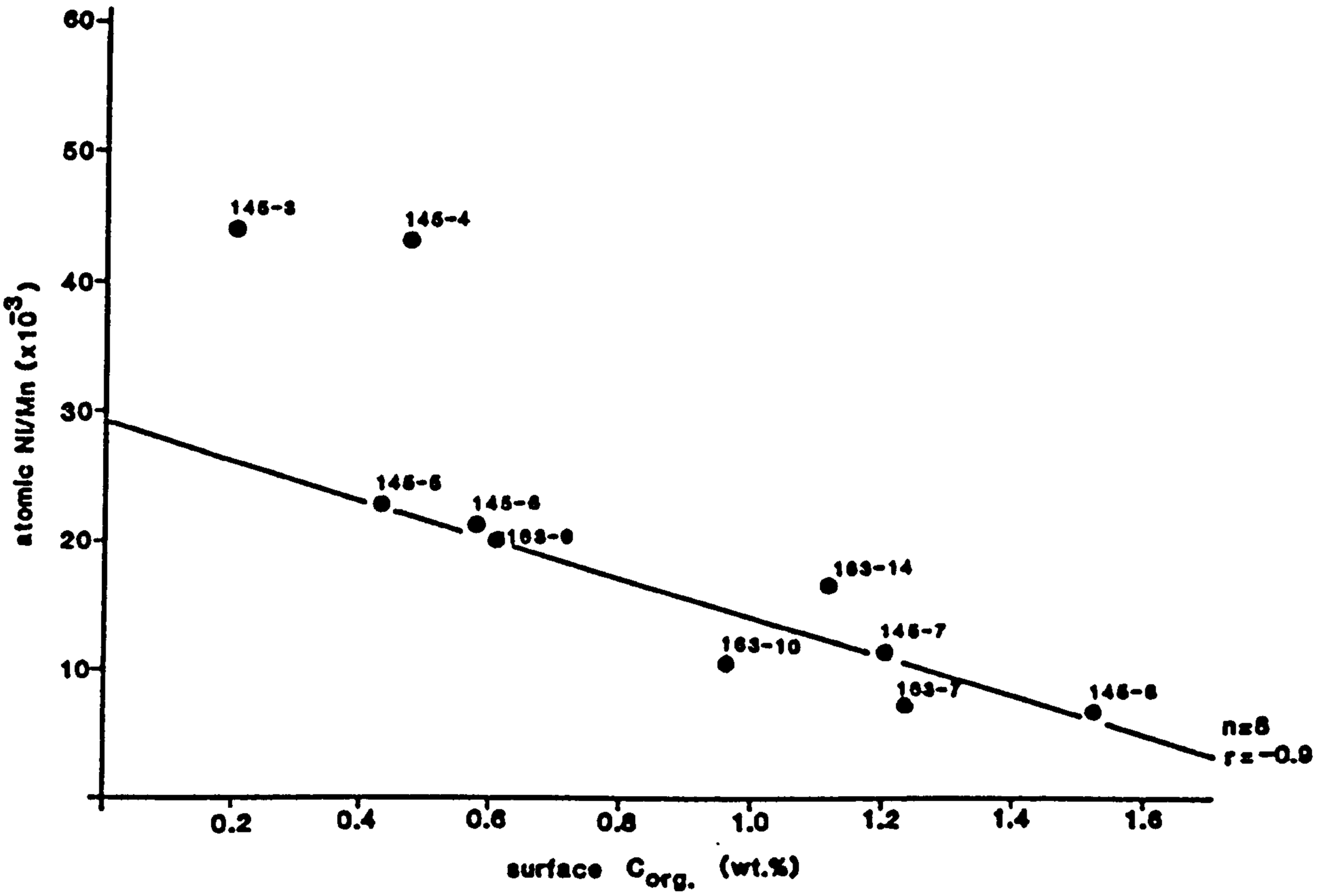

FIGURE 6.6 The correlation between Ni/Mn and surface organic C content in sediments from the Baja California transect (salt-free). The regression line does not include stations 145-3 and 145-4.

TABLE 6.5

BOTTOM SEAWATER CONCENTRATIONS

Mn^{2+}	Mo^{6+}	Ni^{2+}	Zn^{2+}	Cu^{2+}
0.2-3.0[@]	110[+]	10-12[*]	3-4[*]	8-9[*]

all in nmol/kg

[@] Open ocean concentration. Bottom waters may be much higher.

[+] Sugawara and Okabe (1966)

[*] Bruland (1980)

6.4.2 *The partitioning of Ni and Zn between oxic and suboxic zones*

Sawlan (1982) believes Ni to be a "passive participant" in the Mn reduction-oxidation cycle. If so then the release of Ni to pore waters during the redox event, and its lack of incorporation into the reprecipitating oxide during extreme diagenesis must mean that an alternative sink exists for dissolved Ni. Figure 6.7 indicates the Ni/Al ratio with depth in the suboxic zone of the three hemipelagic stations. In core, 163-7 the level of Ni relative to Al increases with depth. 163-14 has a higher carbonate content and displays a lower Ni/Al ratio at depth, whilst 163-10 displays a maximum in Ni/Al at 23 cm depth. This data qualitatively supports Figure 6.4; the greater the integrated Ni content relative to Al in the deeper suboxic sediment, the less the enrichment in the surficial MnO_2 layer. A similar arguement may be put forward for Zn which also displays suboxic fixation.

The mechanism by which these two trace elements become

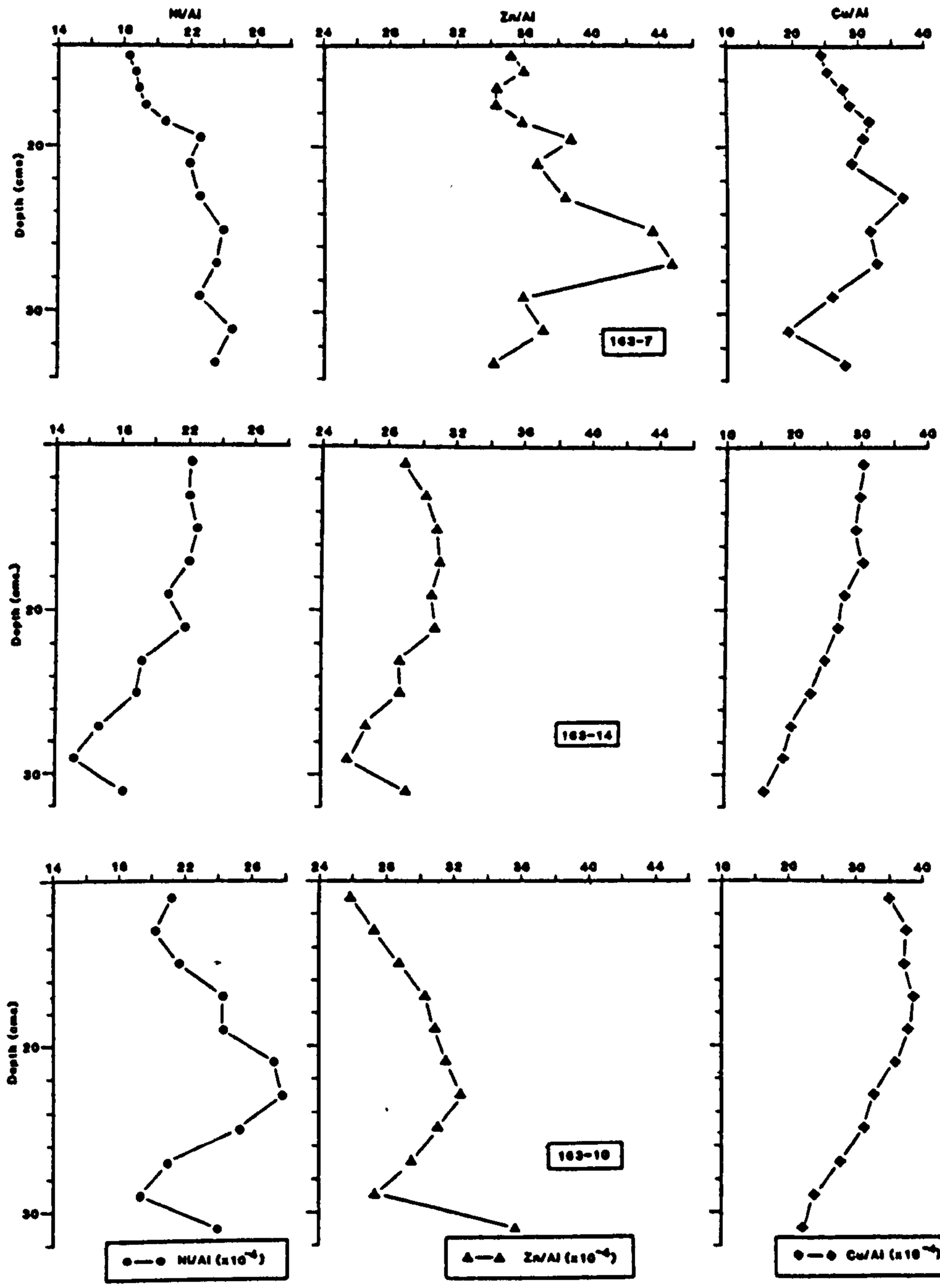

FIGURE 6.7 Profiles of Ni/Al, Zn/Al and Cu/Al in suboxic sediment from hemipelagic cores off Baja California. Note the scale change for Cu/Al.

incorporated at depth to concentrations greater than typical shale values (Table 6.1) may be due to uptake by diagenetic smectite. The highest concentration of diagenetic smectite and zeolite (hydrous Ca Na alumino-silicate) in present-day surface sediments seems to be in slowly accumulating, deep-sea clays of the south and east Pacific. These clays are extremely trace element-rich (Table 6.6). Chester *et al* (1976) studied the partioning of Mn, Cu, Ni, Co, and Zn in the "lattice-held" fraction of smectite, clinoptilite-rich, calcareous clays from the Bermuda Rise (DSDP Leg 2, Site 9) and concluded that the formation of zeolites controlled the lattice fixation of these trace elements. Dymond and Eklund (1978) looked at smectite compositions of the Bauer Basin with an electron microprobe. This data was used by Graybeal and Heath (1984) to suggest that smectite formation is a viable hypothesis for explaining excess, fixed trace metal concentrations from MANOP site M, even though they were not able to quantify the presence of diagenetic smectite because of a large detrital clay component.

TABLE 6.6
CHEMISTRY OF DOMES SMECTITES

Sample No.	Al wt.%	Fe wt.%	Mg wt.%	Cu ppm	Ni ppm	Mn ppm	Zn ppm	Ba ppm	Mo ppm
47-10	7.5	7	2.0	1500	150	2000	300	1500	b.d.
47-10*	7.45	6.47	3.14	1100	500	3300	1300	500	b.d.
48-19	6.6	7	3.0	1500	150	2000	300	1000	b.d.
52-42	7.1	7	3.0	1000	70	1000	300	1000	b.d.
55-53	5.9	7	3.0	1500	150	2000	300	1000	b.d.
16B-49	7.6	7	2.0	1000	100	1500	300	700	b.d.
18A-36	4.0	10	2.0	1000	100	3000	500	2000	b.d.
18B-37	6.2	7	2.0	700	100	2000	300	1000	b.d.

* <0.1 μm fraction analysed by atomic absorption spectroscopy, all other samples are the <1.0 μm fraction analysed by emission spectroscopy.

b.d. - below detetection limit (5 ppm)

from Hein *et al* (1979)

It would therefore appear that the initial precipitation of hydrogenous Mn and Fe oxides with associated trace metals from water column leads to the increased availability of these metals for clay adsorbtion during Mn redox mobilisation, in turn controlling the character of the diagenetically reprecipitated MnO_2.

6.4.3 The partioning of Cu between oxic and suboxic zones

Apart from a suboxic maximum in Cu/Al at 23 cm in 163-7, Cu apparently decreases in concentration downcore in the suboxic zone. Sawlan (1982) and Sawlan and Murray (1983) identified a sulphide phase as a possible agent for limiting Cu and Ni pore water concentrations at depth in 145-7 and 145-8. They detected the onset of the Fe^{2+} pore water gradient at the depth of NO_3^- consumption in 145-8. With further lowering in pE SO_4^{2-} reduction would occur together with the formation of sulphides acting as a sink for Cu and Ni. Due to the short cores taken this effect is only seen in the bottom few centimeters of 163-7. However, the colour change in the sediment (Appendix A) due to the Fe^{3+}/Fe^{2+} transition (Lyle, 1983) is not accompanied by any measurable increase in the Fe/Al ratio (Figure 3.12) of the suboxic sediment, indicating that sulphide control may not be as important as clay adsorption in controlling trace metal concentrations.

6.4.4 The partioning of Mo between oxic and suboxic zones

Figure 6.8 illustrates the dichotomous behaviour of Mo in the hemipelagic environment. The uptake of Mo by oxic sediment

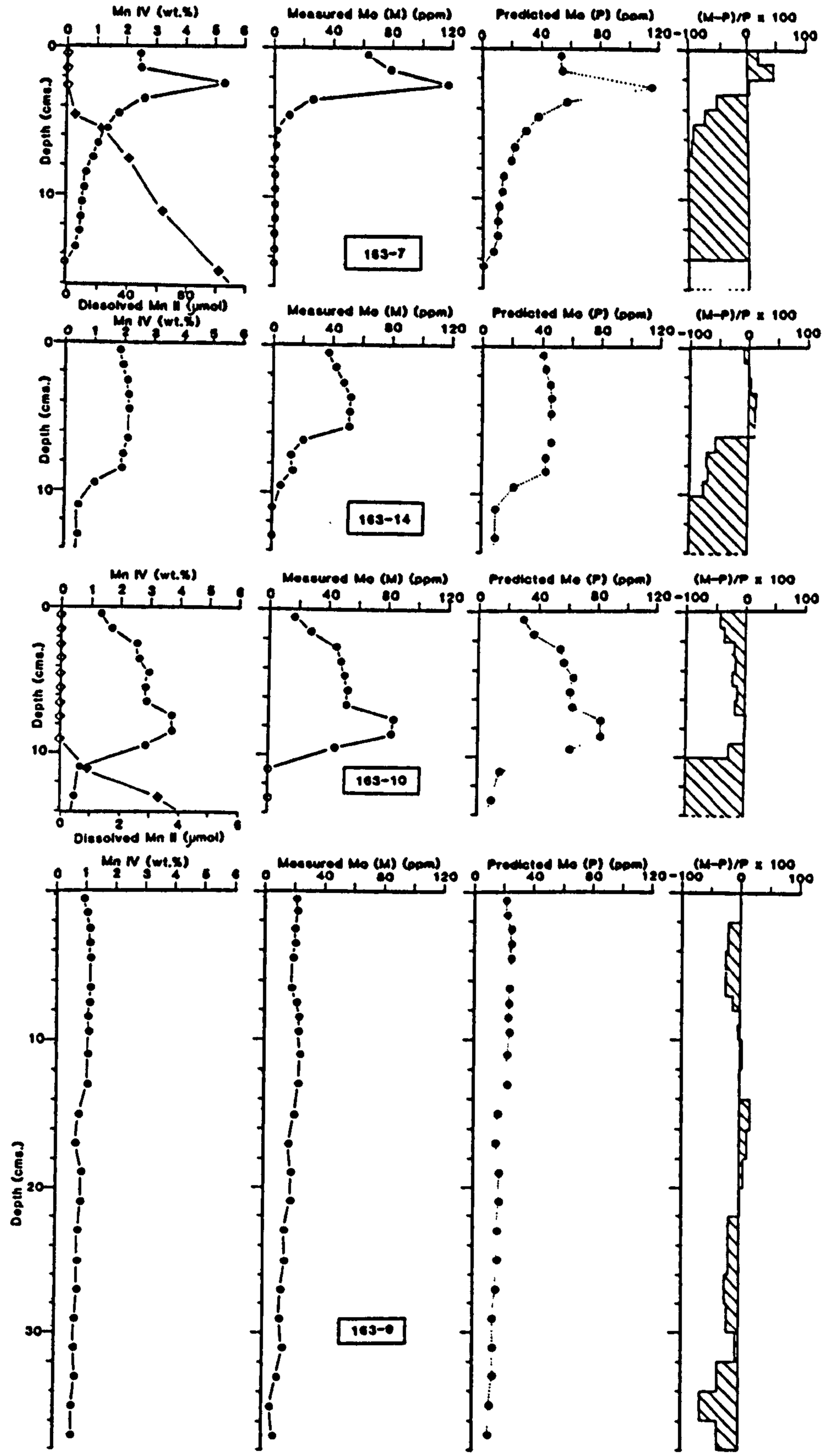

FIGURE 6.8 Profiles of Mo and Mn^{4+} with depth in oceanic sediments off Baja California (salt-free). Predicted Mo (obtained from the hydrogenous ratio of 0.00218 in 163-9) is compared with measured Mo and expressed as a percentage difference. Dissolved Mn from unpublished cruise report.

in 163-9 has been used to define the hydrogenous ratio of Mo/Mn^{4+} (0.00218) which is very similar to that found by Bischoff *et al* (1979) (Mo/Mn = 0.002) for the DOMES area. From this ratio the concentration of Mo in the oxic sediment of 163-10, 163-14 and 163-7 is predicted based on the Mn^{4+} profiles for these sediments. Whilst the predicted concentrations generally agree with the measured Mo values above the redoxcline they fall off sharply when dMn^{4+}/dZ = max, ie the site of Mn^{4+} reduction due to diagenetic remobilisation. Cruise report data (unpub.) for dissolved Mn^{2+} indicates that the disappearance of Mo in 163-7 and 163-10 is at the first appearance of Mn^{2+} (Figure 6.8). The reprecipitating Mn^{4+} at this level appears to be depleted in Mo despite the fact that the pore water concentration should be greater than the large quantity of Mo in seawater. Envoking the same arguement that was used for Ni, Zn and Cu it would seem that a substantial sink for Mo exists at depth, beyond that cored.

Mo associated with Mn above the redoxcline shows large enrichments relative to shale, attributed to the high concentrations of Mo in bottom seawater (Section 6.4.1). Scavenging of Mo by hydrous oxides of Mn has been well documented experimentally (Krauskopf, 1956; Chan and Riley, 1966) and in the natural environment (Berrang and Grill, 1974; Bischoff *et al*, 1979).

Several mechanisms have been proposed to account for the fixation of Mo in deeper-buried sediments. These include co-precipitation with Fe-sulphides (Bertine, 1972) or Mo-sulphides (Goldschmidt, 1954) and sorption onto particulate organic

matter (Szilagyi, 1967) or dissolved organic matter (DOM) (Contreras *et al*, 1978). Contreras *et al* and Brumsack and Gieskes (1983) have shown that the pore water behaviour of Mo and Mn are not comparable in anoxic sediments. In particular they point out that the mobilisation of Mo into the interstitial water phase does not seem to be associated with Mn mobilisation or sulphide precipitation. They argue that the degradation of organic matter generates dissolved humics which act as adsorbtion or ion exchange sites. Thus, a significant part of the Mo may be mobilised prior to Mn reduction and transfered to the dissolved organic carbon pool which builds up with depth.

CHAPTER 7

THE ACCUMULATION AND DISTRIBUTION OF RADIOISOTOPES OFF BAJA CALIFORNIA

7.1 INTRODUCTION AND OBJECTIVES

7.1.1 *The Mechanism of Radionuclide Production*

Both ^{230}Th and ^{231}Pa are naturally occuring, daughter radioisotopes (or radionuclides) of the cosmogenic uranium series, produced during the step-wise decay to the stable isotopes of lead (Figure 7.1). Many other daughters are produced, each having a different half-life and distinct chemical propeties.

The fathers of ^{230}Th and ^{231}Pa are the primordial isotopes of uranium, ^{238}U and ^{235}U. These occur in a constant ratio of 137.88/1 and may be released to the geochemical cycle *via* weathering. On entering an oxidising aqueous system U tends to form a stable uranyl carbonate complex, $[UO_2(CO_3)_3^{4-}]$. Although the concentration of U in rivers seems to vary quite considerably (<0.01 µg/l - 1.22 µg/l; Bertine *et al*, 1970), the average is about 0.03 µg/l. Turekian and Chan (1971) have shown that the annual river influx of dissolved U is 3 $\mu g/cm^2/kyr$, giving an average oceanic concentration of 3.3 µg/l.

7.1.2 *Behaviour and removal within the water column*

Alpha-recoil decay of ^{234}U and ^{235}U produces ^{230}Th and ^{231}Pa (*via* ^{231}Th). Both isotopes are hydrolysed strongly by particle surfaces, particularly oxides of Mn and Fe. At a first approximation it seems that the concentration of Th and Pa isotopes is controlled by particle absorbtion and that the flux of particles within the water column influences the residence time of the radionuclides. Table 7.1 summarises the residence times for the U/Th series nuclides in the oceans. Closer to the continental margins the increased flux of detrital and

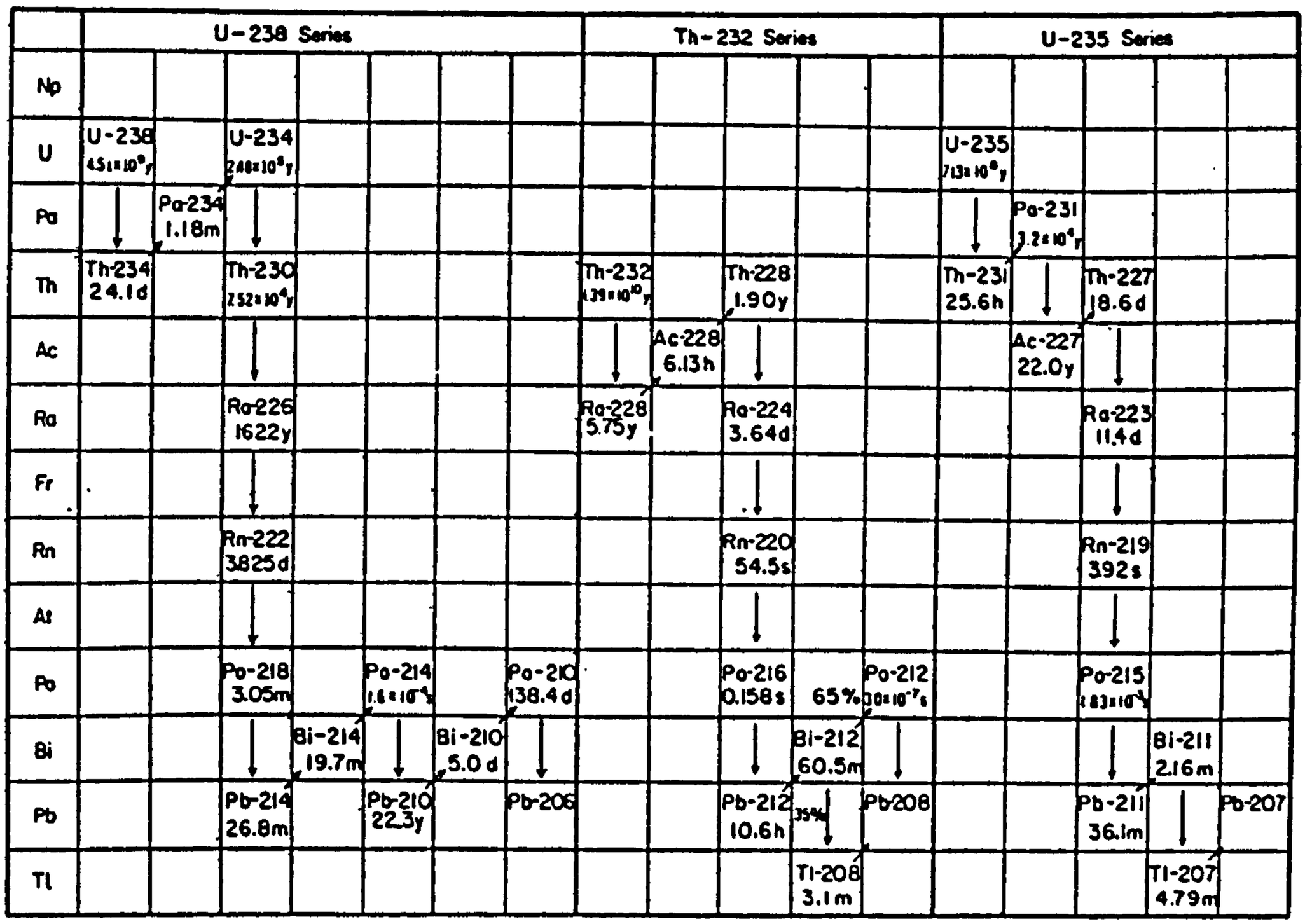

FIGURE 7.1 ^{238}U, ^{232}Th and ^{235}U decay series.

biogenically-produced particles results in lower residence times. Evidence for this is given by Bhat *et al* (1969) for $^{234}Th/^{238}U$, by Broecker *et al* (1973) for $^{228}Th/^{228}Ra$, and by Anderson *et al* (1983a,b) for $^{230}Th/^{231}Pa$.

The residence time, or transfer rate, can be described by a simple box model where:

Flux-into-box = decay-in-box + flux-out-of-box

In terms of an algebraic material balance this may be written:

$$\lambda_P N_P = \lambda_D N_D + k_D N_D$$

where the subscripts refer to parent (P) and daughter (D), λ is the decay constant of the nuclide, N is the atomic concentration, and k is a first-order removal constant. Flux-into-box ($\lambda_P N_P$) refers to production *via* the parent nuclide.

Since the activity (A) is identical to λN we have:

$$A_P = A_D \left(1 + \frac{k_D}{\lambda_D} \right)$$

By measuring the activity ratio A_D/A_P in a given water mass k_D, or the first-order removal constant of the daughter product, may be calculated. The reciprocal of k_D, in units of time, is called the "mean residence time".

Alternatively, the removal rate of the nuclide may be modelled by curve-fitting a set of data according to the expression:

$$K_Z = \frac{d^2N}{dZ^2} + W \frac{dN}{dZ} - \lambda N + J = 0$$

an example of the familiar advection-diffusion equation. K_Z is the vertical eddy diffusion coefficient for the water column of interest, W is the advective velocity, Z is the depth and J is the production (or removal) term assumed to follow first-order kinetics, ie J = kN.

TABLE 7.1

RESIDENCE TIMES

Nuclide	T (years)	Author	Location
^{234}Th	> 0.75	Amin *et al* (1974)	S. Pacific
^{230}Th	41 ± 3	Anderson *et al* (1983a)	Pacific
^{231}Pa	130 ± 11	"	"
^{230}Th	20 ± 4	"	N. Atlantic
^{231}Pa	50 ± 15	"	nr. Bermuda
^{210}Pb	50	Craig *et al* (1973)	Pacific
^{210}Pb	100	Thomson & Turekian (1976)	S. Pacific
^{210}Pb	< 96	Nozaki & Tsunogai (1976)	N.W. Pacific

In spite of their short residence times ^{230}Th and ^{231}Pa appear to be fractionated on incorporation into seafloor deposits. Theoretically, they should be produced in an activity ratio of 10.8; a ratio fixed by their half-lives and the isotopic compostion of U in seawater. However, Anderson *et al* (1983,a) have shown that particles in the open ocean preferentially scavenge ^{230}Th relative to ^{231}Pa leading to the high activity ratios commonly observed in deep-sea sediments

(Ku, *et al*, 1972; Cochran and Krishnaswami, 1980; Anderson *et al*, 1983a). In contrast, manganese nodules (Sackett, 1966; Ku and Broecker, 1969; Krishnaswami and Cochran, 1978; Moore *et al*, 1981), metalliferous sediments (Kadko, 1980b) and recently, particulate material from the ocean margins (Anderson *et al*, 1983b) have much lower values suggesting a preferential sink for ^{231}Pa in these deposits. The mechanism by which these two isotopes become fractionated is unknown but must be due to the mechanism of removal from seawater and behaviour towards particulate material.

7.1.3 *Physical and chemical processes within the sediment*

The most common use of radionuclides within sediments is the dating of sedimentary layers, and/or growth bands in chemical accumulations such as ferromanganese nodules. However, physical disruption of the sediment pile, together with chemical remobilisation effects can lead to complications. Nevertheless, several models exist which not only describe the process of sediment accumulation quantitatively (Osmond, 1979), but also allow the determination of rates of reworking by organisms (Goldberg and Koide, 1962; Guinasso and Schink, 1975; Officer, 1982; Officer and Lynch,1983) and rates of chemical remobilisation (Burdidge and Gieskes, 1983).

The distibution of ^{230}Th and ^{231}Pa in the oceanic and hemipelagic sediment off the continental margin of Baja California, Mexico was carried out with the following aims:

(1) To investigate the behaviour of ^{230}Th and ^{231}Pa in sediments along a transect normal to the continetal margin, and with depth down to a maximum of 50 cm.

(2) To relate the sediment inventory to the water column production of the nuclides.

(3) To compare the accumulation of ^{230}Th and ^{231}Pa in sediments with the bulk chemical composition, where some elements are controlled by glacial/interglacial conditions.

7.2 ACCUMULATION MODELS OF ^{230}Th AND ^{231}Pa IN DEEP-SEA SEDIMENTS

7.2.1 *Introduction*

From the legacy of analytical development and descripition of radionuclides (^{230}Th and ^{231}Pa) in the marine environment several models to account for their accumulation in sediments have been produced. The most commonly used model assumes a constant sediment accumulation rate, an assumption that is blatantly untenable in view of the glacial cycles of the late Pleistocene. Alternative models which consider the possibility of fluctuating sediment supply have been known since soon after the discovery of excess radioactivity in marine sediments, but have been largely neglected, in favour of models concerned with the distribution of the nuclide in the sediment (Goldberg and Koide, 1962; Kadko, 1980a,b; Officer, 1982). The evolution of the three nuclide accumulation models available is outlined below.

7.2.2 *Constant Activity Model*

Piggot and Urry (1941, 1942), in their attempt to determine rates of deep sea sediment accumulation, decided to assume that the activity of depositing sediment (in

disintegrations per minute per gram, dpm/g) remained constant with time. In this way the activity of ^{230}Th and ^{231}Pa, unsupported by ^{234}U and assumed to be in equilibrium with ^{226}Ra, would decay away with time according to their respective half-lives as more sediment accumulated above. At this time ^{226}Ra was the only isotope capable of being measured and it is now known that the assumption that ^{226}Ra does not migrate away from the loci where it is produced is false. By the 1950's ^{230}Th was being analysed leading to the work by Kulp, in particular Holland and Kulp (1954) and Volchok and Kulp (1957) who suggested that the main mechanism of ^{230}Th transport to the sea floor is as ions adsorbed on clay particles. They applied a "surface correction" to their initial ^{230}Th activities. The Russians Baranov and Kuz'mina (1958) estimated the rate of sedimentation in some Indian Ocean cores by advocating the scavenging by Fe and Mn oxides in ^{230}Th transport and suggested that the ratio ^{230}Th/(Fe, Mn) should be used as a dating parameter.

Today the constant activity model is the most commonly used in the determination of sediment accumulation rates and may be found in many papers, for example the work of Muller and Mangini (1980) in the DOMES area.

7.2.3 *Activity Ratio Model*

In order to eliminate the assumption of constant precipitation of ^{230}Th made by Piggot and Urry (1941, 1942) and other workers (see above), Picciotto and Wilgain (1954) suggested the use of a normalisation ratio, ionium-thorium ($^{230}Th/^{232}Th$) with two provisos; (1) The $^{230}Th/^{232}Th$ ratio of

the oceans had remained constant over the time span of interest (some 350,000 years); (2) ^{232}Th is precipitated from sea water in the same ratio as ^{230}Th. To avoid this second assumption that all the ^{232}Th is from sea water precipitation and not continental weathering Goldberg and Koide (1962) also used the $^{230}Th/^{232}Th$ ratio but leached the sediment with acid to remove only the authigenic Th.

Sackett (1960) and Rosholt *et al* (1961) chose a different normalisation procedure; the $^{231}Pa/^{230}Th$ ratio. The rationale behind this choice is that both elements are daughters of U, that their incorporation into sediments is nearly identical, and since they decay at different rates (a half-life ratio of 60,100 years) then their ratio should be a function of time only and independant of geological conditions. From this method investigators believed they could ascertain if the fluctuations in decay curve with depth was due to changing sediment accumulation rates or changing sediment characteristics. However, even this seemingly infallible tool now seems to present problems. Not only is the time resolution limited by the shorter life of ^{231}Pa (some 150,000 years as opposed to 300,000 years for ^{230}Th alone) but, more worryingly, the contemporary sea bed $^{231}Pa/^{230}Th$ ratios do not match their known production ratios by U in sea water (see Sections 7.1.2 and 7.2.3).

7.2.4 *Constant Flux Model*

Due to the very long residence time of U (10^6 years) in the oceans and the relatively rapid removal of ^{230}Th (and

^{231}Pa) the overall flux of ^{230}Th to the sea floor, at any one place, must be fairly constant. Several early workers (Kroll, 1953, 1954; Pettersson, 1954, ; Koczy, 1954, 1956) realised that as a result the excess ^{230}Th in a sediment column should remain constant and equal in activity to the parent U in the water column. Koczy (1956) in a scalding attack on the work of Holland and Kulp (1954), termed this the "European Model" as opposed to the "American Model" of constant activity advocated by his proponents.

Whilst Sackett (1960, 1965) also applied a constant accumulation model to his study of ^{231}Pa, later work by Kadko (1983) using a large compilation of literature data, demonstrated that the sediment inventories of $^{230}Th_{excess}$ and $^{231}Pa_{excess}$ are generally less than the overlying water column production, especially in regions of low sediment accumulation rate. Anderson *et al* (1983a,b) have shown that more active removal occurs in areas of high particle flux and that ^{230}Th is removed in preference to ^{231}Pa in the open ocean (Section 7.1.2).

7.3 METHODS AND RESULTS

Presented here is a study of the alpha-emitting isotopes of uranium and thorium in oceanic and hemipelagic sediments from the Baja California transect. The analyses were performed by Dr. John Thomson of the Institute of Oceanographic Sciences, Wormley, U.K., using a method developed by him (Thomson, 1982).

7.3.1 *Analytical Methods*

Briefly, total dissolution of the sample is effected by fusion with potassium fluoride (to dissolve silicates) and with sodium/potassium pyrosulphate (to dissolve other refractory minerals and convert to the sulphate system). The Fe and Al naturally present in the system is used as carriers for U and Th, first in a mixed hydroxide precipitate and subsequently in preparing U and Th for final purification by anion exchange for electroplating. Final concentrations were measured by alpha-spectrometry using an Ortec multi-channel analyser connected to 450 mm^2 silicon surface barrier detectors. The electroplated sources were counted for 1-2 days to collect at least 1000 counts at each peak of interest. These peaks were ^{238}U, ^{234}U and ^{232}U, and ^{232}Th, ^{230}Th, ^{228}Th and ingrown ^{224}Ra on two separate mounts. Total tracer yields for both U and Th through the entire process was about 60-80% and generally similar for both elements in a single analysis.

7.3.2 *Results: The Distribution of ^{230}Th and ^{231}Pa*

Appendix C lists the data obtained for four cores; 163-7, 163-14, 163-10 and 163-9. The quoted errors are based on 1 σ counting uncertainties only. Figure 7.2 displays the change in activity of $^{230}Th_{excess}$ and $^{231}Pa_{excess}$ with depth. In the outermost core the change in activity may be used to calculate the overall sedimentation rate (0.45 cm kyr^{-1}). For this several assumptions have been made. These are that there has been a constant accumulation rate of the sediment, that there has been constant production and removal of nuclides from the

overlying water column, and that the profile of activity has not been disrupted by biomixing. There is no evidence of such a biomixed layer within the resolution of the data. This is unexpected as such layers a decimeter or more thick are commonly observed, even in oceanic red clays (DeMaster and Cochran, 1982). However, the organic carbon decay rate (Chapter 4) also suggests there has been no benthic activity, and that the surface of sedimentation has been preserved during core collection.

In the three hemipelagic cores the activity distribution is very different. Over the uppermost ~15 cm the activities of the two nuclides remain constant; below they show marked but variable decrease. The upper constant activity region is thought to represent a zone of biomixing which varies in thickness from 18 cm in 163-10 through 11 cm in 163-14 to 8 cm in 163-7. The trend in decreasing activity for both isotopes below the biomixed zone can be tentatively used to estimate apparent sediment accumulation rates in the manner applied to 163-9. Despite the inaccuracy involved using only three or four points it is apparent that rates of sediment accumulation that can be calculated are an order of magnitude less than those estimated from ^{14}C (Sawlan, 1982) and the trends of the $CaCO_3$ and Zr/Al profiles (Chapter 3). Only in one of these cores can this inconsistency be partly accounted for. In 163-7 U contents at depth (maximum 6.57 ppm) exceed the average of 2.3-3.0 ppm.. Here, U is likely to have precipitated within the reduced zone as a consequence of diffusion via interstitial water from overlying seawater (Heye, 1969; Bertine *et al*, 1970; Turekian and Bertine, 1971; Bonatti *et al*, 1971; Kadko, 1980b; Weber and Sackett, 1981; Yamada and Tsunogai, 1984). This

enrichment will affect the calculation of $^{230}Th_{excess}$ and $^{231}Pa_{excess}$.

TABLE 7.2

SURFACE $^{230}Th_{excess}/^{231}Pa_{excess}$ ACTIVITY RATIOS

Core	Mixed layer depth (cm)	Mean weight dry sediment/ unit volume (g/cm3)	Mixed layer mean activity $^{230}Th_{excess}$ (dpm/g)	Mixed layer mean activity $^{231}Pa_{excess}$ (dpm/g)	Activity ratio $\frac{^{230}Th_{excess}}{^{231}Pa_{excess}}$	Scavenging ratio
7	13	0.50	19.7	3.0	6.6	1.64
14	11	0.52	21.3	3.0	7.1	1.52
10	18	0.53	23.8	3.0	7.9	1.37
9	0	0.56	38.2+	4.1+	9.3	1.16

+Regression line surface intercept value.
Scavenging ratio = 1/(mixed layer ratio/10.8).

Table 7.2 presents the mean activity ratios for $^{230}Th_{excess}$ and $^{231}Pa_{excess}$ within the biomixed layer of the three hemipelagic cores, and from the estimated surface activities for the oceanic core, 163-9 (Figure 7.2). Two points may be noted: (a) The activity ratio decreases landwards and is below the theoretical production ratio of 10.8. (b) The decrease in activity ratio for the hemipelagic cores is due to a decrease in mean $^{230}Th_{excess}$ upslope whilst $^{231}Pa_{excess}$ seems to have reached a limit of some kind. (In actual fact the mixed layer activity will underestimate the delivery ratio because of the faster decay of ^{231}Pa relative to ^{230}Th during the

residence time of the biomixed layer, although without precise accumulation rates this is unquantifiable).

7.3.3 *The Relationship between Sediment Composition and Isotope Distribution*

Inspection of Figure 7.2 indicates that the remobilisation of Mn occurs within sediment characterised by constant $^{230}Th_{excess}$ and $^{231}Pa_{excess}$ activity. This implies that the redox boundary and the recycling of Mn occurs within the zone of biomixing. From this it would appear that dissolution/reprecipitation reactions involving Mn proceed faster than the turnover of sediment by benthic mixing. Isotopes such as ^{210}Pb ($t_{1/2}$ = 22.3 years) and ^{234}Th ($t_{1/2}$ = 24 days) would display much shallower depths of mixing due to their short half-lives, and because of the exponential fall off in abundance of organisms (Rhoads, 1974) and the frequency of physical reworking (Smith, 1977; Berger and Heath, 1968). The redoxcline of MnO_2 in core 163-7 occurs at only 3 cm depth and deepens oceanwards (9 cm depth in 163-14 and 163-10; Chapter 6). This trend follows the thickness of the biomixed zone defined by ^{230}Th and ^{231}Pa. It appears that both are indirectly related to the organic matter content of the sediments and its availability to the benthos. In the nearshore environment where organic matter is more plentiful biomixing occurs to a shallower depth and is probably more vigorous. In this situation dissolved oxygen incorporated into the sediment by diffusion, and more importantly, advection, is rapidly consumed leading to a shallow position of the redoxcline. More distal sediments with lower organic carbon contents appear to have a

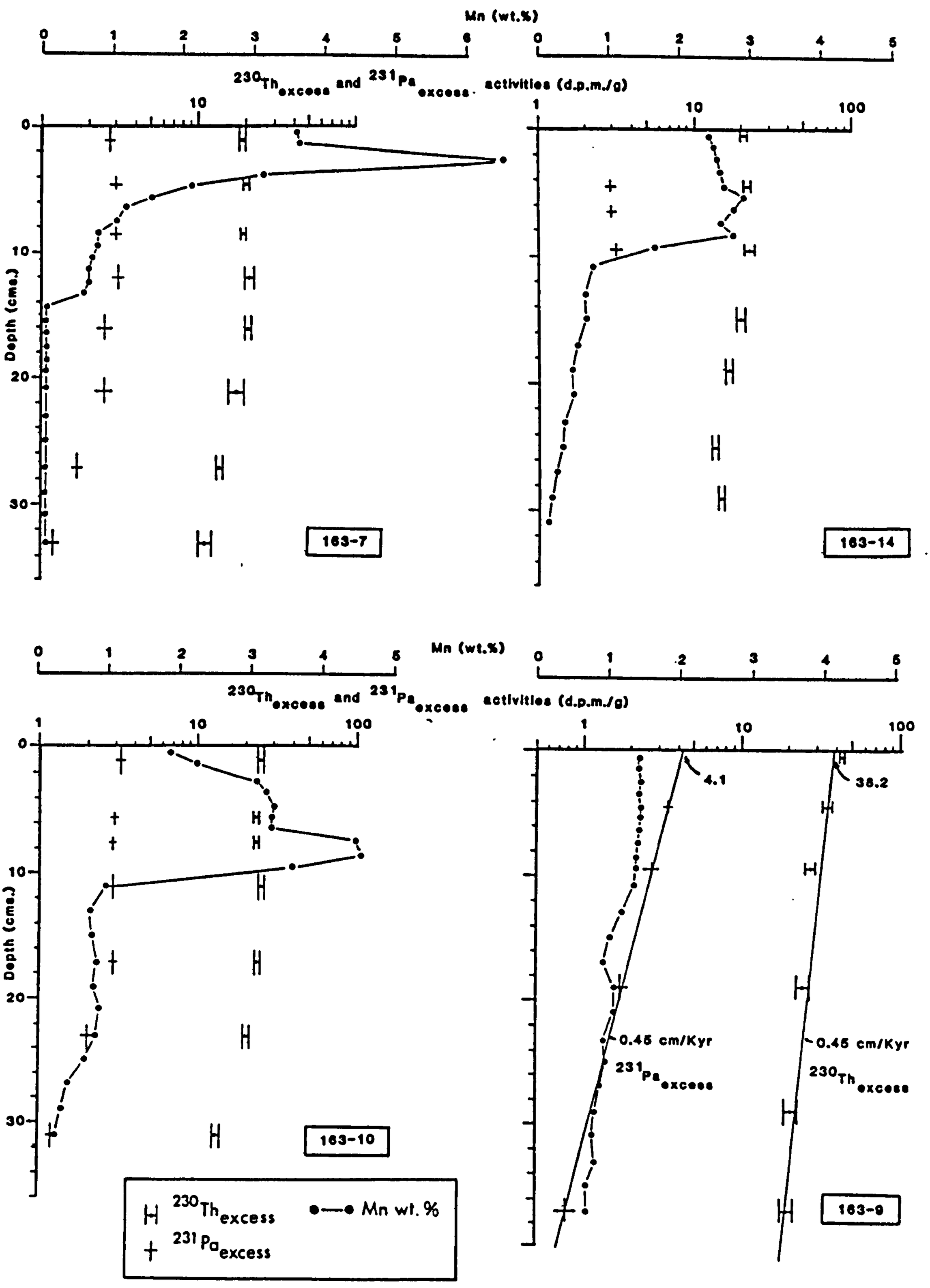

FIGURE 7.2 Excess ^{230}Th and ^{231}Pa activities for oceanic sediments from the Baja California transect, together with solid phase Mn (salt-free). The position of the Mn redoxcline indicates that diagenetic remobilisation occurs faster than sediment mixing by benthic activity.

less abundant benthic community that penetrates deeper into the sediment and allows for a deeper redoxcline.

Beneath the biomixed zone in the three hemipelagic cores the radionuclide distribution occurs within sediment deposited under different conditions to that existing today. The higher $CaCO_3$ levels and the increasing amount of Zr relative to Al (Figure 3.2) indicates that the sediment is coarser in overall grain size and probably accumulated more rapidly. This pattern of sedimentation will have an influence on the activity of ^{230}Th and ^{231}Pa in the sediment, and will be discussed below.

7.4 DISCUSSION

Two different approaches may be taken towards the understanding of the processes involved in radionuclide accumulation in sediments from the Baja California margin, elaborating on the "constant flux" and "constant activity" models outlined in Section 7.2. In a "constant flux" model the total integrated activity of the radionuclide at any one site should be more or less constant, and hence the rate of accumulation of the nuclide in the sediment would also be constant and independant of the rate of supply of bulk sediment. Dissolved ^{234}U and ^{235}U in the oceans should give rise to a $^{230}Th/^{231}Pa$ activity ratio of 10.8, but this ratio is rarely seen in the deep sea. In addition Kadko (1980a, 1983) suggested that the addition of ^{230}Th to the sediment is

linearly proportional to water depth due to the high solubility and extremely long residence times of U in the oceans. As 2.8 atoms of ^{230}Th are produced per minute per litre of seawater then at steady state the standing crop of ^{230}Th from this source, N_{sw}, in sediments would be:

$$N_{sw} = (2800 \text{ atoms/min/m}^3) \times Z$$
$$= 0.28.Z \text{ atoms/cm}^2\text{/min.}$$

where Z is the water depth in metres.

In contrast, the commonly used "constant activity" (Osmond, 1979) model considers that radionuclides are carried to the seafloor by adsorbtion on settling particles. If the particle flux increases so too will the activity. In this case the ratio of nuclide to sediment, in other words the concentration of the nuclide, is used in the model. The relationship that combines the generation of the nuclide from seawater (nuclide flux, F), the rate of bulk sediment supply (S) together with the scavenging of the former by the latter, resulting in nuclide activity within the sediment, (A), is represented in Figure 7.3. The implications of the constant flux and constant activity model treatment of radionuclide accumulation is now discussed in detail.

7.4.1 *Constant Flux Model*

A simple application of the constant flux model, used by Kadko (1980a, 1983) to balance the inventory of accumulated radionuclide in the sediment to that of the overlying water column production, is repeated for 163-9. In this core it is found that the sediment column inventory balances the water column supply to within 20% (Table 7.3). The surface

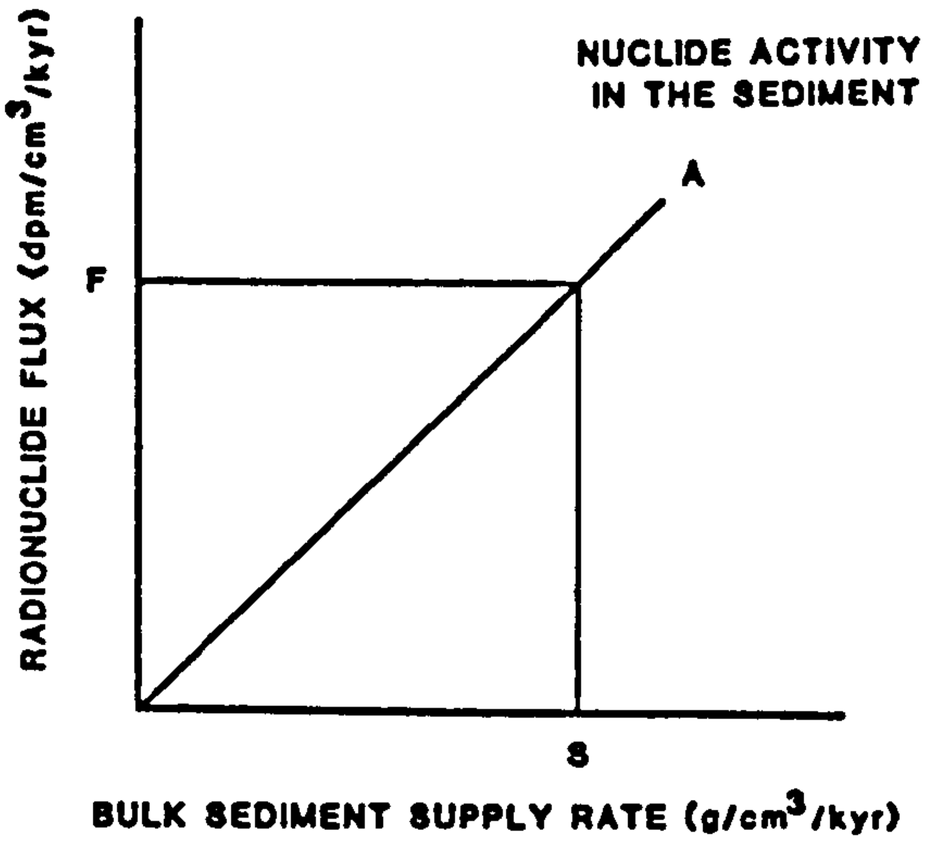

FIGURE 7.3 The relationship between bulk sediment supply rate (S) and the generation of the radionuclide from seawater (F) resulting in nuclide activity within the sediment (A)

after Osmond (1979)

$^{230}Th_{excess}/^{231}Pa_{excess}$ activity ratio implied by the regression line intercepts in Figure 7.2 is somewhat lower than the theoretical value of 10.8; this is caused by the additional $^{231}Pa_{excess}$ present relative to $^{230}Th_{excess}$.

TABLE 7.3

COMPARISON OF SEDIMENT INVENTORY AND WATER COLUMN SUPPLY FOR 163-9

Nuclide	Water coluan supply (P^*)	Sediment inventory (Σ^+)	Σ/P
$^{230}Th_{excess}$	1000	1046	1.0
$^{231}Pa_{excess}$	41	51	1.2

*For ^{230}Th: $P = 0.28.z$ (atoms.cm^{-2}.min^{-1}) where z is the water column depth (m) (Kadko 1980). For ^{231}Pa: $P = 0.011.z$ (atoms.cm^{-2}min^{-1}).

+$\Sigma = A_o.\rho.s/\lambda$ (dpm.cm^{-2}); where A_o is the surface value of excess activity (dpm g-1). ρ is the mean weight dry sediment per unit volume (g cm^{-3}), s is the sediment accumulation rate (cm kyr^{-1}) and λ is the disintergration constant (kyr^{-1}) (Krishnaswami et al, 1971).

Work on the removal and fractionation of the two nuclides from the water column has shown that activity ratios of 20-30 commonly occur in open-ocean sediments (Ku, 1966; Ku *et al*, 1972; Cochran, 1979; Cochran and Krishnaswami, 1980; Kadko, 1983), whilst analyses of sediment trap and suspended particulate material can be higher still, 40-50 (Anderson *et al*, 1983a). These authors propose that there is a preferential association of ^{230}Th with particulate material in this environment relative to ^{231}Pa. In contrast,

$^{230}Th_{excess}/^{231}Pa_{excess}$ activity ratios in trap and particulate material from the marginal environment of the Guatemala and Panama Basins (Anderson *et al*, 1983b) are much lower (4-8) and suggest a more active removal of ^{230}Th and particularly ^{231}Pa at ocean margins. In the hemipelagic cores off the Baja California continental margin there is a monotonic decrease in the mean $^{230}Th_{excess}/^{231}Pa_{excess}$ activity ratio of the biomixed layer landwards along the transect (Table 7.2). This activity ratio could be described as a stripping or scavenging ratio indicating the preferential removal of ^{231}Pa over ^{230}Th, relative to average water column production (Table 7.2). This is confirmation from the sediment record that Anderson *et al*'s hypothesis of preferential removal of ^{231}Pa removal at ocean margins is operating off Baja California. However, the box model approach of the open ocean and ocean margin scavenging of isotopes (Anderson *et al*, 1983b) oversimplifies the margin removal process as a continuum in the degree of removal exists.

7.4.2 *Constant Activity Model*

Usually, the rate of accumulation of sediment is determined by observation of the exponential decrease of $^{230}Th_{excess}$ or $^{231}Pa_{excess}$ with depth in the core. In this way the constant activity model (Osmond, 1979) is applied to the concentration of the nuclide per unit of total sediment. This method was used to calculate the accumulation rate in 163-9 of 0.45 cm kyr^{-1} and requires certain assumptions which have been outlined above. In particular it assumes that there has been

constant accumulation of the sediment with time; a reasonable proposition for the open ocean but clearly invalid for sediments reflecting glacial/interglacial variations in sediment input, recently pointed out by Bacon (1984). Indeed, application of the constant activity model to nuclide data obtained from beneath the biomixed layer results in accumulation rates that are considerably lower than those obtained by ^{14}C (Sawlan, 1982) or from compositional trends (Chapter 3).

A complication arises in considering accumulation rates of the two nuclides in 163-9 and the sub-biomixed sediment in the three hemipelagic cores. The discrepancy between the apparent $^{230}Th_{excess}$ and $^{231}Pa_{excess}$ accumulation rates increases landwards. This is shown in Figure 7.4 in which the nuclide activities and horizon core depths have been normalised so that the curves for $^{230}Th_{excess}$ and $^{231}Pa_{excess}$ should be congruent, consistent with the same sediment accumulation rate within each core. (The higher U contents at depth in 163-7 will tend to affect the plot for this core).

7.4.3 *Implications of the Constant Flux and Constant Activity Models*

The Pacific margin off Baja California is complicated by variations in overall sediment flux to the seafloor with time (depth in the core) and space (distance from the shelf), and the non-uniformity of nuclide supply to the margin. The result is that constant flux and constant activity models must be considered in tandem if a unifying hypothesis is to be erected.

Taking the relationship:

$$A = F/S$$

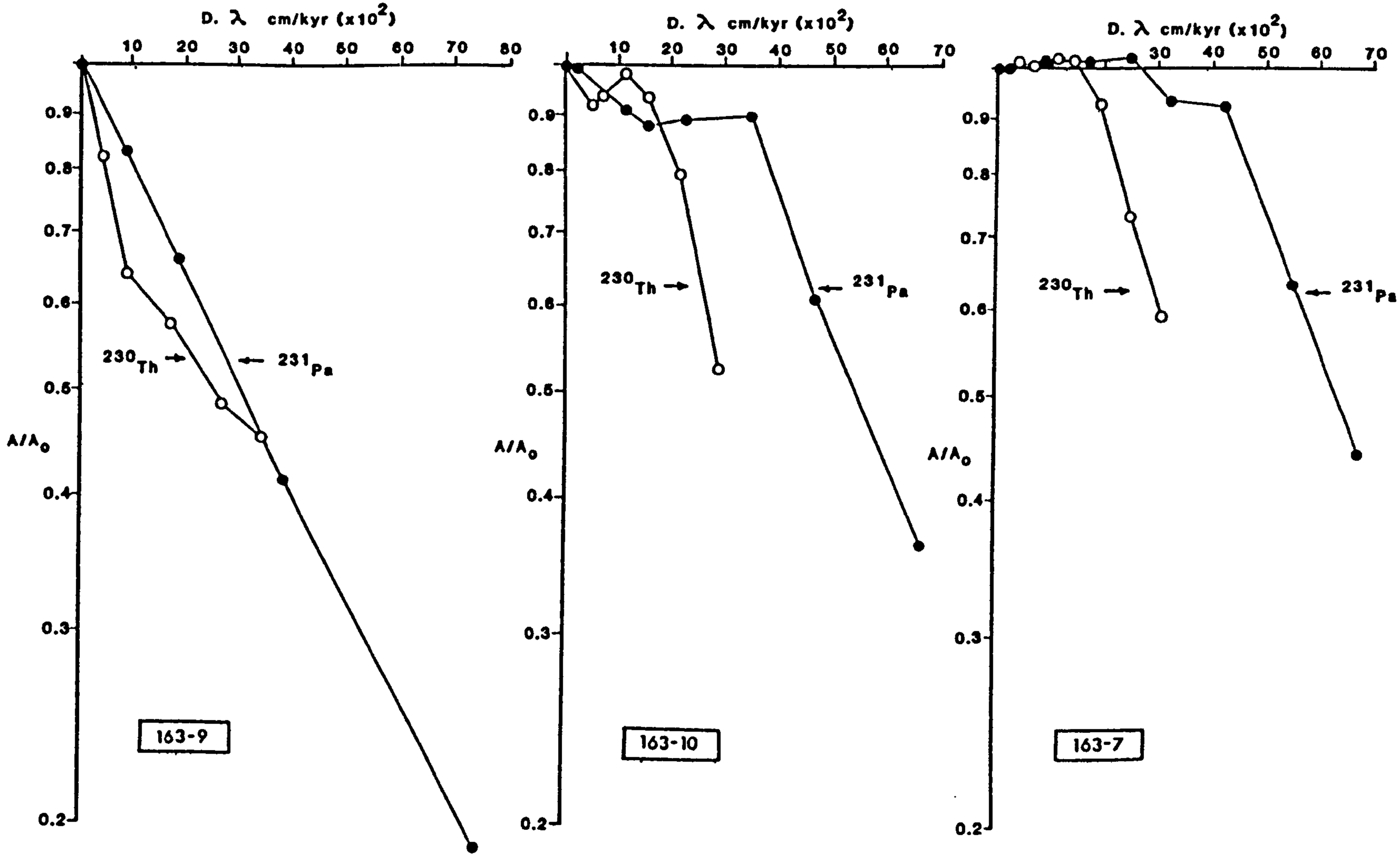

FIGURE 7.4 Profiles of excess ^{230}Th and ^{231}Pa in oceanic sediments off Baja California. The activity values (A) are normalised to those at the core top (A_o), and core horizon depths (D) are normalised in terms of the respective decay constants. If the two nuclides were behaving similarly then the normalised curves would all be congruent, corresponding to a single average sediment accumulation rate.

of Osmond (1979) several scenarios are possible if the bulk sediment supply decreases from its average value (S), analogous to the change in sedimentation from glacial to interglacial episode at the ocean margin. These are depicted in Figure 7.5.

(1) The bulk sediment supply (S) may change from S to S' resulting in a change in nuclide activity within the sediment, A'(1), whilst the nuclide flux, F'(1), remains constant, corresponding to "constant flux".

(2) The nuclide flux, F'(2), decreases proportionately with S, producing no change in nuclide activity within the sediment, A'(2), corresponding to "constant activity".

(3) The nuclide activity in the sediment, A'(3), increases while the nuclide flux, F'(3), decreases.

If $^{230}Th_{excess}$ and $^{231}Pa_{excess}$ accumulation of Baja California were to be described by a constant flux model then in a situation where the bulk sediment supply rate increases, such as moving upslope at the present day or downcore to glacial sediments, we would expect the nuclide activity in the sediment to decrease (Case 1). Here, the nuclide activity is apparently "diluted" by the higher input of oxide, aluminosilicate and organic particles. However, if the water column supply of the nuclide at ocean margins is indeed higher (especially ^{231}Pa) then cases 2 and 3 are possible. This is probably a more realistic situation as many lines of evidence (Bhat *et al*, 1969; Broecker *et al*, 1973; Anderson *et al*, 1983b) have suggested that with a greater bulk sediment supply rate there will be a lower residence time of the nuclide, indicative of greater scavenging at ocean margins.

The decreasing $^{230}Th_{excess}$ activity within the sediment

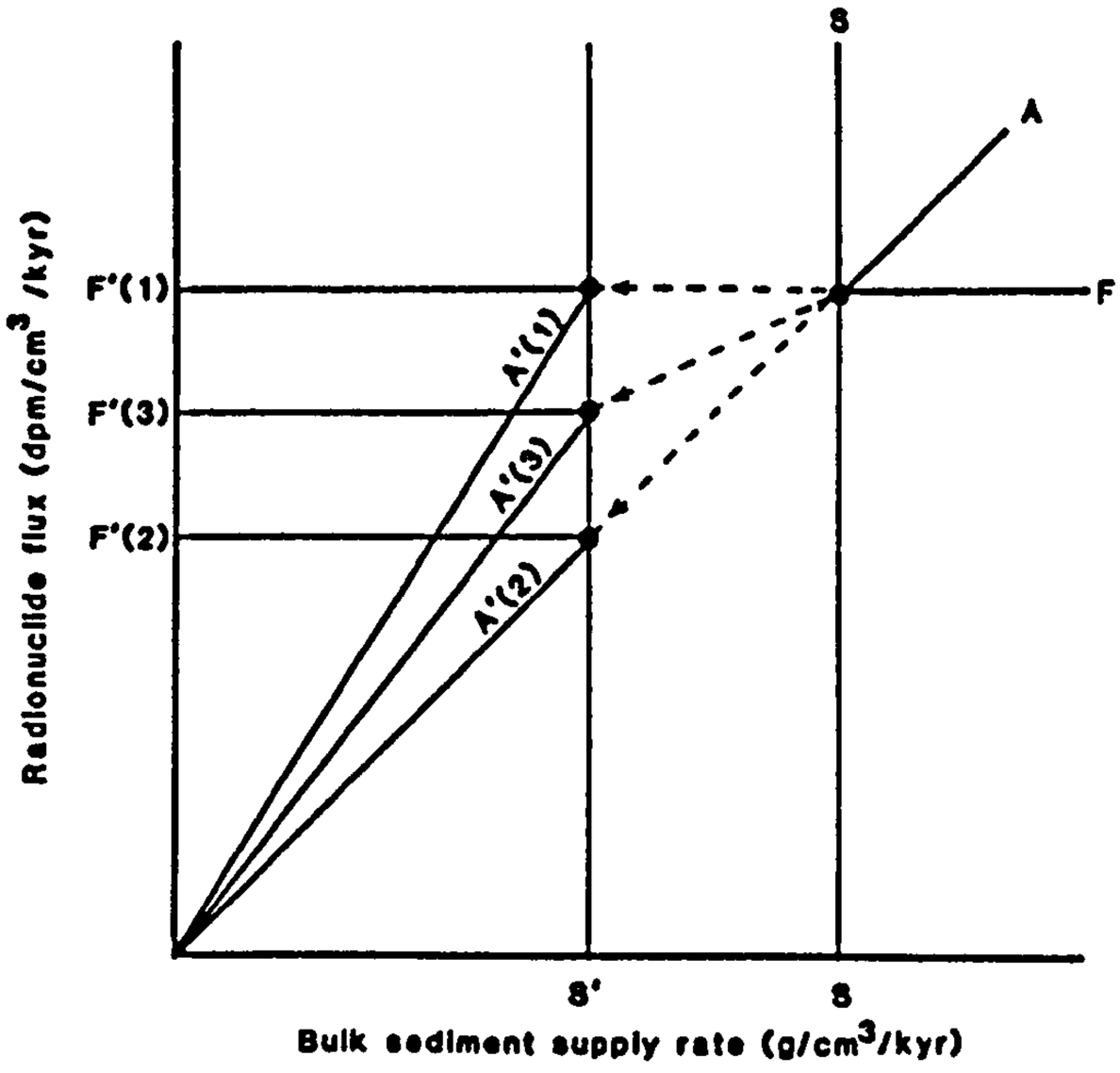

FIGURE 7.5 The relationship between radionuclide flux (F) and nuclide activity within the sediment when the bulk sediment supply drops from S to S', as would happen at the termination of a glacial episode:
(1) The bulk sediment supply (S) may change from S to S' resulting in an increase in nuclide activity within the sediment, A'(1), whilst the nuclide flux, F'(1), remains constant, corresponding to "constant flux".
(2) The nuclide flux, F'(2), decrease proportionately with S, producing no change in nuclide activity within the sediment, A'(2), corresponding to "constant activity".
(3) The nuclide activity in the sediment, A'(3), increases whilst the nuclide flu, F'(3), decreases.

biomixed layer upslope to environments of higher bulk sediment supply rate is reasonable evidence of this process. The distribution of $^{230}Th_{excess}$ and $^{231}Pa_{excess}$ activity beneath the biomixed layer results from a complex interplay of dilution by increased bulk sediment supply during glacial episodes and increased radionuclide scavenging. Off Baja California the net result is a dominance of the former over the latter at depth creating excessively low nuclide activities within the sediment column resulting in apparent low sediment accumulation rates. In this case the constant activity model is unsuitable for determining sediment accumulation rates.

A major outstanding question concerns the discrepancy between the average mixed layer activities of $^{230}Th_{excess}$ and $^{231}Pa_{excess}$, and the non-congruency of the curves in Figure 7.4 These must relate to the mechanism of nuclide incorporation by particles into the sediment and perhaps the preference of oxides over aluminosilicates. In the open ocean aluminosilicate flux dominates over oxide flux and in this situation ^{230}Th is preferentially scavenged (Anderson *et al*, 1983a). On the other hand, the higher activity of ^{231}Pa in oxide related systems such as Mn nodules (Sackett, 1966; Ku and Broecker, 1969; Krishnaswami and Cochran, 1978; Moore *et al*, 1981) and metalliferous oxide deposits (Kadko, 1980b) suggests that this nuclide has a greater affinity for these types of chemical deposit. Table 7.4 indicates the relative amounts Mn and Al in filtered, suspended particulate (>0.4 um) matter and in surface sediments along the Baja California transect (N.B. Price, unpub. data). All the Mn/Al ratios are higher than average shale or oceanic sediment. The increase in Mn over Al in

TABLE 7.4

SUSPENDED PARTICULATE MATTER AND SURFACE SEDIMENT COMPOSITION

Station TGT-145 - 5				Station TGT-145 - 6				Station TGT-145 - 7			
Depth (m)	Mn	Al	Mn/Al	Depth (m)	Mn	Al	Mn/Al	Depth (m)	Mn	Al	Mn/Al
200	14.73	0.27	0.055	200	23.56	0.81	0.029	217	20.16	0.22	0.094
1000	14.19	0.17	0.083	1046	18.73	0.24	0.078	990	19.29	0.19	0.102
2994	16.39	0.18	0.091	3070	43.81	0.31	0.141	2934	80.11	0.32	0.250

Station TGT-163 - 9				Station TGT-163 - 10				Station TGT-163 - 14				Station TGT-163 - 7			
Depth (cm)	Mn	Al	Mn/Al	Depth (cm)	Mn	Al	Mn/Al	Depth (cm)	Mn	Al	Mn/Al	Depth (cm)	Mn	Al	Mn/Al
0-1	1.43	7.92	0.181	0-1	1.83	7.91	0.231	0-1	2.40	7.67	0.313	0-1	3.58	7.49	0.478

Water depth in meters

Particulate Al in µg/l
Particulate Mn in ng/l

Sediment Mn and Al in wt.%

Average shale Mn/Al = 0.011
Lithogenous clay Mn/Al = 0.080
(Turekian and Wedepohl, 1961)

suspended particulates must be related to two processes within the marginal environment. The increase in particulate Al landwards is due to the greater influence of resuspended aluminosilicates at the top of the slope and continental rise, whilst the anomalously high concentrations of particulate Mn may occur due to the recycling of the element within organic-rich sediment and overlying water column. In this way fractionation of ^{231}Pa over ^{230}Th will be enhanced in marginal sediments. Consequently, ^{231}Pa in the hemipelagic environment does not conform to a modified constant flux model, as is the case with ^{230}Th, due to chemical controls on its behaviour making it less suitable for the determination of sediment accumulation rates.

CHAPTER 8

DIAGENETIC MINERAL FORMATION OFF BAJA CALIFORNIA

8.1 INTRODUCTION

Berner (1981 a,b) has classified sedimentary environments in which diagenetic minerals are forming into three categories: oxic, anoxic-nonsulphidic, and anoxic-sulphidic. This classification is based on the presence or absence of detectable dissolved oxygen or detectable hydrogen sulphide. In Chapter 4 the diagenesis of organic matter was discussed with reference to oxic, sub-oxic, and anoxic environments. As the process of formation of many diagenetic minerals initially originates with organic matter decomposition and involvement of organic and inorganic species it is important to relate Berner's classification to the terminology used in this thesis. Common to both approaches is the characterisation of the oxic environment by aerobic respiration, nitrification and the onset of denitrification. The anoxic-nonsulphidic zone of Berner can preceed sulphate reduction, equivalent to suboxic diagenesis and the first appearance of dissolved Mn^{2+}, or succeed sulphate reduction in the case of methane formation, the criterion being the lack of H_2S. Anoxic-sulphidic environments are equivalent to the zone of anoxic diagenesis in which sulphate is consumed.

In the study of Baja California diagenetic mineral formation the sequence of oxic, sub-oxic and anoxic diagenetic zones is adhered to. For each zone the characteristic diagenetic mineral assemblage is described morphologically and geochemically in relation to its depositional environment. In this way it is hoped that a clear understanding of the interplay between mineral genesis and geochemical environment is achieved, rather than persue an indepth appraisal of our present knowledge of diagenetic mineral formation, which is outside the scope of this chapter.

8.2 OXIC MINERAL FORMATION

The formation of Mn oxyhydroxides (primarily vernadite) in the surficial sediment of the hemipelagic environment, and throughout the oxic sediment of the oceanic red-clay is discussed at length in Chapter 6. Instead, this section deals with the formation of apatite in shallow-water shelf sediments, in particular core 145-17.

8.2.1 *Diagenetic apatite formation*

As the availability of P is not limited by redox dissolution/reprecipitation reactions in the same way as Mn and Fe, but instead has an important source in the decomposition of organic matter through oxic, suboxic and anoxic diagenesis (Table 4.4) the formation of apatite is not strictly limited to aerobic respiration. In this respect the general formation of apatite does not conform to the classification used here, however the particular environment of apatite formation off Baja California appears to favour oxic/suboxic conditions (see below). At this point it is important to note that the occurrence of large phosphorite nodules and crusts, and smaller pellets in the surface lag of 163-13 is not proof of oxic formation *per se*, but results from removal of the original mud matrix by current action. The occurrence of many such nodules in the geological record appears to be related to concentration by current and storm action and are not considered here. In contrast, the diagenetic apatite in 145-17 is undoubtedly of *in situ* origin (Jahnke *et al*, 1983).

Results

Figure 8.1 displays the depth profile of solid phase P in core 145-17. From an initial concentration of 0.60 wt.%, P increases to a core maximum of 2.16 wt.% at 5-6 cm depth. A smaller increase (0.71-0.73 wt.%) occurs some 10 cm deeper. Figure 8.1 also indicates the increase in P and Sr relative to Al as several lines of evidence (Si/Al, Zr/Al, Figure 3.4; C_{org}, Figure 4.2) indicate a grain size and sediment type change from silt in the upper ~6 cm to mud below. Also shown in Figure 8.1 is NO_3^-, PO_4^{3-} and dissolved U from Jahnke *et al* (1983) who analysed a sub-core from the same boxcore. Assuming the analysis of the sample from between 12-14 cm depth contains little, if any, diagenetic apatite then the difference in P and Sr between this sample and the enrichment at 5-6 cm depth is an indication of the Sr uptake in the apatite, calculated at 124 ppm per wt.% P, or 3840 ppm per mole P. XRD was unable to reveal the presence of crystalline apatite in the core, unlike Jahnke *et al* (1983). However, SEM examination identified microcrystalline growths of apatite (EDAX confirmed the presence of P) in foraminifera tests (Plate 8.1a,b).

Discussion

The sudden increase in pore water PO_4^{3-} in the top few cm of 145-17 above normal seawater (marked by an arrow on the abcissa, Figure 8.1) indicates probable release during decomposition of organic matter, and/or possible dissolution of phosphatic bone and teeth debris (Suess, 1981). With regard to the age of the deposit, Jahnke *et al*, (1983) used $^{230}Th/^{234}U$ activity ratios to show that its maximum age is 3000-4000

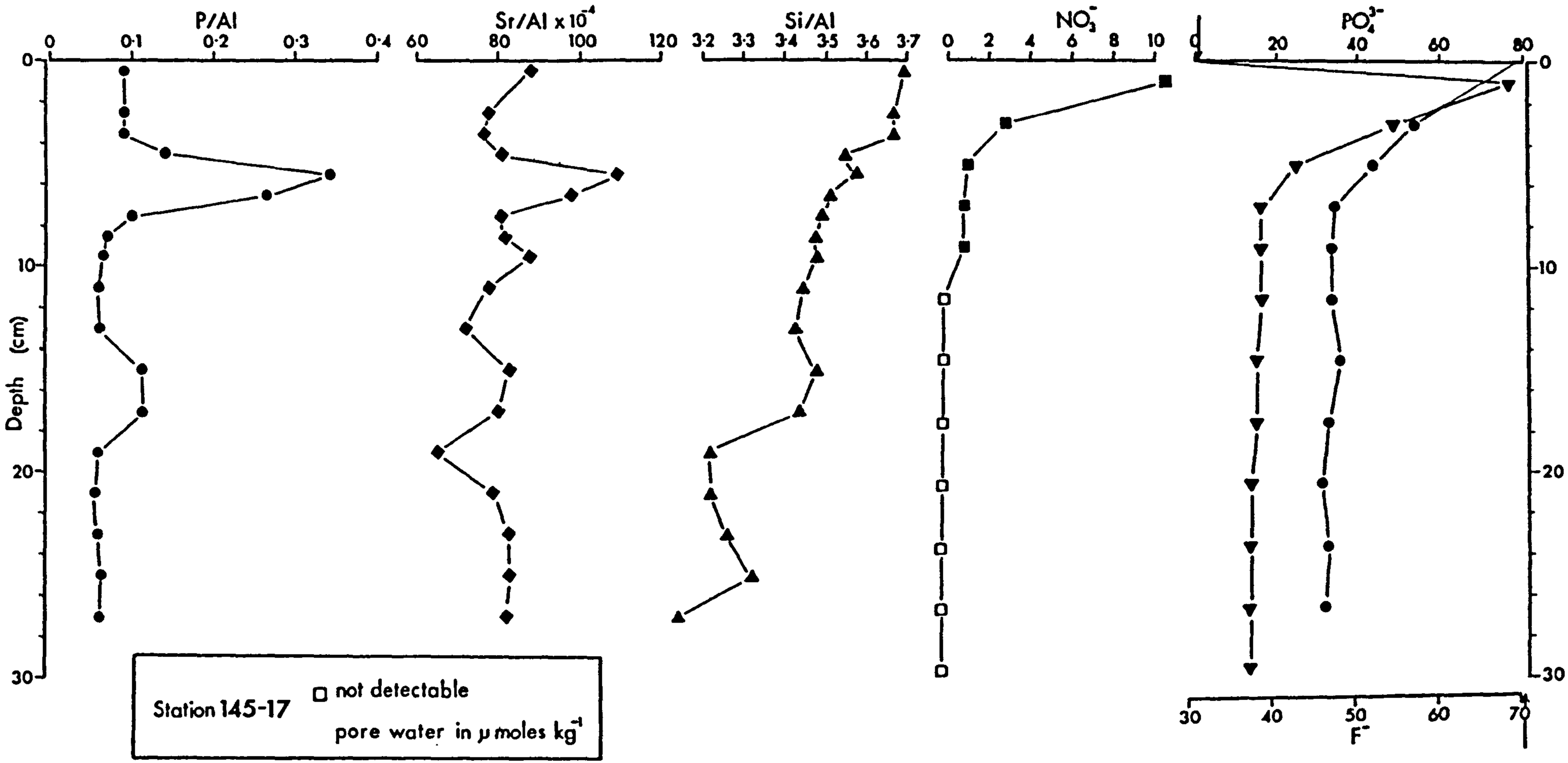

FIGURE 8.1 Profiles of P/Al, Sr/Al ($x10^{-4}$) and Si/Al with depth in core 145-17 from the continetal shelf off Baja California. Also shown are nitrate, phosphate and fluoride pore water concentrations for a sub-core from the same box-core in umole/kg (Jahnke *et al*, 1983). Bottom water phosphate and fluoride concentrations are indicated by arrows.

years; this occurrence therefore represents Recent diagenetic apatite formation. The curvature of the dissolved PO_4^{3-} and soluble U profiles (Figure 8.1) at 6 cm depth is indicative of diagenetic precipitation within the sediment. Calculation of the current rate of formation from the PO_4^{3-} gradient indicates thet 300-600 years would be required to produce the measured P maximum (Jahnke *et al*, 1983). The pore water NO_3^- profile suggests that the apatite peak is at the boundary between oxic and suboxic conditions (absence of the pore water Mn^{2+} makes this statement equivocable). As outlined above, it is not the diagenetic environment (redox system) that controls P regeneration, rather the availability of PO_4^{3-} and the presence of a suitable locus of precipitation.

The origins and conditions of phosphorite formation have been hotly debated over the years. A summary of some of the proposed factors influencing formation are reproduced in Table 8.1. Most authors believe the supply of dissolved PO_4^{3-}, either directly through organic matter decay, or by upwelling and the supply of nutrient-rich waters, is necessary. Jahnke *et al*'s study revealed that the Baja California apatite is not controlled by pH, nor by pore water Mg^{2+} content. As chemical activity of PO_4^{3-} increases with pH (Roberson, 1966; Pytkowicz and Kester, 1967), high pH had been suggested (Guldbrandsen, 1969; Burnett, 1977) as a controlling factor. Likewise, laboratory studies by Martens and Harriss (1970) found that amorphous calcium phosphate did not convert to crystalline apatite when allowed to react with seawater for up to eight months. However, in the absence of Mg^{2+} conversion occured in four days suggesting to several workers (Burnett, 1977; Kastner *et al*, 1984) that phosphorite cannot form in the presence of

TABLE 8.1

FACTORS LEADING TO DIAGENETIC APATITE FORMATION

Large supply of PO_4^{3-} (nutrient-rich waters and organic matter)	1 2 3 4 5 6 8
Clay mineral transport	7
Warm temperatures	1 4 7
High salinity	1
High pH	1 4 7
High bacteriological activity	7
High pore water Ca/Mg ratios	4 7 9
Suitable nucleation sites	4 7
Low terrigenous accumulation rates	1 2
Association with boundaries of the oxygen minimum zone	2 4 8

1 Guldbrandsen (1969)
2 Manheim *et al* (1975)
3 Piper and Codispoti (1975)
4 Burnett (1977)
5 Price and Calvert (1978)
6 Baturin and Bezrukov (1979)
7 Bremner (1980)
8 Jahnke *et al* (1983)
9 Kastner *et al* (1984)

seawater concentrations of Mg^{2+}. Depletion of Mg^{2+} in pore fluids by diagenetic reactions and the formation of Mg-bearing clay minerals sepiolite, palygorskite, smectites or glauconite, or by dolomite formation have been envoked (Guldbrandsen, 1960; Burnett, 1977; Baturin, 1982; Kastner *et al*, 1984). The near seawater values of Mg^{2+} recorded by Jahnke *et al* (1983) suggest that crystalline apatite formation is not limited by the presence of Mg^{2+}. A recent note by Guldbrandsen *et al* (1984) on a "fortuitous" ten year long experiment on carbonate fluorapatite synthesised in seawater conceeded that:

> "..the effect of magnesium in seawater is to reduce the rate of reaction to a time of probably little consequence in the natural environment but one that is discouragingly long for laboratory study."

The availability and suitability of substrate for apatite formation has not received much attention in the literature. The presence of calcite has been shown to catalyse the precipitation of apatite (Stumm and Leckie, 1970) and act as a nucleating agent (Stumm and Morgan, 1970). SEM studies by Burnett (1977) indicate that many surfaces act as nucleation sites in the absence of carbonate; siliceous tests, feldspar crystals, fish-bone apatite. In each case the morphology of the acicular, hexagonal apatite cystals (see Burnett, 1977, Figure 7) is identical to that in Plate 8.1a,b. Similar morphologies are reported for nodules from the East Australian continental shelf (Marshall and Cook, 1980; Figure 3, E,F), and from precipitation from interstitial fluids in diatomaceous mud of the Namibian shelf (Bremner, 1980; Figure 8).

Jahnke *et al* (1983) state that the apatite spike is not a steady state feature and that some textural control on its precipitation may be operating. They measured C_{org} and found it to increase downcore, agreeing with determinations made in this study (Figure 4.2). They felt that the lower surface C_{org} levels are due to more O_2 respiration at the present day and that apatite precipitation began when oxic respiration became important, possibly due to a shift in the oxygen minimum. Evidence presented here (Si/Al, Zr/Al, Cl concentration; Chapters 3 and 4) indicate that the C_{org} profile relates to grain size. Therefore it is believed that the change in lithology from mud to silt in core 145-17 provides a more open sediment framework for diagenetic mineral precipitation, in common with other diagenetic mineral occurrences (see below). The coincidence of both the major apatite peak (5-6 cm) and the lower peak (15-17 cm) with the increase in Si/Al (Figure 8.1)

PLATE 8.1 Scanning electron micrographs of apatite and manganese carbonate:

(a) Microcrystalline apatite growing within a foraminifera test; core 145-17.

(b) Close-up of microcrystalline apatite in (a) showing the acicular, hexagonal habit.

(c) Botryoidal Mn-Ca-carbonate growing in a sponge spicule cavity resulting from Si dissolution: 28-30 cm depth, core 163-10.

(d) Botryoidal Mn-Ca-carbonate in a more open sediment framework: 28-30 cm depth, core 163-10.

(e,f) Close-up of Mn-Ca-carbonate showing a "cornflake" texture.

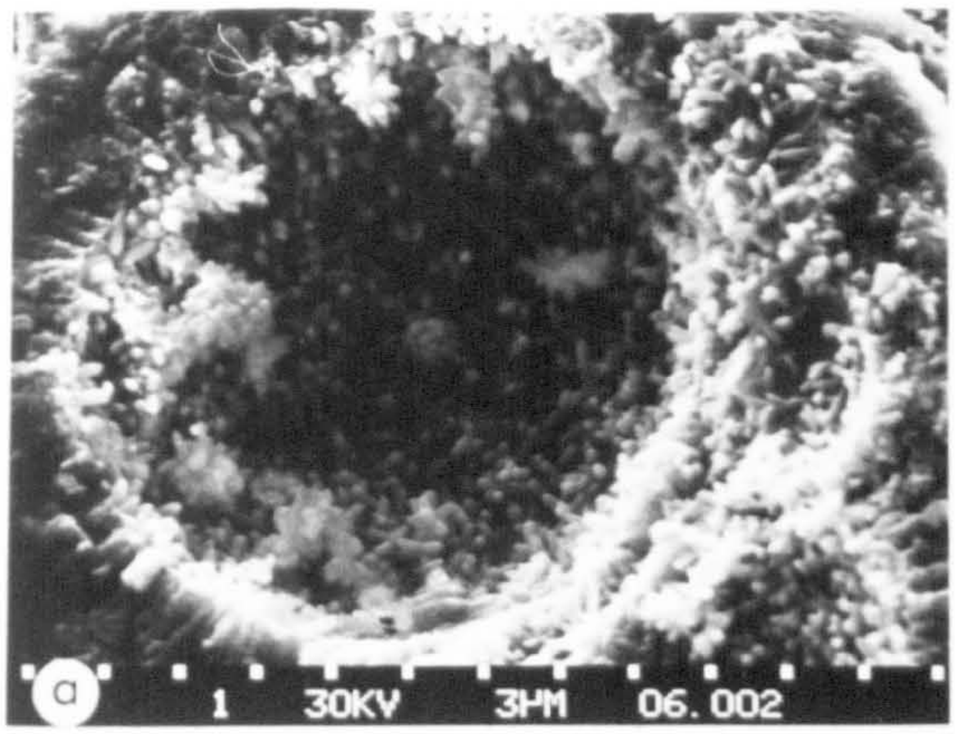
a
1 30KV 3HM 06.002

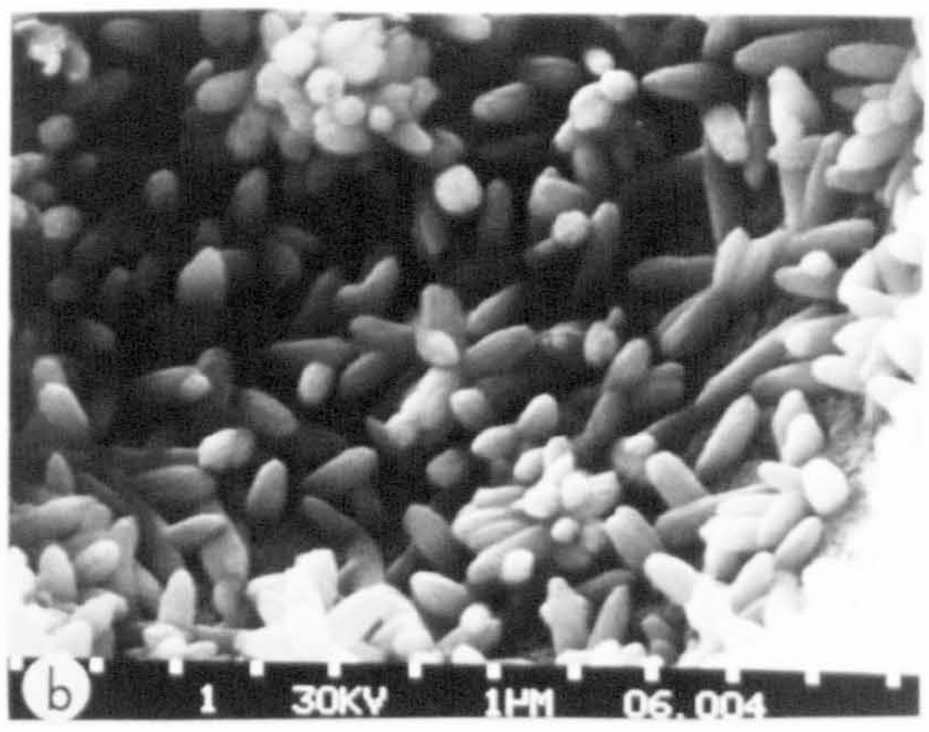
b
1 30KV 1HM 06.004

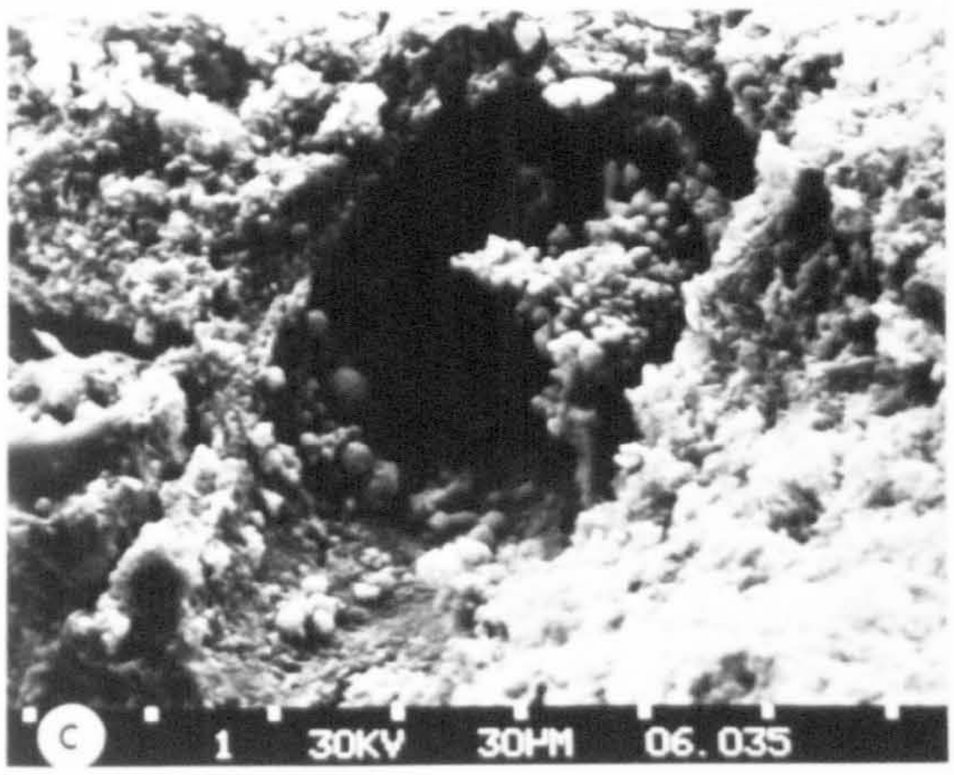
c
1 30KV 30HM 06.035

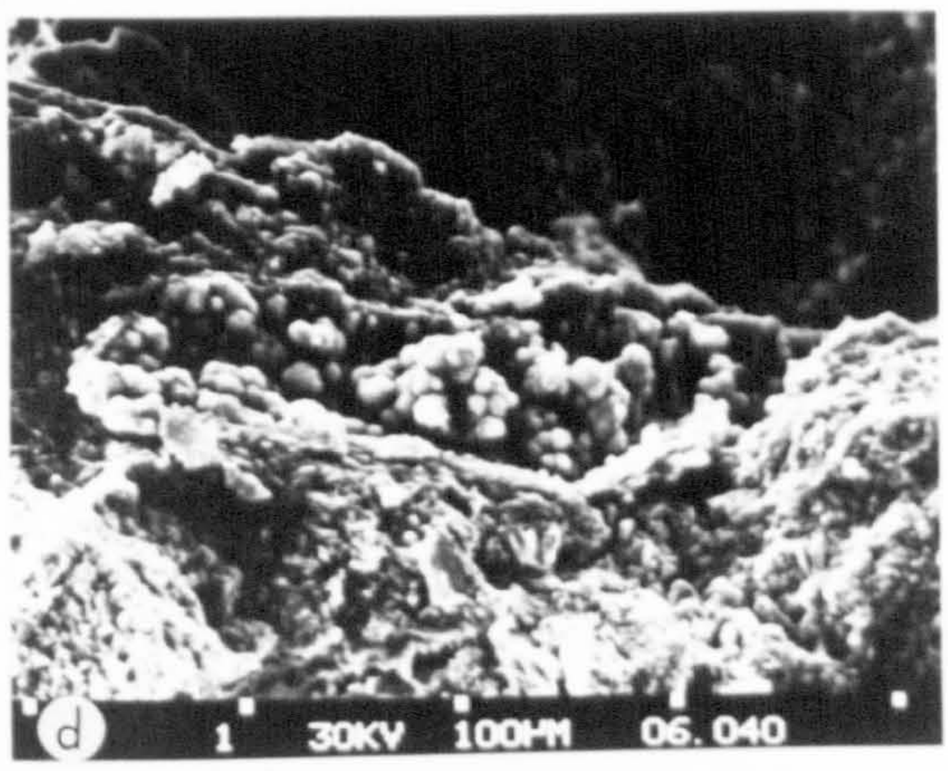
d
1 30KV 100HM 06.040

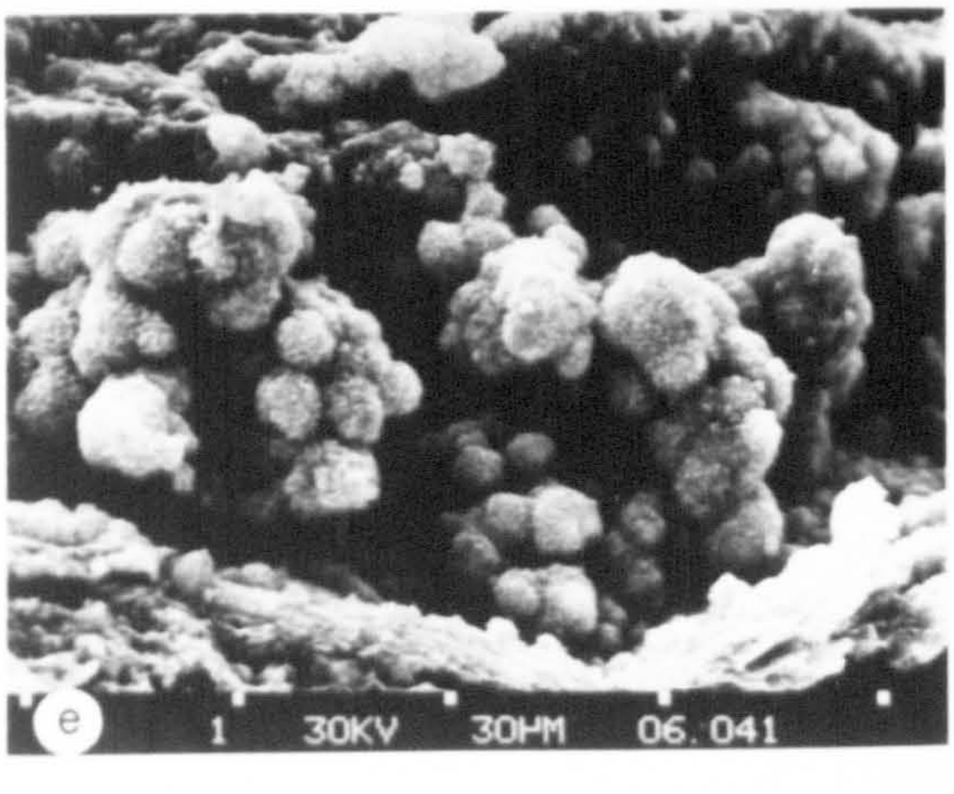
e
1 30KV 30HM 06.041

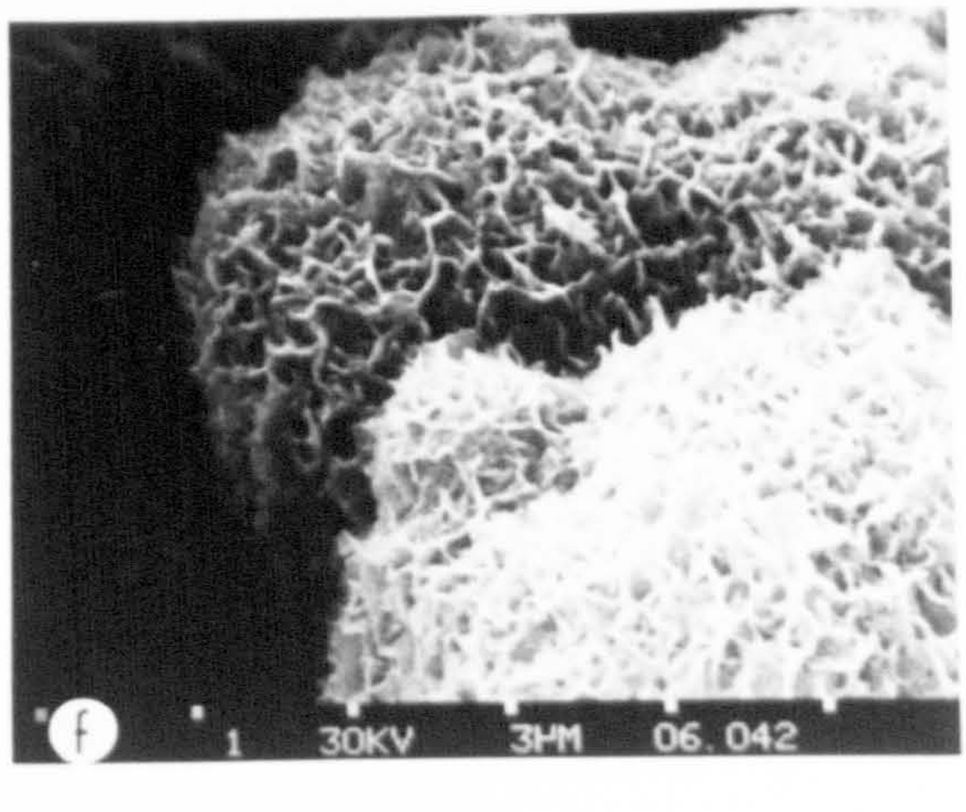
f
1 30KV 3HM 06.042

is striking.

8.3 SUBOXIC MINERAL FORMATION

Prior to the consumption of SO_4^{2-} and after utilisation of available O_2 (under marine conditions) NO_3^-, MnO_2 and Fe_2O_3 are the preferred electron acceptors in order of their thermodynamic free energy yield (Chapter 4). The reduction of Mn^{4+} and Fe^{3+} to their more soluble species, Mn^{2+} and Fe^{2+}, provides a major source of these cations for diagenetic mineral formation, together with any passive trace elements participating in the redox reactions (Chapter 6). As these reactions are linked with organic matter degradation, mineral formation may occur in a macro Eh environment or in a microenvironment where there is a high concentration of reactive organic matter which, during breakdown, sets up strong chemical gradients between the site of mineral precipitation and the enclosing environment. Examples of both these forms of diagenetic mineral formation are described and discussed below.

8.3.1 *Manganese Carbonate Formation*

Results

Inspection of the solid phase Mn profiles below the Mn redoxcline (Figures 6.1 and 6.2) reveal substantial Mn concentrations over and above average shale in the hemipelagic sediments at stations 163-14 and 163-10. Two mechanisms (Chapter 6) have been advocated for these observed

concentrations; (1) the formation of a mixed Mn-Ca-Mg carbonate phase, accounting for the elevated Mn profile at depth; (2) stabilisation of the vernadite (δ-MnO_2) by minor metal cations, accounting for the elevated oxidation states measured below the redoxcline (Figure 6.3). Mineralogical evidence has been found for precipitation of a mixed Mn carbonate phase.

Investigation of samples from 30-32 cm depth in 163-10 reveals the presence of lithified, creamy-white crusts often with black lustrous flecks and streaks. The crusts were too friable to obtain electron microprobe analyses, and too impure for wet chemical analysis, however observation with SEM and EDAX indicates a Mn, Ca, Si and Al bearing phase (Plate 8.1c,d,e,f; Figure 8.2). The black streaks suggest oxidation of the carbonate (Pedersen, 1979). The botryoids are 5-10 μm in diameter, have a "cornflake" surface texture (Plate 8.1e,f) (although this may be an artifact of sample preparation) and often occurs in cavities introduced by sponge spicule dissolution (Plate 8.1c) or an open sediment framework (Plate 8.1d). A similar morphology was described by Pedersen and Price (1982; Figure 3) for manganese carbonate from the Panama Basin, except that the botryoids were much larger (~100 μm in diameter). In the Baja California samples XRD analysis was inconclusive as to the mineralogy, possibly because of the amounts of impurities in the sample (quartz, feldspar, clays) and/or poor crystallinity of the carbonate.

Discussion

The constancy of interstitial Mn^{2+} pore water profiles have often been interpreted as being due to solubility control

by a rhodochrosite-type mineral phase (Li *et al*, 1969; Robbins and Callender, 1975; Murray *et al*, 1978; Klinkhammer, 1980; Sawlan and Murray, 1983). However, the pressure effect on alkalinity during core retrieval from deep water, and the lack of solubility data on natural mixed Mn-Mg-Ca carbonate phases which are often found (Manheim, 1961; Lynn and Bonatti, 1965; Calvert and Price, 1970b; Logvinenko *et al*, 1972; Suess, 1979; Pedersen and Price, 1982), as opposed to pure rhodochrosite has precluded accurate calculation of the degree of saturation of interstitial waters. Recently Johnson (1982) measured the apparent solubility of rhodochrosite in seawater at 3.3°C, which when corrected for pressure effects, gives a K_{sp} = 4.8 x 10^{-9} at 380 bars (Sawlan, 1982), compared with 2 x 10^{-10} at 0°C and 380 bars (Li *et al* (1969) using Garrels and Christ's (1965) K_{sp} for rhodochrosite), and 10.7 x 10^{-11} at 2.4°C and 414 bars (Pedersen and Price (1982) using Morgan's (1967) K_{sp} for rhodochrosite).

Ion concentration products (ICP)* have been calculated by Sawlan (1982) from Mn^{2+}, pH and alkalinity pore water measurements made at stations 145-7 and 145-8 at the top of the constant Mn^{2+} concentration zone, giving ICP's of 5.4 and 7.3 x 10^{9} respectively. The resulting saturation index,

$$\frac{\text{ICP}}{K_{sp}\text{ (in situ)}} = \Omega$$

is 1.16 for 145-7 and 1.61 for 145-8, theoretically confirming the precipitation of rhodochrosite in these cores.

---

* $\text{ICP} = a[Mn^{2+}].a[CO_3^{2-}]$
where a = total activity coefficient, and the species in brackets are the total analytical concentrations of each ion including free and complexed forms.

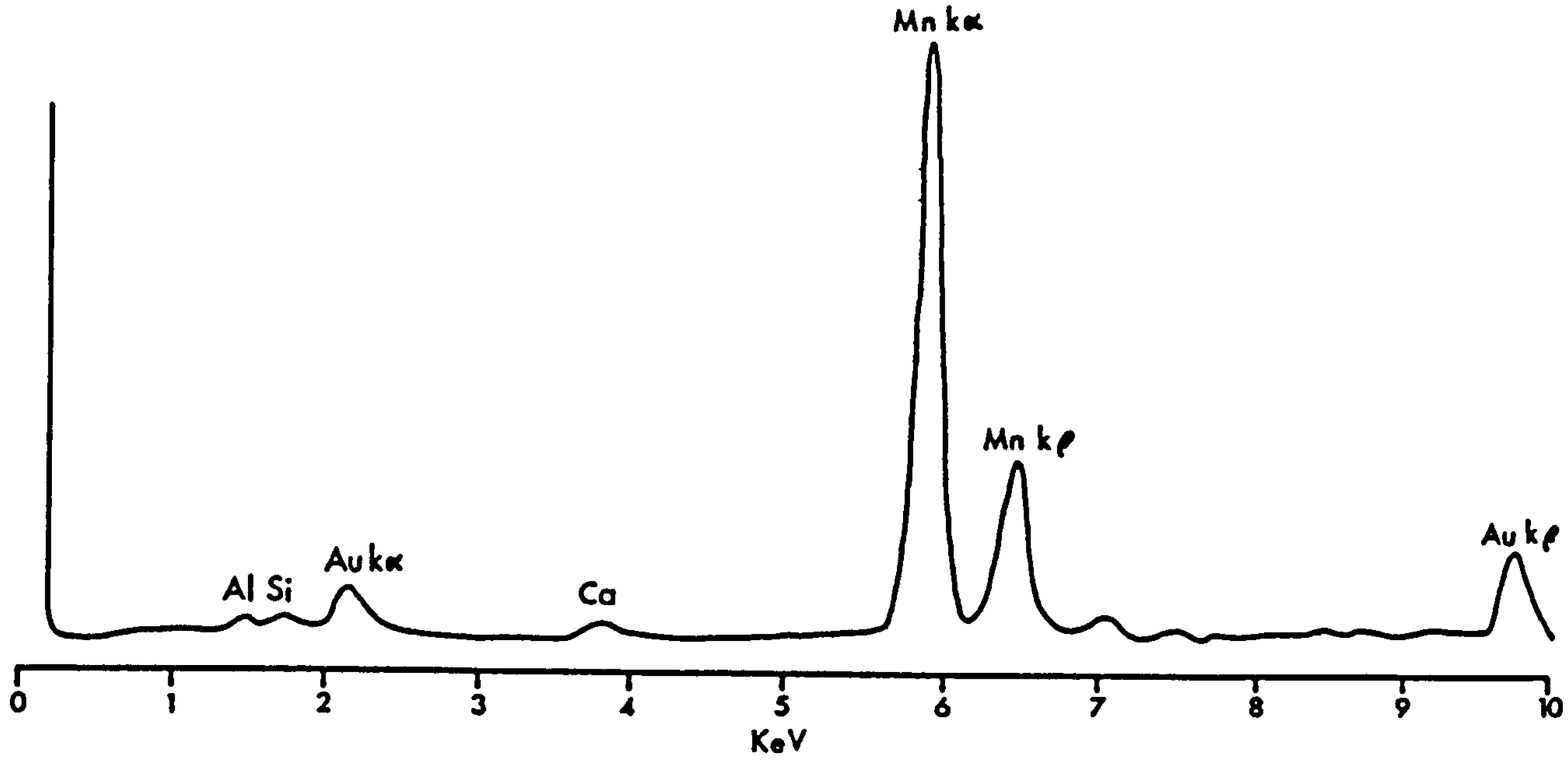

FIGURE 8.2 EDAX trace of botryoidal Mn-Ca carbonate from the base of core 163-10 as displayed in Plate 8.1.

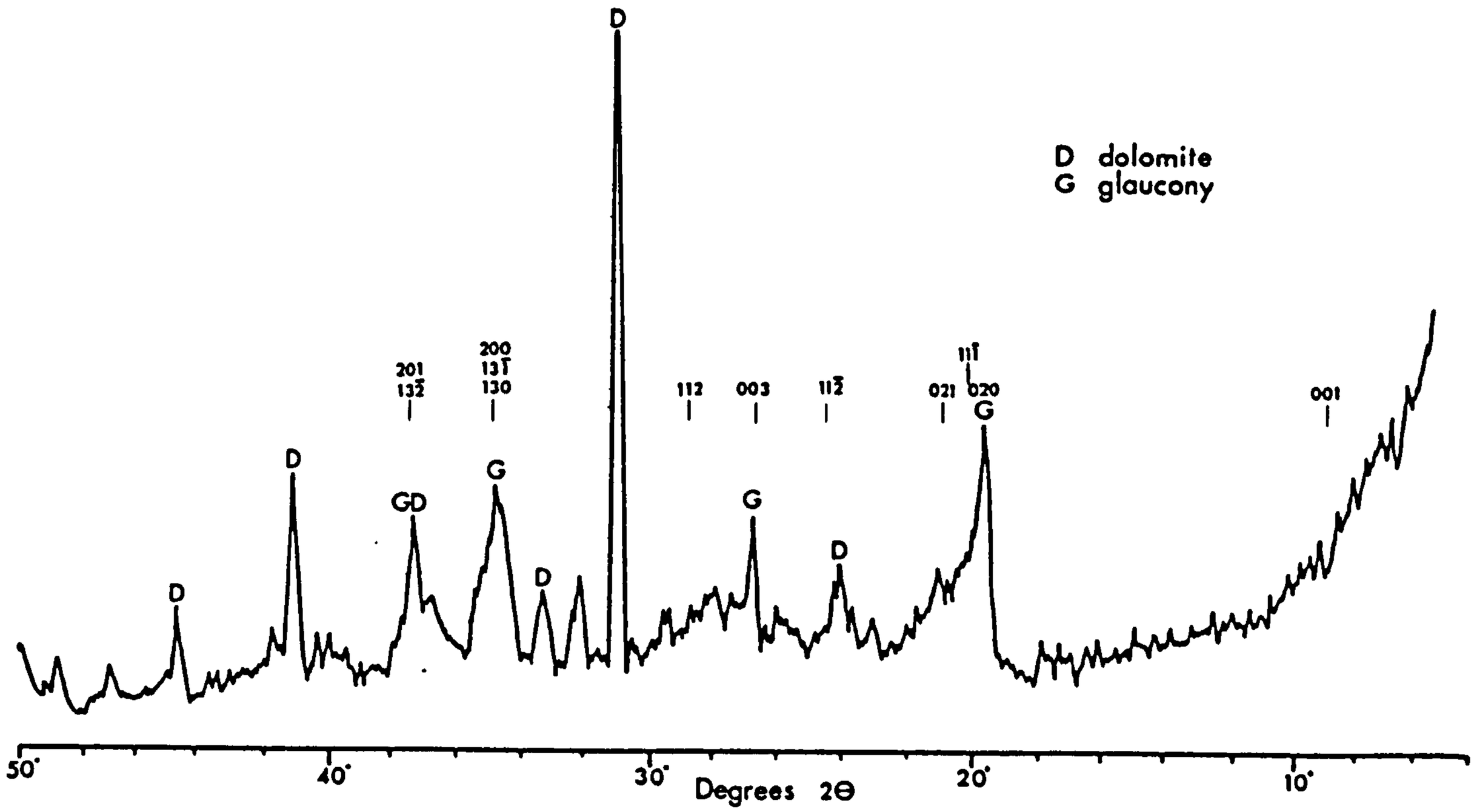

FIGURE 8.3 XRD trace of a dolomite-containing glaucony pellet from core 163-13, indicating the poor crystallinity of the glaucony (Cu Kα radiation).

TABLE 8.2

FACTORS INFLUENCING THE PRECIPITATION OF DIAGENETIC Mn-CARBONATE

Textural difference between Mn-carbonate horizons and surrounding sediment	1 2 3 5 6 7 8
Non-dependance on substrate type	7
Regulation by CO_2 distribution	3 4
High organic matter concentrations	3
Supply of Mn by surface oxide reduction	4 7 8
Mn supply by alteration of ferromagnesian silicates	5

1 Zen (1959)
2 Lynn and Bonatti (1965)
3 Strakhov (1969)
4 Logvinenko *et al* (1972)
5 Hein *et al* (1979)
6 Suess (1979)
7 Pedersen and Price (1982)
8 Yamada and Tsunogai (1984)

Table 8.2 outlines some of the proposed factors influencing the precipitation of diagenetic Mn-carbonate. Nearly all authors have remarked on the close association of the carbonate and coarse grain size of the host sediment, even though the substrate may be variable (Pedersen and Price, 1982). Quite how nucleation occurs is questionable but the evidence from Baja California (Plate 8.1c,d,e,f) suggests that a large pore volume is required. Strakhov (1969) and Logvinenko *et al* (1972) suggest that large pore volumes enable rapid diffusion of CO_2 out of the system, raising the pH and inducing Mn-carbonate precipitation. Pedersen and Price (1982) indicate that high levels of C_{org} are not required for sulphate reduction and consequent alkalinity increase. In both Loch Fyne and the Panama Basin Mn-carbonate precipitation occurs in suboxic sediments prior to major sulphate consumption

(Pedersen, 1979).

The occurrence of Mn-carbonate off Baja California is therefore attributed to two main factors: (1) a suitable locus for precipitation; (2) a surficial concentration of MnO_2 to supply the required Mn^{2+}. In addition, sufficient organic matter is necessary to act as an electron donor and reduce the oxides. Chapter 3 describes geochemical evidence for an increase in grain size downcore in stations 163-7, 163-14 and 163-10. Likewise the elevated Si/Al, Fe/Al, K/Al and Mg/Al (Figures 3.5, 3.8, 3.12) ratios in the basal samples of 163-14, and particularly 163-10, have been attributed to the presence of an extra-sedimentary input such as an ash band. The occurrence of the Mn-carbonate at this horizon is similar to that found by Pedersen and Price (1982) in the Panama Basin. Pore water data on Mn^{2+} from Sawlan and Murray (1983) for a nearby core, 145-7, suggests the reduction of surficial oxides are the main source of Mn^{2+}, not the alteration of the ferromagnesian silicates which may be associated with the ash band, and advocated by Hein *et al* (1979) for a manganous ion source in the Bering Sea.

This occurrence of Mn-carbonate, and the apatite in 145-17 (see above), suggests that even with a plentiful supply of Mn^{2+} and PO_4^{3-} respectively, the mechanism of diagenetic mineral formation can often depend on a suitable locus for precipitation.

8.3.2 *Diagenetic glauconite formation*

Results

Glauconite pellets occur in abundance on the outer part of the Baja California shelf, particularly in core 163-13 in both the upper lag deposit and in the undisturbed clay below. It is felt that the pellets from the lag deposit would provide little information with regard to the process of *in situ* glauconitisation. Instead pellets were removed by gentle seiving of the fine-grained clay at the base of the core with the hope that they have suffered little transport and are effectively characteristic of the depositional environment.

Using the terminology of Triplehorn (1966) the dark-green to light-grey pellets are spheroidal to ellipsoidal or ovoid (Plate 8.2a,b) in shape, occasionally lobate or mamillated, and range in size from 1-8 mm in diameter. Many of the pellets bear internal and surface cracks creating a somewhat bulbous habit. The durability of the pellets is quite variable with the lighter green variety tending to be the most friable.

Investigations with SEM reveal a "cornflake" texture composed of webby, highly crenulated blades <1 μm in diameter (Plate 8.2c). This texture is very similar to smectite and perhaps is a result of the drying out of the sample during preparation. In all cases the texture lacks any well-defined morphology such as rosettes or the sub-parallel, sinuous alignment of crystallites characteristic of ancient glauconite (Odin and Matter, 1981). Many of the pellets contain well-preserved dolomite (Section 8.3.3).

Figure 8.3 is a reproduction of the XRD trace of some dark green glauconite pellets from the basal clay of 163-13. Dolomite also appears on the diffraction pattern. The first

PLATE 8.2 Scanning electron micrographs of glaucony pellets and diagenetic dolomite:

(a,b) Morphology of glaucony pellets from the basal clay of 163-13 indicating the bulbous, cracked nature of the pellets.

(c) "Cornflake" texture of early-formed glaucony from the broken inside surface of a pellet at 20 cm depth in 163-13.

(d) Dolomite rhomb showing evidence of dissolution, from the oxidised zone of core 163-14.

(e) Grain mount of rhombohedral dolomite displaying step-growth dislocations (core 163-13).

(f) Isolated, *in situ* rhomb with a small intergrowth at the top left of the central face. Note adhering Fe-rich smectites (163-7).

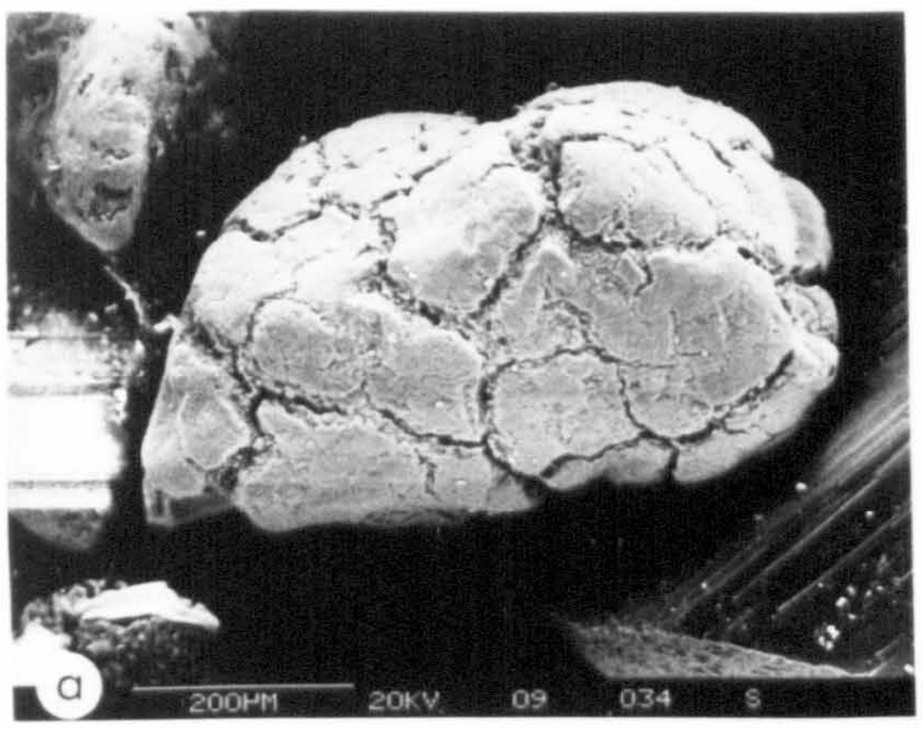
a
200PM 20KV 09 034 S

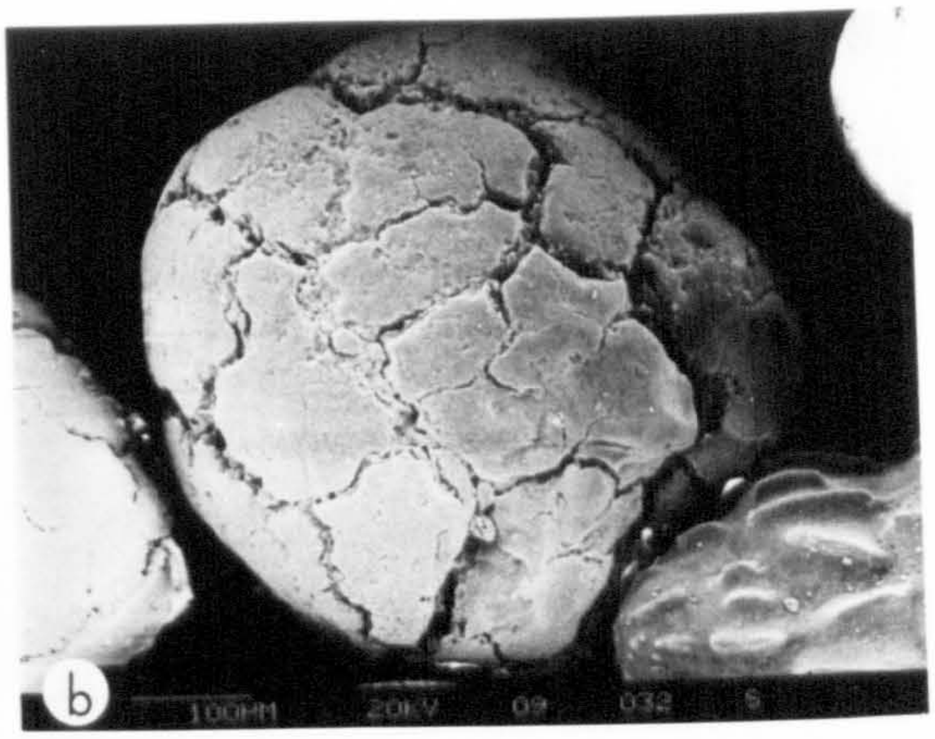
b
100PM 20KV 09 032 S

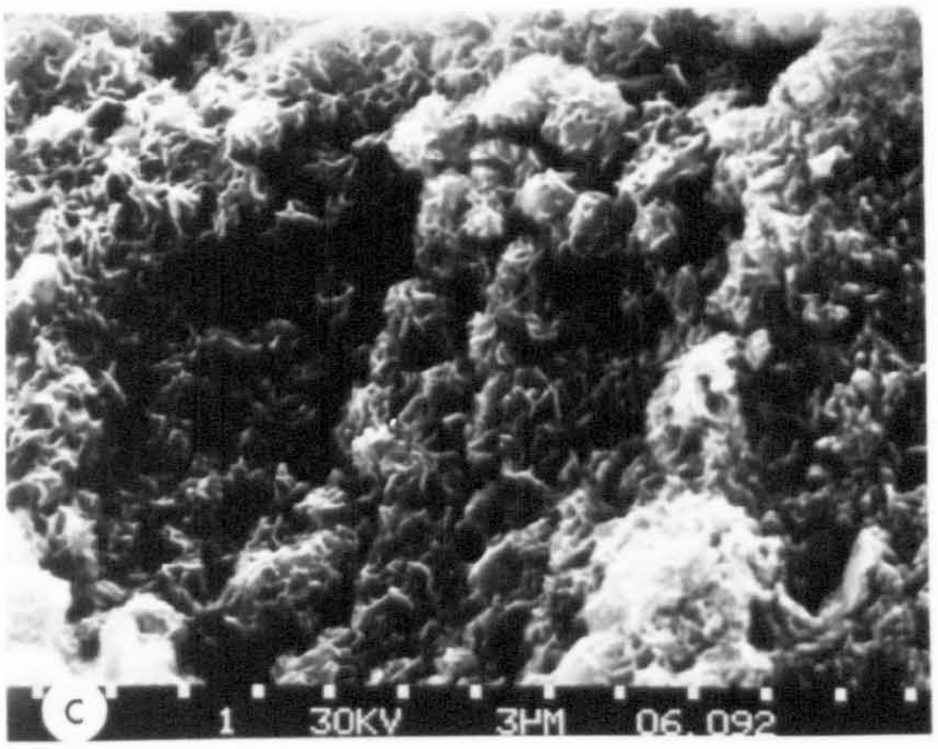
c
1 30KV 3PM 06.092

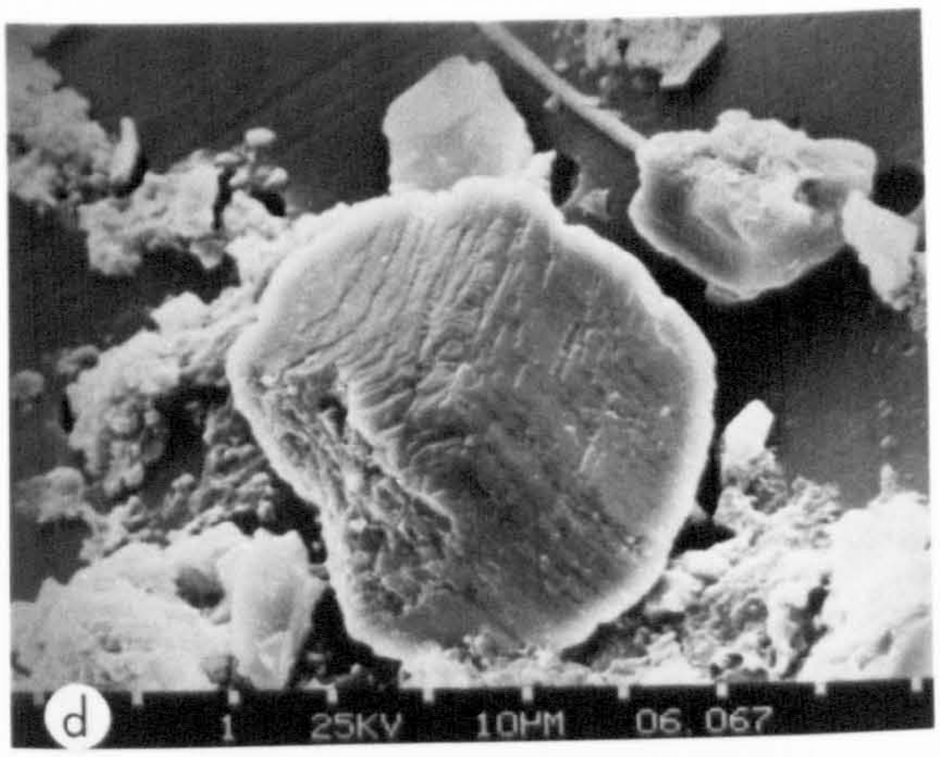
d
1 25KV 10PM 06.067

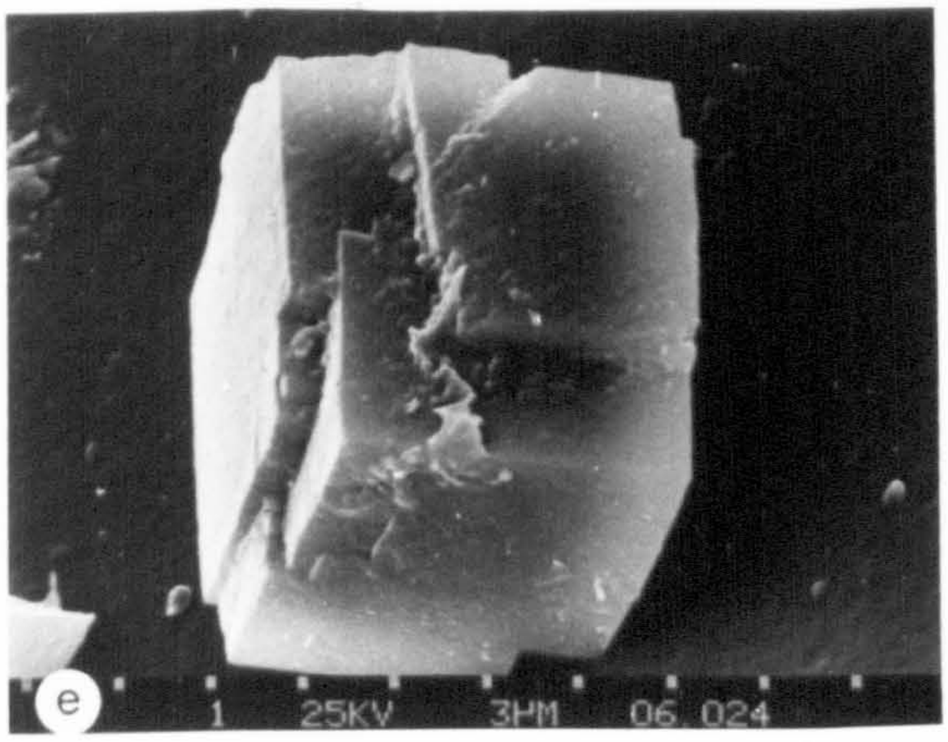
e
1 25KV 3PM 06.024

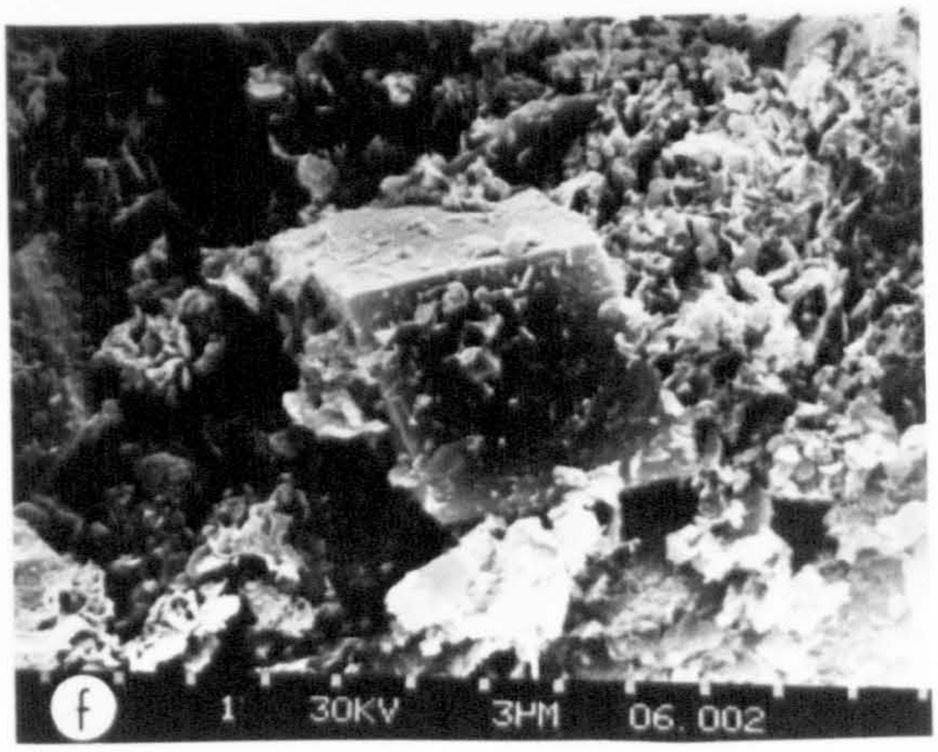
f
1 30KV 3PM 06.002

TABLE 8.3

GLAUCONY ANALYSES

Cations calculated from oxide analyses assuming 22 oxygens in a formula unit

Pellet 1, 2, 3, 4, 5 from this study.

Birch 1, 2, 3, 4 from Birch *et al* (1972)

G312A, G313A, G318A, G319A, G362A, G490cA, G490hA, G448FF from Odin and Matter (1981)

GLAUCONY ANALYSES

Cation	Pellet 1	Pellet 2	Pellet 3	Pellet 4	Pellet 5	Pellet 6	Pellet 7
Si	7.60	7.62	7.72	7.52	7.61	7.49	7.52
Ti	0.02	0.03	0.09	0.01	0.02	0.02	0.02
Al	0.86	1.12	1.06	0.78	0.87	0.84	0.83
Fe3	2.41	2.12	1.98	2.52	2.37	2.53	2.52
Mg	1.09	1.12	1.22	1.13	1.09	1.09	1.08
Ca	0.10	0.15	0.12	0.05	0.08	0.05	0.04
Na	0.05	0.06	0.08	0.03	0.11	0.05	0.05
K	1.27	1.08	0.91	1.56	1.26	1.52	1.51
Octahedral total	3.98	4.01	4.07	3.96	3.96	3.97	3.97
Interlayer total	1.42	1.29	1.11	1.64	1.45	1.62	1.60
Total	13.40	13.30	13.17	13.61	13.42	13.59	13.57

Cation	Birch 1	Birch 2	Birch 3	Birch 4
Al	7.57	7.58	7.61	7.59
Ti	-	-	-	-
Al	1.07	0.78	0.80	0.75
Fe3	2.27	2.59	2.46	2.35
Fe2	-	-	-	-
Mg	0.95	0.97	1.00	1.21
Ca	0.28	0.05	0.05	0.03
Na	0.04	0.06	0.02	0.02
K	1.05	1.32	1.52	1.71
P	0.03	0.03	0.03	0.02
Octahedral total	3.86	3.92	3.87	3.90
Interlayer total	1.37	1.43	1.59	1.76
Total	13.26	13.38	13.49	13.69

Cation	G312A	G313A	G318A	G319A	G362A	G490cA	G490hA	G448FF
Si	7.17	6.98	7.24	7.25	7.12	7.18	7.32	6.35
Ti	0.08	0.09	0.09	0.05	0.05	0.03	0.06	0.13
Al	1.76	1.76	1.18	1.15	1.17	1.11	1.27	4.00
Fe3	2.42	2.48	2.62	2.73	2.78	2.76	2.58	1.37
Fe2	-	0.14	0.14	-	-	0.15	-	-
Mg	0.69	0.66	0.63	0.64	0.81	0.96	0.84	0.39
Ca	0.23	0.23	0.23	0.23	0.23	0.23	0.23	0.43
Na	0.06	0.15	0.12	0.04	0.03	0.06	0.09	0.05
K	0.45	0.58	0.99	1.28	1.31	0.79	0.68	0.30
P	0.03	0.04	0.03	0.03	-	-	-	-
Octahedral total	4.12	4.11	3.90	3.82	3.93	4.19	4.07	4.24
Interlayer total	0.74	0.96	1.34	1.55	1.57	1.08	1.00	0.78
Total	12.88	13.11	13.27	13.39	13.51	13.28	13.08	13.01

order basal reflection (001) at 10 Å is poorly defined or absent, whereas the (020) peak at 19.60°28 is quite distinct but assymetric towards higher angles, merging with the $(11\bar{1})$ and (021) reflections. The (003) reflection is quite sharp despite the small size of the (112) and $(11\bar{2})$ reflections indicating the poor ordering of the layer silicate lattice (Bentor and Kastner, 1965). Crystallographically the mineral is very similar to smectite.

The chemistry of several glauconite pellets (light and dark green varieties) from the basal clay of 163-13 is presented in Table 8.3 together with published analyses of other Cenozoic glauconites (Birch *et al*, 1976; Odin and Matter, 1981). Analysis was by electron microprobe using polished sections cut from selected pellets. It should be stressed that the samples are somewhat impure due to the mode of formation (see below) of the pellets which may incorporate clay, carbonates, oxides and sulphides in varying degrees. Nevertheless the similarity with other published microprobe analyses (of which there are few), especially those of Birch et al (1976) is encouraging. The cations have been recalculated assuming 20 oxygens and 4 hydroxyls in the unit cell and a general formula of:

$$(K,Na,Ca)_{1.2-2.0}(Fe^{3+},Al,Fe^{2+},Mg)_{4.0}[Si_{7-7.6}Al_{0.4-1}O_{20}](OH)_4.n(H_2O)$$

(Deer *et al*, 1961). The role of water in the structure is uncertain and has therefore been disregarded. Glauconite may be considered as a di-octahedral mica, but differs from muscovite by having a considerable quantity of divalent (and trivalent) ions (Fe^{3+}, Fe^{2+}, Mg^{2+}, Ti^{+} and Al^{3+}) in the octahedral sites, the total number of ions being very close to four.

In all cases Si is less than that required (8) for the tetrahedral site, the deficit being balanced by sufficient Al allowing calculation of tetrahedral Al. The remaining Al, together with Fe, Mg and Ti, is used to calculate the octahedral total which in every case is near the theoretical value of four for a dioctahedral mica. K, Na and Ca are assumed to enter interlayer sites only, the sum being always less than two, but greater than the number of Al ions in the tetrahedral positions. Most published analyses of glauconite indicate a greater proportion of Fe^{3+} to Fe^{2+} (Deer *at al*, 1961, Odin and Matter, 1981; Ireland *et al*, 1983) and like Birch *et al* (1976) Fe is reported here as all Fe^{3+}. Even taking a low Fe^{2+}/Fe^{3+} ratio of 1/4 (Ireland *et al*, 1983; determined by wet chemistry) would only lower the octahedral total by a small amount. Apart from Pellet 2 (Table 8.3) the Fe^{3+}/octahedral Al ratios are quite high compared to most glauconites (Deer *et al*, 1961) confirming that the process of glauconitisation has occured in an environment containing avalilable Fe^{3+} (perhaps before major sulphide genesis). In summary, the glauconite chemistry off Baja California is very similar to typical values cited by Deer *et al* (1961):

$$Fe^{3+}_{2-2.2},\ [Al]^{6}_{0.6-0.8},\ [Al]^{4}_{0.4-1.0} \text{ and } (K,Ca,Na)_{1.2-2.0}$$

Discussion

The term "glauconite" has created some confusion in the geological literature (eg McRae, 1972). *Glauconitic minerals* generally contain more than 15% Fe_2O_3 (Van Houten and Purucker, 1984) and include green smectite, mixed-layer glauconite and smectite, and "glauconite". Odin and Matter (1981) and Berg-

Madsen (1983) propose the general facies of *glaucony* (pl. glauconies) for these minerals, for which *glauconitic smectite* and *glauconitic mica* are the principal end members of the family. This proposed nomenclature is followed below.

The mechanism of formation of glaucony

Ideas on the formation of glaucony have followed a distinct evolutionary trend, facilitated by the advance in analytical techniques and methods of observation. The earliest theory advocated the co-precipitation of Mg-, Fe-, Al- and Si-gels which subsequently absorbed K (Murray and Renard, 1891) modified by Takahashi (1939) to describe the precipitation and hydration of gelatinous Si allowing absorbtion of bases. The pre- and post-war years saw the development of ideas advocating the evolution of glaucony from biotite or Fe-mica parent material (Galliher, 1935; Hendricks and Ross, 1941) with K and Mg being supplied from seawater (Hendricks and Ross, 1941). Modification of this idea led to the "layer lattice theory" of Burst (1958 a,b) supported by Hower (1961). In this model a degraded 2:1 layer lattice structure with low lattice charge (high alumina smectite, illite or degraded mica) is "glauconitized" by Fe substitution for Al in the octahedral position. This increase in the octahedral charge necessitates interlayer cation (mainly K) substitution to balance the charge, collapsing the expanded layers to a 10 Å non-expandable clay. Serious flaws exist in this model, particularly the dependance on a 2:1 clay mineral substrate which does not explain the glauconitisation and neomorphic replacement of carbonate (McRae, 1972) and non-micaceous silicates (Ojakangas and Keller, 1964; Dapples, 1967). Furthermore, there is often a

lack of K and Fe correlation and no inverse relationship to the number of expanded layers contrary to that predicted by Burst's theory (Bentor and Kastner, 1965; Foster, 1969; Weaver and Pollard, 1973; Birch *et al*, 1976).

Recently, Odin and Matter (1981) have proposed the neoformation of glaucony, resulting from the precipitation of crystallites of Fe- and K-rich glauconitic smectite in a granular, highly porous substrate under slightly reducing, semi-confined conditions. This nascent glaucony evolves by a recrystallisation process related to progressive equilibrium with bottom seawater. In this scheme the evolution and alteration of the substrate is critically important, unlike the previous models which considered the substrate as an impurity.

Glaucony formation off Baja California

Figure 8.4 indicates some of the cation relationships in four published sets of glaucony analyses: (1) the Baja California glauconies; (2) the average 1st, 2nd, 3rd and 4th stage glauconies (light yellow to dark green) of Birch *et al* (1976) from the Namibian shelf; (3) Pleistocene-Holocene glauconies of Odin and Matter (1981); (4) the averages of six populations of glaucony given by Ireland *et al* (1983). Insofar as these analyses span a wide range of glaucony types they may not be strictly comparable, nevertheless they serve to identify several factors pertinent to the proposed models of glaucony formation.

(1) Figure (8.4a) clearly illustrates the antipathetic relationship between Al and Fe in the octahedral site. The more aluminous nature of Ireland *et al*'s and Odin and Matter's data

FIGURE 8.4 The relationship between cations in Baja California glauconies compared with other published analyses: Birch *et al* (1972), west South Africa shelf; Odin and Matter (1981), Pleistocene-Holocene glaucony; Ireland *et al* (1983), Lower Cretaceous Sand Formation, Alberta, Canada.

(a) The inverse correlation between octahedral Al and total Fe indicating Fe substitution in the octahedral site.

(b) The inverse correlation between octahedral Al and Mg indicating some Mg substitution for Al. Note the Mg-rich nature of the Baja California glauconies.

(c) The lack of dependance of interlayer K^+ substitution to balance the octahedral coordination of Fe.

(d) The lack of dependance of total interlayer occupancy on the Fe content of the glaucony.

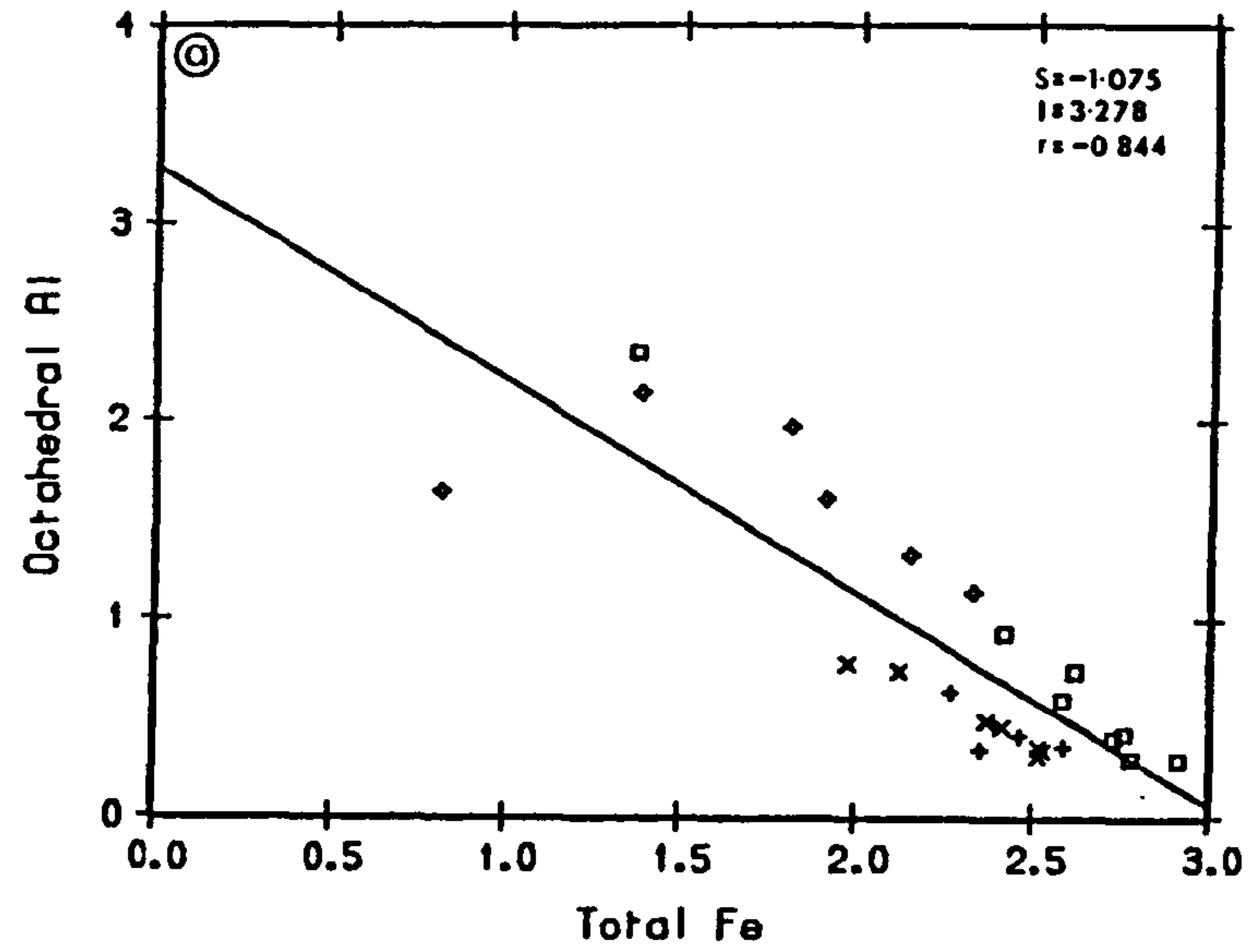

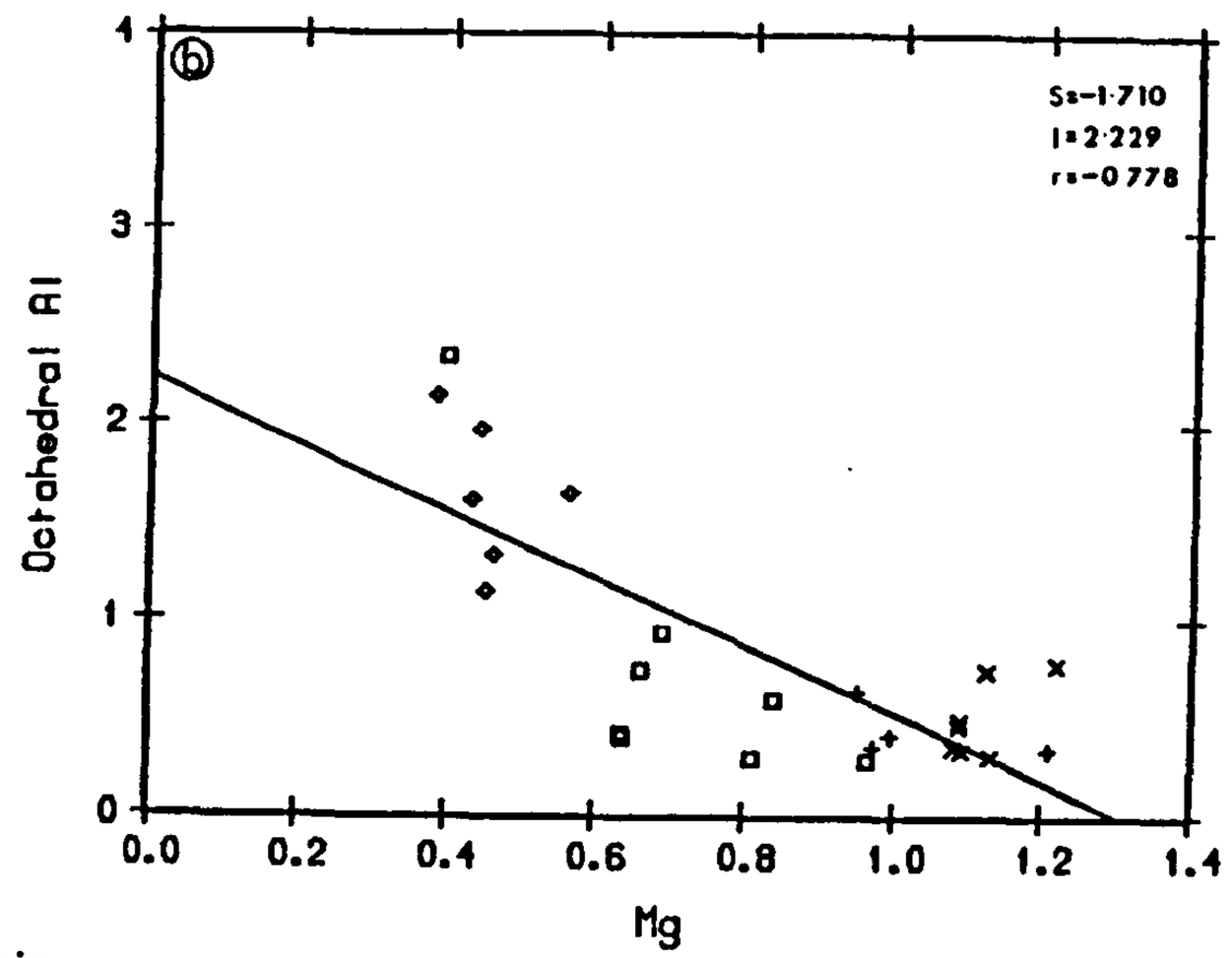

× Baja California
+ Birch et al (1972)
□ Odin and Matter (1981)
◆ Ireland et al (1983)

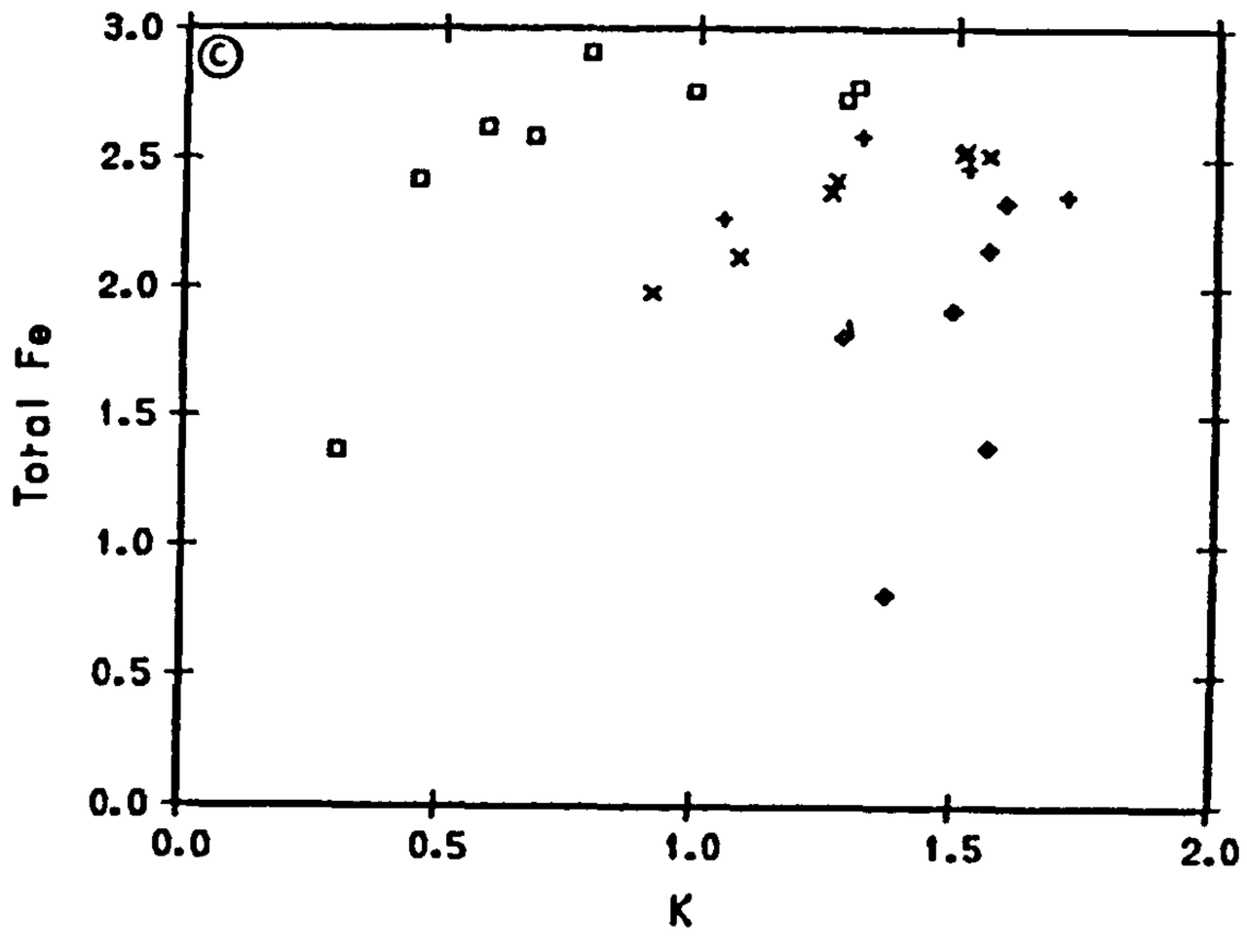

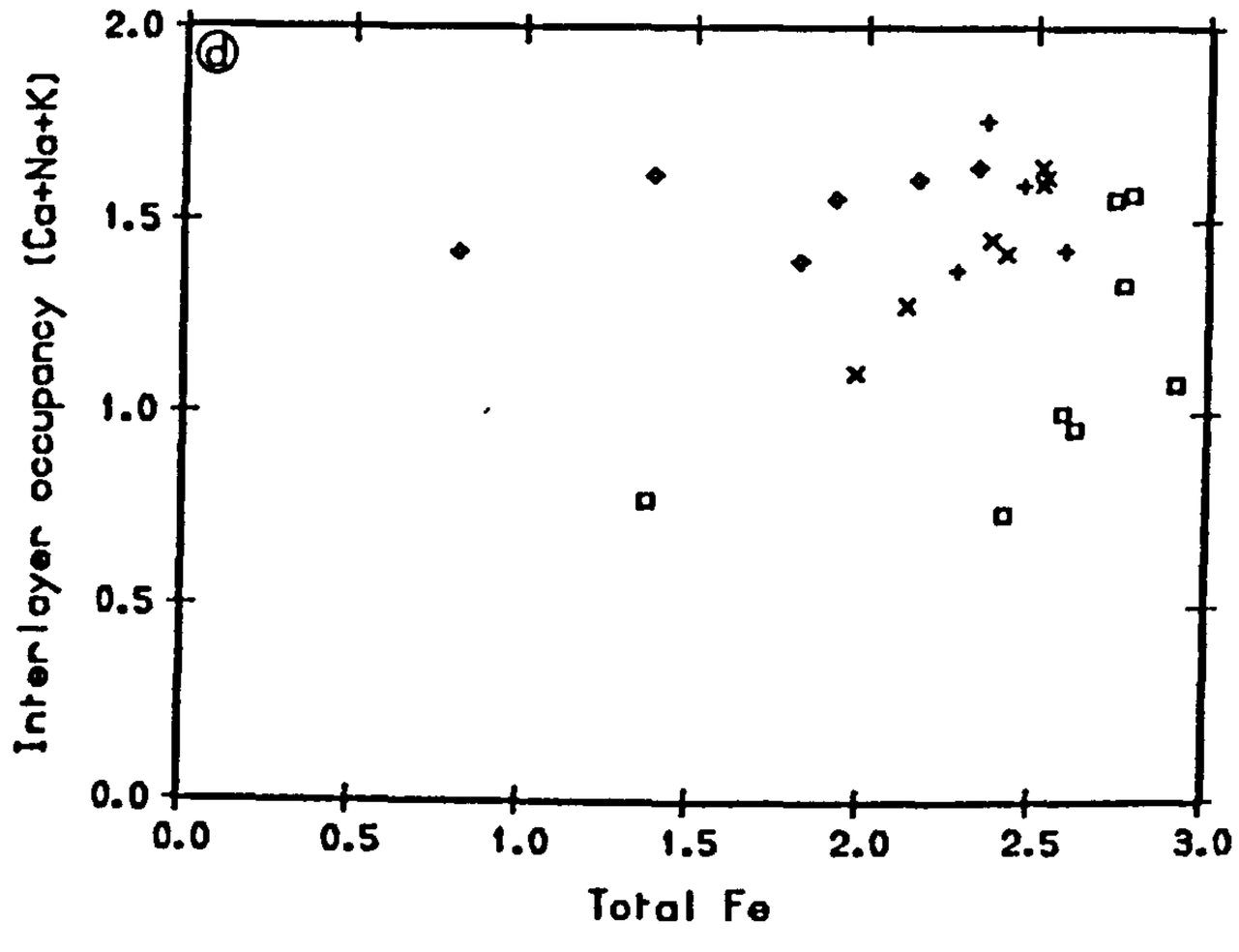

may be due to greater diagenetic alteration (Ireland *et al*, 1983).

(2) The other important octahedral cation, Mg, also displays an inverse relationship with octahedral Al (Figure 8.4b); Baja California glauconies being rich in Mg compared with the other published analyses.

(3) If the "layer lattice theory" is correct then Fe and K should be proportional to each other. Figure (8.4c) indicates that for all the glauconies taken as a whole, there is little dependance of K on the Fe content. However, there does appear to be some linear relationship for the *in situ* Baja California glauconies, although the sample set is not large enough to provide any conclusive evidence.

(4) Similarly, the charge balance of the interlayer cations (Ca^{2+}, Na^{+}, K^{+}) is unrelated to Fe, although the Baja California glauconies again define a complimentary increase (Figure 8.4d). Previous authors (Ehlmann *et al*, 1963; Foster, 1969; Birch *et al*, 1976; Odin and Matter, 1981) have interpreted the lack of correlation between octahedral Al and interlayer occupancy (especially K^{+}) as indicative of incorporation of the two cations at different times in the glauconitisation process; the fixation of Fe preceeding that of K. The relatively high interlayer charge and high levels of octahedral Fe is similar to that found by Odin and Matter (1981) and Ireland *et al* (1983) confirming their suggestion that the glaucony does not evolve from precursor illite.

The morphology of the glaucony pellets and their scattered distribution in fine grained sediment, which itself displays no evidence of glauconitisation, suggests that formation does

indeed occur in confined microenvironments as suggested by Odin and Matter (1981). They also suggest that the bulbous and cracked nature of the pellets results from preferential crystal growth at the centre of the grain, causing differential expansion.

In determining the controlling factor on glaucony formation off Baja California several points must be accounted for: (1) The assumed presence of high levels of Fe^{3+} in the structure; (2) Sufficient supply of interlayer cations throughout the evolution of the glaucony (not necessarily at the time of Fe^{3+} incorporation); (3) Formation in semi-confined micro-environments in disseminated pockets throughout the fine-grained sediment; (4) A restricted zone of occurrence towards the outer shelf and slope (D'Anglejan, 1967) in sediments containing abundant organic matter.

The presence of Fe^{3+} indicates formation prior to advanced sulphate reduction (Chapter 4) and the formation of sulphides which are highly efficient sinks for Fe, but not necessarily under fully reducing conditions. Faecal pellets accumulating in the upper few cm provide a semi-permeable microenvironment into which seawater K, Mg and Na are free to diffuse down a geochemical gradient towards the more reducing centre of the pellet. Low overall sediment accumulation rates on the outer shelf, away from any major source of clastic input, allow the pellets to reside for sufficient time in the zone of cation diffusion, increasing the "maturity" of the grains manifested by a greater K content and darker green colour. The ageing process may well occur below the Fe^{3+}/Fe^{2+} redox boundary, explaining the lack of correlation between total Fe and the

interlayer occupancy of the glaucony. Such situations may well occur during major marine transgressions (Odin and Matter, 1981), such as the present Flandrian transgression (Chapter 3). It should be emphasised that the concentration of glaucony in the surface of 163-13 and in other deposits around the world arises through winnowing and reworking, and does not necessarily reflect the original environment of formation.

The common locus of glaucony formation on the outer shelf and slope may be due to the critical geochemical balance between Fe sulphide formation or flocculation of Fe^{3+} in nearshore environments and sufficient reactive Fe^{3+} in the outer shelf zone to form glaucony, and the presence of suitable microenvironment substrates. Recent evidence (Ireland *et al*, 1983) suggests that in organic-rich, fine-grained facies glaucony may not be well preserved due to Fe^{3+} reduction to its more stable ferrous state, and the substitution of Al into the octahedral site. For this reason the geological record of ancient glaucony in coarse-grained sediments low in organic matter may be a result of geochemical bias.

8.3.3 *Diagenetic dolomite formation*

Distribution in the sediments

Visual observation of smear slides of surface and subsurface samples show that dolomite distribution, along the transect studied, appears to be limited to those sediments associated with the hemipelagic environment. Distal cores (145-6, 163-9, and 163-15) have only trace amounts in them, whilst the shelf silts are devoid of dolomite. In order to determine

the vertical distribution of dolomite in these sediments the silt-size fraction at 5 cm intervals was extracted by wet sieving. An estimate of the dolomite content in this fraction was made by line counting 300 grains (Galehouse, 1969). Results of this are shown in Figure 8.5 together with C_{org} and solid phase Mn in the sediment. The vertical distribution of dolomite appears to be related to the Mn redox boundary and/or C_{org} within the sediment. It is present in significant amounts only in the reduced sediment, and here is broadly correlatable with the abundance of C_{org}. Within the oxidising zone authigenic dolomite is either absent or present in small quantities. Moreover, inspection of the dolomite within oxidising sediment shows evidence of corrosion, (Plate 8.2,d) whereas dolomite at depth occurs as perfect rhombs (Plates 8.2e,f; 8.3a,b). Pore water NO_3^- data from Sawlan and Murray (1983) indicates that total consumption does not occur until 40 cm and 20 cm in 145-7 and 145-8 respectively. Only on total depletion of O_2 and NO_3^- (Gieskes, 1975) will the process of sulphate reduction predominate indicating that in these cores dolomite occurs in the presence of SO_4^{2-} ions.

Physiography and chemistry of the dolomite

The dolomite occurs as discrete rhombohedra, or with small interpenetrating crystals, (Plates 8.2e,f and 8.3a,b) growing displacively in the sediment. The rhombs vary in size from one or two microns up to a maximum of 40 μm, and show no evidence of size sorting in the sediment. Occasionally, minute inclusions of pyrite and clay material can be seen. Crystal terminations are sharp and well defined, which indicate that no

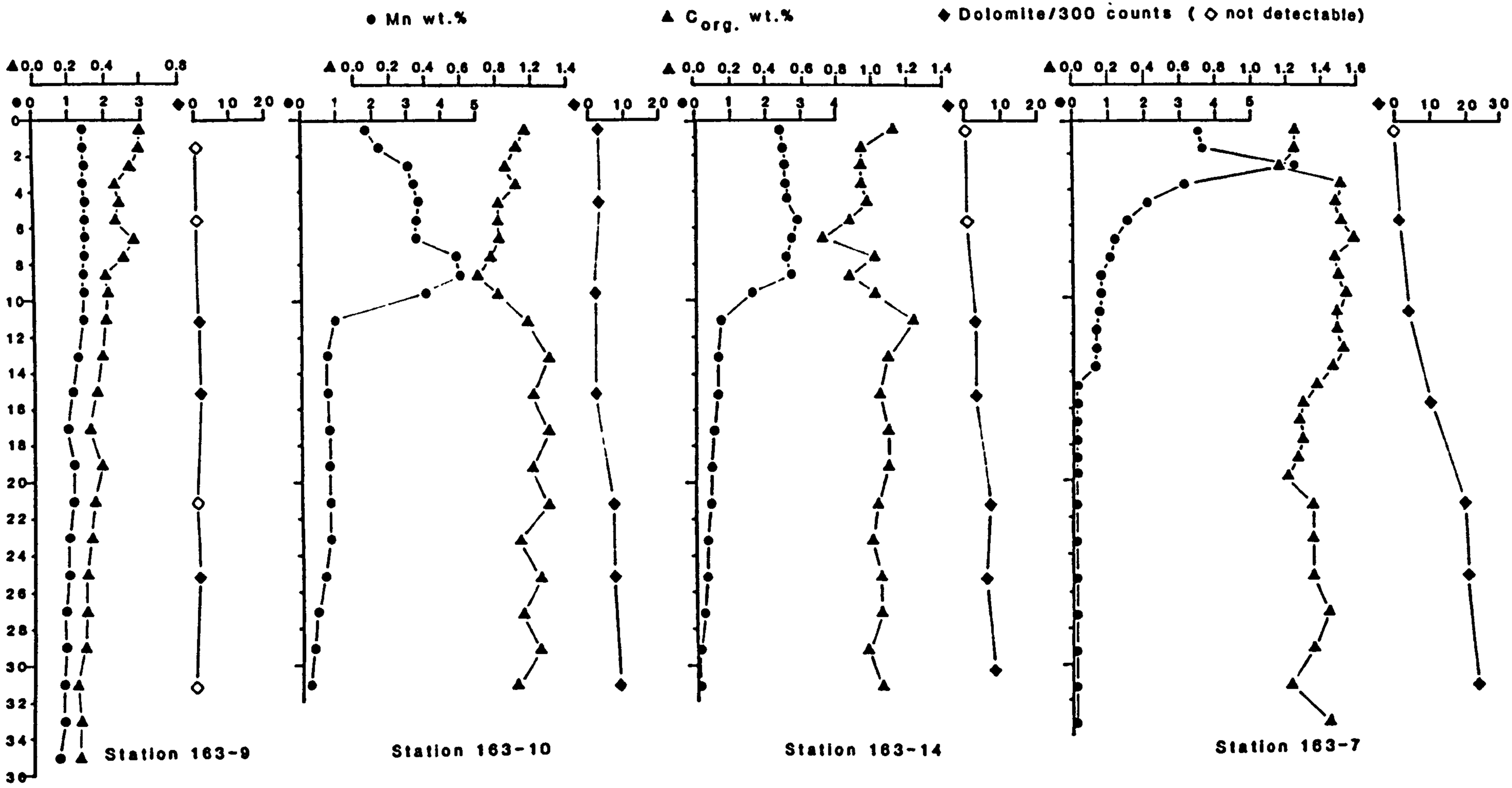

FIGURE 8.5 The vertical distribution of the frequency of dolomite estimated from counting 300 grains, solid phase Mn (wt.%) and organic C (wt.%) in oceanic cores off Baja California.

PLATE 8.3 Scanning electron micrographs of dolomite and dolomite/Mn-Carbonate, dolomite/glaucony relationships:

(a,b) Interpenetrating dolomite rhombs, morphology suggests *in situ* precipitation (163-13).

(c) Dolomite rhomb surrounded by diagenetic Mn-Ca-carbonate (identified by EDAX): 28-30 cm depth, core 163-10.

(d,e,f) Broken inside surfaces of glaucony pellets from core 163-13 showing uncorroded euhedral dolomite predating the formation of the glaucony pellet. Upwards of 70% (e) of the pellet may be composed of dolomite.

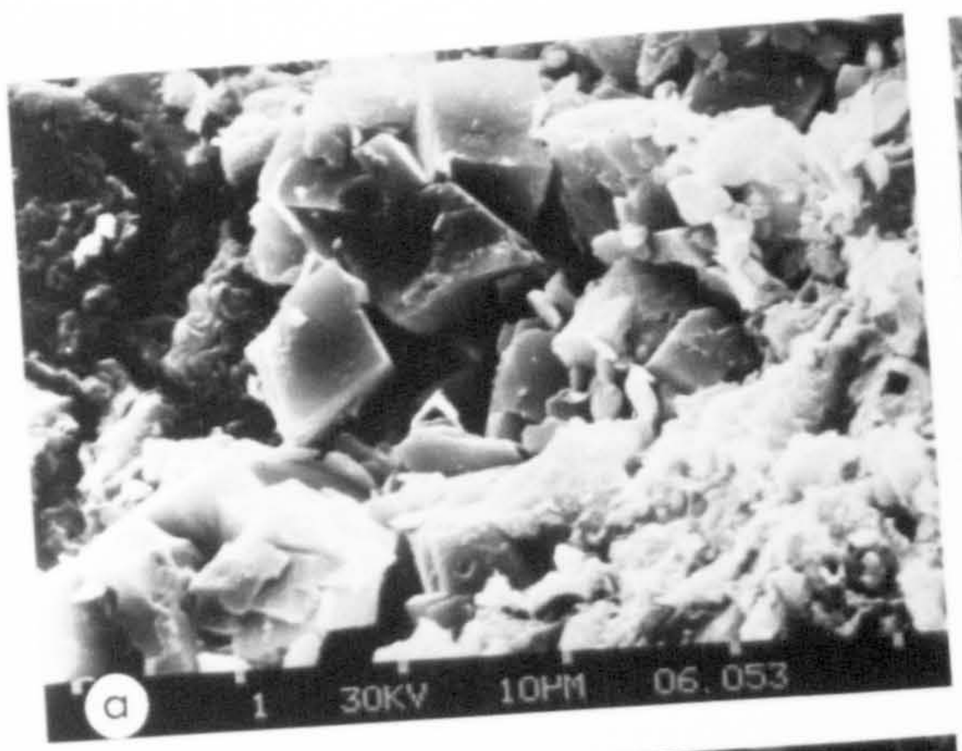
a
1 30KV 10PM 06.053

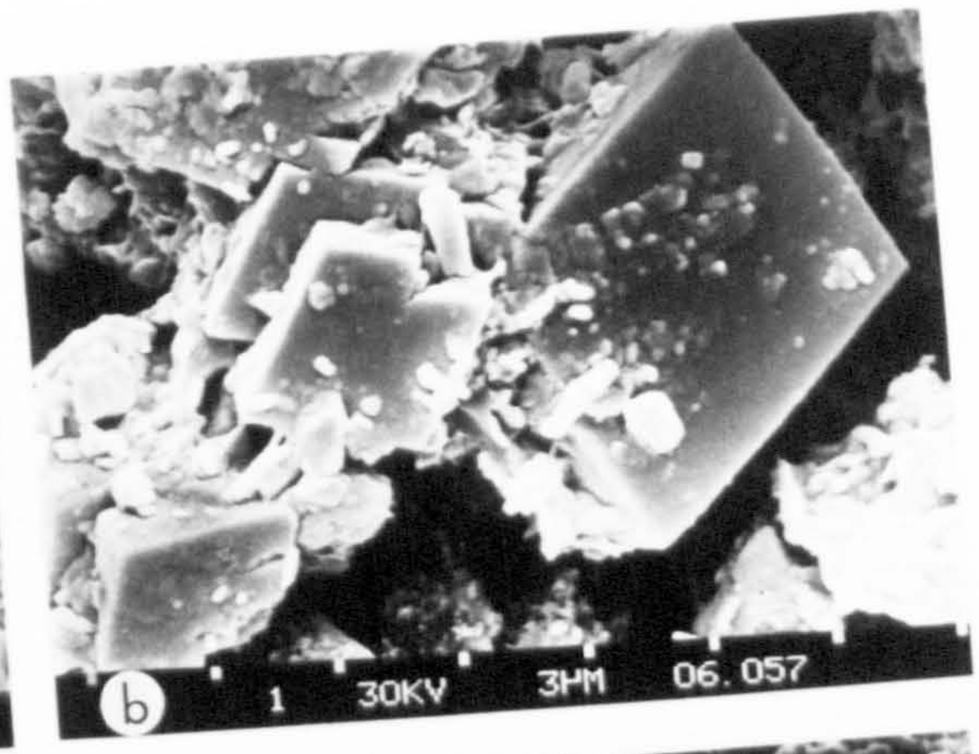
b
1 30KV 3PM 06.057

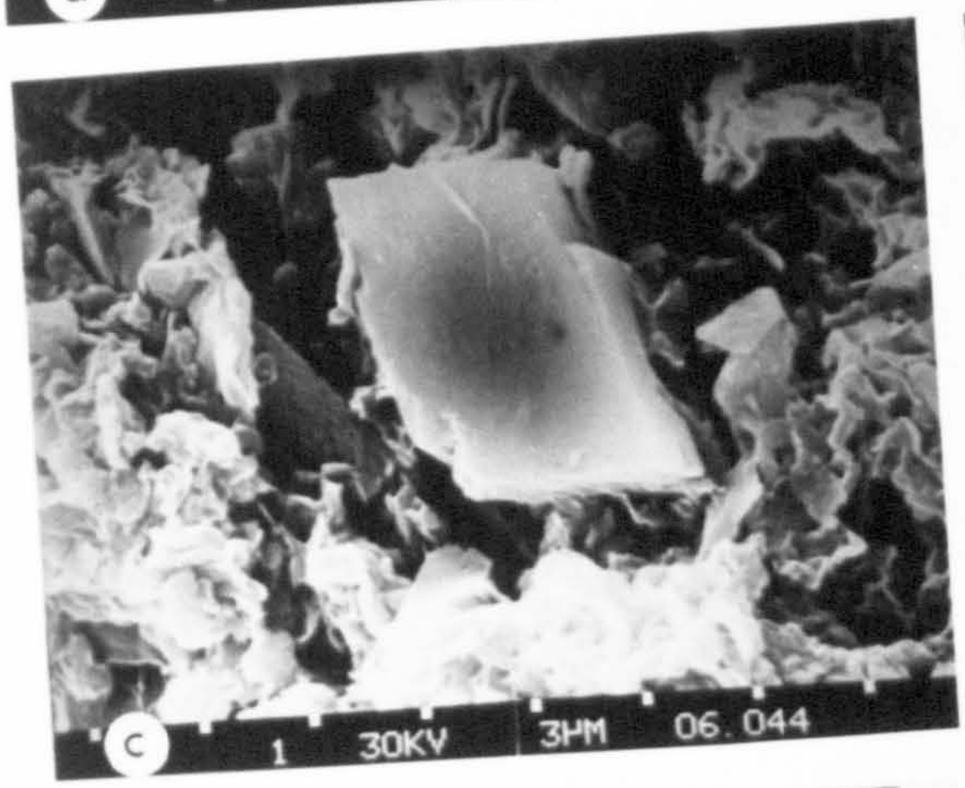
c
1 30KV 3PM 06.044

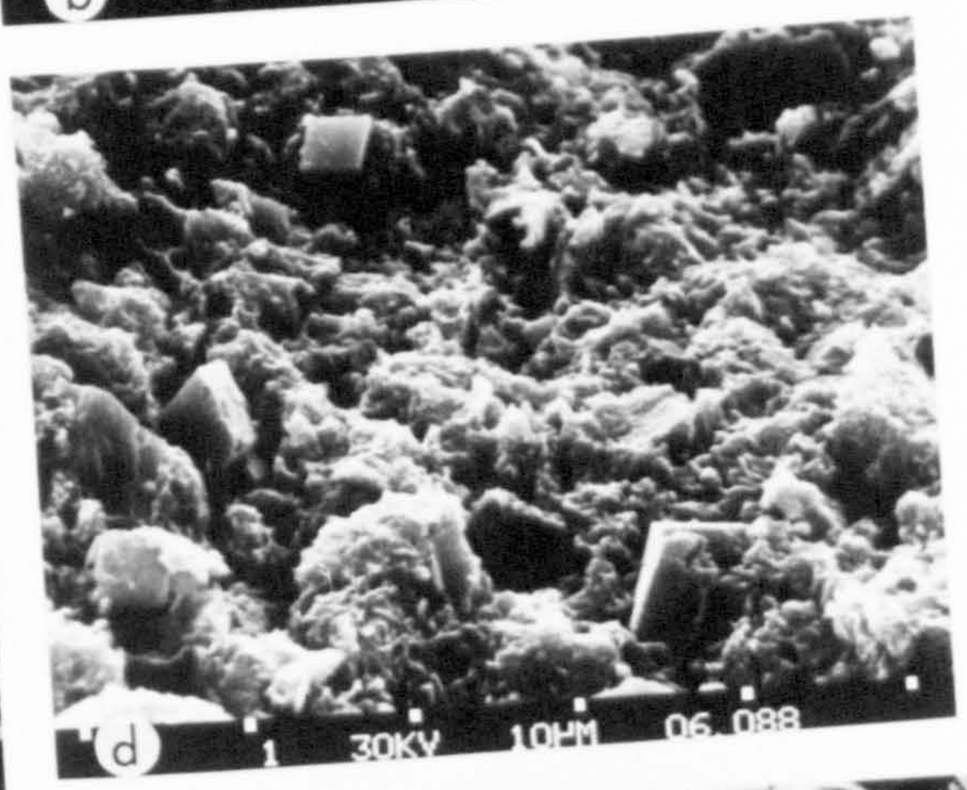
d
1 30KV 10PM 06.088

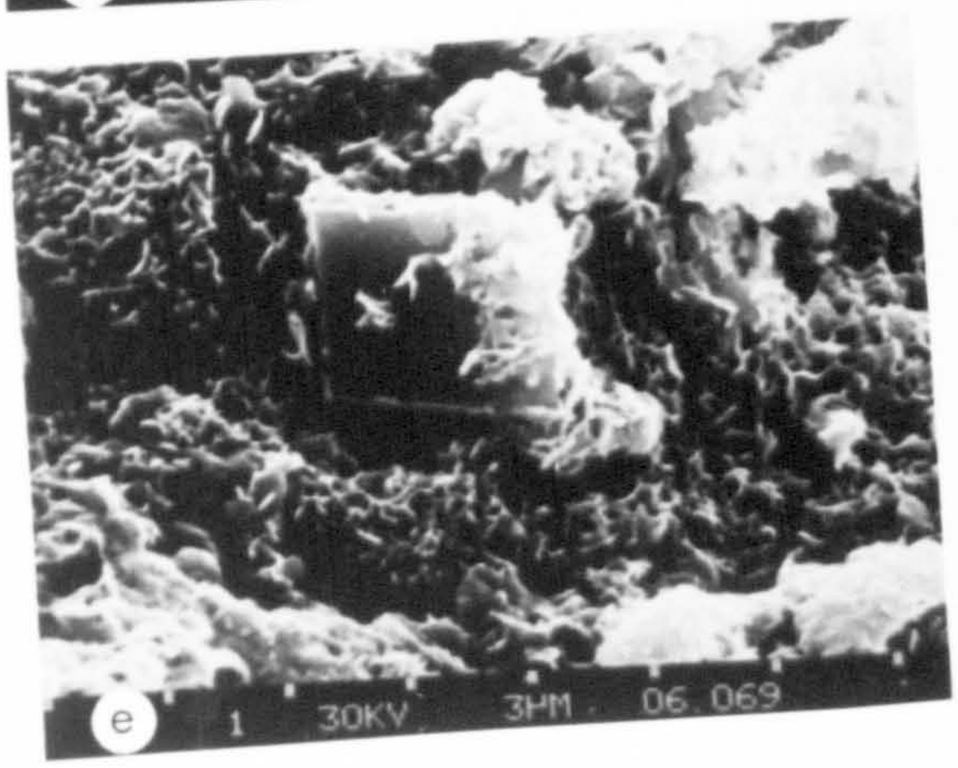
e
1 30KV 3PM 06.069

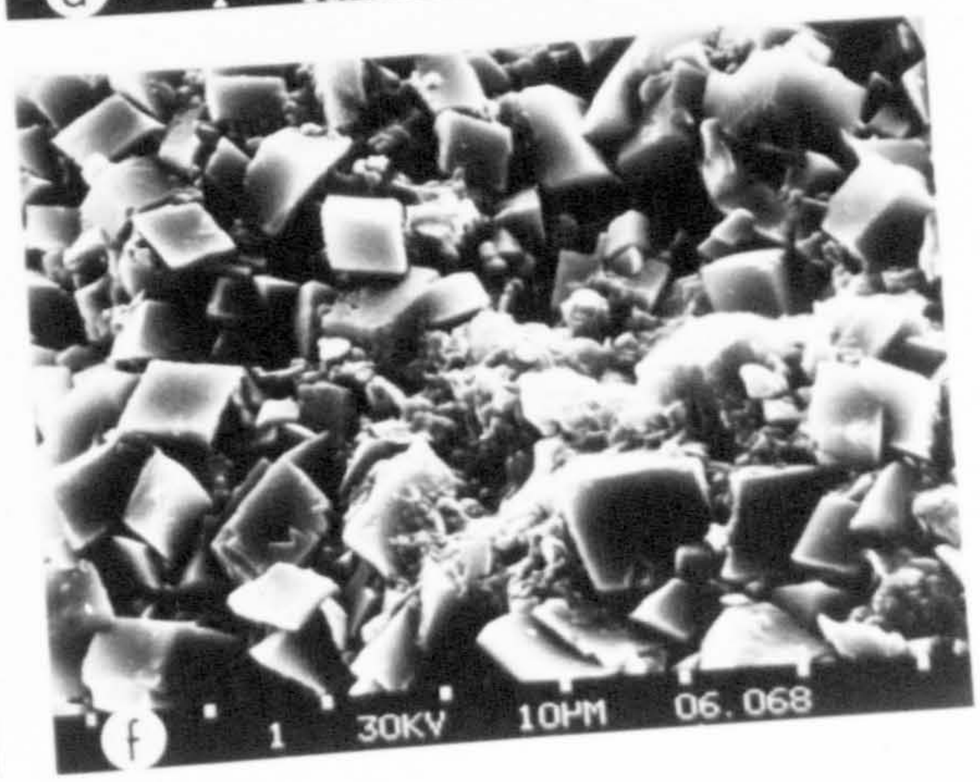
f
1 30KV 10PM 06.068

abrasion or other transport effects have taken place. Close inspection of certain surfaces of the dolomite grains sometimes show dislocations (Plate 8.2e) due to step growth along a spiral path (Nielsen, 1964). Such dislocations indicate that dolomite growth could take place at very low levels of supersaturation (<1.01) where two-dimension surface nucleation would be nearly impossible (Burton *et al*, 1951; Berner, 1981). Visual observation on the dolomite using the SEM and cathode luminesence failed to reveal any evidence of an earlier carbonate precursor phase. Foraminifera tests are unaltered and do not have dolomite associated with them. Spatial arrangement of the rhombs in the sediment indicate direct precipitation, rather than some physico-chemical alteration from another carbonate. There is, however, a close association between growth of dolomite and other diagenetic phases such as glaucony, manganese carbonate and pyrite. These will be discussed below.

Chemical and mineralogical examination shows that the dolomite from Baja California is not a "protodolomite" as defined by Graf and Goldsmith, (1956) and Gaines, (1977). This is illustrated in Figure 8.6 where the (211) and (111) superstructure reflections are clearly visible, confirming the degree of ordering compared with synthetic protodolomite or other naturally occuring protodolomites.

The Mg/Ca ratio of the dolomite was estimated using XRD by measuring the shift of the (211) reflection relative to a quartz internal standard (Goldsmith and Graf, 1958) giving a composition of 56 mole % $CaCO_3$. The use of a fluorite internal standard and slow chart scans of $1/8^{o}$ 2θ/min. showed the a_o and c_o unit cell parameters to be 4.8291 Å and 16.1521 Å

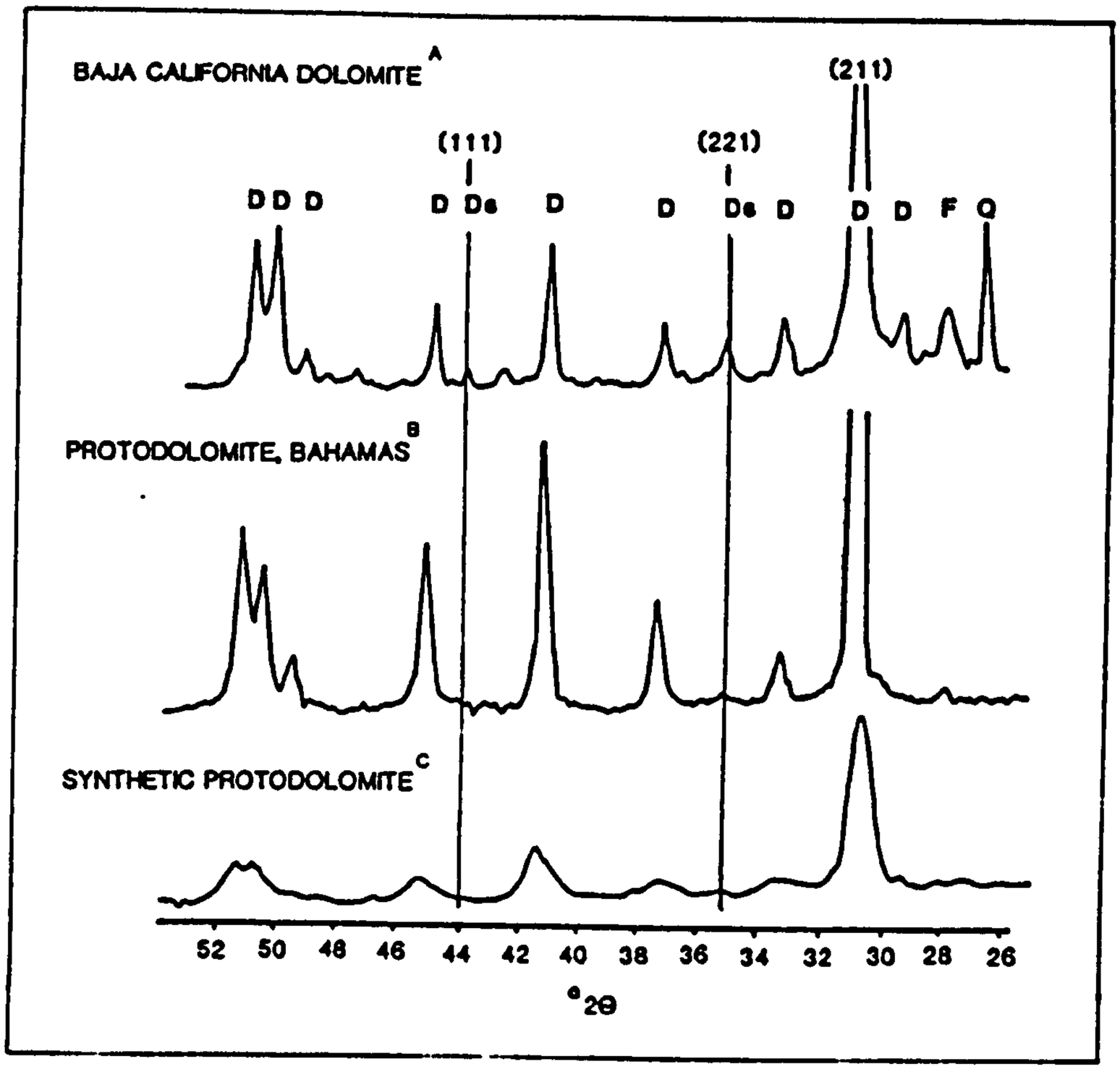

FIGURE 8.6 X-ray diffractograms of dolomite (A) and a comparison with published spectra of protodolomites (B: Illing *et al*, 1977; C: Glover and Sippel, 1967) all using Cu Kα radiation. The superstructure reflections (111) and (221) reveal that the Baja California variety is an ordered dolomite. (D-dolomite, Ds-dolomite superstructure reflection, F-feldspar, Q-quartz).

respectively. These have been plotted in Figure 8.7 and compared to other published dolomites and protodolomites. The Baja California dolomite hexagonal unit cell parameters are consistent with ordered dolomite (Land, 1980) and contrast with the measurements on protodolomites that show expanded parameters departing from the calcite - magnesite trend. It would appear that the excess of calcium over that of stoichiometric dolomite does not result in disordering.

Electron microprobe analyses of dolomite from two cores (163-7 and 163-13) are shown in Table 8.4. Results for the Ca/Mg ratios, shown as a histogram in Figure 8.8, confirm the 56 mole % $CaCO_3$ obtained by the XRD method. Both stations have seemingly similar dolomite compositions, and show a smaller range of excess Ca than that found in IPOD core material from the Gulf of California by Kelts and MacKenzie, (1982). Dolomite of near stoichiometric composition, 50-52 mole% $CaCO_3$, is more common in sediments that contain evaporites, whereas less stoichiometric dolomite, 55-56 mole% $CaCO_3$, is typical of dolomite formed under non-evaporite conditions (Lumsden and Chiamhusky, 1980). While Sr tends to show reasonably consistent values, and somewhat lower than those of Behrens and Land, (1972) (800 ppm) from Baffin Bay, Texas the microprobe analyses (Table 8.4) do suggest incorporation of the element within the dolomite structure; the greater variability of Ba may be due to impurities such as barite.

Si and Al contents of the dolomites (Figure 8.9) are, in all probability, due to the presence of clay inclusions as the Si/Al ratio (3.3) is identical to that of the host sediment (Figure 3.3). Fe contents appear to be in excess, both of the

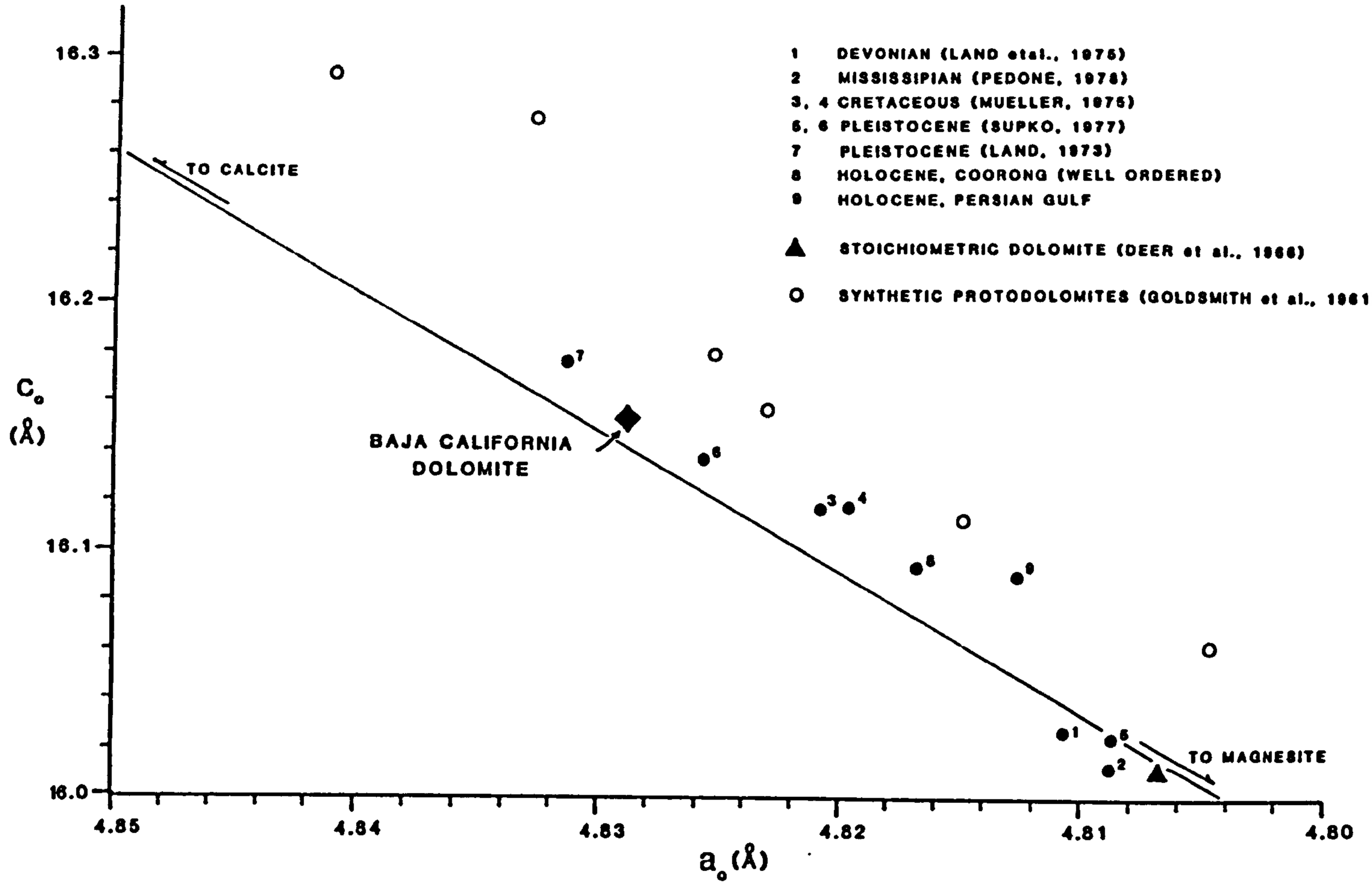

FIGURE 8.7 A plot of unit cell parameters a_o and c_o (in Å) of Baja California dolomite, and published dolomite of various ages. The sloping line extrapolates to values for pure calcite and magnesite. Expansion of the unit cell due to disordering will result in an increase of the a_o and c_o parameters relative to this line (after Land, 1980).

TABLE 8.4

ELECTRON MICROPROBE ANALYSES OF BAJA CALIFORNIA DOLOMITE

Core number and depth interval	Ca	Mg	Fe	Si	Al	Na	K	Ba	S	Sr
13:15-16	21.07	9.93	0.47	1.22	0.35	0.13	0.11	n.d.	n.d.	412
13:15-16	22.52	10.92	0.39	0.35	0.09	0.06	0.04	n.d.	n.d.	431
13:15-16	22.74	10.67	0.27	0.74	0.25	0.08	0.10	n.d.	n.d.	545
13:15-16	22.06	11.04	0.77	0.26	0.08	0.05	0.04	n.d.	n.d.	736
13:15-16	21.82	10.06	0.59	0.43	0.08	0.05	0.02	n.d.	n.d.	n.d.
13:15-16	22.98	11.43	0.12	0.59	0.11	0.12	0.05	n.d.	n.d.	n.d.
13:15-16	23.00	10.85	0.16	0.27	0.08	0.07	0.05	n.d.	n.d.	n.d.
13:15-16	22.78	10.92	0.22	0.27	0.09	0.05	0.03	n.d.	n.d.	n.d.
13:18-19	22.50	10.63	1.19	0.50	0.15	0.06	0.08	1161	960	n.d.
13:18-19	23.72	10.93	0.36	0.25	0.08	0.06	0.06	450	740	n.d.
13:18-19	23.15	11.08	0.43	0.21	0.08	0.06	0.06	1348	700	n.d.
13:20-21	23.17	11.12	0.15	0.32	0.06	0.04	0.08	508	150	n.d.
13:20-21	22.64	10.76	1.10	0.32	0.15	0.05	0.08	590	350	n.d.
13:20-21	23.02	11.47	0.45	0.83	0.25	0.15	0.11	450	740	n.d.
13:21-22	22.81	10.81	0.23	0.87	0.26	0.08	0.13	758	630	376
13:21-22	23.12	11.36	0.12	0.17	0.09	0.06	0.05	391	380	298
13:21-22	23.08	11.07	0.19	0.36	0.09	0.05	0.08	616	440	464
13:22-24	22.47	10.72	0.25	0.55	0.17	0.07	0.10	1405	680	390
13:22-24	23.36	10.85	0.69	0.36	0.13	0.07	0.08	697	330	317
13:22-24	20.89	10.03	1.09	2.53	0.32	0.06	0.14	688	280	221
13:25-26	22.58	10.75	0.90	0.62	0.23	0.07	0.13	797	290	265
13:25-26	23.48	11.66	0.15	0.37	0.08	0.06	0.07	892	630	339
13:25-26	21.00	10.66	0.55	0.27	0.07	0.03	0.05	862	650	479
7:30-34	23.08	11.65	0.06	0.21	0.09	0.06	0.10	437	460	339
7:30-34	23.75	11.45	0.01	0.06	0.03	0.02	0.06	651	310	166
7:30-34	23.47	11.81	0.17	0.61	0.31	0.14	0.07	625	60	n.d.
7:30-34	23.55	10.92	0.22	0.14	0.06	0.03	0.09	275	n.d.	n.d.
7:30-34	19.70	9.80	0.11	1.94	0.83	0.15	0.09	208	n.d.	n.d.
Detection limit	0.015	0.08	0.033	0.014	0.009	0.014	0.01	560	122	127
Precision (±2 σ)	0.175	0.08	0.056	0.027	0.016	0.017	0.019	573	277	163

Major elements in wt.%; Ba, S and Sr in ppm
Counting statistics in the same units
(n.d. = not determined)

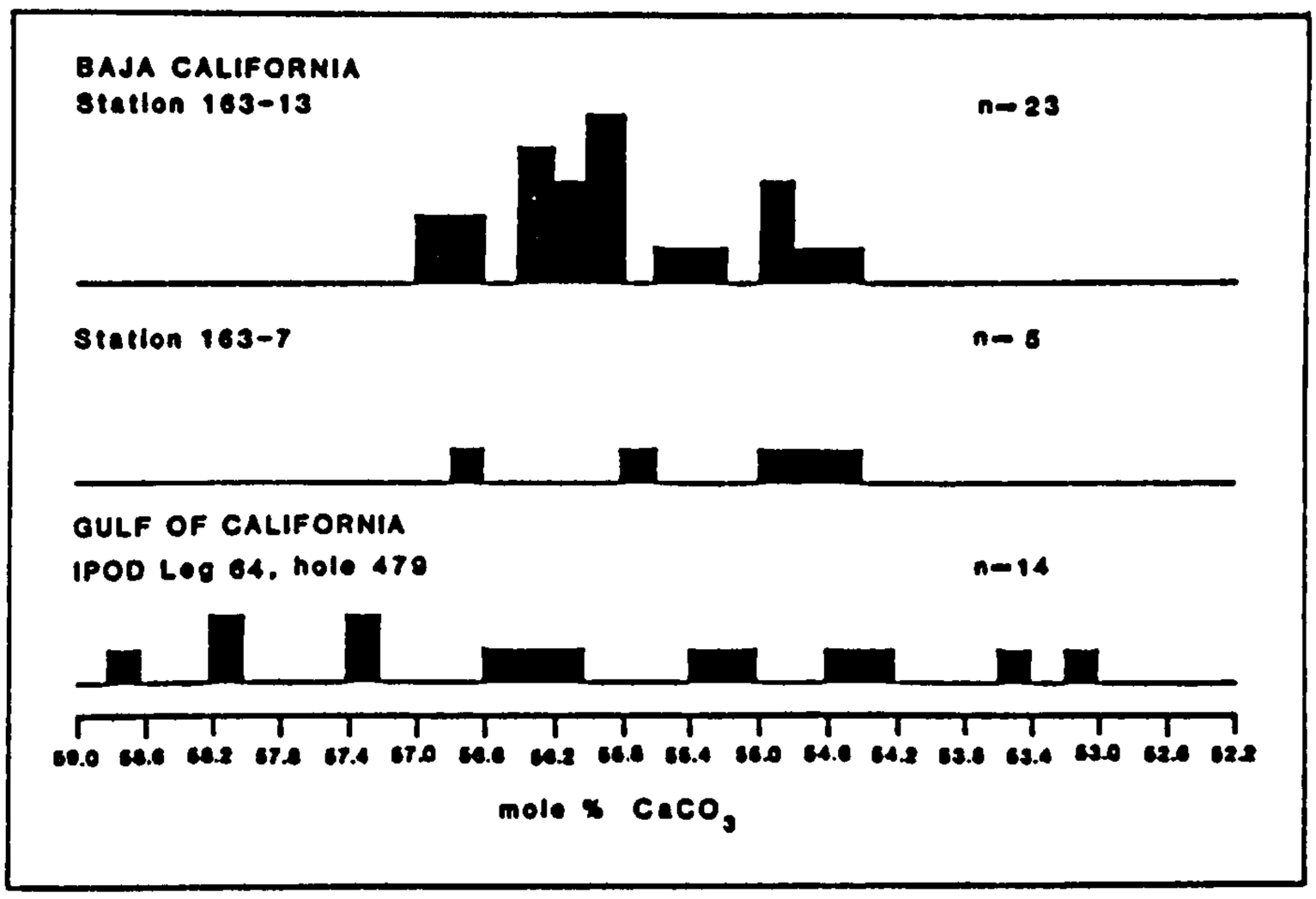

FIGURE 8.8 A histogram of the distribution of analyses for mole % $CaCO_3$ in Baja California dolomite, stations 163-13 and 163-7, and the Gulf of California, IPOD (DSDP) Leg 64, hole 479 (Kelts and McKenzie, 1982) performed by electron microprobe. (n=number of analyses)

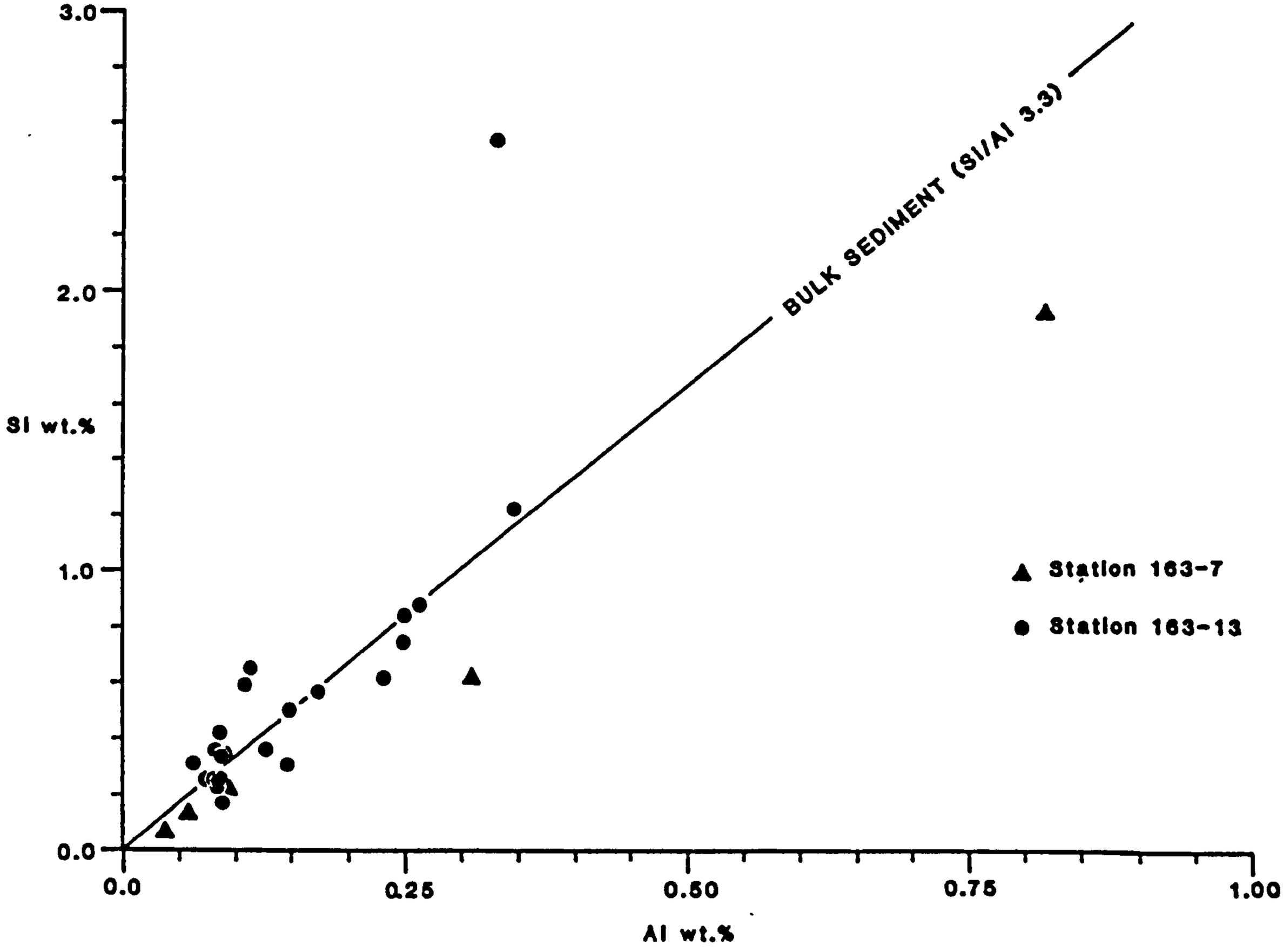

FIGURE 8.9 A plot of Si and Al content of Baja California dolomites as measured from electron microprobe analyses. The Si/Al ratio (3.3) of bulk sediment is based on the regression data for all samples analysed by XRF (Figure 3.3).

level of S that can be accommodated as pyrite (FeS_2), barite ($BaSO_4$), and Fe-rich smectite. The analyses suggest that a very small amount of Fe (<0.6 wt.%) is incorporated within the dolomite lattice.

Oxygen and carbon stable isotope mass ratios were kindly provided by E. Suess (Oregon State University) on dolomite from the base of the three hemipelagic cores (163-7, 163-14, 163-10) and from clay underlying the lag deposit in 163-13. In all cases dolomite was separated from the fine clay fraction by repeated settling of the coarse material and decantation of the suspended fines. The prepared samples were checked by XRD and revealed only quartz and feldspar impurities; clay was undetectable.

Table 8.5 presents the $d^{18}O$ and $d^{13}C$ in $^{o}/oo$ relative to PDB. The $d^{18}O$ signature varies from near 0.0 $^{o}/oo$ to +1.34 $^{o}/oo$ PDB in the hemipelagic samples, but are somewhat enriched in ^{18}O in the dolomite-rich clay of 163-13 (+3.45 - +5.33 $^{o}/oo$ PDB). These values are within the -2.8 to +4.7 $^{o}/oo$ PDB range (+28 - +35.5 $^{o}/oo$ SMOW) of normal marine limestone (NML; Friedman and Murata, 1979; Land, 1980). The most recent estimate of benthic conditions off Baja California at present is given by Shackleton and Hall (1982) who predict a $d^{18}O$ for *Uvigerina* of +2.3 + 0.2 $^{o}/oo$ PDB for a bottom water temperature of 6.5^{o}C in the Gulf of California. Also given in Table 8.5 are the estimated palaeotemperatures of formation using experimentally determined expressions for geothermometry (Fritz and Smith, 1970; Friedman and O'Neill, 1977; Matthews and Katz, 1977). There is a marked uncertainty in these geothermometers: originally it was believed that the fractionation of oxygen isotopes between dolomite and calcite was zero (Friedman and

TABLE 8.5

OXYGEN AND CARBON STABLE ISOTOPES OF BAJA CALIFORNIA DOLOMITES
TOGETHER WITH PALAEOTEMPERATURES OF FORMATION

Sample	Depth cm	$\delta^{13}C$ °/oo(PDB)	$\delta^{18}O$ °/oo(PDB)	$\delta^{18}O$ °/oo(SMOW)	Temperature °C N+C	F+S	M+K
163-7	30-34	-0.76	-0.07	30.79	44	31	29
163-14	30-32	-0.59	+0.80	31.68	40	27	25
163-10	30-32	-0.31	+1.34	32.24	37	24	23
"	32+	-1.45	+1.08	31.97	39	36	35
163-13	15-16	-14.33	+5.07	36.09	21	8	8
"	18-19	-11.74	+5.33	36.35	20	7	7
"	20-21	-8.79	+3.45	34.42	22	9	9
"	21-22	-10.00	+4.78	35.79	22	9	9
"	22-24	-12.27	+4.99	36.00	22	8	8
"	24-26	-17.30	+5.31	36.33	20	7	7

Temperatures calculated assuming bottom water is 0 °/oo SMOW

Geothermometry equations used:

N+C Northrup and Clayton (1966) (extrapolated dolomite/water line)
$1000 \ln a_{d-w} = 3.20(10^6 T^{-2}) - 1.50$

F+S Fritz and Smith (1970) (protodolomite/water pair using a constant $a_{dol-cal}$ of 3.1 o/oo given by Friedman and O'Neill (1977)
$1000 \ln a_{d-w} = 2.78(10^6 T^{-2}) + 0.21$

M+K Matthews and Katz (1977) (extrapolated dolomite/water line)
$1000 \ln a_{d-w} = 3.06(10^6 T^{-2}) - 3.24$

All expressions use 1.0412 for the fractionation factor for CO_2-H_2O at 25°C (Friedman and O'Neill, 1977)

Hall, 1963; Degens and Epstein, 1964; Epstein *et al*, 1964) because dolomitisation occured by solid state cation exchange without altering the integrity of the C and O isotopic composition. Later experiments and theory (Weber, 1964; Clayton *et al*, 1968; Shepard and Schwarcz, 1970) indicated that dolomite formation by dissolution/reprecipitation results in a marked enrichment in $d^{18}O$. However it should be stressed that there is still uncertainty in the fractionation effects of formation of dolomite at very low temperatures. Similarly, the calculated temperature will depnd on the $d^{18}O$ (H_2O) of the precipitating fluid, assumed to be 0.0 $^{o}/oo$ (SMOW) in this case.

The $d^{18}O$ of the Baja California dolomites are within the range of similar dolomites from the East Pacific (Pisciotto and Mahoney, 1981; Kelts and McKenzie, 1982; Kelts and McKenzie, 1984; Figure 8.10). On the Peruvian margin Kulm *et al* (1984) have found dolomites to be 2-3 $^{o}/oo$ PDB heavier. Dolomites from DSDP Leg 63 have been interpreted by Pisciotto and Mahoney (1981) as forming in equilibrium with pore water under a range of temperatures and depths of formation, except those from Hole 471 (near the TGT-163 transect; Figure 1.2) which were consistently found to be ~13^{o}C too high. They attributed this effect to either a high geothermal gradient in the area, isotopic exchange between dolomite and ^{18}O-depleted water, or isotopic non-equilibrium during precipitation of the diagenetic carbonate.

The $d^{13}C$ isotopic signature for dolomite separates the hemipelagic sediments from station 163-13. In the former environment $d^{13}C$ varies between -0.31 and -1.45 $^{o}/oo$ PDB. In 163-13 the signature is much lighter, -8.79 - -17.30 $^{o}/oo$ PDB.

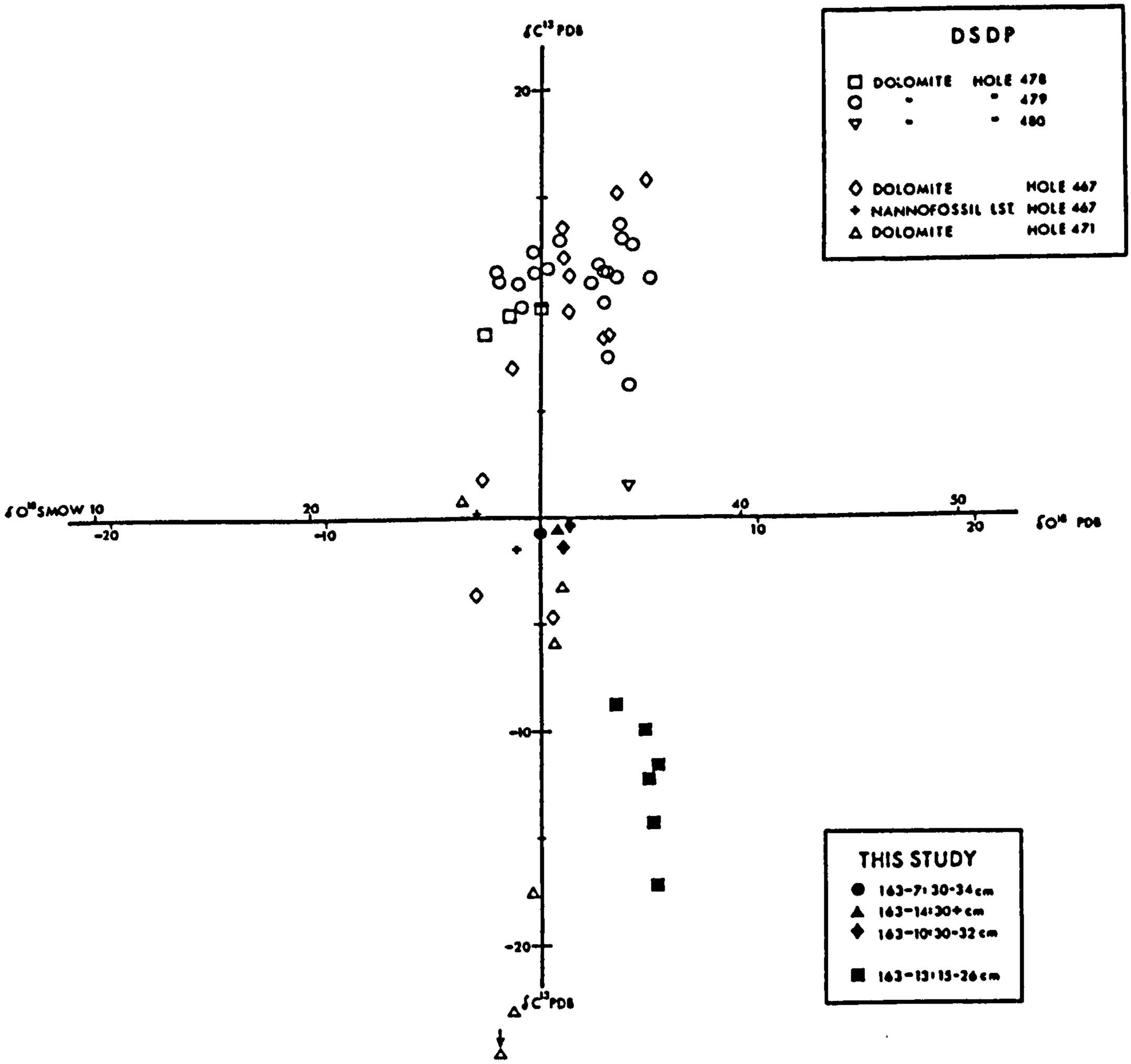

FIGURE 8.10 Carbon and oxygen isotopes of Baja California dolomites. Filled symbols are from this study; DSDP dolomites from Sites 467 and 471 are from Pisciotto and Mahoney (1981), and Sites 478, 479 and 480 are from Kelts and McKenzie (1982).

Average marine limestone varies between -4 and +4 $^{o}/_{oo}$ (Friedman and Murata, 1979; Land, 1980) with Pleistocene benthonic foraminifera averaging <-1.0 to ~0.0 $^{o}/_{oo}$ PDB (Savin *et al*, 1975). Light $d^{13}C$ carbonate values as low as -25 $^{o}/_{oo}$ can derive from CO_2 evolved (as dissolved bicarbonate) in shallow zones of aerobic oxidation of organic matter, or anaerobic sulphate reduction (Claypool, 1974; Claypool and Kaplan, 1974; Irwin *et al*, 1977; Curtis, 1978; Irwin, 1980; Dickson and Coleman, 1980; Pisciotto, 1981; Kelts and McKenzie, 1982; Kulm *et al*, 1984). With further diagenesis isotopically heavy (^{13}C enriched) carbonates form by a variety of proposed mechanisms (Reitsema, 1980): (1) Reduction of CO_2 to CH_4 leaving ^{13}C enriched CO_3 (Claypool and Kaplan, 1974); (2) By late stage oxidation of refractory organic matter to produce CO_2 in organic-poor sediment (Deuser, 1970); (3) Equilibrium between carbonate and CO_2 especially in bacterial systems (Friedman and Murata, 1979); (4) Anaerobic fermentation producing light methane but heavy CO_2 (Irwin *et al*, 1977; Coleman *et al*, 1979; Pisciotto and Mahoney, 1981; Kelts and McKenzie, 1982; Kulm *et al*, 1984). The lack of a heavy ^{13}C signature in the TGT-163 dolomites suggests that carbonate reduction and fermentation reactions have not yet occured. It should be noted that there is evidence to suggest light isotopic carbonates (~-10 $^{o}/_{oo}$ PDB) result from formation at depth during thermocatalytic decarboxylation (Irwin *et al*, 1977, Curtis, 1978), however the relatively heavy $d^{18}O$ values negate this possibility.

The relation of dolomite to other authigenic phases

All the above evidence suggests that dolomite is an early diagenetic phase. In order to understand the genesis of this dolomite it is important to relate it to the occurrences of other diagenetic minerals that have been identified by SEM and EDAX, and XRD techniques.

The coexistence of rare pyrite inclusions within the dolomite does suggest some sulphate reduction in core 163-13 has occured before the formation of dolomite. The existence of minor quantities of Ba within the dolomite also implies some barite formation before its crystallisation. In cores 163-10 and 163-14 $MnCO_3$ has been identified by EDAX (Plate 8.1c,d,e,f) towards their base (28-32 cm) and its formation depth in these sediments is consistent with that calculated on thermodynamic grounds by Sawlan, (1982). Examination of the carbonate reveals that dolomite can be associated with this mineral phase (Plate 8.3c) and that its depth of formation may be prior to that of the $MnCO_3$. Recent evidence (Pedersen and Price, 1982; Sawlan and Murray, 1983) suggests $MnCO_3$ formation after Mn reduction but before SO_4^{2-} reduction.

The association of dolomite with glaucony, in 163-13, is of particular interest as this mineral pair provides a valuable clue to the timing of dolomite growth, and its stability in the marine environment. SEM, XRD and chemical evidence (Section 8.3.2) suggests that the glaucony forms early in the depositional history of the sediment, and that newly formed "nascent" glaucony occurs off Baja California in the vicinity of 163-13. Dolomite is seen to be intimately associated with this glaucony (Plate 8.3d,e,f; Plate 8.4a,b) which acts as a non-corrosive cement binding the earlier formed dolomite

PLATE 8.4 Scanning electron micrographs of dolomite/glaucony dissolution relationships (core 163-13):

(a,b) Dolomite rhombs enclosed within a glaucony pellet showing no evidence of dissolution.

(c) Surface of a glaucony pellet with dolomite rhombs beginning to corrode (surface lag deposit).

(d) Dolomite rhomb from (c) showing the orientation of dissolution.

(e) Glaucony with rhombohedral pits in which there is some relict dolomite remaining.

(f) Close-up of rhombohedral pits from which all dolomite has been completely corroded away.

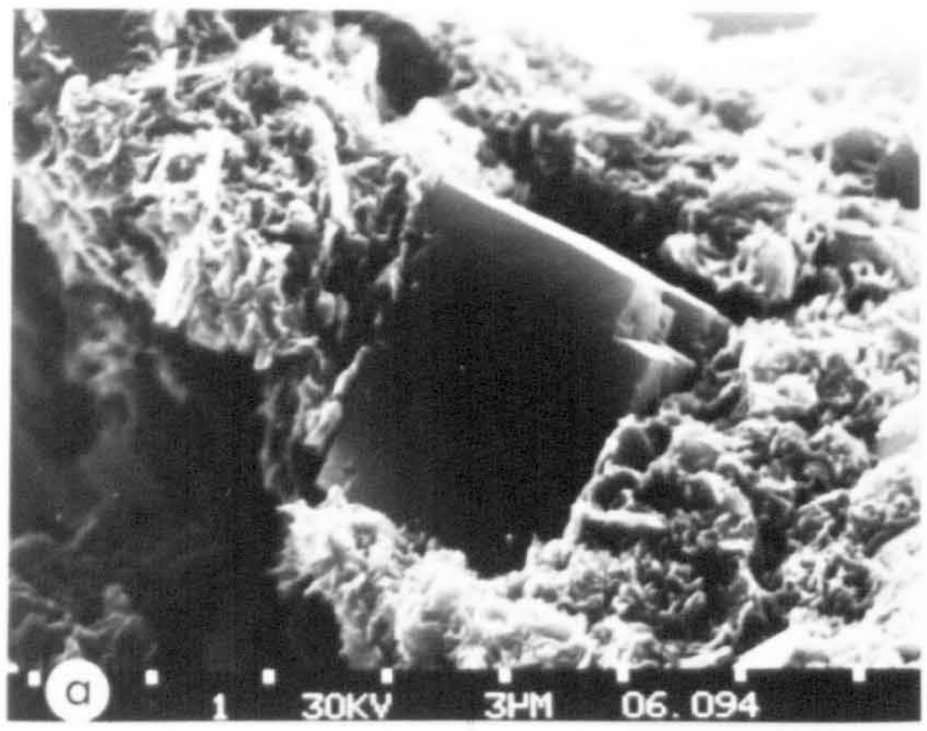
a
1 30KV 3MM 06.094

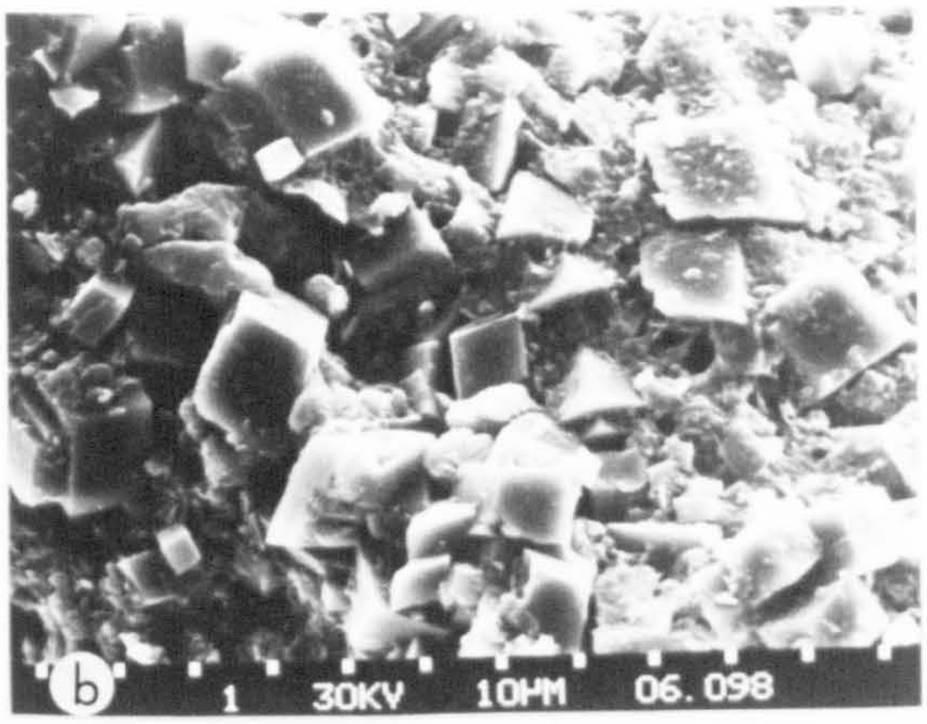
b
1 30KV 10MM 06.098

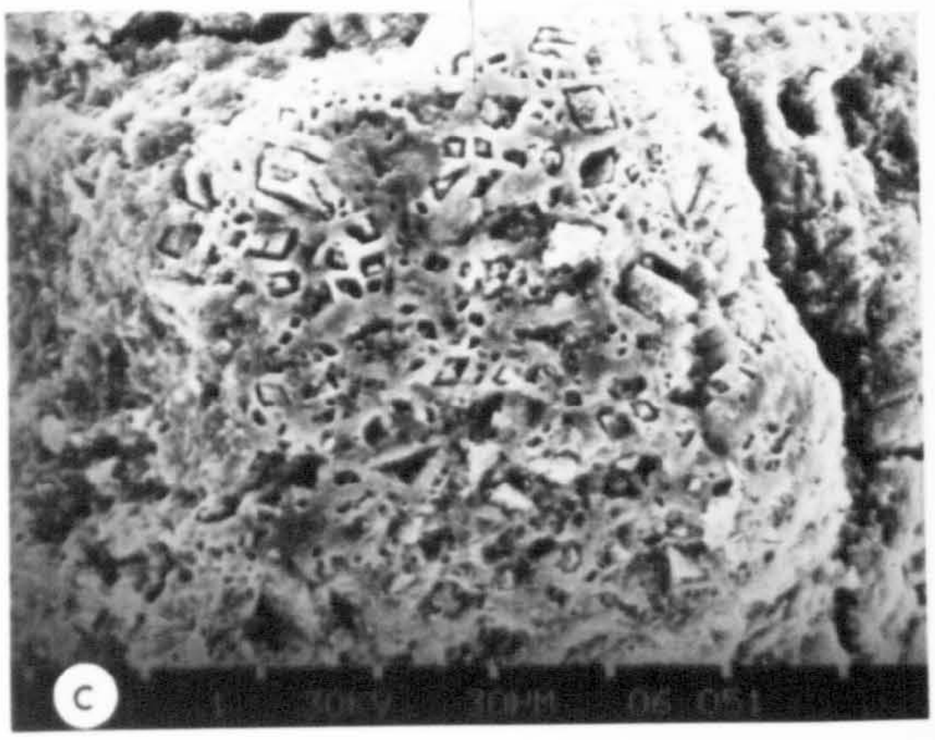
c

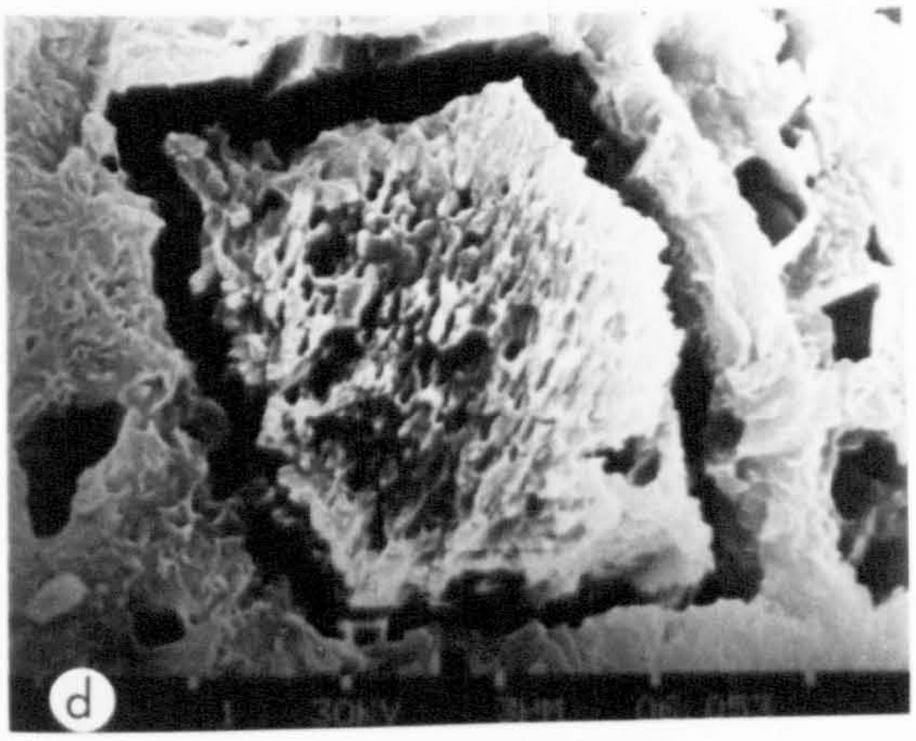
d

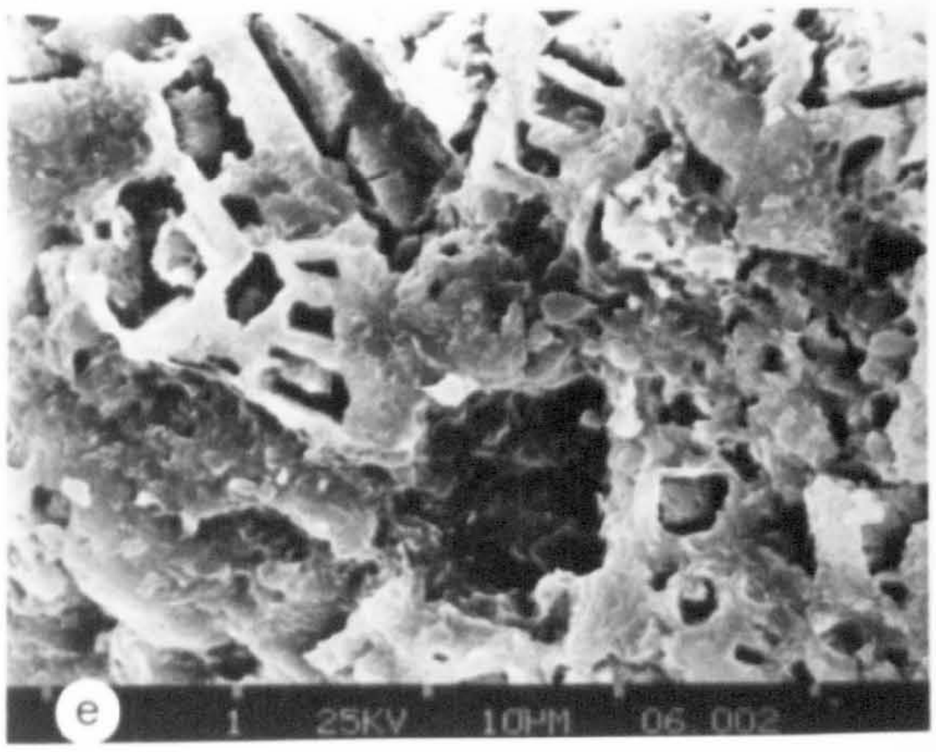
e
1 25KV 10MM 06.002

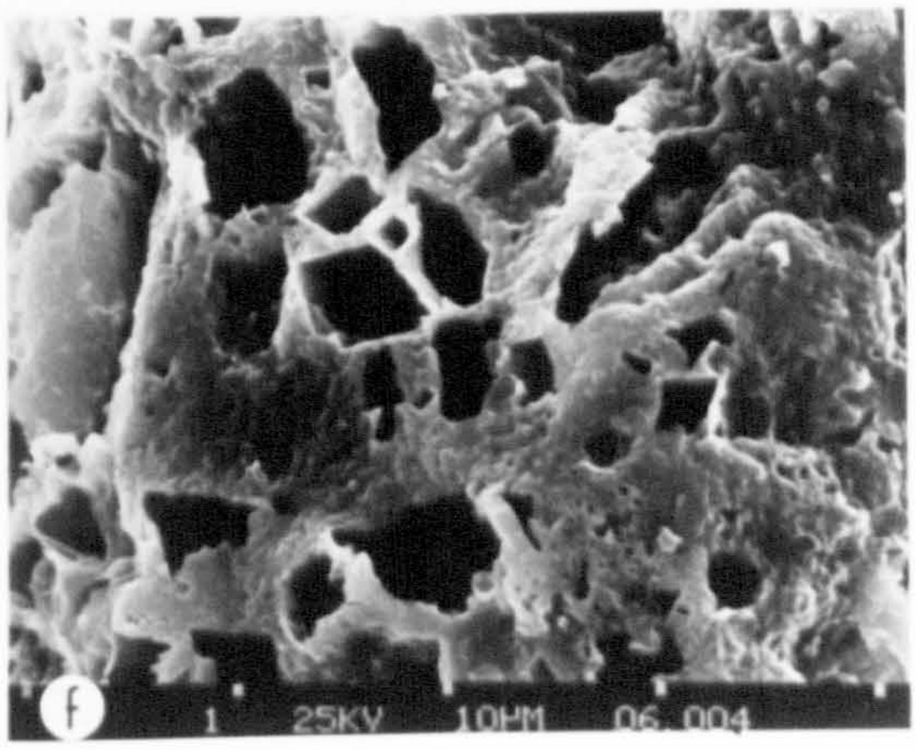
f
1 25KV 10MM 06.004

together. Broken grains mounted in the SEM show that up to 70 % of the inside of these pellets is composed of perfectly formed dolomite rhombs (Plate 8.3e). Glaucony extracted from this lag deposit shows dolomite to be unstable at the surface of the pellet. Here, dolomite is only recognised as highly pitted remains or rhombohedral impressions (Plate 8.4c,d,e,f). Clearly, formation of the dolomite preceeds that of the glaucony. Within the lag deposit only, dolomite at the surface of glaucony pellets is unstable and prone to dissolution.

Possible origin of dolomite and the source of magnesium

Reports of trace amounts of dolomite rhombohedra (5-40 μm) in unconsolidated deep-sea sediments have existed over the last century (Correns, 1939; Fairbridge, 1957; Bonatti, 1966). Various conflicting views have been proposed on their origins, including detrital sources, formation due to hydrothermal metamorphism and submarine volcanism, and organic formation. Recent discoveries have focused attention on the association of dolomite with organic-rich sediment (Friedman and Murata, 1979; Pisciotto and Mahoney, 1981; Kelts and McKenzie, 1982; Garrison *et al*, 1984). The formation of dolomite off Baja California seems to be consistent with these latter observations. Dolomite in DSDP cores from the Gulf of California (Kelts and McKenzie, 1982) shows that it is associated with organic - rich horizons extending from Late Pleistocene to Late Pliocene. Similar dolomite - bearing hemipelagic sediments extending down to the Miocene have been noted on the Pacific side of Baja California (Pisciotto and Mahoney, 1981). Kelts and McKenzie, (1982) have interpreted dolomite formation to be a result of low

temperature, early diagenesis with primary precipitation of dolomite occuring in the interstitial spaces of anoxic, diatomaceous oozes. They claim that the process takes place in a subsurface system, closed to sea water exchange and characterised by low sulphate concentration. Experimental data on the replacement of calcite and aragonite by dolomite (Baker and Kastner, 1981) also suggests that dolomite formation is favoured by low dissolved sulphate concentrations. Here, it is implied that the common site of dolomite formation is where the dissolved sulphate concentration is reduced by microbial sulphate reduction. Kushnir and Kastner (1982) from adsorbtion experiments of SO_4^{2-} on carbonates show that the residence time of adsorbed SO_4^{2-} is very short. In fact 50% of the adsorbed SO_4^{2-} is desorbed or exchanged in about ten minutes.

The observations on morphology, location, geochemistry and mineral associations indicate that the Baja California dolomite formation is not related to detrital input, evaporative reflux (Adams and Rhodes, 1960), evaporative pumping (Hsu and Siegenthaler, 1969), mixed water or schizohaline (Folk and Land, 1975) processes. Hence, any interpretation of dolomite formation must be related to normal hemipelagic accumulation.

The first appearance of significant dolomite in the Baja California sediment, beneath the zone of Mn reduction in the three hemipelagic cores and often in the presence of NO_3^-, clearly indicates that dolomite nucleation and growth can occur in the presence of SO_4^{2-} ions. Moreover, the formation of dolomite rhombs predating the development of glaucony pellets also suggests growth in the immediate subsurface environment. This hypothesis is supported by the near zero $\delta^{13}C$ values; the

$d^{18}O$ may be a result of isotopic disequilibrium or fractionation. While this dolomite may usually occur in small quantities, its preponderance in the glaucony suggests development within this zone can be extensive. Glaucony typically forms in a non-sulphidic environment common under fluctuating oxic-anoxic conditions (Odin and Matter, 1981; Berner, 1981 a,b; Section 8.3.1). It is most likely to occur in semi-reducing microenvironments in an overall oxidising regime (Odin and Matter, 1981). In sediments of high sulphide activity, or post sulphide activity, it is extremely unlikely that sufficient Fe^{3+} ions would be present to account for the amount of glaucony seen.

The association of dolomite with early diagenetic manganese carbonate formed from the precipitation of Mn^{2+} under mildly reducing conditions is also consistent with SO_4^{2-} being present in the sediment. The inclusion of pyrite in some dolomite rhombs does suggest sulphate reduction, although it is not known if this is due to local reduction in microenvironments or an overall reduction of the sediment. Dolomites analysed from the bulk sediment at depth in 163-13 do display $d^{13}C$ values (Figure 8.10) indicating some aerobic and/or SO_4^{2-} reduction, with the $d^{18}O$ indicating bottom water temperatures.

Thermodynamic and stability calculations have suggested that dolomite could be the stable phase in sea water (Garrels *et al*, 1960 ;Baker and Kastner, 1981). Observation of dolomite dissolution in the uppermost sediments, particularly 163-13, implies that this may not be correct. Within a lag deposit pore water conditions relating to alkalinity, Mg^{2+} and Ca^{2+} activity would not be significantly different from that of the overlying

sea water.

The relationship between the amount of dolomite and organic matter may be significant both in respect of our understanding of dolomite formation and the source of Mg. It has been suggested that the source of Mg for dolomitisation could come from sea water, organic matter or ion exchange in sediments (Milliman, 1974). With deeply formed dolomite the sea water source of Mg is obviously somewhat limited (Kelts and McKenzie, 1982) and here one may resort to an organic or ion exchange source of Mg involving clay minerals for dolomite precipitation or replacement within a sedimentary sequence. Organic-rich, diatomaceous sediments are known to have Mg concentrations in excess of those held in terrigenous silicates, but even in such instances the amount of organically bound Mg tends to be modest and rarely exceeds 1 or 2 % of the sediment (Calvert, 1976). With lower $C_{org.}$ found in the sediments off Baja California this source of Mg would be somewhat limited.

Accumulation estimates of Baja California hemipelagic sediments indicate rates of 1.5 to 2.0 cm kyr^{-1} (Chapter 3) for those sediments existing in the reducing zone. Moreover, radionuclide measurements (Chapter 7) show that the oxidising layer may be entirely bioturbated. Estimates of bioturbation in Pacific sediments suggest the top 10 to 20 cm may be entirely biomixed every 1000 years. Certainly the rate of biomixing is considerably greater than sediment accumulation (Turekian *et al.*, 1978). The profiles of solid phase Mn in Figure 8.5 could be interpreted in terms of a surface bioturbated layer and an underlying zone of steady state accumulation. If extensive

bioturbation occurs in the Baja California sediment irrigation of this surface could bring sufficient Mg within the entrained waters for significant amounts of dolomite to form at, or near, this redox boundary. Due to the low sedimentation rate Mg may also reach this zone by diffusing in from the overlying sea water (Gieskes, 1975). The presence of minor amounts of dolomite within the oxidising layer could be caused by precipitation within microenvironments, or alternatively, could have formed at the locus of dolomite precipitation within the reduced sediment and been subsequently transported by benthic activity.

The mechanism of dolomitisation within the uppermost reduced sediment, or at the redox boundary, is unknown, but higher alkalinity in the reduced sediment may be one factor leading to its precipitation. Elevated Mg/Ca ratios that have previously been considered important in the formation of supratidal dolomite are not a limiting requirement. This view is also held by Baker and Kastner, (1981) and Kelts and McKenzie, (1982) in the formation of deep-sea dolomite.

Variation in input of C_{org} to the sediments will affect the subsurface environment in two ways. Firstly, it is likely to produce variation in the total dissolved C in the reduced sediment which may have some bearing on the dolomite formation. Secondly, and perhaps more importantly, it may induce a range of benthic activity and corresponding entrainment of sea water Mg to the zone of reduction leading to dolomitisation. The occurrence of dolomite in many ancient sediments is often associated with bioturbation as seen in the dolomite bands of the Monterey Formation of southern California (Friedman and Murata, 1979).

Laboratory experiments on dolomite kinetics (Gaines, 1980) show it to be extremely slow growing. Within the rapidly accumulating sediments of the shelf conditions conducive to dolomite growth are changing too rapidly for precipitation to take place. Here, incipient dolomite formed would be rapidly buried before significant crystal growth could be achieved. Within organic-poor oceanic red clays a low rate of sediment mixing from bioturbation again reduces the liklihood of significant quantities of dolomite. It would seem that the slowly accumulating hemipelagic sediments, with high C_{org} contents due to elevated biological productivity as is seen here, represent an ideal locus for dolomite precipitation. In the eastern Pacific the generally low terrigenous supply coupled with high biological productivity, suggests that this area of the ocean is highly conducive towards early diagenetic dolomite formation. Reports of some rhombohedral dolomite in late Cenozoic hemipelagic sediments from DSDP cores (Pisciotto and Mahoney, 1981; Kelts and McKenzie, 1982) and in dredge hauls (Kulm *et al*, 1981, 1984) may have formed in the manner described.

Dolomite formation in deeply buried sediments undoubtedly occurs. Such late formation has been evidenced by the isotopic composition (especially the heavy ^{13}C dolomites of Pisciotto and Mahoney (1981) and Kelts and McKenzie (1982); Figure 8.10) of the mineral and its pervasive growth in certain horizons. This suggests that the earliest formed dolomite, as is seen in the immediate subsurface environment off Baja California, may act as a substrate for further dolomite precipitation, especially during methanogenesis after sulphate has been

consumed. Growth of this dolomite is obviously limited by the amount of residual sea water and organic Mg within the sediment and the extent of ion exchange involving Mg from clay minerals, during diagenesis. Such dolomite is not likely to be uniformly precipitated within the sediment, but is going to be confined to those horizons with prior dolomite. In the exceptional case (as in 163-13) of very high C_{org} and benthic activity, early dolomite formation can be extensive.

8.4 ANOXIC MINERAL FORMATION

8.4.1 *Pyrite Formation*

Pyrite formation has received considerable attention in the literature and is commonly believed to be characteristic of anoxic-sulphidic diagenesis, formed as a result of the reduction of seawater sulphate by anaerobic bacteria using organic matter as a substrate. In this section some of the pyrite morphology found in anoxic sediment off Baja California is described together with an outline on its importance in influencing the geochemical pathway of iron, rather than details concerning its diagenetic formation which have been recently reviewed (Berner, 1984).

8.4.2 *Results*

Pyrite morphology has been documented from the basal clay of 163-13, underlying the coarse lag deposit. Apart from discrete microspherules of framboidal pyrite, most of the

concretions display biological affinities, either as pyritised worm tubes or infillings within foraminifera tests. The microspherules are some 10 μm in diameter composed of welded pyritohedra. It is uncertain whether these framboids form separately in fine grained sediment, or have been disaggregated from larger pyrite masses during sample preparation. The pyritised worm tubes (Plate 8.5a,b,c) are composed of hundreds of microspherules in a form suggesting replacement of the inner mucosal lining of the tube (Thomsen and Vorren, 1984). Similar pyritised worm tubes have been described by Hein and Griggs (1972) and Jorgensen (1977). However, none of these authors have noted the occurrence of a dendritic sulphide (Plate 8.5d,e) covering the external surface of the framboidal pyrite tube. EDAX confirms the presence of Fe and S in the dendrites but this qualitative method is not sufficient to determine the stoichiometry of this phase. Within foraminifera tests well-defined, euhedral, octahedra of pyrite (Plate 8.5f) are found growing into the cavity formed by the test. Similar infillings have been described by Love (1962) and Hein and Griggs (1972).

Discussion

Formation of pyrite depends on the sources of sulphide and iron. Sulphide is produced by bacterial metabolisation of organic matter. In this way the quantity of available organic matter in the sediment accessible to sulphate reducing bacteria (*Desulfovibrio desulfuricans*) limits the total amount of pyrite that can be formed (Berner, 1970; Calvert, 1976); there being a stoichiometric relationship between pyrite formed and the

PLATE 8.5 Scanning electron micrographs of sulphide morphology from core 163-13:

(a) Pyritised worm tube composed of framboidal pyrite.

(b) Close-up of the end of the pyritised tube suggesting framboids form as a result of bacterial degradation of the mucosal lining of the tube.

(c) Pyritised worm tube displaying well formed framboids.

(d) Dendritic sulphide (identified by EDAX) growth interlinking framboidal pyrite.

(e) Close-up of dendrite terminations in (d).

(f) Well developed pyrite octahedra inside a foraminifera test.

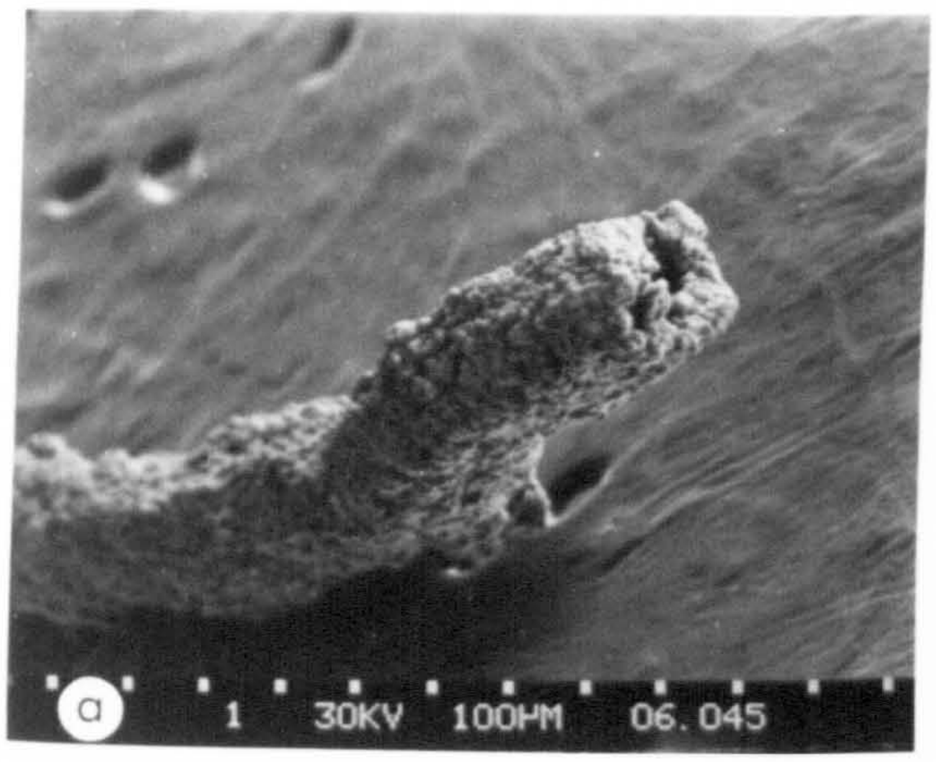
a
1 30KV 100µM 06.045

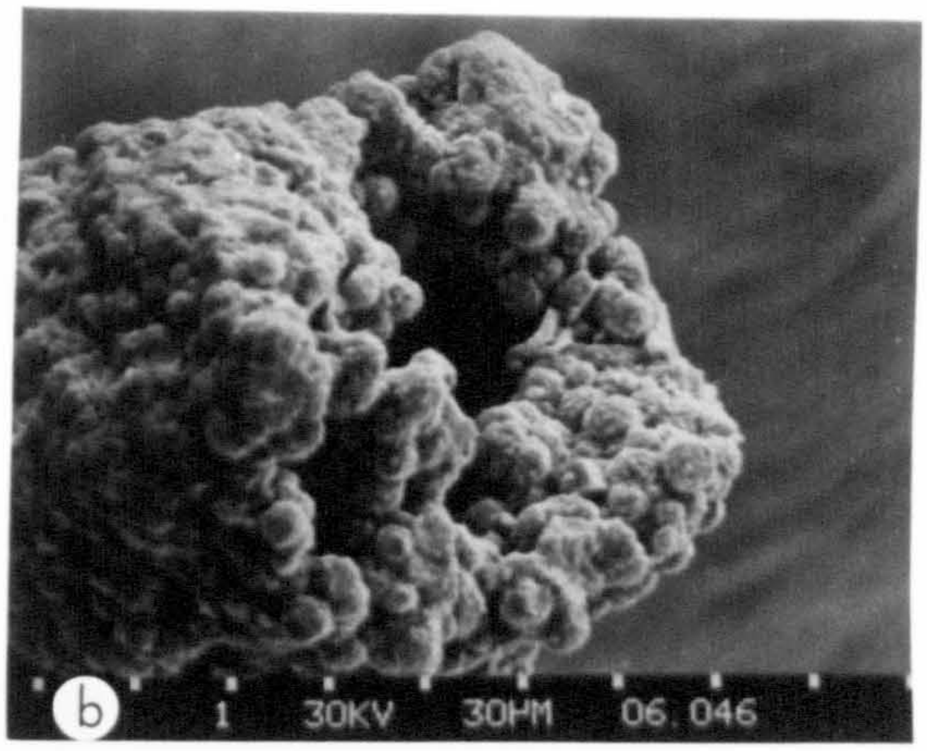
b
1 30KV 30µM 06.046

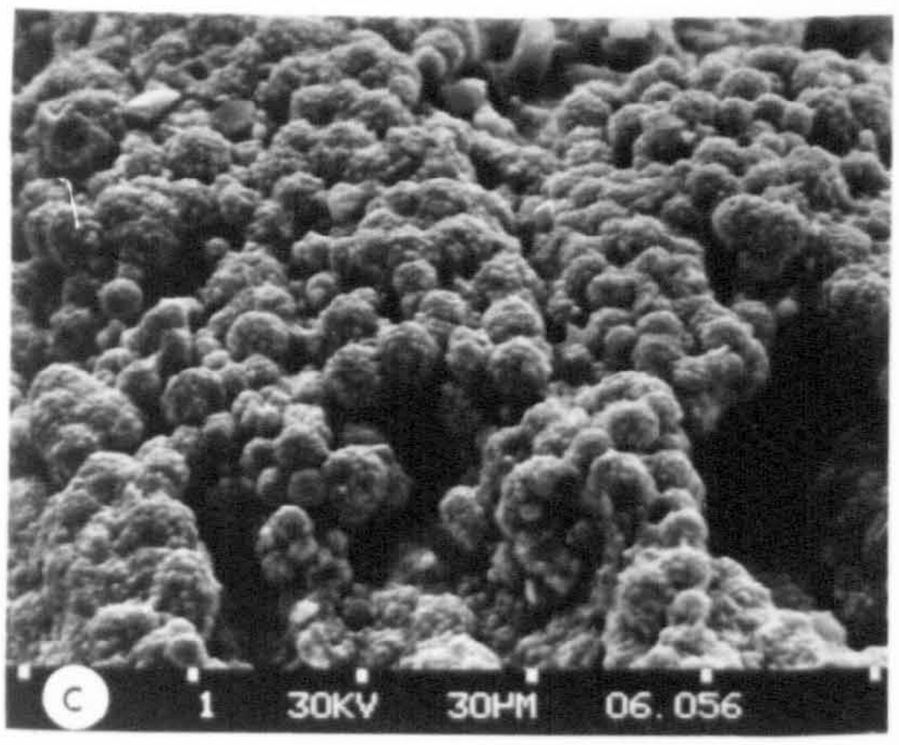
c
1 30KV 30µM 06.056

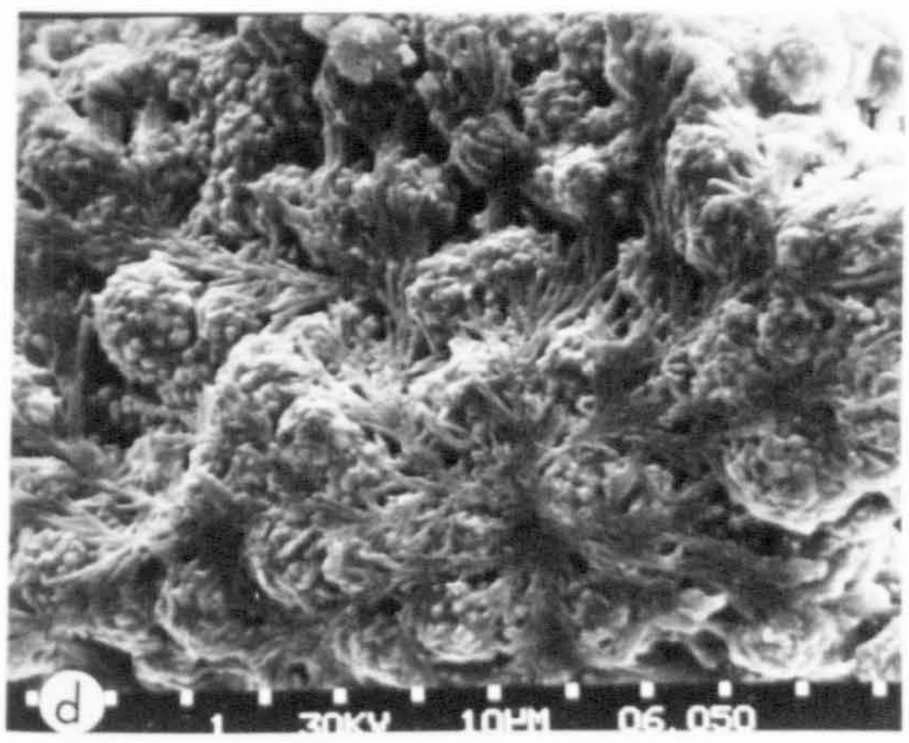
d
1 30KV 10µM 06.050

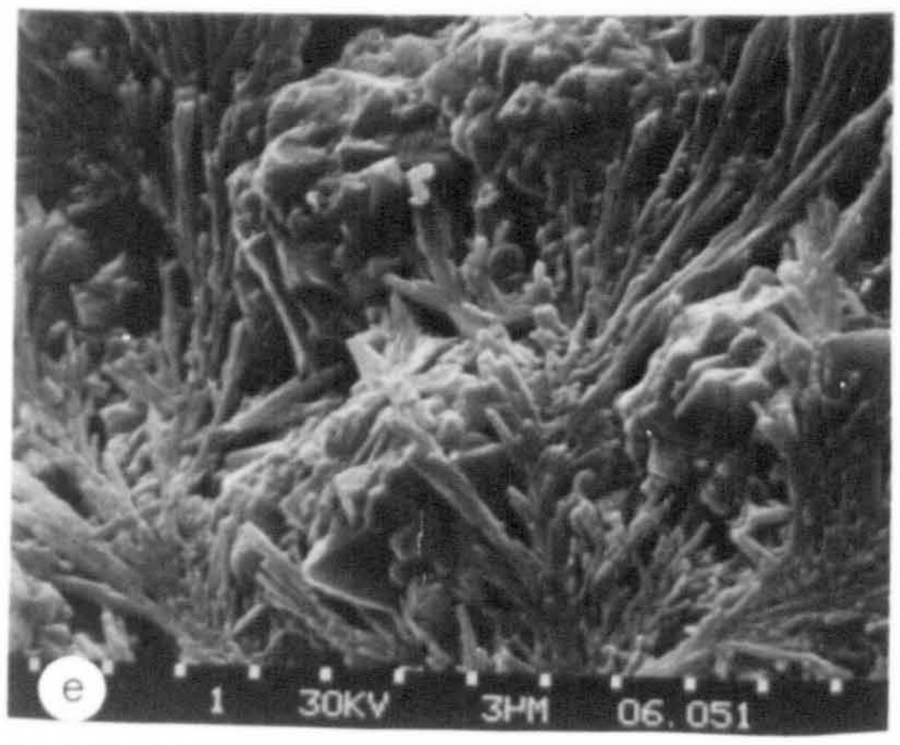
e
1 30KV 3µM 06.051

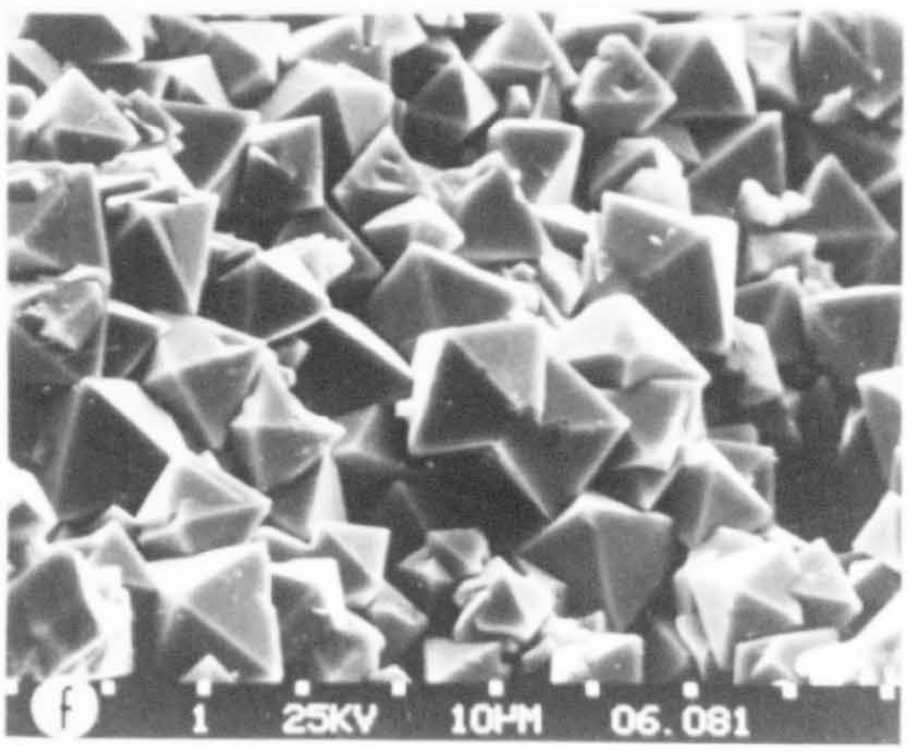
f
1 25KV 10µM 06.081

amount of organic matter oxidised to CO_2 (Berner, 1981,a). Usually, because there is often excess organic matter in anoxic sediments, there is a positive correlation between the amount of pyrite formed and the concentration of C_{org} (Berner, 1970; Goldhaber and Kaplan, 1974).

However, it is the role of Fe, and particularly its availability, which is of interest off Baja California. Berner (1970, 1981 a,b, 1984) indicates that only in special circumstances (high carbonate sediments - Florida Bay, or "euxinic" (anoxic) sediments - Black Sea) does the quantity of detrital Fe in the sediment limit the formation of pyrite. More important is the amount of Fe_2O_3 formed during continental weathering which may be substantial in the semi-arid climate of northern Mexico (Chapter 2).

Pyritisation does not abundantly occur in the zone of SO_4^{2-} depletion, but rather in microenvironments in the top few cm near the sediment/water interface (Berner 1970, 1981 a). In this zone SO_4^{2-} may be constantly replenished by diffusion, or by irrigation by infaunal organisms. This may well be the mechanism by which worm tubes have become pyritised in 163-13, initiated by the reduction of SO_4^{2-} by bacteria metabolising the mucosal lining of the tubes.

One may speculate on the role of pyrite formation in influencing the distribution of Fe and Mn off Baja California. Given that Fe oxyhydroxides can be important electron acceptors during organic matter breakdown (Table 4.4) the absence of a distinct solid phase Fe redoxcline in the hemipelagic sediments at the depth of Fe^{2+} release (shown by Sawlan and Murray, 1983) is slightly puzzling, considering that Fe is also subject to dissolution/reprecipitation during redox changes in the same

way as Mn. Although at the same pH and temperature oxidation of Fe is more rapid than Mn (Stumm and Morgan, 1970; Hem 1978) their rate laws are different; oxygenation of Fe^{2+} is first order with respect to Fe^{2+} and O_2, whereas Mn undergoes an autocatalytic reaction. If Fe and Mn are both derived from terrestrial weathering and supplied to the Baja California shelf, slope and rise as oxyhydroxides (submarine exhalative inputs of juvenile Fe and Mn are considered unimportant in this area) then the dominance of Mn over Fe in the oxic hemipelagic sediments, and *vice versa* in the more reducing shelf sediments is attributable to the different geochemical behaviour of the two metals. Fe has a stronger tendency to form organic complexes (especially with phosphate ions) affecting the solubility and colloid chemical propeties of the dispersed oxides (Stumm and Morgan, 1970). Sholkovitz (1978) confirmed previous studies which have shown that almost total removal of dissolved Fe (95%) occurs during estuarine mixing. In contrast, Mn behaves more conservatively and independantly of Fe. Only 25-45% appears to be removed by flocculation during estuarine mixing. Fe sinks on the shelf in the form of glaucony, and possibly to a greater extent, pyrite, are more efficient than for Mn. MnS is more soluble than FeS_2 and is stabilised by only very high concentrations of H_2S (Holdren, 1977). To date, alabandite has only been reported from the Baltic Sea (Suess, 1979). Thus Mn recycling occurs rapidly on the shelf promoting a net flux to the oceanic environment which may be greater than the Fe flux helping to sustain the surficial enrichments in diagenetically remobilised sediment in the hemipelagic environment. However, the capacity of Fe to be taken up by

smectite in reduced sediment is probably greater than the sink for Mn in mixed Mn-Ca-Mg carbonate. It must be stressed that without accurate accumulation rates and figures for the relative inputs of Mn and Fe to the marine environment these conclusions are rather speculative.

CHAPTER 9

CONCLUSIONS

This thesis investigates the geochemical distribution of sediments along a transect normal to the continental margin off Baja California, Mexico. Consideration of the influence of diagenesis in modifying the bulk chemistry and promoting mineral formation is of prime importance. By studying a suite of box-cores from the oceanic environment to the shallow water conditions of the shelf valuable information has been gained on the role of ocean margins in influencing metal and radionuclide geochemistry.

The study area (Chapter 2), situated at the confluence of the southward flowing California Current and northward California Undercurrent, experiences upwelling and a high level of biological surface productivity. Detrital sedimentation at the present day is minimal due to the aridity of the climate and lack of major river systems. Shelf sediments are consequently fine-grained (clay-silt) with occasional tongues of coarser material radiating outwards from Santo Domingo bay. The tectonic evolution of the margin has resulted in a series of longituidinal basins, landward of the main shelf break, characterised by low levels of oxygen and high organic matter contents. Abundant foraminifera together with glaucony and phosphorite occur on raised banks of the outer shelf and upper slope. The predominantly lithogenous sediments of the oceanic environment are divided into hemipelagic facies, identified by a red-brown oxidised layer overlying grey-green reduced sediment, and pelagic facies which are oxidising throughout and with manganese nodules at the surface. The clay fraction of the sediment increases oceanwards, dominating the oceanic environment. Smectite, illite and chlorite are all present; the smectite being poorly-ordered as opposed to the crystalline

detritál illite and chlorite.

Bulk sediment inorganic geochemistry reveals variation in detrital input to both the shelf and oceanic environment (Chapter 3). Zr, believed to be enriched in the coarser, heavy-mineral fraction of the sediment, has higher concentrations relative to Al in the nearshore shelf sands and with depth in the hemipelagic sediments. Similarly, Si/Al ratios follow the same pattern; Si being present in detrital minerals not in biogenic remains. K/Al and Mg/Al ratios in the oceanic sediments suggest that smectite and illite concentrations have changed in the past, being dominated by the former at present. The correlation between Fe and Al in the oceanic sediments indicates that Fe-rich smectite may be the major host for this metal and that diagenetic reduction of smectite causes the colour change seen in hemipelagic sediments. On the shelf Fe is precipitated by diagenetic pyrite formation.

Biogenic elements such as Ca and Sr are strongly controlled by the level of carbonate in the sediments. A well defined increase in $CaCO_3$ occurs in the lower decimeter of the three hemipelagic cores, having a Sr content similar to average pelagic foraminifera. The close similarity between the level of carbonate concentration in the sediments and the Zr/Al and Si/Al profiles suggests that climatic and physiographic conditions off the Baja California peninsula have changed over the time span sampled by the cores. ^{14}C dates from sediments along this transect (TGT-145) reveal ages compatible with the last Wisconsin glaciation for sediments with elevated Si, Zr and $CaCO_3$. These findings have been interpreted as resulting from sea level changes which at low stands promoted greater

discharge of detritus off the shelf into deeper water. The origin of the $CaCO_3$ increases at this time, either through productivity changes, or through detrital carbonate being washed from the shelf, is unresolved. Ba in the oceanic sediments is also a clear indicator of biogenic productivity as opposed to occuring as a detrital element in feldspars of the shelf sediments. However, the decrease in Ba/Al over the region of high $CaCO_3$ and Zr and Si/Al ratios assigned to the last glacial episode, suggests that dilution by terrigenous debris dominated any increased Ba productivity signal at this time.

Organic carbon is the prime mediator in diagenetic reactions occuring within the sediments off Baja California (Chapter 4). The low sedimentation rates and high organic matter contents ensure a sequence of observable reactions within 30-40 cm of the surface of the sediment column. The breakdown and release of C_{org}, N, P, I and Br provides valuable information on the rate of these processes. Oxic diagenesis, characterised by core 163-9, is the most efficient method of organic matter breakdown. However, bioturbation and sedimentation rate are important; in hemipelagic sediments suffering bioturbation oxic diagenesis degrades C_{org} 6-14 times more quickly than in the pelagic environment. This is probably due to the longer residence time of the detrital organic matter at the sediment/water interface in more slowly accumulating sediments. Under oxic conditions in pelagic sediments N release from organic matter, and its expulsion from sediment *via* pore waters, is not effective. Instead, N appears to be held in the sediment, possibly by smectite absorbtion. I and Br are both intimately associated with organic matter; I responding to

redox variability more readily than Br. Like N, I fixation occurs in the pelagic red clays, possibly by IO_3^- reacting with Fe- and Mn-hydroxides, or by the uptake of organic compounds containing I by smectites.

The utilisation of NO_3^- and MnO_2 as electron acceptors at a shallow depth within the sediment column qualitatively indicates faster rates of diagenesis. Under these conditions N and I uptake after organic matter release is minimal, whilst the presence of a substantial surficial layer of MnO_2 plays an important part in limiting the outward flux of dissolved I as it oxidises from I^- to IO_3^-. Br is not susceptible to redox changes in the same way, nor to absorbtion processes, but maintains a relatively constant Br/C_{org} in all diagenetic environments. P contents in oceanic sediments occurs in excess of either detrital or organic contributions and is believed to result from accumulation of skeletal fish debris. On the shelf, where dilution of such material by terrigenous detritus is more pronounced, the level of P in the sediment can be accounted for by the degree of organic matter preserved in the suboxic/anoxic intrashelf basins, or by diagenetic apatite formation (Core 145-17).

Assessment of C_{org} fluxes both to the sea bed and during burial reveal that over 90% of C_{org} produced by surface productivity is destroyed within the water column, and that of the amount reaching the seafloor an equal percentage is consumed by benthic processes prior to burial. Once within the sediment approximately 30% of the buried C_{org} is consumed during oxic diagenesis. Within hemipelagic cores there is a suggestion that the last glaciation increased the level of

organic matter within the sediment, either through productivity or sedimentation rate increases, although dilution by terrigenous debris makes this statement equivocable.

Trace metal enrichments in the organic-rich facies found on the Baja California shelf (Chapter 5) do not appear to be excessive. Realisation that C_{org} levels within the sediment apparently depend on grain size and clay content suggest that the excellent correlation between heavy metal and C_{org} is not an *à priori* association with organic matter, but due to textural control. Thus fine grained sediments have higher trace metal contents, and C_{org}, than coarse grained ones. Mo has the greatest enrichment over average shale off Baja California and its precipitation with FeS under anoxic conditions is believed responsible.

During the diagenesis of organic matter in oceanic sediments the fate of Mn plays an important part in influencing the distribution of associated trace metals (Chapter 6). The high surficial Mn concentrations result from dissolution/ reprecipitation reactions occuring at a critical Eh within the sediment column. Measurements of the oxidation state of the solid phase Mn suggests that although above the Mn redoxcline oxidation states are high (~$MnO_{1.80}$), there appears to be a ubiquitous lower oxidation state at, and immediately below, the sediment/water interface, and that Mn^{4+} metastably exists below the critical redox level. The low initial oxidation state may result from hydrogenous precipitation of a low stoichiometric Mn oxide such as hausmannite, or utilisation of Mn oxide as an electron acceptor in microenvironments at sites of local organic matter breakdown. The existence of Mn^{4+} below the

redoxcline may be due to the stabilisation of the vernadite lattice by trace metal substitution.

Examination of the uptake of trace metals by vernadite reveals that the order of metal enrichment is Mo>Ni>Zn=Cu, very similar to their respective concentrations in seawater. Furthermore, Ni and Mo exhibit preferential metal uptake depending on the degree of diagenesis. Sediments with low organic matter contents (thereby slower diagenesis) have high Ni/Mn atomic ratios; an increasing Ni/Mn ratio is seen in sediments oceanwards. Mo release from the surficial Mn oxide layer occurs at the first appearance of Mn^{2+} in solution. Thus Mo may be transferred to the dissolved organic carbon pool which builds up with depth. Whether this source supplies Mo for coprecipitation with FeS at depth, and the fate of Mo on monosulphide/sulphide transformation, is not resolved by this study.

Below the Mn redoxcline trace metal concentrations are still high relative to average shale. This may be due to diagenetic uptake by smectite. It appears that the initial precipitation of hydrogenous Mn oxides with associated trace metals from the water column leads to increased availability of these metals for clay absorbtion during Mn redox mobilisation, in turn controlling the trace metal character of the diagenetically reprecipitated MnO_2.

The study of the radionuclides (Chapter 7), ^{230}Th and ^{231}Pa, in association with the bulk sediment geochemistry reveals that the kinetics of Mn remobilisation are faster than the rate of benthic mixing defined by ^{230}Th and ^{231}Pa. Radionuclide removal is greater in the hemipelagic environment

than in the open ocean, whilst the preferential scavenging of ^{231}Pa relative to ^{230}Th increases landwards. Due to the increased flux of particles near the continental margin, both at the present day and in the past during glacial episodes, the concentration of radionuclides in the sediment has been modified. There appears to be a complex interplay between changing bulk sediment supply rate which acts as a "dilutent" towards the nuclides, and the scavenging of nuclides by particles. During the last glaciation dilution of the nuclide activity by terrigenous and biogenic material has influenced the activity within the sediment causing low apparent sediment accumulation rates. The composition of suspended particles in the water column, particularly Mn oxides, seems to influence the fractionation of ^{230}Th and ^{231}Pa in the sediment, the latter being preferentially enriched in marginal sediments. The combination of varying sediment accumulation rate temporally and laterally, together with non-uniform particle composition makes the determination of bulk sediment accumulation rates in marginal sediments difficult.

Diagenetic mineral formation occurs in a variety of sediments off Baja California (Chapter 8). Mineral formation is often considered, as in this thesis, as occuring within defined diagenetic zones. However, availability of reactants, suitable sites of precipitation and the preservation potential once formed are extremely important. Diagenetic apatite formation occurs in shelf sediments of core 145-17 in a zone where pH and pore water Mg^{2+} controls are unimportant. Given the availability of PO_4^{3-} *via* biological vectoring, the main control on precipitation appears to be grain size; formation

occurs in layers where a lithologic change provides a more open sediment framework.

Manganese carbonate formation occurs at depth in the hemipelagic cores (163-14, 163-10) and is attributed to two main factors; a suitable locus for precipitation (a possible ash band occurs in the basal sample interval of both cores), and a surficial concentration of MnO_2 to supply the required Mn^{2+}. In addition, sufficient organic matter is necessary to act as an electron donor and reduce the oxides.

Glaucony formation is characterised by ovoid, cracked, bulbous pellets occuring on the outer shelf and slope off Baja California. XRD analysis indicates that the material is non-crystalline and smectitic in nature. Electron microprobe analyses reveal substantial Fe and some Mg substitution for octahedral Al without equivalent substitution by charge balancing cations in the interlayer position. This is taken as further evidence of Fe fixation preceeding K uptake suggested by other authors. Therefore the glaucony does not seem to evolve from precursor illite. The high level of Fe (probably mostly Fe^{3+}) indicates formation prior to advanced sulphate reduction, possibly in microenvironments such as faecal pellets which are semi-permeable allowing diffusion of K, Na and Mg. Low overall sediment accumulation rates on the outer shelf may allow the pellets to reside for sufficient time in the zone of cation diffusion and uptake.

Studies on the distribution and geochemistry of dolomite indicates that precipitation principally occurs in the hemipelagic sediments, whilst little or no genesis occurs in the pelagic red clays or shelf sediments. Within the

hemipelagic environment the abundance of dolomite broadly correlates with the level of C_{org} in the sediment. Vertical distribution in the silt fraction from the cores indicates that formation occurs below the zone of Mn reduction, and that dolomite within the zone of oxidising sediment shows evidence of dissolution. Structurally, the dolomite is well-ordered and therefore not proto-dolomite and has an average composition of 56 mole% $CaCO_3$. Association with glaucony pellets indicates extensive prior formation in sediments from the upper slope (163-13), while dolomite formation also associated with Mn carbonate genesis in the hemipelagic setting. This suggests that major dolomite growth can occur within the presence of SO_4^{2-} ions. Supply of Mg may be achieved through benthic mixing and entrainment of bottom waters to the base of the oxidised zone. Slow sedimentation rates enable suitable formation conditions to be maintained during the important early stages of mineral growth. This early dolomite may be an important substrate for futher dolomite precipitation during burial.

Formation of pyrite in the organic-rich shelf sediments indicates the importance of biogenic substrates (mucosal linings of worm tubes, foraminifera chambers) in providing a suitable locus for SO_4^{2-} reduction in a zone of Fe and S supply. Pyrite formation may also play an important part in limiting the amount of Fe reaching the oceanic environment in contrast to Mn which is rapidly recycled in organic-rich shelf sediments due to the lack of a substantial Mn sink.

This thesis has attempted to convey the value of an integrated approach to the geochemistry of marine sediments, and the importance of continental margins in ocean chemistry.

Only by studies sampling a range of environments, but containing essentially similar geochemical inputs, can the complex interplay between sedimentation and diagenesis be unravelled.

APPENDICES

APPENDIX A

SAMPLE COLLECTION AND CORE DESCRIPTION

Samples were collected during cruise TGT-163 of R/V *Thomas G. Thompson* in November 1981 under the auspices of the University of Washington (Dr. James W. Murray). A suite of 10 box-cores were recovered from the shelf, slope and abyssal plain, mostly along a transect normal to the strike of the Baja California peninsula (Figure 1.1). This same transect was occupied the previous year by cruise TGT-145 from which some samples were obtained (in particular core 145-17). A stainless steel box-corer was used which minimises disruption of the sediment/water interface enabling the very topmost material to be recovered. On deck the box-core was opened, described and any nodules or clasts removed prior to sub-sampling with 2.5" butyl acetate liner. Sediment was then extruded from the liner using a rubber plunger, sectioned into 1 cm and 2 cm slices, bagged in self-sealing polythene and stored wet at $4^{o}C$ aboard ship. Subsequently, the samples were transported back to Edinburgh as personal baggage aboard a commercial flight. The sediments collected and used in this thesis are briefly described in Table A.1.

On arrival at the Grant Institute the sediment was unsealed, any shells or nodules removed, and a portion weighed wet before drying at $60^{o}C$ overnight in order to calculate the water content of each sample. The results are given in Table A.2. This dried portion of sediment was subsequently ground to pass 200 mesh in a tungsten carbide Tema disc mill for 2 minutes, this material being used for XRF, carbon and wet chemical analysis (see below). The remaining wet sediment was stored at $4^{o}C$ and used for mineralogy, XRD and kept as an archive.

Sample numbers in the following tables refer to core number and depth range (in cm) of the samples. For example, 7:12-14 refers to a 2 cm thick sample from core 7 at 12-14 cm depth. In the text cores are prefixed by the cruise number; 163- refers to cores collected and analysed by myself, whilst data (mainly pore water) for 145- cores from the previous year have been published elsewhere. However, one sub-core from core 145-17 on the shelf was analysed by me and reported in this thesis.

TABLE A.1

DESCRIPTION OF CORES INVESTIGATED IN THIS STUDY

Station	Core length cm	Core description	Microscopic description
163-5	24	Olive green silt/fine sand; many biogenic fragments (bivalves, gastropods, scaphapods); upper surface rippled; grazing trails and bioturbation evidence.	Abundant detrital grains, especially quartz and feldspar, poorly sorted, sub-rounded to well-rounded, biogenic micro-fauna tests quite abundant, both siliceous and calcareous.
163-12	20	Olive green silt/fine sand; many biogenic remains including large infaunal bivalves.	Abundant detrital grains; quartz, feldspar and heavy minerals; poorly sorted; sub-rounded to well-rounded.
145-17	28	Olive green mud/silt; few biogenic remains.	Similar to 163-5 and 163-12 except with diagenetic apatite manifested as micro-crystalline growths within foram tests.
163-8	49	Foram ooze; dark green throughout with black particles at 26-28 cm and deeper. H_2S noted in sections deeper than 38 cm. Little evidence of bioturbation.	Fine-grained, organic-rich mud with abundant benthic and planktonic forams. Several species of siliceous diatoms; detrital grains include quartz, feldspar, biotite and some glaucony.
163-11	24	Green foram mud/silt; live infauna (worms), large gastropods, lithified sandy nodules at 3-5 cm depth	Abundant planktonic and benthic calcareous forams in well-sorted silt. Detrital quartz feldspar, biotite, glaucony, chlorite, all abraded and well rounded. Planktonic forams show evidence of dissolution.
163-13	26	14 cm coarse lag deposit consisting of a large gabbro clast and phosphorite nodules overlying fine-grained dark clay. Lag contains abundant forams and glaucony pellets which are present, but reduced in concentration in the underlying clay.	Clay contains abundant dolomite both within the sediment fabric and within glaucony pellets. Quite abundant benthic forams, glaucony and barite pellets, and sulphides often forming around micro-worm tubes or concretionary masses. Large crystals of gypsum may be an artifact of sulphide oxidation on collection.
163-7	34	12 cm of dark, chocolate-brown ooze overlying pale greyish, olive green mud. The top 3 cm is very soupy. Black mottling below 26 cm.	Clay; few forams or siliceous diatoms; rhombic dolomite increases in concentration downcore; detrital quartz, feldspar and mica; poorly sorted and sub-rounded.
163-14	32	10 cm of chocolate-brown ooze overlying creamy, greyish mud. At 6 cm depth there is a creamy-yellow transition. Upper surface of the box-core was sharply sloping, possibly disturbed.	Very similar to 163-7, except no dolomite in the top 10 cm.
163-10	32	10 cm of chocolate-brown ooze overlying creamy-grey mud; at the core base are hard lithified lumps of Mn carbonate occuring in a stiff clay.	Very similar to 163-7 and 163-14; dolomite increases downcore. SEM evidence of foram dissolution.

TABLE A.1 (cont.)

Station	Core length cm	Core description	Microscopic description
163-9	38	Uniform moderate brown clay with 7 Mn nodules at the surface. The nodules are mushroom-shaped with a smooth upper surface covered in encrusting organisms (serpulids) and a knobbly, friable lower surface in contact with the sediment.	Fragments of radiolaria and diatoms; no calcareous forams; fine-grained detritus.
163-15	35	Uniform moderate brown clay with 2 large Mn nodules at the surface. A further 2 rounded nodules occur between 5 and 10 cm depth.	Similar to 163-9 with occasional micronodules.

TABLE A.2

WATER CONTENTS OF BAJA CALIFORNIA SEDIMENTS REPORTED IN THIS THESIS

Depth cm	163-5	163-12	163-11	163-14	163-10	163-9	163-15	Depth cm	163-8	Depth cm	163-13	Depth cm	163-7
0-1	33.94	37.56	43.96	67.10	62.19	68.32	69.14	0-1	69.05	1-2	33.01	0-1	67.77
1-2	37.33	42.28	43.36	65.59	62.89	67.40	66.98	1-2	68.13	2-3	29.99	1-2	64.33
2-3	36.87	42.05	45.21	65.87	63.58	63.57	65.34	2-3	68.22	3-4	38.24	2-3	65.03
3-4	37.56	39.21	47.67	65.99	64.82	62.21	64.79	3-4	71.20	4-5	33.22	3-4	63.46
4-5	37.70	38.11	47.82	65.55	66.58	60.73	63.31	4-5	70.56	5-6	40.38	4-5	64.42
5-6	36.48	37.09	49.44	65.36	67.78	61.39	62.71	5-6	73.36	6-7	44.85	5-6	65.21
6-7	37.20	36.16	49.23	64.27	63.21	61.58	62.46	6-7	72.23	7-8	40.79	6-7	65.83
7-8	36.76	35.57	47.67	63.48	61.13	62.24	62.34	7-8	73.88	8-9	39.56	7-8	62.64
8-9	39.95	35.15	47.57	60.73	58.52	61.13	64.07	8-9	74.20	9-10	39.56	8-9	64.45
9-10	37.78	34.76	45.65	61.06	59.12	60.60	60.75	9-10	69.13	10-11	47.72	9-10	63.64
10-12	38.29	35.02	46.89	61.39	60.42	57.42	60.90	10-11	69.07	11-12	40.68	10-11	63.02
12-14	38.00	36.86	48.10	62.09	60.60	56.97	57.74	11-12	67.50	12-13	45.94	11-12	63.06
14-16	39.09	34.91	48.36	60.49	59.38	56.08	57.10	12-13	69.84	13-14	56.08	12-13	62.99
16-18	39.60	34.80	45.36	59.59	59.19	56.02	57.18	13-14	70.20	14-15	50.68	13-14	63.81
18-20	39.06	36.22	47.52	58.17	58.13	56.49	56.22	14-15	70.48	15-16	51.41	14-15	64.69
20-22	40.48		47.16	56.77	58.41	56.19	57.83	15-16	69.57	16-17	54.36	15-16	64.60
22-24	39.29		44.51	57.57	59.46	56.55	58.41	16-18	68.58	17-18	43.15	16-17	63.11
24-26				58.10	58.29	57.48	58.60	18-20	69.16	18-19	54.82	17-18	62.81
26-28				58.72	58.78	56.62	57.70	20-22	70.36	19-20	48.59	18-19	63.30
28-30				59.29	58.89	54.87	56.94	22-24	70.63	20-21	47.14	19-20	63.16
30-32				58.29	58.63	54.97	58.43	24-26	70.68	21-22	58.49	20-22	62.04
32-34						57.89	55.93	26-28	68.55	22-24	56.90	22-24	60.20
34-36						58.76	56.31	28-30	68.08	24-26	56.75	24-26	59.43
36-38						53.94		30-32	71.14			26-28	58.41
								32-34	68.06			28-30	57.88
								34-36	68.37			30-32	59.41
								36-38	69.18			32-34	58.22
								38-40	66.19				
								40-42	70.04				
								42-44	72.27				
								44-46	67.68				
								46-48	67.64				
								48-49	68.12				

Water contents obtained from drying sediment at 60°C.

Expressed as a percentage of the wet weight.

APPENDIX B

ANALYTICAL TECHNIQUES

B.1 BULK GEOCHEMISTRY: X-RAY FLUORESCENCE SPECTROMETRY

X-ray fluorescence spectrometry was performed on a Phillips PW 1450 sequential automatic X-ray spectrometer.

B.1.1 *Major elements: Method*

Fused, 45 mm diameter glass discs were prepared by a method similar to that of Norrish and Hutton (1969). Approximately 1 gram of ground, pre-dried sediment powder was accurately weighed (± 0.001 g) into a 95% Pt/5% Au crucible, covered with a Pt lid, and pre-ignited in a muffle furnace at 1100^{o}C for 1 hour. The sample was then allowed to cool in the crucible and reweighed to calculate the pre-ignition volatile loss. An ultra-pure flux, Spectroflux 105 (Johnson-Matthey Chemicals Ltd.) was added in a ratio 5.3333:1 (by weight, flux:sample), the crucible re-covered and placed back in the muffle furnace for a further 20 minutes. The flux consists of $Li_2B_4O_2$, La_2O_3 and Li_2CO_3, in which the tetraborate helps dissolve the sample whilst the La acts as a heavy absorber of the X-rays helping to minimise matrix effects between different samples and standards of varying composition. The crucible was then withdrawn from the furnace, allowed to cool to room temperature and reweighed. Any slight weight loss (from H_2O absorbed by the Spectroflux) is made up with further flux and the crucible plus lid placed over a Meker burner to melt and re-fuse the sample. On a hot plate at 220^{o}C a disc-shaped, slightly concave, graphite mould was placed inside a brass sleeve and the molten glass poured into the centre of the mould. An Al plunger, also at 220^{o}C, was used to press the glass into a ~1 mm thick disc. This technique results in a

reproducible "orange peel" surface texture of each glass disc. The discs are then allowed to cool progressively by covering with Vitreosil crucibles which helps prevent shattering. The discs can then be presented directly to the X-ray beam.

International rock and sediment standards (Table B.1) were used for calibration of the samples as these cover the range in composition of the Baja California sediments. For all elements the calibration lines are linear over the range of compositions investigated. Table B.2 lists the analytical conditions for the XRF major and minor element analyses. For major elements matrix effects were overcome by use of La as a heavy absorber and the use of theoretical absorbtion coefficients (Theisen and Vollach, 1967) based on a flux:sample ratio of 5.3333:1 following the correction procedures of Thirlwall (1979). Precision (based on replicate analyses) and accuracy of the method is given in Table B.3.

Although the fusion method provides a very consistent and accurate method of analysis for most rocks and sediments a problem exists with samples containing large quantities of organic matter and/or high carbonate contents, manifested by a loss of halogens and alkalies. Cl analyses from fusion discs were always far less than than that predicted from the salt content (see below). Na and K loss appears to have occured in the organic-rich shelf sediments (Chapter 3; Appendix C) and in the calcareous sediments from the lower decimeter of the hemipelagic cores (especially 163-14). During heating of salt in the presence of reactive organic matter, Na, K and Mg chlorides are probably hydrolysed and the Cl lost as volatile HCl. This may occur at temperatures < 400^{o}C. Pedersen (1979) found that no loss of alkalies (or even Cl) occured when

samples were immediately fused with Spectroflux rather than taken through a pre-ignition step at 1100°C. It may be that the melt eutectic of 700°C for a $Li_2O:B_2O_3$ ratio in Spectroflux 105 (Norrish and Hutton, 1969) is sufficiently low to prevent major alkali loss.

However, it should be stressed that this artifact only appears to occur in high organic matter samples and that the majority of analyses presented in this thesis are unaffected. The advantage of having a constant heavy-absorber flux to sample ratio for matrix corrections is of prime consideration.

B.1.2 *Minor Elements*

Pressed powder discs, 32 mm in diameter, were used for minor element analysis in preference to 45 mm discs as these proved to be less prone to swelling and cracking. A minimum of 3 g of ground, dried sediment was placed in a stainless stell sleeve resting on a highly polished tungsten carbide disc. Both the sleeve and cylinder were enclosed within a larger stainless steel cylinder. A leucite plunger was inserted into the sleeve and, using hand pressure, the sediment was compacted into a semi-competent disc. The leucite plunger and sleeve were removed and boric acid added sufficient to cover the disc and a large stainless steel plunger lowered onto the powder. A hydraulic press was used to compact the sample at 10 tons for a minute before releasing the pressure slowly for a further half minute.

This pressed-powder disc with its boric acid backing was

then presented to the X-ray beam after masking down the beam to 28 mm. Due to the unstable nature of the Baja California sediments the normal Grant Institute minor element analysis procedure of running a pressed disc twice through the XRF using Cr Kα radiation (for lighter elements) and W Kα radiation (for heavier elements) was unsuitable. This, together with the need to analyse Mo, As, I, Br and S resulted in the development of alternative software for the analysis of sediment trace metals with W Kα radiation. This work was carried out in conjunction with S.C.R Rainey, and I gratefully acknowledge the computing expertise of A. Walker.

Operating conditions for the minor elements are given in Table B.2. Count times (Table B.4) were optimised by statistical analysis of count rates (fluorescent yield) of standards approximating in composition to a typical sediment. Table B.4 also gives the theoretical peak to background detection limit (in ppm) for each element. Raw count data from the XRF was fed to an online Apple microcomputer which was programmed to recieve the count data, flag spurious counts*, perform average peak minus background calculations, present

---

*The program detects spurious counts by performing the following checks once the first peak and background have been measured for each element. Peak (n) will be flagged if:

$$Peak(1) - ((Peak(1) + \ldots\ldots Peak(n))/n) > \sqrt{Peak(1)} \times Factor\ (EL)$$

The factors for each element were determined by analysing the same sample several times to determine the mean ($\bar{x}$) and standard deviation (σ) of the counts, and using the equation:

$$Factor\ (EL) = \sigma/\sqrt{\bar{x}}$$

A Background (n) will be flagged if:

$$Back(1) - ((Back(1) + \ldots Back(n))/n) > \sqrt{Back(1)} \times 0.02$$

approximate concentrations relative to a standard of the operators choice, and finally to output the peak-background counts for later data processing and calculation of final concentrations. The microcomputer program, written in Applesoft Basic, is listed in Table B.5.

The average peak-background data was converted to initial minor element concentrations using theoretical mass absorbtion coefficients (Theisen and Vollach, 1967) calculated from the major element data and calibration against international and synthetic standards (Table B.1). These intial concentrations were then re-run using their additional mass absorbtion contribution to obtain the final concentration of the minor elements. The program (TRACE 15) also calculates interference corrections for Ti on V, V on Cr, Rb on Y, Sr on Zr and the effect of the W K$\alpha_2$tube line on As, and produces calibration graphs of count data against concentration of the element in the selected standards (Figure B.1). Table B.6 presents a listing of the data processing program TRACE 15, written in IMP to run under the Edinburgh Multiple Access System (EMAS). Precision and accuracy of this method is given in Table B.3.

TABLE B.1

STANDARDS USED IN ANALYSES PRESENTED IN THIS THESIS

Element	Standard
Al	G2 GSP1 AGV1 BCR1 PCC1 DTS1 GA GH BR
As	MA1 MA2 MA3 MA4 MA5
Ba	MAG1 SGR1 SCO1 G2 GSP1 AGV1 GA GH BR BCR1 PCC1 SY2 SY3 JB1
Br	BP1 BP2 BP3 BP4 BP5
Ca	G2 GSP1 AGV1 BCR1 PCC1 DTS1 GA GH BR
Cl	SGR1 SCO1 G2 BR BCR1 SY2 JB1
Cu	BCSS1 MESS1 SGR1 SCO1 G2 GSP1 AGV1 GA GH BR BCR1 PCC1 SY2 SY3 JB1
Cr	BCSS1 MESS1 MAG1 SGR1 SCO1 G2 GSP1 AGV1 GA BR BCR1 SY2 JB1
Fe	G2 GSP1 AGV1 BCR1 PCC1 DTS1 GA GH BR
I	BCSS1 MESS1 I1 I2 I3 I4 I5
K	G2 GSP1 AGV1 BCR1 PCC1 DTS1 GA GH BR
Mg	G2 GSP1 AGV1 BCR1 PCC1 DTS1 GA GH BR
Mn	G2 GSP1 AGV1 BCR1 PCC1 DTS1 GA GH BR
Mo	BR MA1 MA2 MA3 MA4 MA5
Na	G2 GSP1 AGV1 BCR1 PCC1 DTS1 GA GH BR
Ni	BCSS1 MESS1 MAG1 SGR1 SCO1 G2 GSP1 AGV1 GA GH BR BCR1 SY2 SY3 JB1
P	G2 GSP1 AGV1 BCR1 PCC1 DTS1 GA GH BR
Pb	BCSS1 MESS1 MAG1 SGR1 SCO1 G2 GSP1 AGV1 GA GH BR BCR1 PCC1 SY2 SY3 JB1
Rb	MAG1 SGR1 SCO1 G2 GSP1 AGV1 PCC1 GA GH BR SY2 SY3 JB1
S	MAG1 SG1 SCO1
Si	G2 GSP1 AGV1 BCR1 PCC1 DTS1 GA GH BR
Sr	BCSS1 MESS1 MAG1 SGR1 SCO1 G2 GSP1 AGV1 GA GH BR BCR1 SY2 SY3 JB1 JG1
Th	MAG1 SGR1 SCO1 G2 GSP1 AGV1 BCR1 GA BR
Ti	G2 GSP1 AGV1 BCR1 PCC1 DTS1 GA GH BR
V	BCSS1 MESS1 MAG1 SGR1 SCO1 AGV1 PCC1 BA GH BR SY2 SY3
Y	SGR1 SCO1 G2 GSP1 AGV1 BCR1 GA EH BR SY2 JB1
Zn	BCSS1 MESS1 MAG1 SGR1 SCO1 G2 GSP1 AGV1 GA BR BCR1 PCC1 SY2 SY3 JB1
Zr	MAG1 SGR1 SCO1 G2 GSP1 AGV1 GA BCR1 GH BR SY2 SY3 JB1

Standards prefixed I-, MA- and BP- are synthetic dilution-series standards made up from the following Specpure compounds diluted with bulk sediment from this study to maintain similar mass absorbtion characteristics:

As - As_2O_3, Br - NaBr, I - $Ba(IO_3)_2$, Mo - MoO_3

TABLE B.2

ANALYTICAL CONDITIONS FOR XRF MAJOR AND MINOR ELEMENT ANALYSES

Element	Line	Tube	kV	mA	Crystal	Peak $^{o}_{2\theta}$	Background $^{o}_{2\theta}$	Counter	Pulse Height LL	Pulse Height Window	Collimator	Sample	Notes
Al	Kα	Cr	50	45	PE	144.73	139.01	F	250	600	Coarse	Fusion	
As	Kβ_1	W	90	30	LiF200	30.48	31.20	FS	200	600	Fine	P.D.	Interference from W Kα_2 tube line (30.80)
Ba	Lβ_2	W	60	45	LiF200	73.32	74.70	F	150	600	Fine	P.D.	
Br	Kα	W	90	30	LiF200	29.98	28.60	FS	200	600	Fine	P.D.	
Ca	Kα	Cr	50	30	LiF200	113.09	110.00	F	200	600	Fine	Fusion	
Cl	Kα	W	90	30	PE	66.51	66.60	F	200	600	Coarse	P.D.	
Cr	Kα	W	60	45	LiF200	69.36	70.50	F	150	600	Fine	P.D.	Interference from V Kβ_1 (69.13)
Cu	Kα	W	60	45	LiF200	45.00	45.48	FS	400	300	Fine	P.D.	
Fe	Kα	Cr	50	45	LiF200	57.52	55.81	F	150	700	Fine	Fusion	
I	Lα_1	W	60	45	LiF200	102.88	103.80	FS	300	500	Fine	P.D.	
K	Kα	Cr	50	45	LiF200	136.63	131.78	F	200	600	Fine	Fusion	
Mg	Kα	Cr	50	45	TLAP	45.26	43.28	F	200	600	Coarse	Fusion	
Mn	Kα	Cr	50	45	LiF200	62.98	62.08	F	150	600	Fine	Fusion	Al filter used to eliminate Cr Kβ_1 tube line (62.36)
Mo	Kα	W	90	30	LiF200	20.28	20.70	S	200	600	Fine	P.D.	Avoid Zr Kβ_1 (20.07)
Na	Kα	Cr	50	45	TLAP	55.22	53.22	F	250	500	Coarse	Fusion	
Ni	Kα	W	60	45	LiF200	48.65	46.50	FS	150	600	Fine	P.D.	
P	Kα	Cr	50	45	GE	141.07	144.27	F	330	400	Coarse	Fusion	Discriminate against Ca Kα escape peak with P.H.S.
Pb	Lβ_1	W	90	30	LiF200	28.22	28.50	FS	200	600	Fine	P.D.	
Rb	Kα	W	90	30	LiF200	26.56	27.00	FS	200	600	Fine	P.D.	Avoid Br Kβ_2 (26.43)
S	Kα	W	60	45	GE	110.72	111.30	F	250	500	Coarse	P.D.	
Si	Kα	Cr	50	45	PE	109.04	115.49	F	250	600	Coarse	Fusion	
Sr	Kα	W	90	30	LiF200	25.10	25.85	FS	200	600	Fine	P.D.	
Ti	Kα	Cr	50	45	LiF200	86.14	90.80	F	250	600	Fine	Fusion	
Th	Lα_1	W	90	30	LiF200	27.43	27.95	FS	200	600	Fine	P.D.	Interference from Pb Lβ_1 on Th background
V	Kα	W	60	45	LiF200	76.94	78.00	F	300	500	Fine	P.D.	Interference from Ti Kβ_1 (77.26)
Y	Kα	W	90	30	LiF200	23.75	24.35	FS	200	600	Fine	P.D.	Interference from Rb Kβ_1 (23.75)
Zn	Kα	W	60	45	LiF200	41.77	42.35	FS	200	600	Fine	P.D.	
Zr	Kα	W	90	30	LiF200	22.50	22.95	FS	200	600	Fine	P.D.	Interference from Sr Kβ_1 (22.42)

F = flow, S = scintillation, LL = lower level, P.D. = pressed disc

TABLE B.3

XRF ANALYTICAL PRECISION AND ACCURACY FOR MAJOR AND MINOR ELEMENTS

Element	Mean (n=8)	1σ	Estimated total precision[1] (as % relative std. dev., 1σ)	Accuracy[2]
Si	26.24	0.12	0.5	0.097
Al	7.99	0.03	0.4	0.075
Fe	5.29	0.03	0.6	0.032
Mg	2.10	0.03	1.4	0.059
Ca	1.14	0.01	1.0	0.048
Na	1.34	0.02	1.5	0.053
K	2.39	0.01	0.4	0.019
Ti	0.45	0.004	1.0	0.009
Mn	2.15	0.02	0.7	0.004
P	0.10	0.002	2.0	0.013
As	16.3	5.89	36.2	4.5
Ba	2736.5	36.83	1.3	42.5
Br	153.6	1.49	1.0	7.4
Cl	9194.0	214.60	2.3	39.1
Cr	107.9	1.83	1.7	14.4
Cu	112.3	0.83	0.7	4.7
I	144.1	2.52	1.7	19.8
Mo	25.3	0.12	0.5	2.0
Ni	120.0	0.71	0.6	4.7
Pb	16.1	1.36	8.5	1.8
Rb	80.8	0.43	0.5	3.8
S	2804.3	58.90	2.1	157.7
Sr	400.8	3.77	0.9	10.7
Th	7.4	1.22	16.5	2.1
V	114.8	2.11	1.8	10.8
Y	30.8	0.43	1.4	3.8
Zn	193.6	0.99	0.5	6.1
Zr	126.5	1.12	0.9	7.2

[1]Total precision includes counting error, disc reproducibility, error in regression line and error in matrix mass absorbtion determinations.

[2]Accuracy determined from r.m.s.d. of international standards about the regression line.

Major element mean concentrations and accuracy in wt.%, minor elements in ppm.

TABLE 8.4

XRF TRACE ELEMENT COUNTING STATISTICS

Element	Conc. (ppm)	Standard[1]	Peak Count Rate (R_p)	Background Count Rate (R_b)	$1/(\sqrt{R_p} - \sqrt{R_b})$	Number of Counts	Count Time per Peak (s)	Precision[2] %	Detection[3] Limit (ppm)
As	11	BCSS-1	96.09	76.48	0.946	100000	62.7	6.90	0.20
Ba	330	BCSS-1	122.08	71.02	0.381	10000	50.5	3.10	5.05
Cl	31200	MAG-1	7575.77	191.40	0.014	-	4.0	0.40	49.30
Cr	105	MAG-1	129.90	26.96	0.161	4000	16.1	2.20	1.72
Cu	30	MAG-1	212.20	88.75	0.194	40000	16.0	2.79	0.58
I	100	BCSS-1	108.97	30.84	0.205	-	40.0	1.87	1.40
Mo	2	MAG-1	38.02	31.43	1.786	400000	40.0	16.25	0.08
Ni	54	MAG-1	52.19	17.74	0.332	200000	20.9	4.19	1.53
Pb	23	BCSS-1	43.01	37.91	2.495	200000	47.5	20.88	0.72
Rb	80	BCSS-1	44.36	22.29	0.516	400000	43.3	4.53	2.24
S	4600	MAG-1	645.30	255.33	0.106	-	10.0	1.94	67.81
Sr	156	MAG-1	583.08	227.89	0.110	40000	4.0	3.18	3.35
Th	13	MAG-1	44.21	40.02	3.096	200000	38.8	28.72	0.40
V	140	MAG-1	228.25	40.61	0.114	20000	14.1	1.76	1.29
Y	35	MESS-1	46.79	28.91	0.683	400000	34.6	6.70	0.68
Zn	120	BCSS-1	178.72	51.99	0.162	100000	9.8	2.98	2.23
Zr	130	MAG-1	71.67	31.77	0.353	400000	31.7	3.63	2.42

[1] Composition chosen to reflect an average sediment

[2] detection limit $= \frac{3}{m}\sqrt{\frac{R_b}{T_b}}$

[3] precision $\sigma = \frac{100}{\sqrt{T_p}} \times \frac{1}{\sqrt{R_p} - \sqrt{R_b}}$

where m = counts sec^{-1} $\%^{-1}$

R_b = background count rate

T_b = total time on background (secs)

R_p = peak count rate

T_p = total time on peak (secs)

TABLE B.5

APPLE MICROCOMPUTER PROGRAM

```
100  REM  USER DEFINABLE ELEMENT COUNT AVERAGES
110  CLEAR
120 D$ = CHR$ (4): REM  CNTRL-D
130  PRINT D$;"PR#3"
140  PRINT " "
150  PRINT D$;"PR#0"
155  DIM PM$(900)
160  HOME
170  VTAB 4
180  INVERSE
190  PRINT "DEEP THROAT - AVERAGE COUNT CALCULATIONS"
200  PRINT : PRINT : PRINT
210  NORMAL
220 K$ = ""
230  VTAB 6: HTAB 9
240  PRINT "PLEASE SELECT OPTION"
250  PRINT : PRINT
260  PRINT "1. AVERAGE COUNTS FOR W-TRACES": PRINT
270  PRINT "2. AVERAGE COUNT FILE TO TAPE PUNCH": PRINT
275  PRINT "3. VISUAL DISPLAY OF COUNT AVERAGE FILE": PRINT
280  PRINT "4. STOP": PRINT
290  PRINT : INPUT K$
300  IF  VAL (K$) < 1 OR  VAL (K$) > 4 THEN  PRINT "INVALID": GOTO 290
310  ON  VAL (K$) GOTO 500,3000,14000,8000
500  HOME : REM  AVERAGE COUNTS FOR W-TRACES
510  PRINT : PRINT : INPUT "DO YOU WANT APP. CONCS.?(Y OR N) :";X$
520  IF X$ = "N" THEN 550
530  PRINT : INPUT "SELECT STANDARD OF SIMILAR MU: ";S$
540  GOSUB 16000: PRINT
550  PRINT : INPUT "NO. OF ELEMENTS: ";NOELS: GOSUB 19000
560  PRINT : PRINT : PRINT "Z=ATOMIC NO., P=NO. OF PEAKS"
570  PRINT "B=NO. OF BACKGROUNDS"
580  PRINT "FT=FIXED TIME(1), FC=FIXED COUNTS(0)": PRINT : PRINT
590  DIM CODE(NOELS,4)
600  DIM AV(NOELS,3)
610  DIM NAV(3,NOELS)
613  DIM APP$(NOELS,3)
615  DIM STD(NOELS)
617  DIM CAL(NOELS)
620  FOR C = 1 TO NOELS
630  INVERSE
640  PRINT "ENTER ELEMENT CODE-Z,P,B,FT/FC ";
650  NORMAL
660  INPUT CODE(C,1),CODE(C,2),CODE(C,3),CODE(C,4)
670  NEXT C
1000  HOME : VTAB 4
1010  INVERSE : PRINT "AVERAGE COUNTS FOR W-TRACES - SEDIMENTS"
1020  NORMAL : VTAB 8
1030  GOSUB 6000: REM  OUTPUT SPECIFICATION
1040  PRINT : PRINT "SET PROGRAM NO. ON THUMBWHEELS"
1050  FLASH
1060  PRINT : PRINT "PRESS START BUTTON ON PROGRAMMER"
1070  NORMAL
1080 Y = 0
1090 TRIC = 0
1100  GOSUB 9000: REM  INPUT FROM SPECTROMETER
2000  REM  DATA LOGGING
2010  HOME : PRINT " THIS IS YOUR FRIENDLY PW 1450 SPEAKING...."
2020  INVERSE : PRINT "I'M WAITING FOR FURTHER INSTRUCTIONS": NORMAL
2030  PRINT : PRINT "EITHER, LOAD MORE SAMPLES AND PRESS"
2040  PRINT : PRINT "START BUTTON ON PROGRAMMER"
2050  PRINT : PRINT "OR, PRESS 'RESET' AND TYPE 'RUN'"
2060  IF  LEN (RX$) = 0 THEN 1100
2070  HOME : PRINT RX$: GOSUB 12000
2080  FOR X = 1 TO 3
2090  GOSUB 9000: PRINT RX$: GOSUB 12000
2100  NEXT X
2110  FOR C = 1 TO NOELS
2120 W$ = "":P = 0:B = 0
2130  FOR A = 1 TO 3
2140 PEAK(A) = 0:BACK(A) = 0:PF(A) = 0:BF(A) = 0
2150  NEXT A
2160 LX$ = "": IF CODE(C,4) = 0 THEN 4000
2170  GOSUB 9000
2180  IF  MID$ (RX$,3,3) = " 1 " THEN  GOTO 2370
2190 B = B + 1
2200 E = 1
2210 BACK(E) = BACK(E) +  VAL ( MID$ (RX$,6,7))
2220  IF B = 1 THEN BF(E) = BACK(E): GOTO 2240
2230  GOSUB 18000
2240 LX$ = LX$ + RX$
2250  IF  LEN (LX$) = 21 THEN LX$ =  LEFT$ (LX$,4) + "                    " +  RIGHT
$ (LX$,17)
2260  FOR E = 2 TO 3
2270  GOSUB 9000
2280  IF  LEN (RX$) >  = 16 GOTO 2310
2290 RX$ = " " + RX$
2300  GOTO 2280
2310 BACK(E) = BACK(E) +  VAL ( LEFT$ (RX$,7))
2320  IF B = 1 THEN BF(E) = BACK(E): GOTO 2340
```

```
2330  GOSUB 18000
2340 LX$ = LX$ + RX$
2350  NEXT E
2360  GOTO 2480
2370 LX$ = LX$ + RX$: P = P + 1
2380  FOR A = 1 TO 3
2390  GOSUB 9000
2400  IF  LEN (RX$) >  = 16 THEN  GOTO 2430
2410 RX$ = " " + RX$
2420  GOTO 2400
2430 PEAK(A) = PEAK(A) +  VAL ( LEFT$ (RX$,7))
2440  IF P = 1 THEN PF(A) = PEAK(A): GOTO 2460
2450  GOSUB 17000
2460 LX$ = LX$ + RX$
2470  NEXT A
2480  PRINT LX$
2490 RX$ = LX$: GOSUB 12000
2500  IF P + B < CODE(C,2) + CODE(C,3) THEN 2160
3000  REM  PEAK - BACKGROUND CALCULATIONS
3010  FOR A = 1 TO 3
3020 PEAK(A) =  INT (PEAK(A) / CODE(C,2))
3030 BACK(A) =  INT (BACK(A) / CODE(C,3))
3040 AV(C,A) = PEAK(A) - BACK(A)
3050  IF X$ = "N" THEN 3100
3060  IF TRIO > 0 THEN 3080
3070  IF X$ = "Y" AND W$ <  > "NO" THEN STD(C) = AV(C,1):W$ = "NO": GOSUB 15100
3080 APP$(C,A) =  STR$ ( INT (AV(C,A) / CAL(C)))
3090  IF APP$(C,A) =  STR$ (AV(C,A)) THEN APP$(C,A) = "  N/A"
3100  NEXT A
3110 W$ = ""
3120  PRINT "AVERAGE COUNTS": SPC( 1):AV(C,1): SPC( 1):AV(C,2): SPC( 1):AV(C,3)
3130  GOSUB 12100
3140  IF X$ = "Y" THEN  GOSUB 12200
3150  NEXT C
3160  GOSUB 7000:TRIO = TRIO + 1: GOTO 1100
4000  REM  COUNTING FOR FIXED TIME - NO MONITOR
4010  GOSUB 9000:LX$ = "":P = P + 1
4020 A = 1
4030 PEAK(A) =  VAL ( MID$ (RX$,6,7)) + PEAK(A)
4040  IF P = 1 THEN PF(A) = PEAK(A): GOTO 4060
4050  GOSUB 17000
4060 LX$ = LX$ + RX$
4070  FOR A = 2 TO 3
4080  GOSUB 9000
4090  IF  LEN (RX$) >  = 16 THEN 4120
4100 RX$ = " " + RX$
4110  GOTO 4090
4120 PEAK(A) = PEAK(A) +  VAL ( LEFT$ (RX$,7))
4130  IF P = 1 THEN PF(A) = PEAK(A): GOTO 4150
4140  GOSUB 17000
4150 LX$ = LX$ + RX$
4160  NEXT A
4170 LX$ =  LEFT$ (LX$,4) + "                    " +  RIGHT$ (LX$,49)
4180  PRINT LX$:RX$ = LX$: GOSUB 12000
4190  GOSUB 9000:LX$ = "":E = E + 1
4200 E = 1
4210 BACK(E) =  VAL ( MID$ (RX$,6,7)) + BACK(E)
4220  IF E = 1 THEN BF(E) = BACK(E): GOTO 4240
4230  GOSUB 18000
4240 LX$ = LX$ + RX$
4250  FOR E = 2 TO 3
4260  GOSUB 9000
4270  IF  LEN (RX$) >  = 16 THEN 4300
4280 RX$ = " " + RX$
4290  GOTO 4270
4300 BACK(E) = BACK(E) +  VAL ( LEFT$ (RX$,7))
4310  IF E = 1 THEN BF(E) = BACK(E): GOTO 4330
4320  GOSUB 18000
4330 LX$ = LX$ + RX$
4340  NEXT E
4350 LX$ =  LEFT$ (LX$,4) + "                    " +  RIGHT$ (LX$,49)
4360  PRINT LX$:RX$ = LX$: GOSUB 12000
4370  IF P + E < CODE(C,2) + CODE(C,3) THEN 4000
4380  GOTO 3000
5000  REM  AVERAGE COUNT FILE TO TAPE
5010  HOME : VTAB 4: HTAB 5
5020  INVERSE : PRINT "AVERAGE COUNT FILE TO TAPE"
5030  NORMAL
5040  PRINT : INPUT "NAME OF AVERAGE COUNT FILE?:";NM$
5050  PRINT : INPUT "WHICH DISC DRIVE?:(D1 OR D2):";DR$
5060  IF DR$ = "D1" OR DR$ = "D2" THEN 5080
5070  PRINT "INVALID": GOTO 5050
5080  PRINT D$;"APPEND";NM$;",";DR$
5090  PRINT D$;"WRITE";NM$
5100  PRINT "999"
5110  PRINT D$;"CLOSE";NM$
5120  PRINT D$;"OPEN";NM$;",";DR$
5130  PRINT D$;"READ";NM$
5140  FOR X = 1 TO 900
5150  INPUT TX$
5160 PM$(X) = TX$
5170  IF TX$ = "999" THEN 5190
5180  NEXT X
```

```
5190  PRINT D$."CLOSE".NM$
5200  PRINT D$."OPEN":NM$:".".DR$
5210  PRINT D$:"WRITE".NM$
5220  FOR X = 1 TO 900
5230  IF PM$(X) = "999" THEN 5260
5240  PRINT PM$(X)
5250  NEXT X
5260  PRINT D$:"CLOSE":NM$
5270  PRINT D$:"PR#3"
5280  FOR X = 1 TO 900
5290  IF PM$(X) = "999" THEN 5320
5300  PRINT PM$(X)
5310  NEXT X
5320  PRINT D$:"PR#0"
5330  HOME : GOTO 160
6000  REM  OUTPUT SPECIFICATION
6010 K$ = "":NM$ = "":DR$ = ""
6020  PRINT   INPUT "OUTPUT TO PRINTER OR TT?(PT OR TT):".K$
6030  IF K$ = "PT" THEN SL = 1: GOTO 6060
6040  IF K$ = "TT" THEN SL = 3: GOTO 6060
6050  PRINT "INVALID": GOTO 6020
6060  PRINT . INPUT "NAME FOR AVERAGE COUNT FILE?:";NM$
6070  PRINT : INPUT "TO WHICH DISC DRIVE?(D1 OR D2):";DR$
6080  IF DR$ = "D1" OR DR$ = "D2" THEN 6100
6090  PRINT "INVALID": GOTO 6070
6100  PRINT : INPUT "NEW FILE? (Y OR N):";K$
6110  IF K$ = "N" THEN 6130
6120  GOSUB 6500
6130  RETURN
6500  REM  CREATE NEW DISC FILE
6510  PRINT D$:"OPEN";NM$:",";DR$
6520  PRINT D$:"WRITE";NM$
6523  PRINT D$;"DELETE":NM$
6525  PRINT D$:"OPEN";NM$
6530  PRINT TX$
6550  PRINT D$:"CLOSE";NM$
6560 TX$ = ""
6570  RETURN
7000  REM  ASSEMBLE OUTPUT STRING
7020  FOR C = 1 TO NOELS
7030  FOR A = 1 TO 3
7040 NAV(A,C) = AV(C,A)
7050  NEXT A
7060  NEXT C
7080  FOR A = 1 TO 3
7090  FOR C = 1 TO NOELS
7095  IF C = 1 THEN TX$ = TX$ +  STR$ (NAV(A,C)): GOTO 7105
7100 TX$ = TX$ + " " +  STR$ (NAV(A,C))
7105  IF C = NOELS THEN TX$ = TX$ +  CHR$ (13)
7110  NEXT C
7120  GOSUB 13000
7130  NEXT A
7140  RETURN
8000  REM  STOP ROUTINE
8010  HOME
8020  IF PT = 1 THEN 8040
8030  END
8040  PRINT D$:"PR#1"
8050  PRINT  CHR$ (12): REM  PAGE THROW
8060  PRINT D$."PR#0"
8070  GOTO 8030
9000  REM  INPUT FROM SPECTROMETER
9010 RX$ = ""
9020  PRINT D$:"IN#2"
9030  PRINT D$:"PR#2"
9040  INPUT RX$
9050  POKE  - 16224.64
9060  PRINT D$:"IN#0"
9070  PRINT D$:"PR#0"
9080  RETURN
12000  REM  GENERAL OUTPUT ROUTINE
12010  REM  RX$ IS DATA. SL IS DATA
12020  PRINT D$;"PR#";SL
12030  PRINT RX$
12040  PRINT D$:"PR#0"
12050 RX$ = ""
12060  RETURN
12100  REM  AVERAGE COUNT OUTPUT AS AV
12110  PRINT D$:"PR#";SL
12112 A$ = "AV.COUNTS"
12114  PRINT  CHR$ (1)
12120  PRINT A$. TAB( 2):AV(C,1): TAB( 5):AV(C,2); TAB( 5):AV(C,3) CHR$ (2)
12125  IF X$ = "N" THEN  PRINT : PRINT
12130  PRINT D$."PR#0"
12140 AV = 0
12150  RETURN
12200  REM  APP  CONC. OUTPUT
12210  PRINT D$:"PR#":SL
12220 A$ = "APP CONC "
12240  PRINT  CHR$ (1)A$: TAB( 2):APP$(C,1). TAB( 5):APP$(C,2); TAB( 5):APP$(C,3)
```

```
12250  PRINT  CHR$ (2) : PRINT
12260  PRINT D$:"PR#0"
12270 APP = 0
12280  RETURN
13000  REM  OUTPUT TO DISC
13010  PRINT D$:"APPEND".NM$.",":DR$
13020  PRINT D$:"WRITE":NM$
13030  PRINT TX$
13040  PRINT D$:"CLOSE":NM$
13050 TX$ = ""
13060  RETURN
14000  REM  OUT TO VDU
14010  PRINT D$:"MON C,I,O"
14020  PRINT : INPUT "NAME OF AVERAGE COUNT FILE ?:":NM$
14030  PRINT : INPUT "WHICH DISC DRIVE?(D1 OR D2): ":DR$
14040  PRINT D$."OPEN":NM$;",":DR$
14050  PRINT D$:"READ":NM$
14060  DIM TX$(500)
14070  FOR I = 1 TO 500
14080  INPUT TX$(I)
14090  NEXT I
14100  PRINT D$:"CLOSE":NM$
14110  PRINT D$:"NOMON C,I,O"
14120  GOTO 8000
15000  REM  APP. CONC. CALIBRATIONS
15100  IF S = 1 AND ANAL(C) = 0 THEN 15190
15110  IF S = 2 AND ANAL(C + NOELS) = 0 THEN 15190
15120  IF S = 3 AND ANAL(C + NOELS * 2) = 0 THEN 15190
15130  IF S = 1 THEN 15160
15140  IF S = 2 THEN 15170
15150  IF S = 3 THEN 15180
15160 CAL(C) = STD(C) / ANAL(C): GOTO 15200
15170 CAL(C) = STD(C) / ANAL(C + NOELS): GOTO 15200
15180 CAL(C) = STD(C) / ANAL(C + NOELS * 2): GOTO 15200
15190 CAL(C) = 1
15200  RETURN
16000  IF S$ = "BCSS-1" THEN S = 1: GOTO 16040
16010  IF S$ = "MESS-1" THEN S = 2: GOTO 16040
16020  IF S$ = "MAG-1" THEN S = 3: GOTO 16040
16030  PRINT : PRINT "STANDARD NOT RECOGNISED - TRY AGAIN": GOTO 530
16040  RETURN
17000  REM  SPURIOUS COUNT CHECK ON PEAKS
17010  IF  ABS (PF(A) - PEAK(A) / P) <  SQR (PF(A)) * FACT(C) THEN 17060
17020  IF CODE(C,4) = 0 AND A = 1 THEN RIX$ = RIX$ +  LEFT$ (RX$,12) + "**" +  R
IGHT$ (RX$,7): GOTO 17040
17030 RIX$ = RIX$ +  LEFT$ (RX$,7) + "**" +  RIGHT$ (RX$,7)
17040 RX$ = RIX$
17050 RIX$ = ""
17060  RETURN
18000  REM  SPURIOUS COUNT CHECK ON BACKGROUNDS
18005 BG = 0.01
18010  IF  ABS (BF(E) - BACK(E) / B) < BF(E) * BG THEN 18050
18020  IF E = 1 THEN RIX$ = RIX$ +  LEFT$ (RX$,12) + "**" +  RIGHT$ (RX$,7): GOT
O 18030
18025 RIX$ = RIX$ +  LEFT$ (RX$,7) + "**" +  RIGHT$ (RX$,7)
18030 RX$ = RIX$
18040 RIX$ = ""
18050  RETURN
19000  REM  READ IN DATA FOR STANDARDS AND FLAGGING ROUTINE
19010  DATA  11200,2,350,50,96,80,9,23,11,119,19,55,229,123,93,330,7340,100,3600
,210
19020  DATA  8200,2,500,35,89,100,20,34,11,191,25,30,513,71,72,270,9050,40,7200,
200
19030  DATA  31200,2,130,41,156,152,13,25,6,126,30,54,810,105,142,490,4300,0,460
0,0
19040  DIM ANAL(NOELS * 3)
19050  FOR R = 1 TO NOELS * 3
19060  READ ANAL(R)
19070  NEXT R
19080  DATA  1.877,0.093,0.118,0.08,0.7,0.234,0.322,0.198,0.362,0.428,0.359,0.27
2,1,0.758,0.687,1 548,1.802,1.258,0.797,1.29
19090  DIM FACT(NOELS)
19100  FOR F = 1 TO NOELS
19110  READ FACT(F)
19120  NEXT F
19130  RETURN
```

TABLE B.6

TRACE 15 - A PROGRAM FOR THE CORRECTION OF XRF COUNT DATA

```
                ERCC.  Imp80 Compiler Release1 Version 30 Aug 84


  1023  3069
     1          %dynamic %string %fn %spec DATE
     2          %dynamic %string %fn %spec TIME
     3          %dynamiclongrealfnspec LOGTEN(%longreal X)
     4          %externallongrealfnspec EXPTEN(%longreal R)
     5          %dynamicstringfnspec ITOS(%integer I)
     6          %dynamicroutinespec reporton(%integer i)
     7          %dynamicintegerfnspec RETURNCODE
     8          %DYNAMICROUTINESPEC GPLIST(%STRING(64) S)
     9          %dynamicstringfnspec RTOSTR(%longreal Z, %integer M,N)
    10          !
    11          ! preliminary versi  on of trace-element correction program for sediments
    12          !
    13          ! see Graham Shimmield or Steve Rainey re XRF aspects of the program
    14          !
    15          ! see Andy Walker re programming
    16          !
    17          %dynamicroutinespec axis(%longreal x,y,%integer idir,%longreal %c
     C          ticint,%integer intono)
    19          %DYNAMICROUTINESPEC SCALE(%LONGREAL XO,YO,XS,YS,TH)
    20          %DYNAMICROUTINESPEC OPENPLOTTER(%INTEGER ICHAN)
    21          %DYNAMICROUTINESPEC GRAPHPAPER(%LONGREAL XLNGTH,%INTEGER IUNITS)
    22          %DYNAMICROUTINESPEC SETPLOT(%LONGREAL XMIN,YMIN,XMAX,YMAX,%INTEGER IUNITS)
    23          %DYNAMICROUTINESPEC CLOSEPLOTTER
    24          %DYNAMICROUTINESPEC PLOT(%INTEGER IPEN,%LONGREAL TX,TY,DASH,GAP)
    25          %DYNAMICROUTINESPEC ANNOTATE(%LONGREAL X,Y,SIZE,TH)
    26          %DYNAMICROUTINESPEC PLOTSYMBOL(%INTEGER I)
    27          %DYNAMICROUTINESPEC PLOTSTRING(%STRING(225) S)
    28          %DYNAMICROUTINESPEC PLOTNUMBER(%LONGREAL X,%INTEGER M,N)
    29          %DYNAMICROUTINESPEC POINTSYMBOL(%INTEGER ICODE,%LONGREAL SIZE)
    30          %externalintegerfnspec exist(%string (32) s)
    31          %externalroutinespec define(%string (64) s)
    32          %externalroutinespec list(%string (64) s)
    33          %dynamicintegerfnspec outstream
    34          %dynamicroutinespec destroy(%string(64) s)
    35          %externalroutinespec prompt(%string (64) s)
    36
    37          %externalstring (12) %array elnames(1:12)="SI","AL","FE","MG","CA","NA","K",
     C           "TI","MN", "P","LOI", "O"
    39          %externalstring (12) %array elemtrace(1:20)="CL","MO","ZR","Y","SR","RB",
     C           "TH","PB", "AS","ZN","CU","NI","MN","CR","V","BA","TI","I","S","BR"
    41
    42          !
    43          ! mass absorbtion coeffs for trace elements against major elements
    44          ! Si Al Fe Mg Ca Na K Ti Mn P LOI O
    45          !
    46          %externalrealarray mu1(1:240)= %c
     C          { Cl } 1400.93,1144.65,806.24,920.24,376.70,725.90,
     C           324.64,496.65,719.56,1690.84,254.55,297.158,
     C          { Mo } 7.060,5.769,39.331,4.638,20.576,3.658,
     C           18.128,26.036,35.700,8.521,1.015,1.169,
     C          { Zr } 9.395,7.676,51.626,6.171,27.008,4.868,
     C           23.795,34.175,46.860,11.339,1.365,1.577,
     C          { Y } 10.895,8.902,59.443,7.157,31.098,5.645,
     C           27.398,39.350,53.956,13.150,1.591,1.841,
     C          { Sr } 12.685,10.365,68.706,8.333,35.944,6.573,
     C           31.668,45.482,62.364,15.310,1.863,2.159,
     C          { Rb } 14.818,12.107,79.663,9.734,41.676,7.678,
     C           36.718,52.736,72.318,17.885,2.806,2.541,
     C          { Th } 16.154,13.199,86.484,10.611,45.244,8.370,
     C           39.862,57.251,78.500,19.497,2.597,3.016,
     C          { Pb } 17.455,14.262,93.102,11.466,48.707,9.044,
     C           42.912,61.632,84.508,21.067,2.597,3.016,
     C          { As } 21.38,17.47,112.939,14.045,59.085,11.079,
     C           52.055,74.763,102.513,25.806,3.209,3.729,
     C          { Zn } 50.294,41.093,254.969,33.037,133.389,26.060,
     C           107.520,168.785,231.434,60.702,7.836,9.131,
     C          { Cu } 61.359,50.131,308.093,40.303,161.181,31.792,
     C           142.005,203.952,279.653,74.053,9.648,11.243,
     C          { Ni } 75.252,61.485,374.185,49.431,195.757,38.992,
     C           172.468,247.703,339.644,90.824,11.939,13.921,
     C          { Mn } 145.887,119.199,90.555,95.830,367.631,75.593,
     C           323.894,465.185,80.819,176.077,23.860,27.838,
     C          { Cr } 185.276,151.382,114.090,121.704,461.561,96.003,
     C           406.650,584.041,101.823,223.618,30.638,35.751,
     C          { V } 237.727,194.239,145.173,156.181,585.181,123.181,
     C           515.564,89.427,129.564,286.924,39.767,46.411,
     C          { Ba } 254.795,208.184,155.236,167.370,625.110,132.025,
     C           550.742,95.625,138.545,307.524,42.759,49.904,
     C          { Ti } 308.463,252.034,186.736,202.623,749.863,159.833,
     C           660.653,115.030,166.658,372.298,52.229,60.958,
     C          { I } 450.249,367.882,269.145,295.759,125.752,233.301,
     C           946.968,165.793,240.206,543.426,77.589,90.566,
     C          { S } 2000.76,1634.75,1137.81,1314.26,531.62,1036.72,
     C           458.13,700.83,1015.47,2414.81,369.807,431.527,
     C          { Br } 20.490,16.741,108.452,13.459,56.738,10.617,
     C           49.988,71.793,98.441,24.730,3.070,3.567
```

```
87
88          !
89          ! mass absorbtion coeffs for trace elements against trace elements
90          ! Cl Mo Zr Y Sr Rb Th Pb As Zn Cu Ni Mn Cr V Ba Ti I S Br
91          !
92          %externalrealarray mu2(1:400)= %c
 C          { Cl } 202.514,1762.011,2766.261,2571.695,2386.288,2209.832,0.0,1609.776,
 C          1220.131,
 C           1106.654,999.566,0,639.213,564.987,1253.779,0,1160.710,2016.120,1909.325,
 C          { Mo } 11.986,19.532,16.971,107.046,100.395,93.997,104.736,128.931,70.862,
 C          56.002,
 C           51.504,47.229,0,32.277,29.075,44.376,0,38.173,10.160,81.944,
 C          { Zr } 15.951,25.717,22.345,20.773,19.276,123.380,63.841,0.0,93.014,73.508,
 C           67.605,61.993,0,42.376,38.140,58.401,0,50.262,13.521,107.560,
 C          { Y } 18.497,29.658,25.770,23.957,22.230,20.586,73.382,121.117,107.098,84.638,
 C           77.841,71.380,0,48.782,43.916,67.335,0,57.966,15.679,123.846,
 C          { Sr } 21.536,34.337,29.835,27.736,25.737,23.833,84.667,139.722,123.788,97.825,
 C           89.972,82.504,0,56.384,50.759,77.937,0,67.109,18.256,143.146,
 C          { Rb } 25.158,39.880,34.651,32.214,29.891,27.681,97.992,161.686,143.528,
 C          113.429,
 C           104.320,95.661,0,65.376,58.854,90.495,0,77.943,21.325,27.429,
 C          { Th } 84.695,43.335,37.653,35.004,32.481,30.079,106.275,68.888,155.817,
 C          123.140,
 C           113.251,103.857,0,70.973,63.893,98.320,0,84.695,28.247,25.559,
 C          { Pb } 29.634,46.690,40.568,37.715,34.996,32.408,114.305,73.945,167.741,
 C          132.564,
 C           121.918,111.798,0,76.405,68.782,105.919,0,91.253,25.120,27.546,
 C          { As } 36.300,56.763,49.320,45.851,42.546,39.400,138.332,89.023,28.256,160.808,
 C           147.894,135.618,0,92.683,83.436,128.726,0,110.940,30.770,33.514,
 C          { Zn } 85.387,129.343,112.384,104.479,96.947,89.778,304.205,194.656,64.591,
 C          48.992,
 C           44.404,306.171,0,209.241,188.367,292.896,0,252.793,72.379,76.611,
 C          { Cu } 104.168,156.629,136.092,126.520,117.399,108.717,372.766,233.472,
 C          78.276,59.371,
 C           53.811,48.604,0,252.837,227.614,354.566,0,306.122,88.299,92.842,
 C          { Ni } 127.760,190.651,165.653,154.002,142.899,132.332,451.657,281.401,
 C          95.351,72.323,
 C           65.550,59.207,0,307.076,276.442,431.433,0,372.616,108.297,113.094,
 C          { Mn } 247.683,360.622,313.338,291.299,270.298,250.311,841.702,515.559,
 C          180.806,137.139,
 C           124.297,112.269,0,71.795,319.155,322.646,0,704.819,207.751,214.451,
 C          { Cr } 314.557,453.938,394.418,366.667,340.241,315.082,1053.825,641.531,
 C          227.796,172.780,
 C           156.600,141.446,0,90.454,79.950,392.416,0,887.195,266.637,270.184,
 C          { V } 403.608,577.075,501.410,466.143,432.536,400.552,1332.203,809.812,
 C          289.859,219.854,
 C           199.266,179.983,0,115.098,101.732,255.422,0,641.160,342.121,343.796,
 C          { Ba } 432.585,616.915,536.026,498.324,462.398,428.205,1421.9427,858.568,
 C          309.950,235.093,
 C           213.078,192.459,0,123.076,108.784,271.811,0,684.308,366.684,367.626,
 C          { Ti } 523.701,741.568,644.335,599.015,555.829,514.728,1701.946,1022.582,
 C          372.844,282.798,
 C           256.315,231.512,0,148.050,130.858,322.646,0,308.727,443.919,442.224,
 C          { I } 764.422,1067.320,927.375,862.148,799.991,740.835,0.0,1445.183,537.385,
 C          407.600,
 C           369.430,333.681,0.0,213.386,188.607,452.951,0.0,429.849,647.968,637.382,
 C          { S } 287.447,707.626,2146.420,1998.689,3363.170,3114.478,0.0,0.0,2271.798,
 C          1723.131,
 C           1561.767,1410.639,0.0,902.090,797.338,1726.047,0.0,1585.538,239.208,2694.538,
 C          { Br } 34.787,54.483,47.339,44.010,40.837,37.817,132.903,85.623,195.397,
 C          154.420,
 C           142.019,130.231,0,89.002,80.123,123.564,0,106.484,29.487,32.163
149
150
151         ! presents a table of values in DATA, with WID columns and HT rows, each
152         !     location in the table showing LINES values.
153         ! column titles in T2, row titles in T3, header title in T1
154         ! values printed to D2 decimal places, with D1 spaces reserved for integral
155         !     part.
156         ! COL spaces reserved for row titles, printed to channel CHAN
157         ! PAGENO incremented for each page of table printed, CONT = 0
158         !     for continuation pages separated by 'newpages' and headers
159         ! CONT = 1 for no header or newpage between table segments
160         !
161         %routine printval(%real r,%integer bp,dp,zero)
162         %if r=0 %thenstart;%if zero=0 %thenstart
163         %if dp=0 %then spaces(bp+1) %else spaces(bp+dp+2);%return;%finish;%finish
164         print(r,bp,dp)
165         %end
166
```

```
167         %routine TABLE(%stringarrayname t1,t2,t3, %realarrayname data, %integer d1,
  C            d2,col,wid,ht,lines,chan,cont,cll,zero, %integername pageno)
169            %integer i,j,k,och
170            %string (30) temp
171            %integer totwidth
172            och=outstream { store original output channel }
173            selectoutput(chan)
174         ! define width of each column (special cases: D2=0 for integer,
  C         !      D1=0 for standard form
176            totwidth=d1+d2+3
177            %if d2=0 %then totwidth=totwidth-1
178            %if d1=0 %then totwidth=d2+8
179         ! print header if requested
180            %if cont=0 %thenstart
181               newpage; printstring(t1(1)); spaces(totwidth*wid-length(t1(1)))
182               pageno=pageno+1
183               printstring("page "); write(pageno,1); newlines(2)
184               %if t1(2)#"" %then printstring(t1(2)) %and newline
185               %if t1(3)#"" %then printstring(t1(3)) %and newline
186            %finishelse newline
187             newline
188         ! row of column titles:
189             spaces(cll)
190            %for i=1,1,col %cycle
191               %if t2(i)="" %thencontinue
192         ! truncate long titles
193               temp=t2(i); %if length(temp)>totwidth %then length(temp)=totwidth-1
194         ! pad column titles to <totwidth> with spaces
195               %cycle; %if length(temp)<totwidth %then temp=" ".temp %elseexit
196                  %if length(temp)<totwidth %then temp=temp." " %elseexit
197               %repeat
198               printstring(temp); %repeat; newlines(2)
199         ! main body of table: HT rows
200             %for i=1,1,ht %cycle
201               %if t3(i)="" %thencontinue
202               printstring(t3(i)); spaces(cll-length(t3(i)))
203         ! for each row, print K values
204               %for k=1,1,lines %cycle
205                  %if k#1 %then spaces(cll)
206                  %for j=1,1,col %cycle
207         printval(data(i,j,k),d1,d2,zero)
208                     space; %repeat
209                  newline; %repeat
210         ! no newline at base of table: allows 20 (WID) x 2 (LINES) table on
211         !     one line-printer page: just!!
212               %if i#ht %then newline
213            %repeat
214            selectoutput(och)
215         %end
216
217
218         ! read a line of text from current input stream, ignoring initial
219         !     newlines or spaces, and terminating at the next newline.
220         !
221         %routine RLINE(%stringname s)
222            %string (1) t
223            s=""
224            { delete initial spaces/newlines}
225         11:%if nextsymbol=10 %or nextsymbol=32 %then skipsymbol %and ->11
226            %cycle; readitem(t); %if t=tostring(nl) %thenstart
227                  %if s="STOP" %or s="QUIT" %thenstop
228                  %return; %finish
229               s=s.t
230            %repeat
231         %end
232
233
234         ! performs first order regression on NOSAMS coordinates contained
235         !      in XX and YY, with regression parameters being returned in array
236         !      RES
237         !
238         %routine LINEAR(%realarrayname xx,yy,res, %integer nosams)
239            %integer v
240            %real sumx,sumy,sumxy,sumx2,sumy2
241            sumx=0; sumy=0; sumxy=0; sumx2=0; sumy2=0
242            %cycle v=1,1,nosams
243               sumx=sumx+xx(v)
244               sumy=sumy+yy(v)
245               sumxy=sumxy+xx(v)*yy(v)
246               sumx2=sumx2+(xx(v))**2
247               sumy2=sumy2+(yy(v))**2
248            %repeat
249            { Meanx }res(1)=sumx/nosams
250            { Meany }res(2)=sumy/nosams
251            { Cscp }res(3)=sumxy-(sumx*sumy/nosams)
252            { Cssx }res(4)=sumx2-(sumx**2/nosams)
253            { Cssy }res(5)=sumy2-(sumy**2/nosams)
254            { Classical regression slp }res(6)=res(3)/res(4)
255            { Classical regression ipt }res(7)=(sumy/nosams)-(res(6)*sumx/nosams)
256            { Pearson's correlation coeff }res(8)=res(3)/((res(4)*res(5))**0.5)
257            { Classical std dev }res(9)=(1/(nosams-2))*(res(5)-res(3)**2/res(4))
258         %end
```

```
259
260
261         ! read an 'atom' of text, ignoring initial spaces or newlines and
262         !     terminating at the next space or newline, and converting all
263         !     lower-case characters to upper-case.
264         %routine UPPER(%stringname s)
265            %integer i
266            s=""
267            { delete leading spaces/newlines }
268         11:%if nextsymbol=10 %then skipsymbol %and ->11
269            %if nextsymbol=32 %then skipsymbol %and ->11
270            %cycle
271               readsymbol(i)
272               %if 96<i<123 %then i=i-32 { i.e. change case lower to upper }
273               %if i=10 %or i=32 %thenstart
274                  %if s="STOP" %or s="QUIT" %thenstop; %return; %finish
275               s=s.tostring(i)
276            %repeat
277         %end
278
279
280         ! define file FILE to channel CHAN, checking that file exists
281         !
282         %routine CHANNEL(%string (32) text, %stringname file, %integer CHAN)
283            %integer i
284            %for i=1,1,10 %cycle { allow 10 attempts to enter a filename }
285               prompt(text.": "); upper(file)
286               %if charno(file,1)#'.' %and exist(file)=0 %then %c
  C                  printstring("file ".file." not accessible
288"            ") %andcontinue
289            ! ok for channels 1-9
290               define(tostring(chan+48).",".file)
291               %return
292            %repeat
293         %end
294
295
296         ! reads a 'normfile' style trace element analysis and returns element
297         !     values in 'ELEMTRACE' order in TR, title in TITL, with FAIL = 1
298         !     if %event 9 (endoffile) detected, otherwise FAIL = 0
299         !
300         %routine READTR(%realarrayname tr, %stringname titl, %integername fail)
301            %real re
302            %integer j
303            %string (20) elem
304            %onevent 9 %start; fail=1; %return; %finish { end-of-file }
305            fail=0; tr(j)=0 %for j=1,1,20
306            rline(titl) { title must be on one line only }
307            tr(12)=0
308            %cycle
309         ! read next element name
310               upper(elem)
311         ! escape if analysis terminator read
312               %if elem="-1" %thenexit
313               %if elem="-2" %then fail=1 %andexit
314               read(re) { read value associated with name ELEM }
315               %for j=1,1,20 %cycle { now identify ELEM }
316                  %if elem=elemtrace(j) %then tr(j)=re %andexit
317               %repeat
318            %repeat
319         %end
320
321
322         ! read 'normfile' style major-element analysis, returning data in
323         !     'ELNAMES' order in MAJ, title in TITL and FAIL = 1 for
324         !     %event 9 (endoffile), otherwise FAIL = 0
325         !
326         %routine READMAJ(%realarrayname maj, %stringname titl, %integername fail)
327            %real re
328            %integer j
329            %string (20) elem
330            %onevent 9 %start; fail=1; %return; %finish { end-of-file }
331            fail=0; maj(j)=0 %for j=1,1,12
332            rline(titl) { title must be on one line }
333            maj(12)=0
334            %cycle
335               upper(elem) { read element label }
336         ! escape if name is analysis terminator
337               %if elem="-1" %then maj(12)=1-maj(12) %andexit
338               %if elem="-2" %then maj(12)=1-maj(12) %andexit
339               read(re) { read value associated with ELEM }
340               %for j=1,1,11 %cycle { now identify label }
341         ! element percent => element fractions
342                  %if elem=elnames(j) %then %c
  C                     maj(j)=re*0.01 %and maj(12)=maj(12)+maj(j) %andexit
344               %repeat
345            %repeat
346         %end
347
```

```
348
349         ! print all values of ra(i) for which ok(i)=1
350         !
351         %routine PRINTAV(%realarrayname ra, %integerarrayname ok, %integer bp,dp)
352            %integer i
353         ! only print values specified by user
354            %for i=1,1,20 %cycle; %if ok(i)=1 %then print(ra(i),bp,dp)
355            %repeat
356            newline
357         %end
358
359
360         ! read 20 values into array MUTR, FAIL = 1 for %event 9 (endoffile),
  C         !     FAIL = 0 otherwise
362         !
363         %routine READAV(%realarrayname mutr, %integerarrayname ok, %integername fail)
364            %integer i
365            %onevent 9 %start; newline; fail=1 { end-of-file }
366               %return; %finish
367            fail=0
368         ! read values for user-specified elements
369            %for i=1,1,20 %cycle; %if ok(i)#0 %then read(mutr(i)) %else mutr(i)=0
370            %repeat
371         %end
372
373
374         !#########################################################################
375         {TR15}
376
377         ! trace-element correction program for XRF data from APPLE program
378         !  DEEPTHROAT ( 'SEDIMENT' in XRF user guide ).
379         !
380         ! MAJORS ANALYSES must be entered as ELEMENT PERCENT WEIGHTS
381         !
382
383         %ROUTINE PLOTSYMB(%REAL X,Y,ERROR,SC,%INTEGER SYMB)
384         %REAL INC
385         PLOT(1,X,Y,0,0);POINTSYMBOL(SYMB,.1);INC=SC*ERROR
386         PLOT(1,X-.1,Y+INC,0,0);PLOT(2,X+.1,Y+INC,0,0)
387         PLOT(1,X,Y+INC,0,0)
388         PLOT(2,X,Y-INC,0,0);PLOT(1,X-.1,Y-INC,0,0);PLOT(2,X+.1,Y-INC,0,0)
389         %END
390
391         %dynamicroutine TR15(%string (64) s)
392            %ownstring (10) %array t3(1:6)="slope","intercept","pearson cc",
  C          "std dev","points","+/- ppm".
394            %integer rep,pageno2,error,noel,N,OP
395         %STRING(5) AA
396            %integer i,j,k,l,m,FAIL1,FAIL2,fail,cnt,stds,sets,max,pageno,line,wid,ht,
  C             cur,con,ct,col,NOX,NOY,CYC,nmm,plotno
398            %integerarray diln(0:20,1:2)
399            %string (32) name1,name2,name3,name4,name5
400            %string (10) elem,NMB
401            %string (100) name
402            %realarray ref2(1:35,1:20),ref(1:4,1:35,1:20),lreg(1:4,1:20,1:5),
  C             data(1:20,1:20,1:2),blankan(1:4,1:20,1:20),rco(0:10,1:4)
404            %realarray xdat(1:20,1:12,1:4)
405            %integerarray id(0:5,0:35),xref(1:105),ok(0:20),din(1:20)
406            %string (100) %array t4,t1(1:3)
407            %string (30) %array rti(1:35),tt,t2(1:20),dil(0:20,0:10),BLANTI(1:20),
  C             dilc(1:20)
409            %real re,temp,min,maxx,rval,rvam,may,xam,INX,INY,XSC,YSC,X1,X2,Y1,Y2
410         %REAL CUX,CUY
411            %realarray res,muconc,mutr,maj,mumaj,mutot(1:20),x,y(1:105)
412
413         plotno=0;CYC=1
414            {[[ output at top of program ]]}
415            printsymbol('*') %for j=1,1,50
416            printstring("
417"         * trace element correction program for sediments *
418"         ")
419            printsymbol('*') %for j=1,1,50
420            newlines(2); printstring("preliminary version, no on-line help
421"
422"         ")
423            pageno=0; max=0
424
```

```
425          {[[ SET UP CHANNELS ]]}
426
427          channel("         standards file",name4,8)
428          channel("   average counts file",name1,3)
429          channel("major element normfile",name2,9)
430       ! i.e. output 'normfile' of trace and major elements
431          PROMPT("     combined normfile: "); UPPER(name5); DEFINE("5,".NAME5."1000")
432       prompt("    regression graphs?: ");upper(aa);length(aa)=1
433       %IF AA="Y" %OR AA="1" %THEN GP=1 %ELSE GP=0
434       %if gp=1 %thenstart;prompt("        which plotter?: ");upper(aa)
435       %finish
436       define("12,.null")
437       ! consists of tables of intermediate values
438          PROMPT(" interactive output to: "); UPPER(NAME3); DEFINE("2,".name3."1000")
439       ! two work-files created by the program, destroyed by logging-off
440          define("6,t#temp2,1000")
441          define("7,t#temp1,1000")
442
443          {[[ READ CONTROL DATA ]]}
444
445          selectinput(8)
446
447          {[[ LIST OF ELEMENTS ANALYSED FOR ]]}
448
449          prompt("element: ")
450          ok(i)=0 %for i=1,1,20
451          %cycle; upper(elem) { read element name }
452             ok(0)=0
453             %if elem="-1" %thenexit { for end of element list }
454             %for j=1,1,20 %cycle
455                %if elem=elemtrace(j) %then ok(0)=1 %and ok(j)=1 %andexit
456             %repeat
457             %if ok(0)#1 %then printstring(elem." not valid name") %and newline
458          %repeat
459          {[[ set up array of elements to be analysed ]]}
460          %for i=1,1,20 %cycle; %if ok(i)=1 %then tt(i)=elemtrace(i) %else tt(i)=""
461             %repeat
462       printstring("* The following elements are to be corrected:");newline
463       %for j=1,1,j %cycle
464       %if tt(j)="" %thencontinue
465       printstring(" ".tt(j))
466       %repeat;newlines(2)
467
468          {[[ READ INTERFERENCE CORRECTION FACTORS ]]}
469
470          %for i=1,1,10 %cycle { allow up to 10 inteference corrections }
471       nextint:
472             prompt("interfered element: "); upper(elem)
473             %if elem="-1" %then rco(0,1)=i-1 %andexit { end of list }
474             %for j=1,1,21 %cycle; %if j=21 %then %c
  C                printstring(elem." is not a valid element
476"       ") %and ->nextint
477                %if elem=elemtrace(j) %then rco(i,1)=j %andexit
478             %repeat
479       nextint2:prompt("interfering element: "); upper(elem)
480             %for j=1,1,21 %cycle { must be one of specified elemenets }
481                %if j=21 %then printstring(elem." is not a valid element name
482"       ") %and ->nextint2
483                %if elem=elemtrace(j) %then rco(i,2)=j %andexit; %repeat
484             read(rco(i,3)); read(rco(i,4)) { read 'SLOPE' and 'INTERCEPT' }
485          %repeat
486       %if rco(0,1)>0 %thenstart
487       printstring("* The following interference corrections are to be applied:")
488       newline
489       %for j=1,1,int(rco(0,1)) %cycle
490       printstring("  on ".elemtrace(int(rco(j,1))).", by ".elemtrace(int(rco(j,2))))
491       newline;%repeat
492       newline
493       %finish
```

```
494
495          {[[ READ DILUTION SERIES INFO ]]}
496
497          %for i=1,1,20 %cycle
498       nextdil:prompt("dilution element: "); upper(dil(i,0)) { read diluted element }
499             %if dil(i,0)="-1" %then diln(0,1)=i-1 %andexit { end of list }
500             %for j=1,1,21 %cycle { must be one of specified list of elements }
501                %if j=21 %then printstring("element not recognised") %and ->nextdil
502                %if dil(i,0)=elemtrace(j) %then diln(i,2)=j %andexit
503             %repeat
504             prompt("empty: "); upper(dilc(i))
505                { analysis title with none of trace element }
506             prompt("blank: "); upper(blanti(i))
507                { un-spiked dilution series composition }
508             prompt("titles: ") { enter series of analysis titles of dilution series }
509       next: %for j=1,1,10 %cycle
510                upper(dil(i,j))
511                %if dil(i,j)="-1" %then diln(i,1)=j-1 %andexit { end of list }
512                %if j>1 %thenstart
513                   %for k=1,1,j-1 %cycle
514                      %if dil(i,j)=dil(i,k) %then %c
  C                       printstring("duplicate title rejected") %and ->next
516                   %repeat
517                %finish
518             %repeat
519          %repeat
520       %if diln(0,1)>0 %thenstart
521       printstring("* The following elements are to be calibrated by dilution series:")
522       newline
523       %for j=1,1,diln(0,1) %cycle
524       printstring("  element=".dil(j,0)." blank=".blanti(j))
525       newline
526       printstring("   series=")
527       %for i=1,1,diln(j,1) %cycle;printstring(" ".dil(j,i))
528       %repeat;newline
529       %repeat
530       newline
531       %finish
532
533          {[[ READ STANDARD CONCENTRATIONS ]]}
534
535       ! allows up to 35 different standards to be used for calibrations
536          %for stds=1,1,35 %cycle
537       nextone:readtr(mutr,rti(stds),fail) { read concentrations of standards }
538             %if fail=1 %then id(0,0)=stds-1 %andexit { end-of-file }
539             %if stds>1 %thenstart
540                %for j=1,1,stds-1 %cycle
541       ! reject duplicate entries in standards file
542                   %if rti(j)=rti(stds) %then %c
  C                    printstring(rti(stds)." entered twice, ignored
544"       ") %and ->nextone
545                %repeat; %finish
546             { store standards concentrations }
547             ref2(stds,j)=mutr(j) %for j=1,1,20
548          %repeat
549          selectoutput(0)
550          %if id(0,0)=0 %then %c
  C          printstring("standards file ".name4." is empty") %andstop
552          newline
553          write(id(0,0),3); printstring(" analyses read from standards file ".name4."
554"       ")
555
556
557          {[[ READY TO READ AVERAGE COUNTS FILE ]]}
558
559          selectinput(3)
560          id(0,j)=0 %for j=1,1,35 { record no. times each standard read }
561          { constants for tabulation, channel 2 }
562          wid=12; con=4; ct=0; cur=0
563          ti(1)="table 1 : correction for absorption by major elements"
564          ti(2)= %c
  C             " Line 1: average counts corrected for interferences, Line 2: major-el".%c
  C             "ement corrected average counts"
567          ti(3)=""
568
569          {[[ READ PAIRS OF AVERAGE-COUNTS/MAJORS ANALYSES ]]}
570
571          din(cnt)=0 %for cnt=1,1,20
572          %for cnt=1,1,1000 %cycle { up to 1000 analyses }
573             selectinput(9)
574             readmaj(maj,name,fail1) { read MAJORS analysis }
575             %for k=1,1,20 %cycle { major-element correction factor }
576                mumaj(k)=0
577                mumaj(k)=mumaj(k)+(mul(k*12-12+j)*maj(j)) %for j=1,1,12
578             %repeat
579             selectinput(3)
580             readav(mutr,ok,fail2) { read AVERAGE COUNTS analysis }
581
```

```
582               {[[ IN CASE OF DIFFERENT NUMBERS OF ANALYSES ]]}
583               %if fail1=1 %or fail2=1 %thenstart
584                  %unless fail1=1 %and fail2=1 %thenstart
585                     %if fail=1 %then printstring( %c
  C                        "mismatch- too few average counts analyses")
587                     %if fail=2 %then printstring("mismatch- too few majors analyses")
588                     %stop; %finishelse cnt=cnt-1 %andexit; %finish
589
590               {[[ CORRECTION FOR INTERFERENCE ]]}
591
592               %if rco(0,1)>0 %thenstart
593          nmm=0
594                  %for l=1,1,int(rco(0,1)) %cycle
595                     mutr(int(rco(1,1)))=mutr(int(rco(1,1)))-(rco(1,3)*mutr(int(rco(1,
  C                     2)))+rco(1,4))
597                  %repeat
598               %finish
599
600               { save values for tabulation }
601               cur=cur+1; data(1,cur,1)=mutr(1) %for l=1,1,20
602               t2(cur)=name
603
604               {[[ CORRECTION FOR MAJOR-ELEMENT ABSORPTION ]]}
605
606               mutr(j)=mutr(j)*mumaj(j) %for j=1,1,20
607
608               {[[ SAVE DILUTION SERIES CORRECTED COUNTS ]]}
609
610               %if diln(0,1)>0 %thenstart; %for i=1,1,diln(0,1) %cycle
611                     %if name=blanti(i) %thenstart
612                        din(i)=din(i)+1
613                        blankan(din(i),i,j)=mutr(j) %for j=1,1,20; %finish
614                  %repeat; %finish
615
616               { tabulate data }
617               data(l,cur,2)=mutr(l) %for l=1,1,20
618               %if cur=wid %then table(t1,t2,tt,data,8,0,cur,wid,20,2,2,ct,6,
  C                  1,pageno) %and cur=0
620
621               {[[ SEND CORR. COUNTS TO T#TEMP1 ]]}
622
623               selectoutput(7); printstring("
624"            ".name."
625"            "); printav(mutr,ok,6,0); printav(mumaj,ok,3,3)
626
627               {[[ SAVE CORR. COUNTS OF ALL STANDARDS ]]}
628
629                  %for j=1,1,id(0,0) %cycle; %if name=rti(j) %thenstart
630            %if id(0,j)=4 %thenstart
631            printstring("WARNING: standard ".name." has been read more than four times")
632            newline
633            printstring(" (current analysis will be processed, but not used for." %c
  C            " calibrations"); newline; %exit; %finish
635                        id(0,j)=id(0,j)+1
636                        %if max<id(0,j) %then max=id(0,j)
637                        id(id(0,j),j)=cnt; ref(id(0,j),j,k)=mutr(k) %for k=1,1,20
638                        %exit; %finish
639
640                     { go and get next pair of analyses }
641                  %repeat
642               %repeat
643               %if cur#0 %then table(t1,t2,tt,data,8,0,cur,wid,20,2,2,ct,6,1,pageno)
644
645
646               {[[ COMPENSATE DILUTION ANALYSES ]]}
647
648               %for k=1,1,diln(0,1) %cycle { for each dilution element }
649                  %for n=1,1,id(0,0) %cycle; %if dilc(k)=rti(n) %thenexit
650                  %repeat
651                  %for j=1,1,id(0,0) %cycle { for each standard }
652                     %for l=1,1,diln(k,1) %cycle { for each member of dilution series }
653                        %if dil(k,l)=rti(j) %then %c
  C                        %start { if standard is dilution series member }
655                        %for i=1,1,id(0,j) %cycle { for each reading of K'th standard }
656                           %if i<=din(k) %then m=i %else m=din(k)
657
658                           { correct for effect of un-spiked trace_element }
659                           ref(i,j,diln(k,2))=ref(i,j,diln(k,2))-(blankan(m,k,diln(k,
  C                           2))-ref(i,n,diln(k,2)))
661            ! ref(i,n,diln(k,2))
662            ! blankan(m,k,diln(k,2))
663                        %repeat
664                     %finish
665                  %repeat
666               %repeat
667            %repeat
668            selectoutput(0)
669            write(cnt,3); printstring( %c
  C               " trace element analyses read from average-counts file ".name1."
671"            ")
672               printstring("  * Correction for absorption by major elements completed
673"            ")
674               closestream(7)
675               closestream(9)
```

```
676
677           { constants for tabulation }
678           wid=18; pageno=0; ti(1)="table 2 : standards data used for first regression"
679           ti(2)="   line 1: number of times standard used"
680           ti(3)="   line 2: (range of limits)/(average of limits) x 100"
681
682           {{[ CHECK CONSISTENCY OF STANDARDS COUNTS ]}}
683
684           cur=0; %for i=1,1,id(0,0) %cycle
685              cur=cur+1; %for j=1,1,20 %cycle
686                 %if ref2(i,j)=0 %then %c
  C                    data(cur,j,1)=0 %and data(cur,j,2)=0 %andcontinue
688                 data(cur,j,1)=id(0,i); %if id(0,i)#0 %thenstart
689                    min=ref(1,i,j); maxx=min
690                    %for k=1,1,id(0,i) %cycle
691                       %if ref(k,i,j)<min %then min=ref(K,i,j)
692                       %if ref(k,i,j)>maxx %then maxx=ref(K,i,j)
693                    %repeat
694                    data(cur,j,2)=200*(maxx-min)/(maxx+min) { estimate of range }
695                 %finishelse data(cur,j,2)=0; %repeat
696              t2(cur)=rti(i)
697
698              { and tabulate results }
699              %if cur=wid %thenstart; table(ti,elemtrace,t2,data,3,0,20,20,cur,2,2,0,
  C                  10,0,pageno)
701                 cur=0
702              %finish; %repeat
703           %if cur#0 %then table(ti,elemtrace,t2,data,3,0,20,20,cur,2,2,0,10,0,pageno)
704
705           { constants for tabulation }
706           wid=11; pageno=0; cur=0; ct=0; col=10; rep=0
707           ti(1)= %c
  C              "table 3 : data for first regression on standards of counts against co". %c
  C              "ncentration"
710           ti(2)=""; ti(3)=""
711
712
713           {{[ FIRST REGRESSION OF COUNTS AGAINST CONC. ]}}
714
715           %for l=1,1,20 %cycle { for all elements }
716              lreg(i,1,1)=1 %and lreg(i,1,2)=0 %for i=1,1,max
717              %if tt(l)="" %thencontinue
718              k=0
719              %for j=1,1,id(0,0) %cycle { for all readings of standard }
720                 %for i=1,1,id(0,j) %cycle { average standards counts }
721                    %if i#1 %then ref(1,j,l)=ref(1,j,l)+ref(i,j,l); %repeat
722                 ref(1,j,l)=ref(1,j,l)/id(0,j)
723                 %if ref2(j,1)#0 %thenstart { if standard conc. not zero... }
724                    k=k+1; x(k)=ref2(j,1); y(k)=ref(1,j,
  C                     1) { COUNTS and CONCs into arrays }
726                    xref(k)=j
727                 %finish
728              %repeat
729              %cycle
730                 linear(x,y,res,k) { regress }
731                 res(9)=sqrt(res(9)) { std dev }
732                 m=0; %for j=1,1,k %cycle; temp=res(6)*x(j)+res(7)
733                    %if mod(temp-y(j))>RES(9)*4 %thencontinue { accept 4 x std dev }
734                    M=M+1; y(m)=y(j); x(m)=x(j)
735                 %repeat
736                 %if m<3 %then error=1 %andexit { number of accepted points }
737                 %if m=k %then error=0 %andexit
738                 k=m
739              %repeat
740              lreg(1,1,m)=res(m+5) %for m=1,1,3 { slope, intpt, corr. coeff., std dev }
741
742              { data for tabulation }
743              cur=cur+1
744              xdat(m,cur,1)=res(m+5) %for m=1,1,4
745              xdat(6,cur,1)=xdat(4,cur,1)/xdat(1,cur,1)
746              xdat(5,cur,1)=k
747              t2(cur)=elemtrace(1)
748              %if cur=wid %thenstart
749                 table(ti,t2,t3,xdat,0,3,cur,wid,5,1,2,ct,11,1,pageno)
750                 cur=0; rep=rep+1; %if rep/3=rep//3 %then ct=0 %else ct=1
751              %finish
752
753              { go for next element }
754           %repeat
755           %if cur#0 %then table(ti,t2,t3,xdat,0,3,cur,wid,5,1,2,ct,11,1,pageno)
756           selectoutput(0)
757           printstring("  * First regression on standards completed
758"        ")
759
760           { constants for tabulation }
761           selectinput(7); max=0
762           t4(1)="table 5 : first approximation to trace element concentration"
763           t4(2)=""; t4(3)=""
764           ti(1)="table 4 : total mass absorption coefficients of samples"
765           ti(2)=""; ti(3)=""
766           cur=0; pageno2=0; pageno=0; wid=12
767           id(0,k)=0 %for k=1,1,id(0,0) { count no times each standard read }
768           din(m)=0 %for m=1,1,20
769
```

```
770
771          {[[ CORRECTION OF COUNTS FOR ABSORPTION BY TRACE ELEMENTS ]]}
772
773          %for cnt=1,1,cnt %cycle
774        ! retrieve data from workfile T#TEMP1
775             rline(name); readav(mutr,ok,fail); readav(mumaj,ok,fail)
776             cur=cur+1
777
778             {[[ FIRST ESTIMATE OF CONCENTRATION ]]}
779
780             muconc(j)=(mutr(j)-LREG(1,J,2))/lreg(1,j,1) %for j=1,1,20
781             xdat(j,cur,1)=muconc(j) %for j=1,1,20
782
783             {[[ CALCULATE ABSORPTION COEFFS FOR TRACE ELEMENTS ]]}
784
785             %for j=1,1,20 %cycle { for 20 elements }
786
787                {[[ TRACE ELEMENT MASS ABSORPTION COEFFS ]]}
788
789                mutot(j)=0; mutot(j)=mutot(j)+(muconc(k)*mu2(j*20-20+k)*.000001) %c
  C                %for k=1,1,20
791
792                {[[ TOTAL MASS ABSORPTION COEFFICIENT ]]}
793                mutot(j)=mutot(j)+mumaj(j)
794                data(j,cur,1)=mutot(j) { save for tabulation }
795             %repeat
796
797             {[[ CORRECT FOR TOTAL MASS-ABSORPTION ]]}
798
799             %for j=1,1,20 %cycle; %if ok(j)=0 %thencontinue
800                mutr(j)=mutr(j)/mumaj(j)*mutot(j); %repeat
801
802             {[[ SAVE COUNTS FOR 'BLANK' COMPOSITIONS ]]}
803
804             %if diln(0,1)>0 %thenstart; %for i=1,1,diln(0,1) %cycle
805                   %if name=blanti(i) %thenstart
806                      din(i)=din(i)+1
807                      blankan(din(i),i,j)=mutr(j) %for j=1,1,20; %finish
808                %repeat; %finish
809
810             { tabulation }
811             t2(cur)<-name
812             %if cur=wid %thenstart
813                table(t1,t2,tt,data,4,3,cur,wid,20,1,2,0,6,1,pageno)
814                table(t4,t2,tt,xdat,7,0,cur,wid,20,1,2,0,6,1,pageno2)
815                cur=0
816             %finish
817
818                {[[ STORE COUNTS FOR ALL STANDARDS ]]}
819
820                %for j=1,1,id(0,0) %cycle; %if name=rti(j) %thenstart
821                      id(0,j)=id(0,j)+1
822                      %if max<id(0,j) %then max=id(0,j)
823                      id(id(0,j),j)=cnt; ref(id(0,j),j,k)=mutr(k) %for k=1,1,20
824                      %exit; %finish
825                %repeat
826                selectoutput(6)
827
828                {[[ SAVE ALL COUNTS IN T#TEMP2 ]]}
829
830                printav(mutr,ok,6,0)
831
832                { go for next analysis }
833          %repeat
834          %if cur#0 %thenstart
835             table(t1,t2,tt,data,4,3,cur,wid,20,1,2,0,6,1,pageno)
836             table(t4,t2,tt,xdat,7,0,cur,wid,20,1,2,0,6,1,pageno2)
837          %finish
838
839
840          {[[ CORRECT DILUTION SERIES ]]}
841
842          %for k=1,1,diln(0,1) %cycle { for each diltuion series... }
843             %for n=1,1,id(0,0) %cycle; %if dilc(k)=rti(n) %thenexit
844             %repeat
845             %for j=1,1,id(0,0) %cycle { for each standard... }
846                %for i=1,1,diln(k,1) %cycle { for each member of K'th diln series }
847                   %if dil(k,1)=rti(j) %then %c
  C                   %start { check on whether standard id in series }
849                      %for i=1,1,id(0,j) %cycle { for each reading of standard }
850                         %if i<=din(k) %then m=i %else m=din(k)
851                         { apply correction }
852                         ref(i,j,diln(k,2))=ref(i,j,diln(k,2))-(blankan(m,k,diln(k,
  C                         2))-ref(i,n,diln(k,2)))
854                      %repeat
855                   %finish
856                %repeat
857             %repeat
858          %repeat
859          selectoutput(0); printstring( %c
  C             "  * Correction for absorption by trace elements completed
861"       ")
862          selectinput(0)
863
```

```
        { constants for tabulation }
        closestream(7); closestream(6)
        wid=18; pageno=0; ti(1)= %c
          "table 6 : standards data used for second regression"
        ti(2)="   line 1: number of times standard used"
        ti(3)="   line 2: (range of limits)/(average of limits) x 100"

        {[[ CHECK CONSISTENCY OF STANDARDS DATA ]]}

        cur=0; %for i=1,1,id(0,0) %cycle
           cur=cur+1; %for j=1,1,20 %cycle
              %if ref2(i,j)=0 %then %c
                 data(cur,j,1)=0 %and data(cur,j,2)=0 %andcontinue
              data(cur,j,1)=id(0,i); %if id(0,i)#0 %thenstart
                 min=ref(1,i,j); maxx=min
                 %for k=1,1,id(0,i) %cycle
                    %if ref(k,i,j)<min %then min=ref(K,i,j)
                    %if ref(k,i,j)>maxx %then maxx=ref(K,i,j)
                 %repeat
                 data(cur,j,2)=200*(maxx-min)/(maxx+min)
                    { approximation of variation }
                 %finishelse data(cur,j,2)=0; %repeat
              t2(cur)=rti(i)

              { tabulate results }
              %if cur=wid %thenstart; table(t1,elemtrace,t2,data,3,0,20,20,cur,2,2,0,
                    10,0,pageno)
                 cur=0
              %finish; %repeat
        %if cur#0 %then table(t1,elemtrace,t2,data,3,0,20,20,cur,2,2,0,10,0,pageno)

        { constants for tabulation }
        wid=12; t1(1)="table 7 : final regression data for standards"
        t1(2)=""; t1(3)=""; pageno=0; ct=0; rep=0; cur=0; col=11


        {[[ SECOND REGRESSION OF CONCS AGAINST COUNTS ]]}

        %for l=1,1,20 %cycle
           lreg(i,1,1)=1 %and lreg(i,1,2)=0 %for i=1,1,max
           %if tt(l)="" %thencontinue
           k=0
           %for j=1,1,id(0,0) %cycle { for each standard }
              %for i=1,1,id(0,j) %cycle; %if i#1 %then %c
                    ref(i,j,1)=ref(i,j,1)+ref(i,j,1)
              %repeat; ref(i,j,1)=ref(i,j,1)/id(0,j) { average of all readings }
              %if ref2(j,1)#0 %thenstart { ignore elements with zero concn }
                 k=k+1 %and x(k)=ref2(j,1) %and %c
                    y(k)=ref(i,j,1) { conc & counts into array }
              %finish
           %repeat
           %cycle
              linear(x,y,res,k) { regress }
              res(9)=sqrt(res(9)) { std dev }
              m=0; %for j=1,1,k %cycle; temp=res(6)*x(j)+res(7)
                 %if mod(temp-y(j))>RES(9)*4 %thencontinue { reject 4 x std dev }
                 M=M+1; y(m)=y(j); x(m)=x(j)
              %repeat
              %if m<3 %then error=1 %andexit { m values left }
              %if m=k %then error=0 %andexit
              k=m
           %repeat

           { tabulation }
           lreg(1,l,m)=res(m+5) %for m=1,1,3
           cur=cur+1; xdat(m,cur,1)=res(m+5) %for m=1,1,4
           xdat(5,cur,1)=k
           xdat(6,cur,1)=xdat(4,cur,1)/xdat(1,cur,1)
           t2(cur)=elemtrace(1)
        %IF GP=1 %THENSTART
        xam=x(1);%for m=1,1,k %cycle;%if x(m)>xam %then xam=x(m);%repeat
        may=y(1);%for m=1,1,k %cycle;%if may<y(m) %then may=y(m);%repeat
        rval=1@-10;%cycle;rvam=rval*10;%if rvam>xam>=rval %thenexit;rval=rvam;%repeat
        rval=expten(int(logten(rval)))
        inx=rval;nox=intpt(xam/inx)+1
        rval=1@-10;%cycle;rvam=rval*10;%if rvam>may>=rval %thenexit;rval=rvam;%repeat
        rval=expten(int(logten(rval)))
        iny=rval;noy=intpt(may/iny)+1
        XSC=15/(NOX*INX);YSC=15/(NOY*INY)
        %IF CYC=1 %THENSTART
        plotno=plotno+1
        %if charno(aa,1)='.' %thenstart
        %if exist("t#GP")=1 %THEN destroy("T#GP")
        define("45,t#GP")
        %finishelsestart
        %if exist(aa.itos(plotno))=1 %then destroy(aa.itos(plotno))
        define("45,".aa.itos(plotno))
        %finish
        openplotter(45);graphpaper(100,0)
        nmm=nmm+1
        setplot(0,0,80,60,0);%FINISH
        %IF cyc=1 %then CUX=3 %ELSE CUX=23
```

```
      CUY=3
      scale(CUX,CUY,1,1,0)
      axis(0,0,1,15/NOX,nox)
      rval=0
      RVAM=0
      %for i=1,1,NOX+1 %cycle
      NMB=RTOSTR(RVAM,1,0)
      ANNOTATE(RVAL-(LENGTH(NMB)*.15/2),-.4,.1,0)
      PLOTSTRING(NMB)
      RVAM=RVAM+INX
      rval=rval+(15/nox);%repeat
      rval=0
      RVAM=0
      %for i=1,1,NOY+1 %cycle
      NMB=RTOSTR(RVAM,1,0)
      annotate(-(LENGTH(NMB)*.15),rval,.1,0)
      PLOTSTRING(NMB)
      RVAM=RVAM+INY
      rval=rval+(15/noy);%repeat
      axis(0,0,2.15/NOY,noy)
      %for m=1,1,k %cycle
      plotSYMB(XSC*x(m),YSC*y(m),RES(9),YSC,2)
      %repeat
      X1=0;X2=xam;Y1=RES(6)*X1+RES(7);Y1=Y1*YSC
      Y2=RES(6)*X2+RES(7);Y2=Y2*YSC;X2=X2*XSC
      PLOT(1,X1,Y1,0,0);PLOT(2,X2,Y2,0,0)
      ANNOTATE(5,-1,.15,0)
      PLOTSTRING("PPM conc.")
      annotate(-((length(nmb)*1.5*.1)+.2),5,.15,90);plotstring("counts")
      annotate(10,1,.15,0);plotstring(" errors= +- 1 std dev")
      annotate(10,2,.15,0);plotstring("std dev=".rtostr(res(9),0,3))
      annotate(10,2.5,.15,0);plotstring("  intpt=".rtostr(res(7),0,3))
      annotate(10,3,.15,0);plotstring("  slope=".rtostr(res(6),0,3))
      %for nox=1,1,5 %cycle
      annotate(10+nox*.01,4,.3,0);plotstring(elemtrace(1))
      %repeat
      annotate(-1,-2.8,.1,0)
      plotstring("TR15 final calibration on ".elemtrace(1). %c
C     " for traces file ".name1.", plotted ".time." ".date.".")
      printstring("* ".elemtrace(1)." calibration curve plotted")
      newline
      %IF (CYC=2 %OR L=20) %THENstart
      CYC=0;reporton(12);CLOSEPLOTTER
      %if charno(aa,1)='.' %then GPLIST("T#GP,".AA)
      %if returncode#0 %thenstart;reporton(0);printstring("WARNING: GPLIST fails")
      newline;%finishelse reporton(0)
      %finish
      CYC=CYC+1
      %FINISH
            %if cur=wid %thenstart
               table(t1,t2,t3,xdat,0,3,cur,wid,6,1,2,ct,11,1,pageno)
               cur=0; rep=rep+1; %if rep/3=rep//3 %then ct=0 %else ct=1
            %finish

            { next standard }
         %repeat
         %if cur#0 %then table(t1,t2,t3,xdat,0,3,cur,wid,6,1,2,ct,11,1,pageno)
         selectoutput(0)
         printstring("
       * Second regression on standards completed
")

         { constants for tabulation }
         t1(1)="table 8 : final correction for trace elements"
         t1(2)=" line 1: final correction of counts, Line 2: final concentrations"
         t1(3)=""; pageno=0; cur=0; wid=11


      {[[ CALCULATE FINAL CONCENTRATIONS ]]}

      %for cnt=1,1,cnt %cycle
         selectinput(6); readav(mutr,ok,fail) { from T#TEMP2 }
         selectinput(9); readmaj(maj,name,fail) { re-read MAJORS }

         { save for tabulation }
         cur=cur+1
         t2(cur)<-name

         {[[ FINAL CONCENTARTION ]]}

         muconc(j)=(mutr(j)-LREG(1,J,2))/lreg(1,j,1) %for j=1,1,20

         { tabulation }
         data(j,cur,2)=muconc(j) %and data(j,cur,1)=mutr(j) %for j=1,1,20
         %if cur=wid %then table(t1,t2,elemtrace,data,9,0,cur,wid,20,2,2,0,6,
C           1,pageno) %and cur=0
```

```
1043              {{[ GENERATE 'NORMFILE' COMBINED MAJORS/TRACE ELEMENTS ANALYSES ]}
1044
1045              selectoutput(5); %if cnt>1 %then printstring("-1
1046"
1047"        ")
1048              printstring(name."
1049"        ")
1050              %for j=1,1,12 %cycle
1051                 spaces(3-length(elnames(j)))
1052                 printstring(elnames(j)." ")
1053                 print(100*maj(j),2,3); space
1054                 %if j/6=j//6 %then newline; %repeat
1055              %for j=1,1,20 %cycle
1056                 spaces(3-length(tt(j)))
1057                 printstring(tt(j)." ")
1058                 print(muconc(j),5,0); spaces(2)
1059                 %if j/6=j//6 %then newline; %repeat
1060              %unless j/6=j//6 %then newline
1061              { next analysis }
1062           %repeat
1063           printstring("-2
1064"        ")
1065           %if cur#0 %then table(t1,t2,tt,data,9,0,cur,wid,20,2,2,0,6,1,pageno)
1066
1067           {{[ END OF PROGRAM ]}}
1068
1069           selectoutput(0)
1070           printstring("  calculation of trace element concentrations completed
1071"        ")
1072           printstring("  tabulated output file ".name3." completed
1073"        combined major and trace element normfile ".name5." completed
1074"        ")
1075           newlines(2)
1076           printstring("*************************************************
1077"        * end of XRF trace element correction program, *
1078"        ")
1079           printstring("* comments to Steve Rainey, Graham Shimmield   *
1080"        *  or Andy Walker                                *
1081"        *************************************************
1082"        ")
1083           %end
1084           %endoffile

1084 LINES ANALYSED IN  3928 MSECS  -  SIZE= 54461
```

FIGURE B.1

Calibration graphs for XRF minor element analyses. Standards used are indicated in Table B.1. Error bars are 1σ deviations on the best fit line.

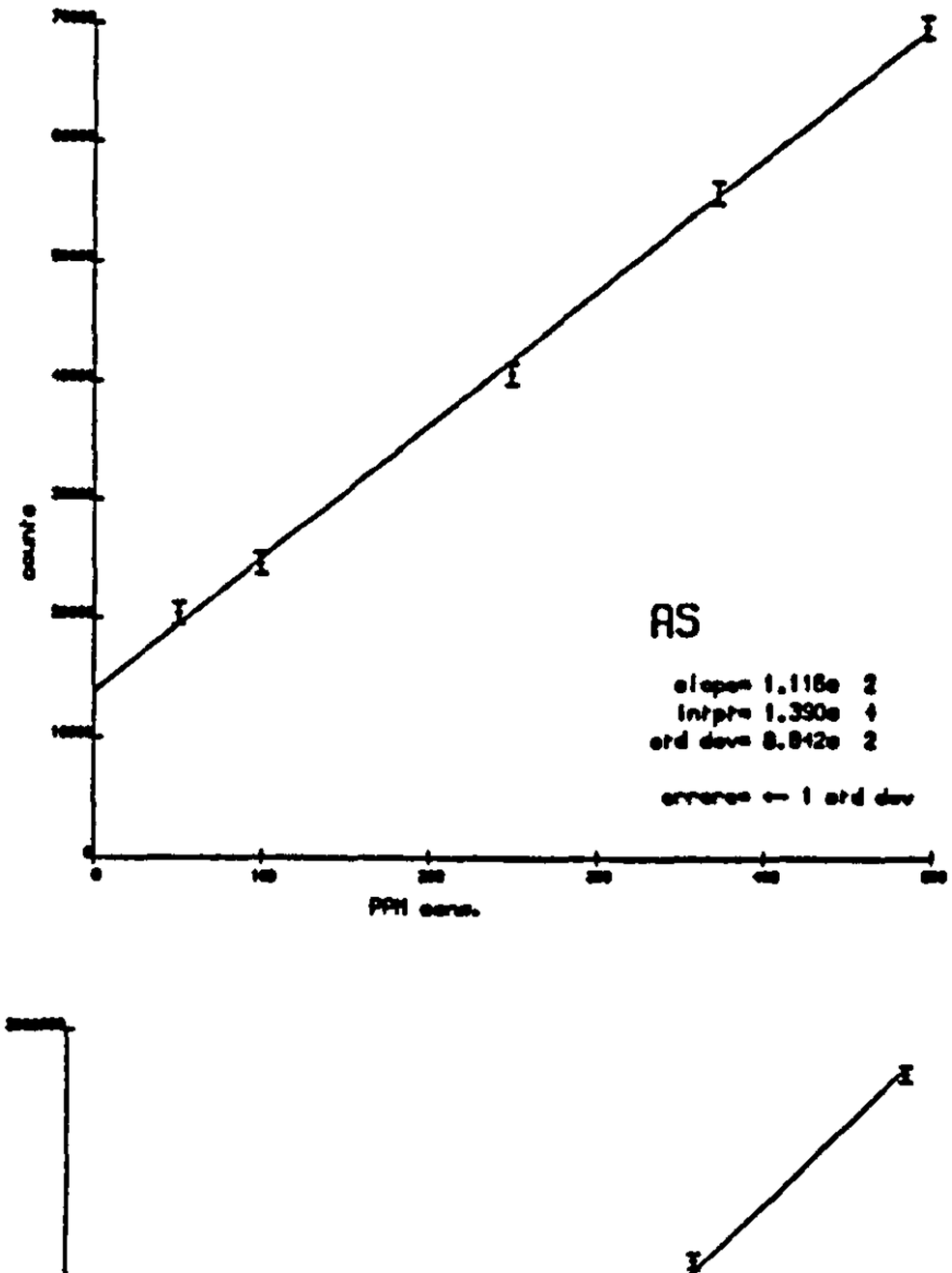
AS
counts
PPM conc.

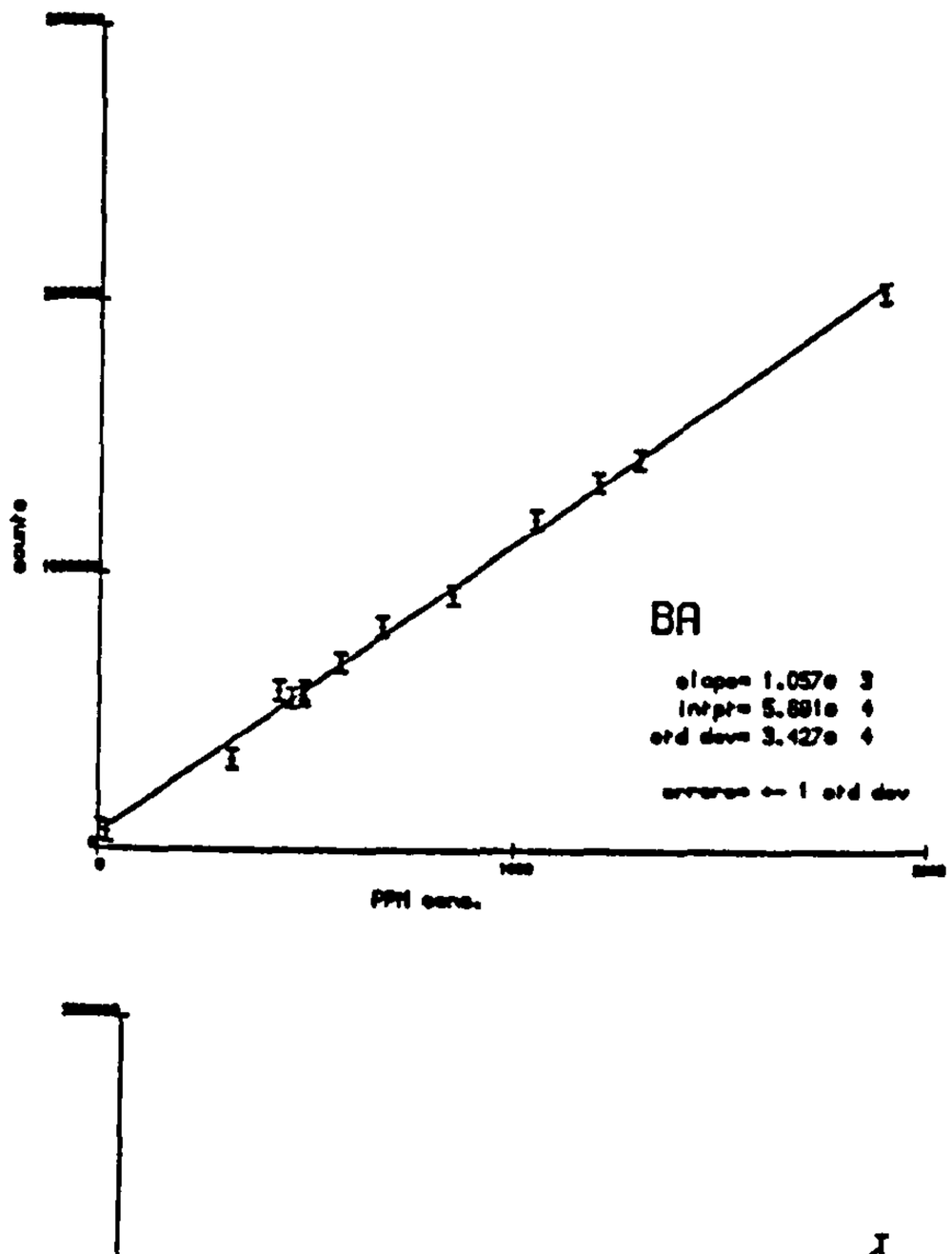
BA
counts
PPM conc.

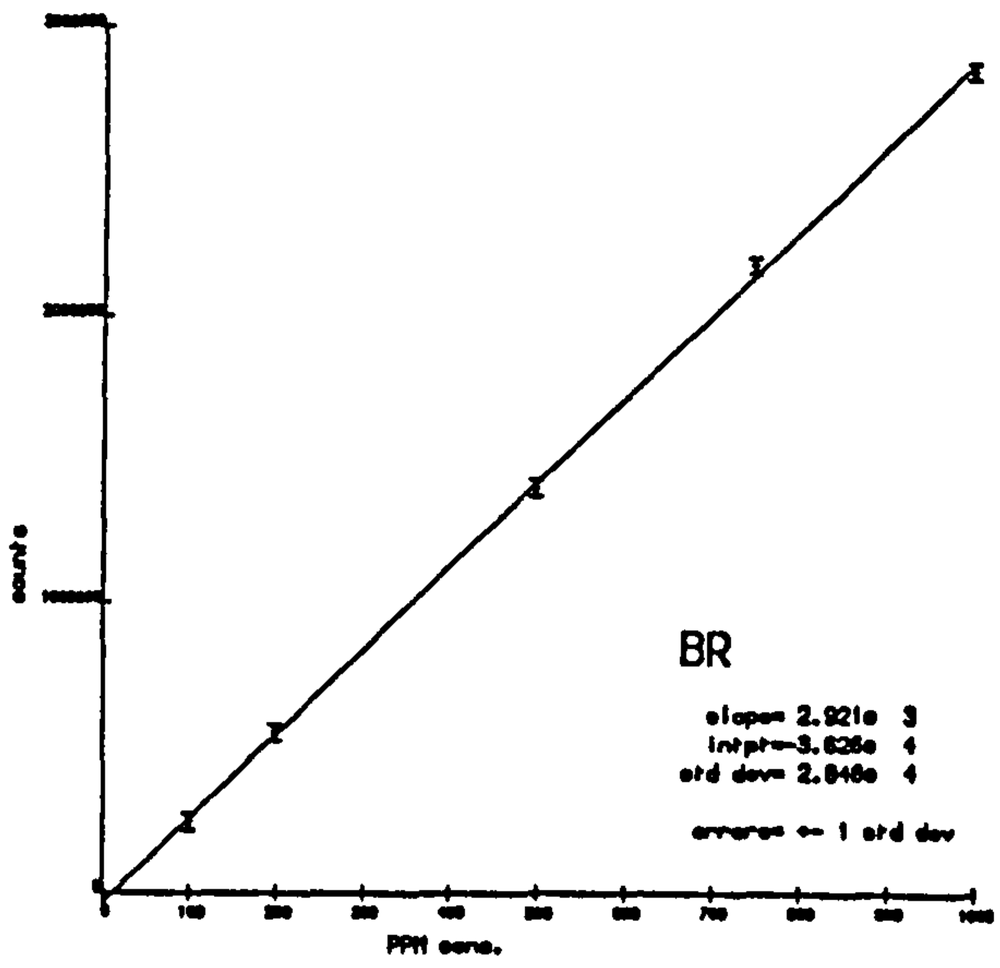
BR
counts
PPM conc.

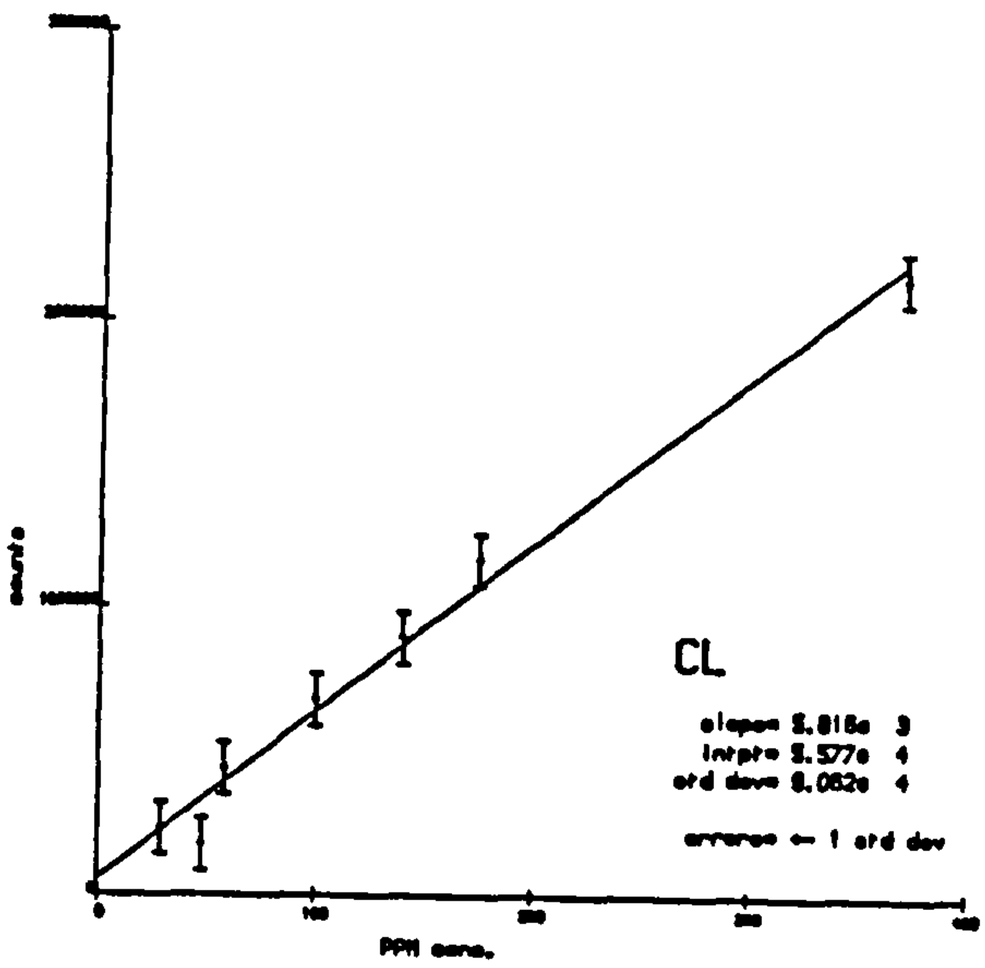
CL
counts
PPM conc.

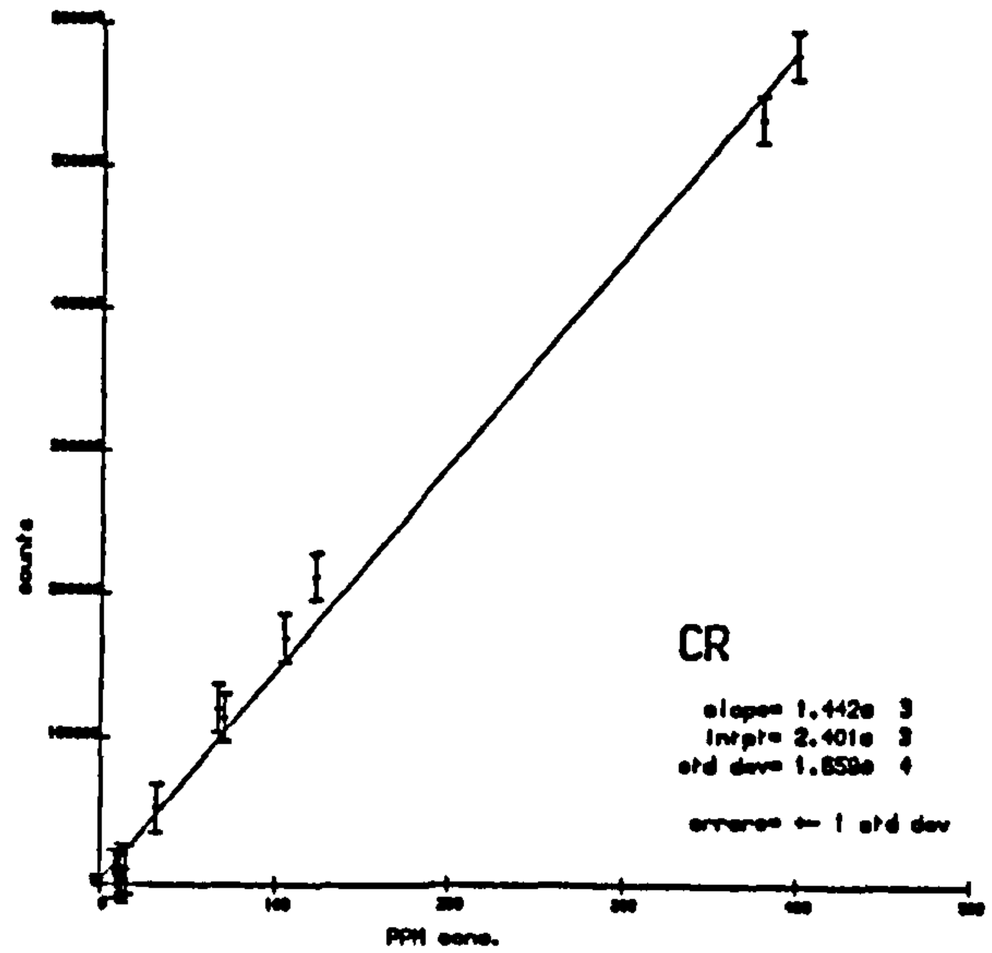
CR
counts
PPM conc.

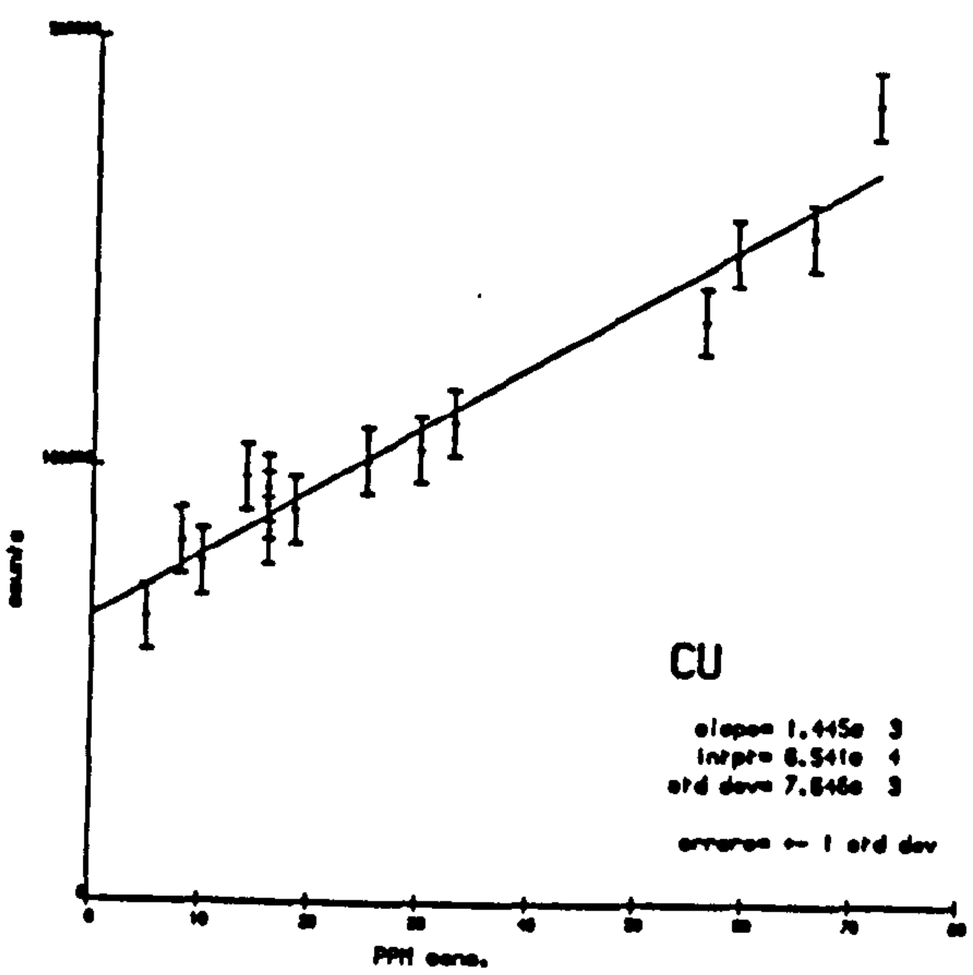
CU
counts
PPM conc.

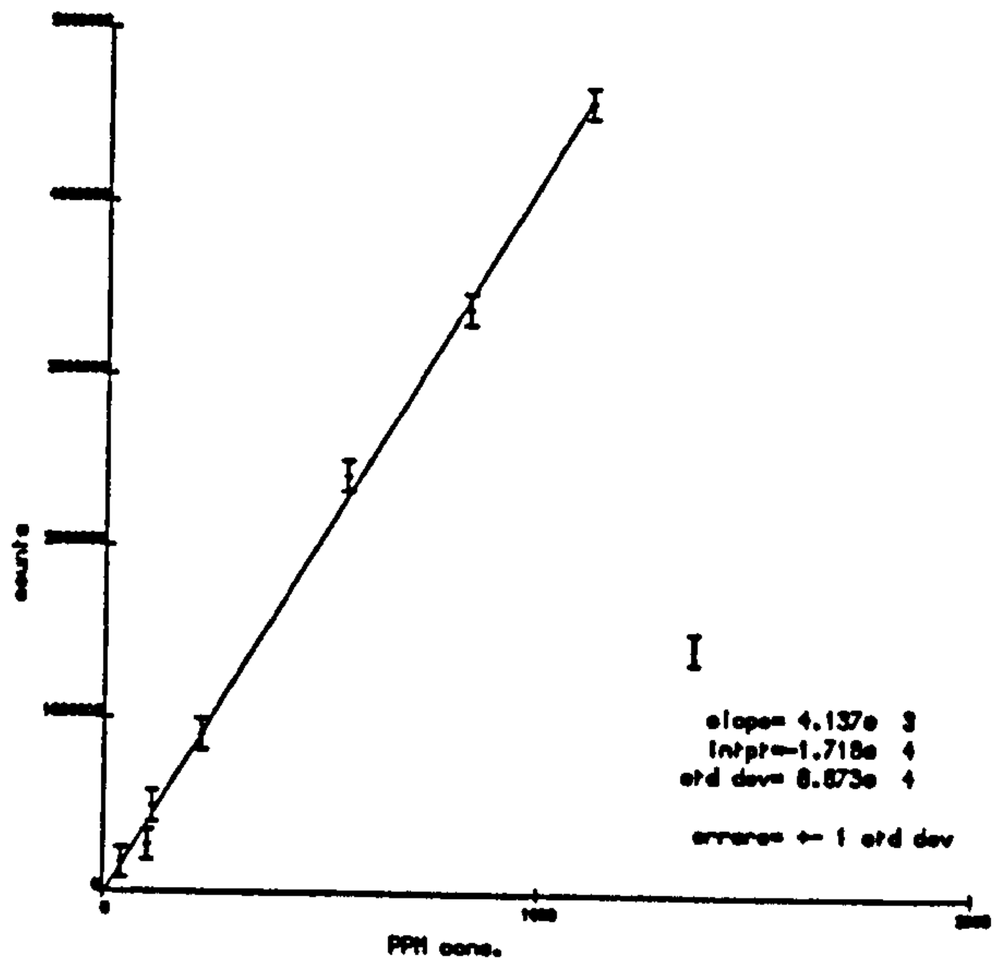
counts
PPM conc.
I
slope= 4.137e 3
intpt=-1.718e 4
std dev= 8.873e 4
errors <- 1 std dev

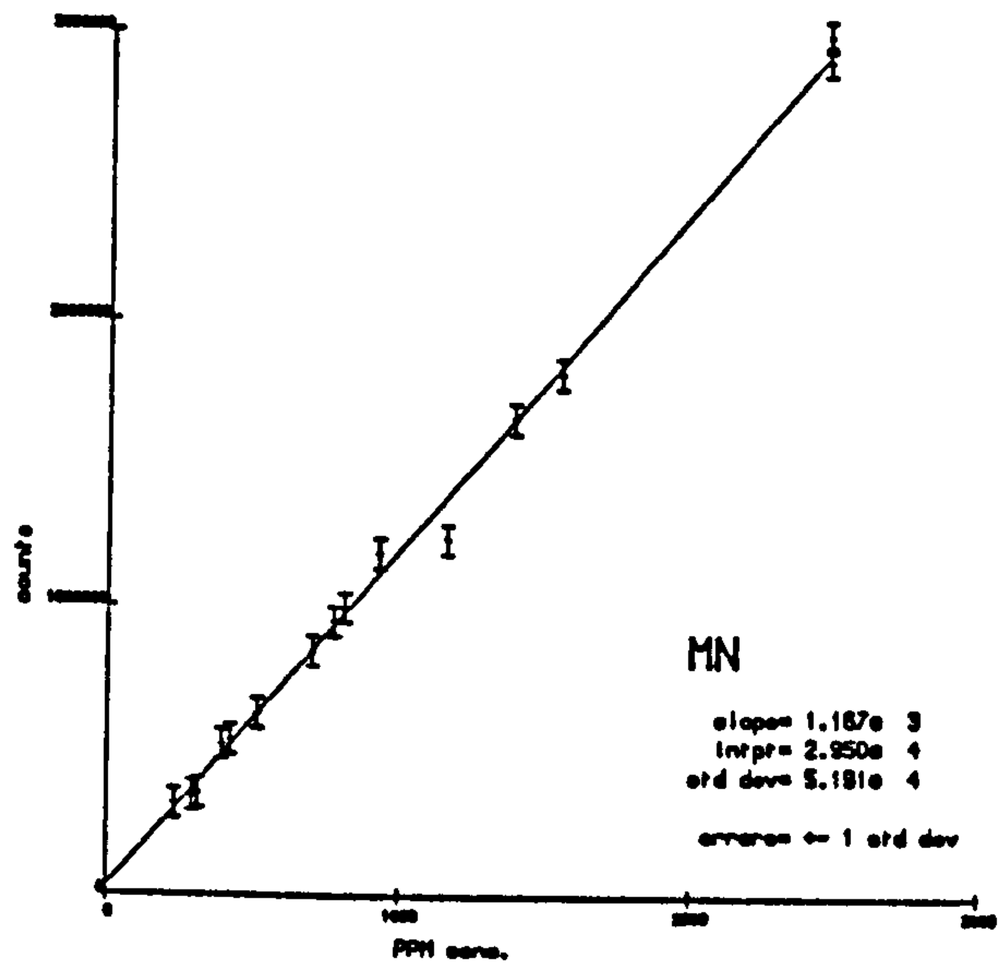
counts
PPM conc.
MN
slope= 1.167e 3
intpt= 2.950e 4
std dev= 5.181e 4
errors <- 1 std dev

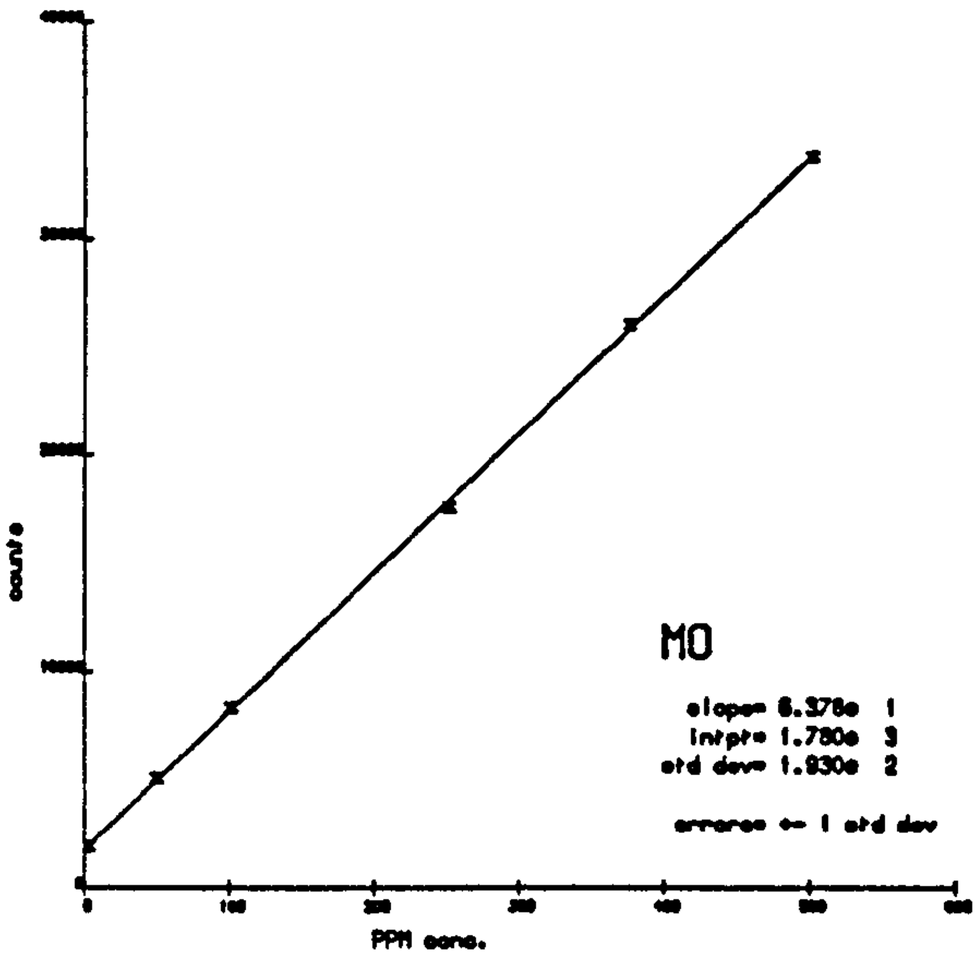
counts
PPM conc.
MO
slope= 8.378e 1
intpt= 1.780e 3
std dev= 1.830e 2
errors <- 1 std dev

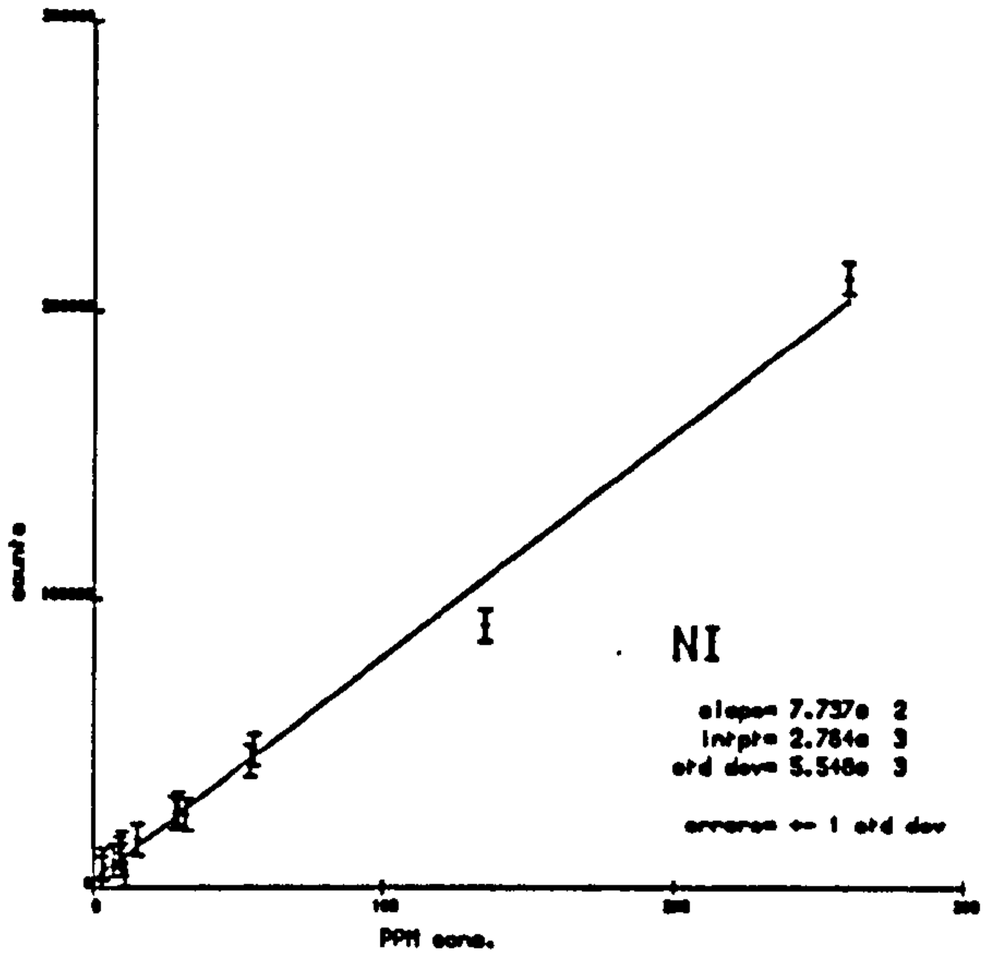
counts
PPM conc.
NI
slope= 7.737e 2
intpt= 2.784e 3
std dev= 5.548e 3
errors <- 1 std dev

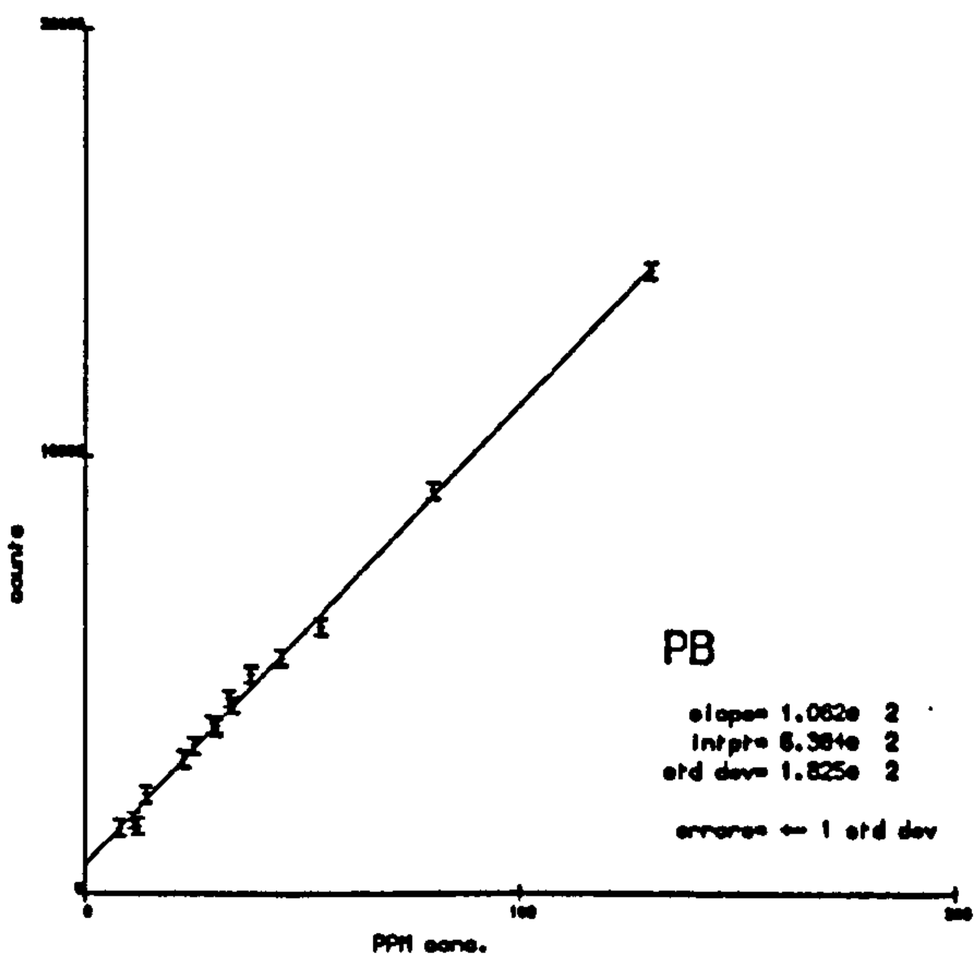
counts
PPM conc.
PB
slope= 1.062e 2
intpt= 6.384e 2
std dev= 1.825e 2
errors <- 1 std dev

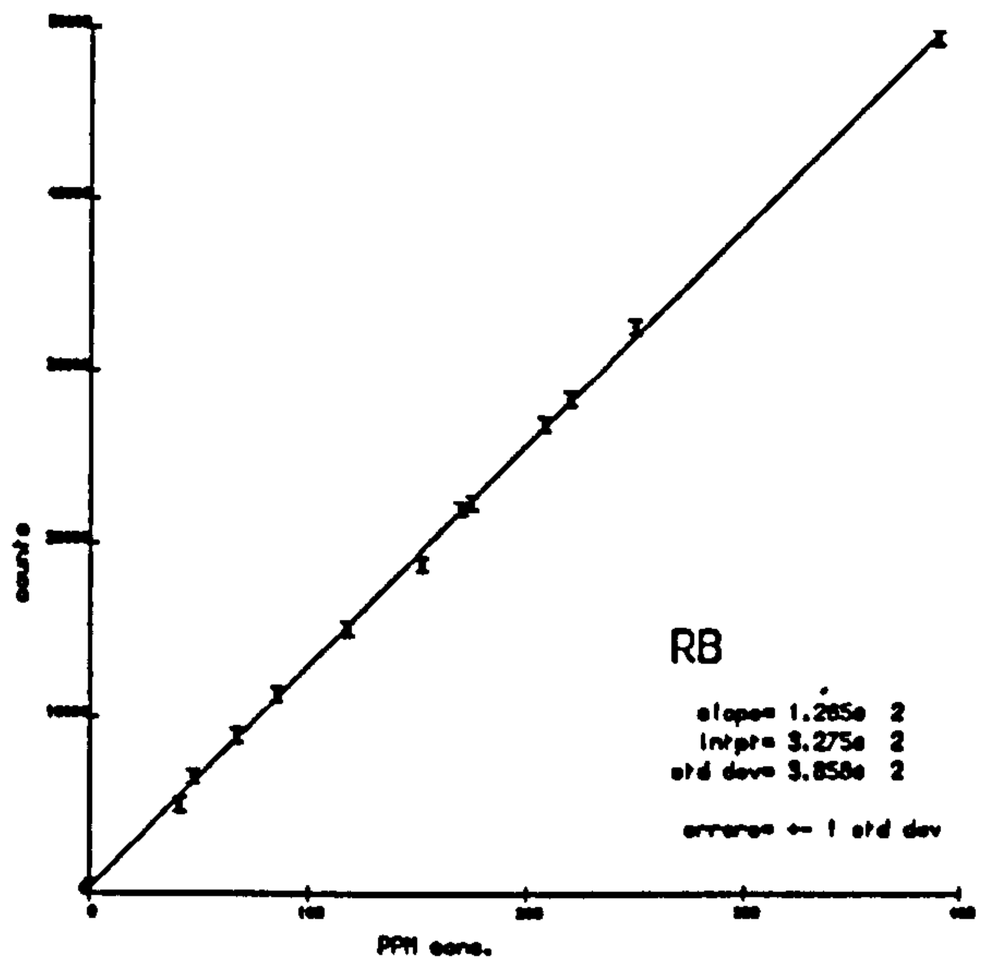
counts
PPM conc.
RB
slope= 1.285e 2
intpt= 3.275e 2
std dev= 9.858e 2
errors <- 1 std dev

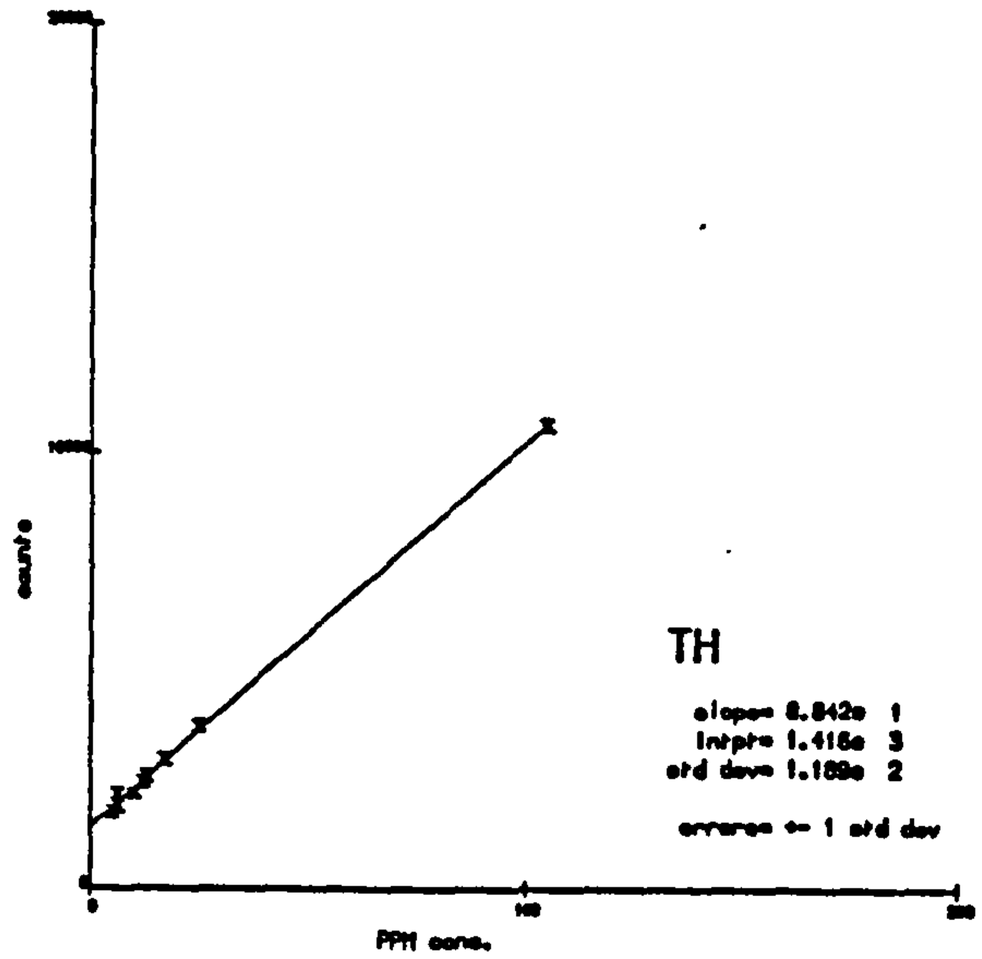
counts
PPM conc.
TH
slope= 8.842e 1
intpt= 1.416e 3
std dev= 1.189e 2
errors <- 1 std dev

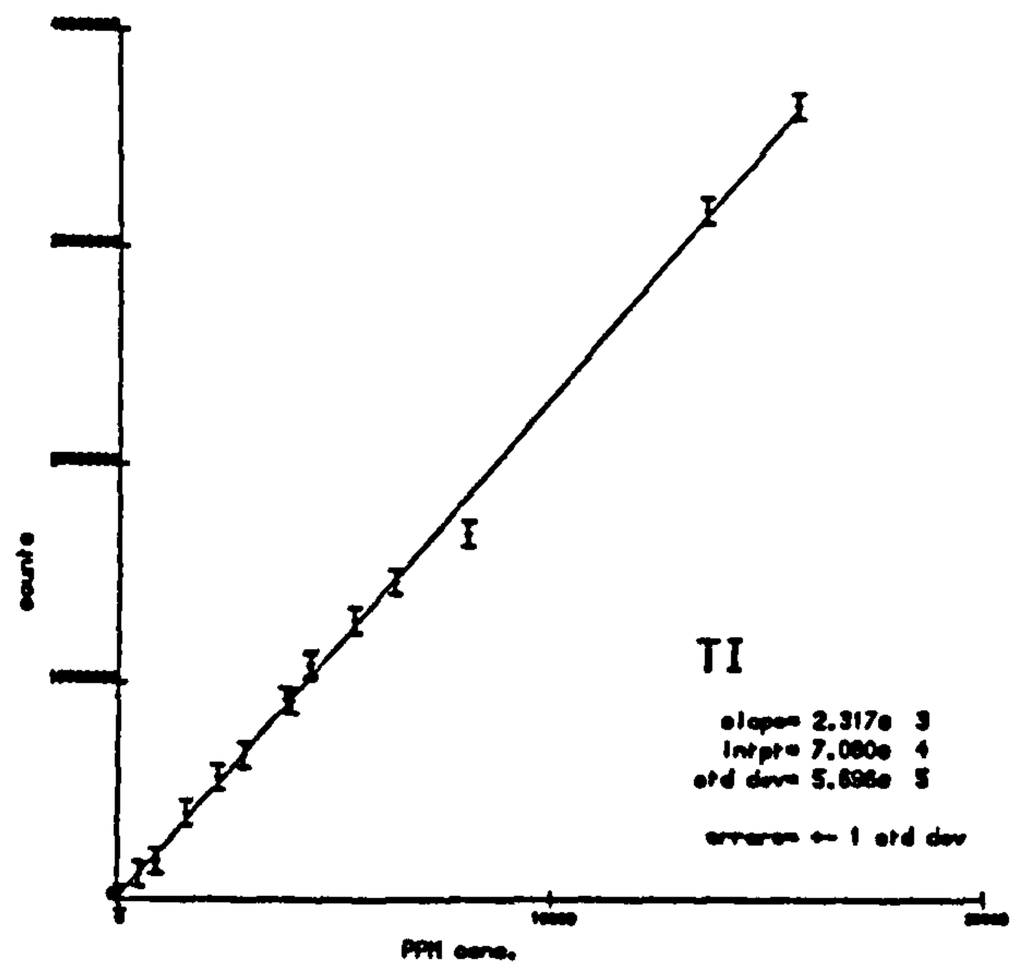
counts
PPM conc.
TI
slope= 2.317e 3
intpt= 7.080e 4
std dev= 5.696e 3
errors <- 1 std dev

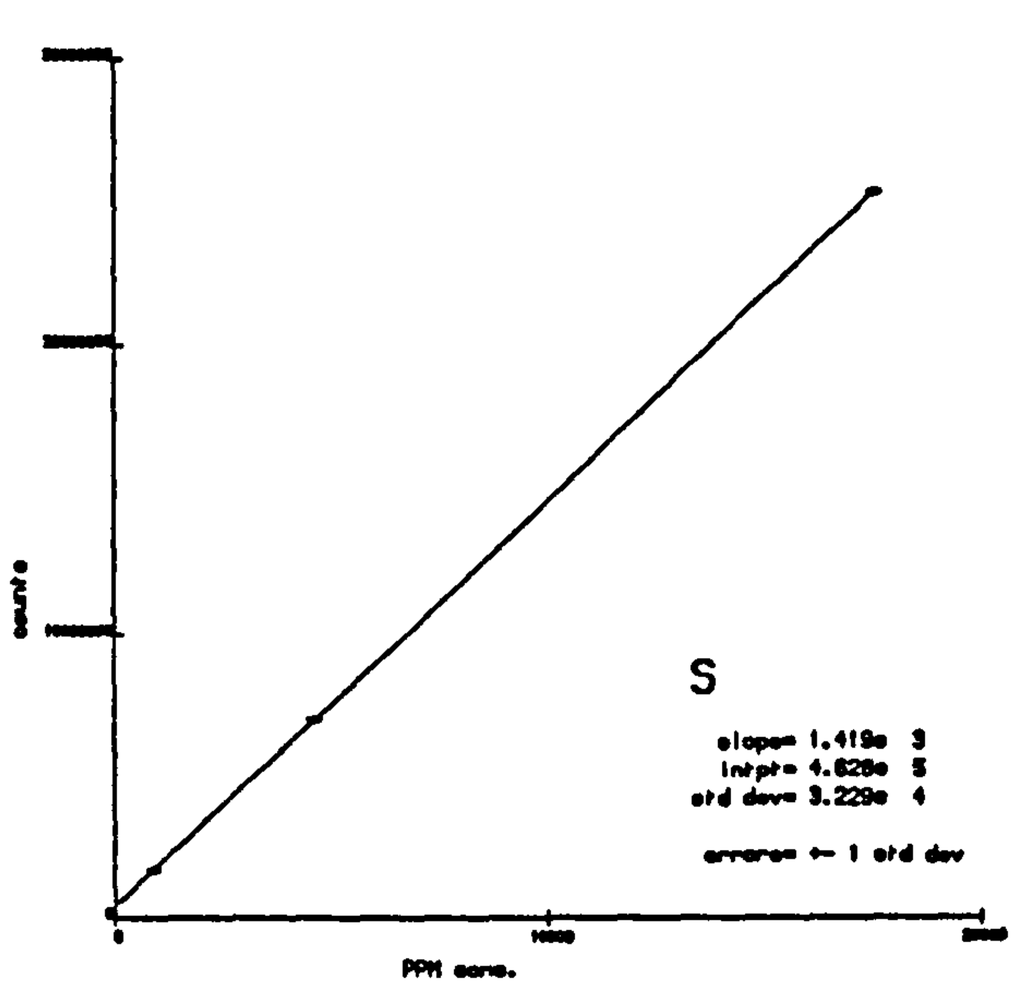
counts
PPM conc.
S
slope= 1.419e 3
intpt= 4.628e 3
std dev= 3.229e 4
errors <- 1 std dev

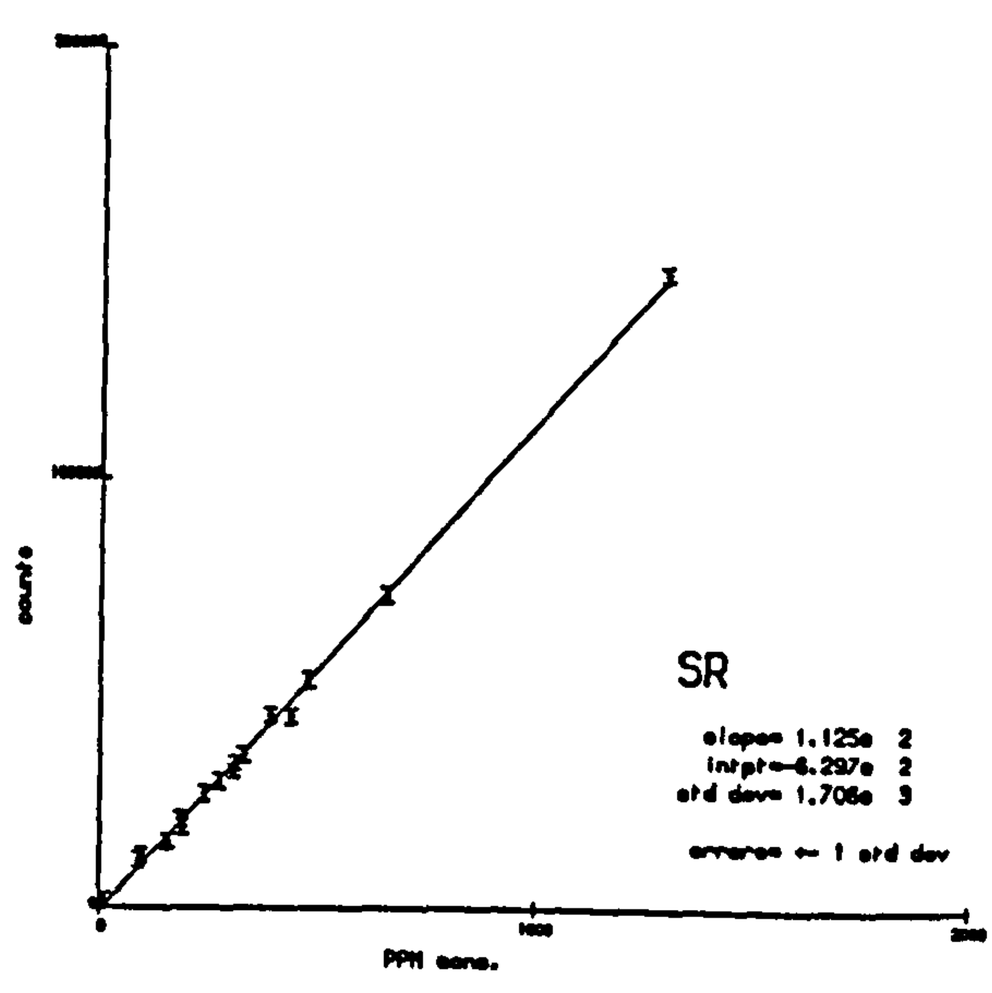
counts
PPM conc.
SR
slope= 1.125e 2
intpt=-6.297e 2
std dev= 1.708e 3
errors <- 1 std dev

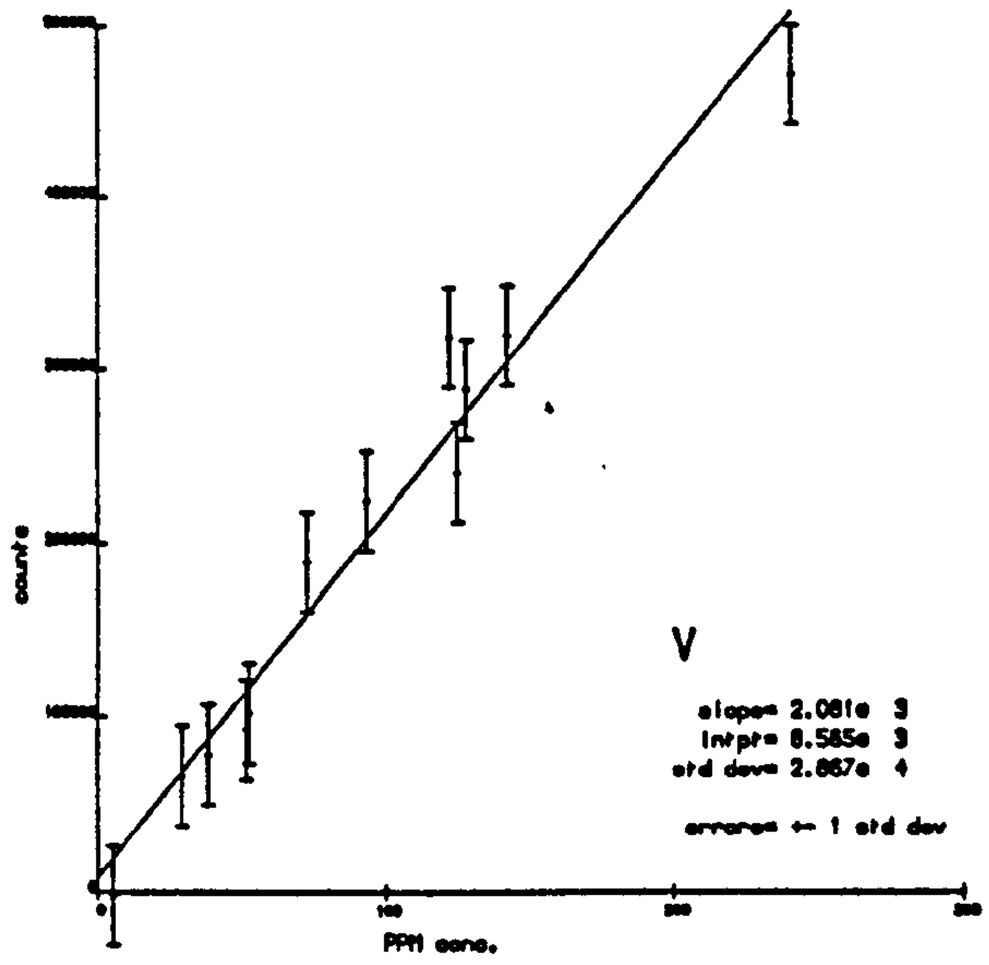
counts
PPM conc.
V
slope= 2.081e 3
intpt= 8.585e 3
std dev= 2.867e 4
errors <- 1 std dev

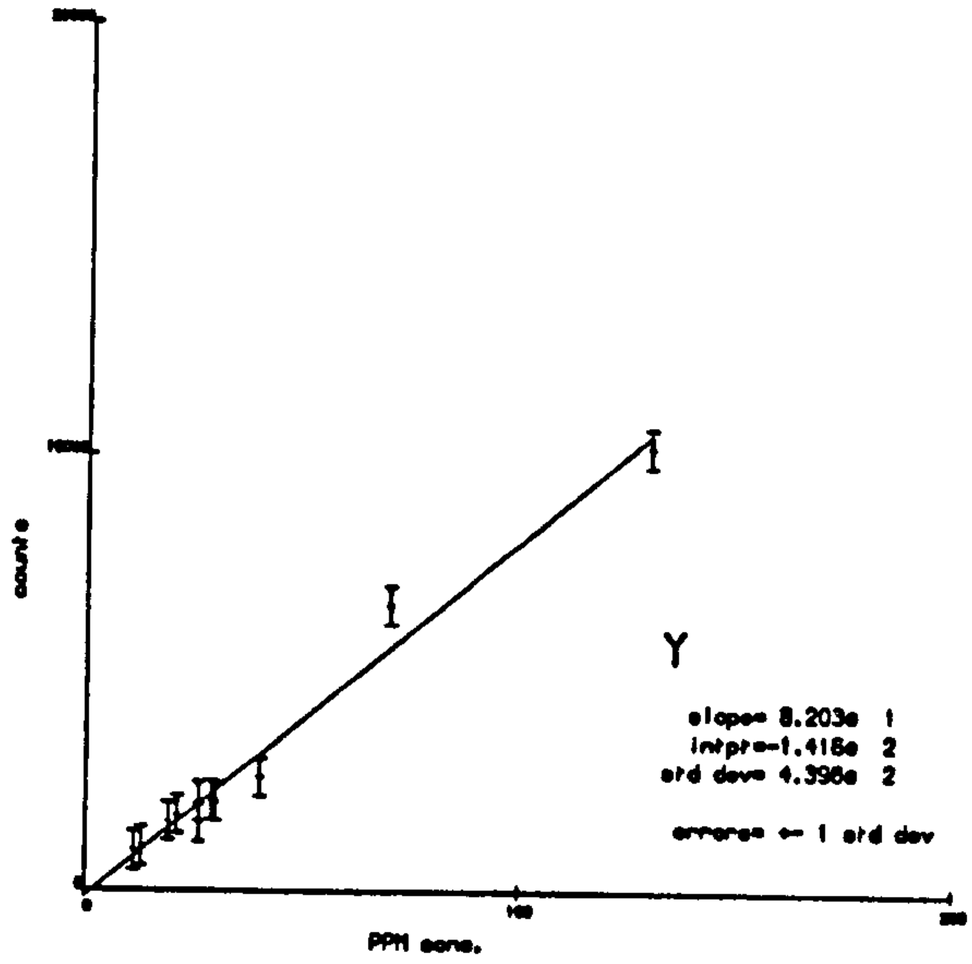
counts
PPM conc.
Y
slope= 8.203e 1
intpt=-1.418e 2
std dev= 4.398e 2
errors <- 1 std dev

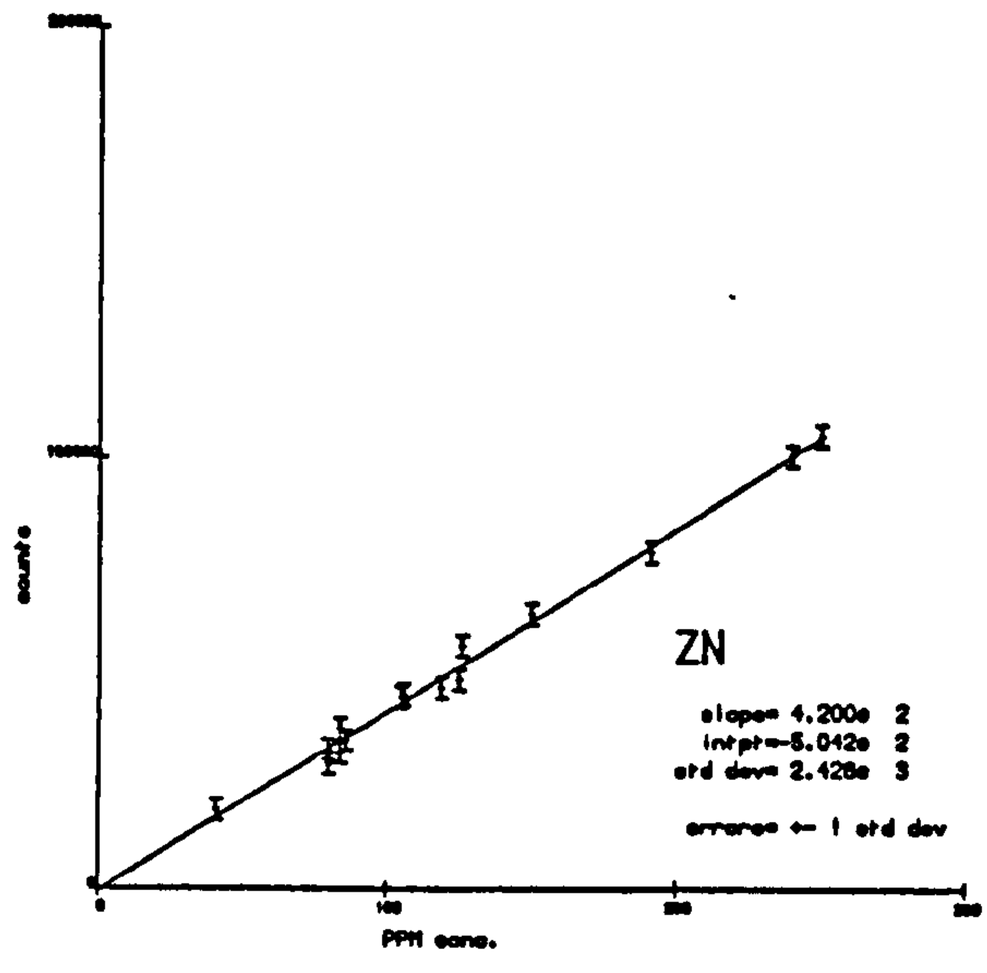
counts
PPM conc.
ZN
slope= 4.200e 2
intpt=-5.042e 2
std dev= 2.428e 3
errors <- 1 std dev

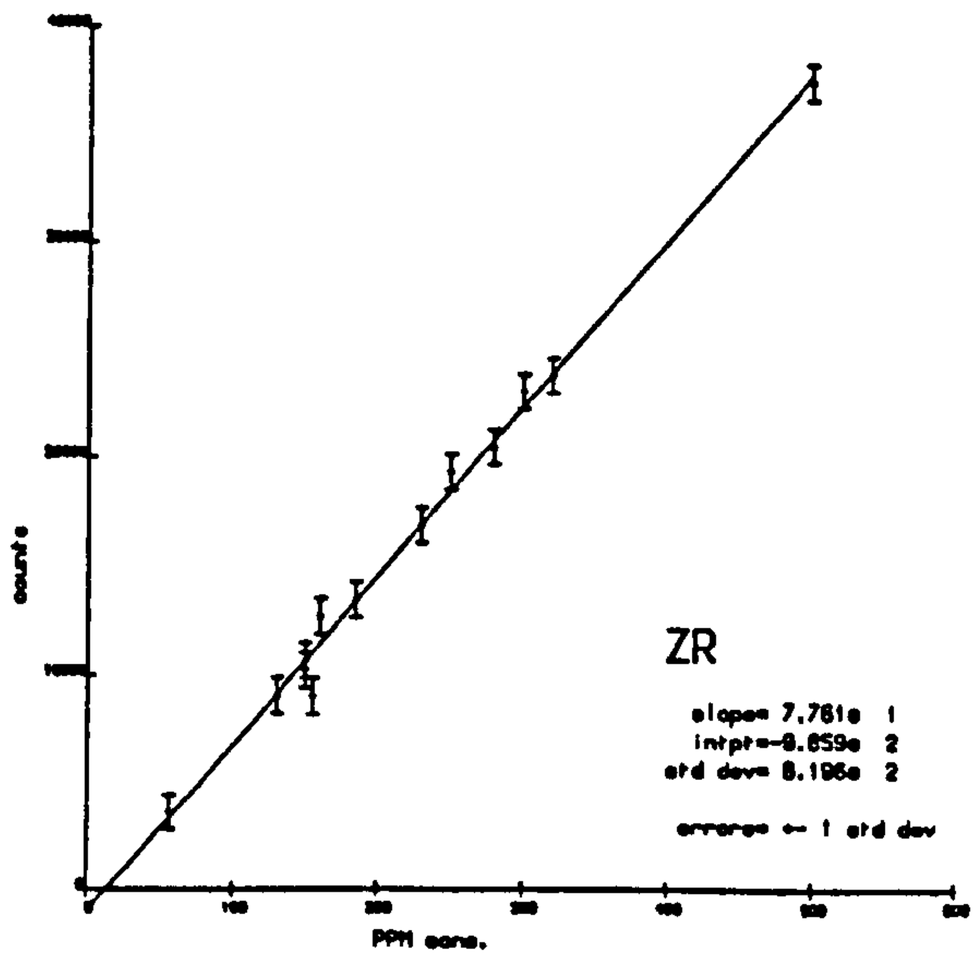
counts
PPM conc.
ZR
slope= 7.761e 1
intpt=-8.659e 2
std dev= 8.196e 2
errors <- 1 std dev

B.2 CORRECTION FOR THE DILUTION AND CONTRIBUTION OF RESIDUAL SEA-SALT

Allowance must be made for the effect of residual sea-salt when reporting elemental concentrations in marine sediments. This salt can act both as a direct contributor of certain elements (Na, Mg, Ca, K, S, Br; other elements occur but at concentrations that are insignificant), and as a dilutent of the overall concentration of all elements present in a sample.

An assumption is made that the salinity of interstitial water is constant and the same as that of normal marine sea water, ie 35 $^{o}/_{oo}$. Using the water contents given in Table A.2 the salt content of each sample is calculated from the relationship:

$$\text{Salt} = \frac{3.513 \times W}{(100 - W)}$$

where W is the water content (% of wet weight)

Due to the exponential increase in salt relative to sediment with increasing water content, a small change in W results in a large fluctuation in the percentage of salt present when the sediment is dried (for samples with >65% water).

Individual element corrections are applied first using the following equations based on the concentration of the elements present in normal sea water:

$$(\text{wt.\% Na})_{sed} = (\text{wt.\% Na})_{sed+salt} - 0.306(\text{wt.\% salt})$$

$$(\text{wt.\% Mg})_{sed} = (\text{wt.\% Mg})_{sed+salt} - 0.037(\text{wt.\% salt})$$

$$(\text{wt.\% Ca})_{sed} = (\text{wt.\% Ca})_{sed+salt} - 0.012(\text{wt.\% salt})$$

$$(\text{wt.\% K})_{sed} = (\text{wt.\% K})_{sed+salt} - 0.011(\text{wt.\% salt})$$

$$(\text{ppm S})_{sed} = (\text{ppm S})_{sed+salt} - 258(\text{wt.\% salt})$$

$$(\text{ppm Br})_{sed} = (\text{ppm Br})_{sed+salt} - 19(\text{wt.\% salt})$$

All elemental concentrations are then corrected for total dilution by sea-salt using the equation:

$$(\text{El. conc.})_{\text{salt-free}} = (\text{El. conc.})_{\text{sed+salt}} \times (100/100-\text{salt})$$

B.3 TOTAL CARBON AND NITROGEN ANALYSIS

Total carbon and nitrogen analyses were determined on dried, powdered sediment samples using a Perkin-Elmer 240 Elemental Analyser. Approximately 10 mg of sample was used for each analysis. Temperatures of combustion and reduction were 950^{o}C and 700^{o}C respectively. Combustion was held for an extra minute to ensure complete reaction of the sample, otherwise operating conditions were followed according to the manufacturers recommendations. Acetanilide was used as the working standard for instrument calibration.

	Carbon	Nitrogen
mean (n=8)	2.25	0.17
std. dev. (1σ)	0.019	0.01
% precision	0.84	5.88

B.4 ORGANIC CARBON ANALYSIS

Organic carbon analysis was performed on a Leco 521-200 induction furnace equipped with a dust trap, sulphur trap (SO_2 absorbtion by MnO_2 powder) and catalyst furnace. This was connected to a Leco 572-100 carbon analyser using a gas burette to measure the change in volume when the O_2-CO_2 mixture from combustion is flushed through CO_2-absorbing KOH.

For a sample containing approximately 1% of organic carbon, 1 gram of pre-dried sediment was accurately weighed out into a disposable Leco ceramic crucible. Carbonate digestion was performed by damping the sample with slightly acidified, de-ionized water, and then adding a 50% solution of HCl dropwise to just wet the sample entirely. If too much is added there is a risk of washing out hydrolysable organic material. The sample was then placed on a hot plate at $60^{o}C$ and evaporated to dryness before acid was again added dropwise. Acidification was continued until the sample no longer effervesced.

The samples were analysed using tin and iron accelerators spread evenly (one spatula of each) over the surface of the acidified, dried sediment. The oxygen flow rate was 1.5 l/min.

Analytical precision based on replicates of two samples, one with high carbonate (Station 163-14, bottom), were as follows:

(a) 163-14 (top) n = 9

mean = 0.973 wt.%

σ = 0.022

% relative std. dev., 1σ = 2.26 %

(b) 163-14 (bottom) n = 10

mean = 1.013

σ = 0.036

% relative std. dev., 1σ = 3.54 %

B.5 CARBONATE ANALYSIS

Carbonate carbon was calculated from total carbon (Section B.3) - organic carbon x 8.333. Carbonate contents of four oceanic cores off Baja California are presented in Appendix C.

B.6 THE DETERMINATION OF THE OXIDATION STATE OF MANGANESE IN BAJA CALIFORNIA SEDIMENTS

Several methods exist for the determination of the oxidising capacity of manganese. In each of these decomposition of the Mn-bearing phase is effected by acids containing an excess of a reducing agent. A direct determination by simple acid decomposition is not generally possible as ions in high oxidation states are not sufficiently stable under these conditions (Wilson, 1964).

The method outlined below was modified from Wilson, (1964) in an attempt to overcome some analytical problems. These were:

(1) To decompose only the Mn oxides and leave the silicates intact.

(2) To lower the reducing power of the vanadyl by using more

acidic conditions.

(3) To have as little effect on the organics as possible.

The method proved accurate on inorganic mangannic compounds but no organic-containing sediment standard was available.

Approximately 100 mg of pre-dried (110^{o}C), powdered sample of known weight was digested in a teflon crucible overnight using a mixture of 1 ml of 25% w/v vanadyl sulphate, 0.6 ml of 1+1 H_2SO_4 and 2.4 ml of deionized water. This results in the VO^{2+} being oxidised by the MnO_2 as it decomposes in the acid medium:

$$2\ VO^{2} + Mn^{4+} + 4\ H_2O = 2\ VO_3^{-} + Mn^{2+} + 8\ H^{+}$$

Both VO^{2+} and VO_3^{-} are stable under normal atmospheric conditions allowing the experiment to be carried out without special conditions.

The crucible containing the digested sample is transfered, in its entirety, to a polythene beaker containing 100 ml of orthophosphoric acid, 100 ml of deionized water and 5 ml of indicator (0.02 g of sodium diphenylamine p-sulphonate in 100 ml of water). The contents of the crucible are mixed well with the beaker solution and left for a few minutes to allow the indicator colour (a pale lilac) to develop.

Titration is by a potentiometric method using a standard ferrous ammonium sulphate solution (0.05 N in 2 N sulphuric acid):

$$VO_3^{-} + Fe^{2+} + 4\ H^{+} = VO^{2+} + Fe^{3+} + 2\ H_2O$$

Thus, V^{5+} generated by the oxidation of vanadyl sulphate is directly titrated by standard ferrous ammonium sulphate solution. A standard platinum calomel electrode is used

connected to a chart recorder. An exponential decrease in relative mV is observed at the end-point corresponding to a colour change from lilac to pale-green.

Some pure aluminium turnings were immersed in the ferrous ammonium sulphate solution to prevent deterioration; nevertheless, standardisation was periodically carried out using about 100 mg of ammonium metavanadate. Since 0.1 g of this vanadate contains 61.48 mg of FeO and

$$Mn^{4+} = 2\ Fe^{2+}$$

then the equivalence of 1 ml of ferrous ammonium sulphate solution in weight (g) of MnO_2 may be calculated (x). Hence, (x.titre)/sample wt. may be converted to wt.% MnO_2.

The relative precision (1σ) of this method based on a sample containing a mean of 2.95 wt.% MnO_2 is 0.5% (n=6). A sample containing <0.5 wt.% MnO_2 will be subject to larger errors.

Checks were made for the effects of salt, variation in sample weight, and the presence of organics, but they had no determinable influence. The effect of Fe^{3+} on the MnO_2 determination is also negligible (Wilson, 1955).

The oxidation state of Mn is quoted as MnO_x where:

$$x = 1 + 1/2 \frac{[\ 2\ Mn^{4+} + Mn^{3+}\ ]}{[\ Mn^{4+} + Mn^{3+} + Mn^{2+}\ ]}$$

$[\ Mn^{4+} + Mn^{3+} + Mn^{2+}\ ]$ is taken as the total Mn, as determined by XRF, less the aluminosilicate fraction (Mn/Al = 0.011; Turekian and Wedepohl, 1961). Several samples were checked for total Mn using flame atomic adsorbtion spectroscopy. Good agreement was found.

Finally a comparison was made with the iodometric method used by Murray *et al* (1984):

Sample	Iodometric method	Adapted Wilson method
14 Top	3.10	2.97
7:0-1	3.74	3.56
7:1-2	3.87	3.32
7:2-3	8.18	7.81
14:24-26	0.52	0.14

(All analyses in wt.% MnO_2)

The increase in MnO_2 by the iodometric method is attributable to absorbed oxygen on the surface of the sample causing induced oxidation of the iodide (Pantony and Siddiqi, 1962). This error is large when samples have little MnO_2.

B.7 ELECTRON MICROPROBE TECHNIQUES

Dolomite and glaucony analyses were performed on a Cambridge Instruments Microscan Mk.5 electron microprobe. Wavelength dispersive spectrometry techniques were used with Z.A.F. corrections following Sweatman and Long (1969). Table B.7 lists the analysing conditions for each element.

TABLE B.7

ELECTRON MICROPROBE ANALYSIS

Conditions: 20 KV, 30 nA, WDS

Element	Line	Standard	Crystal
Na	Kα	$NaAlSi_2O_6$	RAP
Mg	Kα	MgO	RAP
Al	Kα	Al_2O_3	RAP
Si	Kα	$CaSiO_3$	RAP
S	Kα	FeS_2	PET
K	Kα	$KAlSi_3O_8$	QTZ
Ca	Kα	$CaSiO_3$	QTZ
Ti	Kα	TiO_2	QTZ
Fe	Kα	metal	QTZ
Sr	Lα	$SrSO_4$	PET
Ba	Lα	$BaSO_4$	RAP

APPENDIX C

DATA

Elemental analyses are listed both uncorrected and corrected for salt contributions. Elemental ratios are also corrected. All trace element to Al ratios are $\times 10^{-4}$ except K/Rb.

Radionuclide data provided by the kind permission of Dr.J. Thomson.

STATION 163-5 Uncorrected major element data, Wt.%

	Si	Al	Fe	Mg	Ca	Na	K	Ti	Mn	P	LOI
5:0-1.	27.17	6.37	1.80	1.08	6.74	2.32	1.07	0.34	0.03	0.39	9.30
5:1-2.	23.87	5.95	1.82	1.08	6.74	2.20	0.96	0.31	0.03	0.29	11.60
5:2-3.	25.80	6.61	2.01	1.17	7.14	2.38	1.04	0.34	0.03	0.28	10.80
5:3-4.	26.00	6.68	2.03	1.15	7.06	2.41	1.06	0.33	0.03	0.30	10.80
5:4-5.	25.34	6.51	2.01	1.15	7.31	2.43	1.04	0.33	0.03	0.32	11.70
5:5-6.	25.57	6.50	1.98	1.13	7.24	2.43	1.05	0.33	0.03	0.30	11.60
5:6-7.	25.69	6.55	2.04	1.22	7.29	2.36	1.04	0.34	0.04	0.30	12.30
5:7-8.	25.90	6.46	1.94	1.18	7.17	2.41	1.05	0.33	0.03	0.32	11.60
5:8-9.	24.54	6.13	1.94	1.17	7.14	2.40	1.01	0.33	0.03	0.34	12.50
5:9-10.	25.46	6.29	1.97	1.22	7.55	2.28	1.03	0.33	0.03	0.40	12.10
5:10-12.	25.40	6.31	2.02	1.22	7.60	2.28	0.99	0.34	0.03	0.36	12.80
5:12-14.	24.95	6.36	2.03	1.22	7.43	2.28	0.99	0.34	0.03	0.28	13.10
5:14-16.	24.87	6.38	2.06	1.19	7.67	2.33	0.98	0.34	0.04	0.31	13.30
5:16-18.	25.02	6.43	2.09	1.19	7.57	2.33	0.98	0.34	0.04	0.29	13.60
5:18-20.	24.76	6.38	2.11	1.24	7.69	2.32	0.99	0.34	0.03	0.31	14.00
5:20-22.	24.84	6.37	2.09	1.25	7.65	2.37	0.98	0.34	0.03	0.30	13.10
5:22-24.	24.76	6.25	2.07	1.24	7.81	2.31	1.01	0.34	0.03	0.32	13.40

STATION 162-5 Salt corrected major element data, Wt.% Element

	Si	Al	Fe	Mg	Ca	Na	K	Ti	Mn	P	LOI	Salt
5:0-1.	27.67	6.49	1.84	1.03	6.84	1.80	1.07	0.35	0.03	0.40	9.30	1.82
5:1-2.	24.38	6.08	1.86	1.02	6.87	1.60	0.96	0.32	0.03	0.30	11.60	2.09
5:2-3.	26.34	6.75	2.05	1.12	7.26	1.79	1.04	0.34	0.03	0.29	10.80	2.05
5:3-4.	26.53	6.82	2.07	1.10	7.17	1.83	1.06	0.34	0.03	0.30	10.80	2.01
5:4-5.	25.90	6.66	2.05	1.10	7.45	1.80	1.04	0.34	0.03	0.33	11.70	2.17
5:5-6.	26.10	6.63	2.02	1.07	7.36	1.85	1.04	0.34	0.03	0.31	11.60	2.02
5:6-7.	26.24	6.69	2.09	1.17	7.42	1.76	1.04	0.34	0.04	0.31	12.30	2.08
5:7-8.	26.44	6.60	1.98	1.12	7.29	1.82	1.05	0.34	0.03	0.33	11.60	2.04
5:8-9.	25.13	6.28	1.98	1.10	7.28	1.72	1.01	0.33	0.03	0.35	12.50	2.34
5:9-10.	26.01	6.43	2.02	1.17	7.69	1.66	1.03	0.34	0.03	0.41	12.10	2.13
5:10-12.	25.97	6.45	2.06	1.17	7.74	1.65	0.99	0.34	0.03	0.37	12.80	2.18
5:12-14.	25.50	6.50	2.07	1.17	7.57	1.66	0.99	0.34	0.03	0.29	13.10	2.15
5:14-16.	25.44	6.53	2.11	1.14	7.82	1.68	0.98	0.35	0.04	0.31	13.30	2.25
5:16-18.	25.61	6.58	2.14	1.13	7.72	1.67	0.98	0.36	0.04	0.30	13.60	2.30
5:18-20.	25.33	6.52	2.15	1.19	7.85	1.67	0.99	0.35	0.03	0.32	14.00	2.25
5:20-22.	25.45	6.53	2.14	1.19	7.81	1.68	0.98	0.35	0.03	0.30	13.10	2.39
5:22-24.	25.33	6.40	2.12	1.19	7.96	1.66	1.00	0.34	0.03	0.32	13.40	2.27

STATION 163-5 Salt- free ratios to aluminium

	Si/Al	Fe/Al	Mg/Al	Ca/Al	Na/Al	K/Al	Ti/Al	Mn/Al	P/Al
5:0-1.	4.263	0.284	0.159	1.054	0.277	0.165	0.054	0.005	0.062
5:1-2.	4.010	0.306	0.168	1.130	0.263	0.158	0.053	0.005	0.049
5:2-3.	3.902	0.304	0.166	1.076	0.265	0.154	0.050	0.004	0.043
5:3-4.	3.890	0.304	0.161	1.051	0.268	0.155	0.050	0.004	0.044
5:4-5.	3.889	0.308	0.165	1.119	0.270	0.156	0.051	0.005	0.050
5:5-6.	3.937	0.305	0.161	1.110	0.279	0.157	0.051	0.005	0.047
5:6-7.	3.922	0.312	0.175	1.109	0.263	0.155	0.051	0.006	0.046
5:7-8.	4.006	0.300	0.170	1.105	0.276	0.159	0.052	0.005	0.050
5:8-9.	4.002	0.315	0.175	1.159	0.274	0.161	0.053	0.005	0.056
5:9-10.	4.045	0.314	0.182	1.196	0.258	0.160	0.053	0.005	0.064
5:10-12.	4.026	0.319	0.181	1.200	0.256	0.153	0.053	0.005	0.057
5:12-14.	3.923	0.318	0.180	1.165	0.255	0.152	0.052	0.005	0.045
5:14-16.	3.896	0.323	0.175	1.198	0.257	0.150	0.054	0.006	0.047
5:16-18.	3.892	0.325	0.172	1.173	0.254	0.149	0.055	0.006	0.046
5:18-20.	3.885	0.330	0.183	1.204	0.256	0.152	0.054	0.005	0.049
5:20-22.	3.897	0.328	0.182	1.196	0.257	0.150	0.054	0.005	0.046
5:22-24.	3.958	0.331	0.186	1.244	0.259	0.156	0.053	0.005	0.050

STATION 163-5 Uncorrected trace element data, ppm

	I	Br	Mo	Zr	Y	Sr	Rb	Th	Pb	As	Zn	Cu	Ni	Cr	V	Ba
5:0-1.	220	155	3	172	24	546	35	N.D.	9	1	29	8	23	111	59	433
5:1-2.	207	155	3	141	20	534	33	N.D.	10	3	29	5	24	100	55	389
5:2-3.	215	162	4	146	22	571	37	2	8	3	33	8	26	105	64	413
5:3-4.	215	158	5	135	22	577	37	2	12	2	33	9	26	109	65	439
5:4-5.	227	156	5	137	22	585	37	5	11	2	33	9	27	103	63	418
5:5-6.	214	151	5	135	21	580	38	1	10	1	32	9	27	114	63	410
5:6-7.	224	157	4	140	23	582	37	2	11	1	34	10	28	111	65	395
5:7-8.	210	148	3	141	22	571	37	3	9	1	33	9	28	109	66	391
5:8-9.	210	147	5	134	21	558	35	3	8	2	32	8	27	109	61	386
5:9-10.	217	153	4	132	22	585	37	3	9	2	33	9	27	116	65	404
5:10-12.	197	156	5	138	22	586	36	2	11	1	34	9	30	120	67	404
5:12-14.	168	157	6	142	22	579	37	3	8	1	34	10	30	113	64	404
5:14-16.	166	162	6	148	22	588	38	2	10	1	34	10	30	114	69	409
5:16-18.	222	164	5	145	23	585	38	1	9	1	36	10	31	116	67	414
5:18-20.	199	158	6	136	21	587	38	1	10	2	38	11	32	117	66	401
5:20-22.	190	163	6	140	21	583	38	3	10	2	36	11	31	118	69	399
5:22-24.	204	158	5	136	22	586	37	N.D.	8	3	36	10	31	114	70	377

N.D. - Not detectable

STATION 163-5 Salt corrected trace element data, ppm

	I	Br	Mo	Zr	Y	Sr	Rb	Th	Pb	As	Zn	Cu	Ni	Cr	V	Ba
5:0-1.	224	123	3	175	24	556	36	N.D.	9	1	30	8	23	113	60	441
5:1-2.	211	118	3	144	20	545	34	N.D.	10	3	30	5	25	102	56	397
5:2-3.	219	126	4	149	22	583	38	2	8	3	34	8	27	107	65	422
5:3-4.	219	123	5	138	22	589	38	2	12	2	34	9	27	111	66	448
5:4-5.	232	118	5	140	22	598	38	5	11	2	34	9	28	105	64	427
5:5-6.	218	116	5	138	21	592	39	1	10	1	33	9	28	116	64	418
5:6-7.	229	120	4	143	23	594	38	2	11	1	35	10	29	113	66	403
5:7-8.	214	112	3	144	22	583	38	3	9	1	34	9	29	111	67	399
5:8-9.	215	107	5	137	22	571	36	3	8	2	33	8	28	112	62	395
5:9-10.	222	116	4	135	22	598	38	3	9	2	34	9	28	119	66	413
5:10-12.	201	159	5	141	22	599	37	2	11	1	35	9	31	123	68	413
5:12-14.	172	119	6	145	22	592	38	3	8	1	35	10	31	115	65	413
5:14-16.	170	123	6	151	23	602	39	2	10	1	35	10	31	117	71	418
5:16-18.	227	124	5	148	24	599	39	1	9	1	37	10	32	119	69	424
5:18-20.	204	119	6	139	21	601	39	1	10	2	39	11	33	120	68	410
5:20-22.	195	122	6	143	22	597	39	3	10	2	37	11	32	121	71	409
5:22-24.	209	119	5	139	23	600	38	N.D.	8	3	37	10	32	117	72	386

N.D. - Not detectable

STATION 163-5 Salt- free trace element ratios to aluminium (X10-4)

	Mo/Al	Zr/Al	Y/Al	Sr/Al	Rb/Al	Th/Al	Pb/Al	As/Al	Zn/Al	Cu/Al	Ni/Al	Cr/Al	V/Al	Ba/Al	K/Rb
5:0-1.	0.46	26.96	3.70	85.67	5.55	N.D.	1.39	0.15	4.62	1.23	3.54	17.41	9.24	67.95	297.22
5:1-2.	0.49	23.68	3.29	89.64	5.59	N.D.	1.64	0.49	4.93	0.82	4.11	16.78	9.21	65.30	282.35
5:2-3.	0.59	22.07	3.26	86.37	5.63	0.30	1.19	0.44	5.04	1.19	4.00	15.85	9.63	62.52	273.68
5:3-4.	0.73	20.23	3.23	86.36	5.57	0.29	1.76	0.29	4.99	1.32	3.96	16.28	9.68	65.69	278.95
5:4-5.	0.75	21.02	3.30	89.79	5.71	0.75	1.65	0.30	5.11	1.35	4.20	15.77	9.61	64.11	273.68
5:5-6.	0.75	20.81	3.17	89.29	5.88	0.15	1.51	0.15	4.98	1.36	4.22	17.50	9.65	63.05	266.67
5:6-7.	0.60	21.38	3.44	88.79	5.68	0.30	1.64	0.15	5.23	1.49	4.33	16.89	9.87	60.24	273.68
5:7-8.	0.45	21.82	3.33	88.33	5.76	0.45	1.36	0.15	5.15	1.36	4.39	16.82	10.15	60.45	276.32
5:8-9.	0.80	21.82	3.50	90.92	5.73	0.48	1.27	0.32	5.25	1.27	4.46	17.83	9.87	62.90	280.56
5:9-10.	0.62	21.00	3.42	93.00	5.91	0.47	1.40	0.31	5.29	1.40	4.35	18.51	10.26	64.23	271.05
5:10-12.	0.78	21.86	3.41	92.87	5.74	0.31	1.71	0.16	5.43	1.40	4.81	19.07	10.54	64.03	267.57
5:12-14.	0.92	22.31	3.38	91.08	5.85	0.46	1.23	0.15	5.38	1.54	4.77	17.69	10.00	63.54	260.53
5:14-16.	0.92	23.12	3.52	92.19	5.97	0.31	1.53	0.15	5.36	1.53	4.75	17.92	10.87	64.01	251.28
5:16-18.	0.76	22.49	3.65	91.03	5.93	0.15	1.37	0.15	5.62	1.52	4.86	18.09	10.49	64.44	251.28
5:18-20.	0.92	21.32	3.22	92.18	5.98	0.15	1.53	0.31	5.98	1.69	5.06	18.40	10.43	62.88	253.85
5:20-22.	0.92	21.90	3.37	91.42	5.97	0.46	1.53	0.31	5.67	1.68	4.90	18.53	10.87	62.63	251.28
5:22-24.	0.78	21.72	3.59	93.75	5.94	N.D.	1.25	0.47	5.78	1.56	5.00	18.28	11.25	60.31	263.16

N.D. - Not detectable

STATION 163-12 Uncorrected major element data, Wt.%

	Si	Al	Fe	Mg	Ca	Na	K	Ti	Mn	P	LOI
12:0-1.	25.25	7.67	2.41	1.39	6.73	3.00	1.29	0.36	0.03	0.25	9.60
12:1-2.	24.74	7.75	2.53	1.43	6.63	3.14	1.26	0.38	0.04	0.19	10.90
12:2-3.	24.54	7.68	2.51	1.43	6.64	3.05	1.26	0.38	0.04	0.19	10.80
12:3-4.	25.05	7.84	2.52	1.41	6.66	3.08	1.29	0.37	0.04	0.20	10.70
12:4-5.	25.06	7.82	2.53	1.43	6.66	3.04	1.30	0.38	0.03	0.20	10.40
12:5-6.	24.83	7.74	2.50	1.43	6.64	3.03	1.32	0.37	0.03	0.21	10.50
12:6-7.	24.94	7.73	2.52	1.45	6.70	3.05	1.35	0.37	0.04	0.21	9.70
12:7-8.	24.79	7.69	2.49	1.43	6.74	2.99	1.33	0.37	0.04	0.21	10.60
12:8-9.	24.86	7.68	2.53	1.46	6.85	2.91	1.33	0.36	0.03	0.22	10.60
12:9-10.	24.96	7.69	2.52	1.46	6.85	3.00	1.34	0.36	0.03	0.22	10.10
12:10-12.	24.95	7.72	2.51	1.44	6.82	2.98	1.33	0.36	0.04	0.22	10.40
12:12-14.	24.90	7.70	2.53	1.47	6.83	2.97	1.30	0.36	0.03	0.22	10.70
12:14-16.	25.02	7.67	2.46	1.46	6.82	3.13	1.36	0.35	0.03	0.22	9.10
12:16-18.	24.84	7.66	2.52	1.47	6.98	2.96	1.32	0.36	0.04	0.22	9.90
12:18-20.	24.80	7.65	2.54	1.46	6.87	2.99	1.31	0.36	0.03	0.22	10.10

STATION 163-12 Salt-corrected major element data, Wt.% Element

	Si	Al	Fe	Mg	Ca	Na	K	Ti	Mn	P	LOI	Salt
12:0-1.	25.79	7.83	2.46	1.34	6.85	2.40	1.29	0.37	0.03	0.25	9.60	2.11
12:1-2.	25.39	7.95	2.59	1.37	6.78	2.41	1.26	0.39	0.04	0.20	10.90	2.57
12:2-3.	25.18	7.88	2.57	1.38	6.78	2.32	1.26	0.39	0.04	0.20	10.80	2.55
12:3-4.	25.63	8.02	2.58	1.35	6.79	2.44	1.29	0.39	0.04	0.21	10.70	2.27
12:4-5.	25.61	7.99	2.58	1.38	6.78	2.43	1.31	0.39	0.03	0.21	10.40	2.16
12:5-6.	25.36	7.90	2.55	1.38	6.76	2.44	1.32	0.38	0.03	0.21	10.50	2.07
12:6-7.	25.45	7.88	2.58	1.41	6.81	2.49	1.36	0.38	0.04	0.21	9.70	1.99
12:7-8.	25.28	7.84	2.55	1.38	6.84	2.44	1.33	0.37	0.04	0.21	10.60	1.94
12:8-9.	25.34	7.83	2.58	1.41	6.96	2.37	1.34	0.37	0.03	0.22	10.60	1.90
12:9-10.	25.43	7.84	2.57	1.42	6.95	2.47	1.35	0.37	0.03	0.22	10.10	1.87
12:10-12.	25.43	7.87	2.56	1.40	6.93	2.44	1.33	0.37	0.04	0.22	10.40	1.89
12:12-14.	25.43	7.86	2.58	1.42	6.95	2.40	1.31	0.37	0.03	0.22	10.70	2.05
12:14-16.	25.50	7.82	2.51	1.42	6.93	2.60	1.37	0.36	0.04	0.23	9.10	1.88
12:16-18.	25.31	7.81	2.57	1.43	7.09	2.43	1.32	0.37	0.04	0.23	9.90	1.88
12:18-20.	25.30	7.80	2.59	1.41	6.98	2.44	1.32	0.37	0.03	0.22	10.10	1.99

STATION 163-12 Salt-free ratios to aluminium

	Si/Al	Fe/Al	Mg/Al	Ca/Al	Na/Al	K/Al	Ti/Al	Mn/Al	P/Al
12:0-1.	3.294	0.314	0.171	0.875	0.307	0.165	0.047	0.004	0.032
12:1-2.	3.194	0.326	0.172	0.853	0.303	0.158	0.049	0.005	0.025
12:2-3.	3.195	0.326	0.175	0.860	0.294	0.160	0.049	0.005	0.025
12:3-4.	3.196	0.322	0.168	0.847	0.304	0.161	0.049	0.005	0.026
12:4-5.	3.205	0.323	0.173	0.849	0.304	0.164	0.049	0.004	0.026
12:5-6.	3.210	0.323	0.175	0.856	0.309	0.167	0.048	0.004	0.027
12:6-7.	3.230	0.327	0.179	0.864	0.316	0.173	0.048	0.005	0.027
12:7-8.	3.224	0.325	0.176	0.872	0.311	0.170	0.047	0.005	0.027
12:8-9.	3.236	0.330	0.180	0.889	0.303	0.171	0.047	0.004	0.028
12:9-10.	3.244	0.328	0.181	0.886	0.315	0.172	0.047	0.004	0.028
12:10-12.	3.231	0.325	0.178	0.881	0.310	0.169	0.047	0.005	0.028
12:12-14.	3.235	0.328	0.181	0.884	0.305	0.167	0.047	0.004	0.028
12:14-16.	3.261	0.321	0.182	0.886	0.332	0.175	0.046	0.005	0.029
12:16-18.	3.241	0.329	0.183	0.908	0.311	0.169	0.047	0.005	0.029
12:18-20.	3.244	0.332	0.181	0.895	0.313	0.169	0.047	0.004	0.028

STATION 163-12 Uncorrected trace element data, ppm

	I	Br	Mo	Zr	Y	Sr	Rb	Th	Pb	As	Zn	Cu	Ni	Cr	V	Ba
12:0-1.	120	148	3	137	20	728	34	1	11	2	30	8	30	116	70	490
12:1-2.	112	179	3	123	18	721	36	3	11	2	33	9	30	120	79	489
12:2-3.	62	174	6	112	19	695	36	5	13	1	31	10	29	117	77	502
12:3-4.	128	162	4	125	19	734	36	3	11	2	33	10	30	120	78	518
12:4-5.	62	165	12	111	21	693	36	2	14	N.D.	34	11	30	119	72	488
12:5-6.	140	152	4	121	19	732	36	3	12	1	32	9	30	121	74	494
12:6-7.	144	149	4	124	9	735	36	2	11	1	32	11	30	121	73	493
12:7-8.	136	139	3	126	20	733	35	2	10	1	33	10	30	122	78	501
12:8-9.	131	139	3	127	19	733	37	2	10	3	33	11	32	120	76	492
12:9-10.	118	132	3	127	19	733	35	5	10	2	33	11	34	123	75	471
12:10-12.	105	131	6	124	19	737	35	1	12	1	33	10	34	115	75	509
12:12-14.	122	133	5	122	19	732	35	6	8	2	32	10	34	117	78	486
12:14-16.	111	124	4	123	19	733	36	N.D.	10	2	33	10	33	117	75	483
12:16-18.	121	121	3	130	20	746	34	6	5	5	32	10	33	122	72	481
12:18-20.	99	114	4	129	19	730	36	3	7	3	32	10	37	121	77	482

N.D. - Not detectable

STATION 163-12 Salt-corrected trace element data, ppm

	I	Br	Mo	Zr	Y	Sr	Rb	Th	Pb	As	Zn	Cu	Ni	Cr	V	Ba
12:0-1.	123	110	3	140	20	744	35	1	11	2	31	8	31	119	72	501
12:1-2.	115	135	3	126	18	740	37	3	11	2	34	9	31	123	81	502
12:2-3.	64	131	6	115	19	713	37	5	13	1	32	10	30	120	79	515
12:3-4.	131	123	4	128	19	751	37	3	11	2	34	10	31	123	80	530
12:4-5.	63	128	12	113	21	708	37	2	14	N.D.	35	11	31	122	74	499
12:5-6.	143	116	4	124	19	747	37	3	12	1	33	9	31	124	76	504
12:6-7.	147	114	4	127	9	750	37	2	11	1	33	11	31	123	74	503
12:7-8.	139	105	3	128	20	748	36	2	10	1	34	10	31	124	80	511
12:8-9.	134	106	3	129	19	747	38	2	10	3	34	11	33	122	77	502
12:9-10.	120	99	3	129	19	747	36	5	10	2	34	11	35	125	76	480
12:10-12.	107	98	6	126	19	751	36	1	12	1	34	10	35	117	76	519
12:12-14.	125	97	5	125	19	747	36	6	8	2	33	10	35	119	80	496
12:14-16.	113	90	4	125	19	747	37	N.D.	10	2	34	10	34	119	76	492
12:16-18.	87	123	3	132	20	760	35	6	5	5	33	10	34	124	73	490
12:18-20.	101	78	4	132	19	745	37	3	7	3	33	10	38	123	79	492

N.D. - Not detectable

STATION 163-12 Salt-free trace element ratios to aluminium (x10-4)

	Mo/Al	Zr/Al	Y/Al	Sr/Al	Rb/Al	Th/Al	Pb/Al	As/Al	Zn/Al	Cu/Al	Ni/Al	Cr/Al	V/Al	Ba/Al	K/Rb
12:0-1.	0.38	17.88	2.55	95.02	4.47	0.13	1.40	0.26	3.96	1.02	3.96	15.20	9.20	63.98	368.57
12:1-2.	0.38	15.85	2.26	93.08	4.65	0.38	1.38	0.25	4.28	1.13	3.90	15.47	10.19	63.14	340.54
12:2-3.	0.76	14.59	2.41	90.48	4.70	0.63	1.65	0.13	4.06	1.27	3.81	15.23	10.03	65.36	340.54
12:3-4.	0.50	15.96	2.37	93.64	4.61	0.37	1.37	0.25	4.24	1.25	3.87	15.34	9.98	66.08	348.65
12:4-5.	1.50	14.14	2.63	88.61	4.63	0.25	1.75	N.D.	4.38	1.38	3.88	15.27	9.26	62.45	354.05
12:5-6.	0.51	15.70	2.41	94.56	4.68	0.38	1.52	0.13	4.18	1.14	3.92	15.70	9.62	63.80	356.76
12:6-7.	0.51	16.12	1.14	95.18	12.44	0.25	1.40	0.13	4.19	1.40	3.93	15.61	9.39	63.83	138.78
12:7-8.	0.38	16.33	2.55	95.41	4.59	0.26	1.28	0.13	4.34	1.28	3.95	15.82	10.20	65.18	369.44
12:8-9.	0.38	16.48	2.43	95.40	4.85	0.26	1.28	0.38	4.34	1.40	4.21	15.58	9.83	64.11	352.63
12:9-10.	0.38	16.45	2.42	95.28	4.59	0.64	1.28	0.26	4.34	1.40	4.46	15.94	9.69	61.22	375.00
12:10-12.	0.76	16.01	2.41	95.43	4.57	0.13	1.52	0.13	4.32	1.27	4.45	14.87	9.66	65.95	369.44
12:12-14.	0.64	15.90	2.42	95.04	4.58	0.76	1.02	0.25	4.20	1.27	4.45	15.14	10.18	63.10	363.89
12:14-16.	0.51	15.98	2.43	95.52	4.73	N.D.	1.28	0.26	4.35	1.28	4.35	15.22	9.72	62.92	370.27
12:16-18.	0.38	16.90	2.56	97.31	4.48	0.77	0.64	0.64	4.23	1.28	4.35	15.88	9.35	62.74	377.14
12:18-20.	0.51	16.92	2.44	95.51	4.74	0.38	0.90	0.38	4.23	1.28	4.87	15.77	10.13	63.08	356.76

N.D. - Not detectable

STATION 145-17 Uncorrected major element data, Wt.% Element

	Si	Al	Fe	Mg	Ca	Na	K	Ti	Mn	P	LOI	Corg.
17:0-1.	23.82	6.44	1.93	1.00	8.76	2.54	1.11	0.294	0.04	0.59	12.90	1.93
17:2-3.	24.43	6.65	2.04	1.08	7.19	2.62	1.20	0.310	0.04	0.61	11.90	2.45
17:3-4.	24.45	6.65	2.05	1.07	6.87	2.58	1.21	0.314	0.04	0.61	11.50	2.32
17:4-5.	24.51	6.71	2.08	1.08	7.15	2.55	1.23	0.315	0.04	0.93	11.00	2.23
17:5-6.	22.05	6.16	2.07	1.14	9.30	2.55	1.12	0.301	0.04	2.11	12.00	2.70
17:6-7.	21.63	6.15	2.26	1.23	8.77	2.53	1.10	0.309	0.04	1.62	14.50	3.38
17:7-8.	21.80	6.23	2.35	1.24	8.20	2.51	0.98	0.316	0.04	0.63	16.80	3.57
17:8-9.	21.43	6.15	2.35	1.21	8.87	2.44	0.95	0.308	0.04	0.43	18.00	3.45
17:9-10.	20.91	6.00	2.39	1.18	9.61	2.40	0.90	0.302	0.04	0.39	18.70	3.36
17:10-12.	20.79	6.02	2.48	1.32	8.22	2.46	0.87	0.311	0.04	0.36	20.40	4.21
17:12-14.	21.49	6.26	2.45	1.34	7.51	2.46	0.94	0.318	0.04	0.39	19.70	3.73
17:14-16.	21.52	6.18	2.32	1.25	8.35	2.44	0.97	0.311	0.04	0.69	17.70	3.67
17:16-18.	21.43	6.22	2.40	1.32	8.05	2.48	1.00	0.315	0.04	0.71	18.30	4.17
17:18-20.	19.80	6.14	2.74	1.57	6.67	2.52	0.98	0.322	0.04	0.36	23.70	6.12
17:20-22.	18.55	5.74	2.57	1.48	8.75	2.34	0.76	0.305	0.03	0.31	24.70	5.53
17:22-24.	18.47	5.65	2.49	1.44	8.99	2.50	0.77	0.296	0.03	0.33	24.80	6.35
17:24-26.	19.39	5.82	2.48	1.42	9.04	2.46	0.80	0.307	0.03	0.37	22.30	4.72
17:26-28.	18.86	5.69	2.49	1.40	8.78	2.45	0.90	0.305	0.03	0.34	21.40	5.16

STATION 163-17 Salt-corrected major element data, Wt.% Element

	Si	Al	Fe	Mg	Ca	Na	K	Ti	Mn	P	LOI	Corg.	Salt
17:0-1.	24.30	6.57	1.96	0.94	8.91	1.97	1.11	0.300	0.04	0.60	12.90	1.97	1.97
17:2-3.	24.99	6.80	2.09	1.02	7.33	1.98	1.20	0.317	0.04	0.63	11.90	2.51	2.24
17:3-4.	25.02	6.81	2.09	1.01	7.01	1.92	1.21	0.321	0.04	0.63	11.50	2.37	2.28
17:4-5.	25.04	6.85	2.12	1.03	7.28	1.96	1.23	0.322	0.04	0.94	11.00	2.28	2.09
17:5-6.	22.53	6.29	2.12	1.08	9.48	1.94	1.13	0.308	0.04	2.16	12.00	2.76	2.12
17:6-7.	22.17	6.30	2.31	1.17	8.95	1.84	1.10	0.317	0.04	1.67	14.50	3.46	2.42
17:7-8.	22.42	6.41	2.42	1.17	8.40	1.72	0.98	0.325	0.04	0.65	16.80	3.67	2.75
17:8-9.	22.01	6.32	2.42	1.14	9.08	1.67	0.95	0.316	0.04	0.45	18.00	3.54	2.63
17:9-10.	21.47	6.16	2.46	1.11	9.83	1.64	0.89	0.310	0.04	0.40	18.70	3.45	2.61
17:10-12.	21.46	6.22	2.56	1.24	8.44	1.55	0.86	0.321	0.04	0.37	20.40	4.35	3.14
17:12-14.	22.19	6.46	2.53	1.27	7.71	1.55	0.94	0.328	0.04	0.40	19.70	3.85	3.12
17:14-16.	22.13	6.35	2.39	1.18	8.55	1.64	0.97	0.320	0.04	0.71	17.70	3.77	2.74
17:16-18.	22.00	6.39	2.46	1.26	8.23	1.73	1.00	0.323	0.04	0.73	18.30	4.28	2.59
17:18-20.	20.48	6.35	2.84	1.50	6.86	1.55	0.97	0.333	0.04	0.37	23.70	6.33	3.32
17:20-22.	19.15	5.93	2.65	1.41	8.99	1.42	0.75	0.315	0.03	0.32	24.70	5.71	3.14
17:22-24.	19.11	5.84	2.58	1.36	9.26	1.53	0.76	0.306	0.03	0.35	24.80	6.57	3.34
17:24-26.	20.10	6.03	2.57	1.34	9.33	1.43	0.79	0.318	0.03	0.38	22.30	4.89	3.54
17:26-28.	19.45	5.87	2.57	1.33	9.01	1.57	0.89	0.314	0.03	0.35	21.40	5.32	3.00

- Not analysed

STATION 145-17 Salt-free ratios to aluminium

	Si/Al	Fe/Al	Mg/Al	Ca/Al	Na/Al	K/Al	Ti/Al	M/Al	P/Al	Corg./Al
17:0-1.	3.701	0.299	0.143	1.357	0.301	0.169	0.046	0.007	0.092	0.300
17:2-3.	3.674	0.307	0.149	1.077	0.291	0.177	0.047	0.006	0.092	0.368
17:3-4.	3.677	0.308	0.148	1.029	0.283	0.178	0.047	0.006	0.092	0.349
17:4-5.	3.656	0.310	0.150	1.062	0.286	0.180	0.047	0.006	0.138	0.333
17:5-6.	3.582	0.337	0.172	1.507	0.309	0.179	0.049	0.006	0.343	0.439
17:6-7.	3.517	0.367	0.186	1.421	0.291	0.175	0.050	0.006	0.264	0.550
17:7-8.	3.498	0.377	0.183	1.311	0.268	0.152	0.051	0.006	0.101	0.573
17:8-9.	3.483	0.383	0.180	1.437	0.265	0.150	0.050	0.006	0.071	0.561
17:9-10.	3.484	0.398	0.180	1.595	0.266	0.145	0.050	0.006	0.065	0.560
17:10-12.	3.450	0.412	0.200	1.357	0.249	0.138	0.052	0.006	0.059	0.699
17:12-14.	3.432	0.391	0.196	1.193	0.240	0.145	0.051	0.006	0.062	0.596
17:14-16.	3.486	0.376	0.186	1.347	0.259	0.152	0.050	0.006	0.112	0.594
17:16-18.	3.444	0.385	0.197	1.289	0.271	0.156	0.051	0.006	0.114	0.670
17:18-20.	3.223	0.447	0.235	1.080	0.244	0.153	0.052	0.006	0.059	0.996
17:20-22.	3.229	0.447	0.237	1.516	0.239	0.127	0.053	0.006	0.055	0.963
17:22-24.	3.271	0.441	0.233	1.584	0.262	0.130	0.052	0.005	0.059	1.124
17:24-26.	3.331	0.426	0.221	1.546	0.237	0.130	0.053	0.006	0.063	0.811
17:26-28.	3.315	0.437	0.226	1.536	0.268	0.153	0.054	0.006	0.060	0.907

STATION 145-17 Uncorrected trace element data, ppm

	Mo	Zr	Y	Sr	Rb	Th	Pb	As	Zn	Cu	Ni	Cr	V	Ba	S	I	Br	Cl
17:0-1.	N.D.	201	32	568	59	7	13	20	54	10	26	58	62	550	4579	255	235	11925
17:2-3.	N.D.	209	36	519	63	8	11	24	60	12	32	70	72	568	5436	232	248	13602
17:3-4.	N.D.	201	34	513	62	6	13	22	59	11	32	70	70	573	5660	221	240	13847
17:4-5.	N.D.	197	35	543	63	10	11	26	61	12	33	69	72	561	5905	209	231	12645
17:5-6.	2	178	30	671	62	9	14	33	62	15	37	69	74	516	7658	219	269	12847
17:6-7.	3	162	29	604	65	10	11	31	71	18	44	75	91	533	8408	237	335	14694
17:7-8.	5	163	28	502	67	6	9	27	74	19	46	79	92	521	8618	227	361	16690
17:8-9.	3	161	28	502	64	9	8	27	70	17	44	76	87	504	9833	236	340	15943
17:9-10.	3	161	27	528	64	7	10	32	68	16	44	70	80	496	10680	247	329	15843
17:10-12.	7	152	26	469	66	7	11	27	79	22	53	86	96	472	11716	233	402	19072
17:12-14.	10	152	28	453	69	8	8	31	82	21	56	86	106	498	10889	236	413	18909
17:14-16.	8	159	28	512	66	7	8	24	73	19	50	79	87	504	9403	220	342	16608
17:16-18.	8	157	27	498	69	6	10	26	78	20	55	83	97	492	9512	215	360	15677
17:18-20.	15	122	26	398	75	9	10	24	98	31	74	104	132	462	11574	232	536	20157
17:20-22.	8	118	25	453	70	9	8	25	88	26	69	98	117	431	10714	259	519	19071
17:22-24.	12	115	25	468	69	8	7	26	88	28	71	95	128	444	11312	276	595	20268
17:24-26.	8	125	25	480	68	11	9	32	82	24	61	92	107	441	10245	248	529	21484
17:26-28.	7	130	27	467	69	9	9	26	83	24	63	91	108	450	10018	229	476	18219

N.D. - Not detectable

STATION 145-17 Salt-corrected trace element data, ppm

	Mo	Zr	Y	Sr	Rb	Th	Pb	As	Zn	Cu	Ni	Cr	V	Ba	S	I	Br	Cl
17:0-1.	N.D.	205	33	579	60	7	13	20	55	10	27	59	63	561	4149	260	202	11925
17:2-3.	N.D.	214	37	531	64	8	11	25	61	12	33	72	74	581	4964	237	210	13602
17:3-4.	N.D.	206	35	525	63	6	13	23	60	11	33	72	72	586	5185	226	201	13847
17:4-5.	N.D.	201	36	555	64	10	11	27	62	12	34	70	74	573	5477	213	195	12645
17:5-6.	2	182	31	686	63	9	14	34	63	15	38	70	76	527	7261	224	234	12847
17:6-7.	3	166	30	619	67	10	11	32	73	18	45	77	93	546	7971	243	296	14694
17:7-8.	5	168	29	516	69	6	9	28	76	20	47	81	95	536	8126	233	317	16690
17:8-9.	3	165	29	516	66	9	8	28	72	17	45	78	89	518	9396	242	298	15943
17:9-10.	3	165	28	542	66	7	10	33	70	16	45	72	82	509	10269	254	287	15843
17:10-12.	7	157	27	484	68	7	11	28	82	23	55	89	99	487	11252	241	353	19072
17:12-14.	10	157	29	468	71	8	8	32	85	22	58	89	109	514	10403	244	365	18909
17:14-16.	8	163	29	526	68	7	8	25	75	20	51	81	89	518	8936	226	298	16608
17:16-18.	8	161	28	511	71	6	10	27	80	21	56	85	100	505	9074	221	319	15677
17:18-20.	16	126	27	412	78	9	10	25	101	32	77	108	137	478	11078	240	489	20157
17:20-22.	8	122	26	468	72	9	8	26	91	27	71	101	121	445	10218	267	474	19071
17:22-24.	12	119	26	484	71	8	7	27	91	29	73	98	132	459	10804	286	550	20268
17:24-26.	8	130	26	498	70	11	9	33	85	25	63	95	111	457	9666	257	479	21484
17:26-28.	7	134	28	481	71	9	9	27	86	25	65	94	111	464	9523	236	432	18219

N.D. - Not detectable

STATION 145-17 Salt-free trace element ratios to aluminium (x10-4)

	Mo/Al	Zr/Al	Y/Al	Rb/Al	Sr/Al	Th/Al	Pb/Al	As/Al	Z/Al	Cu/Al	Ni/Al	Cr/Al	V/Al	Ba/Al
17:0-1.	N.D.	31.23	5.03	9.14	88.19	1.07	1.98	3.05	8.38	1.52	4.11	8.99	9.60	85.45
17:2-3.	N.D.	31.45	5.44	9.41	78.05	1.18	1.62	3.67	8.97	1.76	4.85	10.58	10.88	85.40
17:3-4.	N.D.	30.27	5.14	9.26	77.13	0.88	1.91	3.38	8.82	1.62	4.85	10.58	10.58	86.10
17:4-5.	N.D.	29.35	5.26	9.34	81.04	1.46	1.61	3.94	9.05	1.75	4.96	10.22	10.80	83.66
17:5-6.	0.32	28.93	4.93	10.02	109.06	1.43	2.23	5.41	10.02	2.38	6.04	11.13	12.08	83.78
17:6-7.	0.48	26.34	4.76	10.63	98.23	1.59	1.75	5.08	11.58	2.86	7.14	12.22	14.76	86.64
17:7-8.	0.78	26.21	4.52	10.77	80.51	0.94	1.40	4.37	11.86	3.12	7.33	12.64	14.82	83.63
17:8-9.	0.47	26.12	4.59	10.45	81.67	1.42	1.27	4.43	11.40	2.69	7.12	12.35	14.09	81.99
17:9-10.	0.49	26.77	4.54	10.71	87.93	1.14	1.62	5.35	11.36	2.60	7.30	11.68	13.30	82.58
17:10-12.	1.13	25.24	4.34	10.93	77.81	1.13	1.77	4.50	13.18	3.70	8.84	14.31	15.91	78.29
17:12-14.	1.55	24.29	4.49	10.98	72.41	1.24	1.24	4.95	13.15	3.40	8.97	13.77	16.86	79.52
17:14-16.	1.26	25.67	4.57	10.71	82.85	1.10	1.26	3.94	11.81	3.15	8.03	12.76	14.02	81.59
17:16-18.	1.25	25.20	4.38	11.11	79.98	0.94	1.57	4.23	12.52	3.29	8.76	13.30	15.65	79.04
17:18-20.	2.52	19.83	4.25	12.28	64.84	1.42	1.57	3.93	15.89	5.04	12.12	17.00	21.56	75.23
17:20-22.	1.35	20.57	4.38	12.14	78.90	1.52	1.35	4.38	15.34	4.55	11.97	17.03	20.40	75.02
17:22-24.	2.05	20.37	4.45	12.15	82.84	1.37	1.20	4.62	15.58	4.96	12.50	16.77	22.59	78.57
17:24-26.	1.33	21.55	4.31	11.60	82.54	1.82	1.49	5.47	14.09	4.14	10.44	15.74	18.40	75.74
17:26-28.	1.19	22.84	4.77	12.10	81.99	1.53	1.53	4.60	14.66	4.26	11.08	16.02	18.92	79.10

N.D. - Not detectable

STATION 163-8 Uncorrected major element data, Wt.% Element

	Si	Al	Fe	Mg	Ca	Na	K	Ti	Mn	P	LOI	Corg.
8:0-1.	14.89	4.41	2.27	1.74	11.92	1.96	0.28	0.261	0.03	0.24	32.40	6.36
8:1-2.	14.97	4.44	2.23	1.73	11.78	2.03	0.33	0.266	0.02	0.22	31.80	6.76
8:2-3.	14.61	4.34	2.26	1.79	11.90	1.97	0.30	0.265	0.02	0.22	33.10	6.30
8:3-4.	14.15	4.17	2.20	1.77	11.56	2.08	0.31	0.252	0.02	0.21	34.60	6.63
8:4-5.	14.32	4.26	2.23	1.77	11.53	2.11	0.31	0.256	0.02	0.21	33.70	6.80
8:5-6.	13.81	4.09	2.20	1.81	11.12	2.33	0.38	0.248	0.02	0.21	34.40	6.98
8:6-7.	14.33	4.28	2.24	1.80	10.75	2.41	0.41	0.253	0.02	0.21	33.50	7.34
8:7-8.	14.46	4.31	2.33	1.89	9.55	2.48	0.46	0.254	0.02	0.22	34.50	7.55
8:8-9.	15.43	4.67	2.28	1.86	10.95	2.30	0.38	0.273	0.02	0.24	31.10	7.49
8:9-10.	15.81	4.82	2.26	1.78	9.45	2.88	0.72	0.273	0.02	0.25	28.10	8.02
8:10-11.	14.73	4.55	2.12	1.68	8.88	2.31	0.55	0.257	0.02	0.23	30.80	7.40
8:11-12.	15.77	4.79	2.25	1.76	9.70	2.39	0.57	0.273	0.02	0.24	30.90	8.02
8:12-13.	15.34	4.68	2.21	1.78	9.87	2.56	0.57	0.267	0.03	0.23	30.90	7.86
8:13-14.	14.40	4.34	2.24	1.85	8.66	3.03	0.65	0.254	0.02	0.23	33.60	7.71
8:14-15.	14.66	4.45	2.17	1.74	10.88	2.55	0.58	0.257	0.02	0.23	31.10	7.61
8:15-16.	14.89	4.52	2.22	1.78	10.86	2.06	0.34	0.266	0.02	0.23	33.70	7.57
8:16-18.	16.15	4.93	2.51	1.97	8.75	2.43	0.61	0.290	0.03	0.24	30.80	7.93
8:18-20.	16.19	4.89	2.46	1.97	8.90	2.19	0.50	0.292	0.02	0.24	32.10	7.98
8:20-22.	15.53	4.68	2.39	1.91	8.84	2.45	0.60	0.276	0.02	0.23	32.70	8.42
8:22-24.	15.72	4.75	2.55	2.02	8.84	2.22	0.52	0.286	0.03	0.24	33.00	7.90
8:24-26.	14.97	4.53	2.53	1.98	9.70	2.21	0.51	0.272	0.02	0.24	33.20	8.08
8:26-28.	14.06	4.26	2.28	1.76	11.65	1.90	0.27	0.251	0.02	0.22	34.90	7.45
8:28-30.	14.57	4.41	2.14	1.74	11.77	2.48	0.59	0.253	0.02	0.23	31.60	7.38
8:30-32.	14.53	4.40	2.15	1.78	11.03	2.26	0.40	0.256	0.02	0.22	33.90	7.51
8:32-34.	14.71	4.44	2.46	1.96	10.55	1.93	0.38	0.271	0.02	0.22	34.40	7.49
8:34-36.	14.08	4.25	2.18	1.76	11.49	2.29	0.46	0.248	0.02	0.21	33.00	7.83
8:36-38.	14.54	4.35	2.10	1.75	10.69	2.20	0.41	0.250	0.02	0.22	34.50	8.13
8:38-40.	16.65	5.06	2.29	1.88	9.53	2.22	0.55	0.293	0.03	0.25	29.90	6.90
8:40-42.	15.95	4.76	2.41	1.99	8.53	2.46	0.59	0.279	0.03	0.24	31.80	8.45
8:42-44.	15.44	4.60	2.49	2.10	7.79	2.34	0.51	0.275	0.02	0.23	35.30	9.42
8:44-46.	15.18	4.61	2.40	2.05	10.35	2.02	0.40	0.279	0.03	0.22	33.20	8.35
8:46-48.	15.19	4.61	2.19	1.90	11.15	2.00	0.31	0.270	0.03	0.24	32.70	7.27
8:48-49.	14.53	4.41	2.24	1.76	11.73	2.46	0.54	0.260	0.02	0.23	32.30	6.92

STATION 163-8 Salt-corrected major element data, Wt.% Element

	Si	Al	Fe	Mg	Ca	Na	K	Ti	Mn	P	LOI	Corg.	Salt
8:0-1.	16.16	4.79	2.46	1.57	12.84	-0.48	0.21	0.283	0.03	0.26	32.40	6.90	7.84
8:1-2.	16.18	4.80	2.42	1.56	12.64	-0.29	0.27	0.288	0.02	0.24	31.80	7.31	7.51
8:2-3.	15.80	4.69	2.45	1.63	12.77	-0.37	0.23	0.287	0.02	0.24	33.10	6.81	7.54
8:3-4.	15.50	4.56	2.41	1.59	12.54	-0.63	0.23	0.276	0.03	0.23	34.60	7.26	8.68
8:4-5.	15.64	4.65	2.43	1.60	12.48	-0.51	0.24	0.280	0.02	0.23	33.70	7.43	8.42
8:5-6.	15.28	4.53	2.43	1.60	12.18	-0.70	0.31	0.275	0.02	0.23	34.40	7.73	9.67
8:6-7.	15.77	4.71	2.47	1.61	11.71	-0.43	0.34	0.278	0.03	0.23	33.50	8.08	9.14
8:7-8.	16.06	4.79	2.58	1.69	10.47	-0.63	0.39	0.282	0.02	0.24	34.50	8.38	9.94
8:8-9.	17.17	5.20	2.54	1.66	12.05	-0.89	0.30	0.304	0.03	0.26	31.10	8.33	10.11
8:9-10.	17.16	5.24	2.45	1.62	10.16	0.51	0.69	0.296	0.02	0.27	28.10	8.71	7.87
8:10-11.	15.99	4.93	2.30	1.51	9.54	-0.09	0.50	0.279	0.02	0.25	30.80	8.03	7.85
8:11-12.	17.02	5.17	2.42	1.61	10.37	0.17	0.53	0.294	0.03	0.26	30.90	8.65	7.30
8:12-13.	16.70	5.09	2.40	1.61	10.64	0.07	0.52	0.291	0.03	0.25	30.90	8.56	8.14
8:13-14.	15.70	4.74	2.44	1.68	9.33	0.54	0.61	0.277	0.02	0.25	33.60	8.41	8.28
8:14-15.	16.00	4.86	2.37	1.56	11.77	-0.02	0.54	0.281	0.02	0.25	31.10	8.31	8.39
8:15-16.	16.19	4.92	2.41	1.61	11.71	-0.43	0.27	0.289	0.02	0.25	33.70	8.23	8.03
8:16-18.	17.49	5.33	2.72	1.83	9.38	0.09	0.57	0.314	0.03	0.26	30.80	8.59	7.67
8:18-20.	17.57	5.30	2.67	1.82	9.55	-0.24	0.45	0.317	0.02	0.26	32.10	8.66	7.88
8:20-22.	16.94	5.10	2.61	1.75	9.53	-0.11	0.55	0.301	0.03	0.25	32.70	9.19	8.34
8:22-24.	17.17	5.19	2.79	1.87	9.55	-0.40	0.46	0.312	0.03	0.26	33.00	8.63	8.45
8:24-26.	16.35	4.95	2.77	1.82	10.49	-0.42	0.46	0.297	0.02	0.26	33.20	8.83	8.47
8:26-28.	15.22	4.61	2.47	1.60	12.51	-0.49	0.20	0.272	0.03	0.23	34.90	8.07	7.66
8:28-30.	15.75	4.77	2.32	1.59	12.62	0.20	0.55	0.273	0.02	0.25	31.60	7.98	7.49
8:30-32.	15.91	4.82	2.35	1.60	11.97	-0.43	0.33	0.280	0.02	0.25	33.90	8.22	8.66
8:32-34.	15.91	4.80	2.66	1.82	11.31	-0.39	0.33	0.293	0.02	0.24	34.40	8.10	7.49
8:34-36.	15.24	4.60	2.36	1.60	12.34	-0.03	0.40	0.268	0.03	0.23	33.00	8.47	7.59
8:36-38.	15.78	4.73	2.28	1.59	11.50	-0.23	0.35	0.271	0.02	0.24	34.50	8.83	7.89
8:38-40.	17.88	5.43	2.46	1.74	10.14	0.13	0.51	0.315	0.03	0.26	29.90	7.41	6.88
8:40-42.	17.38	5.19	2.62	1.84	9.19	-0.06	0.54	0.304	0.03	0.26	31.80	9.21	8.21
8:42-44.	17.00	5.07	2.74	1.94	8.45	-0.51	0.45	0.303	0.03	0.25	35.30	10.37	9.15
8:44-46.	16.39	4.98	2.59	1.91	11.07	-0.25	0.34	0.301	0.03	0.24	33.20	9.01	7.36
8:46-48.	16.39	4.97	2.36	1.76	11.94	-0.26	0.24	0.291	0.03	0.25	32.70	7.85	7.34
8:48-49.	15.71	4.76	2.42	1.60	12.59	0.17	0.49	0.281	0.02	0.25	32.30	7.48	7.51

STATION 163-8 Salt-free ratios to aluminium

	Si/Al	Fe/Al	Mg/Al	Ca/Al	Na/Al	K/Al	Ti/Al	Mn/Al	P/Al	Corg./Al
8:0-1.	3.374	0.514	0.329	2.681	-0.100	0.043	0.059	0.006	0.055	1.441
8:1-2.	3.368	0.503	0.326	2.630	-0.061	0.056	0.060	0.005	0.050	1.521
8:2-3.	3.368	0.521	0.348	2.722	-0.079	0.049	0.061	0.005	0.051	1.452
8:3-4.	3.397	0.527	0.348	2.750	-0.138	0.051	0.060	0.006	0.051	1.591
8:4-5.	3.362	0.523	0.343	2.682	-0.110	0.052	0.060	0.004	0.050	1.596
8:5-6.	3.375	0.538	0.354	2.690	-0.154	0.068	0.061	0.005	0.050	1.706
8:6-7.	3.347	0.524	0.342	2.485	-0.091	0.073	0.059	0.006	0.049	1.715
8:7-8.	3.355	0.540	0.354	2.188	-0.131	0.082	0.059	0.005	0.050	1.752
8:8-9.	3.305	0.489	0.319	2.319	-0.171	0.058	0.058	0.005	0.050	1.604
8:9-10.	3.278	0.468	0.309	1.939	0.098	0.131	0.057	0.005	0.051	1.662
8:10-11.	3.242	0.467	0.306	1.934	-0.019	0.102	0.057	0.005	0.051	1.628
8:11-12.	3.292	0.469	0.311	2.006	0.033	0.102	0.057	0.005	0.050	1.674
8:12-13.	3.281	0.472	0.317	2.089	0.015	0.102	0.057	0.006	0.048	1.681
8:13-14.	3.315	0.515	0.355	1.971	0.114	0.129	0.058	0.005	0.052	1.775
8:14-15.	3.296	0.487	0.322	2.424	-0.004	0.111	0.058	0.005	0.051	1.711
8:15-16.	3.293	0.490	0.327	2.381	-0.087	0.055	0.059	0.005	0.051	1.674
8:16-18.	3.278	0.510	0.343	1.758	0.017	0.107	0.059	0.005	0.049	1.610
8:18-20.	3.314	0.504	0.344	1.802	-0.044	0.085	0.060	0.005	0.048	1.634
8:20-22.	3.319	0.511	0.342	1.868	-0.021	0.108	0.059	0.005	0.049	1.800
8:22-24.	3.307	0.537	0.360	1.839	-0.078	0.089	0.060	0.006	0.050	1.662
8:24-26.	3.301	0.558	0.368	2.117	-0.085	0.093	0.060	0.005	0.053	1.782
8:26-28.	3.301	0.535	0.347	2.713	-0.105	0.044	0.059	0.006	0.051	1.749
8:28-30.	3.300	0.486	0.332	2.645	0.043	0.115	0.057	0.004	0.052	1.672
8:30-32.	3.301	0.488	0.332	2.483	-0.088	0.069	0.058	0.005	0.051	1.706
8:32-34.	3.312	0.554	0.378	2.356	-0.082	0.068	0.061	0.005	0.050	1.686
8:34-36.	3.314	0.513	0.349	2.685	-0.007	0.088	0.058	0.006	0.051	1.843
8:36-38.	3.338	0.481	0.335	2.433	-0.049	0.075	0.057	0.005	0.050	1.867
8:38-40.	3.293	0.453	0.321	1.868	0.023	0.094	0.058	0.005	0.048	1.365
8:40-42.	3.350	0.506	0.355	1.771	-0.011	0.104	0.059	0.006	0.050	1.774
8:42-44.	3.354	0.540	0.383	1.668	-0.100	0.089	0.060	0.005	0.049	2.046
8:44-46.	3.294	0.520	0.385	2.226	-0.050	0.069	0.061	0.006	0.048	1.812
8:46-48.	3.295	0.475	0.354	2.401	-0.053	0.049	0.059	0.006	0.051	1.578
8:48-49.	3.297	0.509	0.336	2.643	0.036	0.103	0.059	0.005	0.052	1.571

STATION 163-8 Uncorrected trace element data, ppm

	Mo	Zr	Y	Sr	Rb	Th	Pb	As	Zn	Cu	Ni	Cr	V	Ba	S	I	Br	Cl
8:0-1.	N.D.	72	17	656	40	3	11	29	69	23	56	120	70	257	8588	482	752	23913
8:1-2.	N.D.	71	17	657	40	6	12	25	68	22	57	118	75	250	9134	473	753	22925
8:2-3.	1	71	17	645	40	6	12	27	71	22	59	122	86	253	8959	478	780	22137
8:3-4.	3	67	17	630	41	5	9	26	70	24	59	121	96	238	9844	473	838	26325
8:4-5.	2	69	17	625	41	5	10	24	72	25	60	122	88	236	9184	490	836	24934
8:5-6.	2	67	16	591	41	2	9	20	73	25	66	117	102	235	9669	508	974	28717
8:6-7.	3	70	18	575	42	6	12	20	78	28	68	127	119	241	9585	542	915	26989
8:7-8.	8	72	17	512	43	7	9	21	78	30	68	131	137	278	10334	557	851	29213
8:8-9.	8	78	19	532	45	7	11	29	84	35	74	147	136	303	10632	537	881	30839
8:9-10.	2	79	19	542	43	3	9	24	77	30	69	142	98	312	9156	478	697	23898
8:10-11.	3	74	18	515	40	4	6	15	74	26	68	139	97	325	9085	468	678	22654
8:11-12.	5	78	20	546	42	3	7	17	74	29	73	143	108	336	9254	514	719	22619
8:12-13.	5	76	19	553	41	2	10	23	75	30	72	141	110	330	9741	514	751	25241
8:13-14.	2	71	18	538	37	5	6	16	67	24	68	128	99	265	9596	530	708	25045
8:14-15.	6	73	18	594	40	5	8	30	70	27	70	135	110	306	10077	493	743	24942
8:15-16.	4	74	19	587	40	5	7	21	73	26	68	135	105	307	9751	455	710	23817
8:16-18.	5	82	20	502	46	5	9	22	74	30	78	148	135	315	10084	449	761	21712
8:18-20.	5	81	20	507	44	5	7	18	77	30	73	143	114	329	10409	449	750	23040
8:20-22.	7	78	20	506	43	6	6	26	76	31	73	143	139	306	10851	455	762	24496
8:22-24.	7	78	19	497	44	6	8	22	79	29	74	140	154	323	11866	443	767	24150
8:24-26.	12	73	18	535	45	5	7	24	78	29	70	132	160	284	11574	421	793	23379
8:26-28.	12	70	18	610	40	5	6	23	73	28	70	129	132	311	12300	436	670	22365
8:28-30.	7	73	19	613	40	2	7	33	70	28	71	138	106	297	11629	434	637	22399
8:30-32.	10	73	18	581	39	7	4	31	68	25	68	132	112	322	11962	410	664	24831
8:32-34.	8	72	20	565	44	3	11	25	80	28	74	139	128	277	11762	423	736	20742
8:34-36.	9	69	17	612	39	6	5	29	72	31	73	133	128	302	11685	450	641	22576
8:36-38.	10	72	17	574	38	5	7	24	71	31	76	140	124	337	11943	436	676	23995
8:38-40.	1	82	21	563	41	6	7	23	75	28	69	146	100	337	9885	407	591	19919
8:40-42.	12	78	20	498	42	4	6	24	85	33	82	150	133	353	12691	439	725	23434
8:42-44.	24	75	19	467	42	5	6	24	87	38	93	155	196	343	14739	430	780	26681
8:44-46.	7	74	19	557	41	N.D.	6	26	77	30	76	143	144	276	11558	408	650	20381
8:46-48.	8	74	19	608	38	6	6	20	73	28	69	137	113	313	11076	399	592	20898
8:48-49.	11	73	18	630	38	3	5	26	71	29	71	135	124	306	11901	398	593	23660

N.D. - Not detectable

STATION 163-8 Salt-corrected trace element data, ppm

	Mo	Zr	Y	Sr	Rb	Th	Pb	As	Zn	Cu	Ni	Cr	V	Ba	S	I	Br	Cl
8:0-1.	N.D.	78	18	712	43	3	12	31	75	25	61	130	76	279	7107	523	654	23913
8:1-2.	N.D.	77	18	710	43	6	13	27	74	24	62	128	81	270	7765	511	660	22925
8:2-3.	1	77	18	698	43	6	13	29	77	24	64	132	93	274	7569	517	689	22137
8:3-4.	3	73	19	690	45	5	10	28	77	26	65	133	105	261	8308	518	737	26325
8:4-5.	2	75	19	682	45	5	11	26	79	27	66	133	96	258	7638	535	738	24934
8:5-6.	2	74	18	654	45	2	10	22	80	28	73	130	113	260	7921	562	875	28717
8:6-7.	3	77	20	633	46	7	13	22	86	31	75	140	131	265	7934	597	816	26989
8:7-8.	9	80	19	569	48	8	10	23	87	33	76	145	152	309	8605	618	735	29213
8:8-9.	9	87	21	592	50	8	12	32	93	39	82	164	151	337	8904	597	766	30839
8:9-10.	2	86	21	588	47	3	10	26	84	33	75	154	106	339	7717	519	594	23898
8:10-11.	3	80	20	559	43	4	7	16	80	28	74	151	105	353	7644	508	574	22654
8:11-12.	5	84	22	589	45	3	8	18	80	31	79	154	117	362	7935	554	626	22619
8:12-13.	5	83	21	602	45	2	11	25	82	33	78	153	120	359	8300	560	649	25241
8:13-14.	2	77	20	587	40	5	7	17	73	26	74	140	108	289	8115	578	600	25045
8:14-15.	7	80	20	648	44	5	9	33	76	29	76	147	120	334	8619	538	637	24942
8:15-16.	4	80	21	638	43	5	8	23	79	28	74	147	114	334	8332	495	606	23817
8:16-18.	5	89	22	544	50	5	10	24	80	32	84	160	146	341	8762	486	666	21712
8:18-20.	5	88	22	550	48	5	8	20	84	33	79	155	124	357	9075	487	652	23040
8:20-22.	8	85	22	552	47	7	7	28	83	34	80	156	152	334	9473	496	658	24496
8:22-24.	8	85	21	543	48	7	9	24	86	32	81	153	168	353	10561	484	662	24150
8:24-26.	13	80	20	585	49	5	8	26	85	32	76	144	175	310	10239	460	691	23379
8:26-28.	13	76	19	661	43	5	6	25	79	30	76	140	143	337	11164	472	568	22365
8:28-30.	8	79	21	663	43	2	8	36	76	30	77	149	115	321	10465	469	535	22399
8:30-32.	11	80	20	636	43	8	4	34	74	27	74	145	123	353	10631	449	547	24831
8:32-34.	9	78	22	611	48	3	12	27	86	30	80	150	138	299	10609	457	642	20742
8:34-36.	10	75	18	662	42	6	5	31	78	34	79	144	139	327	10509	487	538	22576
8:36-38.	11	78	18	623	41	5	8	26	77	34	83	152	135	366	10739	473	571	23995
8:38-40.	1	88	23	605	44	6	8	25	81	30	74	157	107	362	8694	437	494	19919
8:40-42.	13	85	22	543	46	4	7	26	93	36	89	163	145	385	11501	478	620	23434
8:42-44.	26	83	21	514	46	6	7	26	96	42	102	171	216	378	13605	473	667	26681
8:44-46.	8	80	21	601	44	N.D.	6	28	83	32	82	154	155	298	10411	440	551	20381
8:46-48.	9	80	21	656	41	6	6	22	79	30	74	148	122	338	9894	451	488	20898
8:48-49.	12	79	19	681	41	3	5	28	77	31	77	146	134	331	10756	450	487	23660

N.D. - Not detectable

STATION 163-8 Salt-free trace element ratios to aluminium (x10-4)

	Mo/Al	Zr/Al	Y/Al	Rb/Al	Sr/Al	Th/Al	Pb/Al	As/Al	Zn/Al	Cu/Al	Ni/Al	Cr/Al	V/Al	Ba/Al
8:0-1.	N.D.	16.29	3.76	8.98	148.69	0.63	2.51	6.47	15.66	5.22	12.74	27.15	15.87	58.27
8:1-2.	N.D.	16.03	3.75	8.95	147.77	1.25	2.71	5.62	15.40	4.99	12.90	26.64	16.86	56.19
8:2-3.	0.21	16.41	3.84	9.17	148.77	1.28	2.77	6.18	16.41	5.12	13.64	28.13	19.82	58.40
8:3-4.	0.66	16.00	4.16	9.86	151.25	1.10	2.19	6.14	16.88	5.70	14.25	29.15	23.02	57.21
8:4-5.	0.43	16.12	4.08	9.67	146.61	1.07	2.36	5.59	16.98	5.80	14.19	28.59	20.64	55.46
8:5-6.	0.44	16.34	3.97	9.94	144.40	0.44	2.21	4.86	17.66	6.18	16.12	28.70	24.95	57.41
8:6-7.	0.64	16.34	4.24	9.76	134.35	1.49	2.76	4.67	18.25	6.58	15.92	29.71	27.80	56.24
8:7-8.	1.88	16.72	3.97	10.03	118.90	1.67	2.09	4.81	18.18	6.90	15.88	30.30	31.76	64.57
8:8-9.	1.73	16.75	4.04	9.62	113.95	1.54	2.31	6.16	17.90	7.51	15.78	31.57	29.07	64.87
8:9-10.	0.38	16.42	4.01	8.97	112.27	0.57	1.91	4.96	16.04	6.30	14.32	29.41	20.24	64.73
8:10-11.	0.61	16.22	4.06	8.72	113.34	0.81	1.42	3.24	16.22	5.68	15.00	30.62	21.29	71.57
8:11-12.	0.97	16.25	4.26	8.71	113.96	0.58	1.55	3.48	15.48	6.00	15.29	29.80	22.64	70.04
8:12-13.	0.98	16.30	4.12	8.84	118.24	0.39	2.16	4.91	16.11	6.48	15.32	30.05	23.57	70.51
8:13-14.	0.42	16.26	4.22	8.45	123.94	1.06	1.48	3.59	15.41	5.49	15.62	29.56	22.80	61.02
8:14-15.	1.44	16.48	4.12	9.06	133.46	1.03	1.85	6.80	15.65	5.97	15.65	30.28	24.71	68.79
8:15-16.	0.81	16.27	4.27	8.75	129.76	1.02	1.63	4.68	16.07	5.69	15.05	29.90	23.19	67.93
8:16-18.	0.94	16.69	4.12	9.37	101.98	0.94	1.87	4.50	15.01	6.00	15.75	30.00	27.37	63.93
8:18-20.	0.94	16.59	4.15	9.05	103.72	0.94	1.51	3.77	15.84	6.22	14.90	29.23	23.38	67.32
8:20-22.	1.57	16.65	4.31	9.21	108.16	1.37	1.37	5.49	16.26	6.66	15.68	30.57	29.78	65.44
8:22-24.	1.54	16.37	4.04	9.25	104.59	1.35	1.73	4.62	16.56	6.16	15.60	29.47	32.36	67.99
8:24-26.	2.62	16.15	4.04	9.89	118.12	1.01	1.62	5.25	17.16	6.46	15.35	29.08	35.34	62.59
8:26-28.	2.82	16.48	4.12	9.32	143.31	1.08	1.30	5.42	17.13	6.50	16.48	30.35	31.00	73.07
8:28-30.	1.68	16.56	4.40	9.01	138.95	0.42	1.68	7.54	15.93	6.29	16.14	31.23	24.10	67.28
8:30-32.	2.28	16.60	4.15	8.92	131.94	1.66	0.83	7.05	15.35	5.60	15.35	30.08	25.52	73.23
8:32-34.	1.87	16.24	4.58	10.00	127.25	0.62	2.50	5.62	17.91	6.25	16.66	31.24	28.74	62.27
8:34-36.	2.18	16.32	3.92	9.14	144.01	1.31	1.09	6.74	16.97	7.40	17.19	31.33	30.24	71.13
8:36-38.	2.33	16.50	3.81	8.67	131.77	1.06	1.69	5.50	16.29	7.19	17.55	32.15	28.55	77.41
8:38-40.	0.18	16.21	4.24	8.10	111.43	1.11	1.47	4.60	14.92	5.53	13.63	28.92	19.71	66.67
8:40-42.	2.51	16.38	4.24	8.87	104.67	0.77	1.35	5.01	17.93	6.94	17.16	31.42	27.95	74.21
8:42-44.	5.13	16.38	4.14	9.08	101.45	1.18	1.38	5.13	18.95	8.29	20.13	33.75	42.63	74.61
8:44-46.	1.61	16.08	4.22	8.84	120.80	N.D.	1.21	5.63	16.68	6.43	16.48	30.95	31.15	59.90
8:46-48.	1.81	16.09	4.22	8.24	131.91	1.21	1.21	4.42	15.89	6.03	14.88	29.76	24.53	67.97
8:48-49.	2.52	16.58	3.99	8.61	142.95	0.63	1.05	5.88	16.16	6.51	16.16	30.65	28.13	69.48

N.D. - Not detectable

STATION 163-11 Uncorrected major element data, Wt.%

	Si	Al	Fe	Mg	Ca	Na	K	Ti	Mn	P	LOI
11:0-1.	10.86	3.18	1.22	0.73	22.58	1.09	0.28	0.15	0.02	0.22	31.10
11:1-2.	9.89	2.89	1.11	0.64	23.61	1.01	0.24	0.14	0.01	0.21	32.20
11:2-3.	9.75	2.86	1.11	0.66	23.68	0.99	0.23	0.14	0.01	0.20	32.20
11:3-4.	10.88	3.22	1.25	0.77	22.31	1.17	0.26	0.15	0.01	0.19	31.20
11:4-5.	12.20	3.66	1.36	0.88	20.52	1.36	0.32	0.18	0.02	0.19	29.20
11:5-6.	12.50	3.73	1.43	0.87	19.85	1.35	0.31	0.18	0.02	0.19	30.10
11:6-7.	12.49	3.74	1.42	0.90	19.74	1.42	0.31	0.18	0.02	0.19	29.70
11:7-8.	12.10	3.59	1.41	0.86	20.64	1.41	0.33	0.18	0.01	0.19	29.60
11:8-9.	12.49	3.73	1.46	0.86	20.19	1.44	0.35	0.18	0.02	0.19	28.80
11:9-10.	10.69	3.17	1.31	0.76	22.55	1.17	0.27	0.15	0.01	0.19	31.40
11:10-12.	10.52	3.12	1.26	0.75	22.64	1.14	0.26	0.15	0.01	0.19	31.70
11:12-14.	10.46	3.12	1.33	0.73	22.42	1.16	0.27	0.15	0.02	0.23	31.50
11:14-16.	9.67	2.85	1.21	0.69	23.54	1.04	0.22	0.14	0.01	0.22	32.30
11:16-18.	9.17	2.75	1.21	0.72	24.03	0.98	0.21	0.14	0.01	1.03	31.20
11:18-20.	9.38	2.80	1.19	0.71	24.01	1.00	0.21	0.14	0.01	0.25	32.60
11:20-22.	9.04	2.71	1.19	0.77	24.26	0.98	0.21	0.13	0.01	0.23	32.90
11:22-24.	8.24	2.46	1.12	0.74	25.11	0.90	0.19	0.12	0.01	0.27	33.50

STATION 163-11 Salt-corrected major element data, Wt.% Element

	Si	Al	Fe	Mg	Ca	Na	K	Ti	Mn	P	LOI	Salt
11:0-1.	11.17	3.27	1.26	0.65	23.18	0.26	0.25	0.15	0.02	0.23	31.10	2.76
11:1-2.	10.16	2.97	1.14	0.56	24.23	0.19	0.22	0.14	0.02	0.22	32.20	2.69
11:2-3.	10.05	2.94	1.15	0.57	24.35	0.11	0.21	0.14	0.01	0.21	32.20	2.90
11:3-4.	11.24	3.33	1.29	0.68	23.00	0.20	0.24	0.16	0.02	0.20	31.20	3.20
11:4-5.	12.61	3.78	1.40	0.78	21.16	0.38	0.30	0.19	0.02	0.20	29.20	3.22
11:5-6.	12.95	3.87	1.48	0.77	20.52	0.32	0.28	0.19	0.02	0.19	30.10	3.44
11:6-7.	12.93	3.87	1.47	0.80	20.39	0.39	0.28	0.19	0.02	0.19	29.70	3.41
11:7-8.	12.50	3.71	1.45	0.77	21.28	0.45	0.30	0.19	0.02	0.20	29.60	3.20
11:8-9.	12.90	3.85	1.51	0.76	20.82	0.47	0.32	0.19	0.02	0.19	28.80	3.19
11:9-10.	11.02	3.27	1.35	0.67	23.20	0.28	0.25	0.16	0.02	0.20	31.40	2.95
11:10-12.	10.85	3.22	1.30	0.66	23.33	0.20	0.23	0.15	0.02	0.20	31.70	3.10
11:12-14.	10.81	3.22	1.37	0.63	23.14	0.17	0.24	0.16	0.02	0.23	31.50	3.26
11:14-16.	10.00	2.95	1.26	0.59	24.30	0.03	0.19	0.14	0.02	0.23	32.30	3.29
11:16-18.	9.45	2.83	1.25	0.63	24.72	0.09	0.18	0.14	0.02	1.06	31.20	2.92
11:18-20.	9.69	2.89	1.23	0.61	24.76	0.03	0.19	0.14	0.02	0.26	32.60	3.18
11:20-22.	9.33	2.80	1.23	0.68	25.01	0.03	0.19	0.14	0.01	0.24	32.90	3.14
11:22-24.	8.48	2.53	1.16	0.65	25.80	0.04	0.16	0.12	0.02	0.27	33.50	2.82

STATION 163-11 Salt-free ratios to aluminium

	Si/Al	Fe/Al	Mg/Al	Ca/Al	Na/Al	K/Al	Ti/Al	Mn/Al	P/Al
11:0-1.	3.416	0.385	0.199	7.089	0.080	0.076	0.046	0.006	0.070
11:1-2.	3.421	0.384	0.189	8.158	0.064	0.074	0.047	0.007	0.074
11:2-3.	3.418	0.391	0.194	8.282	0.037	0.071	0.048	0.003	0.071
11:3-4.	3.375	0.387	0.204	6.907	0.060	0.072	0.048	0.006	0.060
11:4-5.	3.336	0.370	0.206	5.598	0.101	0.079	0.050	0.005	0.053
11:5-6.	3.346	0.382	0.199	5.302	0.083	0.072	0.049	0.005	0.049
11:6-7.	3.341	0.380	0.207	5.269	0.101	0.072	0.049	0.005	0.049
11:7-8.	3.369	0.391	0.208	5.736	0.121	0.081	0.051	0.005	0.054
11:8-9.	3.351	0.392	0.197	5.408	0.122	0.083	0.049	0.005	0.049
11:9-10.	3.370	0.413	0.205	7.095	0.086	0.076	0.049	0.006	0.061
11:10-12.	3.370	0.404	0.205	7.245	0.062	0.071	0.047	0.006	0.062
11:12-14.	3.357	0.425	0.196	7.186	0.053	0.075	0.050	0.006	0.071
11:14-16.	3.390	0.427	0.200	8.237	0.010	0.064	0.047	0.007	0.078
11:16-18.	3.339	0.442	0.223	8.735	0.032	0.064	0.049	0.007	0.375
11:18-20.	3.353	0.426	0.211	8.567	0.010	0.066	0.048	0.007	0.090
11:20-22.	3.332	0.439	0.243	8.932	0.011	0.068	0.050	0.004	0.086
11:22-24.	3.352	0.458	0.257	10.198	0.016	0.063	0.047	0.008	0.107

STATION 163-11 Uncorrected trace element data, ppm

	I	Br	Mo	Zr	Y	Sr	Rb	Th	Pb	As	Zn	Cu	Ni	Cr	V	Ba
11:0-1.	412	196	2	67	20	842	19	5	8	N.D.	24	9	25	78	32	153
11:1-2.	378	173	N.D.	64	20	852	19	6	8	N.D.	21	6	22	76	27	148
11:2-3.	351	175	2	68	19	852	18	2	11	N.D.	21	6	25	78	28	144
11:3-4.	349	204	N.D.	71	18	842	21	3	7	N.D.	24	8	26	82	36	168
11:4-5.	365	233	1	75	19	817	25	4	8	N.D.	30	9	30	92	40	217
11:5-6.	380	249	3	78	19	801	25	1	10	N.D.	31	10	31	90	45	200
11:6-7.	377	252	2	77	19	797	26	N.D.	10	N.D.	30	11	32	91	43	198
11:7-8.	353	226	2	79	20	821	24	5	9	N.D.	29	9	30	91	44	190
11:8-9.	320	224	2	80	19	809	23	7	11	N.D.	29	10	31	92	42	194
11:9-10.	345	191	2	75	19	845	21	3	7	N.D.	25	8	28	86	40	170
11:10-12.	326	190	2	70	18	841	21	5	8	N.D.	24	8	27	87	37	155
11:12-14.	301	194	2	69	19	839	21	3	7	N.D.	26	8	29	86	44	156
11:14-16.	291	180	2	65	19	857	19	1	7	N.D.	24	7	26	84	35	119
11:16-18.	232	161	N.D.	66	20	955	17	7	3	N.D.	22	7	28	83	43	124
11:18-20.	252	163	2	67	20	871	19	1	9	N.D.	24	8	26	79	37	135
11:20-22.	201	154	2	62	18	920	19	3	10	N.D.	37	6	27	79	51	146
11:22-24.	213	139	1	58	18	963	16	5	5	N.D.	20	7	29	78	47	127

N.D. - Not detectable

STATION 163-11 Salt-corrected trace element data, ppm

	I	Br	Mo	Zr	Y	Sr	Rb	Th	Pb	As	Zn	Cu	Ni	Cr	V	Ba
11:0-1.	424	148	2	69	21	866	20	5	8	N.D.	25	9	26	80	33	157
11:1-2.	388	126	N.D.	66	21	876	20	6	8	N.D.	22	6	23	78	28	152
11:2-3.	361	124	2	70	20	877	19	2	11	N.D.	22	6	26	80	29	138
11:3-4.	361	150	N.D.	73	19	870	22	3	7	N.D.	25	8	27	85	37	174
11:4-5.	377	179	1	77	20	844	26	4	8	N.D.	31	9	31	95	41	224
11:5-6.	394	193	3	81	20	830	26	1	10	N.D.	32	10	32	93	47	207
11:6-7.	390	196	2	80	20	825	27	N.D.	10	N.D.	31	11	33	94	45	205
11:7-8.	365	172	2	82	21	848	25	5	9	N.D.	30	9	31	94	45	196
11:8-9.	331	170	2	83	20	836	24	7	11	N.D.	30	10	32	95	43	200
11:9-10.	355	141	2	77	20	871	22	3	7	N.D.	26	8	29	89	41	175
11:10-12.	336	137	2	72	19	868	22	5	8	N.D.	25	8	28	90	38	160
11:12-14.	311	139	2	71	20	867	22	3	7	N.D.	27	8	30	89	45	161
11:14-16.	301	123	2	67	20	886	20	1	7	N.D.	25	7	27	87	36	123
11:16-18.	239	111	N.D.	68	21	984	18	7	3	N.D.	23	7	29	85	44	128
11:18-20.	260	108	2	69	21	900	20	1	9	N.D.	25	8	27	82	38	139
11:20-22.	208	99	2	64	19	950	20	3	10	N.D.	38	6	28	82	53	151
11:22-24.	219	89	1	60	19	991	16	5	5	N.D.	21	7	30	80	48	131

N.D. - Not detectable

STATION 163-11 Salt-free trace element ratios to aluminium (x10-4)

	Mo/Al	Zr/Al	Y/Al	Sr/Al	Rb/Al	Th/Al	Pb/Al	As/Al	Zn/Al	Cu/Al	Ni/Al	Cr/Al	V/Al	Ba/Al	K/Rb
11:0-1.	0.61	21.10	6.42	264.83	6.12	1.53	2.45	N.D.	7.65	2.75	7.95	24.46	10.09	48.01	125.00
11:1-2.	N.D.	22.22	7.07	294.95	6.73	2.02	2.69	N.D.	7.41	2.02	7.74	26.26	9.43	51.18	110.00
11:2-3.	0.68	23.81	6.80	298.30	6.46	0.68	3.74	N.D.	7.48	2.04	8.84	27.21	9.86	46.94	110.53
11:3-4.	N.D.	21.92	5.71	261.26	6.61	0.90	2.10	N.D.	7.51	2.40	8.11	25.53	11.11	52.25	109.09
11:4-5.	0.26	20.37	5.29	223.28	6.88	1.06	2.12	N.D.	8.20	2.38	8.20	25.13	10.85	59.26	115.38
11:5-6.	0.78	20.93	5.17	214.47	6.72	0.26	2.58	N.D.	8.27	2.58	8.27	24.03	12.14	53.49	107.69
11:6-7.	0.52	20.67	5.17	213.18	6.98	N.D.	2.58	N.D.	8.01	2.84	8.53	24.29	11.63	52.97	103.70
11:7-8.	0.54	22.10	5.66	228.57	6.74	1.35	2.43	N.D.	8.09	2.43	8.36	25.34	12.13	52.83	120.00
11:8-9.	0.52	21.56	5.19	217.14	6.23	1.82	2.86	N.D.	7.79	2.60	8.31	24.68	11.17	51.95	133.33
11:9-10.	0.61	23.55	6.12	266.36	6.73	0.92	2.14	N.D.	7.95	2.45	8.87	27.22	12.54	53.52	113.64
11:10-12.	0.62	22.36	5.90	269.57	6.83	1.55	2.48	N.D.	7.76	2.48	8.70	27.95	11.80	49.69	104.55
11:12-14.	0.62	22.05	6.21	269.25	6.83	0.93	2.17	N.D.	8.39	2.48	9.32	27.64	13.98	50.00	109.09
11:14-16.	0.68	22.71	6.78	300.34	6.78	0.34	2.37	N.D.	8.47	2.37	9.15	29.49	12.20	41.69	95.00
11:16-18.	N.D.	24.03	7.42	347.70	6.36	2.47	1.06	N.D.	8.13	2.47	10.25	30.04	15.55	45.23	100.00
11:18-20.	0.69	23.88	7.27	311.42	6.92	0.35	3.11	N.D.	8.65	2.77	9.34	28.37	13.15	48.10	95.00
11:20-22.	0.71	22.86	6.79	339.29	7.14	1.07	3.57	N.D.	13.57	2.14	10.00	29.29	18.93	53.93	95.00
11:22-24.	0.40	23.72	7.51	391.70	6.32	1.98	1.98	N.D.	8.30	2.77	11.86	31.62	18.97	51.78	100.00

N.D. - Not detectable

STATION 163-13 Uncorrected major element data, Wt.%

	Si	Al	Fe	Mg	Ca	Na	K	Ti	Mn	P	LOI
13:1-2.	13.94	2.62	9.35	2.40	12.73	0.99	1.23	0.17	0.02	0.70	21.80
13:2-3.	13.74	2.62	8.34	2.97	12.98	1.03	1.07	0.17	0.02	0.41	24.20
13:3-4.	13.34	2.48	8.32	2.73	13.21	0.99	1.09	0.16	0.02	0.40	24.00
13:4-5.	13.22	2.68	7.46	2.81	12.85	1.04	0.99	0.17	0.02	0.44	24.40
13:5-6.	13.84	2.86	6.95	2.66	13.64	1.10	0.97	0.18	0.02	0.32	25.10
13:6-7.	14.74	3.33	6.25	2.95	12.58	1.23	1.12	0.20	0.02	0.49	23.60
13:7-8.	14.32	3.15	6.33	2.93	12.96	1.15	1.08	0.20	0.02	0.49	24.90
13:8-9.	14.05	3.14	7.03	2.76	13.22	1.23	0.97	0.20	0.03	0.37	24.70
13:9-10.	15.01	3.54	6.25	2.87	11.63	1.33	1.15	0.21	0.03	0.33	23.90
13:10-11.	13.69	2.82	7.24	3.01	13.10	1.18	1.10	0.18	0.03	0.35	24.60
13:11-12.	14.29	3.46	5.81	3.15	12.70	1.33	1.00	0.21	0.02	0.93	24.30
13:12-13.	16.94	5.10	3.67	4.16	8.01	1.81	1.13	0.28	0.03	0.32	25.80
13:13-14.	12.96	2.68	6.80	2.43	14.76	1.10	1.00	0.17	0.01	1.28	23.70
13:14-15.	16.21	4.63	4.29	3.83	8.98	1.58	1.11	0.26	0.03	0.30	25.20
13:15-16.	15.81	4.50	4.30	3.85	9.51	1.54	1.08	0.25	0.02	0.45	25.10
13:16-17.	15.90	4.56	4.32	3.74	9.29	1.62	1.04	0.25	0.03	0.41	25.70
13:17-18.	14.38	3.13	6.78	2.54	12.37	1.20	1.32	0.19	0.01	0.35	23.00
13:18-19.	15.97	4.60	4.20	3.84	9.17	1.62	1.06	0.26	0.02	0.31	25.80
13:19-20.	15.20	3.93	5.25	3.19	11.37	1.47	1.26	0.22	0.02	0.51	22.10
13:20-21.	15.10	3.61	6.25	2.84	11.05	1.39	1.42	0.21	0.02	0.40	21.20
13:21-22.	16.95	5.24	3.75	4.16	7.23	2.04	1.18	0.28	0.03	0.31	24.00
13:22-24.	16.52	5.04	3.73	4.24	7.80	1.89	1.16	0.27	0.03	0.32	23.40
13:24-26.	17.12	5.32	3.54	4.31	7.54	2.05	1.25	0.28	0.03	0.31	22.90

STATION 163-13 Salt-corrected major element data, Wt.% Element

	Si	Al	Fe	Mg	Ca	Na	K	Ti	Mn	P	LOI	Salt
13:1-2.	14.19	2.67	9.52	2.38	12.94	0.47	1.23	0.18	0.02	0.71	21.80	1.73
13:2-3.	13.95	2.66	8.47	2.96	13.16	0.57	1.07	0.17	0.02	0.42	24.20	1.51
13:3-4.	13.64	2.54	8.50	2.71	13.48	0.33	1.09	0.17	0.02	0.41	24.00	2.18
13:4-5.	13.45	2.73	7.59	2.79	13.05	0.51	0.99	0.18	0.02	0.45	24.40	1.75
13:5-6.	14.17	2.93	7.11	2.63	13.95	0.38	0.97	0.18	0.02	0.33	25.10	2.38
13:6-7.	15.18	3.43	6.43	2.93	12.91	0.36	1.12	0.21	0.02	0.50	23.60	2.86
13:7-8.	14.68	3.23	6.49	2.91	13.26	0.42	1.08	0.20	0.02	0.51	24.90	2.42
13:8-9.	14.40	3.22	7.20	2.74	13.52	0.50	0.97	0.20	0.03	0.38	24.70	2.43
13:9-10.	15.37	3.63	6.39	2.85	11.87	0.64	1.15	0.21	0.03	0.34	23.90	2.30
13:10-11.	14.14	2.91	7.48	2.99	13.50	0.21	1.10	0.19	0.03	0.36	24.60	3.21
13:11-12.	14.64	3.54	5.96	3.14	12.98	0.61	0.99	0.21	0.02	0.95	24.30	2.41
13:12-13.	17.46	5.25	3.79	4.18	8.21	0.92	1.13	0.29	0.03	0.33	25.80	2.99
13:13-14.	13.43	2.78	7.05	2.38	15.25	0.03	0.99	0.17	0.02	1.33	23.70	3.49
13:14-15.	16.82	4.80	4.46	3.84	9.28	0.49	1.11	0.27	0.02	0.31	25.20	3.61
13:15-16.	16.42	4.67	4.47	3.85	9.83	0.42	1.08	0.26	0.02	0.47	25.10	3.72
13:16-17.	16.60	4.76	4.51	3.74	9.64	0.35	1.03	0.26	0.02	0.42	25.70	4.18
13:17-18.	14.77	3.21	6.97	2.51	12.68	0.40	1.33	0.20	0.02	0.35	23.00	2.67
13:18-19.	16.69	4.80	4.39	3.84	9.52	0.33	1.06	0.27	0.02	0.32	25.80	4.26
13:19-20.	15.72	4.07	5.43	3.17	11.71	0.47	1.27	0.24	0.02	0.52	22.10	3.32
13:20-21.	15.59	3.73	6.45	2.81	11.37	0.44	1.43	0.22	0.02	0.41	21.20	3.13
13:21-22.	17.83	5.51	3.95	4.19	7.54	0.55	1.18	0.30	0.03	0.33	24.00	4.95
13:22-24.	17.51	5.34	3.95	4.27	8.20	0.19	1.17	0.29	0.03	0.34	23.40	5.61
13:24-26.	17.95	5.58	3.71	4.34	7.84	0.67	1.25	0.30	0.03	0.32	22.90	4.61

STATION 163-13 Salt-free ratios to aluminium

	Si/Al	Fe/Al	Mg/Al	Ca/Al	Na/Al	K/Al	Ti/Al	Mn/Al	P/Al
13:1-2.	5.315	3.566	0.891	4.846	0.176	0.461	0.067	0.007	0.266
13:2-3.	5.244	3.184	1.113	4.947	0.214	0.402	0.064	0.008	0.158
13:3-4.	5.370	3.346	1.067	5.307	0.130	0.429	0.067	0.008	0.161
13:4-5.	4.927	2.780	1.022	4.780	0.187	0.363	0.066	0.007	0.165
13:5-6.	4.836	2.427	0.898	4.761	0.130	0.331	0.061	0.007	0.113
13:6-7.	4.426	1.875	0.854	3.764	0.105	0.327	0.061	0.006	0.146
13:7-8.	4.545	2.009	0.901	4.105	0.130	0.334	0.062	0.006	0.158
13:8-9.	4.472	2.236	0.851	4.199	0.155	0.301	0.062	0.009	0.118
13:9-10.	4.234	1.760	0.785	3.270	0.176	0.317	0.058	0.008	0.094
13:10-11.	4.859	2.570	1.027	4.639	0.072	0.378	0.065	0.010	0.124
13:11-12.	4.136	1.684	0.887	3.667	0.172	0.280	0.059	0.006	0.268
13:12-13.	3.326	0.722	0.796	1.564	0.175	0.215	0.055	0.006	0.063
13:13-14.	4.831	2.536	0.856	5.486	0.011	0.356	0.061	0.007	0.478
13:14-15.	3.504	0.929	0.800	1.933	0.102	0.231	0.056	0.004	0.065
13:15-16.	3.516	0.957	0.824	2.105	0.090	0.231	0.056	0.004	0.101
13:16-17.	3.487	0.947	0.786	2.025	0.074	0.216	0.055	0.004	0.088
13:17-18.	4.601	2.171	0.782	3.950	0.125	0.414	0.062	0.006	0.109
13:18-19.	3.477	0.915	0.800	1.983	0.069	0.221	0.056	0.004	0.067
13:19-20.	3.862	1.334	0.779	2.877	0.115	0.312	0.059	0.005	0.128
13:20-21.	4.180	1.729	0.753	3.048	0.118	0.383	0.059	0.005	0.110
13:21-22.	3.236	0.717	0.760	1.368	0.100	0.214	0.054	0.005	0.060
13:22-24.	3.279	0.740	0.800	1.536	0.036	0.219	0.054	0.006	0.064
13:24-26.	3.217	0.665	0.778	1.405	0.120	0.224	0.054	0.005	0.057

STATION 163-13 Uncorrected trace element data, ppm

	I	Br	Mo	Zr	Y	Sr	Rb	Th	Pb	As	Zn	Cu	Ni	Cr	V	Ba
13:1-2.	559	119	N.D.	84	44	818	74	2	N.D.	48	83	20	37	693	300	10261
13:2-3.	568	129	1	79	30	728	72	8	N.D.	37	78	20	36	629	274	8811
13:3-4.	651	129	N.D.	77	29	763	71	3	N.D.	42	76	21	37	621	263	8515
13:4-5.	520	109	N.D.	88	26	994	70	2	N.D.	48	84	23	40	626	290	14558
13:5-6.	523	149	N.D.	80	26	737	74	7	N.D.	25	87	23	40	566	227	8087
13:6-7.	408	149	2	86	28	634	74	10	N.D.	21	108	27	43	527	221	5228
13:7-8.	385	138	1	82	29	657	75	2	N.D.	20	104	27	43	526	230	4891
13:8-9.	469	143	4	80	29	625	69	4	N.D.	27	102	23	43	501	240	4541
13:9-10.	424	116	N.D.	72	26	737	63	5	N.D.	24	76	15	35	518	227	6207
13:10-11.	458	163	9	88	28	579	79	4	N.D.	23	118	28	52	483	238	3971
13:11-12.	428	121	1	73	25	628	68	2	N.D.	25	82	16	38	553	244	6471
13:12-13.	244	110	8	65	23	461	55	1	1	14	91	10	36	387	193	2588
13:13-14.	148	202	35	123	36	421	102	15	9	19	236	47	88	257	216	1316
13:14-15.	165	140	24	87	25	352	73	4	2	18	155	24	57	270	180	1758
13:15-16.	152	134	22	87	25	423	71	1	N.D.	21	148	23	60	285	190	2702
13:16-17.	151	145	33	88	25	369	70	4	1	29	147	23	61	267	179	1707
13:17-18.	409	124	6	84	26	680	74	4	N.D.	32	98	24	44	492	229	9248
13:18-19.	138	150	35	87	25	344	70	3	2	32	142	24	62	256	176	1337
13:19-20.	247	130	18	88	27	560	73	4	N.D.	26	124	25	55	360	197	4192
13:20-21.	291	121	16	86	28	600	76	4	N.D.	32	127	24	53	429	208	5866
13:21-22.	42	152	48	90	24	249	70	5	8	42	157	25	70	182	163	421
13:22-24.	55	143	42	89	24	279	69	4	7	33	162	36	67	196	165	884
13:24-26.	41	147	44	92	25	258	72	5	9	27	156	23	67	188	164	424

N.D. - Not detectable

STATION 163-13 Salt-corrected trace element data, ppm

	I	Br	Mo	Zr	Y	Sr	Rb	Th	Pb	As	Zn	Cu	Ni	Cr	V	Ba
13:1-2.	569	88	N.D.	85	45	832	75	2	N.D.	49	84	20	38	705	305	10442
13:2-3.	577	102	1	80	30	739	73	8	N.D.	38	79	20	37	639	278	8946
13:3-4.	666	91	N.D.	79	30	780	73	3	N.D.	43	78	21	38	635	269	8705
13:4-5.	529	78	N.D.	90	26	1012	71	2	N.D.	49	85	23	41	637	295	14817
13:5-6.	536	108	N.D.	82	27	755	76	7	N.D.	26	89	24	41	580	233	8284
13:6-7.	420	99	2	89	29	653	76	10	N.D.	22	111	28	44	543	228	5382
13:7-8.	395	95	1	84	30	673	77	2	N.D.	20	107	28	44	539	236	5012
13:8-9.	481	101	4	82	30	641	71	4	N.D.	28	105	24	44	513	246	4654
13:9-10.	434	75	N.D.	74	27	754	64	5	N.D.	25	78	15	36	530	232	6353
13:10-11.	473	107	9	91	29	598	82	4	N.D.	24	122	29	54	499	246	4103
13:11-12.	439	78	1	75	26	644	70	2	N.D.	26	84	16	39	567	250	6631
13:12-13.	252	56	8	67	24	475	57	1	1	14	94	10	37	399	199	2668
13:13-14.	153	143	36	127	37	436	106	16	9	20	245	49	91	266	224	1364
13:14-15.	171	76	25	90	26	365	76	4	2	19	161	25	59	280	187	1824
13:15-16.	158	68	23	90	26	439	74	1	N.D.	22	154	24	62	296	197	2806
13:16-17.	158	72	34	92	26	385	73	4	1	30	153	24	64	279	187	1781
13:17-18.	420	76	6	86	27	699	76	4	N.D.	33	101	25	45	505	235	9502
13:18-19.	144	76	37	91	26	359	73	3	2	33	148	25	65	267	184	1396
13:19-20.	255	71	19	91	28	579	76	4	N.D.	27	128	26	57	372	204	4336
13:20-21.	300	66	17	89	29	619	78	4	N.D.	33	131	25	55	443	215	6056
13:21-22.	44	66	50	95	25	262	74	5	8	44	165	26	74	191	171	443
13:22-24.	58	44	44	94	25	296	73	4	7	35	172	38	71	208	175	937
13:24-26.	43	66	46	96	26	270	75	5	9	28	164	24	70	197	172	444

N.D. - Not detectable

STATION 163-13 Salt-free trace element ratios to aluminium (x10-4)

	Mo/Al	Zr/Al	Y/Al	Sr/Al	Rb/Al	Th/Al	Pb/Al	As/Al	Zn/Al	Cu/Al	Ni/Al	Cr/Al	V/Al	Ba/Al	K/Rb
13:1-2.	N.D.	31.84	16.85	311.61	28.09	0.75	N.D.	18.35	31.46	7.49	14.23	264.04	114.23	3910.86	164.00
13:2-3.	0.38	30.08	11.28	277.82	27.44	3.01	N.D.	14.29	29.70	7.52	13.91	240.23	104.51	3363.16	146.58
13:3-4.	N.D.	31.10	11.81	307.09	28.74	1.18	N.D.	16.93	30.71	8.27	14.96	250.00	105.91	3427.17	149.32
13:4-5.	N.D.	32.97	9.52	370.70	26.01	0.73	N.D.	17.95	31.14	8.42	15.02	233.33	108.06	5427.47	139.44
13:5-6.	N.D.	27.99	9.22	257.68	25.94	2.39	N.D.	8.87	30.38	8.19	13.99	197.95	79.52	2827.30	127.63
13:6-7.	0.58	25.95	8.45	190.38	22.16	2.92	N.D.	6.41	32.36	8.16	12.83	158.31	66.47	1569.10	147.37
13:7-8.	0.31	26.01	9.29	208.36	23.84	0.62	N.D.	6.19	33.13	8.67	13.62	166.87	73.07	1551.70	140.26
13:8-9.	1.24	25.47	9.32	199.07	22.05	1.24	N.D.	8.70	32.61	7.45	13.66	159.32	76.40	1445.34	136.62
13:9-10.	N.D.	20.39	7.44	207.71	17.63	1.38	N.D.	6.89	21.49	4.13	9.92	146.01	63.91	1750.14	179.69
13:10-11.	3.09	31.27	9.97	205.50	28.18	1.37	N.D.	8.25	41.92	9.97	18.56	171.48	84.54	1409.97	134.15
13:11-12.	0.28	21.19	7.34	181.92	19.77	0.56	N.D.	7.34	23.73	4.52	11.02	160.17	70.62	1873.16	141.43
13:12-13.	1.52	12.76	4.57	90.48	10.86	0.19	0.19	2.67	17.90	1.90	7.05	76.00	37.90	508.19	198.25
13:13-14.	12.95	45.68	13.31	156.83	38.13	5.76	3.24	7.19	88.13	17.63	32.73	95.68	80.58	490.65	93.40
13:14-15.	5.21	18.75	5.42	76.04	15.83	0.83	0.42	3.96	33.54	5.21	12.29	58.33	38.96	380.00	146.05
13:15-16.	4.93	19.27	5.57	94.00	15.85	0.21	N.D.	4.71	32.98	5.14	13.28	63.38	42.18	600.86	145.95
13:16-17.	7.14	19.33	5.46	80.88	15.34	0.84	0.21	6.30	32.14	5.04	13.45	58.61	39.29	374.16	141.10
13:17-18.	1.87	26.79	8.41	217.76	23.68	1.25	N.D.	10.28	31.46	7.79	14.02	157.32	73.21	2960.12	175.00
13:18-19.	7.71	18.96	5.42	74.79	15.21	0.62	0.42	6.87	30.83	5.21	13.54	55.62	38.33	290.83	145.21
13:19-20.	4.67	22.36	6.88	142.26	18.67	0.98	N.D.	6.63	31.45	6.39	14.00	91.40	50.12	1065.36	167.11
13:20-21.	4.56	23.86	7.77	165.95	20.91	1.07	N.D.	8.85	35.12	6.70	14.75	118.77	57.64	1623.59	183.33
13:21-22.	9.07	17.24	4.54	47.55	13.43	0.91	1.45	7.99	29.95	4.72	13.43	34.66	31.03	80.40	159.46
13:22-24.	8.24	17.60	4.68	55.43	13.67	0.75	1.31	6.55	32.21	7.12	13.30	38.95	32.77	175.47	160.27
13:24-26.	8.24	17.20	4.66	48.39	13.44	0.90	1.61	5.02	29.39	4.30	12.54	35.30	30.82	79.57	166.67

N.D. - Not detectable

STATION 163-7 Uncorrected major element data, Wt.% Element

	Si	Al	Fe	Mg	Ca	Na	K	Ti	Mn	P	LOI	Corg.	N
7:0-1.	22.97	6.88	4.12	2.28	1.57	3.52	1.73	0.379	3.32	0.16	11.20	1.15	0.20
7:1-2.	23.44	7.02	4.21	2.24	1.57	3.41	1.80	0.390	3.38	0.16	11.10	1.14	0.20
7:2-3.	22.09	6.65	4.01	2.17	1.56	3.32	1.69	0.369	6.07	0.16	12.20	1.08	0.17
7:3-4.	23.28	6.99	4.20	2.19	1.56	3.22	1.80	0.388	2.94	0.16	11.80	1.42	0.23
7:4-5.	24.22	7.23	4.34	2.34	1.58	3.31	1.86	0.401	1.99	0.17	11.10	1.39	0.23
7:5-6.	24.19	7.23	4.30	2.35	1.56	3.32	1.86	0.401	1.46	0.16	11.10	1.41	0.22
7:6-7.	24.25	7.23	4.22	2.36	1.56	3.37	1.85	0.403	1.11	0.16	11.50	1.47	0.23
7:7-8.	24.52	7.37	4.40	2.38	1.57	3.21	1.94	0.412	1.01	0.16	11.80	1.38	0.22
7:8-9.	24.49	7.37	4.37	2.41	1.56	3.28	1.89	0.412	0.75	0.16	11.50	1.40	0.22
7:9-10.	24.55	7.38	4.31	2.44	1.56	3.19	1.89	0.411	0.75	0.16	11.60	1.43	0.22
7:10-11.	24.74	7.41	4.37	2.35	1.57	3.18	1.89	0.410	0.68	0.16	11.80	1.40	0.21
7:11-12.	24.79	7.43	4.41	2.42	1.59	3.13	1.92	0.412	0.63	0.16	11.30	1.39	0.21
7:12-13.	24.74	7.46	4.42	2.41	1.58	3.43	1.95	0.415	0.62	0.16	11.20	1.42	0.22
7:13-14.	24.63	7.45	4.42	2.43	1.58	3.44	1.92	0.408	0.58	0.16	10.70	1.36	0.22
7:14-15.	24.76	7.40	4.78	2.41	1.64	3.38	2.05	0.406	0.09	0.15	11.30	1.28	0.20
7:15-16.	25.15	7.50	4.59	2.42	1.68	3.52	1.98	0.405	0.07	0.14	10.30	1.20	0.19
7:16-17.	24.94	7.46	4.56	2.36	1.89	3.41	1.98	0.405	0.07	0.14	10.70	1.19	0.19
7:17-18.	24.94	7.45	4.60	2.36	2.23	3.36	1.98	0.404	0.08	0.14	11.30	1.20	0.18
7:18-19.	24.64	7.29	4.68	2.39	2.42	3.36	1.94	0.399	0.08	0.14	11.80	1.17	0.18
7:19-20.	24.41	7.15	4.85	2.38	2.72	3.29	1.93	0.386	0.08	0.14	12.30	1.12	0.18
7:20-22.	24.04	7.20	4.37	2.27	3.43	3.13	1.90	0.389	0.07	0.13	12.10	1.25	0.19
7:22-24.	23.89	7.17	4.07	2.24	4.08	2.99	1.85	0.387	0.08	0.13	12.10	1.26	0.19
7:24-26.	23.35	6.89	4.00	2.16	4.84	2.86	1.76	0.371	0.07	0.13	13.50	1.27	0.18
7:26-28.	23.90	7.06	4.12	2.21	4.31	2.86	1.86	0.383	0.08	0.14	12.70	1.37	0.18
7:28-30.	23.81	6.99	3.93	2.13	4.65	2.81	1.84	0.379	0.08	0.13	12.90	1.27	0.18
7:30-32.	23.74	6.81	4.04	2.11	4.66	2.90	1.83	0.371	0.08	0.13	13.10	1.15	0.17
7:32-34.	24.16	6.97	3.95	2.12	4.26	2.84	1.89	0.379	0.08	0.13	12.60	1.37	0.17

STATION 163-7 Salt-corrected major element data, Wt.% Element

	Si	Al	Fe	Mg	Ca	Na	K	Ti	Mn	P	LOI	Corg.	N	Salt
7:0-1.	24.81	7.43	4.45	2.17	1.58	1.36	1.78	0.409	3.58	0.17	11.20	1.24	0.22	7.39
7:1-2.	25.03	7.49	4.50	2.14	1.59	1.57	1.85	0.416	3.61	0.17	11.10	1.22	0.21	6.34
7:2-3.	24.66	7.12	4.30	2.06	1.58	1.43	1.72	0.395	6.49	0.17	12.20	1.16	0.18	6.53
7:3-4.	24.77	7.43	4.47	2.09	1.58	1.47	1.85	0.413	3.13	0.17	11.80	1.51	0.24	6.01
7:4-5.	25.86	7.72	4.63	2.25	1.60	1.45	1.91	0.428	2.13	0.18	11.10	1.48	0.25	6.36
7:5-6.	25.89	7.74	4.61	2.25	1.58	1.40	1.91	0.429	1.56	0.18	11.10	1.51	0.24	6.58
7:6-7.	26.01	7.76	4.53	2.26	1.59	1.40	1.91	0.432	1.19	0.18	11.50	1.58	0.25	6.77
7:7-8.	26.06	7.83	4.67	2.30	1.60	1.49	1.99	0.438	1.07	0.17	11.80	1.47	0.23	5.89
7:8-9.	26.15	7.87	4.67	2.32	1.59	1.42	1.94	0.440	0.80	0.17	11.50	1.50	0.23	6.37
7:9-10.	26.15	7.86	4.59	2.36	1.58	1.39	1.94	0.438	0.79	0.17	11.60	1.52	0.23	6.15
7:10-11.	26.32	7.89	4.65	2.27	1.60	1.43	1.94	0.436	0.72	0.17	11.80	1.49	0.22	5.99
7:11-12.	26.37	7.91	4.69	2.34	1.61	1.38	1.97	0.438	0.67	0.17	11.30	1.48	0.22	6.00
7:12-13.	26.32	7.94	4.70	2.33	1.60	1.70	2.00	0.441	0.66	0.17	11.20	1.51	0.23	5.98
7:13-14.	26.26	7.94	4.71	2.35	1.61	1.65	1.98	0.435	0.61	0.17	10.70	1.45	0.23	6.19
7:14-15.	26.47	7.91	5.11	2.33	1.67	1.51	2.11	0.434	0.10	0.16	11.30	1.37	0.21	6.44
7:15-16.	26.88	8.02	4.90	2.33	1.71	1.67	2.04	0.433	0.08	0.15	10.30	1.28	0.20	6.41
7:16-17.	26.53	7.93	4.85	2.27	1.93	1.67	2.04	0.431	0.08	0.15	10.70	1.27	0.20	6.01
7:17-18.	26.51	7.92	4.89	2.27	2.30	1.65	2.04	0.429	0.08	0.15	11.30	1.28	0.19	5.93
7:18-19.	26.23	7.76	4.98	2.30	2.49	1.61	2.00	0.425	0.09	0.15	11.80	1.25	0.19	6.06
7:19-20.	25.98	7.60	5.16	2.30	2.82	1.54	1.99	0.411	0.08	0.15	12.30	1.19	0.19	6.02
7:20-22.	25.50	7.64	4.63	2.18	3.56	1.46	1.94	0.413	0.08	0.14	12.10	1.33	0.20	5.74
7:22-24.	25.23	7.57	4.30	2.16	4.24	1.44	1.89	0.409	0.08	0.14	12.10	1.33	0.20	5.31
7:24-26.	24.61	7.26	4.22	2.07	5.04	1.35	1.79	0.391	0.08	0.13	13.50	1.34	0.19	5.15
7:26-28.	25.41	7.51	4.38	2.12	4.51	1.11	1.91	0.407	0.08	0.14	12.70	1.46	0.19	5.93
7:28-30.	25.01	7.34	4.13	2.05	4.83	1.40	1.87	0.398	0.08	0.14	12.90	1.33	0.19	4.83
7:30-32.	24.96	7.16	4.24	2.03	4.83	1.47	1.87	0.390	0.08	0.13	13.10	1.21	0.18	4.90
7:32-34.	25.25	7.29	4.13	2.05	4.39	1.58	1.92	0.396	0.08	0.14	12.60	1.43	0.18	4.34

STATION 163-7 Salt-free ratios to aluminium

	Si/Al	Fe/Al	Mg/Al	Ca/Al	Na/Al	K/Al	Ti/Al	Mn/Al	P/Al	Corg./Al
7:0-1.	3.337	0.599	0.291	0.213	0.183	0.240	0.055	0.482	0.023	0.167
7:1-2.	3.340	0.600	0.284	0.212	0.208	0.248	0.056	0.482	0.023	0.163
7:2-3.	3.321	0.604	0.285	0.222	0.200	0.242	0.055	0.912	0.023	0.163
7:3-4.	3.332	0.601	0.281	0.212	0.198	0.248	0.056	0.421	0.023	0.203
7:4-5.	3.351	0.600	0.291	0.208	0.188	0.248	0.055	0.275	0.023	0.192
7:5-6.	3.346	0.595	0.291	0.205	0.181	0.247	0.055	0.202	0.023	0.195
7:6-7.	3.352	0.583	0.292	0.205	0.180	0.246	0.056	0.153	0.023	0.203
7:7-8.	3.329	0.597	0.293	0.204	0.191	0.254	0.056	0.137	0.022	0.187
7:8-9.	3.323	0.593	0.294	0.202	0.181	0.247	0.056	0.101	0.022	0.190
7:9-10.	3.326	0.584	0.300	0.201	0.177	0.247	0.056	0.101	0.021	0.194
7:10-11.	3.337	0.589	0.288	0.203	0.182	0.246	0.055	0.092	0.022	0.189
7:11-12.	3.335	0.593	0.295	0.204	0.174	0.250	0.055	0.084	0.021	0.187
7:12-13.	3.316	0.592	0.293	0.202	0.214	0.252	0.056	0.083	0.022	0.190
7:13-14.	3.308	0.594	0.296	0.202	0.208	0.249	0.055	0.077	0.021	0.183
7:14-15.	3.344	0.646	0.294	0.211	0.190	0.267	0.055	0.013	0.020	0.173
7:15-16.	3.353	0.612	0.291	0.213	0.208	0.255	0.054	0.010	0.019	0.160
7:16-17.	3.344	0.611	0.287	0.243	0.210	0.257	0.054	0.010	0.019	0.160
7:17-18.	3.348	0.618	0.287	0.290	0.208	0.257	0.054	0.011	0.019	0.161
7:18-19.	3.378	0.642	0.296	0.321	0.207	0.257	0.055	0.011	0.019	0.160
7:19-20.	3.416	0.679	0.302	0.370	0.202	0.261	0.054	0.011	0.019	0.157
7:20-22.	3.337	0.606	0.285	0.466	0.191	0.254	0.054	0.010	0.019	0.174
7:22-24.	3.330	0.568	0.285	0.559	0.190	0.250	0.054	0.011	0.019	0.176
7:24-26.	3.390	0.581	0.286	0.694	0.187	0.247	0.054	0.011	0.018	0.184
7:26-28.	3.385	0.584	0.282	0.600	0.148	0.255	0.054	0.011	0.019	0.194
7:28-30.	3.407	0.563	0.280	0.657	0.191	0.255	0.054	0.011	0.019	0.182
7:30-32.	3.486	0.593	0.283	0.675	0.205	0.261	0.054	0.011	0.019	0.169
7:32-34.	3.466	0.567	0.282	0.603	0.217	0.264	0.054	0.011	0.019	0.197

STATION 163-7 Uncorrected trace element data, ppm

	Mo	Zr	Y	Sr	Rb	Th	Pb	As	Zn	Cu	Ni	Cr	V	Ba	S	I	Br	Cl
7:0-1.	58	117	38	338	75	11	23	47	266	266	220	110	170	3216	4309	308	221	21894
7:1-2.	74	118	40	360	73	6	22	34	370	302	429	117	167	3203	4187	255	225	14571
7:2-3.	109	114	36	348	71	8	22	29	373	285	480	109	175	3123	4278	298	226	11839
7:3-4.	24	118	37	347	73	10	20	22	238	264	263	113	150	3177	4202	315	243	11781
7:4-5.	9	122	37	355	76	6	24	23	243	278	233	119	147	3242	4244	276	254	11897
7:5-6.	2	123	37	357	76	6	22	13	251	282	206	124	142	3312	4224	266	260	13627
7:6-7.	1	120	39	347	75	11	23	7	252	277	185	125	139	3288	4426	294	269	11864
7:7-8.	N.D.	124	40	361	76	7	23	21	257	285	182	124	146	3320	4141	285	249	15069
7:8-9.	N.D.	124	39	351	76	6	22	12	251	287	163	130	133	3307	4286	271	252	14529
7:9-10.	N.D.	124	37	347	75	6	20	16	250	282	165	129	131	3312	4219	267	249	12261
7:10-11.	N.D.	124	39	353	76	5	19	13	251	281	162	129	128	3329	4167	252	241	16362
7:11-12.	N.D.	126	41	352	78	6	19	13	251	284	159	133	126	3335	4080	246	243	15708
7:12-13.	N.D.	126	39	352	78	5	20	16	249	280	162	136	123	3382	4248	237	235	11119
7:13-14.	N.D.	125	38	341	76	5	20	13	247	259	158	132	115	3369	4227	230	239	11627
7:14-15.	N.D.	124	31	324	76	7	18	15	260	180	136	132	129	3191	3922	188	225	10572
7:15-16.	N.D.	124	30	321	77	8	17	17	270	189	140	130	142	3199	4135	177	220	8717
7:16-17.	N.D.	127	32	330	77	6	18	18	256	209	141	127	151	3185	3973	177	212	11144
7:17-18.	N.D.	127	34	345	78	5	19	19	255	212	144	122	144	3118	3928	169	208	9808
7:18-19.	N.D.	126	34	347	78	5	17	19	261	239	149	123	143	3012	4109	178	216	10069
7:19-20.	N.D.	124	34	355	80	3	18	16	276	218	161	121	145	2929	4135	169	214	11082
7:20-22.	N.D.	128	36	423	83	6	14	9	265	206	157	118	162	2992	3955	184	205	8377
7:22-24.	N.D.	128	37	410	84	6	16	14	275	262	161	115	184	2964	3836	191	192	7608
7:24-26.	N.D.	124	35	425	79	5	15	15	300	217	165	110	153	2759	3831	194	185	7922
7:26-28.	N.D.	127	33	433	78	7	11	23	315	227	166	116	171	2820	3718	205	184	7612
7:28-30.	N.D.	129	34	418	77	11	12	15	250	179	157	115	140	2722	3684	194	175	8068
7:30-32.	N.D.	127	33	437	79	5	11	19	252	129	166	110	136	2557	3842	177	172	12987
7:32-34.	N.D.	130	25	442	80	8	13	15	238	176	164	110	185	2551	3611	187	191	11959

N.D. - Not detectable

STATION 163-7 Salt-corrected trace element data, ppm

	Mo	Zr	Y	Sr	Rb	Th	Pb	As	Zn	Cu	Ni	Cr	V	Ba	S	I	Br	Cl
7:0-1.	63	125	41	365	81	12	25	51	287	287	238	119	184	3473	2578	333	87	21894
7:1-2.	79	126	43	384	78	6	23	36	395	322	458	125	178	3420	2710	272	112	14571
7:2-3.	117	122	39	372	76	9	24	31	399	305	514	117	187	3341	2760	319	109	11839
7:3-4.	26	126	39	369	78	11	21	23	253	281	280	120	160	3380	2808	335	137	11781
7:4-5.	10	130	40	379	81	6	26	25	260	297	249	127	157	3462	2766	295	142	11897
7:5-6.	2	132	40	382	81	6	24	14	269	302	221	133	152	3545	2690	285	144	13627
7:6-7.	1	129	42	372	80	12	25	8	270	297	198	134	149	3527	2859	315	151	11864
7:7-8.	N.D.	132	43	384	81	7	24	22	273	303	193	132	155	3528	2773	303	146	15069
7:8-9.	N.D.	132	42	375	81	6	23	13	268	307	174	139	142	3532	2809	289	140	14529
7:9-10.	N.D.	132	39	370	80	6	21	17	266	300	176	137	140	3529	2792	284	141	12261
7:10-11.	N.D.	132	41	375	81	5	20	14	267	299	172	137	136	3541	2776	268	135	16362
7:11-12.	N.D.	134	44	374	83	6	20	14	267	302	169	141	134	3548	2681	262	137	15708
7:12-13.	N.D.	134	41	374	83	5	21	17	265	298	172	145	131	3597	2864	252	129	11119
7:13-14.	N.D.	133	41	364	81	5	21	14	263	276	168	141	123	3591	2790	245	129	11627
7:14-15.	N.D.	133	33	346	81	7	19	16	278	192	145	141	138	3411	2402	201	110	10572
7:15-16.	N.D.	132	32	343	82	9	18	18	288	202	150	139	152	3418	2637	189	105	8717
7:16-17.	N.D.	135	34	351	82	6	19	19	272	222	150	135	161	3389	2565	188	104	11144
7:17-18.	N.D.	135	36	367	83	5	20	20	271	225	153	130	153	3315	2537	180	101	9808
7:18-19.	N.D.	134	36	369	83	5	18	20	278	254	159	131	152	3206	2697	189	107	10069
7:19-20.	N.D.	132	36	378	85	3	19	17	294	232	171	129	154	3117	2734	180	106	11082
7:20-22.	N.D.	136	38	449	88	6	15	10	281	219	167	125	172	3174	2613	195	102	8377
7:22-24.	N.D.	135	39	433	89	6	17	15	290	277	170	121	194	3130	2593	202	96	7608
7:24-26.	N.D.	131	37	448	83	5	16	16	316	229	174	116	161	2909	2627	205	92	7922
7:26-28.	N.D.	135	35	460	83	7	12	24	335	241	176	123	182	2998	2313	218	76	7612
7:28-30.	N.D.	136	36	439	81	12	13	16	263	188	165	121	147	2860	2551	204	87	8068
7:30-32.	N.D.	134	35	460	83	5	12	20	265	136	175	116	143	2689	2700	186	83	12987
7:32-34.	N.D.	136	26	462	84	8	14	16	249	184	171	115	193	2667	2595	195	113	11959

N.D. - Not detectable

STATION 163-7 Salt-free trace element ratios to aluminium (x10-4)

	Mo/Al	Zr/Al	Y/Al	Rb/Al	Sr/Al	Th/Al	Pb/Al	As/Al	Zn/Al	Cu/Al	Ni/Al	Cr/Al	V/Al	Ba/Al
7:0-1.	8.48	16.82	5.52	10.90	49.13	1.62	3.36	6.86	38.63	38.63	32.03	16.02	24.76	468.10
7:1-2.	10.55	16.82	5.74	10.41	51.27	0.80	3.07	4.81	52.74	42.99	61.15	16.69	23.77	456.61
7:2-3.	16.43	17.13	5.47	10.67	52.25	1.26	3.37	4.35	56.04	42.84	72.19	16.43	26.26	469.24
7:3-4.	3.50	16.95	5.25	10.49	49.65	1.48	2.83	3.09	34.04	37.81	37.67	16.14	21.53	454.75
7:4-5.	1.30	16.84	5.18	10.50	49.11	0.78	3.37	3.24	33.69	38.48	32.26	16.46	20.34	448.57
7:5-6.	0.26	17.06	5.17	10.47	49.37	0.78	3.10	1.81	34.76	39.03	28.56	17.19	19.64	458.12
7:6-7.	0.13	16.63	5.41	10.31	47.94	1.55	3.22	1.03	48.20	38.28	25.52	17.27	19.20	454.55
7:7-8.	N.D.	16.86	5.49	10.35	49.06	0.89	3.07	2.81	34.88	38.71	24.66	16.86	19.80	450.75
7:8-9.	N.D.	16.77	5.34	10.29	47.64	0.76	2.92	1.65	34.05	39.00	22.11	17.66	18.04	448.71
7:9-10.	N.D.	16.78	4.96	10.17	47.05	0.76	2.67	2.16	33.82	38.15	22.38	17.42	17.80	448.72
7:10-11.	N.D.	16.74	5.20	10.27	47.56	0.63	2.54	1.78	33.86	37.92	21.81	17.37	17.25	449.06
7:11-12.	N.D.	16.94	5.56	10.50	47.29	0.76	2.53	1.77	33.76	38.19	21.37	17.83	16.94	448.63
7:12-13.	N.D.	16.88	5.17	10.46	47.12	0.63	2.65	2.14	33.39	37.55	21.67	18.27	16.51	453.22
7:13-14.	N.D.	16.75	5.16	10.20	45.85	0.63	2.65	1.76	33.13	34.77	21.16	17.76	15.49	452.36
7:14-15.	N.D.	16.80	4.17	10.23	43.72	0.88	2.40	2.02	35.12	24.26	18.32	17.81	17.44	430.97
7:15-16.	N.D.	16.47	3.99	10.23	42.78	1.12	2.25	2.25	35.92	25.20	18.71	17.34	18.96	426.35
7:16-17.	N.D.	17.02	4.29	10.34	44.24	0.76	2.39	2.39	34.28	27.98	18.91	17.02	20.29	427.16
7:17-18.	N.D.	17.05	4.55	10.48	46.35	0.63	2.53	2.53	34.22	28.41	19.32	16.42	19.32	418.64
7:18-19.	N.D.	17.26	4.64	10.69	47.53	0.64	2.32	2.58	35.81	32.72	20.48	16.87	19.58	412.96
7:19-20.	N.D.	17.36	4.73	11.18	49.71	0.39	2.50	2.24	38.66	30.51	22.49	16.96	20.25	409.87
7:20-22.	N.D.	17.79	4.97	11.51	58.75	0.79	1.96	1.31	36.77	28.65	21.85	16.36	22.51	415.30
7:22-24.	N.D.	17.82	5.15	11.75	57.17	0.79	2.24	1.98	38.29	36.57	22.44	15.98	25.61	413.25
7:24-26.	N.D.	18.04	5.10	11.43	61.71	0.69	2.20	2.20	43.53	31.54	23.97	15.98	22.18	400.70
7:26-28.	N.D.	17.99	4.66	11.06	61.28	0.93	1.60	3.20	44.63	32.11	23.45	16.39	24.25	399.41
7:28-30.	N.D.	18.52	4.90	11.03	59.80	1.63	1.77	2.18	45.82	25.61	22.47	16.48	20.02	389.56
7:30-32.	N.D.	18.72	4.89	11.59	64.25	0.70	1.68	2.79	37.01	18.99	24.44	16.20	19.97	375.57
7:32-34.	N.D.	18.67	3.57	11.53	63.41	1.10	1.92	2.20	34.17	25.25	23.47	15.78	26.49	366.03

N.D. - Not detectable

STATION 163-14 Uncorrected major element data, Wt.% Element

	Si	Al	Fe	Mg	Ca	Na	K	Ti	Mn	P	LOI	Corg.	N
14:0-1.	23.79	7.12	4.40	2.37	1.66	3.45	1.79	0.398	2.23	0.16	11.40	1.04	0.17
14:1-2.	23.67	7.11	4.42	2.33	1.60	3.31	1.82	0.400	2.32	0.16	11.40	0.87	0.18
14:2-3.	23.76	7.14	4.41	2.36	1.61	3.33	1.82	0.401	2.34	0.16	11.30	0.88	0.18
14:3-4.	23.60	7.07	4.37	2.36	1.60	3.41	1.78	0.399	2.37	0.16	11.80	0.88	0.18
14:4-5.	23.63	7.13	4.37	2.41	1.60	3.42	1.83	0.401	2.43	0.16	11.30	0.91	0.18
14:5-6.	23.88	7.13	4.35	2.35	1.61	3.28	1.84	0.400	2.70	0.16	11.00	0.81	0.18
14:6-7.	23.25	7.03	4.35	2.31	1.58	3.18	1.88	0.397	2.54	0.16	11.70	0.68	0.19
14:7-8.	24.17	7.29	4.46	2.42	1.62	3.35	1.88	0.408	2.41	0.16	9.50	0.99	0.19
14:8-9.	24.15	7.28	4.51	2.38	1.61	3.03	1.93	0.414	2.58	0.16	10.20	0.82	0.17
14:9-10.	24.57	7.45	4.61	2.42	1.59	3.05	1.95	0.421	1.53	0.16	8.70	1.00	0.18
14:10-12.	25.17	7.59	4.57	2.48	1.61	3.30	1.98	0.428	0.70	0.16	9.90	1.16	0.19
14:12-14.	24.78	7.49	4.51	2.42	1.84	3.09	1.95	0.419	0.61	0.15	9.30	1.03	0.18
14:14-16.	24.51	7.42	4.53	2.38	2.83	2.94	1.88	0.413	0.61	0.15	9.80	0.98	0.18
14:16-18.	22.47	6.76	4.14	2.10	5.70	2.50	1.45	0.374	0.51	0.13	14.30	1.04	0.17
14:18-20.	21.58	6.50	3.91	1.98	7.37	2.25	1.26	0.357	0.45	0.12	16.10	1.04	0.15
14:20-22.	21.68	6.48	3.88	1.98	7.51	2.23	1.30	0.356	0.46	0.12	14.50	0.99	0.15
14:22-24.	21.96	6.49	3.82	1.93	7.38	2.27	1.39	0.358	0.33	0.12	14.30	0.96	0.15
14:24-26.	22.13	6.51	3.84	1.93	7.02	2.26	1.41	0.363	0.31	0.11	15.30	1.00	0.15
14:26-28.	22.90	6.74	3.96	2.03	6.08	2.37	1.54	0.373	0.23	0.12	14.00	1.00	0.15
14:28-30.	23.85	6.96	4.07	2.11	4.90	2.64	1.74	0.391	0.15	0.12	12.20	0.92	0.15
14:30-32.	23.74	6.73	4.81	2.12	4.28	2.60	1.81	0.377	0.11	0.11	11.90	0.99	0.14

STATION 163-14 Salt-corrected major element data, Wt.% Element

	Si	Al	Fe	Mg	Ca	Na	K	Ti	Mn	P	LOI	Corg.	N	Salt
14:0-1.	25.63	7.67	4.74	2.27	1.69	1.36	1.84	0.429	2.40	0.17	11.40	1.12	0.18	7.16
14:1-2.	25.37	7.62	4.73	2.23	1.63	1.36	1.87	0.429	2.49	0.17	11.40	0.93	0.19	6.70
14:2-3.	25.49	7.66	4.73	2.26	1.64	1.34	1.88	0.430	2.51	0.17	11.30	0.94	0.19	6.78
14:3-4.	25.33	7.58	4.69	2.27	1.63	1.42	1.83	0.428	2.54	0.17	11.80	0.94	0.19	6.82
14:4-5.	25.32	7.64	4.68	2.31	1.63	1.47	1.88	0.430	2.61	0.17	11.30	0.98	0.19	6.68
14:5-6.	25.57	7.64	4.66	2.26	1.64	1.34	1.89	0.428	2.89	0.17	11.00	0.87	0.19	6.63
14:6-7.	24.82	7.51	4.64	2.22	1.61	1.33	1.93	0.424	2.71	0.17	11.70	0.73	0.20	6.32
14:7-8.	25.74	7.77	4.75	2.34	1.64	1.57	1.93	0.435	2.57	0.17	9.50	1.05	0.20	6.11
14:8-9.	25.53	7.70	4.77	2.31	1.64	1.45	1.97	0.438	2.73	0.16	10.20	0.87	0.18	5.43
14:9-10.	26.00	7.88	4.88	2.34	1.61	1.44	2.00	0.446	1.61	0.17	8.70	1.06	0.19	5.51
14:10-12.	26.66	8.04	4.84	2.41	1.64	1.68	2.04	0.453	0.74	0.17	9.90	1.23	0.20	5.59
14:12-14.	26.29	7.94	4.78	2.34	1.88	1.41	2.00	0.445	0.65	0.16	9.30	1.09	0.19	5.75
14:14-16.	25.90	7.84	4.79	2.30	2.92	1.36	1.92	0.436	0.64	0.16	9.80	1.04	0.19	5.38
14:16-18.	23.70	7.13	4.37	2.01	5.95	0.97	1.47	0.394	0.53	0.14	14.30	1.10	0.18	5.18
14:18-20.	22.69	6.83	4.11	1.90	7.69	0.79	1.27	0.375	0.47	0.13	16.10	1.09	0.16	4.89
14:20-22.	22.72	6.79	4.07	1.90	7.82	0.86	1.31	0.373	0.48	0.12	14.50	1.04	0.16	4.61
14:22-24.	23.05	6.81	4.01	1.84	7.69	0.85	1.40	0.376	0.35	0.12	14.30	1.01	0.16	4.77
14:24-26.	23.27	6.85	4.04	1.84	7.31	0.81	1.42	0.382	0.32	0.12	15.30	1.05	0.16	4.87
14:26-28.	24.10	7.10	4.17	1.94	6.33	0.89	1.56	0.393	0.24	0.12	14.00	1.05	0.16	5.00
14:28-30.	25.14	7.34	4.29	2.03	5.10	1.14	1.77	0.412	0.15	0.12	12.20	0.97	0.16	5.12
14:30-32.	24.97	7.08	5.06	2.04	4.44	1.16	1.84	0.396	0.12	0.11	11.90	1.04	0.15	4.91

STATION 163-14 Salt-free ratios to aluminium

	Si/Al	Fe/Al	Mg/Al	Ca/Al	Na/Al	K/Al	Ti/Al	Mn/Al	P/Al	Corg./Al
14:0-1.	3.340	0.618	0.296	0.221	0.177	0.240	0.056	0.313	0.022	0.146
14:1-2.	3.329	0.621	0.293	0.213	0.178	0.246	0.056	0.326	0.022	0.122
14:2-3.	3.329	0.617	0.295	0.215	0.175	0.245	0.056	0.328	0.022	0.123
14:3-4.	3.340	0.619	0.299	0.215	0.188	0.242	0.056	0.336	0.022	0.125
14:4-5.	3.312	0.612	0.303	0.213	0.192	0.246	0.056	0.341	0.022	0.128
14:5-6.	3.347	0.610	0.296	0.215	0.175	0.247	0.056	0.378	0.023	0.114
14:6-7.	3.306	0.619	0.296	0.214	0.177	0.257	0.056	0.361	0.022	0.097
14:7-8.	3.313	0.611	0.301	0.212	0.202	0.248	0.056	0.330	0.022	0.136
14:8-9.	3.315	0.619	0.299	0.212	0.188	0.256	0.057	0.354	0.021	0.113
14:9-10.	3.298	0.619	0.297	0.204	0.183	0.253	0.057	0.205	0.021	0.134
14:10-12.	3.316	0.602	0.300	0.204	0.209	0.253	0.056	0.092	0.021	0.153
14:12-14.	3.310	0.602	0.295	0.237	0.177	0.252	0.056	0.082	0.020	0.138
14:14-16.	3.305	0.611	0.294	0.373	0.174	0.245	0.056	0.082	0.020	0.132
14:16-18.	3.325	0.613	0.282	0.835	0.136	0.206	0.055	0.075	0.020	0.154
14:18-20.	3.321	0.602	0.278	1.126	0.116	0.186	0.055	0.069	0.019	0.160
14:20-22.	3.346	0.599	0.279	1.151	0.126	0.193	0.055	0.070	0.018	0.153
14:22-24.	3.385	0.589	0.271	1.130	0.125	0.206	0.055	0.051	0.018	0.148
14:24-26.	3.399	0.590	0.268	1.068	0.118	0.208	0.056	0.047	0.017	0.154
14:26-28.	3.396	0.587	0.273	0.892	0.125	0.220	0.055	0.034	0.017	0.148
14:28-30.	3.426	0.584	0.277	0.695	0.155	0.242	0.056	0.021	0.017	0.132
14:30-32.	3.528	0.715	0.289	0.627	0.164	0.260	0.056	0.017	0.016	0.147

STATION 163-14 Uncorrected trace element data, ppm

	Mo	Zr	Y	Sr	Rb	Th	Pb	As	Zn	Cu	Ni	Cr	V	Ba	S	I	Br	Cl
14:0-1.	34	125	39	359	82	7	20	41	309	273	400	110	149	3420	4502	197	238	28546
14:1-2.	39	125	37	361	91	9	22	31	316	280	410	110	150	3438	4323	207	228	28658
14:2-3.	44	125	38	379	80	8	22	35	317	274	412	111	149	3461	4409	204	234	24961
14:3-4.	48	124	36	374	90	7	23	30	325	269	419	109	152	3399	4338	214	233	22633
14:4-5.	48	128	37	368	89	5	19	36	343	275	445	112	148	3409	4408	223	220	22728
14:5-6.	48	123	42	379	78	9	22	34	358	286	475	114	156	3553	3928	234	219	37554
14:6-7.	19	123	39	365	74	8	20	22	268	259	370	109	147	3487	4264	224	209	20944
14:7-8.	11	131	41	376	77	10	20	32	264	257	348	110	149	3568	4011	226	210	25056
14:8-9.	12	131	40	375	77	7	20	23	257	241	339	115	145	3562	3656	232	184	18458
14:9-10.	5	132	41	369	79	7	22	28	230	224	225	121	143	3622	3758	229	199	19210
14:10-12.	N.D.	135	41	368	79	9	21	22	220	229	168	127	132	3661	3934	199	214	18606
14:12-14.	N.D.	135	41	363	78	8	19	22	226	225	165	125	127	3592	3698	189	200	15493
14:14-16.	N.D.	134	41	371	78	9	19	20	229	218	167	124	126	3487	3643	189	189	13133
14:16-18.	N.D.	125	38	479	73	8	17	21	210	206	149	111	108	3147	3386	235	178	13615
14:18-20.	N.D.	121	35	521	73	6	18	18	199	182	135	102	103	2932	3133	232	165	11634
14:20-22.	N.D.	121	35	528	72	6	19	21	199	174	141	104	103	2863	3124	216	153	10895
14:22-24.	N.D.	124	34	514	72	8	17	25	186	161	125	103	103	2772	3145	213	157	11522
14:24-26.	N.D.	123	34	506	74	8	17	19	186	147	123	101	102	2806	3028	203	157	11503
14:26-28.	N.D.	128	34	477	78	9	19	26	180	134	112	104	107	2788	3128	195	159	11256
14:28-30.	N.D.	132	36	430	77	7	17	22	178	130	105	110	112	2878	3344	177	163	11751
14:30-32.	N.D.	129	31	396	79	10	18	18	196	107	122	107	106	2697	2946	158	155	10984

N.D. - Not detectable

STATION 163-14 Salt-corrected trace element data, ppm

	Mo	Zr	Y	Sr	Rb	Th	Pb	As	Zn	Cu	Ni	Cr	V	Ba	S	I	Br	Cl
14:0-1.	37	135	42	387	88	8	22	44	333	294	431	118	160	3684	2844	212	110	28546
14:1-2.	42	134	40	387	98	10	24	33	339	300	439	118	161	3685	2766	222	108	28658
14:2-3.	47	134	41	407	86	9	24	38	340	294	442	119	160	3713	2839	219	113	24961
14:3-4.	52	133	39	401	97	8	25	32	349	289	450	117	163	3648	2753	230	111	22633
14:4-5.	51	137	40	394	95	5	20	39	368	295	477	120	159	3653	2862	239	100	22728
14:5-6.	51	132	45	406	84	10	24	36	383	306	509	122	167	3805	2361	251	100	37554
14:6-7.	20	131	42	390	79	9	21	23	286	276	395	116	157	3722	2798	239	95	20944
14:7-8.	12	140	44	400	82	11	21	34	281	274	371	117	159	3800	2580	241	100	25056
14:8-9.	13	139	42	397	81	7	21	24	272	255	358	122	153	3767	2373	245	85	18458
14:9-10.	5	140	43	391	84	7	23	30	243	237	238	128	151	3833	2461	242	100	19210
14:10-12.	N.D.	143	43	390	84	10	22	23	233	243	178	135	140	3878	2627	211	114	18606
14:12-14.	N.D.	143	44	385	83	8	20	23	240	239	175	133	135	3811	2337	201	96	15493
14:14-16.	N.D.	142	43	392	82	10	20	21	242	230	176	131	133	3685	2372	200	92	13133
14:16-18.	N.D.	132	40	505	77	8	18	22	221	217	157	117	114	3319	2151	248	84	13615
14:18-20.	N.D.	127	37	548	77	6	19	19	209	191	142	107	108	3083	1957	244	76	11634
14:20-22.	N.D.	127	37	554	75	6	20	22	209	182	148	109	108	3001	2018	226	69	10895
14:22-24.	N.D.	130	36	540	76	8	18	26	195	169	131	108	108	2911	2000	224	70	11522
14:24-26.	N.D.	129	36	532	78	8	18	20	196	155	129	106	107	2950	1852	213	68	11503
14:26-28.	N.D.	135	36	502	82	9	20	27	189	141	118	109	113	2935	1924	205	67	11256
14:28-30.	N.D.	139	38	453	81	7	18	23	188	137	111	116	118	3033	2121	187	69	11751
14:30-32.	N.D.	136	33	416	83	11	19	19	206	113	128	113	111	2836	1756	166	65	10984

N.D. - Not detectable

STATION 163-14 Salt-free trace element ratios to aluminium (x10-4)

	Mo/Al	Zr/Al	Y/Al	Rb/Al	Sr/Al	Th/Al	Pb/Al	As/Al	Zn/Al	Cu/Al	Ni/Al	Cr/Al	V/Al	Ba/Al
14:0-1.	4.82	17.60	5.47	11.47	50.44	1.04	2.87	5.73	43.40	38.32	56.18	15.38	20.85	480.17
14:1-2.	5.51	17.58	5.25	12.86	50.78	1.31	3.15	4.33	44.48	39.37	57.61	15.48	21.13	483.56
14:2-3.	6.14	17.50	5.35	11.23	53.15	1.18	3.13	4.96	44.40	38.40	57.72	15.54	20.90	484.91
14:3-4.	6.86	17.54	5.14	12.79	52.88	1.05	3.30	4.22	46.02	38.11	59.34	15.43	21.49	481.07
14:4-5.	6.67	17.92	5.23	12.43	51.54	0.65	2.62	5.10	48.14	38.59	62.40	15.70	20.80	477.85
14:5-6.	6.67	17.28	5.89	10.99	53.14	1.31	3.14	4.71	50.13	40.05	66.62	15.97	21.86	498.00
14:6-7.	2.66	17.45	5.60	10.52	51.96	1.20	2.80	3.06	38.10	36.77	52.62	15.45	20.92	495.84
14:7-8.	1.54	18.02	5.66	10.56	51.49	1.42	2.70	4.38	36.17	35.27	47.76	15.06	20.47	489.14
14:8-9.	1.69	18.05	5.45	10.52	51.55	0.91	2.73	3.12	35.32	33.11	46.49	15.84	19.87	489.15
14:9-10.	0.63	17.76	5.45	10.66	49.60	0.89	2.92	3.81	30.82	30.06	30.19	16.24	19.15	486.21
14:10-12.	N.D.	17.78	5.35	10.45	48.50	1.24	2.74	2.86	28.97	30.22	22.14	16.79	17.41	482.25
14:12-14.	N.D.	18.00	5.54	10.45	48.47	1.01	2.52	2.90	30.21	30.09	22.03	16.74	16.99	479.75
14:14-16.	N.D.	18.12	5.49	10.46	50.01	1.28	2.55	2.68	30.88	29.35	22.46	16.71	16.97	470.17
14:16-18.	N.D.	18.52	5.61	10.81	70.87	1.12	2.53	3.09	31.01	30.45	22.03	16.42	16.00	465.75
14:18-20.	N.D.	18.59	5.42	11.27	80.22	0.88	2.78	2.78	30.60	27.96	20.79	15.66	15.81	451.32
14:20-22.	N.D.	18.70	5.45	11.04	81.58	0.88	2.95	3.24	30.78	26.80	21.79	16.05	15.90	441.90
14:22-24.	N.D.	19.09	5.29	11.16	79.28	1.17	2.64	3.82	28.63	24.81	19.23	15.86	15.86	427.40
14:24-26.	N.D.	18.84	5.26	11.39	77.72	1.17	2.63	2.92	28.63	22.64	18.84	15.48	15.65	430.95
14:26-28.	N.D.	19.02	5.07	11.55	70.73	1.27	2.82	3.80	26.63	19.87	16.62	15.36	15.92	413.50
14:28-30.	N.D.	18.94	5.18	11.04	61.74	0.95	2.45	3.13	25.62	18.67	15.13	15.81	16.08	413.35
14:30-32.	N.D.	19.22	4.66	11.73	58.79	1.55	2.68	2.68	29.11	15.97	18.09	15.97	15.69	400.77

N.D. - Not detectable

STATION 163-10 Uncorrected major element data, Wt.% Element

	Si	Al	Fe	Mg	Ca	Na	K	Ti	Mn	P	LOI	Corg.	N
10:0-1.	24.31	7.45	4.53	2.32	1.51	3.14	1.98	0.404	1.73	0.14	10.40	0.90	0.17
10:1-2.	24.07	7.39	4.51	2.31	1.51	3.22	1.94	0.403	2.10	0.14	10.40	0.86	0.16
10:2-3.	23.67	7.24	4.51	2.30	1.51	3.34	1.89	0.395	2.88	0.15	10.90	0.80	0.15
10:3-4.	23.32	7.15	4.48	2.28	1.49	3.43	1.87	0.389	2.99	0.15	11.30	0.86	0.16
10:4-5.	23.43	7.13	4.45	2.29	1.50	3.35	1.87	0.389	3.10	0.15	11.40	0.75	0.15
10:5-6.	23.30	7.19	4.49	2.29	1.48	3.38	1.89	0.389	3.04	0.15	10.90	0.75	0.14
10:6-7.	23.18	7.15	4.44	2.27	1.48	3.22	1.87	0.386	3.09	0.14	10.90	0.77	0.14
10:7-8.	23.05	7.13	4.45	2.29	1.50	3.08	1.89	0.389	4.19	0.15	10.80	0.73	0.13
10:8-9.	22.92	7.10	4.45	2.27	1.48	2.99	1.90	0.389	4.30	0.14	10.60	0.67	0.12
10:9-10.	23.59	7.27	4.55	2.32	1.49	3.01	1.97	0.398	3.38	0.14	10.10	0.77	0.14
10:10-12.	24.64	7.56	4.67	2.32	1.52	2.98	2.05	0.412	0.91	0.15	10.30	0.93	0.16
10:12-14.	25.10	7.69	4.74	2.35	1.48	3.00	2.07	0.419	0.69	0.14	9.50	1.04	0.16
10:14-16.	25.14	7.72	4.68	2.34	1.50	3.01	2.10	0.420	0.72	0.14	9.80	0.96	0.16
10:16-18.	24.87	7.60	4.56	2.29	1.56	2.98	2.06	0.414	0.77	0.14	10.10	1.04	0.17
10:18-20.	25.41	7.71	4.58	2.35	1.67	2.92	2.09	0.417	0.75	0.14	9.10	0.96	0.16
10:20-22.	24.98	7.56	4.42	2.27	2.21	2.87	2.03	0.408	0.82	0.13	10.60	1.04	0.15
10:22-24.	24.01	7.23	4.26	2.17	3.34	2.75	1.90	0.392	0.79	0.12	11.60	0.89	0.14
10:24-26.	24.51	7.34	4.26	2.15	3.48	2.73	1.96	0.397	0.63	0.12	11.30	1.00	0.14
10:26-28.	24.65	7.34	4.20	2.12	3.19	2.79	1.97	0.404	0.41	0.11	11.20	0.90	0.15
10:28-30.	25.29	7.50	4.27	2.16	2.71	2.82	2.04	0.412	0.32	0.11	10.30	0.98	0.15
10:30-32.	25.45	7.12	5.51	2.25	2.05	2.85	2.09	0.391	0.22	0.10	9.60	0.86	0.14

STATION 163-10 Salt-corrected major element data, Wt.% Element

	Si	Al	Fe	Mg	Ca	Na	K	Ti	Mn	P	LOI	Corg.	N	Salt
10:0-1.	25.80	7.91	4.81	2.24	1.53	1.45	2.03	0.429	1.83	0.15	10.40	0.96	0.18	5.78
10:1-2.	25.59	7.86	4.79	2.23	1.52	1.49	1.99	0.428	2.23	0.15	10.40	0.91	0.17	5.95
10:2-3.	25.22	7.71	4.81	2.20	1.53	1.56	1.94	0.421	3.07	0.16	10.90	0.85	0.16	6.13
10:3-4.	24.93	7.64	4.79	2.18	1.51	1.55	1.92	0.416	3.20	0.16	11.30	0.92	0.17	6.47
10:4-5.	25.19	7.67	4.79	2.18	1.53	1.30	1.93	0.418	3.33	0.16	11.40	0.81	0.16	7.00
10:5-6.	25.16	7.77	4.85	2.17	1.50	1.21	1.95	0.420	3.28	0.16	10.90	0.81	0.15	7.39
10:6-7.	24.67	7.61	4.72	2.18	1.50	1.46	1.92	0.411	3.28	0.15	10.90	0.82	0.15	6.04
10:7-8.	24.40	7.54	4.72	2.21	1.51	1.47	1.94	0.412	4.43	0.15	10.80	0.77	0.14	5.52
10:8-9.	24.12	7.47	4.68	2.19	1.50	1.55	1.94	0.409	4.53	0.15	10.60	0.70	0.13	4.96
10:9-10.	24.85	7.65	4.79	2.25	1.51	1.53	2.01	0.419	3.56	0.15	10.10	0.81	0.15	5.08
10:10-12.	26.03	7.99	4.93	2.25	1.53	1.42	2.10	0.435	0.97	0.15	10.30	0.98	0.17	5.36
10:12-14.	26.53	8.13	5.01	2.27	1.50	1.42	2.13	0.443	0.73	0.15	9.50	1.10	0.17	5.40
10:14-16.	26.50	8.14	4.94	2.27	1.51	1.52	2.15	0.443	0.75	0.15	9.80	1.01	0.17	5.14
10:16-18.	26.20	8.01	4.80	2.21	1.58	1.49	2.12	0.436	0.81	0.14	10.10	1.10	0.18	5.09
10:18-20.	26.72	8.10	4.82	2.28	1.69	1.50	2.14	0.438	0.79	0.14	9.10	1.01	0.17	4.88
10:20-22.	26.27	7.95	4.65	2.20	2.27	1.43	2.08	0.429	0.86	0.14	10.60	1.09	0.16	4.93
10:22-24.	25.31	7.62	4.49	2.09	3.45	1.24	1.94	0.413	0.83	0.13	11.60	0.94	0.15	5.15
10:24-26.	25.77	7.72	4.48	2.07	3.60	1.29	2.00	0.417	0.66	0.13	11.30	1.05	0.15	4.91
10:26-28.	25.95	7.73	4.42	2.04	3.29	1.32	2.01	0.425	0.43	0.12	11.20	0.95	0.16	5.01
10:28-30.	26.63	7.89	4.50	2.08	2.79	1.35	2.09	0.434	0.34	0.12	10.30	1.03	0.16	5.03
10:30-32.	26.79	7.49	5.79	2.17	2.09	1.39	2.14	0.411	0.23	0.11	9.60	0.91	0.15	4.98

STATION 163-10 Salt-free ratios to aluminium

	Si/Al	Fe/Al	Mg/Al	Ca/Al	Na/Al	K/Al	Ti/Al	Mn/Al	P/Al	Corg./Al
10:0-1.	3.262	0.608	0.283	0.194	0.183	0.257	0.054	0.232	0.019	0.121
10:1-2.	3.256	0.610	0.283	0.194	0.190	0.253	0.055	0.284	0.019	0.116
10:2-3.	3.271	0.623	0.286	0.198	0.202	0.252	0.055	0.398	0.020	0.111
10:3-4.	3.262	0.626	0.285	0.197	0.203	0.251	0.054	0.418	0.020	0.120
10:4-5.	3.285	0.625	0.284	0.199	0.170	0.251	0.055	0.434	0.021	0.105
10:5-6.	3.239	0.624	0.280	0.193	0.155	0.251	0.054	0.422	0.020	0.104
10:6-7.	3.240	0.620	0.286	0.197	0.192	0.253	0.054	0.431	0.020	0.108
10:7-8.	3.234	0.625	0.293	0.201	0.195	0.257	0.055	0.587	0.020	0.102
10:8-9.	3.227	0.627	0.293	0.201	0.208	0.260	0.055	0.606	0.020	0.094
10:9-10.	3.246	0.626	0.294	0.197	0.200	0.263	0.055	0.465	0.020	0.106
10:10-12.	3.258	0.617	0.281	0.192	0.178	0.263	0.054	0.121	0.019	0.123
10:12-14.	3.263	0.617	0.279	0.184	0.175	0.262	0.054	0.090	0.019	0.135
10:14-16.	3.255	0.606	0.279	0.186	0.186	0.264	0.054	0.093	0.018	0.124
10:16-18.	3.270	0.600	0.276	0.198	0.186	0.264	0.054	0.101	0.018	0.137
10:18-20.	3.297	0.594	0.281	0.209	0.185	0.264	0.054	0.098	0.018	0.125
10:20-22.	3.304	0.585	0.276	0.285	0.180	0.261	0.054	0.108	0.017	0.138
10:22-24.	3.322	0.590	0.274	0.453	0.162	0.255	0.054	0.109	0.017	0.123
10:24-26.	3.338	0.580	0.268	0.466	0.167	0.259	0.054	0.086	0.016	0.136
10:26-28.	3.357	0.572	0.264	0.426	0.171	0.260	0.055	0.055	0.016	0.123
10:28-30.	3.373	0.569	0.264	0.353	0.172	0.265	0.055	0.043	0.015	0.131
10:30-32.	3.576	0.774	0.290	0.279	0.186	0.285	0.055	0.031	0.014	0.121

STATION 163-10 Uncorrected trace element data, ppm

	Mo	Zr	Y	Sr	Rb	Th	Pb	As	Zn	Cu	Ni	Cr	V	Ba	S	I	Br	Cl
10:0-1.	16	130	39	361	82	12	22	26	240	299	252	114	137	3807	3999	162	199	30910
10:1-2.	23	128	40	368	85	12	23	34	262	314	298	112	144	3774	3941	170	207	45328
10:2-3.	42	126	42	367	81	12	23	34	325	381	431	108	153	3761	4041	166	213	48554
10:3-4.	45	125	40	370	81	13	23	40	331	384	447	108	153	3751	4098	159	211	45503
10:4-5.	47	124	40	366	80	11	25	46	329	380	456	103	154	3795	4045	167	206	33507
10:5-6.	49	125	39	355	78	10	24	40	327	362	449	104	156	3781	4204	167	201	28463
10:6-7.	50	125	39	363	78	10	23	39	728	358	458	103	153	3800	4030	178	191	29135
10:7-8.	79	126	38	362	76	12	22	44	370	352	571	103	168	3687	3685	189	173	22061
10:8-9.	78	128	37	358	78	12	21	41	293	312	479	103	168	3657	3669	213	170	19917
10:9-10.	43	130	39	345	78	8	22	38	218	283	332	105	157	3747	3629	211	171	16936
10:10-12.	N.D.	133	40	357	84	7	22	23	196	264	160	119	133	3822	3743	166	186	16315
10:12-14.	N.D.	136	42	360	85	8	22	20	210	289	154	123	137	3919	3896	171	191	15413
10:14-16.	N.D.	137	40	357	85	8	22	18	222	288	167	121	132	3854	3716	153	177	13644
10:16-18.	N.D.	134	41	326	80	9	22	28	231	294	184	125	133	3839	3626	155	182	13600
10:18-20.	N.D.	138	40	357	85	8	23	27	239	292	187	124	126	3846	3577	156	181	13708
10:20-22.	N.D.	137	38	361	84	7	22	15	239	269	206	116	126	3643	3408	156	168	11728
10:22-24.	N.D.	134	36	393	83	8	21	20	234	237	202	109	120	3370	3317	149	167	14027
10:24-26.	N.D.	136	35	403	84	9	21	19	228	229	185	110	120	3301	3335	158	161	12682
10:26-28.	N.D.	136	35	382	85	8	20	20	217	202	154	109	114	3221	3188	139	165	11754
10:28-30.	N.D.	139	35	369	87	9	20	19	205	179	144	109	118	3201	3262	137	162	12881
10:30-32.	N.D.	131	30	323	85	7	16	27	255	157	170	104	125	2957	3147	109	154	11704

N.D. - Not detectable

STATION 163-10 Salt-corrected trace element data, ppm

	Mo	Zr	Y	Sr	Rb	Th	Pb	As	Zn	Cu	Ni	Cr	V	Ba	S	I	Br	Cl
10:0-1.	17	138	41	383	87	13	23	28	255	317	267	121	145	4041	2649	172	95	30910
10:1-2.	24	136	43	391	90	13	24	36	279	334	317	119	153	4013	2545	181	100	45328
10:2-3.	45	134	45	391	86	13	25	36	346	406	459	115	163	4007	2607	177	103	48554
10:3-4.	48	134	43	396	87	14	25	43	354	411	478	115	164	4010	2583	170	94	45503
10:4-5.	51	133	43	394	86	12	27	49	354	409	490	111	166	4081	2392	180	78	33507
10:5-6.	53	135	42	383	84	11	26	43	353	391	485	112	168	4083	2465	180	65	28463
10:6-7.	53	133	42	386	83	11	24	42	775	381	487	110	163	4044	2618	189	81	29135
10:7-8.	84	133	40	383	80	13	23	47	392	373	604	109	178	3902	2381	200	72	22061
10:8-9.	82	135	39	377	82	13	22	43	308	328	504	108	177	3848	2504	224	80	19917
10:9-10.	45	137	41	363	82	8	23	40	230	298	350	111	165	3948	2432	222	78	16936
10:10-12.	N.D.	141	42	377	89	7	23	24	207	279	169	126	141	4038	2482	175	89	16315
10:12-14.	N.D.	144	44	381	90	8	23	21	222	305	163	130	145	4143	2634	181	93	15413
10:14-16.	N.D.	144	42	376	90	8	23	19	234	304	176	128	139	4063	2509	161	84	13644
10:16-18.	N.D.	141	43	343	84	9	23	30	243	310	194	132	140	4045	2426	163	90	13600
10:18-20.	N.D.	145	42	375	89	8	24	28	251	307	197	130	132	4043	2427	164	93	13708
10:20-22.	N.D.	144	40	380	88	7	23	16	251	283	217	122	133	3832	2236	164	78	11728
10:22-24.	N.D.	141	38	414	88	8	22	21	247	250	213	115	127	3553	2085	157	73	14027
10:24-26.	N.D.	143	37	424	88	9	22	20	240	241	195	116	126	3471	2165	166	71	12682
10:26-28.	N.D.	143	37	402	89	8	21	21	228	213	162	115	120	3391	1985	146	73	11754
10:28-30.	N.D.	146	37	389	92	9	21	20	216	188	152	115	124	3371	2058	144	70	12881
10:30-32.	N.D.	138	32	340	89	7	17	28	268	165	179	109	132	3112	1949	115	62	11704

N.D. - Not detectable

STATION 163-10 Salt-free trace element ratios to aluminium (x10-4)

	Mo/Al	Zr/Al	Y/Al	Rb/Al	Sr/Al	Th/Al	Pb/Al	As/Al	Zn/Al	Cu/Al	Ni/Al	Cr/Al	V/Al	Ba/Al
10:0-1.	2.15	17.45	5.18	11.00	48.42	1.64	2.91	3.54	32.24	40.08	33.76	15.30	18.33	510.93
10:1-2.	3.05	17.30	5.47	11.45	49.75	1.65	3.05	4.58	35.50	42.50	40.33	15.14	19.47	510.58
10:2-3.	5.84	17.38	5.84	11.15	50.72	1.69	3.24	4.67	44.88	52.66	59.54	14.92	21.14	519.74
10:3-4.	6.28	17.53	5.62	11.38	51.80	1.83	3.27	5.62	46.31	53.76	62.53	15.04	21.45	524.55
10:4-5.	6.65	17.34	5.61	11.21	51.38	1.56	3.52	6.39	46.16	53.33	63.90	14.47	21.65	532.16
10:5-6.	6.82	17.38	5.41	10.81	49.30	1.42	3.35	5.54	45.44	50.33	62.44	14.42	21.63	525.61
10:6-7.	6.96	17.47	5.52	10.90	50.69	1.44	3.15	5.52	101.77	50.03	63.95	14.45	21.41	531.06
10:7-8.	11.13	17.63	5.30	10.60	50.77	1.72	3.05	6.23	51.96	49.44	80.06	14.45	23.59	517.20
10:8-9.	10.97	18.06	5.22	10.97	50.44	1.74	2.94	5.75	41.21	43.89	67.44	14.45	23.68	514.87
10:9-10.	5.88	17.90	5.36	10.71	47.43	1.05	3.01	5.23	30.05	38.93	45.73	14.50	21.56	515.82
10:10-12.	N.D.	17.64	5.26	11.14	47.18	0.88	2.88	3.00	25.90	34.91	21.15	15.77	17.64	505.30
10:12-14.	N.D.	17.71	5.41	11.07	46.86	0.98	2.83	2.58	27.30	37.51	20.05	15.99	17.83	509.53
10:14-16.	N.D.	17.69	5.16	11.05	46.18	0.98	2.83	2.33	28.74	37.34	21.62	15.72	17.07	499.05
10:16-18.	N.D.	17.60	5.37	10.48	42.81	1.12	2.87	3.74	30.33	38.69	24.21	16.48	17.47	504.88
10:18-20.	N.D.	17.89	5.18	10.98	46.27	0.99	2.96	3.45	30.97	37.88	24.31	16.04	16.29	498.86
10:20-22.	N.D.	18.11	5.03	11.07	47.79	0.88	2.89	2.01	31.56	35.59	27.29	15.34	16.73	481.89
10:22-24.	N.D.	18.51	4.99	11.55	54.33	1.05	2.89	2.76	32.42	32.81	27.95	15.09	16.67	466.31
10:24-26.	N.D.	18.52	4.79	11.40	54.91	1.17	2.85	2.59	31.08	31.21	25.26	15.02	16.32	449.55
10:26-28.	N.D.	18.50	4.79	11.51	52.00	1.03	2.72	2.72	29.49	27.55	20.96	14.88	15.52	438.66
10:28-30.	N.D.	18.49	4.69	11.65	49.28	1.14	2.66	2.53	27.36	23.82	19.25	14.57	15.71	427.03
10:30-32.	N.D.	18.42	4.27	11.88	45.39	0.93	2.27	3.74	35.78	22.03	23.90	14.55	17.62	415.49

N.D. - Not detectable

STATION 163-9 Uncorrected major element data, Wt.% Element

	Si	Al	Fe	Mg	Ca	Na	K	Ti	Mn	P	LOI	Corg.	N
9:0-1.	24.04	7.32	5.17	2.27	1.30	3.69	2.01	0.406	1.32	0.12	10.00	0.56	0.11
9:1-2.	24.26	7.39	5.22	2.26	1.29	3.56	2.05	0.407	1.32	0.12	9.40	0.54	0.10
9:2-3.	24.52	7.47	5.28	2.23	1.29	3.37	2.13	0.412	1.36	0.12	8.90	0.51	0.10
9:3-4.	24.65	7.49	5.28	2.25	1.29	3.22	2.14	0.415	1.33	0.12	8.90	0.43	0.10
9:4-5.	24.56	7.47	5.28	2.25	1.29	3.31	2.13	0.413	1.37	0.12	9.40	0.46	0.10
9:5-6.	24.74	7.52	5.31	2.24	1.28	3.23	2.15	0.414	1.37	0.12	9.20	0.43	0.10
9:6-7.	24.65	7.50	5.34	2.25	1.28	3.24	2.15	0.413	1.35	0.12	9.40	0.53	0.10
9:7-8.	24.64	7.49	5.27	2.27	1.27	3.28	2.14	0.412	1.33	0.12	10.10	0.47	0.10
9:8-9.	24.83	7.56	5.22	2.25	1.28	3.16	2.17	0.413	1.30	0.12	9.50	0.37	0.09
9:9-10.	24.84	7.58	5.25	2.26	1.27	3.14	2.17	0.416	1.31	0.12	8.50	0.40	0.09
9:10-12.	25.01	7.61	5.17	2.19	1.25	3.02	2.24	0.418	1.29	0.11	8.60	0.39	0.09
9:12-14.	25.41	7.66	4.96	2.16	1.25	3.02	2.26	0.422	1.14	0.11	8.80	0.37	0.08
9:14-16.	25.68	7.74	4.92	2.14	1.23	2.91	2.33	0.426	0.98	0.10	8.60	0.33	0.08
9:16-18.	25.64	7.73	4.96	2.14	1.20	2.88	2.34	0.424	0.88	0.10	8.40	0.30	0.09
9:18-20.	25.66	7.82	5.10	2.16	1.19	3.01	2.35	0.429	1.03	0.10	7.80	0.37	0.08
9:20-22.	25.69	7.84	5.06	2.13	1.19	2.99	2.35	0.430	1.02	0.10	7.70	0.32	0.07
9:22-24.	25.36	7.71	5.05	2.11	1.17	2.98	2.32	0.425	0.89	0.09	8.00	0.31	0.08
9:24-26.	25.59	7.81	5.14	2.17	1.17	3.03	2.34	0.428	0.90	0.10	8.10	0.28	0.07
9:26-28.	25.79	7.84	5.16	2.17	1.19	3.05	2.37	0.432	0.85	0.10	7.90	0.27	0.07
9:28-30.	26.02	7.81	5.17	2.18	1.21	2.80	2.37	0.439	0.78	0.10	7.60	0.27	0.07
9:30-32.	25.70	7.72	5.13	2.20	1.20	2.88	2.36	0.437	0.76	0.09	7.50	0.22	0.07
9:32-34.	25.71	7.69	5.11	2.15	1.20	2.94	2.32	0.433	0.78	0.10	8.10	0.25	0.06
9:34-36.	25.69	7.65	5.26	2.20	1.20	2.87	2.31	0.434	0.67	0.10	7.70	0.25	0.06
9:36-38.	25.86	7.73	5.15	2.15	1.20	2.78	2.35	0.432	0.69	0.10	7.40	0.25	0.06

STATION 163-9 Salt-corrected major element data, Wt.% Element

	Si	Al	Fe	Mg	Ca	Na	K	Ti	Mn	P	LOI	Corg.	N	Salt
9:0-1.	26.01	7.92	5.59	2.15	1.31	1.48	2.09	0.439	1.43	0.13	10.00	0.61	0.12	7.58
9:1-2.	26.15	7.97	5.63	2.15	1.30	1.44	2.13	0.439	1.42	0.13	9.40	0.58	0.11	7.26
9:2-3.	26.12	7.96	5.62	2.14	1.30	1.59	2.19	0.439	1.45	0.12	8.90	0.54	0.10	6.13
9:3-4.	26.16	7.95	5.61	2.16	1.30	1.54	2.20	0.440	1.42	0.13	8.90	0.46	0.10	5.78
9:4-5.	26.11	7.94	5.61	2.16	1.30	1.59	2.19	0.439	1.45	0.13	9.40	0.49	0.10	5.91
9:5-6.	26.20	7.97	5.62	2.15	1.29	1.61	2.21	0.439	1.45	0.13	9.20	0.46	0.11	5.59
9:6-7.	26.12	7.94	5.66	2.17	1.28	1.60	2.21	0.438	1.43	0.13	9.40	0.56	0.11	5.63
9:7-8.	26.16	7.95	5.60	2.18	1.28	1.61	2.20	0.437	1.41	0.13	10.10	0.50	0.11	5.79
9:8-9.	26.28	8.00	5.53	2.17	1.28	1.55	2.24	0.437	1.38	0.13	9.50	0.39	0.10	5.53
9:9-10.	26.26	8.01	5.55	2.17	1.28	1.58	2.23	0.440	1.39	0.13	8.50	0.42	0.10	5.40
9:10-12.	26.26	7.99	5.42	2.11	1.25	1.65	2.30	0.439	1.35	0.12	8.60	0.41	0.09	4.74
9:12-14.	26.67	8.04	5.20	2.08	1.25	1.66	2.31	0.443	1.19	0.11	8.80	0.39	0.08	4.71
9:14-16.	26.88	8.10	5.16	2.07	1.23	1.61	2.39	0.446	1.03	0.10	8.60	0.35	0.08	4.49
9:16-18.	26.84	8.10	5.19	2.07	1.20	1.58	2.39	0.444	0.92	0.10	8.40	0.31	0.09	4.47
9:18-20.	26.89	8.20	5.34	2.09	1.19	1.69	2.41	0.449	1.08	0.10	7.80	0.39	0.08	4.56
9:20-22.	26.90	8.21	5.30	2.06	1.19	1.69	2.41	0.450	1.07	0.10	7.70	0.34	0.08	4.50
9:22-24.	26.58	8.08	5.29	2.03	1.16	1.66	2.38	0.445	0.94	0.10	8.00	0.32	0.08	4.57
9:24-26.	26.86	8.20	5.39	2.09	1.17	1.66	2.40	0.449	0.95	0.10	8.10	0.29	0.08	4.75
9:26-28.	27.03	8.22	5.41	2.10	1.19	1.73	2.43	0.453	0.89	0.10	7.90	0.28	0.07	4.59
9:28-30.	27.18	8.16	5.40	2.11	1.21	1.56	2.42	0.459	0.81	0.10	7.60	0.28	0.07	4.27
9:30-32.	26.85	8.06	5.36	2.13	1.20	1.63	2.42	0.457	0.79	0.10	7.50	0.23	0.07	4.29
9:32-34.	27.01	8.08	5.37	2.07	1.20	1.53	2.38	0.455	0.82	0.10	8.10	0.26	0.07	4.83
9:34-36.	27.05	8.06	5.54	2.12	1.20	1.40	2.38	0.457	0.70	0.10	7.70	0.26	0.07	5.01
9:36-38.	26.97	8.06	5.37	2.09	1.20	1.59	2.40	0.451	0.72	0.10	7.40	0.26	0.06	4.11

STATION 163-9 Salt-free ratios to aluminium

	Si/Al	Fe/Al	Mg/Al	Ca/Al	Na/Al	K/Al	Ti/Al	Mn/Al	P/Al	Corg./Al
9:0-1.	3.285	0.706	0.271	0.165	0.187	0.263	0.055	0.180	0.016	0.077
9:1-2.	3.283	0.707	0.270	0.163	0.181	0.267	0.055	0.178	0.016	0.073
9:2-3.	3.283	0.706	0.269	0.163	0.200	0.276	0.055	0.182	0.016	0.068
9:3-4.	3.290	0.705	0.271	0.163	0.193	0.277	0.055	0.178	0.016	0.057
9:4-5.	3.289	0.707	0.272	0.163	0.201	0.276	0.055	0.183	0.016	0.062
9:5-6.	3.289	0.706	0.270	0.162	0.201	0.278	0.055	0.182	0.016	0.057
9:6-7.	3.288	0.713	0.273	0.161	0.201	0.278	0.055	0.181	0.017	0.071
9:7-8.	3.288	0.703	0.274	0.161	0.202	0.277	0.055	0.177	0.016	0.063
9:8-9.	3.286	0.691	0.271	0.160	0.194	0.280	0.055	0.172	0.016	0.049
9:9-10.	3.278	0.693	0.271	0.160	0.197	0.278	0.055	0.173	0.016	0.053
9:10-12.	3.285	0.679	0.264	0.157	0.207	0.287	0.055	0.169	0.014	0.051
9:12-14.	3.319	0.648	0.259	0.156	0.207	0.288	0.055	0.148	0.014	0.048
9:14-16.	3.317	0.636	0.255	0.151	0.198	0.295	0.055	0.127	0.013	0.044
9:16-18.	3.315	0.642	0.255	0.149	0.195	0.296	0.055	0.114	0.013	0.039
9:18-20.	3.280	0.652	0.254	0.145	0.207	0.294	0.055	0.132	0.012	0.047
9:20-22.	3.278	0.646	0.251	0.145	0.206	0.293	0.055	0.130	0.012	0.041
9:22-24.	3.290	0.655	0.252	0.144	0.205	0.295	0.055	0.116	0.012	0.040
9:24-26.	3.275	0.658	0.255	0.142	0.202	0.293	0.055	0.116	0.012	0.036
9:26-28.	3.290	0.659	0.256	0.145	0.210	0.296	0.055	0.108	0.012	0.034
9:28-30.	3.329	0.661	0.259	0.148	0.191	0.297	0.056	0.099	0.012	0.035
9:30-32.	3.331	0.665	0.265	0.149	0.203	0.300	0.057	0.098	0.012	0.029
9:32-34.	3.343	0.665	0.256	0.148	0.190	0.295	0.056	0.102	0.012	0.033
9:34-36.	3.357	0.688	0.263	0.149	0.174	0.295	0.057	0.087	0.013	0.033
9:36-38.	3.344	0.666	0.259	0.149	0.197	0.298	0.056	0.089	0.013	0.032

STATION 163-9 Uncorrected trace element data, ppm

	Mo	Zr	Y	Sr	Rb	Th	Pb	As	Zn	Cu	Ni	CR	V	Ba	S	I	BR	Cl
9:0-1.	19	142	45	384	93	16	41	51	192	330	279	99	157	5164	4662	107	210	67375
9:1-2.	20	146	47	397	94	24	41	49	194	332	285	99	162	5293	4165	97	204	85424
9:2-3.	19	151	46	376	91	18	36	42	188	315	276	95	151	5223	4209	89	163	38399
9:3-4.	19	161	48	387	95	19	38	39	191	320	278	97	161	5390	4035	98	158	51497
9:4-5.	18	154	44	372	93	17	37	40	193	316	278	97	160	5220	4133	97	163	41901
9:5-6.	18	152	42	369	91	12	38	35	187	310	272	98	154	5158	4286	93	149	19578
9:6-7.	17	159	43	371	93	16	37	40	191	310	271	99	160	5225	4190	95	162	36182
9:7-8.	20	153	43	382	96	14	37	49	190	308	273	98	167	5335	4099	94	171	55426
9:8-9.	22	155	44	390	98	16	37	45	193	308	275	99	171	5358	3678	103	161	65175
9:9-10.	22	154	44	394	97	20	35	54	188	297	270	100	163	5365	3679	96	159	60409
9:10-12.	23	158	44	366	96	16	32	49	184	277	265	98	161	5192	3600	90	137	41272
9:12-14.	22	160	40	357	98	12	29	37	175	243	237	99	162	5058	3493	87	132	39426
9:14-16.	19	164	38	358	101	13	29	36	169	221	194	94	156	4940	3404	84	120	36858
9:16-18.	16	164	37	358	100	10	30	38	165	218	179	95	159	4998	3333	85	117	33609
9:18-20.	18	164	40	367	100	16	30	42	175	252	204	92	158	5144	3532	88	118	35120
9:20-22.	17	165	38	380	101	15	32	41	174	252	205	96	158	5203	3291	83	113	42351
9:22-24.	13	162	39	374	105	15	34	52	173	243	188	95	159	5278	3295	86	113	59752
9:24-26.	13	164	38	379	102	15	33	47	168	250	188	93	161	5354	3494	82	116	48743
9:26-28.	11	167	39	375	102	14	35	43	162	237	175	91	156	5351	3508	85	110	35115
9:28-30.	11	173	40	376	101	14	32	32	161	227	164	95	157	5570	3443	81	101	36108
9:30-32.	12	172	44	419	109	26	41	46	169	249	169	97	153	5777	2887	80	111	100586
9:32-34.	9	169	41	389	102	13	35	35	163	251	173	93	156	5661	3695	86	113	51366
9:34-36.	4	170	39	381	101	13	34	34	157	219	143	91	149	5591	3674	88	109	27847
9:36-38.	74	172	42	387	103	16	36	39	157	230	151	94	155	5558	3345	84	109	40706

N.D. - Not detectable

STATION 163-9 Salt-corrected trace element data, ppm

	Mo	Zr	Y	Sr	Rb	Th	Pb	As	Zn	Cu	Ni	Cr	V	Ba	S	I	Br	Cl
9:0-1.	21	154	49	415	101	17	44	55	208	357	302	107	170	5588	2912	116	71	67375
9:1-2.	22	157	51	428	101	26	44	53	209	358	307	107	175	5707	2456	105	71	85424
9:2-3.	20	161	49	401	97	19	38	45	200	336	294	101	172	5564	2786	95	50	38399
9:3-4.	20	160	51	411	101	20	40	41	203	340	295	103	171	5721	2688	104	51	51497
9:4-5.	19	164	47	395	99	18	39	43	205	336	295	103	170	5548	2759	103	54	41901
9:5-6.	19	161	44	391	96	13	40	37	198	328	288	104	163	5463	3000	99	45	19578
9:6-7.	18	161	46	393	99	17	39	42	202	328	287	105	170	5537	2889	101	58	36182
9:7-8.	21	162	46	405	102	15	39	52	202	327	290	104	177	5663	2753	100	65	55426
9:8-9.	23	164	47	413	104	17	39	48	204	326	291	105	181	5672	2371	109	59	65175
9:9-10.	23	163	47	416	103	21	37	57	199	314	285	106	172	5671	2405	101	60	60409
9:10-12.	24	166	46	384	101	17	34	51	193	291	278	103	169	5450	2485	94	49	41272
9:12-14.	23	168	42	375	103	13	30	39	184	255	249	104	170	5308	2381	91	45	39426
9:14-16.	20	172	40	375	106	14	30	38	177	231	203	98	163	5172	2342	88	36	36858
9:16-18.	17	172	39	375	105	10	31	40	173	228	187	99	166	5232	2272	89	34	33609
9:18-20.	19	172	42	385	105	17	31	44	183	264	214	96	166	5390	2459	92	33	35120
9:20-22.	18	173	40	398	106	16	34	43	182	264	215	101	165	5448	2221	87	29	42351
9:22-24.	14	170	41	392	110	16	36	54	181	255	197	100	167	5531	2208	90	27	59752
9:24-26.	14	172	40	398	107	16	35	49	176	262	197	98	169	5621	2372	86	27	48743
9:26-28.	12	175	41	393	107	15	37	45	170	248	183	95	164	5608	2426	89	24	35115
9:28-30.	11	181	42	393	106	15	33	33	168	237	171	99	164	5818	2437	85	21	36108
9:30-32.	13	180	46	438	114	27	43	48	177	260	177	101	160	6036	1851	84	31	100586
9:32-34.	9	178	43	409	107	14	37	37	171	264	182	98	164	5948	2563	90	22	51366
9:34-36.	4	179	41	401	106	14	36	36	165	231	151	96	157	5886	2496	93	15	27847
9:36-38.	7	179	44	404	107	17	38	41	164	240	157	98	162	5796	2374	88	21	40706

N.D. - Not detectable

STATION 163-9 Salt-free trace element ratios to aluminium (x10-4)

	Mo/Al	Zr/Al	Y/Al	Sr/Al	Rb/Al	Th/Al	Pb/Al	As/Al	Zn/Al	Cu/Al	Ni/Al	Cr/Al	V/Al	Ba/Al
9:0-1.	2.65	19.45	6.19	12.75	52.40	2.15	5.56	6.95	26.26	45.08	38.13	13.51	21.47	705.62
9:1-2.	2.76	19.71	6.40	12.68	53.73	3.26	5.52	6.65	26.24	44.94	38.54	13.43	21.97	716.39
9:2-3.	2.51	20.24	6.16	12.19	50.40	2.39	4.78	5.66	25.14	42.23	36.95	12.70	21.62	699.37
9:3-4.	2.51	20.12	6.41	12.70	51.68	2.51	5.03	5.16	25.53	42.75	37.09	12.95	21.50	719.38
9:4-5.	2.39	20.66	5.92	12.47	49.77	2.27	4.91	5.42	25.83	42.33	37.17	12.98	21.42	699.00
9:5-6.	2.39	20.21	5.52	12.05	49.08	1.63	5.02	4.64	24.85	41.17	36.15	13.05	20.46	685.76
9:6-7.	2.27	20.27	5.79	12.46	49.47	2.14	4.91	5.29	25.43	41.29	36.13	13.22	21.40	696.98
9:7-8.	2.64	20.37	5.78	12.82	50.91	1.89	4.90	6.54	25.39	41.11	36.46	13.07	22.25	711.92
9:8-9.	2.88	20.50	5.88	13.00	51.64	2.13	4.88	6.00	25.51	40.76	36.38	13.13	22.63	709.15
9:9-10.	2.87	20.35	5.87	12.86	51.93	2.62	4.62	7.12	24.84	39.20	35.58	13.23	21.47	707.94
9:10-12.	3.00	20.77	5.76	12.64	48.04	2.13	4.25	6.38	24.15	36.41	34.78	12.89	21.14	681.86
9:12-14.	2.86	20.90	5.23	12.82	46.66	1.62	3.73	4.85	22.90	31.73	30.98	12.94	21.15	660.48
9:14-16.	2.47	21.22	4.94	13.08	46.27	1.73	3.70	4.69	21.84	28.50	25.05	12.09	20.11	638.21
9:16-18.	2.10	21.25	4.82	12.97	46.32	1.24	3.83	4.94	21.37	28.16	23.10	12.23	20.50	646.25
9:18-20.	2.32	20.98	5.12	12.81	46.96	2.07	3.78	5.37	22.32	32.20	26.10	11.71	20.25	657.41
9:20-22.	2.19	21.08	4.87	12.92	48.51	1.95	4.14	5.24	22.18	32.17	26.20	12.31	20.11	663.97
9:22-24.	1.73	21.04	5.08	13.62	48.53	1.98	4.46	6.68	22.41	31.57	24.39	12.38	20.67	684.68
9:24-26.	1.71	20.97	4.88	13.05	48.53	1.95	4.27	5.97	21.46	31.95	24.02	11.95	20.61	685.36
9:26-28.	1.46	21.30	4.99	13.02	47.83	1.83	4.50	5.48	20.69	30.18	22.27	11.56	19.96	682.56
9:28-30.	1.35	22.17	5.14	12.98	48.14	1.84	4.04	4.04	20.58	29.03	20.95	12.13	20.09	712.68
9:30-32.	1.61	22.33	5.71	14.14	54.34	3.35	5.33	5.95	21.96	32.25	21.96	12.53	19.85	748.81
9:32-34.	1.11	22.03	5.32	13.24	50.61	1.73	4.58	4.58	21.16	32.67	22.52	12.13	20.29	736.02
9:34-36.	0.50	22.21	5.09	13.16	49.77	1.74	4.47	4.47	20.48	28.67	18.74	11.91	19.48	730.48
9:36-38.	0.87	22.20	5.46	13.27	50.10	2.11	4.71	5.08	20.34	29.76	19.47	12.15	20.09	718.71

N.D. - Not detectable

STATION 163-15 Uncorrected major element data, Wt.%

	Si	Al	Fe	Mg	Ca	Na	K	Ti	Mn	P	LOI
15:0-1.	23.71	7.14	5.02	2.24	1.41	3.41	1.93	0.40	1.44	0.12	11.60
15:1-2.	24.17	7.35	5.16	2.26	1.29	3.24	2.03	0.41	1.52	0.12	10.40
15:2-3.	24.30	7.43	5.25	2.24	1.27	3.19	2.09	0.41	1.55	0.12	10.00
15:3-4.	24.46	7.47	5.26	2.28	1.29	3.19	2.11	0.41	1.57	0.12	9.60
15:4-5.	24.36	7.40	5.24	2.24	1.27	3.03	2.11	0.41	1.60	0.11	9.80
15:5-6.	24.47	7.45	5.26	2.20	1.28	3.06	2.13	0.41	1.62	0.12	9.60
15:6-7.	24.63	7.49	5.44	2.26	1.27	3.04	2.14	0.42	1.67	0.12	9.20
15:7-8.	24.56	7.50	5.34	2.24	1.27	3.07	2.15	0.42	1.63	0.12	9.70
15:8-9.	24.32	7.42	5.19	2.18	1.25	2.91	2.13	0.41	1.60	0.12	10.10
15:9-10.	24.45	7.44	5.28	2.18	1.23	2.92	2.18	0.41	1.61	0.12	9.70
15:10-12.	24.42	7.45	5.19	2.20	1.23	2.83	2.16	0.41	1.59	0.11	10.00
15:12-14.	25.04	7.60	5.01	2.13	1.19	2.66	2.25	0.41	1.51	0.10	8.90
15:14-16.	25.20	7.62	4.95	2.09	1.17	2.64	2.29	0.42	1.50	0.10	9.00
15:16-18.	25.14	7.58	4.91	2.07	1.17	2.66	2.27	0.41	1.60	0.10	8.90
15:18-20.	25.45	7.72	5.00	2.18	1.16	2.66	2.31	0.42	1.35	0.10	8.30
15:20-22.	25.90	7.83	5.04	2.21	1.15	2.80	2.36	0.43	0.92	0.09	8.70
15:22-24.	25.70	7.83	5.11	2.28	1.13	2.81	2.35	0.43	0.91	0.09	8.40
15:24-26.	25.43	7.78	5.14	2.16	1.12	2.80	2.34	0.43	1.06	0.09	8.00
15:26-28.	25.40	7.80	5.15	2.16	1.13	2.79	2.34	0.43	1.40	0.09	7.90
15:28-30.	24.70	7.58	5.09	2.16	1.14	2.63	2.30	0.42	2.54	0.09	7.70
15:30-32.	25.30	7.77	5.12	2.18	1.14	2.78	2.32	0.42	1.84	0.09	7.90
15:32-34.	25.21	7.66	5.07	2.15	1.15	2.64	2.33	0.43	2.06	0.09	7.90
15:34-35.	25.41	7.71	5.12	2.19	1.15	2.64	2.34	0.43	1.56	0.09	7.20

STATION 163-15 Salt-corrected major element data, Wt.% Element

	Si	Al	Fe	Mg	Ca	Na	K	Ti	Mn	P	LOI	Salt
15:0-1.	25.74	7.75	5.45	2.12	1.43	0.41	2.00	0.43	1.57	0.13	11.60	7.87
15:1-2.	26.03	7.91	5.56	2.15	1.29	1.14	2.10	0.44	1.63	0.13	10.40	7.13
15:2-3.	26.02	7.95	5.63	2.14	1.28	1.24	2.15	0.44	1.66	0.13	10.00	6.62
15:3-4.	26.15	7.99	5.62	2.18	1.30	1.30	2.18	0.44	1.68	0.13	9.60	6.46
15:4-5.	25.93	7.88	5.58	2.15	1.28	1.26	2.17	0.43	1.71	0.12	9.80	6.06
15:5-6.	26.01	7.92	5.59	2.11	1.28	1.33	2.20	0.44	1.72	0.13	9.60	5.91
15:6-7.	26.16	7.95	5.78	2.17	1.28	1.33	2.21	0.44	1.77	0.13	9.20	5.85
15:7-8.	26.08	7.96	5.67	2.15	1.28	1.36	2.21	0.44	1.74	0.13	9.70	5.82
15:8-9.	25.95	7.92	5.54	2.08	1.25	1.07	2.20	0.44	1.70	0.13	10.10	6.26
15:9-10.	25.85	7.87	5.58	2.10	1.24	1.33	2.25	0.44	1.70	0.12	9.70	5.44
15:10-12.	25.84	7.88	5.49	2.11	1.23	1.22	2.22	0.43	1.68	0.12	10.00	5.47
15:12-14.	26.30	7.99	5.27	2.05	1.19	1.25	2.31	0.43	1.59	0.11	8.90	4.80
15:14-16.	26.44	8.00	5.20	2.01	1.17	1.27	2.35	0.44	1.58	0.10	9.00	4.68
15:16-18.	26.37	7.96	5.15	1.99	1.17	1.29	2.32	0.43	1.67	0.10	8.90	4.69
15:18-20.	26.65	8.08	5.24	2.11	1.16	1.34	2.36	0.45	1.41	0.10	8.30	4.51
15:20-22.	27.21	8.22	5.29	2.13	1.15	1.39	2.42	0.45	0.97	0.10	8.70	4.82
15:22-24.	27.04	8.24	5.37	2.20	1.13	1.37	2.41	0.45	0.96	0.10	8.40	4.93
15:24-26.	26.75	8.18	5.40	2.08	1.12	1.35	2.40	0.45	1.12	0.10	8.00	4.97
15:26-28.	26.68	8.19	5.41	2.08	1.13	1.40	2.39	0.45	1.46	0.10	7.90	4.79
15:28-30.	25.90	7.95	5.34	2.09	1.14	1.26	2.36	0.44	2.66	0.10	7.70	4.65
15:30-32.	26.61	8.18	5.39	2.10	1.13	1.34	2.39	0.44	1.94	0.10	7.90	4.94
15:32-34.	26.38	8.02	5.31	2.07	1.15	1.34	2.39	0.45	2.16	0.10	7.90	4.46
15:34-35.	26.61	8.08	5.37	2.12	1.14	1.31	2.40	0.45	1.63	0.10	7.20	4.53

STATION 163-15 Salt-free ratios to aluminium

	Si/Al	Fe/Al	Mg/Al	Ca/Al	Na/Al	K/Al	Ti/Al	Mn/Al	P/Al
15:0-1.	3.321	0.703	0.274	0.185	0.053	0.258	0.055	0.203	0.017
15:1-2.	3.291	0.703	0.272	0.163	0.144	0.265	0.056	0.206	0.016
15:2-3.	3.273	0.708	0.269	0.161	0.156	0.270	0.055	0.209	0.016
15:3-4.	3.273	0.703	0.273	0.163	0.163	0.273	0.055	0.210	0.016
15:4-5.	3.291	0.708	0.273	0.162	0.160	0.275	0.055	0.217	0.015
15:5-6.	3.284	0.706	0.266	0.162	0.168	0.278	0.056	0.217	0.016
15:6-7.	3.291	0.727	0.273	0.161	0.167	0.278	0.055	0.223	0.016
15:7-8.	3.276	0.712	0.270	0.161	0.171	0.278	0.055	0.219	0.016
15:8-9.	3.277	0.699	0.263	0.158	0.135	0.278	0.056	0.215	0.016
15:9-10.	3.285	0.709	0.267	0.158	0.169	0.286	0.056	0.216	0.015
15:10-12.	3.279	0.697	0.268	0.156	0.155	0.282	0.055	0.213	0.015
15:12-14.	3.292	0.660	0.257	0.149	0.156	0.289	0.054	0.199	0.014
15:14-16.	3.305	0.650	0.251	0.146	0.159	0.294	0.055	0.197	0.013
15:16-18.	3.313	0.647	0.250	0.147	0.162	0.291	0.054	0.210	0.013
15:18-20.	3.298	0.649	0.261	0.144	0.166	0.292	0.056	0.175	0.012
15:20-22.	3.310	0.644	0.259	0.140	0.169	0.294	0.055	0.118	0.012
15:22-24.	3.282	0.652	0.267	0.137	0.166	0.292	0.055	0.117	0.012
15:24-26.	3.270	0.660	0.254	0.137	0.165	0.293	0.055	0.137	0.012
15:26-28.	3.258	0.661	0.254	0.138	0.171	0.292	0.055	0.178	0.012
15:28-30.	3.258	0.672	0.263	0.143	0.158	0.297	0.055	0.335	0.013
15:30-32.	3.253	0.659	0.257	0.138	0.164	0.292	0.054	0.237	0.012
15:32-34.	3.289	0.662	0.258	0.143	0.167	0.298	0.056	0.269	0.012
15:34-35.	3.293	0.665	0.262	0.141	0.162	0.297	0.056	0.202	0.012

STATION 163-15 Uncorrected trace element data, ppm

	Mo	Zr	Y	Sr	Rb	Th	Pb	As	Zn	Cu	Ni	Cr	V	Ba
15:0-1.	16	131	37	339	82	8	32	13	169	252	249	85	156	4265
15:1-2.	19	143	39	350	86	8	27	16	177	266	263	89	164	4414
15:2-3.	20	150	40	352	87	9	26	18	182	266	266	88	169	4466
15:3-4.	20	151	39	354	89	8	27	18	179	257	253	83	153	4125
15:4-5.	20	151	40	353	88	9	21	21	186	268	269	92	171	4657
15:5-6.	21	151	39	356	89	9	24	20	192	274	275	92	178	4810
15:6-7.	21	152	41	359	90	9	33	19	215	276	272	93	174	4711
15:7-8.	21	152	41	360	90	9	23	22	185	266	263	89	168	4528
15:8-9.	21	152	39	355	90	8	19	21	182	262	263	91	168	4678
15:9-10.	23	155	39	356	91	5	21	21	181	255	261	92	173	4686
15:10-12.	24	155	40	353	90	9	20	21	180	245	253	90	173	4557
15:12-14.	29	162	38	347	94	9	16	20	176	215	246	92	174	4550
15:14-16.	30	162	36	342	96	8	12	21	177	190	215	89	171	4504
15:16-18.	27	160	35	339	97	10	14	20	178	195	198	90	172	4478
15:18-20.	24	160	37	347	98	10	20	19	165	207	193	91	177	4599
15:20-22.	13	161	34	348	101	10	17	19	152	170	153	94	172	4724
15:22-24.	12	164	36	347	100	5	18	18	155	181	163	92	165	4825
15:24-26.	14	162	36	351	99	10	19	20	156	192	180	89	169	4868
15:26-28.	20	161	36	356	99	10	22	19	168	222	233	88	176	4973
15:28-30.	44	162	38	368	98	10	17	23	205	319	401	88	205	5186
15:30-32.	25	161	37	362	98	12	13	24	180	243	261	88	187	5047
15:32-34.	27	168	38	366	99	14	18	23	180	269	271	88	195	5227
15:34-35.	19	168	36	361	98	11	20	24	166	249	226	88	186	5238

N.D. - Not detectable

STATION 163-15 Salt-corrected trace element data, ppm

	Mo	Zr	Y	Sr	Rb	Th	Pb	As	Zn	Cu	Ni	Cr	V	Ba
15:0-1.	17	142	40	368	89	9	35	14	183	274	270	92	169	4629
15:1-2.	20	154	42	377	93	9	29	17	191	286	283	96	177	4753
15:2-3.	21	161	43	377	93	10	28	19	195	285	285	94	181	4783
15:3-4.	21	161	42	378	95	9	29	19	191	275	270	89	164	4410
15:4-5.	21	161	43	376	94	10	22	22	198	285	286	98	182	4957
15:5-6.	22	160	41	378	95	10	26	21	204	291	292	98	189	5112
15:6-7.	22	161	44	381	96	10	35	20	228	293	289	99	185	5004
15:7-8.	22	161	44	382	96	10	24	23	196	282	279	94	178	4808
15:8-9.	22	162	42	379	96	9	20	22	194	279	281	97	179	4990
15:9-10.	24	164	41	376	96	5	22	22	191	270	276	97	183	4956
15:10-12.	25	164	42	373	95	10	21	22	190	259	268	95	183	4821
15:12-14.	30	170	40	364	99	9	17	21	185	226	258	97	183	4779
15:14-16.	31	170	38	359	101	8	13	22	186	199	226	93	179	4725
15:16-18.	28	168	37	356	102	10	15	21	187	205	208	94	180	4698
15:18-20.	25	168	39	363	103	10	21	20	173	217	202	95	185	4816
15:20-22.	14	169	36	366	106	11	18	20	160	179	161	99	181	4963
15:22-24.	13	173	38	365	105	5	19	19	163	190	171	97	174	5075
15:24-26.	15	170	38	369	104	11	20	21	164	202	189	94	178	5123
15:26-28.	21	169	38	374	104	11	23	20	176	233	245	92	185	5223
15:28-30.	46	170	40	386	103	10	18	24	215	335	421	92	215	5439
15:30-32.	26	169	39	381	103	13	14	25	189	256	275	93	197	5309
15:32-34.	28	176	40	383	104	15	19	24	188	282	284	92	204	5471
15:34-35.	20	176	38	378	103	12	21	25	174	261	237	92	195	5487

N.D. - Not detectable

STATION 163-15 Salt-free trace element ratios to aluminium (x10-4)

	Mo/Al	Zr/Al	Y/Al	Sr/Al	Rb/Al	Th/Al	Pb/Al	As/Al	Zn/Al	Cu/Al	Ni/Al	Cr/Al	V/Al	Ba/Al	K/Rb
15:0-1.	2.19	18.32	5.16	47.48	11.48	1.16	4.52	1.81	23.61	35.35	34.84	11.87	21.81	597.29	224.72
15:1-2.	2.53	19.47	5.31	47.66	11.76	1.14	3.67	2.15	24.15	36.16	35.78	12.14	22.38	600.88	225.81
15:2-3.	2.64	20.25	5.41	47.42	11.70	1.26	3.52	2.39	24.53	35.85	35.85	11.82	22.77	601.64	231.18
15:3-4.	2.63	20.15	5.26	47.31	11.89	1.13	3.63	2.38	23.90	34.42	33.79	11.14	20.53	551.94	229.47
15:4-5.	2.66	20.43	5.46	47.72	11.93	1.27	2.79	2.79	25.13	36.17	36.29	12.44	23.10	629.06	230.85
15:5-6.	2.78	20.20	5.18	47.73	11.99	1.26	3.28	2.65	25.76	36.74	36.87	12.37	23.86	645.45	231.58
15:6-7.	2.77	20.25	5.53	47.92	12.08	1.26	4.40	2.52	28.68	36.86	36.35	12.45	23.27	629.43	230.21
15:7-8.	2.76	20.23	5.53	47.99	12.06	1.26	3.02	2.89	24.62	35.43	35.05	11.81	22.36	604.02	230.21
15:8-9.	2.78	20.45	5.30	47.85	12.12	1.14	2.53	2.78	24.49	35.23	35.48	12.25	22.60	630.05	229.17
15:9-10.	3.05	20.84	5.21	47.78	12.20	0.64	2.80	2.80	24.27	34.31	35.07	12.33	23.25	629.73	234.37
15:10-12.	3.17	20.81	5.33	47.34	12.06	1.27	2.66	2.79	24.11	32.87	34.01	12.06	23.22	611.80	233.68
15:12-14.	3.75	21.28	5.01	45.56	12.39	1.13	2.13	2.63	23.15	28.29	32.29	12.14	22.90	598.12	233.33
15:14-16.	3.87	21.25	4.75	44.87	12.62	1.00	1.62	2.75	23.25	24.87	28.25	11.62	22.37	590.62	232.67
15:16-18.	3.52	21.11	4.65	44.72	12.81	1.26	1.88	2.64	23.49	25.75	26.13	11.81	22.61	590.20	227.45
15:18-20.	3.09	20.79	4.83	44.93	12.75	1.24	2.60	2.48	21.41	26.86	25.00	11.76	22.90	596.04	229.13
15:20-22.	1.70	20.56	4.38	44.53	12.90	1.34	2.19	2.43	19.46	21.78	19.59	12.04	22.02	603.77	228.30
15:22-24.	1.58	21.00	4.61	44.30	12.74	0.61	2.31	2.31	19.78	23.06	20.75	11.77	21.12	615.90	229.52
15:24-26.	1.83	20.78	4.65	45.11	12.71	1.34	2.44	2.57	20.05	24.69	23.11	11.49	21.76	626.28	230.77
15:26-28.	2.56	20.63	4.64	45.67	12.70	1.34	2.81	2.44	21.49	28.45	29.91	11.23	22.59	637.73	229.81
15:28-30.	5.79	21.38	5.03	48.55	12.96	1.26	2.26	3.02	27.04	42.14	52.96	11.57	27.04	684.15	229.13
15:30-32.	3.18	20.66	4.77	46.58	12.59	1.59	1.71	3.06	23.11	31.30	33.62	11.37	24.08	649.02	232.04
15:32-34.	3.49	21.95	4.99	47.76	12.97	1.87	2.37	2.99	23.44	35.16	35.41	11.47	25.44	682.17	229.81
15:34-35.	2.48	21.78	4.70	46.78	12.75	1.49	2.60	3.09	21.53	32.30	29.33	11.39	24.13	679.08	233.01

N.D. - Not detectable

STATION 145-17 and 163-8 Salt-free halogen to organic carbon ratio (x10-4) and K/Rb ratio.

	Br/C	I/C	K/Rb
17:0-1.	102.61	132.07	184.69
17:2-3.	83.79	94.56	187.86
17:3-4.	84.66	95.19	192.63
17:4-5.	85.62	93.52	192.14
17:5-6.	84.83	81.21	178.66
17:6-7.	85.45	70.15	164.79
17:7-8.	86.35	63.47	141.54
17:8-9.	84.11	68.30	143.48
17:9-10.	83.19	73.62	135.08
17:10-12.	81.21	55.44	126.39
17:12-14.	94.80	63.38	132.25
17:14-16.	78.98	59.89	142.11
17:16-18.	74.52	51.63	140.33
17:18-20.	77.25	37.91	124.58
17:20-22.	83.02	46.76	104.31
17:22-24.	83.72	43.53	107.28
17:24-26.	97.89	52.52	112.27
17:26-28.	81.21	44.36	126.03

	Br/C	I/C	K/Rb
8:0-1.	94.77	75.79	47.88
8:1-2.	90.30	69.91	62.71
8:2-3.	101.12	75.88	53.59
8:3-4.	101.51	71.35	52.20
8:4-5.	99.39	72.05	53.96
8:5-6.	113.24	72.73	68.05
8:6-7.	101.01	73.90	74.76
8:7-8.	87.67	73.72	81.81
8:8-9.	91.93	71.65	60.25
8:9-10.	68.24	59.62	146.52
8:10-11.	71.48	63.26	117.01
8:11-12.	72.36	64.03	116.91
8:12-13.	75.85	65.45	115.50
8:13-14.	71.38	68.76	152.89
8:14-15.	76.68	64.77	121.99
8:15-16.	73.62	60.14	62.63
8:16-18.	77.54	56.59	114.29
8:18-20.	75.27	56.22	93.70
8:20-22.	71.63	53.99	117.52
8:22-24.	76.72	56.09	96.27
8:24-26.	78.28	52.11	93.83
8:26-28.	70.40	58.50	47.03
8:28-30.	67.06	58.79	127.61
8:30-32.	66.53	54.61	77.08
8:32-34.	79.29	56.44	68.15
8:34-36.	63.49	57.48	95.98
8:36-38.	64.69	53.59	86.11
8:38-40.	66.67	58.98	115.76
8:40-42.	67.35	51.92	117.63
8:42-44.	64.33	45.62	97.95
8:44-46.	61.13	48.82	77.78
8:46-48.	62.20	54.93	59.03
8:48-49.	65.09	57.47	119.56

STATION 163-7 and 163-14 Salt-free halogen to organic carbon ratio (x10-4) and K/Rb ratio.

	Br/C	I/C	K/Rb
7:0-1.	70.06	268.17	221.12
7:1-2.	92.02	223.47	238.49
7:2-3.	94.34	276.08	230.61
7:3-4.	90.68	221.74	236.78
7:4-5.	95.66	198.73	236.13
7:5-6.	95.41	188.83	235.71
7:6-7.	95.77	199.78	238.19
7:7-8.	99.57	206.63	245.60
7:8-9.	93.63	193.28	239.97
7:9-10.	92.54	186.39	242.59
7:10-11.	90.65	179.96	239.55
7:11-12.	92.65	177.18	237.89
7:12-13.	85.41	166.85	241.20
7:13-14.	88.98	169.00	244.24
7:14-15.	80.40	146.92	260.50
7:15-16.	81.89	147.40	249.07
7:16-17.	82.14	148.49	248.20
7:17-18.	79.18	141.11	245.49
7:18-19.	85.91	151.75	240.39
7:19-20.	88.95	151.04	233.81
7:20-22.	76.92	147.05	220.96
7:22-24.	72.14	151.80	212.59
7:24-26.	68.71	153.10	216.11
7:26-28.	52.18	149.69	230.51
7:28-30.	65.20	152.87	231.41
7:30-32.	68.64	153.81	224.89
7:32-34.	78.90	136.16	229.14

	Br/C	I/C	K/Rb
14:0-1.	98.20	189.25	209.46
14:1-2.	115.82	238.08	191.32
14:2-3.	119.70	231.99	218.54
14:3-4.	117.53	243.54	188.97
14:4-5.	102.55	245.09	198.02
14:5-6.	115.27	289.33	224.92
14:6-7.	130.88	329.26	244.10
14:7-8.	94.84	228.56	235.33
14:8-9.	98.03	282.56	243.76
14:9-10.	94.49	228.67	237.79
14:10-12.	92.78	171.73	242.55
14:12-14.	87.84	183.92	241.06
14:14-16.	88.83	193.10	234.16
14:16-18.	76.59	226.11	190.66
14:18-20.	69.50	223.14	165.11
14:20-22.	66.48	217.76	174.34
14:22-24.	69.44	222.20	184.25
14:24-26.	64.69	202.63	182.67
14:26-28.	63.65	194.75	190.37
14:28-30.	71.16	192.85	218.82
14:30-32.	62.43	159.44	221.98

STATION 163-10 and 163-9 Salt-free halogen to organic carbon ratio (x10-4) and K/Rb ratio.

	Br/C	I/C	K/Rb
10:0-1.	99.45	180.06	233.43
10:1-2.	109.36	197.94	221.22
10:2-3.	120.86	207.69	225.89
10:3-4.	102.23	184.88	220.57
10:4-5.	96.72	223.20	224.06
10:5-6.	80.26	222.26	232.12
10:6-7.	98.84	230.63	231.91
10:7-8.	93.19	258.85	242.55
10:8-9.	113.48	317.75	237.06
10:9-10.	96.15	273.67	245.28
10:10-12.	90.57	178.09	236.03
10:12-14.	84.59	164.64	236.50
10:14-16.	83.00	159.09	239.24
10:16-18.	82.13	148.75	251.87
10:18-20.	92.15	162.50	240.54
10:20-22.	71.30	149.92	236.28
10:22-24.	77.80	167.32	220.73
10:24-26.	67.51	157.85	227.41
10:26-28.	77.05	154.09	226.15
10:28-30.	67.84	139.55	227.61
10:30-32.	68.59	127.06	240.07

	Br/C	I/C	K/Rb
9:0-1.	117.18	191.44	206.51
9:1-2.	121.94	180.33	210.65
9:2-3.	92.03	174.86	226.08
9:3-4.	111.75	227.88	218.09
9:4-5.	110.45	210.68	221.36
9:5-6.	98.80	217.36	230.54
9:6-7.	103.27	179.84	223.28
9:7-8.	130.29	200.45	215.65
9:8-9.	150.64	278.30	215.08
9:9-10.	141.90	238.87	216.40
9:10-12.	119.69	229.60	227.29
9:12-14.	115.89	234.36	224.58
9:14-16.	104.19	254.69	225.66
9:16-18.	108.27	283.41	227.98
9:18-20.	85.12	237.31	229.40
9:20-22.	86.55	259.64	226.96
9:22-24.	83.12	277.05	216.32
9:24-26.	91.85	292.55	224.47
9:26-28.	84.81	314.50	226.91
9:28-30.	74.46	301.37	228.73
9:30-32.	134.86	365.44	211.88
9:32-34.	83.75	342.61	222.51
9:34-36.	56.99	353.66	224.34
9:34-36.	122.74	352.88	225.34

SALT-FREE CALCIUM CARBONATE CONTENTS: OCEANIC CORES, BAJA CALIFORNIA

Depth cm	163-7 wt.%	Depth cm	163-14 wt.%	Depth cm	163-10 wt.%	Depth cm	163-9 wt.%
0-1	1.08	0-1	1.58	0-1	1.75	0-1	0.75
1-2	1.25	1-2	2.25	1-2	1.42	1-2	0.50
2-3	1.00	2-3	2.33	2-3	1.42	2-3	0.58
3-4	1.00	3-4	2.08	3-4	0.92	3-4	1.17
4-5	0.92	4-5	1.75	4-5	1.08	4-5	0.92
5-6	0.42	5-6	2.33	5-6	1.33	5-6	1.17
6-7	0.25	6-7	4.17	6-7	0.75	6-7	1.08
7-8	0.75	7-8	1.75	7-8	1.17	7-8	0.75
8-9	1.25	8-9	2.17	8-9	1.58	8-9	1.58
9-10	0.67	9-10	1.50	9-10	1.67	9-10	1.17
10-11	0.67	10-12	0.92	10-12	1.17	10-12	0.92
11-12	0.58	12-14	1.92	12-14	1.00	12-14	1.00
12-13	0.33	14-16	4.66	14-16	2.17	14-16	1.25
13-14	0.42	16-18	10.16	16-18	1.67	16-18	1.50
14-15	0.75	18-20	14.83	18-20	2.50	18-20	0.42
15-16	0.58	20-22	15.49	20-22	3.75	20-22	0.75
16-17	1.33	22-24	15.74	22-24	6.50	22-24	1.00
17-18	1.92	24-26	14.16	24-26	5.91	24-26	1.08
18-19	3.08	26-28	12.00	26-28	6.25	26-28	1.58
19-20	3.83	28-30	9.83	28-30	5.33	28-30	0.83
20-22	4.50	30-32	7.58	30-32	3.08	30-32	1.25
22-24	7.25					32-34	1.00
24-26	7.41					34-36	0.83
26-28	6.83					36-38	0.67
28-30	7.88						
30-32	8.58						
32-34	6.59						

$$CaCO_3 = (C_{tot} - C_{org}) \times 8.333$$

RADIONUCLIDES IN OCEANIC SEDIMENTS OFF BAJA CALIFORNIA

Depth	U	Th	Th/U	$^{234}U/^{238}U$	$^{230}Th/^{232}Th$	^{230}Th	^{234}U	$^{230}Th_{xs}$	$^{231}Pa_{xs}$
cm	ppm	ppm		activity ratio	activity ratio	dpm/g	dpm/g	dpm/g	dpm/g
163-7									
0-2	3.00±0.11	6.7±0.4	2.2±0.2	0.97±0.04	13.3±0.5	21.0±0.8	2.18±0.08	18.8±0.8	2.73±0.15
4-5	3.10±0.12	6.1±0.5	2.0±0.2	0.91±0.04	14.3±0.7	22.2±1.2	2.11±0.09	20.1±1.2	3.01±0.27
8-9	2.57±0.10	6.7±0.3	2.6±0.2	1.06±0.05	13.2±0.5	21.0±0.6	2.03±0.08	19.0±0.6	3.00±0.27
11-13	2.41±0.09	7.2±0.7	3.0±0.3	1.04±0.05	12.6±0.4	22.9±1.5	1.88±0.07	21.0±1.5	3.10±0.23
15-17	2.37±0.07	7.8±0.4	3.3±0.2	1.04±0.04	12.2±0.4	22.6±0.8	1.85±0.05	20.7±0.8	2.56±0.31
20-22	3.33±0.11	6.9±1.0	2.1±0.3	1.07±0.04	10.6±0.5	20.1±2.0	2.66±0.09	17.4±2.0	2.52±0.31
26-28	6.57±0.19	7.0±0.4	1.1±0.1	1.07±0.03	11.2±0.4	18.9±0.6	5.24±0.15	13.7±0.6	1.72±0.10
32-34	6.24±0.20	7.0±0.6	1.1±0.1	1.07±0.03	9.5±0.3	16.1±1.0	4.99±0.16	11.1±1.0	1.20±0.10
163-14									
0-1	2.82±0.08	6.7±0.5	2.4±0.2	1.17±0.04	14.3±0.8	23.2±1.0	2.46±0.06	20.8±1.0	
4-5	2.94±0.10	6.8±0.4	2.3±0.2	1.00±0.04	14.4±0.7	23.8±1.0	2.20±0.07	21.6±1.0	
9-10	2.83±0.09	7.4±0.6	2.6±0.2	0.99±0.03	13.2±0.8	23.7±1.3	2.09±0.06	21.6±1.3	
14-16	2.61±0.08	7.8±0.5	3.0±0.2	0.99±0.03	11.4±0.5	21.5±0.9	1.93±0.06	19.6±0.9	
18-20	2.44±0.08	6.7±0.4	2.8±0.2	0.99±0.04	11.1±0.5	18.1±0.7	1.80±0.06	16.3±0.7	
24-26	2.62±0.08	7.1±0.4	2.7±0.2	1.01±0.03	8.9±0.4	15.3±0.6	1.98±0.06	13.3±0.6	
28-30	2.70±0.06	8.8±0.3	3.3±0.1	0.97±0.03-	7.7±0.2	16.5±0.5	1.96±0.05	14.5±0.5	
163-10									
0-2	2.68±0.13	8.0±0.2	3.0±0.2	1.11±0.07	14.1±0.3	27.1±0.4	2.22±0.11	24.8±0.4	3.25±0.12
5-6	2.61±0.07	6.9±0.3	2.6±0.1	1.03±0.03	14.8±0.5	25.0±0.7	2.00±0.05	23.0±0.7	2.96±0.17
7-8	2.67±0.06	7.1±0.2	2.7±0.1	1.04±0.03	14.8±0.4	25.4±0.4	2.08±0.05	23.3±0.4	2.88±0.16
10-12	2.65±0.13	8.0±0.4	3.0±0.2	1.14±0.07	13.5±0.4	26.8±0.8	2.27±0.10	24.5±0.8	2.91±0.16
16-18	2.62±0.07	7.7±0.2	2.9±0.1	0.97±0.03	13.3±0.3	25.2±0.5	1.90±0.05	23.3±0.5	2.93±0.14
22-24	2.57±0.11	7.5±0.4	2.9±0.2	1.02±0.50	11.6±0.4	21.7±0.7	1.96±0.08	19.8±0.7	1.99±0.13
30-32	2.65±0.11	7.0±0.3	2.7±0.2	0.90±0.05	8.7±0.2	14.9±0.4	1.79±0.08	13.1±0.4	1.18±0.08
163-9									
0-1	2.66±0.10	9.6±0.4	3.6±0.2	0.94±0.04	19.3±0.5	44.7±1.3	1.86±0.07	42.9±1.3	
4-5	2.60±0.06	8.9±0.6	3.4±0.2	1.00±0.03	17.3±0.6	37.1±1.9	1.94±0.04	35.2±1.9	3.40±0.20
9-10	2.61±0.05	7.0±0.7	2.7±0.3	0.95±0.02	18.2±0.8	29.3±2.1	1.85±0.04	27.4±2.1	2.70±0.30
18-20	2.61±0.11	9.4±1.0	3.6±0.4	0.95±0.05	12.0±0.6	26.5±2.1	1.86±0.08	24.6±2.1	1.70±0.20
28-30	2.57±0.06	9.1±0.9	3.5±0.4	0.96±0.03	10.3±0.8	22.8±1.7	1.84±0.04	20.9±1.7	
36-38	2.62±0.06	10.9±1.1	4.2±0.4	0.97±0.03	7.8±0.3	21.3±1.8	1.90±0.04	19.4±1.8	0.78±0.13

Quoted uncertainties are based on 1-sigma counting statistics.

ACKNOWLEDGEMENTS

I would like to thank Captain William Clampitt and the crew of the R/V *Thomas G. Thompson* for their fine service in November, 1981. Special thanks to Dr. Jim Murray for his support in this project and without whose help this thesis would never have been started.

The Grant Institute of Geology provided excellent facilities under Professor Gordon Craig. In particular the technical help of Mike Saunders in the Wet Lab., Geoff Angell in XRD and Perkin-Elmer analysis and Dr. Pete Hill on the microprobe was gratefully appreciated. Dr. Godfrey Fitton and Dodie James encouraged and supported the developement of XRF techniques in the long winter evenings of 1983/1984. Colin Chaplin, Diana Baty, Flo Tullis, Leo Harrison, Eddie Clark and Thea Grieve all contributed to this thesis from photography, to providing hardware supplies, to finding obscure references and maintaining a sense of humour through the dust and noise of library upheavals.

My colleagues in the Grant Institute provided much inspiration and criticism. Amongst the many John Boyle, John Craven, Alan Kemp, Andrew Martin, Dave Pattison, and Ian Ridgway deserve praise for their patience in answering my unending questions. Special thanks are due to Steve Rainey and Andy Walker, without whose help the XRF software would still be in its infancy.

I gratefully thank Dr. John Thomson for the radionuclide data and many stimulating discussions, together with Dr. Erwin Suess for the stable isotope data on the dolomites. Dr. Alan Ross and Andrew Ross at the Electron Microscope Unit, Western

General Hospital, Edinburgh, provided a fine service on many a Friday morning.

I would particularly like to thank my supervisor, Dr. N.B. Price for constant enthusiasm, encouragement and advice over the three years of this research. It is with great pleasure that I hope to continue to benefit from his wisdom over the years to come.

The financial support of N.E.R.C. is gratefully acknowledged.

Finally, I must thank my parents for their unfailing support, and above all my wife, Clare, for just being there.

REFERENCES

ADAMS, J.E., and RHODES, M.L., 1960, Dolomitization by seepage refluxion. *Am. Assoc. Petrol. Geol. Bull.*, 44, p.1912-1920.

ADELSECK, C.G.,Jr. and ANDERSON, T.F., 1978, The late Pleistocene record of productivity fluctuations in the eastern equatorial Pacific Ocean. *Geology*, 6, p.388-391.

AMIN, B.S., KRISHNASWAMI, S. and SOMAYAJULU, B.L.K., 1974, $^{234}Th/^{238}U$ activity ratios in Pacific Ocean bottom samples. *Earth Planet. Sci. Lett.*, 21, p.342-344.

ANDERSON, B.J., JENNE, E.A. and CHAO, T.T., 1973, The sorption of silver by poorly crystallised maganese oxides. *Geochim. Cosmochim. Acta*, 37, p.611-622.

ANDERSON, R.F., BACON, M.P. and BREWER, P.G., 1983a, Removal of ^{230}Th and ^{231}Pa from the open ocean. *Earth Planet. Sci. Lett.*, 62, p.7-23.

ANDERSON, R.F., BACON, M.P. and BREWER, P.G., 1983b, Removal of ^{230}Th and ^{231}Pa at ocean margins. *Earth Planet. Sci. Lett.*, 66, p.73-90.

AOKI, S., KOHYAMA, N. and SUDO, T., 1974, An iron-rich montmorillonite in a sediment core from the northeastern Pacific. *Deep-Sea Res.*, 21, p.865-875.

ARNOLD, B.A., 1957, Late Pleistocene and Recent changes in landforms, climate and archaeology, Baja California, Mexico., *Univ. California (Berkley) Publ. Geog.*, 10, p.201-318.

ARRHENIUS, G.O.S., 1952, Sediment cores from the East Pacific. *Reports of the Swedish Deep-Sea Exped., ed.* H. Pettersson, 5, 227pp.

ARRHENIUS, G.O.S., 1963, Pelagic Sediments. *The Sea, ed.* M.N. Hill, 3, Wiley, London, p.655-727.

ASCHMAN, H., 1959, *The central desert of Baja California: Demography and Ecology.*, Univ. California Press (Berkley), 315pp.

ATWATER, T., 1970, Implications of plate tectonics for the Cenozoic tectonic evolution of western North America. *Geol. Soc. Amer. Bull.*, 81, p.3513-3536.

ATWATER, T. and MOLNAR, P., 1973, Relative motion of the Pacific and North American plates deduced from sea floor spreading in the Atlantic, Indian and South Pacific Oceans. *in Tectonic Problems of the San Andreas Fault System, California.* Stanford Univ. Publ. Geol. Sci., p.136-148.

BACON, M.P., 1984, Glacial to interglacial changes in carbonate and clay sedimentation in the Atlantic Ocean estimated from ^{230}Th measurements. *Isotope Geoscience*, 2, p.97-111.

BAKER, P.A. and KASTNER, M., 1981, Constraints on the formation of sedimentary dolomite. *Science*, 213, p.214-216.

BAKER, W.E., 1973, The role of humic acids from Tasmanian podzolic soils in mineral degradation and metal mobilization. *Geochim. Cosmochim. Acta*, 37, p269-281.

BALISTRIERI, L.S. and MURRAY, J.W., 1982, The surface chemistry of δ-MnO_2 in major ion seawater. *Geochim. Cosmochim. Acta*, 46, p.1041-1052.

BALISTRIERI, L.S. and MURRAY, J.W., 1984, Marine scavenging: Trace metal adsorption by interfacial sediment from MANOP Site H. *Geochim. Cosmochim. Acta*, 48, p.921-929.

BALZER, W., 1982, On the distribution of iron and manganese at the sediment/water interface: thermodynamic versus kinetic control. *Geochim. Cosmochim. Acta*, 46, p.1153-1161.

BARANOV, V.I. and KUZ'MINA, W.A., 1958, The rate of silt deposition in the Indian Ocean. *Geochemistry (USSR)*, 1958, p.131-140.

BARKLEY, R.A. and THOMPSON, T.G., 1960, The total iodine and iodate content of seawater. *Deep-Sea Res.*, 7, p.24-34.

BARNES, R.O. and GOLDBERG, E.D., 1976, Methane production and consumption in marine sediment. *Geology*, 4, p.297-300.

BARNES, S.S., 1967, Minor element composition of ferromanganese nodules. *Science*, 157, p.63-65.

BATURIN, G.N., 1982, Phosphorites on the sea floor, origin, composition and distribution. *Developments in Sedimentology*, 33, Elsevier, Amsterdam, 343pp.

BATURIN, G.N. and BEZRUKOV, P.L., 1979, Phosphorites on the sea floor and their origin. *Mar. Geol.*, 31, p.317-332.

BEERS, J.R., 1966, Studies on the chemical composition of major zooplankton groups in the Sargasso Sea off Bermuda. *Limnol. Oceanogr.*, 11, p.520-528.

BEHRENS, E.W. and LAND, L.S., 1972, Subtidal Holocene dolomite, Baffin Bay, Texas. *J. Sediment. Petrol.*, 42, p.155-161.

BENDER, M.L., FANNING, K.A., FROELICH, P.N., HEATH, G.R. and MAYNARD, V., 1977, Interstitial nitrate profiles and oxidation of sedimentary organic matter in the eastern equatorial Atlantic. *Science*, 198, p.605-609.

BENNETT, R.M., BRYANT, W.R. and KELLER, G.M., 1981, Clay fabric of selected submarine sediments: Fundamental propeties and models. *J. Sediment. Petrol.*, 51, p.217-231.

BENTOR, Y.K. and KASTNER, M., 1965, Notes on the mineralogy and origin of glauconite. *J. Sediment. Petrol.*, 35, p155-166.

BERGER, W.H., 1968, Planktonic foraminifera: Selective dissolution and palaeolclimatic interpretation. *Deep-Sea Res.*, 15, p31-43.

BERGER, W.H., 1970, Planktonic foraminifera: Selective solution and the lysocline. *Mar. Geol.*, 8, p.111-138.

BERGER, W.H., 1971, Sedimentation of planktonic foraminifera. *Mar. Geol.*, 11, p.325-358.

BERGER, W.H., 1973, Deep-sea carbonates: Pleistocene dissolution cycles. *J. Foram. Res.*, 3, p187-195.

BERGER, W.H., ADELSECK, C.G.Jr. and MAYER, L.A., 1976, Distribution of carbonate in surface sediments of the Pacific Ocean. *J. Geophys. Res.*, 81, p.2617-2627.

BERGER, W.H., FINKEL, R.C., KILLINGLEY, J.S. and MARCHIG, V., 1983, Glacial-Holocene transition in deep-sea sediments: manganese spike in the east-equatorial Pacific. *Nature*, 303, p.231-233.

BERGER, W.H. and HEATH, G.R., 1968, Vertical mixing in pelagic sediments. *J. Mar. Res.*, 26, p.134-143.

BERGER, W.H. and PIPER, D.J.W., 1972, Planktonic foraminifera: differential settling, dissolution and redeposition. *Limnol. Oceanogr.*, 17, p.275-287.

BERG-MADSEN, V., 1983, High alumina glaucony from the Middle Cambrian of Oland and Bornholm, southern Baltoscandia. *J. Sediment. Petrol.*, 53, p875-893.

BERNAL, P.A. and McGOWAN, J.A., 1981, Advection and upwelling in the California Current.*in Coastal Upwelling, ed.* F.A. Richards, Amer. Geophysical Union, Washington D.C., p.381-399.

BERNER, R.A., 1964, An idealized model of dissolved sulphate distribution in recent sediments. *Geochim. Cosmochim. Acta*, 28, p.1497-1503.

BERNER, R.A., 1970, Sedimentary pyrite formation. *Am. J. Sci.*, 268, p.1-23.

BERNER, R.A., 1971, *Priciples of Chemical Sedimentology.* McGraw Hill, New York, 240pp.

BERNER, R.A., 1973, Phosphate removal from sea water by absorption on volcanogenic ferric oxides. *Earth Plan. Sci. Lett.*, 18, p.77-86.

BERNER, R.A., 1975, Diagenetic models of dissolved species in the interstitial waters of compacting sediment. *Am. J. Sci.*, 275, p.88-96.

BERNER, R.A., 1980, *Early Diagenesis - A Theoretical Approach.* Princeton Univ. Press, Princeton, 241pp.

BERNER, R.A., 1981a, Authigenic mineral formation resulting from organic matter decomposition in modern sediments. *Fortschr. Miner.*, 59, p.117-135.

BERNER, R.A., 1981b, A new geochemical classification of sedimentary environments. *J. Sediment. Petrol.*, 51, p.359-365.

BERNER, R.A., 1982, Burial of organic carbon and pyrite sulfur in the modern ocean: its geochemical and environmental significance. *Am. J. Sci.*, 282, p.451-473.

BERNER, R.A., 1984, Sedimentary pyrite formation: An update. *Geochim. Cosmochim. Acta*, 48, p.605-615.

BERNER, R.A., SCOTT, M.R. and THOMLINSON, C., 1970, Carbonate alkalinity in the pore wayers of anoxic marine sediments. *Limnol. Oceanogr.*, 15, p.544-549.

BERRANG, P.G. and GRILL, E.V., 1974, The effect of manganese oxide scavenging on molybdenum in Saanich Inlet, British Columbia. *Mar. Chem.*, 2, p.125-148.

BERTINE, K.K., 1972, The deposition of molybdenum in anoxic waters. *Mar. Chem.*, 1, p.43-53.

BERTINE, K.K., CHAN, L.H. and TUREKIAN, K.K., 1970, Uranium determinations in deep sea sediments and natural waters using fission tracks. *Geochim. Cosmochim. Acta*, 34, p641-648.

BETEKHTIN, A.G., 1940, The South-Urals manganese deposits as a source of raw material of the Magnitogorsk metalurgical combine. *Tr. Inst. Geol. Nauk SSSR*, 30, p.N4.

BEZRUKOV, P.L., 1960, Sedimentation in the northwestern Pacific Ocean. *Intern. Geol. Congr. 21st, Copenhagen, 1960*, Rept. Soviet Geologists, p.45-48.

BHAT, S.G., KRISHNASWAMI, S., LAL, D., RAMA and MOORE, W.S., 1969, $^{234}Th/^{238}U$ ratios in the ocean. *Earth Planet. Sci. Lett.*, 5, p483-491.

BIRCH, G.F., WILLIS, J.P. and RICKARD, R.S., 1976, An electron microprobe study of glauconites from the continental margin off the west coast of S. Africa. *Mar. Geol.*, 22, p.271-284.

BISCHOFF, J.L., 1972, A ferroan nontronite from the Red Sea geothermal system. *Clays Clay Mineral.*, 20, p.217-223.

BISCHOFF, J.L. and KU, T-L., 1970, Pore fluids of recent marine sediments - I. Oxidising sediments of $20^{o}N$, Continental Rise to Mid-Atlantic Ridge. *J. Sediment. Petrol.*, 40, p.960-972.

BISCHOFF, J.L. and KU, T-L., 1971, Pore fluids of recent marine sediments - II. Anoxic sediments of 34° - 45°N, Gibralter to Mid-Atlantic Ridge. *J. Sediment. Petrol.*, 41, p.1008-1017.

BISCHOFF, J.L., HEATH, G.R. and LEINEN, M., 1979, Geochemistry of deep-sea sediments from the Pacific manganese nodule province: DOMES sites A, B and C. *in Marine Geology and Oceanography of the Pacific Manganese Nodule Province, eds.* J.L. Bischoff and D.Z. Piper, Plenum, New York, p.397-473.

BISHOP, J.K., EDMOND, J.M., KETTEN, D.R., BACON, M.P. and SILKER, W.B., 1977, The chemistry, biology and vertical flux of particulate matter from the upper 400m of the equatorial Atlantic ocean. *Deep-Sea Res.*, 24, p.511-548.

BLOOM, A.L., 1977, Atlas of Sea-Level Curves. Project 61, International Geological Correlations Program.

BONATTI, E., 1966, Deep sea authigenic calcite and dolomite. *Science*, 153, p.534-537.

BONATTI, E. and ARRHENIUS, G.O.S., 1965, Eolian sedimentation in the Pacific off Northern Mexico. *Mar. Geol.*, 3, p.337-348.

BONATTI, E., FISHER, D.E., JOENSSU, O., and RYDELL, H.S., 1971, Post-depositional mobility of some transition elements, phosphorus, uranium and thorium in deep sea sediments. *Geochim. Cosmochim. Acta*, 35, p.189-201.

BORDOVSKIY, O.K., 1965a, Sources of organic matter in marine basins. *Mar. Geol.*, 3, p.5-31.

BORDOVSKIY, O.K., 1965b, Accumulation of organic matter in bottom sediments. *Mar. Geol.*, 3, p.33-82.

BORDOVSKIY, O.K., 1965c, Transformation of organic matter in bottom sediments and its early diagenesis. *Mar. Geol.*, 3, p.83-114.

BOSTROM, K., JOENSSU, O. and BROHM, I., 1974, Plankton: its chemical composition and its significance as a source of pelagic sediments. *Chem. Geol.*, 14, p.255-271.

BOSTROM, K., JOENSSU, O., MOORE, C., BOSTROM, B., DALZIEL, M. and HOROWITZ, A., 1973, Geochemistry of barium in pelagic sediments. *Lithos*, 6, p.159-174.

BOSTROM, K. and PETERSON, M.N.A., 1966, Precipitates from hydrothermal exhalations of the East Pacific Rise. *Econ. Geol.*, 61, p.1258-1265.

BOSTROM, K., PETERSON, M.N.A., JOENSSU, O. and FISHER, D.E., 1969, Aluminium-poor ferromanganoan sediments on active ocean ridges. *J. Geophys. Res.*, 74, p.3261-3270.

BOWEN, H.J.M., 1966, *Trace Elements in Biochemistry*, Academic Press, New York.

BOYLE, E.A., 1983, Chemical accumulation variations under the Peru Current during the past 130,000 years. *J. Geophys. Res.*, 88, p.7667-7680.

BREAKER, L.C. and GILLAND, R.P., 1981, A statellite sequence on upwelling along the California coast. *in Coastal Upwelling, ed.* F.A. Richards, Amer. Geophys. Union, Washington, D.C., p.87-94.

BREMNER, J.M., 1980, Concretionary phosphorite from SW Africa. *J. Geol. Soc. Lond.*, 137, p.773-786.

BRICKER, D.P., 1965, Some stability relations in the system Mn-O_2-H_2O at 25°C and one atmosphere total pressure. *Am. Mineral.*, 50, p.1296-1354.

BROECKER, W.S., 1971, Calcite accumulation rates and glacial to interglacial changes in oceanic mixing. *in Late Cenozoic Ice Ages, ed.* K.K. Turekian, Yale Univ. Press, New Haven, p.239-266.

BROECKER, W.S., KAUFMAN, A. and TRIER, R.M., 1973, The residence time of thorium in surface sea water and its implications regarding the rate of reactive pollutants. *Earth Planet. Sci. Lett.*, 20, p.35-44.

BROECKER, W.S., TUREKIAN, K.K. and HEEZEN, B.C., 1958, The relations of deep-sea sedimentation rates to variations in climate. *Am. J. Sci.*, 256, p.503-517.

BRONGERSMA-SANDERS, M., 1965, Metals of the Kupferschiefer supplied by normal seawater. *Geol. Rund.*, 55, p.365-375.

BRONGERSMA-SANDERS, M., 1966, Origin of trace metal enrichment in bituminous shales. *in Advances in Organic Geochemistry, eds.* G.D. Hobson and G.C. Spears. Pergamon, London, p.231-236.

BRONGERSMA-SANDERS, M., STEPHAN, K.M., KWEE, T.G. and DE BRUIN, M., 1980, Distribution of minor elements in cores from the south-west Africa shelf with notes on plankton and fish mortality. *Mar. Geol.*, 37, p.91-132.

BRULAND, K.W., 1983, Trace elements in sea water. *in Chemical Oceanography, Vol. 8, eds.* J.P. Riley and R. Chester, Academic Press, London, p.157-220.

BRUMSACK, H.-J., 1980, Geochemistry of Cretaceous black shales from the Atlantic Ocean (DSDP legs 11, 14, 36 and 41). *Chem. Geol.*, 31, p.1-25.

BRUMSACK, H.-J. and GEISKES, J.M., 1983, Interstitial water trace-metal chemistry of laminated sediments from the Gulf of California, Mexico. *Mar. Chem.*, 14, p.89-106.

BRUMSACK, H.-J. and LEW, M., 1982, Inorganic geochemistry of Atlantic Ocean sediments with special reference to Cretaceous black shales. *in Geology of the Northwest African Continental Margin, eds.* U. Von Rad, K. Hinz, M. Sarnthein and E. Seibold, Springer-Verlag, Berlin, p.661-685.

BURDIDGE, D.J. and GEISKES, J.M., 1983, A pore water/solid phase diagenetic model for manganese in marine sediments. *Am. J. Sci.*, 283, p.29-47.

BURNETT, W.C., 1977, Geochemistry and origin of phosphorite deposits from off Peru and Chile. *Geol. Soc. Amer. Bull.*, 88, p.813-823.

BURNS, R.G., 1976, The uptake of cobalt into ferromanganese nodules, soils, and synthetic manganese (IV) oxides. *Geochim. Cosmochim. Acta*, 40, p.95-102.

BURNS, R.G. and BURNS, V.M., 1979, Manganese oxides. *in Marine Minerals, ed.* R.G. Burns, Min. Soc. Amer. Short Course Notes, 6, p.1-47.

BURST, J.F., 1958, "Glauconite" pellets: Their mineral nature and applications to stratigraphic interpretations. *Am. Assoc. Petrol. Geol. Bull.*, 42, p.310-327.

BURST, J.F., 1958, Mineral heterogeneity in "glauconite" pellets. *Am. Mineral.*, 43, p.481-497.

BURTON, W.K., CABRERA, N. and FRANK, F.C., 1951, The growth of crystals and equilibrium structure of their surfaces. *R. Soc. Lond. Philos. Trans.*, A-243, p.299-358.

BUSCH, W.H. and KELLER, G.H., 1981, The physical propeties of Peru-Chile continental margin sediments - the influence of coastal upwelling on sediment propeties. *J. Sediment. Petrol.*, 51, p.705-719.

BUSER, W. and GRAF, P., 1955, Differenzierung von Mangan(II)-manganit und d-MnO2 durch oberflachenmessung nach Brunauer-Emmet-Teller. *Helv. Chim. Acta*, 38, p.830-834.

BUSER, W. and GRUTTER, A., 1956, Uber die Natur der Manganknollen. *Schweiz Min. Petr. Mitt.*, 36, p.49-62.

CALLENDER, E. and BOWSER, C.J., 1980, Manganese and copper geochemistry of interstitial fluids from manganese nodule-rich pelagic sediments of the northeastern equatorial Pacific. *Am. J. Sci.*, 280, p.1063-1097.

CALVERT, S.E., 1976, The mineralogy and geochemistry of near-shore sediments. *in Chemical Oceanography, Vol. 6, eds.* J.P. Riley and R. Chester, Academic Press, London, p.187-271.

CALVERT, S.E. and BATCHELOR, C.H., 1978, Major and minor element geochemistry of sediments from Hole 379A, Leg 42B, Deep Sea Drilling Project. *Init. Repts. D.S.D.P.*, 42 Pt.2, p.527-541.

CALVERT, S.E. and PRICE, N.B., 1970a, Minor metal contents of Recent organic-rich sediments off south-west Africa. *Nature*, 227, p.593-595.

CALVERT, S.E., and PRICE, N.B., 1970b, Composition of manganese nodules and manganese carbonates from Loch Fyne, Scotland. *Contr. Mineral. Petrol.*, 29, p.215-233.

CALVERT, S.E. and PRICE, N.B., 1983, Geochemistry of Namibian shelf sediments.,*in Coastal Upwelling, Pt. A, eds.* E. Suess and J. Thiede, Plenum, New York, p.337-375.

CHAN, K.M. and RILEY, J.P., 1966, The determination of molybdenum in natural waters, silicates and biological materials. *Anal. Chim. Acta*, 36, p.220-229.

CHESTER, R. and ASTON, S.R., 1976, The geochemistry of deep-sea sediments.,*in Chemical Oceanography, Vol. 6, eds.* J.P. Riley and R. Chester, Academic Press, London, p.281-390.

CHESTER, R, ASTON, S.R. and BRUTY, D., 1976, The trace element partition geochemistry in an ancient deep-sea sediment core from the Bermuda Rise. *Mar. Geol*, 21, p.271-288.

CHESTER, R., GRIFFITHS, A. and STONER, J.H., 1978, Minor metal content of surface seawater particulates and organic-rich shelf sediments. *Nature*, 275, p.308-309.

CHUKHROV, F.V., GORSHKOV, A.I., BERESOVSKAYA, V.V. and SIVTSOV, A.V., 1979, Contributions to the mineralogy of authigenic manganese phases from marine manganese deposits. *Mineral. Deposita*, 14, p.249-261.

CHURCH, T.M., 1970, Marine Barite. *Unpub. Ph.D. Thesis*, University of California, San Diego, 100pp.

CHURCH, T.M., 1979, Marine barite, *Marine Minerals, Min. Soc. Amer. Short Course Notes, Vol.6, ed.* R.G. Burns, p.175-209.

CLAYPOOL, G.E., 1974, Anoxic diagenesis and bacterial methane production in deep sea sediments. *Unpub. Ph.D. Thesis*, University of California, Los Angeles.

CLAYPOOL, C.E. and KAPLAN, I.R., 1974, The origin and distribution of methane in marine sediments. *in Natural Gases in Marine Sediments, ed.* I.R. Kaplan, Plenum, New York, p.99-140.

CLAYTON, R.N., JONES, B.R. and BERNER, R.A., 1968, Isotope studies of dolomite formation under sedimentary conditions. *Geochim. Cosmochim. Acta*, 32, p.415-432.

COCHRAN, J.K., 1979, The geochemistry of ^{226}Ra and ^{228} in marine deposits. *Unpub. Ph.D. Thesis*, Yale University, 260pp.

COCHRAN, J.K. and KRISHNASWAMI,S., 1980, Radium, thorium, uranium and ^{210}Pb in deep-sea sediments and sediment pore waters from the north equatorial Pacific. *Am. J. Sci.*, 280, p.849-889.

COLEMAN, M.L., CURTIS, C.D. and IRWIN, H., 1979, Burial rate, a key to source reservoir potential. *World Oil*, 188, p.83-92.

CONTRERAS, R., FOGG, T.R., CHASTEEN, N.D., GAUDETTE, H.E. and LYONS, W.M.B., 1978, Molybdenum in pore waters of anoxic marine sediments by electron paramagnetic resonance spectroscopy. *Mar. Chem.*, 6, p.365-373.

CORRENS, C.W., 1939, Pelagic sediments of the North Atlantic Ocean. *in Recent Marine Sediments, ed.* P.D. Trask, Am. Assoc. Petrol. Geol., Tulsa, p.373-395.

CORRENS, C.W., 1954, Titan in Tiefseesedimenten. *Deep-Sea Res.*, 1, p.78-85.

CORTECCI, G. and LONGINELLI, A., 1972, Oxygen-isotope variation in a barite slab from the sea bottom off california. *Chem. Geol.*, 9, p.113-117.

CRAIG, H., KRISHNASWAMI, S., and SOMAYAJULU, B.L.K., 1973, ^{210}Pb-^{226}Ra: radioactive disequilibrium in the deep sea. *Earth Planet. Sci. Lett.*, 17, p.295-305.

CRONAN, D.S., 1972, The Mid-Atlantic Ridge near 45°N, XVIII: Al, As, Hg and Mn in ferruginous sediments from the median valley. *Can. J. Earth Sci.*, 9, p.319-323.

CRONAN, D.S., 1977, Deep-sea nodules: distribution and geochemistry. *in Marine Manganese Deposits, ed.* G.P. Glasby, Elsevier, Amsterdam, p.11-44.

CURTIS, C.D., 1966, The incorporation of soluble organic matter into sediments and its effect on trace-element assemblages. *in Advances in Organic Geochemistry, 1964, Eds.*G.D. Hobson and M.C. Louis, Pergamon Press, London, p.1-13.

CURTIS, C.D., 1978, Possible links between sandstone diagenesis and depth-related geochemical reactions occuring in enclosing mudstones. *J. Geol. Soc. Lond.*, 135, p.107-117.

D'ANGLEJAN, B.F., 1967, The origin of marine phosphorites off Baja California. *Mar. Geol.*, 5, p.15-44.

DAMUTH, J.E., 1975, Quaternary climate change as revealed by calcium carbonate fluctuations in western equatorial Atlantic sediments. *Deep-Sea Res.*, 22, p.725-743.

DAMUTH, J.E. and KUMAR, N., 1975, Amazon cone: morphology, sediments, age, and growth patterns. *Geol. Soc. Amer. Bull.*, 86, p.863-878.

DAMUTH, J.E. and EMBLEY, R.W., 1981, Mass transport processes on the Amazon Cone: western equatorial Atlantic. *Am. Assoc. Petrol. Geol. Bull.*, 65, p.629-643.

DAPPLES, E.G., 1967, Diagenesis of sandstones. *in Diagenesis in Sediments, ed.* G.V. Chillingar, Elsevier, Amsterdam, p.91-125.

DEER, W.A., HOWIE, R.A. and ZUSSMAN, J., 1961, *Rock-Forming Minerals, Vol.3, Sheet Silicates.*,Longmans, London, 270pp.

DEER, W.A., HOWIE, R.A. and ZUSSMAN, J., 1966, *An Introduction to Rock Forming Minerals.*,Longmans, London, 528pp.

DEGENS, E.T. and EPSTEIN, S., 1964, Oxygen and carbon isotope ratios in coexisting calcites and dolomites from recent and ancient sediments. *Geochim. Cosmochim. Acta*, 28, p.23-44.

DEGENS, E.T., REUTER, J.H. and SHAW, K.N.F., 1964, Biochemical compounds in offshore California sediments and sea waters. *Geochim. Cosmochim. Acta*, 28, p.45-66.

DEHAIRS, F., CHESSELET, R. and JEDWAB, J., 1980, Discrete suspended particles of barite and the barium cycle in the open ocean. *Earth Planet. Sci. Lett.*, 49, p.528-550.

DE MASTER, D.J. and COCHRAN, J.K., 1982, Particle mixing rates in deep-sea sediments determined from excess ^{210}Pb and ^{32}Si profiles. *Earth Planet. Sci. Lett.*, 61, p.257-271.

DEUSER, W.G., 1970, Extreme $^{13}C/^{12}C$ variations in Quaternary dolomites from the continental shelf. *Earth Planet. Sci. Lett.*, 8, p.118-124.

DICKSON, J.A.D. and COLEMAN, M.A., 1980, Changes in carbon and oxygen isotope composition during limestone diagenesis. *Sedimentology*, 27, p.107-118.

DIESTER-HAAS, L., 1976, Late Quaternary climatic variations in northwest Africa deduced from East Atlantic sediment cores. *J. Quat. Res.*, 6, p.299-314.

DOYLE, L.J. and BANDY, O.L., 1972, Southern continental borderland, Baja California: its tectonic and environmental development. *Geol. Soc. Amer. Bull.*, 83, p.3785-3794.

DOYLE, P.S. and RIEDEL, W.R., 1979, Cretaceous to Neogene icthyoliths in a giant piston core from the central North Pacific. *Micropaleontology*, 25, p.337-364.

DREVER, J.L., 1971, Magnesium - iron relacement in clay minerals in anoxic marine sediments. *Science*, 172, p.1334-1336.

DREVER, J.L., 1976, Chemical and mineralogical studies, Site 323. *Init. Repts. D.S.D.P.*, 35, p.471-477.

DYMOND, J., 1981, The geochemistry of Nazca Plate surface sediments: An evaluation of hydrothermal, biogenic, detrital and hydrogenous sources. *Geol. Soc. Amer. Memoir*, 134, p.133-173.

DYMOND, J. and EKLUND, W., 1978, A microprobe study of metalliferous sediment components. *Earth Planet. Sci. Lett.*, 40, p.243-251.

EDMOND, J.M., 1974, On the distribution of carbonate and silicate in the deep ocean. *Deep-Sea Res.*, 21, p.455-480.

EHLMANN, A.J., HULINGS, N.C. and GLOVER, E.D., 1963, Stages of glauconite formation in modern foraminiferal sediments. *J. Sediment. Petrol.*, 33, p.87-96.

ELDERFIELD, H. and TRUESDALE, V.W., 1980, On the biophilic nature of iodine in seawater. *Earth Planet. Sci. Lett.*, 50, p.105-114.

ELDERFIELD, H., LUEDKTE, N., McCAFFREY, R.J. and BENDER, M., 1981, Benthic fluxes in Narragansett Bay. *Am. J. Sci.*, 281, p.768-787.

EL WAKEEL, S.K. and RILEY, J.P., 1961, Chemical and mineralogical studies of deep-sea sediments. *Geochim. Cosmochim. Acta*, 25, p.110-146.

EMILIANI, C., 1955, Mineralogical and chemical composition of the tests of certain pelagic foraminifera. *Micropalaeontology*, 1, p.377-380.

EMERSON, S.R. and BENDER, M.L., 1981, Carbon fluxes at the sediment/water interface of the deep-sea: calcium carbonate preservation. *J. Mar. Res.*, 39, p.139-162.

EMERSON, S.R., JAHNKE, R.A., BENDER, M.L., FROELICH, P.N., KLINKHAMMER, G.P., BOWSER, C.J. and SETLOCK, G., 1980, Early diagenesis in sediments from the eastern equatorial Pacific, I. Porewater nutrient and carbonate results. *Earth Planet. Sci. Lett.*, 49, p.57-80.

EMERY, K.O, 1960, *The Sea Off Southern California; A Modern Habitat of Petroleum.*, Wiley, New York, 366pp.

EMERY, K.O., STITT,C. and SALTMAN, P., 1964, Amino acids in basin sediments. *J. Sediment. Petrol.*, 34, p.433-437.

EPSTEIN, S., GRAF, D.L. and DEGENS, E.T., 1964, Oxygen isotope studies on the origin of dolomites. *in Isotopic and Cosmic Chemistry*, North Holland, Amsterdam, p.169-180.

ERICSON, D.B., BROECKER, W.S., KULP, J.L. and WOLLIN, G., 1956, Late Pleistocene climates and deep sea sediments. *Science*, 124, p.385-389.

FAIRBRIDGE, R.W., 1957, The dolomite question. *in Regional Aspects of Carbonate Deposition, eds.* R.J. LeBlanc and J.G. Breeding, S.E.P.M. Spec. Publ., 15, p.125-178.

FLEMING, R.H., 1940, The composition of plankton and units for reporting population and production. *Proc. Sxith Pacific Sci. Cong. Calif.*, 1939, 3, p.535-540.

FOLK, R.L. and LAND, L.S., 1975, Mg/Ca ratio and salinity: two controls over crystallization of dolomite. *Am. Assoc. Petrol. Geol. Bull.*, 59, p.60-68.

FOSTER, M.D., 1969, Studies of celadonite and glauconite. *U.S.G.S. Prof. Paper*, 614-F, 17pp.

FOWLER, S.W., 1977, Trace elements in zooplankton particulate products. *Nature*, 269, p.51-53.

FRIEDMAN, I. and HALL. E.W., 1963, Fractionation of O^{18}/O^{16} between coexisting calcite and dolomite. *J. Geol.*, 71, p.238-243.

FRIEDMAN, I. and MURATA, K.J., 1979, Origin of dolomite in Miocene Monterey Shale and related formations in the Temblor Range, California. *Geochim. Cosmochim. Acta*, 43, p.1357-1365.

FRIEDMAN, I. and O'NEILL, J.R., 1977, Compilation of stable isotope fractionation factors of geochemical interest. *U.S.G.S. Prof. Paper*, 440-K, 12pp.

FRITZ, P. and SMITH, D.C.W., 1970, The isotope composition of secondary dolomites. *Geochim. Cosmochim. Acta*, 34, p.1161-1173.

FROELICH, P.N., BENDER, M.L. and HEATH, G.R., 1977, Phosphorus accumulation rates in metalliferous sediments on the East Pacific Rise. *Earth Planet. Sci. Lett.*, 34, p.351-359.

FROELICH, P.N., KLINKHAMMER, G.P., BENDER, M.L., LUEDTKE, N.A., HEATH, G.R., CULLEN, D., DAUPHIN, P., HAMMOND, D., HARTMANN, B., and MAYNARD, V., 1979, Early oxidation of organic matter in pelagic sediments of the eastern equatorial Atlantic: suboxic diagenesis. *Geochim. Cosmochim. Acta*, 43, p.1075-1090.

FROELICH, P.N., BENDER, M.L. and LUEDTKE, N.A., 1982, The marine phosphorus cycle. *Am. J. Sci.*, 282, p.474-511.

GAINES, A.M., 1977, Protodolomite redefined. *J. Sediment. Petrol.*, 47, p.543-546.

GAINES, A.M., 1980, Dolomitization kinetics: recent experimental studies. *in Concepts and Models of Dolomitization, eds.* D.H. Zenger, J.B. Dunham and R.L. Ethington, S.E.P.M. Spec. Publ., 28, p.81-86.

GALEHOUSE, J.S., 1969, Counting grain mounts: number percentage versus number frequency. *J. Sediment. Petrol.*, 39, p.812-815.

GALLIHER, E.W., 1935, Geology of glauconite. *Am. Assoc. Petrol. Geol. Bull.*, 19, p.1569-1601.

GARDNER, J.V. and HAYS, J.D., 1976, Responses of sea-surface temperature and circulation to global climatic changes during the past 200,000 years in the Eastern Equatorial Atlantic ocean. *in Late Quaternary Palaeoceanography and Palaeoclimatology, eds.* R.M. Cline and J.D. Hays, Geol. Soc. Amer. Memoir 145, p.221-246.

GARRELS, R.M. and CHRIST, G.L., 1965, *Solutions, Minerals and Equilibria.*,Harper and Row, New York, 450pp.

GARRELS, R.M., THOMPSON, M.E. and SIEVER, R., 1960, Stability of some carbonates at 25°C and one atmosphere total pressure. *Am. J. Sci.*, 258, p.402-418.

GARRISON, R.E., KASTNER, M., and ZENGER, D.H., 1984, *Dolomites of the Monterey Formation and Other Organic-Rich Units.*,Pacific Section S.E.P.M., 41, 216pp.

GEISKES, J.M., 1975, Chemistry of interstitial waters of marine sediments. *Ann. Rev. Earth Planet. Sci.*, 3, p.433-453.

GIOVANOLI, R., 1980, Vernadite is random-stacked birnessite. *Mineral. Deposita*, 15, p.251-253.

GLOVER, E.D. and SIPPEL, R.F., 1967, Synthesis of magnesium calcites. *Geochim. Cosmochim. Acta*, 31, p.603-613.

GOLDBERG, E.D., 1954, Marine geochemistry I. Chemical scavengers of the sea. *J. Geol.*, 62, p.249-265.

GOLDBERG, E.D. and ARRHENIUS, G.O.S., 1958, Chemistry of Pacific pelagic sediments. *Geochim. Cosmochim. Acta*, 13, p.153-212.

GOLDBERG, E.D. and KOIDE, M., 1962, Geochronological studies of deep sea sediments by the ionium/thorium method. *Geochim. Cosmochim. Acta*, 26, p.417-450.

GOLDHABER, M.B. and KAPLAN, I.R., 1974, The sulfur cycle. *in The Sea*, Vol.5, *ed.* E.D. Goldberg, Wiley, New York, p.569-655.

GOLDHABER, M.B., ALLER, R.C., COCHRAN, J.K., ROSENFELD, J.K., MARTENS, C.S., and BERNER, R.A., 1977, Suplhate reduction, diffusion and bioturbation in Long Island Sound sediments: report of the FOAM group. *Am. J. Sci.*, 277, p.193-237.

GOLDSCHMIDT, V.M., 1954, *Geochemistry, ed.* A. Muir, Clarendon Press, Oxford, 730pp.

GOLDSMITH, J.R. and GRAF, R.E., 1958, Relation between lattice constants and composition of the Ca-Mg carbonates. *Am. Mineral.*, 43, p.84-101.

GOLDSMITH, J.R., GRAF, D.L. and HEARD, H.C., 1961, Lattice constants of the calcium - magnesium carbonates. *Am. Mineral.*, 46, p.453-457.

GORDON, D.C.Jr., 1971, Distribution of particulate organic carbon and nitrogen at an oceanic station in the central Pacific. *Deep-Sea Res.*, 18, p.1127-1134.

GRAF, D.L. and GOLDSMITH, J.R., 1956, Some hydrothermal syntheses of dolomite and protodolomite. *J. Geol.*, 64, p.173-187.

GRAYBEAL, A.L. and HEATH, G.R., 1984, Remobilization of transition metals in surficial pelagic sediments from the eastern Pacific. *Geochim. Cosmochim. Acta*, 48, p.965-975.

GRIFFIN, J.J. and GOLDBERG, E.D., 1963, Clay mineral distribution in the Pacific Ocean. *in The Sea, ed.* M.N. Hill, Wiley, New York, p.728-741.

GRIFFIN, J.J., WINDOM, H.L. and GOLDBERG, E.D., 1968, The distribution of clay minerals in the world ocean. *Deep-Sea Res.*, 15, p.433-459.

GRUNDMANIS, V. and MURRAY, J.W., 1977, Nitrification and denitrification in sediments from Puget Sound. *Limnol. Oceanogr.*, 22, p.804-813.

GRUNDMANIS, V. and MURRAY, J.W., 1982, Aerobic respiration in pelagic marine sediments. *Geochim. Cosmochim. Acta*, 46, p.1101-1120.

GUINASSO, N.L. and SCHINK, D.R., 1975, Quantitative estimate of biological mixing rates in abyssal sediments. *J. Geophys. Res.*, 80, p.3032-3043.

GULDBRANDSEN, R.A., 1960, Petrology of the Mead Peak phosphatic shale member of the Phosphoria Formation at Coal canyon, Wyoming. *U.S.G.S. Bull.*, 111C, p.71-146.

GULDBRANDSEN, R.A., 1969, Physical and chemical factors in the formation of apatite. *Econ. Geol.*, 64, p.365-382.

GULDBRANDSEN, R.A., ROBERSON, C.E. and NEIL, S.T., 1984, Time and crystallization of apatite in sea water. *Geochim. Cosmochim. Acta*, 48, p.213-218.

HARTMANN, M., KOGLER, F.-C., MULLER, P.J. and SUESS, E., 1973, Preliminary results of geochemical and soilmechanical investigations on Pacific Ocean sediments.*in Origin and Distribution of Manganese Nodules in the Pacific and Prospects for Exploration, ed.* M. Morgenstein, Hawaii Inst. Geophysics, p.7.

HARTMANN, M., MULLER, P.J., SUESS, E. and VAN DER WEIJDEN, C.H., 1976, Chemistry of late Quaternary sediments and their interstitial waters from the NW African continental margin. *'Meteor' Forschungsergeb*, 24, p.1-67.

HARVEY, G., 1980, A study of the chemistry of iodine and bromine in marine sediments. *Mar. Chem.*, 8, p.327-332.

HAY, W.W., 1970, Calcareous nannofossils from cores recovered on Leg 4. *in Init. Repts. D.S.D.P.*, 4, p.455-501.

HAYS, J.D., SAITO, T., OPDYKE, N.D. and BURKLE, L.M., 1969, Pliocene - Pleistocene sediments of the equatorial Pacific: their palaeomagnetic, biostratigraphic and climatic record. *Geol. Soc. Amer. Bull.*, 80, p.1481-1514.

HEATH, G.R., 1969, Mineralogy of Cenozoic deep-sea sediments from the equatorial Pacific Ocean. *Geol. Soc. Amer. Bull.*, 80, p.1997-2018.

HEATH, G.R. and DYMOND, J., 1977, Genesis and transformations of metalliferous sediments from the East Pacific Rise, Bauer Deep, and Central Basin, northwest Nazca Plate. *Geol. Soc. Amer. Bull.*, 88, p.723-733.

HEATH, G.R. and LYLE, M., 1981, Profiles of solid-phase manganese at MANOP sites M and H. *EOS*, 62, p.905.

HEATH, G.R., MOORE, T.C.Jr. and DAUPHIN, J.P., 1977, Organic carbon in deep-sea sediments. *in The Fate of Fossil Fuel CO_2 in the Oceans, eds.* N.R. Andersen and A. Malahoff, Plenum Press, New York, p.605-625.

HEATH, G.R., MOORE, T.C.Jr. and ROBERTS, G.L., 1974, Mineralogy of surface sediments from the Panama Basin, Eastern Equatorial Pacific. *J. Geol.*, 82, p.145-160.

HEIN, J.R. and GRIGGS, G.B., 1972, Distribution and scanning electron microscope (SEM) observations of authigenic pyrite from a Pacific deep-sea core. *Deep-Sea Res.*, 19, p.133-138.

HEIN, J.R., O'NEILL, J.R. and JONES, M.G., 1979, Origin of authigenic carbonates from the deep Bering Sea. *Sedimentology*, 26, p.681-705.

HEIN, J.R. and SCHOLL, D.W., 1978, Diagenesis and distribution of late Cenozoic volcanic sediment in the southern Bering Sea. *Geol. Soc. Amer. Bull.*, 89, p.197-210.

HEIN, J.R., YEH, H-W. and ALEXANDER, E., 1979, Origin of iron-rich montmorillonite from the manganese nodule belt of the north equatorial Pacific. *Clays Clay Mineral.*, 27, p.185-194.

HELLER-KALLAI, L. and ROZENSON, I., 1978, Removal of magnesium from interstitial waters in reducing environments - the problem reconsidered. *Geochim. Cosmochim. Acta*, 42, p.1903-1909.

HEM, J.D., 1978, Redox processes at surfaces of manganese oxide and their effects on aqueous metal ions. *Chem. Geol.*, 21, p.199-218.

HEM, J.D., 1981, Rates of manganese oxidation in aqueous systems. *Geochim. Cosmochim. Acta*, 45, p.1369-1374.

HENDRICKS, S.B. and ROSS, C.S., 1941, Chemical composition and genesis of glauconite and celadonite. *Am. Mineral.*, 26, p.683-708.

HEYE, D., 1969, Uranium, thorium and radium in ocean water and deep-sea sediments. *Earth Planet. Sci. Lett.*, 6, p.112-116.

HIRST, D.M., 1962, The geochemistry of modern sediments from the Gulf of Paria - I. The relationship between the mineralogy and the distribution of major elements. *Geochim. Cosmochim. Acta*, 26, p.309-334.

HIRST, D.M., 1962, The geochemistry of modern sediments from the Gulf of Paria - II The location and distribution of trace elements. *Geochim. Cosmochim. Acta*, 26, p.1147-1187.

HOLDREN, G.R., 1977, Distribution and behaviour of manganese in interstitial waters of Chesapeake Bay sediments during early diagenesis. *Unpub. Ph.D. Thesis*, John Hopkins University, Baltimore, 190pp.

HOLLAND, H.D., 1979, Metals in black shales - a reassessment. *Econ. Geol.*, 74, p.1676-1680.

HOLLAND, H.D. and KULP, J.L., 1954, The mechanism of removal of ionium and radium from the oceans. *Geochim. Cosmochim. Acta*, 5, p.214-224.

HOLM-HANSEN, O., STRICKLAND, J.D.H. and WILLIAMS, P.M., 1966, A detailed study of biologically important substances in a profile off southern California. *Limnol. Oceanogr.*, 11, p.548-561.

HONJO, S., 1980, Material fluxes and modes of sedimentation in the mesopelagic and bathypelagic zones. *J. Mar. Res.*, 38, p.53-97.

HOWER, J., 1961, Some factors concerning the origin and nature of glauconite. *Am. Mineral.*, 46, p.313-334.

HSU, K.J. and SIEGENTHALER, C., 1969, Preliminary experiments on hydrodynamic movement induced by evaporation and their bearing on the dolomite problem. *Sedimentology*, 12, p.11-25.

HUNTER, K.A., 1980, Microelectrophoretic propeties of natural surface-active organic matter in coastal sea water. *Limnol. Oceanogr.*, 25, p.807-822.

ILLING, L.V., WELLS, A.J. and TAYLOR, J.C.M., 1965, Penecontemporary dolomite in the Persian Gulf. *in* *Dolomitization and Limestone Genesis: A symposium, eds.* L.C. Pray and R.C. Murray, S.E.P.M. Spec. Publ.13, p.487-499.

IRELAND, B.J., CURTIS, C.D. and WHITEMAN, J.A., 1983, Compositional variation within some glauconites and illites and implications for their stability and origins. *Sedimentology*, 30, p.769-786.

IRWIN, H., 1980, Early diagenetic carbonate precipitation and pore fluid migration in the Kimmeridge Clay of Dorset, England. *Sedimentology*, 27, p.577-591.

IRWIN, H., CURTIS, C.D. and COLEMAN, M., 1977, Isotopic evidence for source of disgenetic carbonates formed during burial of organic-rich sediments. *Nature*, 269, p.209-213.

JAHNKE, R.A, HEGGIE, D., EMERSON, S.R. and GRUNDMANIS, V., 1982a, Pore waters of the central Pacific Ocean: nutrient results. *Earth Planet. Sci. Lett.*, 61, p.233-256.

JAHNKE, R.A., EMERSON, S.R. and MURRAY, J.W., 1982b, A model of oxygen reduction, denitrification and organic matter mineralization in marine sediments. *Limnol. Oceanogr.*, 27, p.610-623.

JAHNKE, R.A., EMERSON, S.R., ROE, K.K. and BURNETT, W.C., 1983, The present day formation of apatite in Mexican continetal margin sediments. *Geochim. Cosmochim. Acta*, 47, p.259-266.

JANACEK, T.R. and REA, D.K., 1982, Eolian deposition in the northeast Pacific Ocean: Cenozoic history of atmospheric circulation. *Geol. Soc. Amer. Bull.*, 94, p.730-738.

JOHNSON, K.S., 1982, Solubility of rhodochrosite ($MnCO_3$) in water and seawater. *Geochim. Cosmochim. Acta*, 46, p.1805-1809.

JORGENSEN, B.B., 1977, Bacterial sulphate reduction within reduced microniches of oxidised marine sediments. *Mar. Biol.*, 41, p.7-17.

JORGENSEN, B.B., 1978, A comparison of methods for the quantification of bacterial sulphate reduction in coastal marine sediments. II. Calculation from mathematical models. *Geomicrobiol. J.*, 1, p.29-47.

KADKO, D., 1980a, ^{230}Th, ^{226}Ra and ^{222}Rn in abyssal sediments. *Earth Planet. Sci. Lett.*, 49, p.360-380.

KADKO, D., 1980b, A detailed study of some uranium series nuclides at an abyssal hill area near the East Pacific Rise at $8^{o}45'N$. *Earth Planet. Sci. Lett.*, 51, p.115-131.

KADKO, D., 1983, A multitracer approach to the study of erosion in the northeast equatorial Pacific. *Earth Planet. Sci. Lett.*, 63, p.13-33.

KALHORN, S. and EMERSON, S., 1984, The oxidation state of manganese in surface sediments of the deep sea. *Geochim. Cosmochim. Acta*, 48, p.897-902.

KAPLAN, I.R., 1974, *Natural Gases in Marine Sediments.* Plenum Press, New York, 324pp.

KASTNER, M., 1976, Diagenesis of basal sediments and basalts of Sites 322 and 323, Leg 35, Bellinghausen Abyssal Plain. *Init. Repts. D.S.D.P.*, 35, p.513-527.

KASTNER, M., MERTZ, K., HOLLANDER, D. and GARRISON, R., 1984, The association of dolomitite-phosphorite-chert: causes and possible diagenetic consequences. *in Dolomites of the Monterey Formation and Other Organic-Rich Units, eds.* R. E. Garrison, M. Kastner and D.H. Zenger, S.E.P.M. Vol. 41, p.75-86.

KAZAKOV, A., 1938, Phosphorite facies and the generation of natural phosphorites. *Soviet Geology*, 8, p.33-47.

KELTS, K.R. and McKENZIE, J.A., 1982, Diagenetic dolomite formation in Quaternary anoxic diatomaceous muds of Deep Sea Drilling Project, Leg 64, Gulf of California. *Init. Repts. D.S.D.P.*, 64 pt.2, p.553-569.

KELTS, K.R. and McKENZIE, J.A., 1984, A comparison of anoxic dolomite from deep-sea sediments: Quaternary Gulf of California and Messinian Tripoly Formation of Sicily. *in Dolomites of the Monterey Formation and Other Organic-Rich Units, eds.* R.E. Garrison, M.Kastner and D.H. Zenger, S.E.P.M. vol. 41, p.19-28.

KLINKHAMMER, G.P., 1980, Early diagenesis in sediments from the Eastern Equatorial Pacific, II. Pore water metal results. *Earth Planet. Sci. Lett.*, 49, p.81-101.

KLINKHAMMER, G.P. and BENDER, M.L., 1980, The distribution of manganese in the Pacific Ocean. *Earth Planet. Sci. Lett.*, 46, p.361-384.

KLINKHAMMER, G.P., HEGGIE, D.T. and GRAHAM, D.W., 1982, Metal diagenesis in oxic marine sediments. *Earth Planet. Sci. Lett.*, 61, p.211-219.

KNAUSS, J.A., 1978, *Introduction to Physical Oceanography.* Prentice-Hall, Englewood Cliffs, N.J., 338pp.

KNAUER, G.A., MARTIN, J.H. and BRULAND, K.W., 1979, Fluxes of particulate carbon, nitrogen and phosphorus in the upper water column of the Northeast Pacific. *Deep-Sea Res.*, 26, p.97-108.

KOBLENTZ-MISHKE, O.J., VOLKOVINSKY, V.V. and KABANOVA, J.G., 1970, Plankton primary production of the world ocean. *in Scientific Exploration of the South Pacific, ed.* W.S. Wooster, N.A.S. Washington, D.C., p183-192.

KOCZY, F.F., 1954, Geochemical balance of uranium and thorium in the hydrosphere. *in Nuclear Geology, ed.* H. Faul, Wiley, New York, p.210.

KOCZY, F.F., 1956, Geochemistry of the radioactive elements in the ocean. *Deep-Sea Res.*, 3, p.93-103.

KOMAR, P.D., KULM, L.D. and HARTLETT, J.C., 1974, Observations and analysis of bottom turbid layers on the Oregon continental shelf. *J. Geol.*, 82, p.104-111.

KOROLEV, D.F., 1958, The role of iron sulphides in the accumulation of molybdenum in the sedimentary rocks of the reduced zone. *Geokhimiya*, 4, p.452-463.

KRAUSE, D.C., 1965, Tectonics, bathymetry and geomagnetism of the southern continental borderland west of Baja California, Mexico. *Geol. Soc. Amer. Bull.*, 76, p.617-650.

KRAUSKOPF, K.B., 1956, Factors controlling the concentrations of thirteen rare metals in seawater. *Geochim. Cosmochim. Acta*, 9, p.1-32B.

KRAUSKOPF, K.B., 1979, *Introduction to Geochemistry*, 2nd Edition. McGraw Hill, New York, 617pp.

KRINSLEY, D., 1960, Trace elements in the tests of planktonic foraminifera. *Micropaleontology*, 6, p.297-300.

KRISHNASWAMI, S., 1976, Authigenic transition elements in Pacific pelagic clays. *Geochim. Cosmochim. Acta*, 40, p.425-434.

KRISHNASWAMI, S. and COCHRAN, J.K., 1978, Uranium and thorium series nuclides in oriented ferromanganese nodules: growth rates, turnover times and nuclide behaviour. *Earth Planet. Sci. Lett.*, 40, p.45-62.

KRISHNASWAMI, S., LAL, D., MARTIN, J.M. and MEYBECK, M., 1971, Geochronology of lake sediments. *Earth Planet. Sci. Lett.*, 11, p.407-414.

KRISTOFFERSON, A., ROLLA, G., SKJORLAND, K., GLANTZ, P. and IVARSSON, B., 1982, Evidence for formation of organic films on metal surfaces in seawater. *J. Colloid. Interface Sci.*, 86, p.196-203.

KROLL, V.S., 1953, Vertical distribution of radium in deep-sea sediments. *Nature*, 171, p.742.

KROLL, V.S., 1954, On the age determination in deep sea sediments by radium measurements. *Deep-Sea Res.*, 1, p.211-215.

KROM, M.D. and SHOLKOVITZ, E.R., 1977, Nature and reactions of dissolved organic matter in interstitial waters of marine sediments. *Geochim. Cosmochim. Acta*, 41, p.1565-1573.

KU, T-L., 1966, Uranium series disequilibrium in deep-sea sediments. *Unpub. Ph.D. Thesis*, Columbia University, New York.

KU, T-L. BISCHOFF, J.L. and BOERSMA, A., 1972, Age studies of mid-Atlantic ridge sediments near 42°N and 20°N. *Deep-Sea Res.*, 19, p.233-247.

KU, T-L. and BROECKER, W.S., 1969, Radiochemical studies on manganese nodules of deep-sea origin. *Deep-Sea Res.*, 16, p.625.

KULM, L.D., RCUSH, R.C., HARTLETT, J.C., NEUDECK, R.H., CHAMBERS, D.M. and RUNGE, E.J., 1975, Oregon continental shelf sedimentation: interelationship of facies distribution and sedimentary processes. *J. Geol.*, 83, p.145-175.

KULM, L.D., SUESS, E. and THORNBURG, T., 1984, Dolomites in organic-rich muds of the Peru forearc basins: Analogue to the Monterey Formation. *in Dolomite of the Monterey Formation and Other Organi-Rich Units, eds.* R.E. Garrison, M. Kastner and D.H. Zenger, S.E.P.M. Vol.41, p.29-44.

KULM, L.D., THORNBURG, T.M., SCHRADER, H., MASIAS, A., RESIG, J.M. and JOHNSON, L., 1981, Late Cenozoic carbonates on the Peru continetal margin: Lithostratigraphy, biostratigraphy and tectonic history. *Geol. Soc. Amer. Memoir*, 154, p.469-509.

KUSHNIR, J. and KASTNER, M., 1982, Adsorption of sulphate ions on calcite, aragonite and dolomite; Their role in inhibiting dolomitization. (abstract) *EOS*, 63, p.999.

KYLIN, H., 1930, Uber die jodidsaltende Fahigkeit der Phaophycean. *Z. Physiol. Chem.*, 191, p.200-210.

LAMBE, T.W. and WHITMAN, R.V., 1969, *Soil Mechanics.* Wiley, New York, 553pp.

LAND, L.S., 1973, Holocene meteoric dolomitization of Pleistocene limestones, North Jamaica. *Sedimentology*, 20, p.418-424.

LAND, L.S., 1980, The isotopic and trace element geochemistry of dolomite: the state of the art. *in Concepts and Models of Dolomitization, eds.* D.H. Zenger, J.B. Dunham and R.L. Ethington, S.E.P.M. Spec. Publ., 28, p.87-110.

LAND, L.S., SALEM, M.R.I. and MORROW, W.F., 1975, Palaeohydrology of ancient dolomites: Geochemical evidence. *Am. Assoc. Petrol. Geol. Bull.*, 59, p.1602-1625.

LANDERGREN, S., 1964, On the geochemistry of deep-sea sediments. *in Reports of the Swedish Deep-Sea Expedition*, Vol.X, Special Investigations, No.5, 154pp.

LARSON, R.L., 1972, Bathymetry, magnetic anomalies and plate tectonic history of the mouth of the Gulf of California. *Geol. Soc. Amer. Bull.*, 83, p.3345-3360.

LEINEN, M., 1977, A normative calculation technique for determining opal in deep-sea sediments. *Geochim. Cosmochim. Acta*, 41, p.671-676.

LI, Y.H., BISCHOFF, J. and MATHIEU, G., 1969, The migration of manganese in Arctic Basin sediment. *Earth Planet. Sci. Lett.*, 7, p.265-270.

LIU, K-K. and KAPLAN, I.R., 1984, Denitrification rates and availability of organic matter in marine environments. *Earth Planet. Sci. Lett.*, 68, p.88-100.

LOGANATHAN, P. and BURAU, P.G., 1973, Sorption of heavy metals by hydrous manganese oxide. *Geochim. Cosmochim. Acta*, 37, p.1277-1293.

LOGVINENKO, N.V., VOLKOV, I.I. and SOKOLOVA, Y.G., 1972, Rhodochrosite in deep-sea sediments of the Pacific Ocean. *Dokl. Akad. Nauk SSSR*, 203, p.178-181.

LOVE, L.G., 1962, Further studies on micro-organisms and the presence of syngenetic pyrite. *Palaeontology*, 5, p.444-459.

LOWENSTAM, H.A., 1974, Impact of life on chemical and physical processes. *in The Sea*, 5, *ed.* M.N. Hill, Wiley, New York, p.715-795.

LUMSDEN D.N. and CHIAMHUSKY, J.C., 1980, Relationship between dolomite nonstoichiometry and carbonate facies parameters. *in Concepts and Models of Dolomitization, eds.* D.H. Zenger, J.B. Dunham and R.L. Ethington, S.E.P.M. Spec. Publ., 28, p.123-137.

LUZ, B. and SHACKLETON, N.J., 1975, $CaCO_3$ solution in the tropical East Pacific during the past 130,000 years. *Cushman Found. Foram. Res. Spec. Publ.*, 13, p.142-150.

LYLE, M., 1983, The brown-green color transition in marine sediments: A marker of the Fe(III) - Fe(II) redox boundary. *Limnol. Oceanogr.*, 28, p.1026-1034.

LYNN, D.C. and BONATTI, E., 1965, Mobility of manganese in diagenesis of deep sea sediments. *Mar. Geol.*, 3, p.457-474.

MANHEIM, F.T., 1961, A geochemical profile in the Baltic Sea. *Geochim. Cosmochim. Acta*, 25, p.52-71.

MANHEIM, F.T., ROWE, G.T. and JIPA, D., 1975, Marine phosphorite formation off Peru. *J. Sediment. Petrol.*, 45, p.243-251.

MARLETT, E.M. and ERDMAN, J.G., 1959, Carbon-nitrogen distribution and nitrogen type relationships in recent and ancient sediments. *Div. Petroleum Chemistry, Amer. Chem. Soc.*, 135th Meeting, p.107-119.

MARSHALL, J.F. and COOK, D.J., 1980, Petrology of iron and phosphorus-rich nodules from the E Australian continental shelf. *J. Geol. Soc. Lond.*, 137, p.765-772.

MARTENS, C.S. and BERNER, R.A., 1974, Methane production in the interstitial waters of sulphate depleted marine sediments. *Science*, 185, p.1167-1169.

MARTENS, C.S. and BERNER, R.A., 1977, Interstitial water chemistry of anoxic Long Island Sound sediments. I. Dissolved gases. *Limnol. Oceanogr.*, 22, p.10-25.

MARTENS, C.S. and HARRISS, R.C., 1970, Inhibition of apatite precipitation in the marine environment by magnesium ions. *Geochim. Cosmochim. Acta*, 34, p.621-625.

MARTENS, C.S. and KLUMP, J.V., 1980, Biogeochemical cycling in an organic-rich coastal marine basin. I. Methane sediment-water exchange processes. *Geochim. Cosmochim. Acta*, 44, p.471-490.

MARTIN, J.H. and KNAUER, G.A., 1973, The elemetal composition of plankton. *Geochim. Cosmochim. Acta*, 37, p.1639-1653.

MATTHEWS, A. and KATZ, A., 1977, Oxygen isotope fractionation during the dolomitization of calcium carbonate. *Geochim. Cosmochim. Acta*, 41, p.1431-1438.

McCAVE, I.N., 1975, Vertical flux of particles in the ocean. *Deep-Sea Res.*, 22, p.491-502.

McCONNELL, D., 1965, Precipitation of phosphates in sea-water. *Econ. Geol.*, 60, p.1054-1062.

McINTYRE, A. and McINTYRE, R., 1971, Coccolith concentration and differential solution in oceanic sediments. *in The Micropalaeontology of the Oceans, eds.* B.M. Funnel and W.R. Riedel, Cambridge Univ. Press, p.253-262.

McRAE, S.G., 1972, Glauconite. *Earth-Science Rev.*, 8, p.397-440.

MELSON, W.G. and THOMPSON,G., 1973, Glassy abyssal basalts, Atlantic sea floor near St. Paul's Rocks: Petrography and composition of secondary clay minerals. *Geol. Soc. Amer. Bull.*, 84, p.703-716.

MILLIMAN, J.D., 1974, *Marine Carbonates.* Springer-Verlag, New York, 365pp.

MOORE, C. and BOSTROM, K., 1978, The elemental composition of lower marine organisms. *Chem. Geol.*, 23, p.1-9.

MOORE, D.G., 1964, Shear strength and related propeties of sediments from the experimental Mohole (Guadalupe Site). *J. Geophys. Res.*, 69, p.4271-4291.

MOORE, J.R., 1963, Bottom sediment studies, Buzzards Bay, Massachusetts. *J. Sediment. Petrol.*, 33, p.511-558.

MOORE, W.S, KU, T-L., MACDOUGALL, J.D., BURNS, V.M., BURNS, R., DYMOND, J., LYLE, M. and PIPER, D.Z., 1981, Fluxes of metals to a manganese nodule: radiochemical, chemical, structural and mineralogical studies. *Earth Planet. Sci. Lett.*, 52, p.157-171.

MORGAN, J.J. and STUMM, W., 1964, Colloid-chemical propeties of manganese dioxide. *J. Colloid Sci.*, 19, p.347-359.

MORGAN, J.J., 1967, Chemical equilibria and kinetic propeties of manganese in natural waters. *in Principles and Applications of Water Chemistry, eds.* S.D. Faust and J.V. Hunter, Wiley, New York, p.561-624.

MUELLER, H.W., 1975, Centrifugal progradation of carbonate banks: A model for deposition and early diagenesis, Ft. Terrett Formation, Edwards Group, Lower Cretaceous, Central Texas. *Unpub. Ph.D. Thesis*, University of Texas, Austin, 300pp.

MULLER, P.J., 1977, C/N ratios in Pacific deep-sea sediments: Effect of inorganic ammonium and organic nitrogen compounds sorbed by clays. *Geochim. Cosmochim. Acta*, 41, p.765-776.

MULLER, P.J. and MANGINI, A., 1980, Organic carbon decomposition rates in sediments of the Pacific manganese nodule belt dated by ^{230}Th and ^{231}Pa. *Earth Planet. Sci. Lett.*, 51, p.94-114.

MULLER, P.J. and SUESS, E., 1979, Productivity, sedimentation rate and sedimentary organic matter in the oceans. I. Organic carbon preservation. *Deep-Sea Res.*, 26, p.1347-1362.

MUNK, W.H., 1950, On the wind-driven ocean circulation. *J. Meteorology*, 2, p.79-83.

MURRAY, J. and RENARD, A.F., 1891, *Report on Deep-Sea Deposits Based on the Specimens Collected During the Voyage of H.M.S. 'Challenger' in the Years 1872-1876.* H.M.S.O., London, 525pp.

MURRAY, J. and RENARD, A.F., 1898, *Deep Sea Deposits,Challenger Reports*, Longmans, London, 525pp.

MURRAY, J.W. and DILLARD, J.G., 1979, The oxidation of cobalt(II) adsorbed on manganese dioxide. *Geochim. Cosmochim. Acta*, 43, p.781-787.

MURRAY, J.W., BALISTRIERI, L.S. and PAUL, B., 1984, The oxidation state of maganese in marine sediments and ferromanganese nodules. *Geochim. Cosmochim. Acta*, 48, p.1237-1248.

MURRAY, J.W., EMERSON, S.R. and JAHNKE, R.A., 1980, Carbonate saturation and the effect of pressure on the alkalinity of interstitial waters from the Guatemala Basin. *Geochim. Cosmochim. Acta*, 44, p.963-972.

MURRAY, J.M., GRUNDMANIS, V. and SMETHIE, W.M.Jr., 1978, Interstitial water chemistry in sediments of Saanich Inlet. *Geochim. Cosmochim. Acta*, 42, p.1011-1026.

MURRAY, J.W., SPELL, B. and PAUL, B., 1983, The contrasting geochemistry of manganese and chromium in the eastern tropical Pacific Ocean. *in Trace Metals in Sea Water, eds.* C.S. Wong, E. Boyle, K. Bruland, J. Burton, and E. Goldberg, NATO Conf. Series, Plenum, New York, p.643-670.

NARDIN, T.R., 1983, Late Quaternary depositional systems and sea level change - Santa Monica and San Pedro basins, California continental borderland. *Am. Assoc. Petrol. Geol. Bull.*, 67, p.1104-1124.

NARDIN, T,R., OSBORNE, R.H., BOTTJER, D.J. and SCHEIDEMANN, R.C.,Jr., 1981, Holocene sea-level curve for Santa Monica shelf, California continental borderland. *Science*, 213, p.331-333.

NEAL, C. and TRUESDALE, V.W., 1976, The sorption of iodate and iodide by riverine sediments: Its implications to dilution gauging and hydrogeochemistry of iodine. *J. Hydrology*, 31, p.281-291.

NICHOLLS, G.D., CURL, H.C. and BOWEN, V.T., 1959, Spectrographic analysis of marine plankton. *Limnol. Oceanogr.*, 4, p.472.

NIELSEN, A.E., 1964, *Kinetics of Precipitation.* MacMillan, New York, 151pp.

NISSENBAUM, A., 1974, The organic geochemistry of marine and terrestrial humic substances: implications for carbon and hydrogen isotope studies. *in Advances in Organic Geochemistry*, 1973, p.39-52.

NISSENBAUM, A. and KAPLAN, I.R., 1972, Chemical and isotopic evidence for the in situ origin of marine humic substances. *Limnol. Oceanogr.*, 17, p.570-582.

NISSENBAUM, A. and SWAINE, D.J., 1976, Organic matter metal interactions in Recent sediments: the role of humic substances. *Geochim. Cosmochim. Acta*, 40, p.809-816.

NISSENBAUM, A., PRESLEY, B.J. and KAPLAN, I.R., 1972, Early diagenesis in a reducing fjord, Saanich Inlet, British Columbia - I. Chemical and isotopic changes in major components of interstitial water. *Geochim. Cosmochim. Acta*, 36, p.1007-1027.

NORMARK, W.R., 1977, Neogene basins and transform motion within the Pacific continental margin off Baja California. *in Proceedings, Offshore Technology Conference, Houston, Texas*, 3, p.93-100.

NORRISH, K. and HUTTON, J.T., 1969, An accurate X-ray spectrographic method for the analysis of a wide range of geological samples. *Geochim. Cosmochim. Acta*, 33, p.431-453.

NORTHRUP, D.A. and CLAYTON, R.M., 1966, Oxygen isotope fractionations in systems containing dolomite. *J. Geol.*, 74, p.174-196.

NOZAKI, Y. and TSUNOGAI, S., 1976, ^{226}Ra, ^{210}Pb and ^{210}Po disequilibria in the western north Pacific. *Earth Planet. Sci. Lett.*, 32, p.313-321.

NOZAKI, Y., COCHRAN. J.K., TUREKIAN, K.K., and KELLER, G., 1977, Radiocarbon and ^{210}Pb distribution in submersible-taken deep-sea cores from Project FAMOUS. *Earth Planet. Sci. Lett.*, 34, p.167-173.

ODIN, G.S. and MATTER, A., 1981, De glauconiarum origine. *Sedimentology*, 28, p.611-641.

OFFICER, C.B., 1982, Mixing, sedimentation rates and age dating for sediment cores. *Mar. Geol.*, 46, p.261-278.

OFFICER, C.B. and LYNCH, D.R., 1983, Determination of mixing parameters from tracer distributions in deep-sea sediment cores. *Mar. Geol.*, 52, p.59-74.

OJAKANGAS, R.W. and KELLER, W.D., 1964, Glauconitization of rhyolite sand grains. *J. Sediment. Petrol.*, 34, p.84-90.

OSMOND, J.K., 1979, Accumulation models of ^{230}Th and ^{231}Pa in deep sea sediments. *Earth-Science Rev.*, 15, p.95-150.

PANTONY, D.A. and SIDDIQI, A., 1962, *Talanta*, 9, p.811.

PARKIN, D.W. and SHACKLETON, N.J., 1973, Trade-wind and temperature correlations down a deep-sea core off the Sahara Coast. *Nature*, 245, p.455-457.

PAVLOVA, G.A and SHISHKINA, O.V., 1973, Accumulation of iodine in interstitial water during metamorphism in relation to the iodine distribution in Pacific sediments. *Geochem. Int.*, 10, p.804-813.

PEDERSEN, T.F., 1979, The geochemistry of sediments of the Panama Basin, Eastern Equatorial Pacific Ocean. *Unpub. Ph.D. Thesis*, University of Edinburgh, 235pp.

PEDERSEN, T.F., 1983, Increased productivity in the eastern equatorial Pacific during the last glacial maximium. *Geology*, 11, p.16-19.

PEDERSEN, T.F. and PRICE, N.B., 1980, The geochemistry of iodine and bromine in sediments of the Panama Basin. *J. Mar. Res.*, 38, p.397-411.

PEDERSEN, T.F. and PRICE, N.B., 1982, The geochemistry of managnese carbonate in Panama Basin sediments. *Geochim. Cosmochim. Acta*, 46, p.59-68.

PEDONE, V.A., 1978, Petrography, chemistry and crystallography of baroque dolomite, Kingsport, Tennessee. *Unpub. M.A. Thesis*, University of Texas, Austin, 142pp.

PENG, T-H., BROECKER, W.S., KIPPHUT, G. and SHACKLETON, N., 1977, Benthic mixing in deep-sea cores as determined by ^{14}C dating and its implications regarding climate, stratigraphy, and the fate of fossil fuel CO_2. *in The Fate of Fossil Fuel CO2 in the Oceans, eds.* N.R. Andersen and A. Malahoff, Plenum, New York, p.355-374.

PETTERSSON, H., 1954, Radioactivity and the chronology of the ocean floor. *in Nuclear Geology, ed.* H. Faul, Wiley, New York, p.329-330.

PHLEGER, F.B. and SOUTAR, A., 1973, Production of benthic foraminifera in three East Pacific oxygen minima. *Micropalaeontology*, 19, p.110-115.

PICCIOTTO, E. and WILGAIN. S., 1954, Thorium determinations in deep-sea sediments. *Nature*, 173, p.632-633.

PIGGOT, C.S. and URRY, W.D., 1941, Radioactivity of ocean sediments. III. Radioactive relations in ocean water and bottom sediments. *Am. J. Sci.*, 239, p.81-91.

PIGGOT, C.S. and URRY, W.D., 1942, Radioactivity of ocean sediments. IV. The radium content of sediments of the Cayman Trough. *Am. J. Sci.*, 240, p.1-12.

PIPER, D.Z. and CODISPOTI, L.A., 1975, Marine phosphorite deposits and the nitrogen cycle. *Science*, 188, p.15-18.

PISCIOTTO, K.A., 1981, Review of secondary carbonates in the Monterey Formation, California. *in The Monterey Formation and Related Siliceous Rocks of California*, S.E.P.M., p.273-284.

PISCIOTTO, K.A. and MAHONEY, J.J., 1981, Isotopic survey of diagenetic carbonates, Deep Sea Drilling Project, Leg 63. *Init. Repts. D.S.D.P.*, 63, p.595-609.

PREMUZIC, E.T., BENKOVITZ, C.M., GAFFNEY, J.S. and WALSH,J.J., 1982, The nature and distribution of organic matter in the surface sediments of world oceans and seas. *Org. Geochem.*, 4, p.63-77.

PRESLEY, B.J., BROOKS, R.R. and KAPLAN, I.R., 1967, Manganese and related elements in interstitial water of marine sediments. *Science*, 158, p.906-909.

PRESLEY, B.J., KOLODNY, Y., NISSENBAUM, A. and KAPLAN, I.R., 1972, Early diagenesis in a reducing fjord, Saanich Inlet, British Columbia- II. Trace element distribution in interstitial water and sediment. *Geochim. Cosmochim. Acta*, 36, p.1073-1090.

PRICE, N.B. and CALVERT, S.E., 1973, The geochemistry of iodine in oxidised and reduced Recent marine sediments. *Geochim. Cosmochim. Acta*, 37, p.2149-2158.

PRICE, N.B. and CALVERT, S.E., 1977, The contrasting geochemical behaviour of iodine and bromine in Recent sediments from the Namibian shelf. *Geochim. Cosmochim. Acta*, 41, p.1769-2158.

PRICE, N.B. and CALVERT, S.E., 1978, The geochemistry of phosphorites from the Namibian shelf. *Chem. Geol.*, 23, p.151-170.

PRICE, N.B., CALVERT, S.E., and JONES, P.G.W., 1970, The distribution of iodine and bromine in the sediments of the Southwestern Barents Sea. *J. Mar. Res.*, 28, p.22-34.

PYTKOWICZ, R.M. and KESTER, D.R., 1967, Relative calcium phosphate saturation in two regions of the North Pacific. *Limnol. Oceanogr.*, 12, p.714-718.

QUINN, W.H., 1971, Late Quaternary meteorological and oceanic development in the equatorial Pacific. *Nature*, 229, p.330-331.

RANKAMA, K. and SAHAMA, T.G., 1950, *Geochemistry*.Univ. of Chicago Press, 912pp.

RASHID, M.A. and LEONARD, J.D., 1973, Modifications in the solubility and precipitation behaviour of various metals as a result of their interaction with sedimentary humic acid. *Chem. Geol.*, 11, p.89-97.

RATEEV, M.A., TIMOFEEV, P.P. and GRECHIN, V.I., 1981, Distribution of clay fraction minerals in Miocene through Pleistocene terrigenous deposits off Southern California and Baja California, Deep Sea Drilling Project Leg 63. *Init. Repts. D.S.D.P.*, 63, p.611-621.

REDFIELD, A.C., KETCHUM, B.H. and RICHARDS, F.A., 1963, The influence of organisms on the composition of sea water. *in The Sea*, 2, *ed.* M.N. Hill, Wiley, New York, p.26-77.

REEBURGH, W.S., 1976, Methane consumption in Cariaco Trench waters and sediments. *Earth Planet. Sci. Lett.*, 15, p.337-344.

REID, J.L., RODEN, G.I. and WYLLIE, J.G., 1958, Studies of the California Current system. *Calif. Coop. Ocean. Fisheries Invest. Progr. Rept.*, 1 July - 1 Jan., 1958, p.27-57.

REID, J.L., 1963, Measurements of the California Counter Current off Baja California, Mexico. *J. Geophys. Res.*, 68, p.4819-4822.

REIMERS, C.E., 1982, Organic matter in anoxic sediments off Central Peru: relations of porosity, microbial decomposition and deformation propeties. *Mar. Geol.*, 46, p.175-197.

REIMERS, C.E. and SUESS, E., 1983, The partitioning of organic carbon fluxes and sedimentary organic matter decomposition rates in the ocean. *Mar. Chem.*, 13, p.141-168.

REITSEMA, R.H., 1980, Dolomite and nahcolite formation in organic-rich sediments: isotopically heavy carbonates. *Geochim. Cosmochim. Acta*, 44, p.2045-2049.

REX, R.W. and GOLDBERG, E.D., 1958, Quartz contents of pelagic sediments of the Pacific Ocean. *Tellus*, 1, 153-159.

RHOADS, D.C., 1974, Organism - sediment relations on the muddy sea floor. *Oceanogr. Mar. Biol. Ann. Rev.*, 12, p.263-300.

RICHARDS, F.A., 1965, Anoxic basins and fjords. *in Chemical Oceanography*, 1, *eds.* J.P. Riley and G. Skirrow, Academic Press, London, p.611-645.

RICHARDS, F.A. and BENSON, B.B., 1961, Nitrogen/argon and nitrogen isotope ratios in two anaerobic environments, the Cariaco Trench in the Caribbean Sea and Dramsfjord, Norway. *Deep-Sea Res.*, 7, p.254-264.

RICHARDS, F.A. and VACCARO, R.F., 1956, The Cariaco Trench, an anaerobic basin in the Caribbean Sea. *Deep-Sea Res.*, 3, p.214-228.

RITTENBERG, S.C., EMERY, K.O. and ORR, W.L., 1955, Regeneration of nutrients in sediments of marine basins. *Deep-Sea Res.*, 3, p.23-45.

RITTENBERG, S.C., EMERY, K.O., HUSLEMANN, J., DEGENS, E.T., FAY, R.C., REUTER, J.H., GRADY, J.R., RICHARDSON, S.H. and BRAY, E.E., 1963, Biogeochemistry of sediments of the Experimental Mohole. *J. Sediment. Petrol.*, 33, p.140-172.

ROBBINS, J.A. and CALLENDER, E., 1975, Diagenesis of manganese in Lake Michigan sediments. *Amer. J. Sci.*, 275, p.512-533.

ROBERSON, C.E., 1966, Solubility implications of apatite in seawater. *U.S.G.S. Prof. Paper*, 550-D, p.178-185.

ROSHOLT, J.N., EMILIANI,C., GEISS, J., KOCZY, F.F. and WANGERSKY, P.J., 1961, Absolute dating of deep sea cores by Pa^{231}/Th^{230} method. *J. Geol.*, 69, p.162-185.

ROZENSON, I. and HELLER-KALLAI, L., 1976a, Reduction and oxidation of Fe 3+ in dioctahedral smectites - 1. Reduction with hydrazine and dithionite. *Clays Clay Miner.*, 24, p.271-282.

ROZENSON. I. and HELLER-KALLAI, L., 1976b, Reduction and oxidation of Fe 3+ in dioctahedral smectites - 2. Reduction with sodium sulphide solutions. *Clays Clay Miner.*, 24, p.283-288.

ROZENSON, I. and HELLER-KALLAI, L., 1978, Reduction and oxidation of Fe 3+ in dioctahedral smectites - 3. Oxidation of octahedral iron in montmorillonite. *Clays Clay Miner.*, 26, p.88-92.

RUDDIMAN, W.F. and HEEZEN, B.C., 1967, Differential solution of planktonic foraminifera. *Deep-Sea Res.*, 14, p.301-308.

RUSSELL, J.D., GODDMAN, B.A. and FRAGER, A.R., 1979, Infrared and Mossbauer studies of reduced nontronites. *Clays Clay Miner.*, 27, p.63-71.

SACKETT, W.M., 1960, Protactinium-231 content of ocean water and sediments. *Science*, 132, p.1761-1762.

SACKETT, W.M., 1965, Deposition rates by the protactinium method. *in Marine Geochemistry, eds.* D.R. Schink and J.T. Corless, Univ. Rhode Island Occas. Publ., 3, p.29-40.

SACKETT, W.M., 1966, Manganese nodules: Th^{230}/Pa^{231} ratios. *Science*, 154, p.646-647.

SARNTHEIN, M., TETZLAFF, G., KOOPMAN, B., WOLTER, K. and GLAUMANN, U., 1981, Glacial and interglacial wind regimes over the eastern subtropical Atlantic and North West Africa. *Nature*, 293, p.193-196.

SAVIN, S.M., DOUGLAS, R.G. and STEHLI, F.G., 1975, Tertiary marine palaeotemperatures. *Geol. Soc. Amer. Bull.*, 86, p.1499-1510.

SAWLAN, J.J., 1982, Early diagenetic remobilization of some transition metals in hemipelagic sediments. *Unpub. Ph.D. Thesis*, University of Washington, 251pp.

SAWLAN. J.J. and MURRAY, J.W., 1983, Trace metal remobilization in the interstitial waters of red clay and hemipelagic marine sediments. *Earth Planet. Sci. Lett.*, 64, p.213-230.

SAYLES, F.L. and BISCHOFF, J.L., 1973, Ferromanganoan sediments in equatorial east Pacific. *Earth Planet. Sci. Lett.*, 19, p.330-336.

SCHEIDEGGER, K.F. and STAKES, D.S., 1977, Mineralogy, chemistry and crystallization sequence of clay minerals in altered tholeiitic basalts from the Peru Trench. *Earth Planet. Sci. Lett.*, 36, p.413-422.

SCHINK, D.R. and GUINASSO, N.L.Jr., 1977, Effects of bioturbation on sediment-sea water interaction. *Mar. Geol.*, 23, p.133-154.

SEYFRIED, W.E., SHANKS, W.C. and BISCHOFF, J.L., 1976, Alteration and vein formation in Site 321 basalts. *Init. Repts. D.S.D.P.*, 34, p.385-392.

SHACKLETON, N.J. and HALL, M.A., 1982, Oxygen istope study of continuous scrape samples from Site 480. *Init. Repts. D.S.D.P.*, 64 Pt.2, p.1251-1254.

SHANKS, A.L. and TRENT, J.D., 1980, Marine snow: sinking rates and potential role in vertical flux. *Deep-Sea Res.*, 27A, p.137-143.

SHAW, T.I., 1962, Halogens in algae. *in Physiology and Biochemistry of Algae, ed.* R.A. Lewis, Academic Press, London, 922pp.

SHEPARD, F.P. and EMERY, K.O., 1941, Submarine topography off the California coast; canyons and tectonic interpretation. *Geol. Soc. Amer. Spec. Paper*, 31, 171pp.

SHEPPARD, S.M.F. and SCHWARTZ, H.P., 1970, Fractionation of carbon and oxygen isotopes and magnesium between metamorphic calcite and dolomite. *Contrib. Mineral. Petrol.*, 26, p.161-198.

SHISHKINA, D.V. and PAVLOVA, G.A., 1965, Iodine distribution in marine and oceanic bottom muds and in their pore fluids. *Geochem. Int.*, 2, p.559-565.

SHOLKOVITZ, E.R., 1973, Interstitial water chemistry of the Santa Barbara Basin sediments. *Geochim. Cosmochim. Acta*, 37, p.2043-2073.

SHOLKOVITZ, E.R., 1978, The fractionation of dissolved Fe, Mn, Al, Cu, Ni, Co and Cd during estuarine mixing. *Earth Planet. Sci. Lett.*, 41, p.77-86.

SILLEN, L.G., 1961, The physical chemistry of sea water. *in Oceanography, ed.* M. Sears, Amer. Assoc. Advance. Sci., p.549-581.

SMITH, J.D., 1977, Modeling of sediment transport on continental shelves. *in The Sea*, 6, *eds.* E.D. Goldberg, I.N. McCave, J.J. O'Brien and J.H. Steele, Wiley, New York, p.539-577.

SMITH, K.L.Jr., 1978, Benthic community respiration in the NW Atlantic Ocean: in situ measurements from 40-5200m. *Mar. Biol.*, 47, p.337-347.

SMITH, K.L.Jr, LAVER, M.B. and BROWN, N.O., 1983, Sediment community oxygen consumption and nutrient exchange in central and eastern North Pacific. *Limnol. Oceanogr.*, 28, p.882-898.

SMITH, P.E., 1971, Distributional atlas of zooplankton volume in the California Current region, 1951 through 1966. *CalCOFI Atlas*, No.13, v-xvi, p.1-144.

SORENSON, J., JORGENSEN, B.B. and REVSBECH, N.P., 1979, A comparison of oxygen, nitrate and sulphate respiration in coastal marine sediments. *Micro. Ecol.*, 5, p.105-115.

SPEARS, D.A. and AMIN, M.A., 1981, Geochemistry and mineralogy of marine and non-marine Namurian black shales from the Tansley Borehole, Derbyshire. *Sedimentology*, 28, p.407-417.

SPENCER, D.W., BREWER, P.G., FLEER, A., HONJO, S., KRISHNASWAMI, S. and NOZAKI, Y., 1978, Chemical fluxes from a sediment trap experiment in the deep Sargasso Sea. *J. Mar. Res.*, 36, p.493-523.

SPENCER, J.E. and NORMARK, W.R., 1979, Tosco-Abreojos fault zone: A Neogene transform plate boundary within the Pacific margin of southern Baja California, Mexico. *Geology*, 7, p.554-557.

STEVENSON, F.J. and CHENG, C-N., 1972, Organic geochemistry of the Argentine Basin sediments: carbon-nitrogen relationships and Quaternary correlations. *Geochim. Cosmochim. Acta*, 36, p.653-671.

STEVENSON, F.J. and DHARWIAL, A.P.S., 1959, Distribution of fixed ammonium in soils. *Soil. Sci. Soc. Amer. Proc.*, 23, p.121-125.

STEVENSON, F.J., KIDDER, G. and TILO, S.N., 1967, Extraction of organic nitrogen and ammonium from soil with hydrofluoric acid. *Soil Sci. Soc. Amer. Proc.*, 31, p.71-76.

STEVENSON, F.J. and TILO, S.V., 1970, Nitrogenous constituents of deep-sea sediments. *Proc. Third Int. Meeting Org. Geochem.*, London, p.227-253.

STRAKHOV, N.M., 1969, *Principles of Lithogenesis, Vol.2*, Oliver and Boyd, Edinburgh, 609pp.

STUMM, W. and GIOVANOLI, R., 1976, On the nature of particulate manganese in simulated lake waters. *Chimia*, 30, p.423-425.

STUMM, W. and LECKIE, J.D., 1970, Phosphate exchange with sediments; its role in the productivity of surface water. *in Advances in Water Pollution Research*, 2, Pergamon Press, New York, p.II126/1-22/16.

STUMM, W. and MORGAN, J.J., 1970, *Aquatic Chemistry.*, Wiley, London, 583pp.

SUESS, E., 1979, Mineral phases formed in anoxic sediments by microbial decomposition of organic matter. *Geochim. Cosmochim. Acta*, 43, p.339-352.

SUESS, E., 1980, Particulate organic carbon flux in the oceans - surface productivity and oxygen utilization. *Nature*, 288, p.260-263.

SUESS, E., 1981, Phosphate regeneration from sediments of the Peru continental margin by dissolution of fish debris. *Geochim. Cosmochim. Acta*, 45, p.577-588.

SUESS, E. and MULLER, P.J., 1980, Productivity, sedimentation rate and sedimentary organic matter in oceans. II, Elemental fractionation. *in Proc. C.N.R.S. Symposium on Benthic Boundary Layer*, Marseille, France, p.17-26.

SUESS, E., MULLER, P.J., POWELL, H.S. and REIMERS, C.E., 1980, A closer look at nitrification in pelagic sediments. *Geochem. J.*, 14, p.129-137.

SUGAWARA, K., KOYAMA, T. and TERADA, K., 1958, Co-precipitation of iodide ions by some metallic hydrated oxides with special reference to iodide accumulation in bottom water layers and in interstitial water of muds in some Japanese lakes. *J. Earth Sci. Nagoya Univ.*, 6, p.52-61.

SUAGAWARA, K. and OKABE, S., 1966, *J. Tokyo Univ. Fish.*, 8, p.165.

SUGAWARA, K., OKABE, S. and TANAKA, M., 1961, Geochemistry of molybdenum in natural waters (II). *J. Earth Sci. Nagoya Univ.*, 9, p.114-128.

SUNDBY, B., SILVERBERG, N. and CHESSELET, R., 1981, Pathways of manganese in an open estuarine system. *Geochim. Cosmochim. Acta*, 45, p.293-307.

SUPKO, P.R., 1977, Subsurface dolomites, San Salvador, Bahamas. *J. Sediment. Petrol.*, 47, p.1063-1077.

SWEATMAN, T.R. and LONG, J.V.P., 1969, Quantitative electron-probe microanalysis of rock forming minerals. *J. Petrol.*, 10, p.332-379.

SYKES, L.R., 1968, Seismological evidence for transform faults, sea floor spreading, and continental drift. *in The History of the Earth's Crust, ed.* R.A. Phinney, Princeton University Press, Princeton.

SZILAGYI, M., 1967, Sorption of molybdenum by humus preparations. *Geochem. Int.*, 4, p.1165-1167.

TAKAHASHI, J.I., 1939, Synopsis of glauconitization. *in Recent Marine Sediments: A Symposium, ed.* P.D. Trask, Am. Assoc. Petrol. Geol., Tulsa, p.502-512.

TAYLOR, S.R., 1965, The application of trace element data to problems in petrology. *in Physics and Chemistry of the Earth*, 6, *eds.* L.H. Ahrens, F. Press, S.K. Runcorn and H.C. Urey, Pergamon Press, Oxford, p.153-214.

THEISEN, R. and VOLLACH, D., 1967, Tables of X-ray Mass Absorption Coefficients. Verlag Stahleisen M.B.H., Dusseldorf.

THIRLWALL, M.F., 1979, The petrochemistry of the British Old Red Sandstone volcanic province. *Unpub. Ph.D. Thesis*, Edinburgh University.

THOMPSON, T.G. and CHOW, T.J., 1956, The strontium-calcium atom ratio in carbonate secreting marine organisms. *Pap. Mar. Biol. Oceanogr., Deep-Sea Res.*, supplement to Vol.3, p.20-39.

THOMPSON, P.R. and SAITO, T., 1974, Pacific Pleistocene sediments: planktonic foraminifera, dissolution cycles, and geochronology. *Geology*, 2, p.333-335.

THOMSEN, E. and VORREN, T.D., 1984, Pyritization of tubes and burrows from Late Pleistocene continental shelf sediments off North Norway. *Sedimentology*, 31, p.481-492.

THOMSON, J., 1982, A total dissolution method for determination of the a-emitting isotopes of uranium and thorium in deep-sea sediments. *Anal. Chim. Acta*, 142, p.259-268.

THOMSON, J. and TUREKIAN, K.K., 1976, ^{210}Po and ^{210}Pb distributions in ocean water profiles from the eastern south Pacific. *Earth Planet. Sci. Lett.*, 32, p.297-303.

TOTH, D.J. and LERMAN, A., 1977, Organic matter reactivity and sedimentation rate in the ocean. *Am. J. Sci.*, 277, p.465-485.

TOURTELOT, H.A., 1979, Black shale - its deposition and diagenesis. *Clays Clay Miner.*, 27, p.313-321.

TRASK, P.D., 1953, Chemical studies of sediments of the western Gulf of Mexico, part 2 of The Sediments of the western Gulf of Mexico.,- *Papers in Phys. Oceanogr. and Meteor., Mass. Inst. Tech. and Woods Hole Oceanogr. Inst.*, 12, p.49-120.

TRIPLEHORN, D.M., 1966, Morphology, internal structure, and origin of glauconite pellets. *Sedimentology*, 6, p.247-266.

TRUESDALE, V.W., 1975, 'Reactive' and 'unreactive' iodine in seawater - a possible indication of an organically bound iodine fraction. *Mar. Chem.*, 3, p.111-119.

TRUESDALE, V.W and SPENCER, C.P., 1974, Studies on the determination of iorganic iodine in seawater. *Mar. Chem.*, 2, p.33-47.

TSUNOGAI, S., 1971, Iodine in the deep water of the ocean. *Deep-Sea Res.*, 18, p.913-919.

TSUNOGAI, S. and SASE, T., 1969, Formation of iodide-iodine in the ocean. *Deep-Sea Res.*, 16, p.489-496.

TUREKIAN, K.K., 1957, The significance of variations in the strontium content of deep-sea cores. *Limnol. Oceanogr.*, 2, p.309-314.

TUREKIAN, K.K., 1964, The marine geochemistry of strontium. *Geochim. Cosmochim. Acta*, 28, p.1479-1496.

TUREKIAN, K.K. and BERTINE, K.K., 1971, Deposition of molybdenum and uranium along the major ocean ridge systems. *Nature*, 229, p.250-251.

TUREKIAN, K.K. and CHAN, L.H., 1971, The marine geochemistry of the uranium isotopes, ^{230}Th and ^{231}Pa. *in Activation Analysis in Geochemistry, eds.* A.D. Brunfelt and E. Steinnes, Universitets Forlaget, Oslo, p.311-320.

TUREKIAN, K.K., COCHRAN, J.K. and DE MASTER, D.J., 1978, Bioturbation in deep-sea deposits: rates and consequences. *Oceanus*, 21, p.34-41.

TUREKIAN, K.K. and WEDEPOHL, K.H., 1961, Distribution of the elements in some major units of the Earth's crust. *Geol. Soc. Amer. Bull.*, 72, p.175-192.

ULLMAN, W.J. and ALLER, R.C., 1980, Dissolved iodine flux from estuarine sediments and implications for enrichment of iodine at the sediment-water interface. *Geochim. Cosmochim. Acta*, 44, p.1177-1184.

ULLMAN, W.J. and ALLER, R.C., 1983, Rates of iodine mineralization in terrigenous near-shore sediments. *Geochim. Cosmochim. Acta*, 47, p.1423-1432.

VALENCIA, M.J., 1977, Pleistocene stratigraphy of the western equatorial Pacific. *Geol. Soc. Amer. Bull.*, 88, p.143-150.

VAN ANDEL, T.H., 1964, Recent marine sediments of the Gulf of California. *in Marine Geology of the Gulf of California, eds.* T.H. Van Andel and G.C. Shar, Jr., Am. Assoc. Petrol. Geol. Memoir 3, p.216-310.

VANDERBORGHT, J-P. and BILLEN, G., 1975, Vertical distribution of nitrate concentration in interstitial water of marine sediments with nitrification and denitrification. *Limnol. Oceanogr.*, 20, p.953-961.

VANDERBORGHT, J-P., WOLLAST, R. and BILLEN, G., 1977a, Kinetic models of diagenesis in disturbed sediments. Part 1. Mass transfer propeties and silica diagenesis. *Limnol. Oceanogr.*, 22, p.787-793.

VANDERBORGHT, J-P., WOLLAST, R. and BILLEN, G., 1977b, Kinetic models of diagenesis in disturbed sediments. Part 2. Nitrogen diagenesis. *Limnol. Oceanogr.*, 22, p.794-803.

VAN HOUTEN, F.B. and PURUCKER, M.E., 1984, Glauconitic peloids and chamositic ooids - favorable factors, constraints and problems. *Earth-Science Rev.*, 20, p.211-244.

VINE J.D. and TOURTELOT, E.B., 1970, Geochemistry of black shale deposits - a summary report. *Econ. Geol.*, 65, p.253-272.

VINOGRADOV, A.P., 1939, Iodine in marine muds. To the problem of the origin of iodine-bromine waters in petroliferous regions (in Russian). *Trans. Biogeochim/Lab. Akad. Nauk SSSR*, 5, p.19-32, (English, p.33-46).

VINOGRADOV, A.P., 1953, The elementary composition of marine organisms. *Sears Found. Mar. Res.*, 2, p.647.

VINOGRADOVA, Z.A. and KOVAL'SKIY, V.V., 1962, Elemental composition of Black Sea plankton. *Dokl. Acad. Nauk SSSR*, 147, p.1458-1460, (English, p.217).

VOLAT, J.L., PASTOURET, L. and VERGNAUD-GRAZZINI, C., 1980, Dissolution and carbonate fluctuations in Pleistocene deep-sea cores: a review. *Mar. Geol.*, 34, p.1-28.

VOLCHOK, H.L. and KULP, J.L., 1957, The ionium method of age determination. *Geochim. Cosmochim. Acta*, 11, p.219-246.

VOLKOV, I.I. and FOMINA, L.S., 1974, Influence of organic material and process of sulphide formation on the distribution of some trace elements in deep-water sediments of the Black Sea. *in The Black Sea - Geology, Chemistry and Biology, eds.* D.A. Ross and E.T. Degens. Am. Assoc. Petrol. Geol. Memoir, 20, p.456-476.

WADSLEY, A.D., 1952, The structure of lithiophorite $(Al,Li)MnO_2(OH)_2$. *Acta Crystallogr.*, 5, p.676-680.

WADSLEY, A.D., 1955, The crystal structure of chalcophanite, $ZnMn_3O_7.3H_2O$. *Acta Crystallogr.*, 8, p.165-172.

WAKEHAM, S.G., LEE, C., FARRINGTON, J.W. and GAGOSIAN, R.B., 1984, Biochemistry of particulate organic matter in the oceans: results from sediment trap experiments. *Deep-Sea Res.*, 31, p.509-528.

WAPLES, D.W. and SLOAN, J.R., 1980, Carbon and nitrogen diagenesis in deep sea sediments. *Geochim. Cosmochim. Acta*, 44, p.1463-1470.

WEAVER, C.E. and POLLARD, L.D., 1973, *The Chemistry of Clay Minerals.*, Elsevier, Amsterdam, 213pp.

WEBER, J.N., 1964, Carbon-oxygen isotopic composition of Flagstaff carbonate rocks and its bearing on the history of Palaeocene-Eocene Lake Flagstaff of Central Utah. *Geochim. Cosmochim. Acta*, 28, p.1219-1242.

WEBER, F.F.Jr. and SACKETT, W.M., 1981, Uranium geochemistry of the Orca Basin. *Geochim. Cosmochim. Acta*, 45, p.1321-1329.

WEDEPOHL, K.H., DELEVAUX, M.H. and DOE, B.R., 1978, The potential source of lead in the Permian Kupferschiefer bed of Europe and some selected Palaeozoic mineral deposits in the Federal Republic of Germany. *Contrib. Mineral. Petrol.*, 65, p.273-281.

WEISS, A., 1969, Organic derivatives of clay minerals, zeolites and related minerals. *in Organic Geochemistry, eds.* G. Eglington and M.T.J. Murphy, Springer-Verlag, New York, p.737-781.

WELLMAN, H.W., 1962, Delayed isostatic response and high sea-levels. *Nature*, 202, p.1322-1323.

WHITE, R.H. and MILLER, S.L., 1976, Inositol isomers: Occurence in marine sediments. *Science*, 193, p.885-886.

WHITE, S.M., 1970, Mineralogy and geochemistry of continental shelf sediments off the Washington-Oregon coast. *J. Sediment. Petrol.*, 40, p.38-54.

WHITEHEAD, D.C., 1974, The influence of organic matter, chalk and sesquioxides on the solubility of iodide, elemental iodine and iodate incubated with soil. *J. Soil. Sci.*, 25, p.461-470.

WILSON, A.D., 1955, A new method for the determination of ferrous iron in rocks and minerals. *Bull. Geol. Survey Great Britain*, 9, p.56-58.

WILSON, A.D., 1964, The titrimetric and spectrophotometric determination of the oxidising capacity of manganese compounds. *Analyst*, 89, p.571-578.

WILSON, D.E., 1980, Surface and complexation effects on the rate of Mn II oxidation in natural waters. *Geochim. Cosmochim. Acta*, 44, p.1311-1317.

WINDOM, H.L., 1969, Atmospheric dust records in permanent snow fields: Implications to marine sedimentation. *Geol. Soc. Amer. Bull.*, 80, p.761-782.

WISHNER, K.F., 1980, The biomass of deep-sea benthopelagic plankton. *Deep-Sea Res.*, 27, p.203-216.

WONG, G.T.F., 1980, The stability of dissolved inorganic species of iodine in seawater. *Mar. Chem.*, 9, p.13-24.

WONG, G.T.F. and BREWER, P.G., 1974, The determination and distribution of iodate in South Atlantic waters. *J. Mar. Res.*, 32, p.25-36.

WONG, G.T.F. and BREWER, P.G., 1977, The marine chemistry of iodine in anoxic basins. *Geochim. Cosmochim. Acta*, 41, p.151-159.

WONG, G.T.F. and DAVIDSON, J.A., 1977, The fate of chlorine in sea-water. *Water Res.*, 11, p.971-978.

WOOSTER, W.S. and JONES, J.H., 1970, California undercurrent off northern Baja California. *J. Mar. Res.*, 28, p.235-250.

WOOSTER, W.S. and REID, J.L.Jr., 1963, Eastern boundary currents. *in The Sea*, 2, *ed.* M.N. Hill, Wiley, New York, p.253-280.

YAMADA, M. and TSUNOGAI, S., 1984, Postdepositional enrichment of uranium in sediment from the Bering Sea. *Mar. Geol.*, 54, p.263-276.

YAMAMOTO, T. and FUJITA, T., 1966, A summary of chemical abundance in seaweeds. *Bull. Hyoto Univ. Educ. Ser.*, B, 29, p.9-12.

YAMAZAKI, H., GOHDA, S. and NISHIKAWA, Y., 1980, Chemical forms of chromium in natural water - interaction of chromium(III) and humic substances in natural water. *J. Oceanogr. Soc. Jpn.*, 35, p.233-240.

YEATS, R.S. and HAQ, B.U., *et al.*, 1981, Site reports, Site 471: Offshore Magdalena Bay. *Init. Repts. D.S.D.P.*, 63, p.269-291.

YEATS, R.S. and HAQ, B.U., 1981, Deep drilling off the Californias: Implications of Leg 63. *Init. Repts. D.S.D.P.*, 63, p.949-962.

ZEN, E.A., 1959, Mineralogy and petrography of marine bottom sediment samples off the coast of Peru and Chile. *J. Sediment. Petrol.*, 29, p.513-539.

RECENT DOLOMITE FORMATION IN HEMIPELAGIC SEDIMENTS OFF BAJA CALIFORNIA, MEXICO

G.B. Shimmield and N.B. Price, Grant Institute of Geology, University of Edinburgh, West Mains Road, Edinburgh, EH9 3JW, Scotland, U.K.

ABSTRACT

Early diagenetic dolomite occurring as euhedral rhombohedral (5-40 μm.) has been identified in shallow 0-40 cm.) cores from hemipelagic sediments off the coast of Baja California, Mexico. The lateral distribution of dolomite appears to be confined only to these sediments, whilst shelf and oceanic sediments show little or no evidence of dolomite precipitation. Its vertical distribution within the cores appears to be confined to the zone of reduction. Dolomite is found to be unstable in oxidising sediments, suggesting that it is not a stable phase in sea water. Mineralogy and composition (56 mole % $CaCO_3$) show it to be dolomite rather than "protodolomite". Coexistence of other diagenetic phases with the dolomite indicates that its formation predates glauconite and manganese carbonate, and postdates some pyrite and barite. We have attributed the precipitation of dolomite to a low sediment accumulation rate and a high flux of C_{org}. In such sediments extensive biomixing occurs allowing abundant Mg^{2+} ions to reach the surface of reduction - the locus of dolomite precipitation. Dolomitization of hemipelagic sediments of the eastern Pacific is discussed.

INTRODUCTION

The problem of the origin of dolomite, and the chemical conditions necessary for precipitation or replacement of limestones, has been debated over the last century (Correns, 1939; Fairbridge, 1957; Milliman, 1974). Many of these reports have considered dolomite genesis to have taken place under unusual environmental mechanisms due to evaporation and ground water control (Curtis et al., 1963; Deffeyes et al., 1964; Illing et al., 1965; Shinn et al., 1965; Von der Borch, 1965; Hsu and Siegenthaler, 1969; Folk and Land, 1975). Interest in the problem has been revived in recent years as extensive dolomitization has been found to occur in several deep-sea cores which are mainly confined to the ocean margins (Kulm et al, 1981; Pisciotto and Mahoney, 1981; Kelts and McKenzie, 1982). In these sediments there has been recognition that the dolomite is associated with organic carbon (C_{org}). Much of the interest in the latter sediments has been concerned with the timing of dolomite growth. The conclusions that have been reached, supported by laboratory work (Baker and Kastner, 1981; Kushnir and Kastner, 1982), indicate that the mineral can form as an early diagenetic phase, but could be restricted by the presence of SO_4^{2-} ions. Dolomite rhombohedral have been noted in surface sediments for decades (Fairbridge, 1957; Taft, 1961; Bonatti, 1966; Milliman, 1974; Behrens and Land, 1972), but due to their lack of abundance, and the possible detrital origin of some of them, there has been little study in respect of their genesis in the marine environment and their relation to more deeply buried dolomites.

In order to gain some insight into the timing of dolomite growth during sediment burial it is imperative that Recent occurrences be carefully examined and attempts made to relate them to other diagenetic phases which are more easily interpreted within the sequence of diagenesis.

Here, we attempt to observe the distribution, composition and mineral strpcture of dolomite in shallow subsurface cores taken from the eastern Pacific off the coast of Baja California, Mexico.

GENERAL ENVIRONMENTAL SETTING

The Pacific margin of the Baja California peninsula, between latitudes 27°N and 23° N, lies within the high productivity zone bordering the eastern Pacific (Figure 1). A semi-arid climate characterizes the region with an annual rainfall of only 12 cm. (Aschman, 1959) mostly occurring during the summer and autumn. The coastline around Magdalena Bay consists mainly of large sand dunes running parallel to the coast and extending some 20 km. back into the hinterland. The promontories forming Cabo San Lazaro, Cedros Island and the Vizcaino peninsula further to the north, are relict ophiolitic terranes and contribute amphibolitic detritus into the coastal environment. Here placer deposits of phosphorite are being commercially exploited at the present. The low lying terrain, lack of major rivers and development of coastal lagoons limits the amount of terrigenous input to the neighboring shelf.

The hydrography of the region is dominated by two main current systems: the California Current and the warmer North Equatorial water (Reid et al, 1958). The intense seasonal upwelling and associated biological productivity within this area promotes a marked oxygen minimum zone between 200 and 1000 meters depth (D'Anglejan, 1967) with a minimum dissolved O_2 concentration of <0.5 ml/l. This surface productivity is reflected in the organic carbon

in Garrison, Robert E.; Kastner, Miriam and Zenger, Donald H., eds., 1984, Dolomites of The Monterey Formation and Other Organic-Rich Units: Pacific Section S.E.P.M., Vol. 41, p. 5-18.

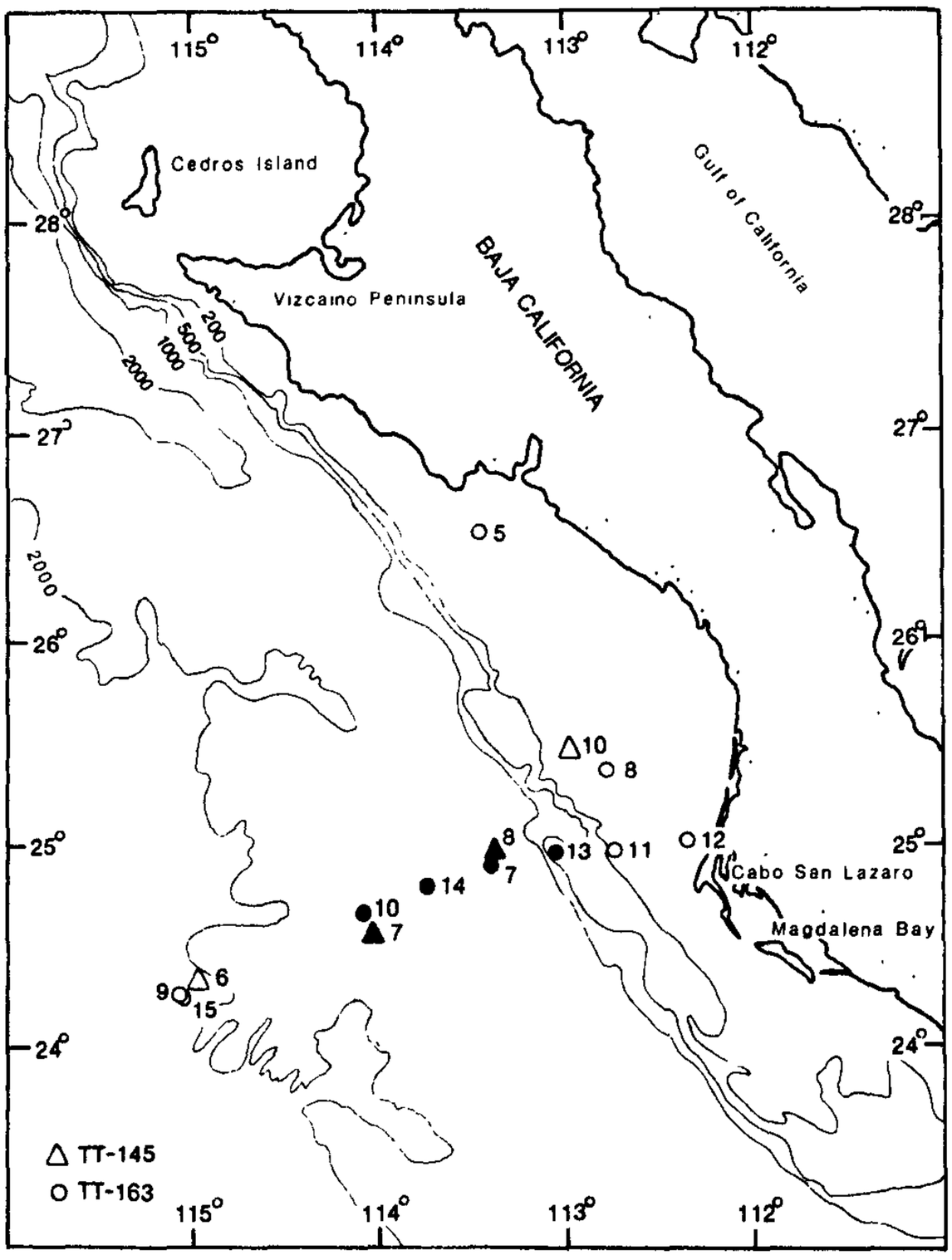

Figure 1 Core location map. Shaded symbols represent the occurrence of dolomite in the sediment. (Bathymetry in fathoms).

content of the sediments which reaches a maximum over the outer shelf. The combination of high C_{org} matter flux and low terrigenous accumulation rate for this continental margin makes it ideal to study the diagenetic processes involved without the obscuring effects of a large detrital component common in many other sediments.

The Baja California shelf and slope is a continuation of the continental borderland developed of southern California (Emery, 1960) resulting in a series of longitudinal intrashelf and slope basins and banks. Published investigations of sediments associated with this complicated topography (D'Anglejan, 1967; Jahnke et al., 1983; Sawlan and Murray, 1983) show that the basins tend to be characterized by greenish muds whilst the longitudinal banks display silts and foraminiferal sands.

METHODS OF STUDY

Sediment samples were collected during the R/V Thomas G. Thompson (University of Washington) cruises TGT-145 and TGT-163 in 1979 and 1980. Fourteen shallow (0-40 cm.) box-cores were sampled from a range of environments along a broad transect at roughly latitude 25°N that encompasses the continental rise, slope and shelf (Fig. 1). These box-cores were subsampled using a 2.5 inch acetate liner and horizontally sectioned into 1 cm. and 2 cm. intervals aboard ship and stored wet at 4° C.

The bulk, dried sediment was investigated for its mineralogy and geochemistry. Subsamples of ground sediment, as glass mounts, were x-ray diffracted using Cu Kα radiation to identify the bulk mineralogy of the sediment. Selected mineral extractions were treated in the same manner to investigate their crystal structure.

Major element content was determined by X-ray fluorescence (XRF) techniques on fused powders using a Cr anode following a technique similar to Norrish and Hutton (1969) and calculating the effects of mass absorption. Salt corrections were made by measuring the water content of the sediment and assuming constant salinity of 35°/00. Analytical precision (2σ, n=8) for Mn and Mg was 2.57% and 1.49% respectively.

Organic carbon was determined by combustion using a Leco induction furnace on residues tat were acidified, using 50% HCI at 60°C, in Leco ceramic crucibles to remove carbonate carbon. The precision (2σ, n=9) of the method was 4.52%.

Investigation of the dolomite and other authigenic phases involved examination of the total sediment, the silt fraction, and hand-picked grains. These included using a scanning electron microscope (SEM) with an energy dispersive analysing system (EDAX) to observe textural features of the dolomite and its host sediment. Accurate analysis of the dolomite (for CA, Mg, Fe, Sr, Ba, Si, Al, Na, K and S) was achieved using electron microprobe techniques on individual dolomite rhombs in polished grain mounts.

SEDIMENT DISTRIBUTION

Cores taken on the continental shelf show sediments to be grey-green, fine sands and silts. Characteristically, these sediments contain much quartz and amphibole and are generally carbonate-poor, except for local accumulations of foraminiferal debris. They are of moderate C_{org} content (1-5 - 2.0%). Cores from the shelf break and continental rise comprise carbonate - and biogenic silica-poor muds and silts with no trace of H_2S within the interval sampled. Typically, these sediments have a red-brown surface oxidising layer over underlying grey-green sediment. This colour change has been attributed to oxidation/reduction of Mn and Fe at depth, although recent evidence (Lyle, 1983) has shown that Fe alone may be the cause of this colour change. The depth of the colour change broadly relates to the C_{org} of the sediment; organic-poor (0.45%) outer continental rise sediments tend to have an oxidising zone in excess of 30 cms. thickness. Landwards, with increasing C_{org} content, the depth of this boundary decreases to a few centimeters and at the shelf break sediments tend to be reducing throughout.

Within these sediments a range of authigenic minerals has been identified and include dolomite, glauconite, barite, apatite, manganese carbonate, and possibly gypsum. The origin of

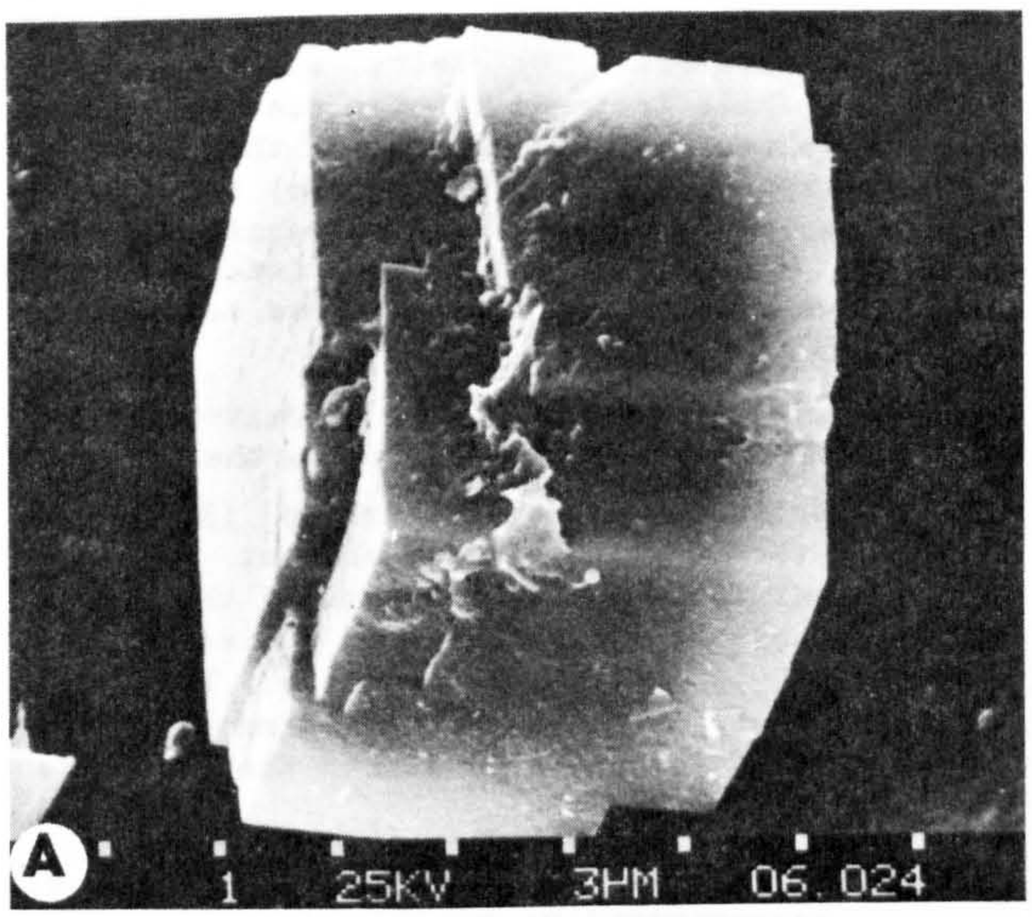

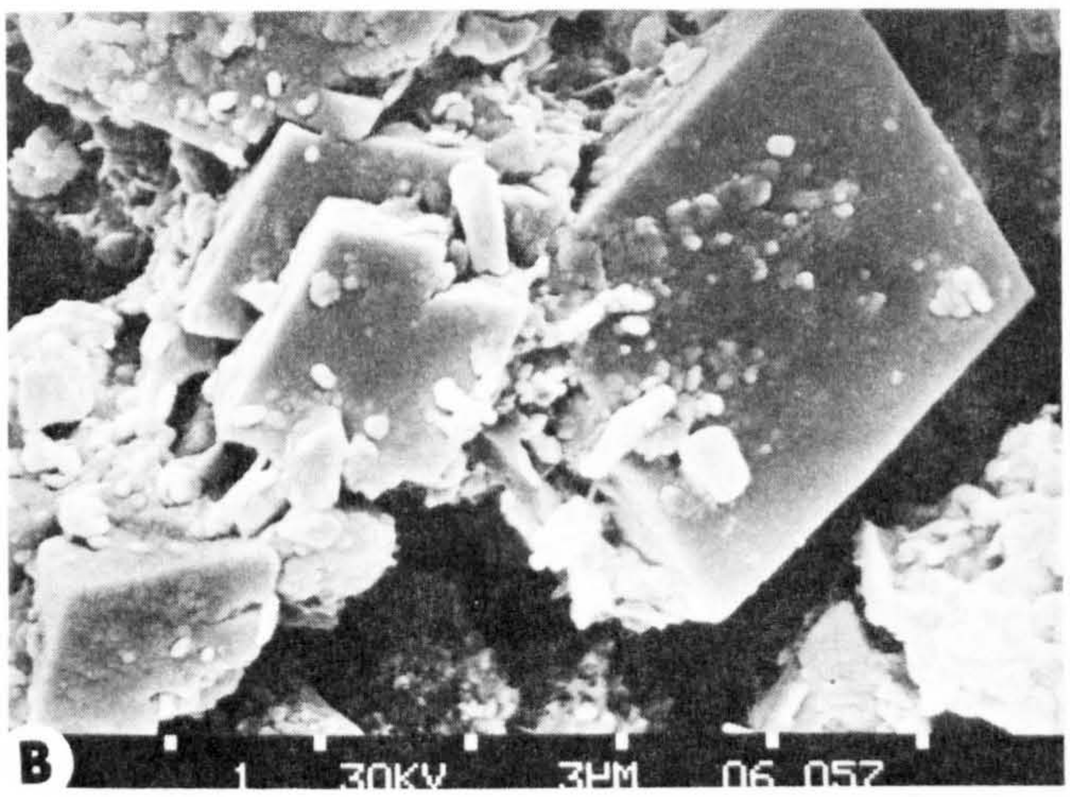

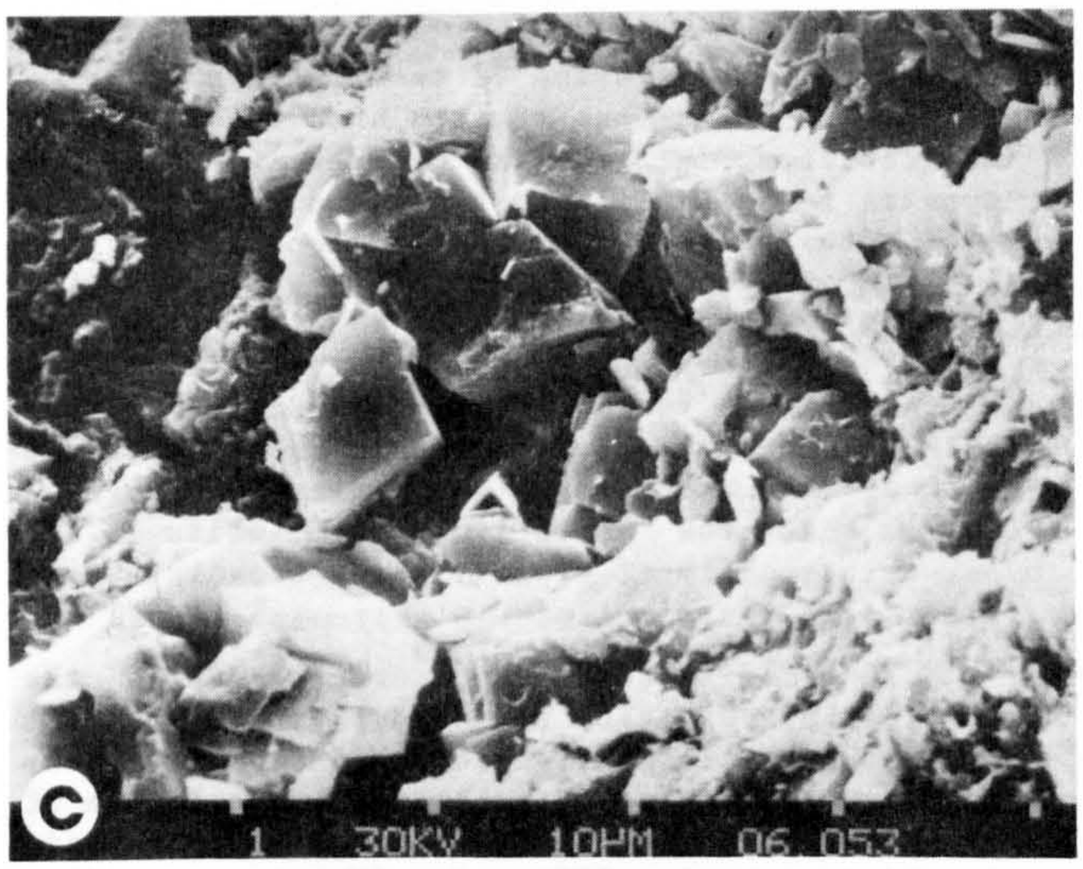

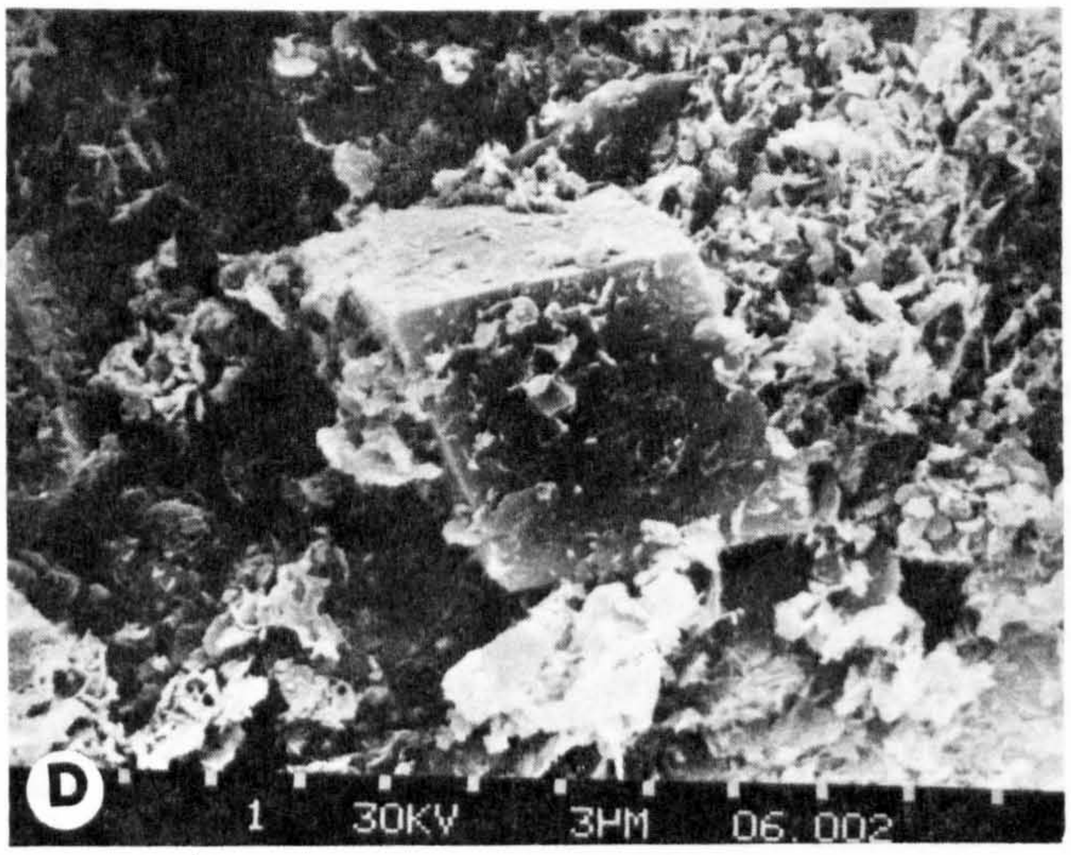

Figure 2 SEM photographs showing dolomite morphology:
(A) Grain mount of rhombohedral dolomite with step dislocations (163-13).
(B) Interpenetrating rhombs (163-13).
(C) Interpenetrating rhombs, morphology suggests *in situ* precipitation (163-13).
(D) Isolated rhomb with small intergrowth at top left of central face. Note adhering Fe-rich smectites (163-7).

gypsum in unknown. It could be a diagenetic phase, an oxidation product, or indeed, an artifact.

PHYSIOGRAPHY AND CHEMISTRY OF THE DOLOMITE

The dolomite occurs as discrete rhombohedra, or with small interpenetrating crystals, (Figure 2: A,B,C,D) growing displacively in the sediment. The rhombs vary in size from one or two microns up to a maximum of 40 μm, and show no evidence of size sorting in the sediment. Occasionally, minute inclusions of pyrite and claymaterical can be seen. Crystal terminations are sharp and well defined which indicate that no abrasion or other transport effects have taken place. Close inspection of certain surfaces of the dolomite grains sometimes show dislocations (Figure 2A) due to step growth along a spiral path (Nielsen, 1964). Such dislocations indicate that dolomite growth could take place at very low levels of supersaturation (<1.01) where two-dimension surface nucleation would be nearly impossible (Burton et al., 1951; Berner, 1981). Visual observation on the dolomite using the SEM and cathode luminescence failed to reveal any evidence of an earlier carbonate precursor phase. Foraminiferal tests are unaltered and do not have dolomite associated with them. Spatial arrangement of the rhombs in the sediment indicate direct precipitation, rather than some physico-chemical alteration from another carbonate. There is, however, a close association between growth of dolomite and other diagenetic phases such as glauconite, manganese carbonate and pyrite. These will be discussed below.

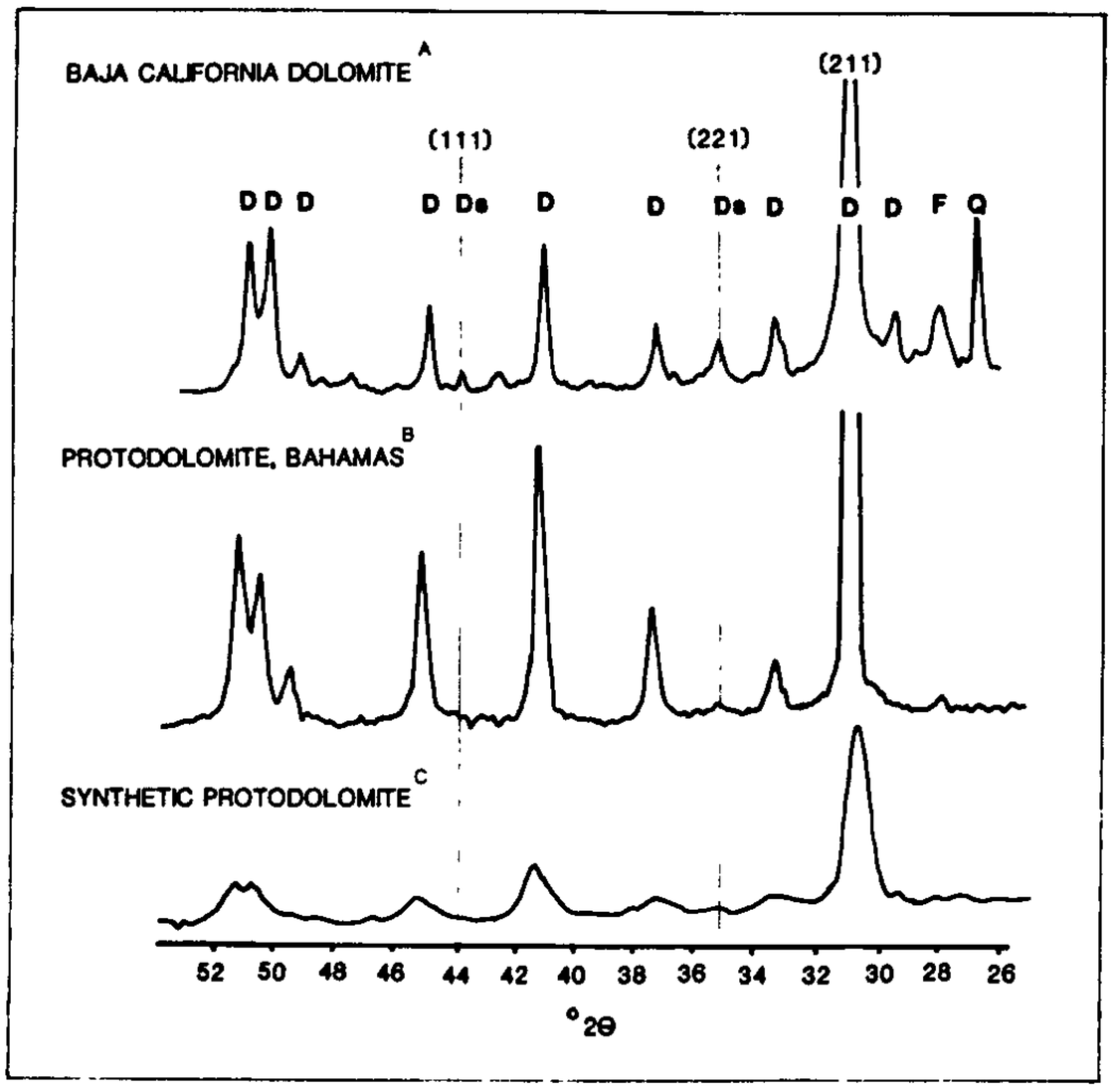

Figure 3 X-ray diffractograms of dolomite (A) and comparison with published spectra of protodolomites (B: Illing et al., 1977; C: Glover and Sippel, 1967) all using Cu Kα radiation. The superstructure reflections (111) and (221) reveal that the Baja California variety is an ordered dolomite. (D-dolomite, Ds-dolomite superstructure reflection, F-feldspar, Q-quartz)

Chemical and mineralogical examination shows that the dolomite from Baja California is not a "protodolomite" as defined by Graf and Goldsmith, (1956) and Gaines, (1977). This is illustrated in Figure 3 where the (211) and (111) superstructure reflections are clearly visible, confirming the degree of ordering compared with synthetic protodolomite or other naturally occurring protodolomites.

The Mg/Ca ratio of the dolomite was estimated using XRD by measuring the shift of the (211) reflection relative to a quartz internal standard (Goldsmith and Graf, 1958) giving a composition of 56 mole % $CaCO_3$. The use of a fluorite internal standard and slow chart scans of 1/8° 2θ/min. showed the a and c unit cell parameters to be 4.8291 Å and 16.1521 Å respectively. These have been plotted in Figure 4 and compared to other published dolomites and protodolomites. The Baja California dolomite hexagonal unit cell parameters are consistent with ordered dolomite (Land, 1980) and contrast with the measurements on protodolomites that show expanded parameters departing from the calcite - magnesite trend. It would appear that the excess of calcium over that of stoichiometric dolomite does not result in disordering.

Electron microprobe analyses of dolomite from two cores (163-7 and 163-13, Figure 1) are shown in Table 1. Results for the Ca/Mg ratios, shown as a histogram in Figure 5, confirm the 56 mole % $CaCO_3$ obtained by the XRD method. Both stations have seemingly similar dolomite compositions, and show a smaller range of excess Ca than that found in IPOD core material from the Gulf of California by Kelts and MacKenzie, (1982). While Sr tends to show reasonably consistent values, and somewhat lower than those of Behrens and Land, (1972) (800 ppm) from Baffin Bay, Texas, they do suggest incorporation of the element within the dolomite structure; the greater variability of Ba may be due to impurities such as barite.

Si and Al contents of the dolomites (Figure 6) are, in all probability, due to the presence of clay inclusion as the Si/Al ratio (3.33) is identical to that of the host sediment. Fe contents appear to be in excess, both of the level of S that can be accommodated as pyrite (FeS_2), barite ($BaSO_4$), and Fe-rich smectite. The analyses suggest that a very small amount of Fe (<0.6 wt.%) is incorporated within the dolomite lattice.

DISTRIBUTION IN THE SEDIMENTS

Visual observation of smear slides of surface and subsurface samples show that dolomite distribution, along the transect studied, appears to be limited to those sediments associated with the hemipelagic environment (Figure 1). Distal cores (145-6, 163-9, and 163-15) have only trace amounts in them, whilst the shelf silts are devoid of dolomite. As a first approximation, the quantity of dolomite in the bulk sediment has been estimated from the excess Mg over that associated with clays. Table 2 shows that the upper limit of dolomite in the subsurface sediment of five cores broadly correlates with the level of C_{org}.

In order to determine, more reliably, the vertical distribution of dolomite in these sediments the silt-size fraction at 5 cm. intervals was extracted by wet sieving. An estimate of the dolomite content in this fraction was made by line counting 300 grains (Galehouse, 1969). Results of this are shown in Fig. 7 together with C_{org} and solid phase Mn in the sediment. The vertical distribution of Mn is used to illustrate the division of the sediment into oxidising and reducing regimes. Incorporation of the Mn into a surface sediment usually occurs as MnO_2 and upon burial and bacterial activity is rapidly reduced to Mn^{2+} at some level in the sediment. The redox of this transition is broadly similar to, but precedes, the reduction of Fe^{3+} to Fe^{2+}. Figure 7 shows very clearly the different depths of this redox change for Mn in the four cores. Inspection of the C_{org}. contents show that those sediments with high organic matter have shallow redox changes (eg. 163-7). The vertical distribution of dolomite appears to be related to these redox boundaries and/or C_{org}. within the sediment. It is present in significant amounts only in the reduced sediment, and here is broadly correlatable with the abundance of C_{org}. Within the oxidising zone authigenic dolomite is either absent or present in small quantities. Moreover, inspection of the dolomite within oxidising sediment shows evidence of corrosion, (Figure 8D) whereas dolomite at depth occurs as perfect rhombs (Figure 2A,B,C,D). Sawlan and Murray (1983) present pore water NO_3 data from two cores, TGT-145-7 and TGT-145 - 8 with similar solid phases Mn

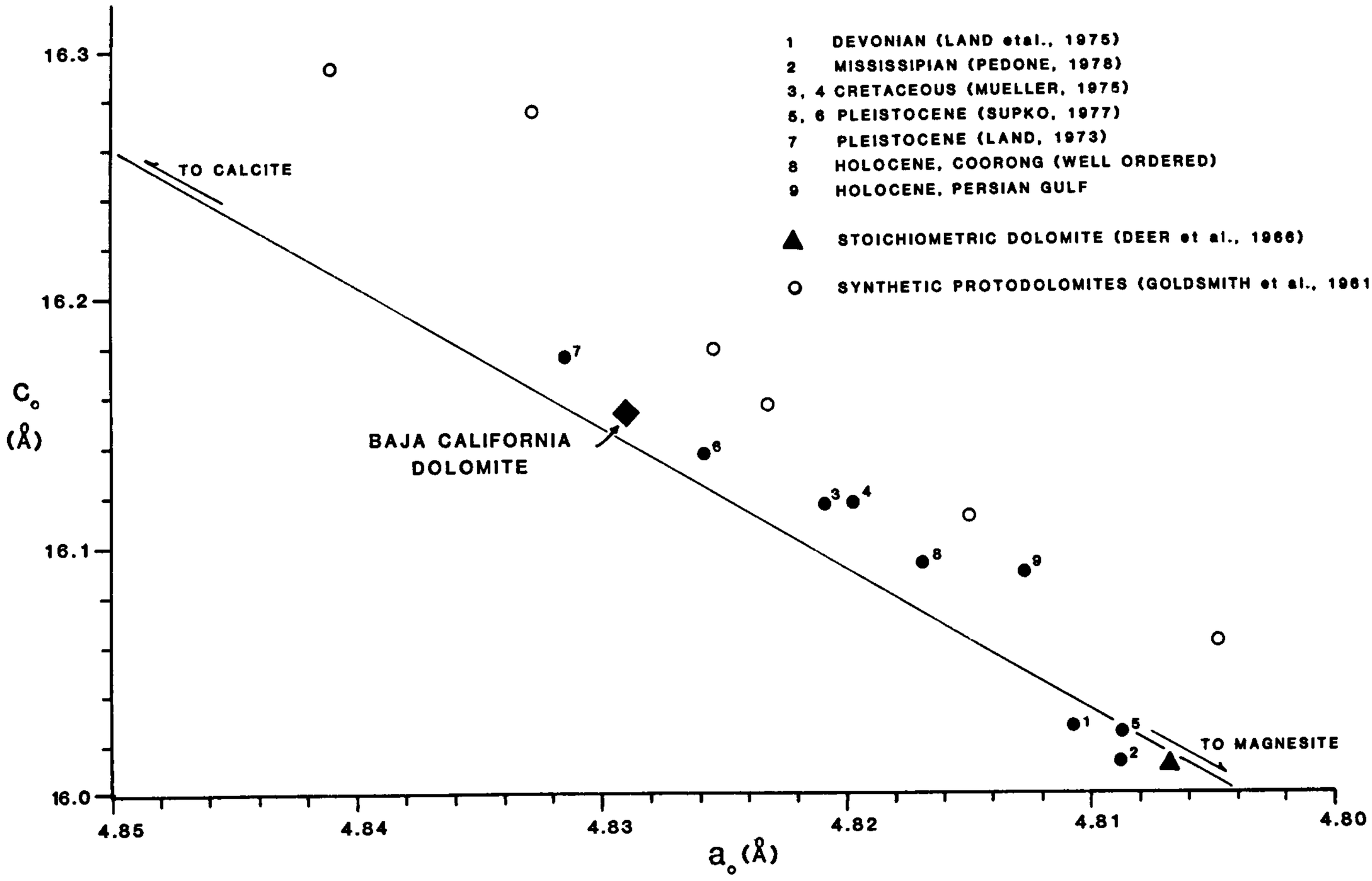

Figure 4 A plot of unit cell parameters a_o and c_o (in A) of Baja California dolomite, and published dolomites of various ages. The sloping line extrapolates to values for pure calcite and magnesite. Expansion of the unit cell due to disordering will result in an increase of the a_o and c_o parameters relative to this line (after Land, 1980).

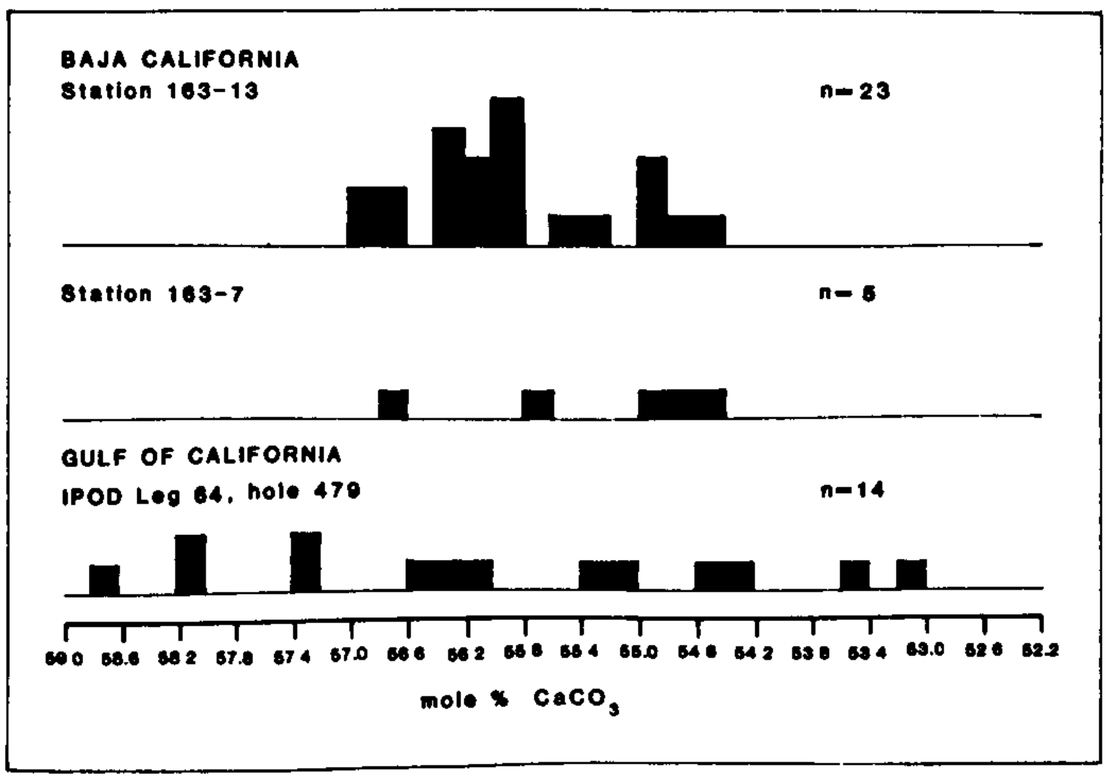

Figure 5 A histogram of the distribution of analyses for mole % $CaCO_3$ in Baja California dolomite, stations 163-13 and 163-7, and the Gulf of California, IPOD Leg 64, hole 479 (Kelts and McKenzie, 1982) performed by electron microprobe. (n=the number of analyses)

profiles. They show that NO_3 is completely consumed at depths greater than 40 cms. and 20 cms. respectively. Only on total depletion of O_2 and NO_3 (Gieskes, 1975) will the process of sulphate reduction predominate indicating that in these cores dolomite occurs in the presence of SO_4^{2-} ions.

Hemipelagic sediments along the studied transect show a maximum development of dolomite of only 3.5 wt.%. The variability of dolomite within these cores is broadly related to the level of C_{org} in the sediment. At station 163-13 the content of dolomite is unusually high and estimated at 25 wt. % in its deeper parts (Table 2) in this organic-rich sediment. The distribution of sediments within this core shows that the upper 20 cms. represents a lag deposit displaying concentrations of phosphorite, pyrite, barite and glauconite, whereas clays are poorly represented. At depth these same minerals are highly diluted by normal clay accumulation.

ELECTRON MICROPROBE ANALYSIS OF BAJA CALIFORNIA DOLOMITE

Core number and depth interval	Ca	Mg	Fe	Si	Al	Na	K	Ba	S	Sr
13:15-16	21.07	9.93	.47	1.22	.35	.13	.11	n.d.	n.d.	412
13:15-16	22.52	10.92	.39	.35	.09	.06	.04	n.d.	n.d.	431
13:15-16	22.74	10.67	.27	.74	.25	.08	.10	n.d.	n.d.	545
13:15-16	22.06	11.04	.77	.26	.08	.05	.04	n.d.	n.d.	736
13:15-16	21.82	10.06	.59	.43	.08	.05	.02	n.d.	n.d.	n.d.
13:15-16	22.98	11.43	.12	.59	.11	.12	.05	n.d.	n.d.	n.d.
13:15-16	23.00	10.85	.16	.27	.08	.07	.05	n.d.	n.d.	n.d.
13:15-16	22.78	10.92	.22	.27	.09	.05	.03	n.d.	n.d.	n.d.
13:18-19	22.50	10.63	1.19	.50	.15	.06	.08	1161	960	n.d.
13:18-19	23.72	10.93	.36	.25	.08	.06	.06	450	740	n.d.
13:18-19	23.15	11.08	.43	.21	.08	.06	.06	1348	700	n.d.
13:20-21	23.17	11.12	.15	.32	.06	.04	.08	508	150	n.d.
13:20-21	22.64	10.76	1.10	.32	.15	.05	.08	590	350	n.d.
13:20-21	23.02	11.47	.45	.83	.25	.15	.11	450	740	n.d.
13:21-22	22.81	10.81	.23	.87	.26	.08	.13	758	630	376
13:21-22	23.12	11.36	.12	.17	.09	.06	.05	391	380	298
13:21-22	23.08	11.07	.19	.36	.09	.05	.08	616	440	464
13:22-24	22.47	10.72	.25	.55	.17	.07	.10	1405	680	390
13:22-24	23.36	10.85	.69	.36	.13	.07	.08	697	330	317
13:22-24	20.89	10.03	1.09	2.53	.32	.06	.14	688	280	221
13:25-26	22.58	10.75	.90	.62	.23	.07	.13	797	290	265
13:25-26	23.48	11.66	.15	.37	.08	.06	.07	892	630	339
13:25-26	21.00	10.66	.55	.27	.07	.03	.05	862	650	479
7:30-34	23.08	11.65	.06	.21	.09	.06	.10	437	460	339
7:30-34	23.75	11.45	.01	.06	.03	.02	.06	651	310	166
7:30-34	23.47	11.81	.17	.61	.31	.14	.07	625	60	n.d.
7:30-34	23.55	10.92	.22	.14	.06	.03	.09	275	n.d.	n.d.
7:30-34	19.70	9.80	.11	1.94	.83	.15	.09	208	n.d.	n.d.
Detection limit	.015	.08	.033	.014	.009	.014	.01	560	122	127
Precision (±2)	.175	.08	.056	.027	.016	.017	.019	573	277	163

Table 1. Electron microprobe analysis of Baja California dolomite. Major elements as wt.%; analysis of Ba, S and Sr in ppm. Counting statistics are given in the same units. (n.d.=not determined)

Station (TGT-163)	9	10	14	7	13
20cm.					
C_{org}	0.34	1.10	1.03	1.33	3.60
excess Mg	0.01	0.20	0.19	0.29	18.73
Dolomite	0.09	1.76	1.68	2.53	18.73
25cm.					
C_{org}	0.29	1.05	1.05	1.42	4.27
excess Mg	0.04	0.14	0.13	0.29	2.95
Dolomite	0.25	1.22	1.13	2.53	25.70

Table 2. $C_{org.}$ determined by combustion in an induction furnace. Mg determined by x-ray fluoresence and salt-corrected. Excess Mg derived from an average pelagic clay Mg/Al ratio of 0.25. Dolomite content calculated from the excess Mg value assuming a stoichiometry for the dolomite of $Mg_{0.44}Ca_{0.56}Co_3$. All values in weight %.

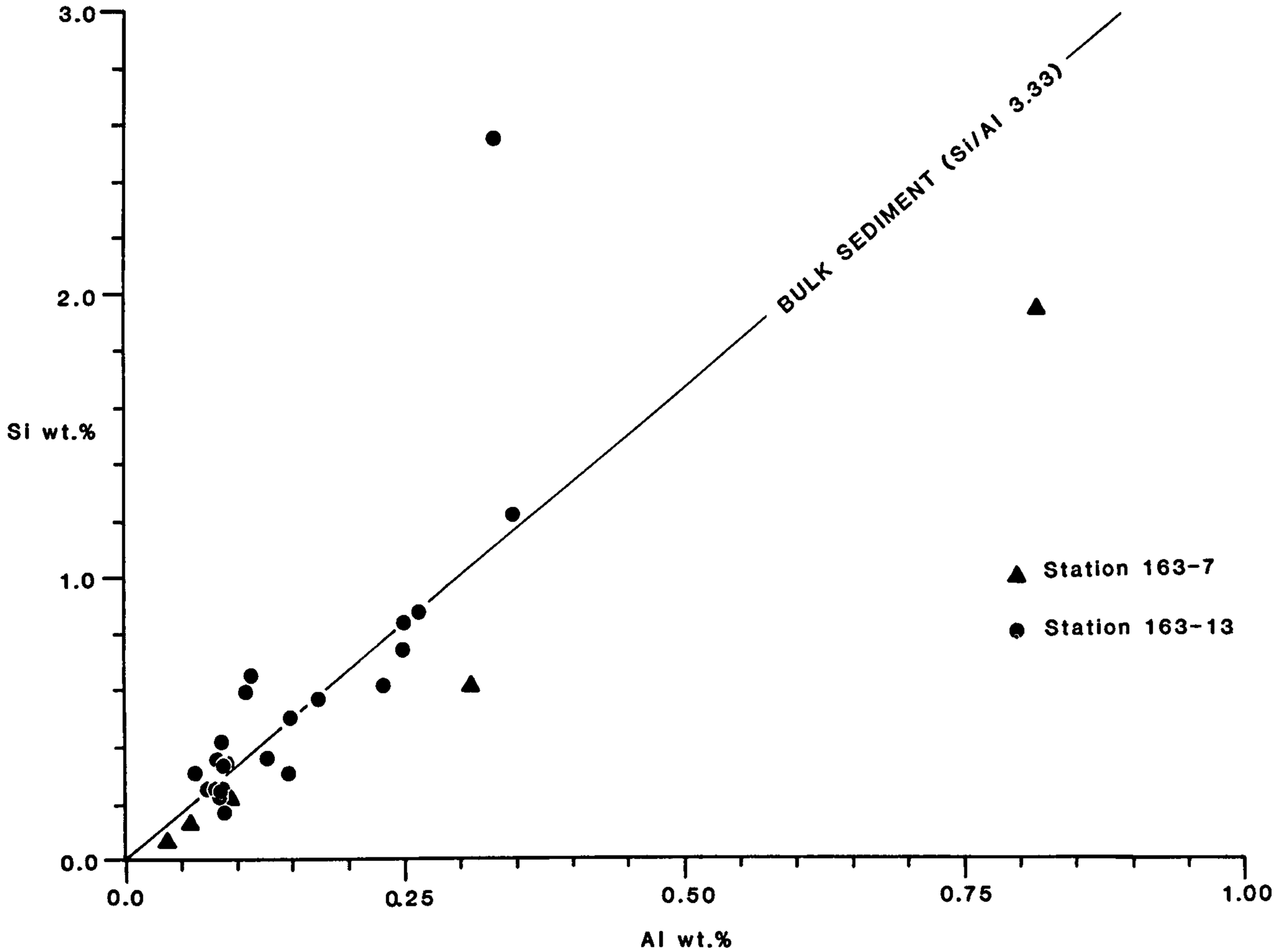

Figure 6 A plot of the Si and Al content of Baja California dolomites as measured from electron microprobe analyses. The Si/Al ratio (3.33) of bulk sediment based on 50 surface (0-10 cm.) analyses (XRF) is depicted by the line.

THE RELATION OF DOLOMITE TO OTHER AUTHIGENIC PHASES

All the above evidence suggests that dolomite is an early diagenetic phase. In order to understand the genesis of this dolomite it is important to relate it to the occurrences of other diagenetic minerals that have been identified by SEM and EDAX, and XRD techniques.

The coexistence of rare pyrite inclusions within the dolomite does suggest some sulphate reduction has occurred before the formation of dolomite. The existence of minor quantities of Ba within the dolomite also implies some barite formation before its crystallization. Recent reports have described the early formation of manganese carbonate (Pedersen and Price, 1982; Sawlan and Murray, 1983) in hemipelagic sediments which appears as a result of Mn reduction and bicarbonate production during burial before SO_4^{2-} exhaustion. In cores 163-10 and 145-7 $MnCO_3$ has been identified by EDAX (Figure 8A,B) towards their base (25-30 cm.) and its formation depth in these sediments is consistent with that calculated on thermodynamic grounds by Sawlan (1982). Examination of the carbonate reveals that dolomite can be associated with this mineral phase (Figure 8C) and that its depth of formation may be prior to that of the $MnCO_3$.

The association of dolomite with glauconite, in 163-13, is of particular interest as this mineral pair provides a valuable clue to the timing of dolomite growth, and its stability in the marine environment. Glauconite occurs both in the lag and the underlying clay in this core. Typically, it forms greenish-grey, very friable, fissured pellets usually 2 to 5 mm. in diameter (Figure 9A). In this respect they are identical to newly formed, "nascent" glauconite that has been identified in other Recent sediments (Odin and Matter, 1981). The structure of the glauconite seen by SEM and XRD analysis supports our contention that it is recently formed. Diffraction patterns show the mineral to be poorly-crystalline and lacking a well defined peak at 10 A; instead a broad hump is seen at

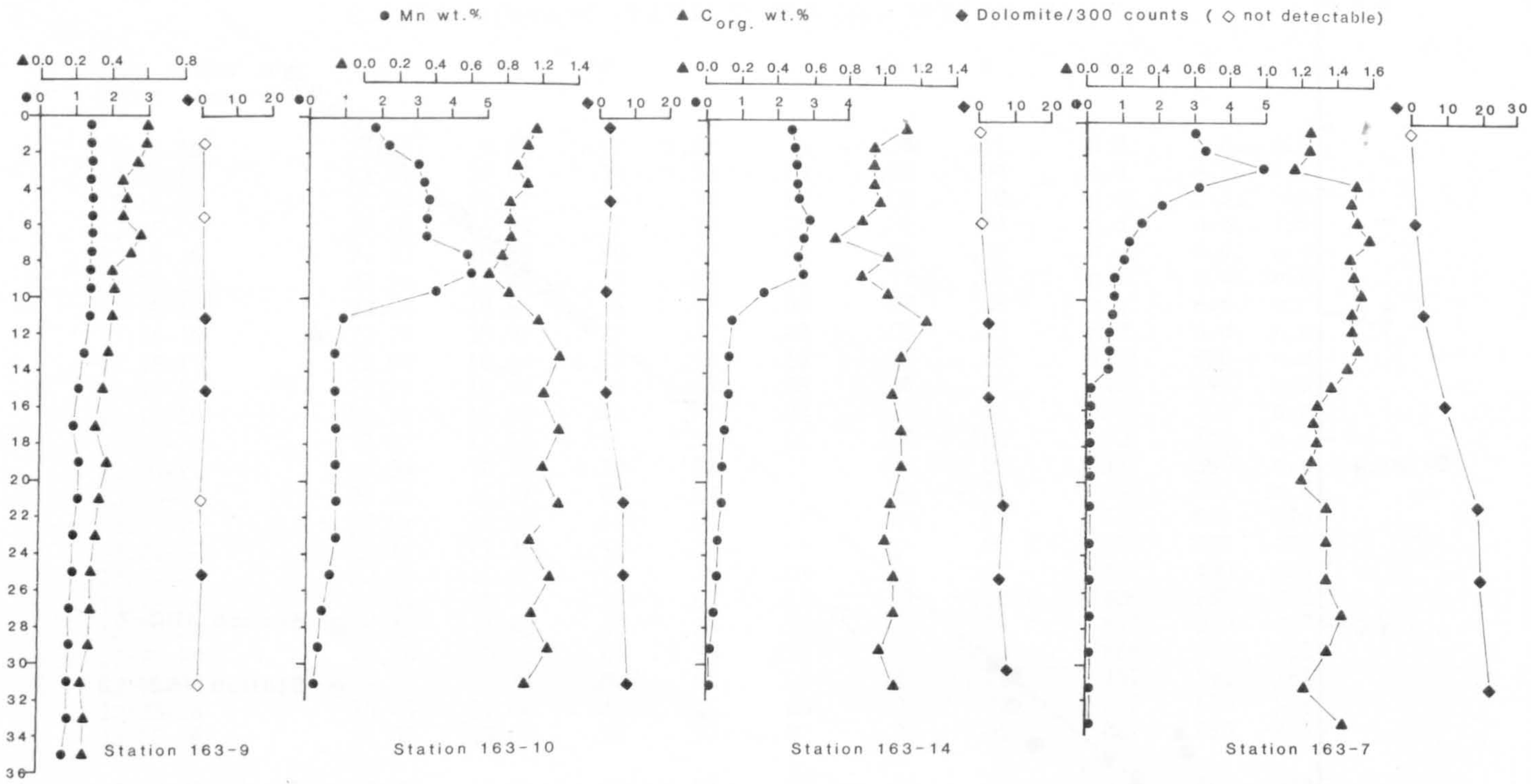

Figure 7 Vertical distribution of the frequency of dolomite estimated from counting 300 grains, solid phase Mn (wt.%) and $C_{org.}$ (wt.%) in four cores off Baja California (163-9, 163-10, 163-14, 163-7).

this wavelength. The mineral appears to be composed of mixed layer smectite phases as noted by Odin and Matter, (1981). SEM observations confirm a box-like morphology typical of early smectite phases (Figure 9B). Dolomite is seen to be intimately associated with this glauconite (Figure 9C,D) which acts as a non-corrosive cement binding the earlier formed dolomite together. Broken grains mounted in the SEM show that up to 70% of the inside of these pellets is composed of perfectly formed dolomite rhombs (Figure 9D). Glauconite extracted from this lag deposit shows dolomite to be unstable at the surface of the pellet. Here, dolomite is only recognised as highly pitted remains or rhombohedral impressions (Figure 10A,B,C,D). Clearly, formation of the dolomite proceeds that of the glauconite. Within the lag deposit only, dolomite at the surface of glauconite pellets is unstable and prone to dissolution.

POSSIBLE ORIGINS OF DOLOMITE AND THE SOURCE OF MAGNESIUM

Reports of trace amounts of dolomite rhombohedral (5-40 um.) in unconsolidated deep-sea sediments have existed over the last century (Correns, 1939; Fairbridge, 1957; Bonatti, 1966). Various conflicting views have been proposed on their origins, including detrital sources, formation due to hydrothermal metamorphism and submarine volcanism, and organic formation. Recent discoveries have focused attention on the association of dolomite with organic-rich sediment (Friedman and Murata, 1979; Pisciotto and Mahoney, 1981; Kelts and McKenzie, 1982). The formation of dolomite off Baja California seems to be consistent with these latter observations. Dolomite in IPOD cores from the Gulf of California (Kelts and McKenzie, 1982) shows that it is associated with organic-rich horizons extending from Late Pleistocene to Late Pliocene. Similar dolomite-bearing hemipelagic sediments extending down to the Miocene have been noted on the Pacific side of Baja California (Pisciotto and Mahoney, 1981). Kelts and McKenzie, (1981). Kelts and McKenzie (1982) have interpreted dolomite formation to be a result of low temperature, early diagenesis with primary precipitation of dolomite occurring in the interstitial spaces of anoxic, diatomaceous oozes. They claim that the process takes place in a subsurface system, closed to sea water exchange and characterized by low sulphate concentration. Experimental data on the replacement of calcite and aragonite by dolomite (Baker and Kastner, 1981) also suggest that dolomite formation is favored by low dissolved sulphate concentrations. Here, it is implied that the common site of dolomite formation is where the dissolved sulphate concentration is reduced by microbial sulphate reduction. Kushnir and Kastner (1982) from adsorption experiments of SO_4^{2-} on carbonates show that the residence time of adsorbed SO_4^{2-} is very short. In fact 50% of the adsorbed SO_4^{2-} is desorbed or exchanged in about ten minutes.

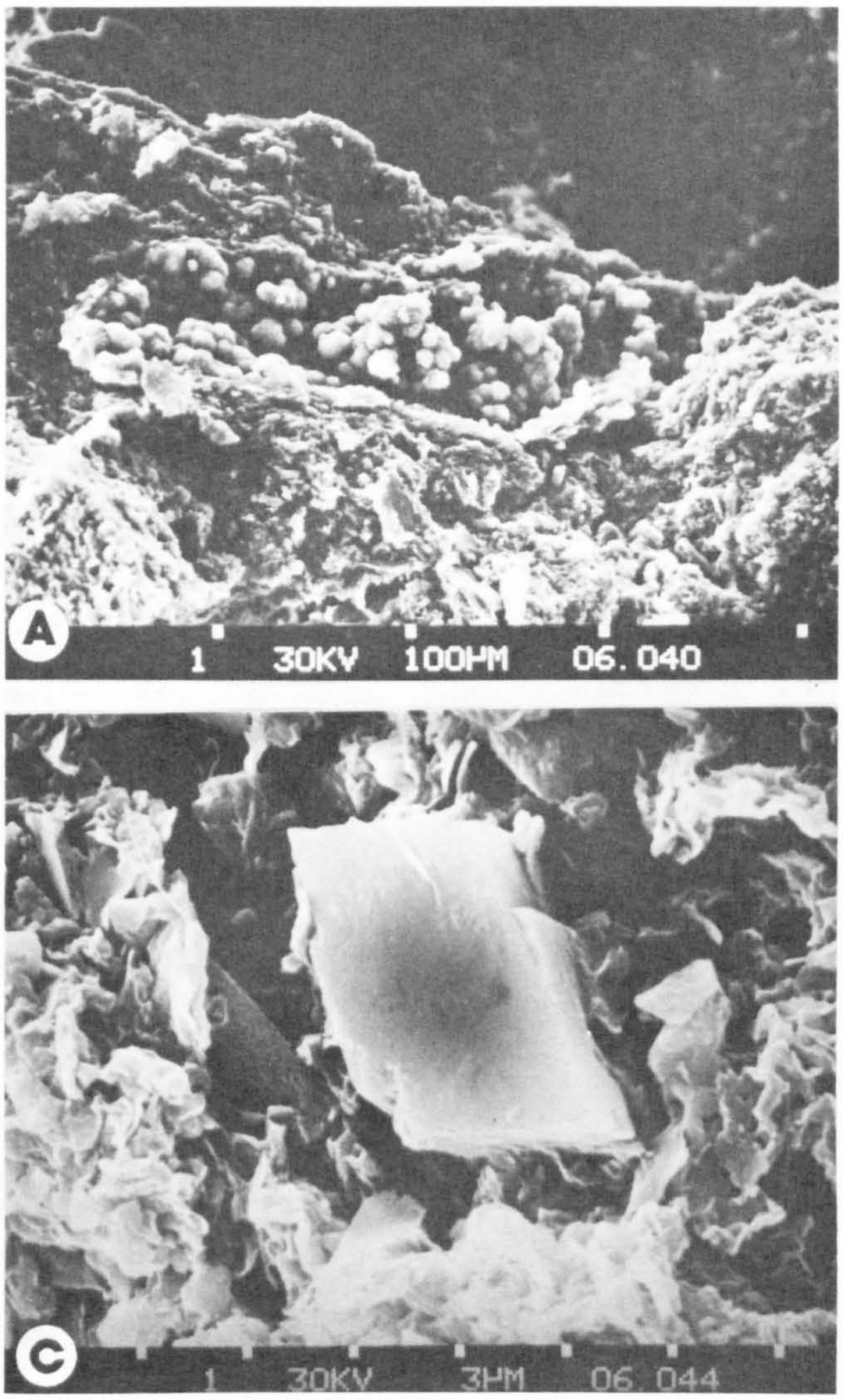

Figure 8 SEM photographs of the occurrence of dolomite in hemipelagic sediments and its association with other diagenetic phases.
(A) Botryoidal manganese carbonate growing in a cavity (163-10, 28-30 cm. depth).
(B) Close-up of the same manganese carbonate.
(C) Dolomite at the edge of the cavity surrounded by manganese carbonate.
(D) Dolomite rhomb showing evidence of dissolution from the oxidised zone of 163-14.

The observations on morphology, location, and mineral associations indicate that the Baja California dolomite formation is not related to detrital input, evaporative reflux (Adams and Rhodes, 1960), evaporative pumping (Hsu and Siegenthaler, 1969), mixed water or schizohaline (Folk and Land, 1975) processes. Hence, our interpretation of dolomite formation must be related to normal hemipelagic accumulation.

The first appearance of significant dolomite in the Baja California sediment, beneath the zone of Mn reduction and often in the presence of NO_3^-, clearly indicates that dolomite nucleation and growth can occur in the presence of SO_4^{2-} ions. Moreover, the formation of dolomite rhombs predating the development of glauconite pellets also suggests growth in the immediate subsurface environment. While this dolomite may usually occur in small quantities, its preponderance in the glauconite suggest development within this zone can be extensive. Glauconite typically forms in a non-suphidic environment common under fluctuating oxic-anoxic conditions (Odin and Matter, 1981; Berner, 1981). One of the major characteristics of glauconite is the excess of Fe^{3+} over Fe^{2+} (Burst, 1958; Odin and Matter, 1981; Ireland et al., 1983). Ideally, glauconite is most likely to occur in reducing microenvironments in an overall oxidising regime (Odin and Matter, 1981). In sediments of high sulphide activity, or post sulphide activity, it is extremely unlikely that sufficient Fe^{3+} ions would be present to account for the amount of glauconite seen.

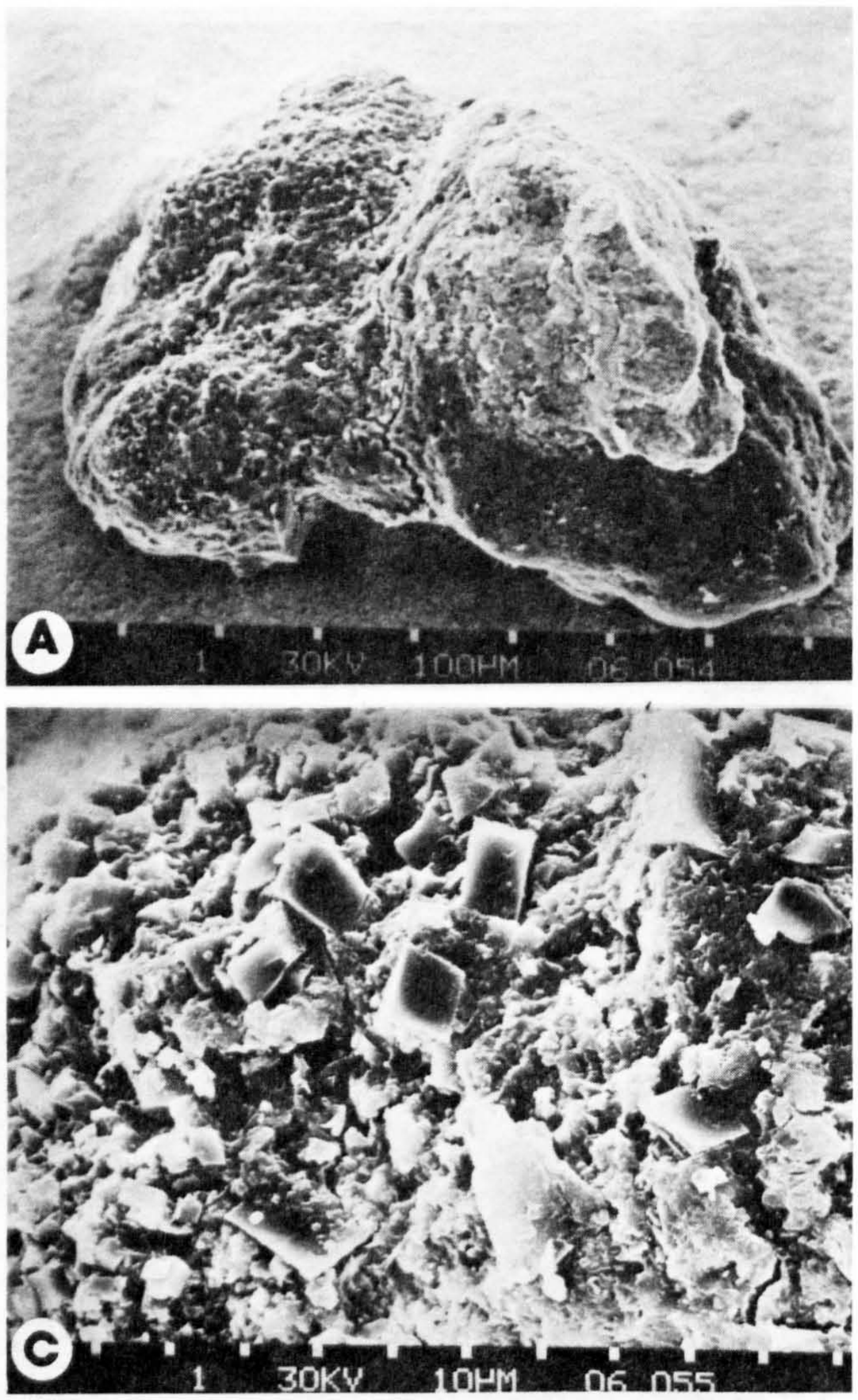

Figure 9 SEM photographs of the dolomite/glauconite association in 163-13.
(A) Grain mount of a glauconite pellet (20 cm. depth).
(B) Broken inside surface of a glauconite pellet showing box-like, smectitic clays (20 cm. depth).
(C) Surface of a glauconite pellet at depth (24 cm.), showing good euheral dolomite with no evidence of corrosion.
(D) A broken glauconite pellet showing 70% dolomite. Some glauconite is visible at the centre of the dolomite cluster (20 cm. depth).

The association of dolomite with early diagenetic manganese carbonate formed from the precipitation of Mn^{2+} under mildly reducing conditions is also consistent with SO_4^{2-} being present in the sediment. The inclusion of pyrite is some dolomite rhombs does suggest sulphate reduction, although it is not known if this is due to local reduction in microenvironments or an overall reduction of the sediment.

Thermodynamic and stability calculations have suggested that dolomite could be the stable phase in sea water (Garrels et al., 1960; Baker and Kastner, 1981). Our observation of dolomite dissolution in the uppermost sediments, particularly 163-13, implies that this is probably not correct. Within a lag deposit pore water conditions relating to alkalinity, Mg^{2+} and Ca^{2+} activity would not be significantly different from that of the overlying sea water.

The relationship between the amount of dolomite and organic matter may be significant both in respect of our understanding of dolomite formation and the source of Mg. It has been suggested that the source of Mg for dolomitization could come from sea water, organic matter or ion exchange in sediments (Milliman, 1974). With deeply formed dolomite the sea water source of Mg is obviously somewhat limited (Kelts and McKenzie, 1982), and here one may resort to an organic or ion exchange source of Mg involving clay minerals for dolomite precipitation or replacement within a sedimentary sequence. Organic-rich, diatomaceous sediments are known to have Mg concentrations in excess of those

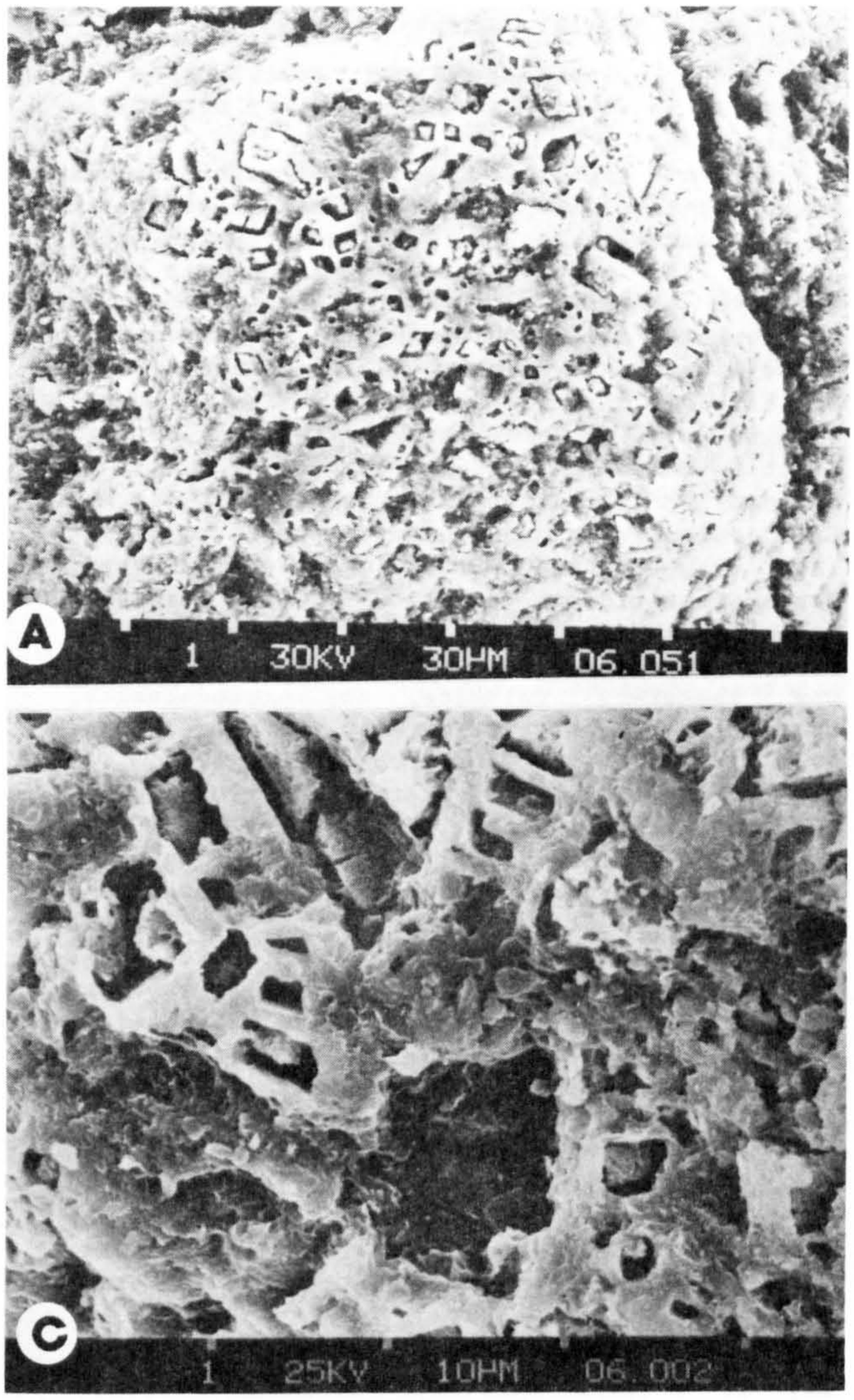

Figure 10 SEM photographs of dolomite dissolution at the surface of 163-13 in glauconite pellets from the lag deposit.

(A) Surface of the pellet with dolomite rhombs beginning to corrode.
(B) Close-up of the dolomite in (A).
(C) Glauconite with rhombohedral pits in which there is some relict dolomite remaining.
(D) Close-up of the rhombohedral pit from which all the dolomite has been completely corroded away.

held in terrigenous silicates, but even in such instances the amount of organically bound Mg tends to be modest and rarely exceeds 1 or 2% of the sediment (Calvert, 1976). With lower C_{org} found in the sediments off Baja California this source of Mg would be somewhat limited.

Preliminary measurements on accumulation of Baja California hemipelagic sediments indicate rates of 0.5 to 1.5 cm./1000 years for those sediments existing in the reducing zone. Moreover, excess ^{230}Th measurements show that the oxidising layer may be entirely bioturbated. Estimates of bioturbation in Pacific sediments suggest the top 10 to 20 cms. may be entirely biomixed every 1000 years. Certainly the rate of biomixing is considerably greater than sediment accumulation (Turekian et al., 1978). The profiles of solid phase Mn in Figure 7 could be interpreted in terms of a surface bioturbated layer and an underlying zone of steady state accumulation. If extensive bioturbation occurs in the Baja California sediment, irrigation of this surface could bring sufficient Mg within the entrained waters for significant amounts of dolomite to form at, or near, this redox boundary. Due to the low sedimentation rate Mg may also reach this zone by diffusing in from the overlying sea water (Gieskes, 1975). The presence of minor amounts of dolomite within the oxidising layer could be caused by precipitation within microenvironments, or alternatively, could have formed at the locus of dolomite precipitation within the reduced sediment and been subsequently transported by benthic activity.

The mechanism of dolomitization within the uppermost reduced sediment, or at the redox boundary, is unknown, but higher alkalinity in the reduced sediment may be one factor leading to its precipitation. Elevated Mg/Ca ratios that have previously been considered important in the formation of supratidal dolomite are not a limiting requirement. This view is also held by Baker and Kastner (1981) and Kelts and McKenzie (1982) in the formation of deep-sea dolomite.

Variation in input of $C_{org.}$ to the sediments will affect the subsurface environment in two ways. Firstly, it is likely to produce variation in the total dissolved C in the reduced sediment which may have some bearing on the dolomite formation. Secondly, and perhaps more importantly, it may induce a range of benthic activity and corresponding entrainment of sea water Mg to the zone of reduction leading to dolomitization. The occurrence of dolomite in many ancient sediments is often associated with bioturbation as seen in the dolomite bands of the Monterey Formation of southern California (Friedman and Murata, 1979).

Laboratory experiments on dolomite kinetics (Gaines, 1980) show it to be extremely slow growing. Within the rapidly accumulating sediments of the shelf, conditions conducive to dolomite growth are changing too rapidly for precipitation to take place. Here, incipient dolomite formed would be rapidly buried before significant crystal growth could be achieved. Within organic-poor oceanic red clays a low rate of sediment mixing from bioturbation again reduces the likelihood of significant quantities of dolomite. It would seem that the slowly accumulating hemipelagic sediments, with high $C_{org.}$ contents due to elevated biological productivity as is seen here, represent an ideal locus for dolomite precipitation. In the eastern Pacific the generally low terrigenous supply coupled wit high biological productivity, suggests that this area of the ocean in highly conducive towards early diagenetic dolomite formation. Reports of some rhombohedral dolomite in late Cenozoic hemipelagic sediments from IPOD cores (Pisciotto and Mahoney, 1981; Kelts and McKenzie, 1982) and in dredge hauls (Kulm et al, 1981) suggests they may have formed in the manner described.

Dolomite formation in deeply buried sediments undoubtedly occurs. Such late formation has been evidenced by the isotopic composition of the mineral and its pervasive growth in certain horizons. We suggest that the earliest formed dolomite, as is seen in the immediate subsurface environment off Baja California, may act as a substrate for further dolomite precipitation, especially during methanogenesis after sulphate has been consumed. Growth of this dolomite is obviously limited by the amount of residual sea water and organic Mg within the sediment and the extent of ion exchange involving Mg from clay minerals, during diagenesis. Such dolomite is not likely to be uniformly precipitated within the sediment, but is going to be confined to those horizons with prior dolomite. In the exceptional case (as in 163-13) of very high $C_{org.}$ and benthic activity, early dolomite formation can be extensive.

SUMMARY AND CONCLUSIONS

Our observations on the distribution of dolomite in subsurface sediments off Baja California show:

1. Dolomite precipitation occurs principally in hemipelagic sediments seen from the shelf break to the continental rise. Sediments on the shelf and in the oceanic setting show little or no dolomite genesis. Within the hemipelagic environment dolomite abundance broadly correlates with the level of $C_{org.}$ in the sediment.
2. Vertical distribution of dolomite in hemipelagic shallow cores show that within the silt fraction dolomite forms in reduced sediment, as defined by the distribution of solid phase Mn. Here, dolomite abundance again appears to correlate with the amount of $C_{org.}$ in the sediment. Trace quantities of dolomite within oxidising sediments show evidence of dissolution.
3. Structurally, the dolomite is well-ordered and therefore dolomite, not protodolomite. Chemically, it contains 56 mole % $CaCO_3$, found by XRD and electron microprobe analysis.
4. The association of other diagenetic minerals and dolomite shows that whereas pyrite and barite can predate dolomite precipitation the growth of glauconite, occurring as "nascent", grey-green, friable, fissured pellets, occurs after dolomite precipitation. Early diagenetic manganese carbonate appears to postdate the formation of dolomite. Some of these associations clearly indicate that dolomite forms as an early diagenetic mineral in the presence of SO_4^{2-} ions.
5. The relationship between dolomite and $C_{org.}$ within these sediments has been interpreted in terms of levels of benthic activity allowing sea water Mg to be entrained within the sediment, and its precipitation as dolomite near the zone of reduction.
6. We believe that this early formed dolomite may be a useful substrate for further dolomite growth during burial.
7. The combination of slow total sediment accumulation and high surface productivity, as occurs along the eastern margin of the Pacific ocean, appears to produce an ideal site for early diagenetic dolomite.

ACKNOWLEDGEMENTS

We wish to thank the University of Washington and crew of the R/V ~~Thomas~~ G. ~~Thompson~~ for their assistance in obtaining core material for this work. We would like to thank, in particular, Dr. Jim Murray for his encouragement and support in this work.

We would also like to thank Andrew Ross and the staff of the M.R.C. Electron Microscope Unit at Western General Hospital, Edinburgh for the use of their facilities.

This research was sponsored by the Natural Environment Research Council, U.K.

REFERENCES CITED

Adams, J.E. and Rhodes, M.L., 1960, Dolomitization by seepage refluxion: Am. Assoc. Petroleum Geologists Bull., v. 44, p. 1912-1920.

Aschman, H., 1959, The Central Desert of Baja California: Demography and Ecology; Univ. Calif. Pres, Berkeley, Calif., 315 pp.

Baker, P.A. and Kastner, M., 1981, Constraints on the formation of sedimentary dolomite: Science, v. 213, p. 214-216.

Behrens, E.W. and Land, .S., 1972, Subtidal Holocene dolomite, Baffin Bay, Texas: Jour. Sed. Petrology, v. 42, p. 155-161.

Berner, R.A., 1981, A new geochemical classification of sedimentary environments: Jour. Sed. Petrology, v. 51, p. 359-365.

_____, 1980, Early Diagenesis: Princeton Univ. Press, Princeton, 241 pp.

Bonatti, E., 1966, Deep sea authigenic calcite and dolomite: Science, v. 153, p. 534-537.

Burst, J.F., 1958, Mineral hereogeneity in "glauconite" pellets: Am. Mineralogist, v. 43, p. 481-497.

Burton, W.K., Cabrera, N. and Frank, F.C., 1951, The growth of crystals and equilibrium structure of their surfaces: Royal Soc. Lond. Philos. Trans. v. A-243, p. 299-358.

Calvert, S.E., 1976, The mineralogy and geochemistry of nearshore sediments: in Riley, J.R. and Chester, R. (eds.) Chemical Oceanography Vol. 6, Academic Press, London, p. 187-271.

Correns, C.W., 1939, Pelagic sediments of the North Atlantic Ocean: in Trask, P.D. (ed.) Recent Marine Sediments, Am. Assoc. Petroleum Geologists, p. 373-395.

Curtis, C.D., Evans, G., Kinsman, D.J.J., and Shearman, D.J., 1963, Association of dolomite and anhydrite in Recent sediments of the Persian gulf: Nature, v. 197, p. 679-680.

D'Anglejan, B.F., 1967, The origin of marine phosphorites off Baja California: Mar. Geol., v. 5, p. 15-44.

Deer, W.A., Howie, R.A. and Zussman, J., 1966, An Introduction to Rock Forming Minerals: Longman, London, 528 pp.

Deffeyes, K.S., Lucia, F.J., and Weyl, P.K., 1964, dolomitization: observations on the island of Bonaire, Netherlands Antilles: Sciences, v. 143, p. 678-679.

Emery, K.O., 1960, The Sea Off Southern California; Wiley, New York, 366 pp.

Fairbridge, R.W., 1957, The dolomite question: in LeBlanc, R.J. and Breeding, J.G. (eds.), Regional Aspects of Carbonate Deposition, Soc. Econ. Paleontologists and Mineralogists Spec. Pub. 15, p. 125-178.

Folk, R.L. and Land, L.S., 1975, Mg/Ca ratio and salinity: Two controls over crystallization of dolomite: Am. Assoc. Petroleum Geologists Bull., v. 59, p. 60-68.

Friedman, I. and Murata, K.J., 1979, Origin of dolomite in Miocene Monterey Shale and related formations in the Temblor Range, California: Geochim. Cosmochim. Acta, v. 43, p. 1357-1365.

Gaines, A.M., 1980, Dolomite kinetics: Recent experimental studies: in Zenger, D.H., Dunham, J.B. and Ethington, R.L., (eds.) Concepts and Models of Dolomitization: Soc. Econ. Paleontologists and Mineralogists Spec. Pub. 28, p. 81-86.

_____, 1977, Protodolomite redefined: Jour. Sed. Petrology, v. 47, p. 543-546.

Galehouse, J.S., 1969, Counting grain mounts: number percentage vs. number frequency: Jour. Sed. Petrology, v. 39, p. 812-815.

Garrels, R.M., Thompson, M.E. and Siever, R., 1960, Stability of some carbonates at 25°C and one atmosphere total pressure: Am. Jour. Sci., v. 258, p. 402-418.

Gieskes, J.M., 1975, Chemistry of interstitial waters of marine sediments: Annual Review of Earth and Planetary Sciences, v.3, p. 433-453.

Glover, E.D. and Sippel, R.F., 1967, Synthesis of magnesium calcites: Geochim. Cosmochim. Acta, v. 31, p. 603-613.

Goldsmith, J.R. and Graf, R.E., 1958, Relation between lattice constants and composition of the Ca-Mg carbonates: Am. Mineralogist, v. 43, p. 84-101.

_____,_____,and Heard, H.C., 1961, Lattice constants of the calcium - magnesium carbonates: Am. Mineralogist, v. 46, p. 453-457.

Graf, D.L., and Goldsmith, J.R., 1956, Some hydrothermal synthesis of dolomite and protodolomite: Jour. Geology, v. 64, p. 173-187.

Hsu, K.J. and Siegenthaler, C., 1969, Preliminary experiments on hydrodynamic movement induced by evaporation and their bearing on the dolomite problem: Sedimentology, v. 12, p. 11-25.

Illing, L.V., Wells, A.J., and Taylor, J.C.M., 1965, Penecontemporary dolomite in the Persian Gulf: in Pray, L.C. and Murray, R.C. (eds.) Dolomitization and Limestone Diagenesis: A Symposium, Soc. Econ. Paleontologists and Mineralogists Spec. Pub. 13, p. 487-499.

Ireland, B.J., Curtis, C.D. and Whiteman, J.A., 1983, Compositional variation within some glauconites and illites and implications for their stabilities and origins: Sedimentology, v. 30, p. 769-787.

Jahnke, R.A., Emerson, S.R., Roe, K.K. and Burnett, W.C., 1983, The present day formation of apatite in Mexican continental margin sediments: Geochim. Cosmochim. Acta, v. 47, p. 259-266.

Kelts, K.R. and McKenzie, J.A., 1982, Diagenetic dolomite formation in Quaternary anoxic diatomaceous muds of Deep Sea Drilling Project Leg 64, Gulf of California: Init. Repts, DSDP, v. 64 pt. 2, p. 553-569.

Kulm, L.D., Thornburg, T.M., Schrader, H., Masias, A., Resig, J.M., and Johnson, L., 1981, Late Cenozoic carbonates on the Peru continental margin: Lithostratigraphy, biostratigraphy, and tectonic history: Geol. Soc. America Memoir 154, p. 469-509.

Kushnir, J. and Kastner, M., 1982, Adsorption of sulfate ions on calcite, aragonite and dolomite: Their role in inhibiting dolomitization: (abs.) EOS, v. 63, p. 999.

Land, L.S., 1973, Holocene meteoric dolomitization of Pleistocene limestones, North Jamaica: Sedimentology, v. 20, p. 411-424.

____, 1980, The isotopic and trace element geochemistry of dolomite: the state of the art: in Zenger, D. H., Dunham, J.B. and Ethington, R.L. (eds.), Concepts and Models of Dolomitization: Soc. Econ. Paleontologists and Mineralogists Spec. Publ. 28, p. 87-110.

____, Salem, M.R.I. and Morrow, W.F., 1975,, Paleohydrology of ancient dolomites: Geochemical evidence: Am. Assoc. Petroleum Geologists Bull., v. 59, p. 1602-1625.

Lyle, M., 1983, The brown-green color transition in marine sediments: A marker of the Fe(III) - Fe(II) redox boundary: Limnol. Oceanography, v. 28, p. 1026-1034.

Milliman, J.D., 1974, Marine Carbonates, Spring Verlag, New York, 375 pp.

Mueller, H.W., 1975, Centrifugal progradation of carbonate banks: A model for deposition and early diagenesis, Ft. Terett Formation, Edwards group, Lower Cretaceous, Central Texas: Ph.D. Diss. Univ. Texas at Austin, 300 pp.

Nielsen, A.E., 1964, Kinetics of Precipitation: MacMillan, new York, 151 pp.

Norrish, K. and Hutton, J.J., 1969, An accurate x-ray spectographic method for the analysis of a wide range of geological samples: Geochim. Cosmochim. Acta, v. 33, p. 431-453.

Odin, G.S. and matter, A., 1981, De glauconiarum origin: Sedimentology, v. 28, p. 611-641.

Pederson, T.F. and Price, N.B., 1982, The geochemistry of manganese carbonate in Panama Basin sediments: Geochim. Cosmochim. Acta, v. 46, p. 59-68.

Pedone, V.A., 1978, Petrography, chemistry and crystallography of baroque dolomite, Kingsport, Tennessee: M.A. Thesis, Univ. Texas at Austin, 142 pp.

Pisciotto, K.A. and Mahoney, J.J., 1981, Isotopic survey of diagenetic carbonates, Deep Sea Drilling Project Leg 63: Init. Repts. DSDP, v. 63, p. 595-609.

Ried, J.L., Roden, G.I., and Wyllie, .G., 1958, Studies of the California Current System: Calif. Coop. Oceanic Fisheries Investigation Progr. Rept., 1 July 1956 - 1 Jan 1958, p. 27-57.

Sawlan, J.J., 1982, Early diagenetic remobilization of some transition metals in hemipelagic sediments: Ph.D. Thesis, Univ. of Washington, 251 pp.

Sawlan, J.J., and Murray, J.W., 1983, Trace metal remobilization in the interstitial waters of red clay and hemipelagic marine sediments: Earth and Planet. Sci. Lett., v. 64, p. 213-230.

Shinn, E., Ginsburg, R.N. and Lloyd, R.M., 1965, Recent supratidal dolomite from Andros Island: in Pary, L.C. and Murray, R.C. (eds.) Dolomitization and Limestone Genesis: Soc. Econ. Paleontologists and Mineralogists Spec. Pub. 13, p. 112-123.

Supko, P.R., 1977, Subsurface dolomite in modern carbonate sediments along the southern coastal of Florida: Science, v. 134, p. 561-562.

Taft, W.H., 1961, Authigenic dolomite in modern carbonate sediments along the southern coast of Florida: Science, v. 134, p. 561-562.

Turekian, K.K., Cochran, J.K. and De Master, D.J., 1978, Bioturbation in deep-sea deposits: Rates and consequences: Oceanus, v. 21, p. 34-41.

Von der Borch, C.C., 1965, The distribution and preliminary geochemistry of modern carbonate sediments of the Coorong area, South Australia: aeochim. Cosmochim. Acta, v. 29, p. 781-799.